Developing *Ex Vivo* Models for Understanding Microbial Infection Associated with Hip and Knee Implants

A Thesis submitted to Cardiff University in fulfilment of the requirements for the degree of Doctor of Philosophy (PhD)

2022

Jabur Salim Khan, B.Sc. (Hons), MSc.

Oral and Biomedical Sciences

School of Dentistry

Cardiff University

Dedication

In memory of my grandparents and Adil
who would have been so proud.

Acknowledgments

First and foremost, I would like to thank ALLAH, the almighty, for providing me with the opportunity, strength and belief that I could complete this Thesis.

I would like to thank my principal supervisor, Professor Rachel Waddington, for her patience with me over the last few years, whilst also giving me belief that I could complete this Thesis, especially when I thought I could not achieve it. Your guidance, advice and encouragement have meant a lot and I have truly learnt a lot from you, I shall always take "research is the sequential acquisition of knowledge" with me everywhere I go. I would like to thank my second supervisor, Professor Alastair Sloan, for your input, knowledge and generosity within this PhD, it has truly been invaluable. You always had time to guide and support me throughout this journey especially when you have been so busy. Finally, I would also like to thank my third supervisor, Mr Stephen Jones, for his valuable feedback and clinical knowledge and allowing me to observe a clinical procedure giving context to the importance of this research.

I would like to thank the Technical Staff for their support during my PhD. To Wendy Rowe for her advice on microscopy imaging and helping me take some amazing SEM images. To Dr Fiona Gagg, who helped me settle back into the lab, after my major leg operations and ensuring that I had a safe environment to work in. To Dr Sarah Youde, for her advice in tissue culture and putting up with me using the wrong prices and product codes on order forms. To Martin Langley, for his various tools that have saved the day. To Dr Sarah Bamford, for her advice and patience with me learning microbiology and calming me down when things got too much. To Dr Maria Stack, for her assistance in molecular biology even if it did not work. I have to thank Alan Lloyd-Jones for washing all my glassware and ensuring that we never run out of PBS and distilled water.

I must praise the whole Pathology Team, especially Hayley Pincott and Sue Wozniak, for their advice on immunohistochemistry, teaching me the importance of positive controls, whilst helping and guiding me when things got too much. You both have made me laugh so much I always looked forward coming into work to see you. To Dr Adam Jones, for your histological advice especially when you were so busy with clinics. I will always remember the various stories you have told me over the years while I was working in the lab.

I would like to thank the various members of MTG, especially Dr Amr Alraies and Dr Wayne Ayre, on their patience, support and advice on the model when things didn't go so well. To Dr Ryan Moseley, who always cheered me on from the side lines. To the various inhabitants of the MTG office; Paul, Lucy, Steven, Zahraa, Ahmed, Mai, Agnes and Carmen who put up with me every day you all deserve a medal. I have to thank my two good friends, Rob and Ed, who have been there every day during lockdown whilst I been writing this Thesis making me laugh, providing moral support and helping to me when things got tough, you both have been amazing. To Daniel Morse, who has always been there for me, made me laugh and filled my phone with his selfies.

I must mention all the wonderful friends in Dental that I have met over the years; Ana, Rae, Helen, Sian, Richard, Emma Woods, Emma BD, Lleucu, Peter, Uzma, Takwa, Katrina,

Yamama, Jordanna, Rhiannon, Joana, Elen and Genevieve, I couldn't have done this journey without you all.

I must give a special mention to the Student Support Team, especially to the dyslexia support workers Diane Dobbs and Terence Morgan, on their advice, guidance and academic counselling. For telling me that it doesn't matter if you are dyslexic, you can do a PhD and write a Thesis, that there may be bumps along the way, but it is possible to achieve and to never tell yourself you can't, you can and you will.

I must give huge gratitude to my family, especially to my parents, who have shared my laughs, my tears and anger over the last five years. For putting up with my constant moaning, listening to my various issues and giving advice. I will always be in indebted you both of you for everything you have done in my life. You both have always pushed me and believed in me, your love and support mean the world and I will always cherish it.

To my wonderful sisters Ariba for always pushing, helping and supporting me, Anila and Rubeena for all your love and support throughout this journey. I apologise I could not always be there for you all when I had to be in the lab at odd hourss. To my nephews and nieces who always shone a light when it got dark.

To my family Rahila Khala, Shuby Khala, Bano (Sarwat) Khala, Hina, Shanaz Phuppo and all the others who are too many to name, for your duas, words of encouragement and additional support.

I would like to dedicate this Thesis to my late cousin Adil Khan and my grandparents Zakia Begum and Muhammad Khursheed Khan, who sadly passed away during this journey, I hope I can make you all proud and you will always be carried within my heart. May ALLAH give you eternal happiness.

Abstract

Bacterial infections surrounding orthopaedic implants hinder the process of bone repair and prevent osteointegration leading to surrounding bone loss and subsequent implant loosening post-loading. However, the relationship between a commonly occurring implant infectious organism, *Staphylococcus aureus* (*S. aureus*) and the local bone marrow cell population is poorly understood. No adequate *ex vivo* model to investigate the mechanism leading to bacterial-induced osteolysis currently exists.

This research sought to develop and characterise a novel, *ex vivo* bone marrow co-culture model to investigate specific cell responses following *S. aureus* infection.

Slices of rat femurs were cultured up to 48 h either submerged within the culture media (base-type culture) or suspended at a liquid/air interface (Trowell-type culture). Both culture models demonstrated significant cell loss and cell death, however, the Trowell-type culture had better maintenance of cell numbers. Cellular analysis indicated the reduced cell numbers of monocytes, macrophages and neutrophil populations over 48 h. Supplementation of the Trowell-type culture with macrophage-colony stimulating factor (M-CSF) and receptor activator of the nuclear factor kappa B ligand (RANKL) to the culture media maintained CD14 and CD68 positive monocyte and macrophage populations but showed no significance when compared to slices without M-CSF and RANKL. The addition of the cytokines at 20 ng/mL M-CSF and 30 ng/mL RANKL maintained low numbers of multinucleated CD68 osteoclast-like cells at 24 h and 48 h. This research further established that the *ex vivo* model could be manipulated by microinjection of cytokines at a concentration of 20 ng/mL M-CSF and 30 ng/mL RANKL with or without tibial bone marrow cells into the bone marrow cavity with improved cell numbers compared to non-injected slices. Microinjection of cytokines into the bone marrow cavity with and without tibial bone marrow cells had reduced extracellular LDH release along with improved CD14 and CD68 cell numbers over 48 h in culture. Following infection with either *S. aureus* NCTC 6571 or the NCTC 7791 strains, cells responded with significant loss of cells along with increased necrosis and apoptosis. Infected slices demonstrated an increase of pro-inflammatory cytokines Tumor Necrosis Factor alpha, interleukin (IL)-1β, and IL-6. The anti-inflammatory levels following infection were low for both IL-4 and IL-10. Histomorphology assessment identified *S. aureus* colonies within the bone marrow cavity and in the case of the NCTC 7791 type strain, there was the presence of a biofilm-like structure attached to the surrounding cortical bone.

This research demonstrates the challenges in developing an *ex vivo* bone marrow culture model which can support immune cell populations which play key roles in bone resorption. Post-infection, there was an increased presence of pro-inflammatory cytokines and increased cellular necrosis and apoptosis. The *ex vivo* bone marrow microenvironment can be manipulated with cells, supplements and bacteria. The model, therefore, has the potential to observe interactions of specific cells to the presence of bacterial species within a three-dimensional model. With all results considered, this model has the potential to further understand the processes involved during early orthopaedic infections whilst aiding in the development and assessment of novel therapeutic interventions.

Table of Contents

Declaration ..... **i**

Dedication ..... **ii**

Acknowledgments ..... **iii**

Abstract ..... **v**

Table of Contents ..... **vi**

Table of Figures ..... **xi**

List of Tables ..... **xii**

List of Abbreviations ..... **xiii**

Chapter 1: General introduction **1**

1.0: Introduction **2**

1.1: Bone Biology and Normal Bone Homeostasis **4**

1.1.1: Role of Mesenchymal Stromal Cells and Osteoblasts in Bone Formation and Repair *5*

1.1.2: Role of Osteoclasts in Bone Remodelling and Repair *9*

1.1.2.1: Osteoclast Differentiation and Signalling Pathways 12

1.1.3: Role of Osteocytes *15*

1.2: Osteoimmunology **17**

1.2.1: Osteoimmunology *17*

1.2.1.1: The Innate Immune Response 17

1.2.1.2: The Adaptive Immune Response 18

1.2.2: Cells Involved in the Immune Response *19*

1.2.2.1: Neutrophils 19

1.2.2.2: Monocytes 21

1.2.2.3: Macrophages 22

1.2.2.4: Dendritic Cells 23

1.2.2.5: Natural Killer Cells 24

1.2.2.6: T-lymphocytes 24

1.2.3: Pro-inflammatory Cytokines *25*

1.2.3.1: Interleukin-1 Beta 28

1.2.3.2: Tumor Necrosis Factor-Alpha 29

1.2.3.3: Interleukin-6 31

1.3 Microorganisms Associated with Orthopaedic Implant Infections **35**

1.4: *Staphylococcus aureus* **38**

1.4.1: Subpopulation of S. aureus *38*

1.4.2: Staphylococcus Binding Proteins and Modes of Attachment *39*

1.5: Process of *Staphylococcus aureus* Induced Dysregulation of Bone Homeostasis and Immune Evasion 41

1.5.1: Dysregulation of the Bone Remodelling Unit 41

1.5.2: Staphylococcus aureus Mechanisms of Immune Evasion 42

1.5.2.1: Abscess Formation 43
1.5.2.2: Development of an *S. aureus* Related Biofilms 44
1.5.2.3: Bacterial Evasion of Immune Cells 48
1.5.2.4: Bacterial Evasion of Phagocytosis and Intracellular Survival 49

1.6: Preclinical *In Vitro, In Vivo* and *Ex Vivo* Models for Prosthetic Joint Infections 51

1.6.1: In Vitro Models 51

1.6.2: In Vivo Models 53

1.6.3: Ex Vivo Models 54

1.7: Aims and Objectives 64

Chapter 2: Development of an *Ex Vivo* Femoral Slice Model 65

2.1: Introduction 66

2.2: Material and Methods 71

2.2.1: Extraction and Obtaining the Semi-Cylindrical Femoral Slices 71
2.2.2: Removal of the Positive Control Tissues 71
2.2.3: Culture of *ex vivo* Semi-Cylindrical Femoral Slices 72
2.2.3.1: Culture of ex vivo Femoral Slices Within Culture Media (Base-Type Cultures) 73
2.2.3.2: Culture of ex vivo Femoral Slices at the Liquid-Air Interface (Trowel-Type Cultures) 73
2.2.3.3: Culture of Hydrogen Peroxide Treated Trowell-type Cultured Positive Control Slice to Induce Necrosis 74
2.2.3.4: Sample Collection and Storage 74
2.2.4: Detection of Necrosis Using the Colorimetric Lactate Dehydrogenase Assay 75
2.2.5: Tissue Decalcification, Processing and Sectioning 76
2.2.5.1: Fixation and Decalcification 76
2.2.5.2: Automated Processing of Semi-Cylindrical Femoral Slices 76
2.2.5.3: Sectioning of Femoral Slices 77
2.2.6: Haematoxylin and Eosin Staining 77
2.2.7: Osteoclast Staining 78
2.2.8: Immunohistochemistry Analysis of Specific Immune, Apoptotic and Necrotic Antibodies 79
2.2.9: Imaging 82
2.2.10: Image Analysis 82
2.2.11: Statistical Analysis 84

2.3: Results 85

2.3.1: Histomorphology Evaluation of Bone Marrow Cells Using H&E of Trowell and Base-Type Cultures 85
2.3.2: Cellular Nuclear Counts of Bone Marrow Cells 89
2.3.3: External Cells Within the Culture Media or Agarose Gel 91
2.3.4: Cellular Necrosis Analysis of Base and Trowell-Type Cultures 92
2.3.4.1: Immunohistochemistry Analysis of LDH localisation for Base- and Trowell-Type Cultures 92
2.3.4.2: LDH Absorbance and Percentage Cytotoxicity Following Culture With Base- and Trowell-Type Cultures 97
2.3.5: Analysis of Apoptosis Cell Localisation Within Base- and Trowell-Type Culture Systems 100
2.3.5.1: Analysis of Cleaved Caspase-3 Immunohistochemistry Localisation 100
2.3.5.2: Analysis of BAX Immunohistochemistry Localisation 105

2.3.6: Immunohistochemical Detection of Bone Marrow Immune Cells Within the Trowell-Type Cultures Over 48 h 110
2.3.6.1: Immunohistochemical Detection of CD14 Cells 110
2.3.6.2: Immunohistochemical Detection of CD68 Cells. 110
2.3.6.3: Detection of Trap Positive Multinucleated Osteoclast-Like Cells 112
2.3.6.4: Immunohistochemical Detection of Neutrophils 112
2.3.7: Immunohistochemical Detection of Bone Marrow Multipotent Mesenchymal Stromal Cell Markers Within the Trowell-Type Culture Over 48 h 119

2.4: Discussion 125

Chapter 3: Manipulation of the Femoral Slice Model with Pro-Osteoclastic Cytokines and Injection of Bone Marrow Cells 133

Chapter 3.1: Introduction 134

3.2: Material and Methods 138

3.2.1: Extraction of Rodent Tibial Bone Marrow Cells 138

3.2.2: Culture of ex vivo Femoral Slices. 139
3.2.2.1: Extraction and Obtaining of Semi-Cylindrical Femoral Slices 139
3.2.2.3: Microinjection of Tibial Mixed Bone Marrow into the *ex vivo* Femoral Slices. 139

3.2.3: Detection of Necrosis Using a Colourimetric Lactate Dehydrogenase Assay 140
3.2.4: *In Vitro* Culture of Osteoclast Precursors with M-CSF and RANKL supplementation 140

3.2.4: In Vitro and Ex vivo Osteoclast staining 141

3.2.5: Haematoxylin and Eosin Staining 142

3.2.6: Immunohistochemistry Analysis of Specific Immune, Apoptotic and Necrotic Antibodies 142

3.2.7: Imaging and Image Analysis 142

3.2.8: Statistical Analysis 143

3.3: Results 144

3.3.1: Bone Marrow Cells Induce Osteoclast-like Cell Formation in the Presence of M-CSF and RANKL 144

3.3.2: Nuclear Cellular Counts of the Bone Marrow Following M-CSF and RANKL Supplementation 146
3.3.2a: Nuclear Cellular Counts of the Bone Marrow Following M-CSF and RANKL Supplementation Within the Surrounding Culture Media 146
3.3.2b: Cellular Counts for Femoral Slices Supplemented With M-CSF and RANKL With Microinjection of Mixed Tibial Bone Marrow Cells 148
3.3.2c: Cellular Counts for Femoral Slices Supplemented With M-CSF and RANKL Without Microinjection of Mixed Tibial Bone Marrow Cells 149

3.3.3: Cellular Viability 151
3.3.3a: Cellular Necrosis of Extracellular LDH Release From Slices Supplemented With M-CSF and RANKL 151
3.3.3b: Extracellular LDH Analysis of Slices Supplemented With M-CSF and RANKL and Injected With Tibial Mixed Bone Marrow Cells. 154
3.3.3c: Extracellular LDH Analysis of Slices Supplemented With M-CSF and RANKL and Without Injection With Tibial Mixed Bone Marrow Cells. 154

3.3.4: Analysis of Apoptosis Cell Localisation Within Slices Supplemented With M-CSF and RANKL 157
3.3.4a: Analysis of Cleaved Caspase-3 Immunohistochemistry Localisation In M-CSF and RANKL Supplemented Femoral Slices 157
3.3.4b: Analysis of Cleaved Caspase-3 Immunohistochemistry Localisation in Slices Injected With M-CSF and RANKL With Or Without Mixed Tibial Bone Marrow Cells. 160

3.3.4d: Analysis of BAX Immunohistochemistry Localisation in M-CSF and RANKL Supplemented Femoral Slices.....163
3.3.4e: Analysis of BAX Immunohistochemistry Localisation in Slices Injected With Or Without M-CSF and RANKL With Mixed Tibial Bone Marrow Cells.....166

3.3.5: Immunohistochemical Detection of Bone Marrow Monocytes, Macrophages and Osteoclasts Following Supplementations With M-CSF and RANKL.....170
3.3.5a: Immunohistochemical Detection of Monocytes and Macrophages Using CD14 Localisation in M-CSF and RANKL Supplemented Femoral Slices.....170
3.3.5b: Immunohistochemical Detection of Monocytes and Macrophages Using $CD14^+$ Localisation in Slices Injected With M-CSF and RANKL With Or Without Mixed Tibial Bone Marrow Cells.....173
3.3.5d: Immunohistochemical Detection of Monocytes and Macrophages Using CD68 Localisation in M-CSF and RANKL Supplemented Femoral Slices.....177
3.3.5e: Immunohistochemical Detection of CD68 Positive Multinucleated Osteoclast-Like Cells in M-CSF and RANKL Supplemented Femoral Slices. 178
3.3.5f: Immunohistochemical Detection of Monocytes and Macrophages using CD68 Localisation in Slices Injected With M-CSF and RANKL With Or Without Mixed Tibial Bone Marrow Cells.....182
3.3.5g: Immunohistochemical Detection of CD68 Positive Multinucleated Osteoclast-Like Cell Localisation in Slices Injected With M-CSF and RANKL With Or Without Mixed Tibial Bone Marrow Cells. 184

3.4: Discussion 188

Chapter 4: Co-Culture of The Femoral Slice Model With *Staphylococcus aureus* 195

4.1: Introduction 196

4.2: Materials and methods 199

4.2.1: Microorganism Culture 199

4.2.2 Bacteria Enumeration of Viable Colony Forming Units (CFU).....199

4.2.3: Bacterial Growth Curves in Tissue Culture Conditions and Bacterial Culture Media.....200

4.2.4 Viability Staining of Bacterial Strains.....201

4.2.5: Co-Culture of the Femoral Slice Model.....202
4.2.5.3: Infection of *ex vivo* Semi-Cylindrical Femoral Slices.....202
4.2.5.4: Sample Collection and Storage 203

4.2.6: Detection of Necrosis Using a Colourimetric Lactate Dehydrogenase Assay.....203

4.2.7: Haematoxylin and Eosin Staining 203

4.2.8: Identification of Secreted Pro-Inflammatory and Anti-Inflammatory Cytokines Using Enzyme-Linked Immunosorbent Assay (ELISA).....203

4.2.9: Modified Gram Stain on Histological Tissue Sections to Identify Attached Bacteria Within the ex vivo Model 207

4.2.10: Scanning Electron Microscopy.....208

4.2.11: Dual Labelled Immunohistochemistry for Apoptosis, Necrosis and Immune Cell Markers Along With Staphylococcus Aureus Protein A.....209

4.2.12: Imaging and Image Analysis 210

4.2.13: Statistical Analysis 211

4.3: Results.....212

4.3.1: Bacteria Enumeration of Staphylococcus aureus.....212

4.3.2: The Growth of Staphylococcus aureus Under Standard Culture Conditions in Various Basal Culture Media. 214

4.3.3: The Viability of Staphylococcus aureus Under Standard Culture Conditions in Various Basal Culture Media. 216

4.3.3.1: The Viability of *Staphylococcus aureus* Grown in BHI Bacterial Broth Culture Media Alone. 216

4.3.3.2: The Viability of Staphylococcus aureus Grown in Tissue Culture Media Supplemented with 20 % BHI Bacterial Broth Culture Media. 217

4.3.3.3: The Viability of *Staphylococcus aureus* Grown in Tissue Culture Media Without Supplementation with BHI Bacterial Broth Culture Media. 219

4.3.4: Modified Gram-Stain of the Co-Cultured Femoral Slice Model 223

4.3.5: Scanning Electron Microscopy of the Co-Cultured Femoral Slice Model 226

4.3.6: Total Bone Marrow Cell Counts and Percentage Loss of Cells Following Infection With NCTC 6571 and NCTC 7791 228

4.3.7: Apoptosis Cell Viability Analysis Following Staphylococcal Aureus Dual-Labelling Immunohistochemistry 231

4.3.7.1: BAX Cell Viability Analysis 231

4.3.7.2: Cleaved Caspase 3 Cell Viability Analysis 235

4.3.8: Necrosis Cell Viability Analysis Following Staphylococcal Aureus Infection 239

4.3.8.1: Lactate Dehydrogenase Immunohistochemistry Necrosis Analysis 239

4.3.8.2: Detection Of Necrosis Using A Colourimetric Lactate Dehydrogenase Assay in Femoral Slices Co-Culture With *Staphylococcus aureus* 243

4.3.9: Pro-Inflammatory Cytokine Secretion 245

4.3.9.1: Interleukin-1 Beta 245

4.3.9.2: Interleukin-6 247

4.3.9.3: Tumor Necrosis Factor-Alpha 249

4.3.10: Anti-Inflammatory Cytokine Release 251

4.3.10.1: Interleukin-10 251

4.3.10.2: Interleukin-4 253

4.3.11: Immune cell analysis 255

4.3.11.1: CD14 Bone Marrow Immunohistochemistry Localisation Following Infection With NCTC 6571 and NCTC 7791 255

4.3.11.2: CD68 Bone Marrow Immunohistochemistry Localisation Following Infection With NCTC 6571 and NCTC 7791 258

4.3.11.3: Multinucleated CD68 Bone Marrow Immunohistochemistry Localisation Following Infection With NCTC 6571 and NCTC 7791 259

4.4: Discussion 262

Chapter 5: General Discussion and Future Work 269

References 281

Appendix I 322

Appendix II 342

Table of Figures

Figure 1.1: The bone remodelling process and osteoclastogenesis _____ *10*
Figure 1.2: 1.2: The molecular downstream signalling network of osteoclast precursors following stimulation with M-CSF and RANK. _____ *11*
Figure 1.3: Illustration of osteoclast, showing a sealing zone once the osteoclast binds to the bone surface using αvβ3 integrins. _____ *14*
Figure 1.4: Various pro-inflammatory signal pathways that either independently or dependently with RANK/RANKL signalling induce osteoclast differentiation. _____ *24*
Figure 1.5: The several mechanisms of S. aureus immune evasion. _____ *43*
Figure 1.6: Development of an S. aureus biofilm. _____ *46*
Figure 1.7: Oxygen and nutrient gradients within S aureus biofilms. _____ *47*
Figure 1.8: Current ex vivo bone models _____ *56*
Figure 2.1: Schematic diagram of obtaining rat semi-cylindrical femoral slices. _____ *72*
Figure 2.2: Schematic diagram of culturing semi-cylindrical femoral slices _____ *75*
Figure 2.3: Cell counts for immunocytochemistry images within the ImageJ software. _____ *83*
Figure 2.4: Haematoxylin and eosin-stained femoral slices of Trowell-type cultures. _____ *87*
Figure 2.5: Haematoxylin and eosin-stained femoral slices of base type cultures. _____ *88*
Figure 2.6: Total cell counts and percentage loss of haematoxylin and eosin stained slices for base- and Trowell- type cultures. _____ *90*
Figure 2.7: Cellular explants from base- and Trowell-type cultures. _____ *91*
Figure 2.8: Base-type cultures stained for LDH. _____ *94*
Figure 2.9: Trowell-type cultures stained for LDH. _____ *95*
Figure 2.10: LDH stained cells in base and Trowell-type cultures _____ *96*
Figure 2.11: Necrosis analysis of LDH extracellular release following culture of Base- and Trowell-type cultures. _____ *99*
Figure 2.12: Base-type cultures stained for cleaved caspase-3. _____ *102*
Figure 2.13: Trowell--type cultures stained for cleaved caspase-3. _____ *103*
Figure 2.14: Cleaved caspase-3 stained cells in base and Trowell-type cultures. _____ *104*
Figure 2.15: Base-type culture stained for BAX. _____ *107*
Figure 2.16: Trowell-type culture stained for BAX. _____ *108*
Figure 2.17: BAX stained cells in base and Trowell-type cultures. _____ *109*
Figure 2.18: Trowell-type cultures stained for CD14. _____ *114*
Figure 2.19: Trowell-type cultures stained wirth CD68. _____ *115*
Figure 2.20: Trowell-type cultures stained for tartrate-resistant acid phosphatase positive osteoclasts. _____ *116*
Figure 2.21: Trowell-type cultures stained with neutrophil elastase. _____ *117*
Figure 2.22: Immunolocalisation of immune cells in Trowell-type cultures. _____ *118*
Figure 2.23: Trowell-type cultures stained with CD73. _____ *121*
Figure 2.24: Trowell-type cultures stained for CD90. _____ *122*
Figure 2.25: Trowell-type cultures stained for CD105. _____ *123*
Figure 2.26: MSC cell markers immunolocalization within Trowell-type cultures. _____ *124*
Figure 3.1: Differentiation potential of bone marrow-derived cells into mature osteoclast-like cells following the addition of M-CSF and RANKL. _____ *145*
Figure 3.2: Total cell counts and percentage loss following culture with M-CSF and RANKL. _____ *147*
Figure 3.3: Total cell counts and percentage loss following microinjection and supplementation with M-CSF and RANKL. _____ *150*
Figure 3.4: Extracellular LDH analysis following culture with M-CSF and RANKL. _____ *153*
Figure 3.5: Extracellular LDH analysis following microinjection and culture with M-CSF and RANKL. _____ *156*
Figure 3.6: Cleaved caspase-3 analysis following culture with M-CSF and RANKL. _____ *159*

Figure 3.7: Cleaved caspase-3 analysis following microinjection and culture with M-CSF and RANKL. ... 162
Figure 3.8: BAX analysis following culture with M-CSF and RANKL. ... 165
Figure 3.9: BAX analysis following microinjection and culture with M-CSF and RANKL. ... 169
Figure 3.10: CD14 analysis following culture with M-CSF and RANKL. ... 172
Figure 3.11: CD14 analysis following microinjection and culture with M-CSF and RANKL. ... 176
Figure 3.12: CD68 analysis following culture with M-CSF and RANKL. ... 181
Figure 3.13: CD68 analysis following microinjection and culture with M-CSF and RANKL. ... 187
Figure 4.1: Bacterial enumeration standard curve. ... 213
Figure 4.2: Absorbance of bacterial suspensions grown in different mammalian and bacterial culture media. ... 215
Figure 4.3: Viability analysis of NCTC 6571 over 24 h in different culture media. ... 221
Figure 4.4: Viability analysis of NCTC 7791 over 24 h in different culture media. ... 222
Figure 4.5: Modified gram staining of NCTC 6571 infected slices. ... 224
Figure 4.6: Modified gram staining of NCTC 7791 infected slices. ... 225
Figure 4.7: Pseudo coloured scanning electron microscopy of femoral slice tissue sections infected with S. aureus after 24 hrs in culture. ... 227
Figure 4.8: Mean cell counts and percentage loss following Trowell-type cultures supplemented with M-CSF and RANKL with and without co-culture of S. aureus strains, NCTC 6571 and NCTC 7791. 230
Figure 4.9: Co-culture of Staphylococcus aureus infected tissue slices stained for BAX. ... 233
Figure 4.10: BAX analysis following microinjection and culture with M-CSF and RANKL ... 234
Figure 4.11: Co-culture of Staphylococcus aureus infected tissue slices stained for cleaved caspase 3. ... 237
Figure 4.12: Cleaved caspase 3 analysis following microinjection and culture with M-CSF and RANKL. ... 238
Figure 4.13: Co-culture of Staphylococcus aureus infected tissue slices stained for LDH. ... 241
Figure 4.14: LDH analysis following microinjection and culture with M-CSF and RANKL. ... 242
Figure 4.15: LDH activity following supplementation with RANKL and M-CSF and co-culture of S. aureus strains NCTC 6571 and NCTC 7791. ... 244
Figure 4.16: IL-1β protein synthesis following supplementation with RANKL and M-CSF and co-culture of S. aureus strains NCTC 6571 and NCTC 7791. ... 246
Figure 4.17: IL-6 protein synthesis following supplementation with RANKL and M-CSF and co-culture of S. aureus strains NCTC 6571 and NCTC 7791. ... 248
Figure 4.18: TNFα protein synthesis following supplementation with RANKL and M-CSF and co-culture of S. aureus strains NCTC 6571 and NCTC 7791. ... 250
Figure 4.19: IL-10 protein synthesis following supplementation with RANKL and M-CSF and co-culture of S. aureus strains NCTC 6571 and NCTC 7791. ... 252
Figure 4.20: IL-4 protein synthesis following supplementation with RANKL and M-CSF and co-culture of S. aureus strains NCTC 6571 and NCTC 7791 ... 254
Figure 4.21: CD14 analysis following microinjection and culture with M-CSF and RANKL. ... 257
Figure 4.22: CD68 analysis following microinjection and culture with M-CSF and RANKL. ... 261

List of Tables

Table 1.1: Microorganisms identified in prosthetic joint infections. ... 37
Table 2.1: Immunohistochemistry primary antibodies. ... 81
Table 2.2: Immunohistochemistry IgG isotype control antibodies. ... 82
Table 2.3: Immunohistochemistry IgG secondary antibodies. ... 82
Table 3.1: ELISA kit reagents, antibodies, standards and horseradish peroxidase (HRP) concentrations. ... 206

List of Abbreviations

3D	Three-Dimensional
ADAM	A Disintegrin and Metalloprotease Domain
AP	Activator Protein
BHI	Brain Heart Infusion
BMP	Bone Morphogenetic Protein
BMU	Basic Multicellular Unit
C-FMS	Colony-Stimulating Factor-1 Receptor
CaMK	Calmodulin-Dependent Protein Kinase
CCL2	Chemotaxis Molecule
CCL7	Monocytic Chemotactic Protein -3
CFU	Colony Forming Units
CHIPS	Chemotaxis Inhibitory Protein of *Staphylococcus Aureus*
Cl^-	Chloride Ions
CLC-7	The Chloride Channel 7
Clf	Clumping Factor
CNA	Collagen-Binding Adhesins
CNTF	Ciliary Inhibitory Factor
CREB	CAMKIV-Stimulated Cyclic AMP-Responsive Element-Binding Protein
CT-1	Cardiotrophin-1
CWA	Cell Wall Adhesins
CXCL	C-X-C motif chemokine
CXCR2	Chemokine Receptor 2
CXCR4	Chemokine Receptor 4
DAB	3,3'-diaminobenzidine
Damps	Damage-Associated Molecular Patterns
Dcs	Dendritic Cells
DMSO	Dimethyl Sulfoxide
DNA	Deoxyribonucleic Acid
ECM	Extracellular Matrix
EDTA	Ethylenediaminetetraacetic Acid
EPS	Extracellular Polymeric Substance
ERK	Extracellular Signal-Regulated Kinase
ESR	Erythrocyte Sedimentation Rate
FGF	Fibroblasts Growth Factor
G-CSF	Granulocyte Colony-Stimulating Factor
GM-CSF	Granulocyte Macrophage-Colony Stimulating Factor
H^+	Hydrogen Ions
$HCO3^-$	Hydrogen Carbonate
HI FBS	Heat-Inactivated Foetal Bovine Serum
HIFs	Hypoxia-Inducible Factors
HSCs	Hematopoietic Stem Cells

Ig	Immunoglobulins
IKK	Iκ-B Kinase
IL	Interleukin
IL-1RI	IL-1 Receptor Type I
IL-6R	Interleukin-6 receptor
IL-IRII	IL-1 Receptor Type II
IFN-γ	Interferon Gamma
IRAKs	Interleukin-1 Receptor-Activated Protein Kinase
ITAM	Immunoreceptor Tyrosine-Based Activation Motif
Jaks	Janus Kinase
JNK	c-Jun N-terminal kinases
LDH	Lactate Dehydrogenase
LIF	Leukaemia Inhibitory Factor
LPS	Lipopolysaccharides
M-CSF	Macrophage-Colony Stimulating Factor
MAMPs	Microbe-Associated Molecular Patterns
MAPK	Mitogen-Activated Protein Kinase
MCP	Monocytic Chemotactic Protein
MHC	Major Histocompatibility Complex
MIP	Macrophage Inflammatory Protein
MIP-1α	Macrophage Inflammatory Protein 1-alpha
MIP-2α	Macrophage Inflammatory Protein 2-alpha
MMP	Matrix Metalloproteases
MSC	Bone Marrow Mesenchymal Stromal Cells
MSCRAMMs	Microbial Surface Components Recognising Adhesive Matrix Molecules
MTT	Thiazolyl Blue Tetrazolium Bromide Powder
NETs	Neutrophil Extracellular Traps
NF-κB	Nuclear Factor Kappa B
NFATc1	Nuclear Factor of Activated T-Cells
NHS	National Health Service
OPG	Osteoprotegerin
OSCAR	Osteoclast Associated Receptor
OSM	Oncostatin M
P55	TNF Receptor 1
P75	TNF Receptor 2
PAMPs	Pathogen Associated Molecular Patterns
PBS	Phosphate-Buffered Saline
PJI	Prosthetic Joint Infection
Plγc2	Phospholipase-C Gamma 2
PMA	Phorbol Myristate Acetate
PMN	Polymorphic Neutrophils
PRR	Pattern Recognition Receptors
PSM	Phenol-Soluble Modulins

RANK	Receptor Activator of The Nuclear Factor Kappa B
RANKL	Receptor Activator of The Nuclear Factor Kappa B Ligand
RGD	Arginylglycylaspartic Acid
Runx2	Runt-Related Transcription Factor-2
SAK	Staphylokinase
SCCmec	Staphylococcal Cassette Chromosome mec
SCIN	Staphylococcus Complement Inhibitor
SCV	Small Colony Variants
Sdr	Serine-Aspartate-Repeat
sIL-6R	Soluble IL-6 Receptor
SpA	Staphylococcal Protein A
SSLs	Superantigen-like Proteins
TAB	Transforming Growth Factor-B Kinase
TAK1	Transforming Growth Factor-B Kinase 1
TCC	T-cytotoxicity Cells
TEM	Transmission Electron Microscopy
TGF-b1	Transforming Growth Factor-Beta 1
Th	T-helper
THA	Total Hip Arthroplasties
THR	Total Hip Replacements
TIMPS	Tissue Inhibitors of Metalloproteases
TKA	Total Knee Arthroplasties
TLR	Toll-Like Receptors
TNF	Tumor Necrosis Factor
TNFα	Tumor Necrosis Factor Alpha
TRAF	TNF Receptor-Associated Factor
TRAF6	Tumor Necrosis Factor Response Associated Factor
TRAP	Tartrate Resistant Acid Phosphatase
Tregs	Regulatory T-Lymphocytes
TREM2	Triggering Receptors Expressed In Myeloid Cells 2
WBC	White Blood Cell
αMEM	Alpha Minimum Essential Medium

Chapter 1:
General Introduction

1.0: Introduction

Within the United Kingdom (UK), the average population was estimated to be 66,796,800 during mid-2019, with the number of people over the age of 65 increased by 22.9 % to 12.4 million between 2009 – 2019 and this increase in over 60s is expected to rise to 21.9 million by 2039 (Letwin et al. 2016; Park 2020). This increase in life expectancy has resulted in a subsequent proportional increase in age-related conditions and illnesses that require medical care and treatment and as a result has seriously impacted social healthcare, within the UK. Typically, on average the National Health Service (NHS) spends £5,200 on healthcare for households housing over 60s, who are typically post-retirement age (Cracknell 2010). This value is doubled when compared to non-retired households which spends on average £2,800 on healthcare (Cracknell 2010). This increase in costs is in response to increasing number of treatments that are required by aged patients. One such treatment commonly used in the elderly are orthopaedic implants, which are used to treat variety age-related conditions such as rheumatoid arthritis and fractures. These implants are crucial to restoring function to joints in the shoulders, elbows, hip, knees and ankles which are mainly joints that suffer high amount of load, wear, fatigue and mechanical stresses (Ribeiro et al. 2012). The surgical procedure that replaces native joints with artificial substitutes within the hip and knees are termed either total hip arthroplasties (THA) or total knee arthroplasties (TKA). These implants are made of biomaterials that adhere to stringent codes; they must not be toxic, carcinogenic, irritant or immunogenic whilst being structurally integrated with the surrounding bone (Williams 2008). Osseointegration is the direct anchorage of the implant metal with bone and this process is vital to providing the artificial implant with anchorage and stability (Mavrogenis et al. 2009; Plecko et al. 2012). The rate and success of osseointegration varies, and is dependent on a variety of factors including; the host, the properties of the material, the location of the implant itself, the quality of the surrounding bone, the ability to endure mechanical load together and the surface roughness of the material. The materials used for these implants are varied and include ceramics, plastics (polyethene) and metals (stainless steel, titanium or its Ti-6Al-4V composite alloy and tantalum; McKellop et al. 1999; NJR 2016; Peroglio et al. 2007; Plecko et al. 2012; Tokarski et al. 2015) .

Prosthetic hip and knee implants can fail. This can occur by dislocation of the implant, or by the implant itself becoming loose from the surrounding bone by either fracture formation, presence of wear particles from the material inducing increased bone resorption or by infections that cause damage to the local bone or implant surface compromising osteointegration (Del Arco and Bertrand 2013). Bacterial infections of the bone following an implant is a serious clinical problem that leads to high rates of morbidity and an economic burden on social healthcare (Dempsey et al. 2007). Orthopaedic biomaterials can be infected by bacteria and lead to two different types of conditions: osteomyelitis or periprosthetic joint infections (PJI). Within the wider literature, the distinction between these two separate conditions is often confused, with either condition being interchanged for the other when reporting hip or knee implant-associated infections. Both forms of infections can occur on prosthetic joints, although, osteomyelitis can occur in the absence of any orthopaedic biomaterial following fractures (Birt et al. 2017). The currently accepted definition of osteomyelitis and PJI is infiltration of an infectious organism around an implant that causes an inflammatory process of the local bone or bone marrow environment, leading to necrosis and destruction of the surrounding environment (Birt et al. 2017). PJI, can occur at any time during the lifespan of the patient with a prosthetic joint. These can occur as early infections within the first 6- 12 weeks following surgery, often caused by direct inoculation of the implant or surrounding tissue during surgery or soon after surgery (Anagnostakos et al. 2009; Tande and Patel 2014; Tsukayama et al. 1996). Delayed infections occur within 3 -24 months following surgery, due to either the low virulence or the low numbers of the bacteria species and can also be caused by a hematogenous source (Anagnostakos et al. 2009; Birt et al. 2017; Tande and Patel 2014). Late infections occur due to inoculation from a remote haematogenous source, such as blood-borne contamination from a urinary catheter, intravenous cannula, via sepsis from dental or skin infections and can occur via indolent infections that are dormant from surgery (Gaine et al. 2000b; Tande and Patel 2014; Tong et al. 2015; Zimmerli et al. 2004).

Current treatments can include irrigation and debridement, though these have an increased failure rate, with success varying in different studies due to various factors, including antibiotic treatment and durations, patient sample selection and microbiological findings (Azzam et al. 2010; Marculescu et al. 2006). Implant replacement surgeries are carried out

in more severe cases, where the inflected implant is removed and the damaged tissue is irrigated and debrided (Tande and Patel 2014). The femur is then either immediately replaced with a new implant (one-stage exchange) or placed with a temporary implant, while the infection is treated and once cleared replaced with a new permeant implant (two-stage exchange; Tande and Patel 2014). These surgical treatment do not guarantee absolute resolution of the infection as there is an increased risk of recolonisation by the bacteria on the implant following treatment (Gaine et al. 2000a; Kapadia et al. 2016).

Modelling such diseases often use *in vivo* animal models, where a material mimicking an orthopaedic implant is inserted within the relevant bone site of the host and is infected (Bernthal et al. 2010; Craig et al. 2005; de Mesy Bentley et al. 2017; Petty et al. 1985; Pribaz et al. 2012). These *in vivo* models do have a variety of ethical concerns, are expensive and subjected to a variety of host systemic influences (Lynch et al. 2018; Smith et al. 2010). As a result, there is a need for a model that allows cells to be cultured in a three-dimensional (3D) space that can be manipulated and controlled with supplements, cells and bacteria. *Ex vivo* models are a good substitute that have the benefits of a controlled and manipulative environment found *in vitro* cultures, alongside the benefits of culturing multiple cell types encased within an extracellular matrix. Previous *ex vivo* models, such as the mandible model, have shown results for inflammatory bone destruction and the tooth slice model has been utilised as an infection co-culture model (Roberts et al. 2013; Sloan et al. 2013; Smith et al. 2010). The overall aim of this current research is to address a need for the development of a new *ex vivo* model, that considers the femurs architecture along with the option to infect the local bone marrow environment.

1.1: Bone Biology and Normal Bone Homeostasis

Bone is a dynamic and complex mineralised tissue, that provides support to vertebrates via mechanical and metabolically active functions. The femur provides load-bearing support and stability of the gait. This is achieved via densely-packed series of surface plates around the outside known as cortices and by internal porous trabecular bone structures that are orientated at a spatial arrangement providing inner support and causes loading forces to dissipate (Parkinson and Fazzalari 2013; Rho et al. 1998). Trabecular bone has a complex

structure of interconnecting plates which are highly elastic, due the presence of a lower mineral density which provides increased mechanical support and strength (Eriksen 2010). In contrast, cortical bone is considerably denser and has high torsional resistance (Eriksen 2010). The femur is constantly remodelled; this is a lifelong process that is vital to maintain bone integrity and structure along with skeletal growth (Martin and Sims 2005). Bone remodelling of the cortical and cancellous bone is a coordinated system of the basic multicellular unit (BMU), consisting of osteoclasts, osteoblasts, osteocytes and osteoblast-derived lining cells (Sims and Gooi 2008). The process of bone turnover starts with bone resorption by osteoclasts and concludes with new bone formation by osteoblast cells. The rate of remodelling in the trabecular bone is consistently higher than cortical bone (Eriksen 2010; Kular et al. 2012). Pathological bone resorption can cause bone loss leading to osteoporosis, a condition marked by low bone mass along with the deterioration of the structure of bone and an increased risk of fractures caused by bone weakening (Logar et al. 2007). In the case of orthopaedic implants, pathological bone resorption caused by bacterial infection causes dysregulation of the BMU and consequently results in implant loosening (discussed further in Section 1.6; Henderson and Nair 2003; Wright and Nair 2010) .

1.1.1: Role of Mesenchymal Stromal Cells and Osteoblasts in Bone Formation and Repair

Bone formation is a process that is heavily reliant on MSC derived osteoblast cells that play roles in modelling, remodelling and fracture repair (Reviewed in Su et al. 2018). Skeletal bone is formed via either endochondral ossification or intramembranous ossification. Endochondral ossification is the process that forms most of the bones of the skeletal system, whereas intramembranous ossification relates to formation of bones of the skull and pelvis (Reviewed in Su et al. 2018). Both processes rely on mesenchymal stromal cells (MSC) to migrate and differentiate into osteoblasts to deposit bone matrix to start the formation of bone. Endochondral ossification starts from during foetal development and growth and continues until early adulthood and is a process that is driven by chondrocytes (Reviewed in Mackie et al. 2011). To initiate this process MSCs differentiate into chondrocytes to initiate cartilage formation. Firstly, chondrocytes proliferate and secrete an ECM which encases the cells (Mackie et al. 2011). The chondrocytes undergo hypotrophy and start to mineralise their ECM (Mackie et al. 2011). This is followed by chondrocyte cell death which causes the

cartilage ECM to be removed, thereby providing an entry point for MSCs to infiltrate and differentiate into bone forming osteoblast cells to ossify the centre which expands during development replacing most of the cartilage, except in the articular surfaces (Reviewed in; Mackie et al. 2008). Intramembranous ossification relies on the direct differentiation of MSCs to osteoblasts (Reviewed in Su et al. 2018). MSCs are directed to the bone surface and differentiate into pre-osteoblasts which start secreting high levels of alkaline phosphatase, until they mature into osteoblasts. Following maturation there are increased levels of cell signalling factors that regulate MSCs and pre-osteoblasts during intramembranous ossification including transforming growth factor-beta 1 (TGF-β1), bone morphogenetic protein (BMP)-2 and WNT family of ligands all of which upregulate pro-osteogenic genes, although high levels of these cell signalling factors can be inhibitory to osteoblast differentiation (further explained in section 1.1.1.1; Su et al. 2018).

During bone repair localised MSCs are recruited from the bone marrow towards the wound site to differentiate into bone forming osteoblasts, by exposure to cell signalling factors. Osteoblasts are primary cells responsible for the deposition of the bone matrix, initially by synthesising osteoid on the surface of the bone. This osteoid is a complex consisting of collagen type I (initially secreted as a procollagen), and a mixture of extracellular proteins including proteoglycans including decorin and biglycan, and glycoproteins and phosphoproteins such as osteopontin (reviewed in (Avery et al. 2020). The presence of these glycoproteins inhibits early mineral deposition which only occurs after the structure of the collagen matrix is formed and these proteins are removed (Avery et al. 2020). These collagen molecule deposited by osteoblasts within an extracellular space, are then assembled into fibrils by decorin, where the tropocollagen molecules align in a quarter-stagger arrangement, with gap zones between the collagen molecules in which intrafibrillar carbonated hydroxyapatite plate-shaped crystals eventually form (Fratzl et al. 2004; Reznikov et al. 2014; Ritchie et al. 2009; Sugars et al. 2003).

At the microstructural level, collagen fibres are layered at different angles and develop into lamellae (Currey 2011). They can be compacted together into concentric lamellae sheets formed by the collagen fibrils, orientated into rings separated by an interlamellar layer, forming strong and dense structures know as osteons (Burr and Akkus 2014; Ritchie et al.

2009). These osteons are typically 10-500 µm in diameter and contain a Haversian canal containing arteries, veins and capillaries along with nerve fibres in communication with osteocytes to form a structure commonly called the Harversian system (Burr and Akkus 2014; Clarke 2008; Currey 2011; Rho et al. 1998). The Harversian system is also a coupling process where the osteoclasts demineralise the bone-forming small pores, which are infiltrated via osteoblasts that get embedded and differentiate into osteocytes, this system is found within humans, though in rats and mice such a system is not found within the cortical bone (Carli et al. 2016).

1.1.1.1: Osteoblast Differentiation

Osteoblasts are derived from bone marrow mesenchymal stromal cells (MSC). To identify mesenchymal stromal cells, they must be plastic-adherent under standard culture and must express the markers CD73, CD90 and CD105, whilst lacking in CD45, CD34, CD14, CD11b, CD79a, CD19 or human leukocyte antigen-DR isotype (Dominici et al. 2006). In the osteoblast differentiation pathway, there are four stages following osteogenic differentiation from MSCs the pre-osteoblast, the osteoblast, the osteocyte and the bone lining cells (Kular et al. 2012). The main transcription factor that activates and regulates MSC differentiation to osteoblasts is runt-related transcription factor-2 (RunX2; Zhang et al. 2012). RunX2 is regulated by various transcription factors that aid in its expression and activation. Studies in mice with RunX2 knocked out have shown impaired osteoblast formation and ossification with little alkaline phosphatase activity (Komori et al. 1997; Otto et al. 1997). The binding of RunX2 to specific gene promotor enhancing regions within the cells, induces the transcription of genes that regulate osteoblast function and matrix deposition, that include osteocalcin and collagen type I (Franceschi et al. 2003). The overexpression of RunX2 can decrease osteocalcin expression and inhibit the formation of mature osteoblasts and RunX2 expression is enhanced during MSC differentiation to pre-osteoblasts before being downregulated for terminal differentiation to osteoblasts (reviewed in Avery et al. 2020). Shui et al. (2003) demonstrated that treatment of MSCs with dexamethasone for up to 14 days induced mature osteoblast formation, indicated by mineralised nodule formation and increased gene expression of alkaline phosphatase and osteocalcin.

Osterix is a downstream signalling molecule of RunX2, coded by the gene *Sp7* and is vital for osteoblast maturation (Sinha and Zhou 2013). In a study by Kawane et al. (2018), mice that were deficient in *RunX2* and *Sp7* had a reduction in collagen type I and maturation of the surrounding bone of both the calvaria and the mandible, due to the inability of MSCs to differentiate into mature osteoblasts. The study further demonstrated that mice deficient in *Sp7* still managed to deposit low levels of collagen type-I, $\alpha 1$ along with an increase in MSCs mobilisation within tissues, than mice deficient in RunX2. Similarly, Nakashima et al. (2002) demonstrated that *Sp7* deficient mice had normal levels of RunX2 and collagen type-I, $\alpha 1$, but completely abolished osteocalcin, osteonectin and osteopontin expression. Taz, another transcription factor is vital for determining the fate of MSCs towards more osteogenic linage by suppressing adipogenesis by downregulating peroxisome proliferator-activated receptor gamma and enhancing RunX2 downstream signalling (Hong et al. 2005).

Osteogenic differentiation is also regulated by various signalling molecules. TGF-β1 and BMP-2, stimulate the expression of RunX2 as a target of their signalling (Lee et al. 2000). Both TGF-β1/BMP signals activate Smad-dependent and -independent pathways (Chen et al. 2012; Hughes et al. 2006). TGF-β1 stimulates a variety of matrix proteins, including fibronectin and its associated receptor, collagen, osteopontin and osteonectin, whilst inhibiting extracellular matrix (ECM) degradation (Lee et al. 2000). TGF-β signalling has been shown to promote osteoblast proliferation and differentiation. Analysis using murine growth plate development studies on Dermo1-Cre mice, by knocking out the TGF-β1 receptor ALK5, has shown that these cells are selectively stimulated towards an osteoblast lineage via the MAPK and SMAD 2/3 pathways (Matsunobu et al. 2009). In addition to the binding of TGF-β1, the binding of parathyroid to its receptor acts as a stimulus for osteoblast differentiation (Sims and Gooi 2008). BMP-2 signalling can also direct cells to an osteoblast lineage and the translocation of Smads into the nucleus is vital for the activation of RunX2 and osterix, both of which are regulated by Dlx5 to induce osteogenesis (Chen et al. 2012; Rahman et al. 2015).

In addition to TGF-β1/BMP signalling, another vital signalling pathway that regulates osteoblast bone formation is the Wnt/β-catenin pathway. The Wnt ligand binds to its receptor complex consisting of Frizzled and an LDL receptor related protein 5/6, initiating a

downstream signalling pathway (Kular et al. 2012; Rahman et al. 2015; Westendorf et al. 2004). This pathway increases bone mass through the renewal of stem cells, stimulates pre-osteoblast proliferation, inhibition of osteocyte and osteoblast apoptosis and induces osteogenesis. Negative regulation of the Wnt signalling can be controlled via the Dickkopfs binding to the LDL receptor-related protein 5/6 receptor and secreted frizzled-related proteins that bind to the Wnts directly preventing binding to its receptor (Westendorf et al. 2004).

1.1.2: Role of Osteoclasts in Bone Remodelling and Repair

Osteoclasts are large multinucleated cells, which are fundamental in bone resorption, including its pathological destruction. Osteoclasts are derived from mononuclear progenitors, monocytes and macrophages. These precursors undergo proliferation, differentiation and fusion into multinucleated polykaryon osteoclast precursors which then undergo maturation into bone resorbing osteoclasts via a process called osteoclastogenesis. This differentiation of osteoclast progenitors is regulated by the cytokines M-CSF and RANKL, which are released by MSCs, osteoblasts and osteocytes (Figure 1.1; Figure 1.2; Boyle et al. 2003; Sims and Gooi 2008; Kular et al. 2012). The osteoclast has two morphological states, the motile and the resorbing states. The motile osteoclasts are non-polarised cells, with podosomes that are formed from actin filaments creating actin turnover used in cell motility. Here, the osteoclast extends its lamellipodia in the direction required and retracts the membrane at the opposite side, pushing the osteoclast (Li et al. 2006). The activated osteoclast matures and becomes rich in mitochondria and undergoes polarisation where the cytoskeleton is reorganised forming different domains once it reaches the resorptive surface. The osteoclasts during polarisation form specialised membranes, the ruffled border, the sealing zone, the functional secretory domain and the basolateral membrane (Figure 1.3; Vaananen et al. 2000; Li et al. 2006) .

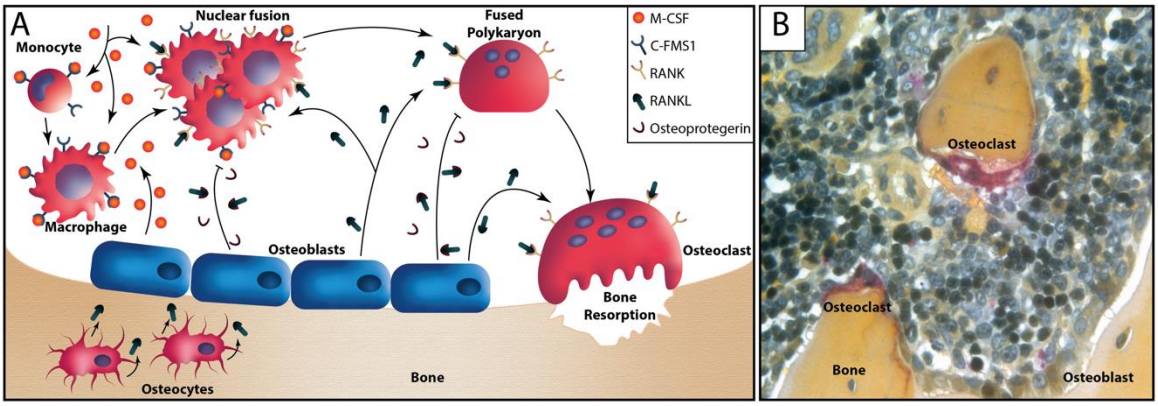

Figure 1.1: The bone remodelling process and osteoclastogenesis.
Image A) The bone remodelling process indicating the differentiation of osteoclasts precursors into mature osteoclasts using RANKL ligand secreted from osteoblasts and osteocytes. First, circulating osteoclast precursors, monocytes and macrophages are stimulated with M-CSF. M-CSF is secreted by osteoblasts into the microenvironment. The binding of M-CSF to its receptor on the surface of osteoclast precursors acts as a survival factor and activates various transcription factors within the cell. The addition of RANKL synthesised from osteoblasts and osteocytes into the microenvironment binds to RANK on the surface of osteoclast precursors. This stimulates these osteoclast precursors (monocytes and macrophages) to undergo differentiation (osteoclastogenesis) and fusion becoming a fused polykaryon. Further stimulation with RANKL/RANK initiates a downstream signalling cascade that drives the cell towards a mature osteoclast. The cell attaches to the bone mineral surface and actively resorbs the bone mineral. Osteoblasts regulate bone resorption by releasing OPG that binds to RANKL preventing RANKL/RANK binding and preventing osteoclastogenesis. B) A microscopy image of a rodent bone marrow tissue section indicating a live view of the bone remodelling unit osteoclasts, osteoblasts and osteocytes *in situ*. Abbreviations: M-CSF (macrophage colony stimulating factor), C-FMS (colony stimulating factor-1 receptor), RANK (receptor activator of the nuclear factor kappa B), RANKL (receptor activator of the nuclear factor kappa B ligand) and OPG (Osteoprotegerin). Image A adapted from Adamopoulos and Mellins (2015); Boyle et al. (2003), Image B was taken from TRAP-stained samples from Section 2.2.3.

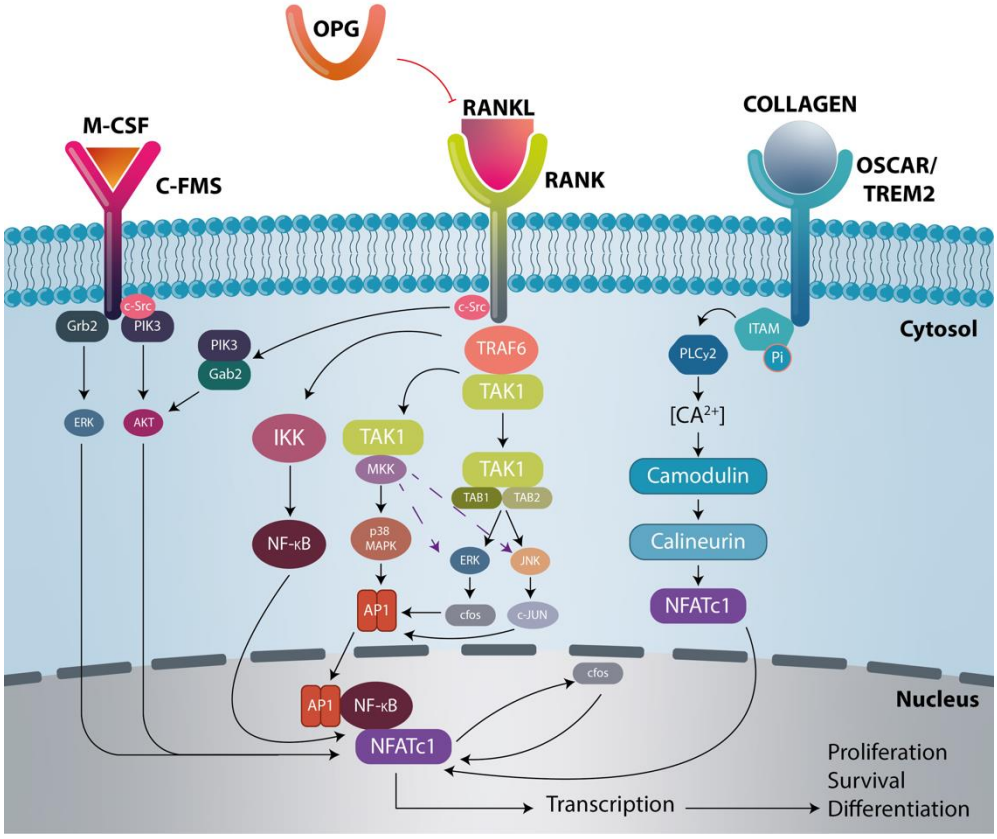

Figure 1.2: The molecular downstream signalling network of osteoclast precursors following stimulation with M-CSF and RANKL. M-CSF/C-FMS binding activates PIK3 and Grb2 which induces ERK and AKT activations, which when translocated to the nucleus regulate proliferation, survival and differentiation. The binding of RANKL/RANK recruits TRAF6 to initiate a downstream signalling cascade of various adaptors and kinases. TRAF6 recruitment activates the phosphorylation of IKK and thus, the translocation of NF-kB into the nucleus for transcription of osteoclastogenesis genes. In addition, TRAF6 also forms complexes with TAK1 that activate MAPKs via the formation of different complexes, TAK1-MKK activates p38 and possibly ERK and JNK, whereas TAK1-TAB1-TAB2 activates ERK and JNK which activates c-fos and c-JUN, respectively. Activation of p38, ERK and JNK translocates AP1 into the nucleus and forms a complex with NF-kB leading to induction of c-fos. RANKL is further enhanced by the OSCAR/TREM2 co-stimulatory pathway with ITAM phosphorylation to induce calcium signalling and subsequent NFATc1 translocation into the nucleus. NFATc1 forms a complex with AP-1/ NF-kB to induce osteoclast transcription factors and subsequent osteoclast proliferation, survival and differentiation. OPG blocks RANKL/RANK binding. Abbreviations: M-CSF (macrophage colony-stimulating factor), C-FMS (colony-stimulating factor-1 receptor), RANK (receptor activator of the nuclear factor kappa B), RANKL (receptor activator of the nuclear factor kappa B ligand), OPG (Osteoprotegerin), Grb2 (growth factor receptor-bound protein 2), PIK3 (phosphoinositide 3-kinase), c-Src (Proto-oncogene tyrosine-protein kinase Src), ERK (extracellular signal-regulated kinases), AKT (protein kinase B), TRAF6 (tumor necrosis factor receptor-associated factor 6), TAK1 (transforming growth factor-β kinase 1), TAB (transforming growth factor-β kinase), JNK (c-Jun N-terminal kinases), MKK (mitogen-activated protein kinase kinase), MAPK (mitogen-activated protein kinase), AP-1 (Activator protein 1), OSCAR (osteoclast associated receptor) / TREM2 (triggering receptors expressed in myeloid cells 2), ITAM (immunoreceptor tyrosine-based activation motif), PLγC2 (phospholipase-C gamma 2), NF-κB (nuclear factor kappa B) and NFATc1 (Nuclear factor of activated T-cells, cytoplasmic 1). Image adapted from Amarasekara et al. (2018); Kular et al. (2012); Park et al. (2017); Takayanagi (2005).

1.1.2.1: Osteoclast Differentiation and Signalling Pathways

Osteoclast differentiation is regulated by the release of M-CSF and RANKL (Figure 1.2; Kular et al. 2012; McArdle et al. 2015). The binding of M-CSF to its ligand induces the production of the receptor activator of the NF-κB (RANK) and activates proliferative and survival signals in the nucleus (Figure 1.2; Novack and Teitelbaum 2008). RANKL homotrimeric protein is membrane-bound on osteoblasts and T-cells and can be secreted via activated T cells. Bound RANKL is proteolytically cleaved by Matrix Metalloproteases (MMP)-3 and -7, or via the A Disintegrin and Metalloprotease Domain (ADAM), allowing binding to its receptor, RANK, which is expressed on the surface of the osteoclast precursor cells (OPC; Boyce and Xing 2008). The binding of RANK/RANKL initiates a downstream signalling cascade essential to the formation of mature osteoclasts. The tumor necrosis factor (TNF) receptor-associated factor (TRAF) -2, -5 and -6 also binds to the cytoplasmic domain of RANK (Figure 1.2; Boyce and Xing 2007). TRAF6 leads to the activation of NF-κB via the phosphorylation of Iκ-B kinase (IKK), which causes IκB to be ubiquitinated via proteasome degradation and releases the NF-κB (Figure 1.2; Kular et al. 2012). This promotes the initial induction Nuclear Factor of Activated T-Cells (NFATc1) into the nucleus and along with activator protein (AP)-1, induces auto-amplification and transcribing genes for osteoclastogenesis (Figure 1.2; Boyce and Xing 2007,2008; Negishi-Koga and Takayanagi 2009) .

Other signalling pathways that TRAF6 activates include the activation of c-Fos, a complex composed of Jun, ATF and FOS family members (Negishi-Koga and Takayanagi 2009). The c-Fos activates the AP-1 and subsequently NFATc1 leading to osteoclast differentiation (Figure 1.2; Takayanagi 2005). The activation of c-Fos can also be induced via the binding of TNF to its receptor, TNFR, downstream signalling of NFκB and the JNK pathways (Figure 1.2; Boyce and Xing 2008). The activation of NFATc1 is also induced via the co-stimulatory pathway of calcium (Figure 1.2). RANKL activates calcium oscillation, an essential component of NFATc1 activation (Kular et al. 2012). The calcium pathways occur through the co-stimulation of the immunoglobulin-like receptor, the osteoclast associated receptor (OSCAR) and the triggering receptor expressed on myeloid cells (TREM) -2, which together work alongside the immunoreceptor tyrosine-based activation (ITAM) motif adaptor molecules (Figure 1.2; Kular et al. 2012) . RANK and ITAM signals activate the phospholipase Cγ (PLCγ) and the

intrasignalling activation of calcium ions. The phosphorylation of the PLCγ occurs via the tyrosine kinases, the Bruton's tyrosine kinase and the Tec kinase family (Kular et al. 2012; Negishi-Koga and Takayanagi 2009). The subsequent calcium ions bind to calmodulin, inducing a conformational change and activating calcineurin and its effector protein calmodulin-dependent protein kinase (CaMK). Calcineurin regulates NFATc1 and its auto-amplification and transcription in the nucleus. CaMK via the CAMKIV-stimulated cyclic AMP-responsive element-binding protein (CREB) activates c-Fos which induces the signalling of AP-1 and NFATc1 (Negishi-Koga and Takayanagi 2009).

Lomaga et al. (1999) have shown that TRAF6 knockout mice develop osteopetrosis. The authors state that osteoclast function was compromised, but not their differentiation capability, as osteoclasts were withdrawn from the bone surface. Although a few were shown to attach to the bone surface and form sealing zones, they had disorganised ruffled borders resulting in limited bone resorption. Osteoblasts regulate osteoclast differentiation, where they express RANKL, M-CSF and OPG, as described above. Interestingly, B-lymphocytes can also synthesise OPG and RANKL in addition to osteoblasts (Titanji 2017). OPG is a soluble decoy for RANKL and inhibits osteoclastogenesis (Boyce and Xing 2007; Boyce and Xing 2008; Matsuo and Irie 2008; Yamashita et al. 2012). OPG-deficient mice have been shown to experience a decrease in bone density, leading to a high incidence of fractures and early-onset osteoporosis (Bucay et al. 1998).

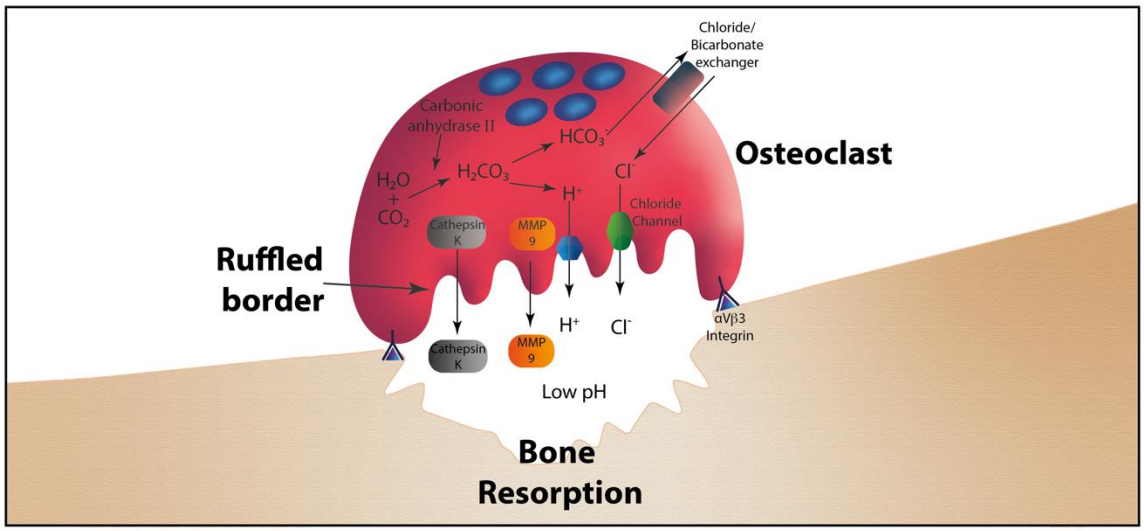

Figure 1.3: Illustration of osteoclast, showing a sealing zone once the osteoclast binds to the bone surface using αvβ3 integrins. The carbonic anhydrase II converts water and carbon dioxide into hydrogen carbonate (HCO_3^-) into hydrogen (H^+) ions and hydrogen carbonate (HCO_3^-). The HCO_3^- is transported out of the cell and allows an influx of chloride ions (Cl^-) into the cell using an HCO_3^-/ Cl^- exchanger. The H^+ ions are released across the ruffled border using an ATPase proton pump and a counter anion channel called the chloride channel 7 (CLC-7) secretes the Cl^- and both play roles in acidifying the resorption lacunae. The proteolytic enzyme, cathepsin K aids in the degradation and destruction of the bone matrix. Image adapted from Vaananen and Laitala-Leinonen (2008) and Athanasou (2011) .

The sealing domain is the site where the osteoclast attaches to the bone mineral and encloses the ruffled border (Figure 1.3; Vaananen et al. 2000) . The sealing zone is made up of podosomes with a core of F-actin surrounded by the integrin αvβ3 and the polarization of the cytoskeleton is controlled by the integrin αvβ3 (Athanasou 2011). This αv integrin family are transmembrane heterodimers that attach to the cell and allow signals to transmit to the extracellular matrix. The β subunit is the focus for the attachment to the cytoskeleton and signalling molecules controlling the behaviour (McHugh et al. 2000; Novack and Teitelbaum 2008). It has been shown in studies using mice deleted for the β3 subunit, that these mice still had differentiated osteoclasts, yet developed osteosclerosis as they aged, indicating the importance of αvβ3 in bone resorption (McHugh et al. 2000). These integrins exist in a low and high-affinity state towards the arginylglycylaspartic acid (RGD) motif of proteins in the bone matrix including bone sialoprotein and osteopontin (Novack and Faccio

2011). The ruffled border is the restorative organelle that has a two-way continuous intracellular vesicle transport system that transfers cathepsin K along with hydrochloric acid (Figure 1.3). The secreted hydrochloric acid dissolves the bone mineral forming a resorption lacuna (Figure 1.3; Athanasou 2011). This system is regulated by the GTPase Rab7 (Vaananen and Laitala-Leinonen 2008).

Within the osteoclast, carbonic anhydrase II generates hydrogen (H^+) ions and hydrogen carbonate (HCO_3^-) from water and carbon dioxide (Figure 1.3). The HCO_3^- is transported out of the cell by the HCO_3^-/ chloride ions (Cl^-) exchanger allowing an influx of Cl^- into the cell and maintaining the electroneutrality of the cell (Figure 1.3; Novack and Teitelbaum 2008; Touaitahuata et al. 2014) . The secretion of H^+ ions acidifies the resorption lacunae across the ruffled border using an ATPase proton pump. However, along with this proton pump a counter anion channel the chloride channel 7 (CLC-7) secretes Cl^- (Figure 1.3; Vaananen and Laitala-Leinonen 2008; Athanasou 2011). These ions result in the acidification of the resorption lacunae by forming hydrochloric acid, however, along with these ions, proteolytic enzymes such as cathepsin K aid in the destruction of the bone matrix (Figure 1.3). It is considered that cathepsin K is the foremost degrader of the bone matrix and is found in high quantities in osteoarthritic bone samples (Figure 1.3; Logar et al. 2007)

1.1.3: Role of Osteocytes

Osteocytes are differentiated osteoblasts that have embedded themselves into the new bone matrix within the lacunae. They are spatially isolated and have long extended filipodia that connect to other osteocytes, the bone marrow and osteoblasts, which together form a dense and bioactive network (Metzger and Narayanan 2019). Osteocytes are mechanosensory cells that reside in the lacunae and can react to fluid flow shear and interstitial hydrostatic pressure changes within the lacuna/canalicular network (Compton and Lee 2014; Kular et al. 2012; Metzger and Narayanan 2019). They can direct osteoblast and osteoclast responses through a variety of mechanisms. Osteocytes can express various genes encoding for proteins required for mineralisation and homeostasis, such as *SOST* (encodes for the protein sclerostin), *PHEX* (encodes for the enzyme phosphate-regulating neutral endopeptidase, x-linked) and *DMP1* (encodes the protein dentine matrix acidic

phosphoprotein 1; Metzger and Narayanan 2019). Osteocytes that have mutations which downregulate the expression of *PHEX*, can cause an increase in osteopontin deposition, inhibiting mineralisation and increasing fibroblast growth factor (FGF)-23 serum expression resulting in a reduction in phosphate resorption and vitamin D synthesis, causing X-linked hypophosphatemia-related rickets (Beck-Nielsen et al. 2019). Sclerostin is an antagonist of the BMP family and prevents the signalling of Wnt/β-Catenin in MSCs and osteoblasts, and can be produced by mature osteocytes (Bonewald and Johnson 2008; Poole et al. 2005; Robling et al. 2006). Sclerostin can be regulated by the parathyroid hormone or local mechanical loading, where areas under considerable strain have down-regulated levels resulting in increased osteogenesis and bone mass (Compton and Lee 2014; Costa et al. 2011). Studies on transgenic mice overexpressing the *SOST* gene and thus sclerostin, with mechanical cyclic axial loading, applied for 1 min a day at 2 Hz on the ulnae, showed wild type mice having an increase in mineralisation response in contrast to transgenic mice which resulted in a reduction in mineralisation by 70-85 % (Tu et al. 2012).

Osteocytes, along with osteoblasts, release the receptor activator of the nuclear factor kappa B (NF-κB) ligand (RANKL) which aids in the initiation of osteoclastogenesis. Studies have shown that RANKL gene expression is increased following the addition of recombinant human sclerostin on mouse osteocyte-like MLO-Y4 cells, whilst suppressing the gene expression of the antagonist of RANKL, osteoprotegerin (OPG; Wijenayaka et al. 2011). Following co-culture of these MLO-Y4 cells with murine splenocytes or human peripheral blood mononuclear cells, along with recombinant human sclerostin and macrophage-colony stimulating factor (M-CSF), there was a significant increase in the number of mature osteoclast-like cells (Wijenayaka et al. 2011). Studies by Nakashima et al. (2011) have shown the importance of RANKL secretion from osteocytes on the local bone marrow microenvironment. The authors showed that transcription of the *Tnfsf11* gene, which encodes RANKL, was significantly higher in murine osteocytes than osteoblasts and MSCs. The authors observed which of the two cells, osteocytes or osteoblasts, had a greater effect on osteoclast differentiation, a basic co-culture experiment. Both cell type was cultured individually within the presence pre-osteoclasts cells. Following treatment with 1,25-dihydroxy vitamin D3 and prostaglandin E2 (PGE2), the results indicated that co-cultures with osteocytes significantly increased the number of mature osteoclast-like cells, compared

to osteoblasts. The authors also preformed genetic knockout experiments on the *Tnfsf11* RANKL gene from osteocytes alone, in the presence of both osteoblasts and pre-osteoclast like cells. The results indicated that genetic suppression of RANKL from osteocytes significantly decreased the number of mature osteoclasts and their resorption capacity. This is surprising, as it is commonly assumed that osteoblasts are the main drivers of osteoclast differentiation secreting significant amounts of RANKL. This study by Nakashima et al. (2011) highlights the importance of osteocyte RANKL, as even with the presence of intact RANKL producing osteoblast was not sufficient in increasing mature osteoclast numbers and preventing over mineralisation. This indicates that the RANKL in osteocytes maybe has a greater impact on bone remodelling than RANKL produced by osteoblasts. This is supported by analysis on transgenic mice deleted for the *Tnfsf11* RANKL gene from osteocytes, leading to a doubled increase in bone density along with a 75 % osteoclast reduction, suggesting that the RANKL produced by osteocytes is the main source for osteoclasts precursors to undergo osteoclast differentiation. (Xiong et al. 2011).

1.2: Osteoimmunology

1.2.1: Osteoimmunology

Osteoimmunology is the interaction between the immune response and the bone, the fact that most of the immune cells that are active in the immune response are derived from the bone marrow give credence to the importance of this relationship. The immune system helps regulate homeostasis and protects the bone marrow microenvironment from trauma, pathogens, bone disorders (Reviewed in Charles and Nakamura 2014). Typically, two different components make up the immune system, the innate and the adaptive immune response (Walsh et al. 2018).

1.2.1.1: The Innate Immune Response

The innate immune response acts against a pathogen or micro-organism, whilst trying to limit and reduce cellular damage that is caused by bacterial invasion (Charles and Nakamura 2014). The immunity produced is more non-specific and utilises a variety of cells, including

neutrophils, monocytes, macrophages and dendritic cells, all of which synthesis cytokines and chemokines, that initiate phagocytosis or push the innate immune response towards an adaptive response (Reviewed in Chaplin 2010) . These cells initiate the immune response when they bind their cell surface pattern recognition receptors (PRR) to specific conserved molecules, such as pathogen associated molecular patterns (PAMPs) on the surface of the micro-organism (Charles and Nakamura 2014). There are many classes of PRR found on the cell surface, one of which are the well characterised Toll-like receptors (TLR) and bind to specific PAMPS on the surface of various microorganisms; initiating the adaptive immune response (Kawasaki and Kawai 2014). Additionally, various immune cells can play a role in injury and trauma, by using PRRs to bind to damage-associated molecular patterns (DAMPs) released from damaged cells, which activates mobilisation and phagocytosis of the innate immune cells and remove any cellular debris (Kawasaki and Kawai 2014). In response to PRR, recognition of PAMPs or DAMPs causes a release of cytokines, especially pro-osteoclastogenesis cytokines interleukin (IL)-1b, IL-6 and tumor necrosis factor alpha (TNFα) which have been shown to affect the local bone microenvironment especially on the BMU cells osteoclasts and osteoblasts, as mentioned previously (Charles and Nakamura 2014).

1.2.1.2: The Adaptive Immune Response

The adaptive immune response is often intertwined within the innate immune response. This form of immunity is directed by T-lymphocytes and B-lymphocytes, which utilises two different responses the humoral response and the cellular response (Chaplin 2010). Firstly, the humoral immune response utilises antibodies that are either produced by B-lymphocytes that produce antigens to target pathogens, toxins or aid in pathogen identification (Amanna et al. 2007). T-lymphocytes can also act as antigen presenting cells and produce antigens that can target the pathogen (Nicholson 2016). Secondly, there is the cellular response where T-lymphocytes, neutrophils, monocytes and macrophages, that can recognise these antigens, are initiated and infiltrate to the site of the pathogen to undergo phagocytosis and destruction. Monocyte and macrophage cells aid in the adaptive immune response by phagocytosing microbial antigens and degrading them into peptide fragments using proteolysis and present them to T-lymphocytes via the major histocompatibility complex (MHC) class I or II, activating them (Chaplin 2010). Once cellular immunity has been

completed, it is vital that the activated cells that respond to bacterial antigens are removed by undergoing, apoptosis, this process has to be carefully managed to prevent inadvertent tissue damage and inflammation (Chaplin 2010). To achieve this, regulatory T-lymphocytes (Tregs) produce a variety of anti-inflammatory cytokines, including Interferon gamma (IFN-γ), IL-4, IL-10, TGFβ and IL-35, to suppress the pro-inflammatory environment and resolve the activated immune response (Romano et al. 2019).

1.2.2: Cells Involved in the Immune Response

1.2.2.1: Neutrophils

The first line of defence against bacteria is provided by the phagocytes that can be found within the bone marrow. These include neutrophils and macrophages. The polymorphic neutrophils (PMN) are the most abundant and fleeting leukocytes that live for a maximum of 24 h and 48 h in tissues (reviewed in Navegantes et al. 2017). Neutrophils are produced in the bone marrow from hematopoietic stem cells (HSCs), that when stimulated with granulocyte colony-stimulating factor (G-CSF), differentiate into myeloid precursors before turning into mature neutrophils in a process termed granulopoiesis (reviewed in Rosales 2018). Knockout mice depleted for G-CSF receptor, showed a reduction in neutropenia along with a subsequent drop in the number of neutrophils and ability to undergo granulopoiesis (Richards et al. 2003). Following maturation, neutrophils leave the bone marrow into circulation (Rosales 2018). Neutrophils are tightly regulated under the control of two chemokine receptors, chemokine receptor 2 (CXCR2) and chemokine receptor 4 (CXCR4) (Eash et al. 2010). CXCR4 is considered to provide a dominant role in neutrophil release, whereas CXCR2 plays an antagonistic secondary role with CXCR4 for neutrophil bone marrow release (Eash et al. 2010). Stromal cells and osteoblasts produce stromal derived factor-1 (SDF-1), also known as C-X-C motif chemokine (CXCL) 12 (CXCL12), that binds to CXCR4 prevents neutrophil mobilisation and maintains the neutrophil cell population within the bone marrow (Summers et al. 2010). G-CSF downregulates osteoblast CXCL12 mRNA expression which subsequently leads to a reduction in CXCL12 release, thus leading to neutrophil mobilisation (Semerad et al. 2005). G-CSF has also been seen to downregulated CXCR4 synthesis by neutrophils (Kim et al. 2006b). Ligands for CXCR2 include

CXCL1 and CXCL2 (also termed the macrophage inflammatory protein (MIP) 2- alpha (MIP-2α) are produced by osteoblasts, megakaryocytes and endothelial cells following G-CSF administration which also results in neutrophils mobilisation (Eash et al. 2010; Kohler et al. 2011).

The number of apoptotic neutrophils regulates the number of neutrophils produced within the wound environment. Macrophages and dendritic cells phagocytose these apoptotic neutrophils and as a result, the secretion of IL-23 is reduced by those cells (reviewed in Borregaard 2010). It has been shown that the production of IL-23 causes effector T-cells to secrete the cytokine IL-17A. The production of IL-17A can induce recruitment of monocytes and neutrophils, whilst also being able to produce G-CSF from IL-17 stimulated stromal cells (Aggarwal et al. 2003).

Neutrophils play a role in the innate immune response by responding to pathogens by migrating from the blood vessels to the site of the infection. This involves the neutrophil recruitment cascade, where free-flowing neutrophils in the blood become tethered to the vessel wall, start rolling along the vessel wall, before coming to a full arrest under firm adhesion and start initiating neutrophil crawling to transmigrate to the site of infection (reviewed in Kolaczkowska and Kubes 2013). Via the neutrophil recruitment cascade, they accumulate at the wound site after injury or after the presence of a pathogen and can eliminate pathogens intracellularly or extracellularly. These cell types are becoming increasingly recognised as important in implant-associated infections, with an increase in the number of activated PMN in the site of infection indicated by the increase of Fc-receptors, CD14, CD64, the chemokine receptor CXCR6 and various adhesion proteins, including CD11b and CD18 and MHC class II molecules (Gaida et al. 2012). Wagner et al. (2004), showed that PMN following implant-associated infections had an increased lifespan, but lost their migratory capability. However, in the presence of biofilms, these PMN were unable to penetrate and phagocytose the biofilm and instead released reactive oxygen species to try and control the biofilm, which consequently also damaged the surrounding tissue, potentially causing areas for the biofilm to spread and infiltrate. Gaida et al. (2012) reported that there is a direct correlation in the number of PMN to the number of osteoclasts. They reported that PMN induced IL-8, which is seen as another form of

osteoclastogenesis inducer. These studies have shown that the presence of biofilms initiates and activation of neutrophils, so the natural next step is to understand how these neutrophils recognise the biofilms.

Neutrophils utilise PAMPs and microbe-associated molecular patterns (MAMPs) to recognise pathogens (Dapunt et al. 2016). At the site of infection, the neutrophils respond to the bacteria and initiate their destruction by phagocytosis and reactive oxygen species. Phagocytosis depends on the opsonisation of the bacteria that is coated with immunoglobulin G (IgG) and a complement C3b/C3bi system (Stroh et al. 2011). Here, the pathogen is engulfed by the neutrophil into a phagosome which results in the formation of reactive oxygen species, a collective term derived from superoxide anions and hydrogen peroxide, which destroy the bacteria (Fuchs et al. 2007). In more recent years, a new form of bacterial destruction was identified by Brinkmann et al. (2004) called neutrophil extracellular traps (NETs), which respond to both Gram-positive and Gram-negative bacteria. They reported that upon stimulation by IL-8, lipopolysaccharides (LPS) or phorbol myristate acetate (PMA), the neutrophils developed extensions of their membranes. The NETs are composed of, deoxyribonucleic acid (DNA), histones and a variety of proteins, including cathepsin G, neutrophil elastase, myeloperoxidase, gelatinase and lactoferrin (Brinkmann et al. 2004). Bacteria that have been shown to induce NET production include *S. aureus,* which induces a morphological change to the neutrophils to initiate NETs via an oxidant-independent reaction rather than an oxidant-dependant manner (Fuchs et al. 2007; Pilsczek et al. 2010). Previous *ex vivo* models have shown that neutrophil elastase positive cells were low in number after culture for 14 days, however, levels were up-regulated significantly in LPS, IL-6 and TNFα supplemented tissues (Sloan et al. 2013).

1.2.2.2: Monocytes

Monocytes are another cell type of the bone marrow that represent about 10 % of leukocytes in the human blood and originate from hematopoietic stem cell precursors and differentiate into macrophages and osteoclasts. In the innate immune response, they play key roles in the removal of apoptotic cells and phagocytosis of bacterial pathogens (Auffray et al. 2009). These cells circulate the bloodstream and can differentiate into tissue

macrophages and dendritic cells (DCs); and together this system is termed the mononuclear phagocyte system (Geissmann et al. 2003). Monocytes produce a range of cytokines that govern immune response and inflammation. These cytokines include the TNF superfamily IL-1 family and IL-6 (Belge et al. 2002). In humans, monocytes are derived into various subsets based on the expression of surface markers, CD14 and CD16. The classical subtype of monocytes have markers that are $CD14^{++}$ and $CD16^{-}$, which account for 80-90 % of circulating monocytes, and are primed for phagocytosis, immune response and migration (Kapellos et al. 2019) The non-classical monocyte subtype have markers that are $CD14^{+}$ and $CD16^{+}$ and these make up the remaining 10 % of circulating monocytes and are actively proliferating within the bloodstream of patients with systemic infections and play an active role in pathogen defence (Fingerle et al. 1993; Kapellos et al. 2019). These $CD14^{+}$ and $CD16^{+}$ monocytes also express the largest number of antigen-presenting molecules and can secrete all known pro-inflammatory cytokines IL-1β, TNFα and IL-6, along with the chemokine macrophage inflammatory protein-1 alpha (MIP-1α, Kapellos et al. 2019). Both these monocytes when they are stimulated with TLR antagonists produce high levels of TNFα and low levels of IL-10 (Belge et al. 2002). Analysis of monocytes using CD14 markers was low in the *ex vivo* mandible slice model, however supplementation with LPS and TNFα significantly increased the number of CD14 stained monocyte-like cells (Sloan et al. 2013).

1.2.2.3: Macrophages

Macrophages are derived from monocytes, and have three main roles; phagocytosis, antigen-presenting and cytokine production. These cells are mainly scavengers that are activated to phagocytose apoptotic cells and respond to an increase in DAMPs following cell necrosis post tissue injury (Charles and Nakamura 2014). Macrophages, dependent upon the cytokine signalling environment, can polarize via two distinct pathways; the classical M1 pro-inflammatory macrophages used in host defence and the alternatively activated M2 anti-inflammatory macrophages involved in regulating the anti-inflammatory responses associated with stimulating tissue repair (Jablonski et al. 2015). This polarisation has been seen *in vitro* and *in vivo* on monocytes derived from the blood and bone marrow (Bertani et al. 2017; Ma et al. 2014; Ying et al. 2013). Macrophages have a role in both the innate and adaptive immune response, where the different macrophages secrete different cytokines

and cell surface markers. In the M1 macrophages, they enhance local inflammation via the secretion of TNFα, IL1-β, IL-6, IL-12 and IL-23, after they are stimulated with either IFN-γ with bacterial products (Reviewed in Arango Duque and Descoteaux 2014). TNFα or GM-CSF have also been seen to induce nitric oxide (Arango Duque and Descoteaux 2014) . Conversely, M2 macrophages secrete anti-inflammatory markers, TGF-β, IL-10, BMP-2 and vascular endothelial growth factor; essentially markers that promote osteoblast differentiation and mineralisation (Avery et al. 2020). These polarised macrophages induce a variety of responses via their cytokines, the M1 macrophages recruit HSCs, neutrophils, natural killer cells and T–lymphocytes especially, the T-helper (Th)-1 using chemokines IL-8, CXCL9, CXCL1 and CXCL2 (Arango Duque and Descoteaux 2014; De Filippo et al. 2013; Lukacs et al. 1995; Moser et al. 1990; Wright et al. 2002). Recently, an investigation into the effect of ageing on the effect of macrophage polarisation has shown that aged *in vitro* macrophages from 70-72-week-old C57BL/6J mice have increased TNFα release when stimulated with LPS or IFN-γ, which is typical of the M1 response, along with reduced M2 cell surface markers when compared to 8- or 10-week-old mouse macrophages (Gibon et al. 2016). Macrophages derived from aged individuals are more likely to induce more pro-inflammatory cytokines, thus prolonging the inflammatory response. Their role in tissue homeostasis has recently been investigated especially after the identification of tissue-resident macrophages throughout the periosteum and endosteum areas of key bone remodelling sites (Chang et al. 2008). These tissue-resident macrophages (also known as osteotissue macrophages or osteomacs for short) play key roles in bone remodelling releasing TNFα following stimulation with LPS. They have key roles in osteoblast differentiation and mineralisation, while depletion of these cells resulted in a reduction of osteocalcin and mineralisation (Chang et al. 2008).

1.2.2.4: Dendritic Cells

Dendritic Cells (DCs) are another bone marrow cell type that provides a crucial link between the innate and the adaptive immune response. These cells stimulate B and T-lymphocytes by presenting antigens such as MHC class I and II to these cells (Regnault et al. 1999). Immature DC are unable to stimulate T-lymphocytes (Wang et al. 2013). DCs differentiation

and maturation can be inhibited by MSC modulation of the immune system by causing secretions of IL-6, PGE2 and a member of the notch signalling family, Jagged-2 (Jiang et al. 2005; Zhang et al. 2004). MSCs can also induce suppression of the innate and adaptive immunity on cells including DCs, B-cells and natural killer cells (NK, Wang et al. 2013) . The presence of MSCs can induce polarization of the pro-inflammatory T helper lymphocytes 1 (Th1) cells to anti-inflammatory Th2 cells, by increasing the number of anti-inflammatory cytokines secretions from DCs (Beyth et al. 2005).

1.2.2.5: Natural Killer Cells

Natural killer (NK) cells are cells found in the bone marrow that play a role in the innate immune response inducing cytotoxicity in cells that are infected by pathogens or are stressed. Their role in bacterial infections is vital, as they require unique cross-communication with other bone marrow cells that identify bacteria using PAMPs, which release a slew of cytokines including, IL-2, IL-12, IL-15 and IL-18 initiating NK cell activation. Furthermore, their activation can lead to the expression of INF-γ, TNFα and GM-CSF (Reviewed in Souza-Fonseca-Guimaraes et al. 2012) .

1.2.2.6: T-lymphocytes

T-lymphocytes are cells whose precursors derive from the bone marrow, but multiply and mature in the thymus and are then distributed to peripheral tissues or circulate in the blood or lymphatic system. These cells are involved in initiating and resolving the innate immune response, have two main types, the $CD4^+$ cells called T-helper cells or the $CD8^+$ cells called T-cytotoxicity cells (TCC, Bennett et al. 1997) . T-helper cells can occur in a variety of subset populations; Th1, Th2 and Th17 (Hedegaard et al. 2008). The Th1 cells induce INF-γ and can activate macrophages (Hedegaard et al. 2008; Mills et al. 2000). They are also a source of IL-2, which is also known as a T-lymphocyte growth factor, facilitating the growth of both CD4 and CD8 cells. These cells can stimulate immunoglobulin switching in B-lymphocytes to express subtypes of IgG from IgM, which can be used to opsonize bacteria (Sha and Compans 2000). The Th2 cells can stimulate B-lymphocyte differentiation into plasma cells by the

production of IL-4 and IL-5. These cells can regulate the Th1 response (Mills et al. 2000; Rincon et al. 1997). Th17 cells release increased levels of IL-17 cytokine, which can increase the numbers of neutrophil progenitors in the bone marrow (Aujla et al. 2007).

Recent studies have investigated the role of *S. aureus* in skewing the host response by manipulating the cytokine response. *In vivo* studies by Prabhakara et al. (2011a); Prabhakara et al. (2011b) have shown that *S. aureus* can persist from an acute infection to more chronic infection by regulating T-lymphocyte response. Here, it was demonstrated that mice that increased levels of Th1 were more susceptible to the microbe, which was able to produce a chronic biofilm on implants. These Th1 biased mice could not efficiently clear the infection, compared to mice that had increased levels of Th2 which had a 75 % clearance rate of infection. Th2 biased mice had reduced neutrophils along with increased Th2 cytokine response of IL-4 and IL-10, both of which inhibit Th1 response and IL-10 inhibits Th17 response. The study also demonstrated that another subset of T-lymphocytes, the regulatory Tregs, play a role in clearing infections, since mice with increased levels of Th2 had increased Treg cells, which played key roles in initiating *S. aureus* clearance. The data from these studies suggest that the bacteria induce Treg downregulation and induce increased Th1 and Th17 responses, so there is an increase in inflammation and chronic infection. The increase in proinflammatory cytokines and the rapid recruitment of neutrophils increase the number of lysed neutrophils and damage to the host tissues, increasing the chance of bacteria to colonise and form biofilms of damaged pieces of bone.

1.2.3: Pro-inflammatory Cytokines

Cytokines are central to the control of bone repair, controlling pathological destruction and its response to bacterial infection. Cytokines are locally produced molecules that can either act antagonistically or synergistically on a variety of cell types and can alter the bone marrow microenvironment often in a cascade. Cytokines are small regulator proteins produced by various cells that are actively involved in cell-to-cell communication (Zhang and An 2007). Cytokine is a generalised term that can also include chemokines and interleukins.

Cytokine regulation within the local bone marrow microenvironment is achieved either by directly stimulating the very same cells that secrete them, known as an autocrine action system, or affecting local cells that are either at close proximity or at a distance, also known as a paracrine or endocrine system respectively (Zhang and An 2007). Multiple cytokines can be produced from a single cell can affect multiple cells in a co-ordinated network, with key roles within the BMU and infections.

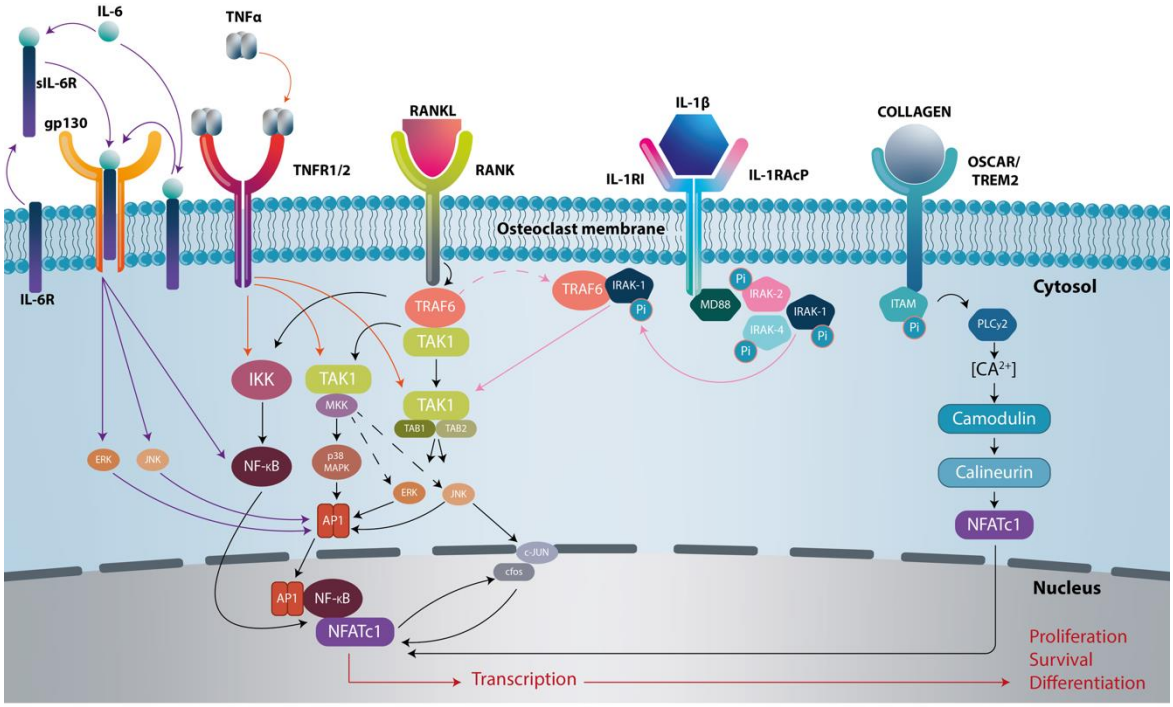

Figure 1.4: Various pro-inflammatory signal pathways that either independently or dependently with RANK/RANKL signalling induce osteoclast differentiation. Binding of IL-6 to membrane-bound or soluble IL-6R homodimerizes with gp130 and induces a signalling cascade. Gp130 signalling induces activation of ERK, JNK activating AP-1 nuclear translocation along with and NF-κB nuclear translocation, that along with NFATc1 induces key osteoclastogenesis transcription factors. TNFα can work independently or decently on RANK/RANKL signalling pathways. TNFα/TNFR1/2 binding initiates similar downstream signal cascades as RANKL/RANK, activating ERK, JNK and MAPK pathways and subsequent AP-1 translocated and initiating NFATc1 activation, along with NF-kB is translocated into the nucleus subsequent transcription and osteoclast differentiation. IL-1 binds to IL-1RI activates a downstream signalling cascade. Two intracellular adaptor proteins are assembled by the conserved cytosolic regions involving IRAK-1,- 2, -4 and MYD88. IRANK 4 phosphorylates IRAK1 and IRAK2 and recruits TRAF6 to activate transcription factors ERK, JNK, AP-1, similarly to RANKL signalling. Image drawn from information obtained from Feng et al. (2017); Osta et al. (2014); Wright and Nair (2010) and Amarasekara et al. (2018).

1.2.3.1: Interleukin-1 Beta

The interleukin-1 (IL-1) is a mediator for inflammation and innate immunity. The Interleukin-1 family consists of cytokines with pro-inflammatory properties (IL-1α, IL-1β, IL-18, IL-36α, IL-36β and IL-36γ), in addition to proteins that are considered receptor antagonists (IL-1Ra, IL-36Ra and IL-38), and anti-inflammatory properties (IL-37) (Garlanda et al. 2013). IL-1 binds to two surface receptors, the IL-1 receptor type I and type II (IL-1RI and IL-IRII). Both IL-1α and IL-1β bind to IL-1RI with equal affinity, whilst the IL-1 RII is also another decoy receptor that can block the effects of IL-1 (Colotta et al. 1993; Lee et al. 2010). The receptor antagonist IL-1Ra is a natural inhibitor by binding to both IL-1α and IL-1β, thereby blocking binding and activation of signalling pathways by IL-1RI (Lee et al. 2010). HSC and its committed cells synthesis IL-1 and its receptor IL-1RI, which helps maintain HSC survival, mobilisation and transendothelial migration (Orelio et al. 2008). IL-1 also plays key roles in inhibiting osteoblast differentiation and promoting bone resorption by increasing osteoclastogenesis, initiating downstream signal cascades on osteoclast precursors and osteoclasts vital for their cell survival, or influence activation of T-lymphocytes to produce RANKL production (Lee et al. 2010; Ruscitti et al. 2015).

When IL-1 binds to IL-1RI, it homodimerizes and undergoes a conformational change activating a downstream signaling cascade (Kim et al. 2009). Here, two intracellular adaptor proteins are assembled by the conserved cytosolic regions, involving interleukin-1 receptor-activated protein kinase (IRAKs) and the myeloid differentiation primary response gene 88 (MYD88), together termed the Toll-like and IL-1R-like domains. MD88 and IRAK4 induce phosphorylation of IRAK1 and IRAK2 and their association with tumor necrosis factor response associated factor (TRAF6, Ruscitti et al. 2015). TRAF6/IL-1β can lead to activation of transcription factors, extracellular signal-regulated kinase (ERK), JNK, AP-1, which is vital for the activation of NF-κB and promoting osteoclastogenesis (Figure 1.4). Although TRAF6 is used as a downstream signalling molecule, IL-1 is unable to directly induce osteoclast differentiation and can only stimulate osteoclastogenesis via prostaglandin E_2 synthesis in osteoblasts (Hofbauer et al. 1999; Lee et al. 2010). IL-1 has also been shown to increase the expression of RANKL in osteoblasts (Hofbauer et al. 1999; Lee et al. 2010). In a study by Kim et al. (2009) has shown that IL-1 can lead to osteoclast differentiation via increasing IL-1RI

and c-Fos expression during RANKL or TNFα initiated osteoclastogenesis. The study reports that osteoclast precursors have decreased levels of IL1RI and increased levels of IL-1RII. When osteoclast precursors are overstimulated with IL-1RI it can lead to IL-1 induced osteoclastogenesis via a RANKL-independent pathway (Kim et al. 2009). Similarly, a different study has reported that IL-1 can induce osteoclastogenesis from osteoclast precursors if they are overexpressing c-Fos and these cells *in vitro* can induce bone resorption (Yao et al. 2008).

IL-1β, along with Tumor necrosis factor-alpha (TNFα) and IL-6 have also been shown to inhibit osteoblast formation and function. This is caused by inhibition of the mitogen activated protein kinases (MAPK) activity. This causes activation of key signaling pathways which include signal transducers and activators of transcription (STATs) and SMAD ubiquitylation regulatory factors 1 and 2. The activation of these two STATs and SMAD ubiquitylation regulatory factors upregulate Dickkopf-related protein 1 and sclerostin, which have been known to which inhibit WNT-frizzled signalling pathways which are vital for the expression of key osteoblast genes required for differentiation and activation (Reviewed in Redlich and Smolen 2012).

1.2.3.2: Tumor Necrosis Factor-Alpha

TNFα is a key pro-inflammatory cytokine produced by many immune cells including monocytes and macrophages (Parameswaran and Patial 2010). TNFα binds to its two receptors; TNF receptor 1 (p55) and TNF receptor 2 (p75, Marahleh et al. 2019). Within the bone marrow, TNFα plays a key role in osteoclastogenesis, stimulating M-CSF and RANKL production in both MSCs and osteoblasts (Hofbauer et al. 1999; Kitaura et al. 2004; 2005) . More recently, TNFα has been linked to inducing RANKL expression in osteocytes (Marahleh et al. 2019). TNFα can stimulate the increased synthesis of the M-CSF receptor on the surface of monocytes and macrophages (Yao et al. 2006). TNFα enhances RANK expression on the surface of osteoclast precursors, with studies showing that the presence of TNFα includes increased $TRAP^{+}$ multinucleated cells, in stroma-free bone marrow cells isolated from 5-7-week-old Sprague-Dawley rats (Komine et al. 2001). TNFα has been seen to play a role within osteoclast differentiation (Figure 1.4). Kobayashi et al. (2000) demonstrated

that treatments of primary murine bone marrow macrophage cultures with 20 ng/mL TNFα, along with 100 ng/mL M-CSF without any RANKL induced a significant number of $TRAP^+$ multinucleated osteoclast-like cells. TNFα treatments between 20-100 ng/mL induced a dose-dependent increase in the number of $TRAP^+$ multinucleated osteoclast-like cells, to numbers similar to M-CSF and RANKL only treated controls. The study demonstrated that TNFα receptors are vital for inducing TNFα dependent osteoclast formation. This has also been demonstrated using C57BL/6J mice which were selectively bred to remove the TNFα receptor gene or by blocking both receptors TNFRI and TNFRII along with treatments with TNFα and M-CSF. Blocking of TNFRI induced no osteoclast-like cells, whereas silencing of TNFRII induced reduced number of osteoclast-like cells to approximately ~ 20 cells when compared to the wild type control which averaged at ~100 osteoclast-like cells. This highlights that these receptors are vital in mediating TNFα induced osteoclast differentiation. The blocking or removal of these receptors had no effect on osteoclast numbers when M-CSF and RANKL were added to cultures alone. Additionally, the presence of the RANKL antagonist, OPG, had no effect on reducing the number of osteoclast-like cells in the presence of TNFα and M-CSF. However, Lam et al. (2000) showed that TNFα alone was not sufficient in inducing osteoclast differentiation along with M-CSF, but differentiation only occurred in macrophages that were previously primed with RANKL before TNFα stimulation within *in vitro* and *in vivo* models. To investigate both these conflicting reports of TNFα-induced osteoclastogenesis with or without RANKL, Luo et al. (2018) showed that osteoclast differentiation was possible in the presence of M-CSF alone without any RANKL. This did cause a marked reduction in the number of mature osteoclasts, when compared to osteoclast precursors stimulated with combinations of either RANKL and TNFα or RANKL, M-CSF and TNFα. These conflicting reports of TNFα induced osteoclastogenesis dependent or independent of RANKL may be explained by the shared downstream signalling pathways that TNFα induce when it is bound to its receptor TNFR1/2 on the preosteoclast surface, in a similar manner to RANKL/RANK as seen in Figure 1.4. Here, following binding of TNFα to its receptor, NF-kB is translocated into the nucleus, along with AP-1 via ERK, JNK and MAPK activation, initiating NFATc1 activation and subsequent transcription and differentiation, in a similar manner to RANKL/RANK binding (Figure 1.4). This may explain why reports have

shown RANKL independent differentiation, if albeit slower causing reduced numbers and why in the presence of RANKL osteoclastogenesis is increased.

TNFα can also induce RANKL expression in BMSCs and osteoblasts and has been shown to be mediated by IL-1 (Hofbauer et al. 1999; Wei et al. 2005). The addition of the IL-1 receptor antagonist on murine and human BMSCs along with TNFα inhibited RANKL gene expression, and similar results were observed in IL-1RI deficient mice and following the addition of IL-4 (Wei et al. 2005). TNFα regulates the synthesis of both IL-1 and IL-1RI expression on BMSCs which suggests that TNFα increase IL-1 synthesis and its receptor to enhance RANKL expression via an autocrine and/or paracrine response on BMSCs (Wei et al. 2005). Studies in transgenic mice with deletions for IL-1R1 and TNFR1/2, caused a significant decrease in the number of osteoclasts and subsequent bone resorption following stimulation of *Porphyromonas gingivalis* and *Escherichia coli* lipopolysaccharide (LPS) stimulation within the parietal bone (Chiang et al. 1999). TNFα has also been seen as an inhibitor for osteoblastic differentiation from primary rat calvaria BMSCs in a dose-dependent response. The presence of the cytokine caused a reduction in both osteoblastic nodule formation and osteocalcin production in primary BMSC cells from either rat calvaria cultures or MC3T3-E1-14 clonal osteoblastic cell lines (Gilbert et al. 2000). Ding et al. (2009) showed in human BMSCs isolated from patients undergoing trabecular bone marrow explants, the presence of IL-1β and TNFα together caused a dose-dependent decrease in the gene expression of RunX2, collagen type I and osteocalcin, which are required for osteoblastic differentiation. The presence of these two cytokines can increase RANKL production from these cells, initiating local osteoclastogenesis. Therefore, these two cytokines, have a dual mode of action; firstly by TNFα promoting IL-1 synthesis which increases RANKL expression in resident BMSCs whilst secondly also suppressing BMSC osteoblastic differentiation, this in turn increases osteoclast differentiation and resorption whilst inhibiting mineralisation.

1.2.3.3: Interleukin-6

Recent studies have focused on IL-6 as a potential synovial fluid biomarker for the diagnosis of PJI. The normal serum IL-6 level is 0-1.0 pg/mL, with levels above this value is considered

elevated (McGrath-Morrow et al. 2016; Yamamura et al. 1998). IL-6 overproduction has been observed in PJI, postmenopausal women, rheumatoid arthritis and other diseases that involve accelerated bone turnover (Davies and Choy 2014; Di Cesare et al. 2005; Kim et al. 2012). IL-6 belongs to a family of cytokines that include IL-11, oncostatin M (OSM), ciliary inhibitory factor (CNTF), cardiotrophin-1 (CT-1) and leukaemia inhibitory factor (LIF, Scheller et al. 2011). The receptors of IL-6 type cytokines are type 1-membrane proteins belonging to the cytokine receptor class I family. All the IL-6 type cytokines signal via binding with the receptor protein gp130 alone or with the receptors LIF and OSM, LIFR and OSMR. The cytokines IL-6, IL-11 and CNTF, all have their specific α receptor subunits, the IL-6R, IL-11R and CNTFR (Heinrich et al. 1998; Scheller et al. 2011). The receptors of IL-6 can be found in both membrane-bound or soluble form and the IL-6R are expressed on certain cell types including; megakaryocytes, hepatocytes, monocytes, macrophages, subtypes of T-cells and B-cells (Garbers et al. 2015; Wolf et al. 2014). The binding of IL-6 to its receptor activates the receptor-associated tyrosine kinase the Janus kinase (Jaks). The activation of Jaks phosphorylates gp130 forming docking sites for STAT factors STAT 1/3, which in turn become phosphorylated and form either homo- or heterodimers and translocate into the nucleus thus activating gene transcription (Scheller et al. 2011). The binding of IL-6 to its receptor and the activation of Jaks also leads to the activation of src-homology domain 2 containing the protease tyrosine phosphatase (SHP2), with subsequent signalling in the mitogen-activated protein kinase–extracellular signal-regulated kinase (MKK) and MAPK/ERK (Kaneshiro et al. 2014).

IL-6 plays a role in acute inflammation, where the increase of pro-inflammatory cytokines can promote neutrophils accumulation and the subsequent release of IL-6. IL-6 can cause a shift from acute to chronic inflammation in rheumatoid arthritis patients (Barnes et al. 2011). During acute inflammation, endothelial cells, monocytes and macrophages release IL-6, causing an increase in neutrophils in synovial fibroblasts (Barnes et al. 2011). As the disease progresses, IL-6 causes a shift towards chronic inflammation (Barnes et al. 2011). IL-6 along with IL-1 have been shown as a key regulator for C-reactive protein production in hepatocytes and both IL-6 and C-reactive protein levels are increased in patients with osteoarthritis in the synovial fluid and serum (Pearle et al. 2007).

IL-6 plays key role in bone homeostasis, affecting the roles of both osteoclasts and osteoblast. Osteoblasts from either MC3T3-E1 cell lines or primary cells can secrete IL-6 following upregulation of IL-1, TNFα and lipopolysaccharides into the *in vitro* microenvironment (Ishimi et al. 1990). Osteoblasts treated with IL-6 upregulated IL-1 serum levels, along with IL-6 gene expression (De Benedetti et al. 2006). McGregor et al. (2019), showed that *in vivo* C57BL/6 mice induced $TRAP^+$ osteoclast formation with three or more nuclei, with the addition of soluble IL-6 Receptor (IL-6R)/IL-6 in co-cultures with osteoblasts but not with osteocytes. Both TNFα and IL-1β regulate the shedding of the sIL-6R either by proteolytic cleavage or by alternative splicing, which is mediated by the TNFα converting enzyme in MG36 human osteogenic sarcoma cell lines and SAOS-2 osteoblast-like cell lines (Franchimont et al. 2005). The inhibition of TNFα converting enzyme into MG36 cells reduced sIL-6R production (Franchimont et al. 2005). Interestingly, TNFα had been shown to reduce IL-6R expression on the surface of osteoblast-like cell lines, indicating that though these cells can produce IL-6 as a proinflammatory response, they become less likely to be stimulated by IL-6 by reducing membrane and thus soluble IL-6R (Vermes et al. 2002).

IL-6 has been seen to induce osteoclastogenesis whilst suppressing osteoblast function and mineralisation which was observed by De Benedetti et al. (2006). Here, osteoblasts from IL-6-transgenic mice, which overexpressed high levels of circulating IL-6, showed a reduction in alkaline phosphatase activity *in vivo*, along with a smaller phenotype, compared to wild type controls. *In vitro* primary cell cultures also showed a similar reduction in alkaline phosphatase, mineralisation and proliferation of osteoblasts, with the gene expression of osteocalcin and collagen type I down-regulated following IL-6 treatment, though RunX2 and alkaline phosphatase were not down-regulated (De Benedetti et al. 2006). Controversially, Franchimont et al. (2005) showed the opposite effect following IL-6 production which osteoblast alkaline phosphatase activity was increased. This variable effect on alkaline phosphatase activity may be due to the type of cells used within studies and the quantity of membrane-bound IL-6R, for example, the MG36 osteoblast-like cell line has reduced membrane-bound IL-6R and thus reduced levels of sIL-6 (Nishimura et al. 1998). Treatment with IL-6 and sIL-6R to these cells induced an increase in alkaline phosphatase activity and reduction in proliferation (Nishimura et al. 1998). Similarly, Brocker et al. (2010) showed

that MG63 cells treated with IL-6 family of cytokines inhibited cell proliferation whilst simultaneously increasing alkaline phosphatase activity, which was further enhanced following the addition of sIL-6R. The study highlighted that IL-6 activated JAK/STAT and MAPK pathways within osteoblastic cells vital for cell survival. More recently, McGregor et al. (2019) have shown similar results on primary osteoblasts derived from C57BL/6 mice, showed that IL-6 alone was not able to increase calvaria thickness of bone *in vivo* and it was only after the addition of IL-6/sIL-6R that such thickness was observed. The authors reported that since sIL-6 can affect both osteoblasts and osteoclasts an additional factor must regulate bone formation/ resorption; this was found to be high circulating levels of soluble GP130-fc which caused a reduction in bone strength along with impaired bone growth. Human bone marrow MSCs cannot undergo osteogenic differentiation to osteoblasts in the presence of IL-6 alone due to them lacking the IL-6R and this is not recovered in the presence of sIL-6 alone, or both IL-6 and sIL-6. The addition of dexamethasone with IL-6 and sIL-6 enhanced alkaline phosphatase activity, again suggesting osteoblasts and their precursors depend on IL-6R availability (Erices et al. 2002).

IL-6 role on osteoclastogenesis is indirect and occurs through osteoblasts via sIL-6R, resulting in increased RANKL expression over OPG and subsequent differentiation of preosteoclasts into mature osteoclasts via osteoclastogenesis (Dayer and Choy 2010). IL-6 role in osteoclast differentiation induces RANKL production on the surface of osteoblasts and MSCs (Yoshitake et al. 2008). IL-6 direct interaction on osteoclasts has seen an inhibitory effect on osteoclastogenesis in mice RAW 246.7 bone marrow monocytic cell line. A reduction of TRAP-positive cells even with the addition of RANKL was observed with IL-6 potentially diverting these cells towards a more macrophage lineage (Duplomb et al. 2008). Inhibition of the IL-6 receptor on the surface of spleen derived osteoclast precursors from 6-week-old wild type mice and human TNFα transgenic mice *in vivo* and *in vitro* have shown a reduction of gene expressions for TRAP, cathepsin K and OSCAR in the presence of both M-CSF and RANKL. Also, numbers of mature osteoclasts were reduced in both mice along with a reduction in resorption (Axmann et al. 2009). Per the above studies, Feng et al. (2017) showed that the addition of IL-6 or its sIL-6R individually on RAW 246.7 cell lines did not induce multinucleated TRAP-positive cells with the addition of 30 ng/mL M-CSF compared to RANKL simulated controls. The addition of both IL-6 and sIL-6R induced a small number

of differentiated osteoclasts with M-CSF. However, the addition of IL-6 at 10 ng/mL alone to 50 ng/mL RANKL reduced the number of mature osteoclasts, but this was not seen at lower concentrations below 20 ng/mL, whereas sIL-6R alone did not have any effect. When both IL-6/ sIL-6R was added at 100 ng/mL to either 10 or 50 ng/mL RANKL both showed similar numbers $TRAP^+$ mature osteoclasts, but this was suppressed at higher RANKL concentrations at 100 ng/mL. Cells pretreated with 100 ng/mL IL-6/sIL-6R with low RANKL dose (10 ng/mL) enhanced NF-kB, ERK and JNK activation in osteoclast precursors, initiating osteoclast differentiation, though this was reduced with the addition of high levels of RANKL (50 ng/mL). Essentially, IL-6/sIL-6R induces osteoclastogenesis via RANKL in a dose-dependent manner and the result can either be positive or negative. This sIL-6R can act as a substitute of IL-6R and the binding of IL-6/sIL-6R and forming a complex with gp130 on osteoclast precursors can induce osteoclast differentiation, via activation of ERK, JNK and NF-kB (Figure 1.4; Feng et al. 2017) .

1.3 Microorganisms Associated with Orthopaedic Implant Infections

Within PJI isolates, a broad range of bacterial species have been identified, as summarised within Table 1.1, consisting of a mix of both gram-positive and gram-negative species, though the former is considered more common. Pathogens cultured from PJI cultures include, though are not limited to, *S. aureus, S. epidermidis*, *Streptococcus, Enterococcus*, *Propionibacterium*, *Escherichia coli*, *P. aeruginosa*, *Serratia marcescens*, *Proteus* species, Klebsiella species, Acinetobacter, *Granulicatella advances*, *Finegoldia Magna, Cutibacterium acnes* and anaerobic species (Table 1.1). *Staphylococcus* is considered the most common species to be frequently detected, with *S. aureus* accounting for between 13 and 75 % of all infections and the coagulase negative *Staphylococcus aureus* (CoNS) accounting for 6 -64 %, of which 16 – 40 % were *S. epidermidis* (Table 1.1). As previously stated, PJI infections can occur throughout the lifespan of the implant, therefore it is safe to assume that microbial species may differ depending on when the infection occurred. For early infections near or directly after the initial surgery, the more virulent organisms are commonly isolated, which include *Escherichia coli* and *S. aureus*. Conversely, delayed infections tend to be caused by less virulent organisms that include CoNS or *Propionibacterium acnes* (Geipel 2009; Zimmerli and Moser 2012). Overall infections tend to be monomicrobial (69-96 %), whilst

polymicrobial infections tend to be less common (4-31 %). The reasoning of this is possibly down to the quality of the diagnostic procedures and the type of antibiotic therapy given to the patients preceding the surgery (Zimmerli and Moser 2012).

Reference	Phillips et al. (2006)	Gallo et al. (2008)	Pulido et al. (2008)	Fink et al. (2013)	Yi et al. (2014)	Bemer et al. (2014)	Langvatn et al. (2015)	Lange et al. (2016)	Flurin et al. (2019)		Average (%)
Country	UK	Czech Republic	USA	Germany	USA	France	Norway	Denmark	USA		
									Monomicrobial	Polymicrobial	
Microorganisms											
Gram-Positive Organisms											
No. (%) of *Staphylococcus aureus* isolates	19 (25)	12 (24)	24 (38)	6 (13)	27 (75)	63 (33)	53 (19)	29 (22)	58 (21)	7 (22)	29.9
No. (%) of *Staphylococcus agalactiae* isolates	N/A	N/A	3 (5)	2 (4)	N/A	N/A	N/A	N/A	N/A	N/A	7
No. (%) of CoNS	27 (36)	19 (38)	13 (20)	29 (64)	2 (6)	45 (23)	113 (41)	26 (20)	17 (6)	8 (25)	27.9
No. (%) of *Staphylococcus epidermidis* isolates	N/A	N/A	12 (19)	18 (40)	N/A	31 (16)	43 (16)	N/A	97 (35)	19 (59)	30.8
No. (%) of *Streptococcus* species isolates	5 (7)	6 (14)	8 (12)	2 (4)	3 (8)	19 (10)	30 (11)	12 (9)	21 (11)	2 (6)	9.2
No. (%) of *Enterococcus* species isolates	7 (9)	1 (2)	N/A	N/A	N/A	3 (2)	26 (9)	8 (6)	16 (6)	9 (28)	8.86
No. (%) of *Corynebacterium* species isolates	1 (1)	1 (2)	1 (2)	N/A	N/A	N/A	N/A	N/A	8 (3)	5 (16)	1.7
No. (%) of *Propionibacterium* species isolates	1 (1)	N/A	N/A	7 (16)	1 (3)	11 (6)	N/A	N/A	N/A	N/A	6.5
Gram-negative organisms											
No. (%) of Gram-negative bacilli	N/A	N/A	N/A	N/A	N/A	N/A	N/A	N/A	21 (8)	3 (9)	8.5
No. (%) of *Escherichia coli* isolates	3 (4)	3 (6)	2 (3)	N/A	N/A	5 (2)	N/A	N/A	N/A	N/A	3.8
No. (%) of *Pseudomonas aeruginosa* isolates	3 (4)	2 (4)	1 (2)	N/A	N/A	4 (1)	N/A	2 (2)	N/A	N/A	2.6
No. (%) of *Serratia marcescens* isolates	N/A	2 (4)	1 (2)	N/A	N/A	N/A	N/A	N/A	N/A	N/A	3
No. (%) of *Proteus* species isolates	N/A	N/A	1 (2)	N/A	N/A	2 (1)	N/A	5 (4)	N/A	N/A	2.3
No. (%) of *Klebsiella* species isolates	2 (3)	N/A	2 (3)	N/A	1 (3)	3 (2)	N/A	N/A	N/A	N/A	2.8
No. (%) of *Acinetobacter* species isolates	1 (1)	1 (2)	N/A	N/A	N/A	N/A	N/A	N/A	N/A	N/A	1.5
No. (%) of *Granulicatella adiacens*	N/A	N/A	N/A	N/A	N/A	N/A	N/A	N/A	6 (2)	0 (0)	1
No. (%) of *Finegoldia magna*	N/A	N/A	N/A	N/A	N/A	N/A	N/A	N/A	4 (1)	6 (19)	10
No. (%) of *Cutibacterium acnes*	N/A	N/A	N/A	N/A	N/A	N/A	N/A	N/A	9 (3)	3 (9)	6
No. (%) of total Gram-negative organism isolates	10 (13)	N/A	7 (11)	N/A	2 (6)	16 (8)	17 (6)	N/A	N/A	N/A	8.8
No. (%) of Anaerobic isolates	N/A	N/A	N/A	1 (2)	N/A	13 (7)	N/A	N/A	N/A	N/A	4.5
No. (%) of Monomicrobial isolates	52 (69)	N/A	59 (94)	42 (93)	34 (94)	163 (85)	251 (90)	125 (96)	278 (90)		88.8
No. (%) of Polymicrobial isolates	23 (31)	N/A	4 (6)	3 (7)	2 (6)	29 (15)	27 (10)	5 (4)	32 (10)		11.1
Total No. of confirmed PJI with positive results	75	42	63	45	36	192	278	130	310		

Table 1.1: Microorganisms identified in prosthetic joint infections.

1.4: *Staphylococcus aureus*

The bacteria of the genus *Staphylococcus* are Gram-positive, facultative aerobes, culturable under aerobic conditions or via fermentation. They are identified by their cocci appearance, with diameters of 0.5 - 1.5 µm and form grape-like bunches (Ribeiro et al. 2012). The bacteria can be present and colonise hosts asymptomatically. Currently, it is predicted that the bacteria is asymptomatically present in 20 – 60 % of hosts, without causing any major tissue damage; 20 – 25 % of the population is considered to have the bacteria persistently present on themselves and 75 – 80 % of the population are either intermittently colonised by the bacteria or never have the bacteria present at all (Archer et al. 2011; Masters et al. 2019). Typically, large communities of *S. aureus* are found on the surface of nasal cavities and the skin, but can be found in virtually every tissue and organ after they spread. The success of these species in being persistent colonisers in multiple conditions is attributed to their resource of virulence factors, toxins, adhesions, biofilm formations and formation of a subpopulation termed small colony variants (SCV; Masters et al. 2019) . In recent years, one particular case study has highlighted these species as persistent colonisers and their ability to remain quiescent for prolonged periods. Here, a patient who had *S. aureus* related osteomyelitis on their left femur as a 10-year-old child was at the time treated surgically without any antibiotics. They later had reoccurring osteomyelitis in the left mid femur when was 85 years old. Culture analysis identified the bacteria as *S. aureus* with gene analysis identifying as sequence type 30, a penicillin-resistant and methicillin-susceptible clone that was prevalent in the 1950 and 1960s, thus suggesting that the strain lay dormant within the femur for 75 years (Libraty et al. 2012). As such, the bacteria must have developed a variety of different strategies to remain undetectable within the host for those 75 years.

1.4.1: Subpopulation of S. aureus

The ability of *S. aureus* to persist and remain asymptomatic and undetectable within a host is often due to the extreme lengths these bacteria alter their lifestyle to remain protected in an otherwise hostile environment. One of these ways is the ability of *S. aureus* to produce a sub-phenotype called *S. aureus* SCV, which are often associated with biofilm formation and chronic infections and have been seen in PJI cases. In a 4-year study on serum

aspirations and tissue biopsies, Sendi et al. (2006) showed that 5/83 patients were positive with SCV, where transmission electron microscopy (TEM) analysis indicated the presence of small cocci cells within patient fibroblasts. They concluded that SCV may be the main cause of relapse and recurrent infections and their ability to persist within cells that lack phagocytic capabilities may be advantageous to their survival. SCV represent an unstable colony variant, possibly due to mutations in a variety of biosynthesis molecules that are essential for nutrient uptake. SCV has been seen with mutations for haemin (an oxidation product for haem), thymidine (a DNA nucleoside) and menadione (a precursor to K_2 and proteolytic aromatic ketone; Sendi and Proctor 2009)

Additional variations of *S. aureus* include the methicillin-resistant *S. aureus* (MRSA) and the methicillin-sensitive *S. aureus* (MSSA). MRSA has emerged due to the bacteria's uptake of the *Staphylococcal* cassette chromosome *mec* (SCC*mec*) DNA element (Foster 2004). This cassette carries the *mec*A gene that encodes the penicillin-binding protein (PBP) 2a and this DNA element is transferred into the bacterial genome, resulting in resistance to b-lactam antibiotics, including amoxicillin, penicillin and oxacillin (Cogen et al. 2008; Foster 2004; Ribeiro et al. 2012). Other antibiotics that MRSA strains have become resistant or less susceptible to include; streptomycin, tetracycline, sulphonamides, cephalosporin, vancomycin and glycopeptide antibiotics (Ribeiro et al. 2012).

1.4.2: Staphylococcus Binding Proteins and Modes of Attachment

S. aureus can express up to 24 different cell-wall anchoring proteins, classified into four groups; the microbial surface components recognising adhesive matrix molecules (MSCRAMMs), the near-iron transporters motif family, the three helical bundle family and the G5-Erepeat family (Ricciardi et al. 2018). These proteins enable the bacteria to bind to the bone matrix, biomaterials and ECM proteins (Arciola et al. 2011; Ribeiro et al. 2012).

MSCRAMMs are vital cell-wall anchoring proteins that are characterised by two IgG-folded domains within the N-terminal region (Foster et al. 2014). These MSCRAMMS are varied and include fibronectin-binding proteins, clumping factor (Clf) A (ClfA) or B (ClfB), fibrinogen-binding proteins, elastin-binding adhesins and collagen-binding adhesins (Ribeiro et al.

2012). Following insertion of an implant, the surface of the biomaterial is covered by a conditioning layer of ECM proteins that include fibronectin, fibrinogen and collagen (Khoo et al. 2010). It is this layer that *S. aureus* can utilise for attachment, colonisation and formation of a biofilm (explained in more detail in Section 1.5.2b).

Both the fibronectin and fibrinogen binding proteins utilise the dock, lock and latch mechanism, where the ligand is docked to an open apo (which has no bound ligand) form and undergo a conformational change to a locked form (Foster et al. 2014). The fibronectin-binding protein allow the bacteria to attach to fibronectin along with other ligands, including fibrinogen, elastin and plasminogen, which occurs wildly on the surface of mammalian cells (Foster 2016). Mutations of the fibronectin-binding proteins on 8325-1 *S. aureus* strain resulted in a reduction of adhesion to fibronectin along with a marked decrease in internalisation within the cells (Brouillette et al. 2003). This indicates that although fibronectin-binding proteins are important in progressive adhesion and internalisation of the bacteria within cells, and the lack of these proteins delays this, it does not prevent infection and disease progression. Genetic analysis of the two genes encoding the fibronecting-binding proteins (*fnbA* and *fnbB*), have identified that both genes were found in high abundance 93-100% in both TKA and THA, thus indicating that *S. aureus* species actively utilised these fibronectin-binding proteins as a method to attach and colonise the implant or surrounding bone or connective tissue (Arciola et al. 2005; Peacock et al. 2002). Similarly, fibrinogen-binding proteins bind to fibrinogen and have a similar structure to fibronectin-binding proteins and allows the bacteria to clump together in the presence of fibrinogen (Hawkins et al. 2012; Scully et al. 2015; Vazquez et al. 2011). The genes that encode these proteins are found in high abundance in PJI isolated species (Peacock et al. 2002). Bacterial species utilise fibrinogen-binding proteins as a protective mechanism increasing their aggregations to each other and thus, protecting themselves from phagocytosis and can be used as a basis for abscess formation linking themselves towards the implant (Muthukrishnan et al. 2019).

Collagen-binding adhesins (CNA) are used by *S. aureus* to colonise and attach to the bone mineral surface (Al-Qtaitat and Aldalaen 2014; Arciola et al. 2011; Boskey 2013; Reznikov et al. 2014; Young 2003). *S. aureus* clinical isolates from PJIs carried low levels of the *cna* gene

26-52 % (Arciola et al. 2005; Montanaro et al. 1999; Peacock et al. 2002). Analysis between TKA and THA isolates showed that within cases of TKA 100 % of isolated *S. aureus* carried the *cna* gene, when compared to the 43 % in THA cases, both species could bind to collagen along with polysaccharide slime production vital for biofilm formation (Montanaro et al. 1999).

The *Staphylococcus aureus* Protein A (SpA) is another important cell-wall anchoring proteins are found in all isolates of *S. aureus*. SpA is bound to the cell wall of the bacteria and can be freely secreted to avoid immune detection and phagocytosis (Kobayashi and DeLeo 2013). The released SpA binds to the surface of the Fc portion of antibodies from B-lymphocytes causing antibody neutralisation, or alternatively, SpA binds to the FAB portion of the bound antibody on B-lymphocytes to induce initiation of cell apoptosis. The interaction of *S. aureus* SpA to a variety of immune and bone marrow cells have been widely studied. The structure of SpA has five immunoglobulins (Ig) binding domains for IgG, IgM, IgA and IgE (Falugi et al. 2013). SpA has enhanced binding capability to IgG on the surface of B-cells via Fcg and fragment antigen binding domains on SpA which alter the adaptive immune response within mice (Falugi et al. 2013). This Fcg is essential for the bacteria to survive in mice blood both *in vivo* and *in vitro* and lack of Fcg resulted in increased opsonisation and phagocytosis (Falugi et al. 2013).

1.5: Process of *Staphylococcus aureus* Induced Dysregulation of Bone Homeostasis and Immune Evasion

1.5.1: Dysregulation of the Bone Remodelling Unit

As commented upon at the start of this Chapter, the bone loss caused by PJIs and osteomyelitis bacterial bone infections results in the loosening of the implant. However, in these conditions, the bone loss is not always the direct action of the bacteria lysing the bone cells, but the indirect action of causing host cells to increase their secretion of pro-inflammatory cytokines, which dysregulates the BMU, leading to pathological septic osteolysis. Three of the most investigated pro-inflammatory cytokines are TNFα, IL-1 and IL-6, due to their direct interplay with osteoclastogenesis and bone resorption. Synovial fluid

analysis in PJI suspected patients indicate high levels of TNFα, IL-1 and IL-6 (Deirmengian et al. 2010; Deirmengian et al. 2014a; Deirmengian et al. 2014b; Di Cesare et al. 2005; Froschen et al. 2020; Garcia-Alvarez et al. 2009; Vicenti et al. 2019). As mentioned previously, these three cytokines have key roles within osteoclast differentiation (Section 1.2.3), with the pathological synthesis of these three pro-inflammatory cytokines can result in an increase in bone resorption over bone formation, resulting in pathological bone loss around the implant and subsequent implant loosening.

Studies looking at the interplay between *S. aureus* and these pro-inflammatory cytokines have been modelled within a variety of animal models. In a study by Morris et al. (2019), twenty-week old male Sprague-Dawley rats implanted with infected or non-infected Ti-6AL-4V implants into the knee showed significantly elevated IL-1β (~300 pg/g tissue) compared to controls. However, IL-6, TNFα and interferon-gamma (IFNγ) were elevated at 28-days post-surgery but were not significant compared to controls. Additionally, the authors showed that infected implants had reduced implant-to-bone contact with decreased bone volume typical of osteolysis. Endorsing this finding, Garcia-Alvarez et al. (2009) reported an increase in IL-1β within the implant tissue, but not circulating in the blood. However, IL-6 levels were elevated in blood circulation in 22-month old Wistar rats implanted with *S. aureus* infected needles within the tibia. Elevated levels of IL-6, TNFα and IL-1β were observed in the murine model of tibial osteomyelitis in a female 5-week old ICR mouse. Over 28-days, IL-1β levels peaked at 7-14 days, before dropping by 28 days post-infection of the tibial implants with *S. aureus*. IL-6 peaked within the first 24 h before dropping to control levels by 28 days. TNFα levels were significantly elevated by 3 days and steadily rose over 28 days (Yoshii et al. 2002).

1.5.2: *Staphylococcus aureus* Mechanisms of Immune Evasion

Following infection, *S. aureus* utilises its vast array of binding proteins to invade, persist and colonise the tissue via dysregulating the innate and adaptive immune responses. Mechanisms that induce immune response dysregulation include the formation of an abscess, biofilm or develop techniques for intracellular evasion (Figure 1.5).

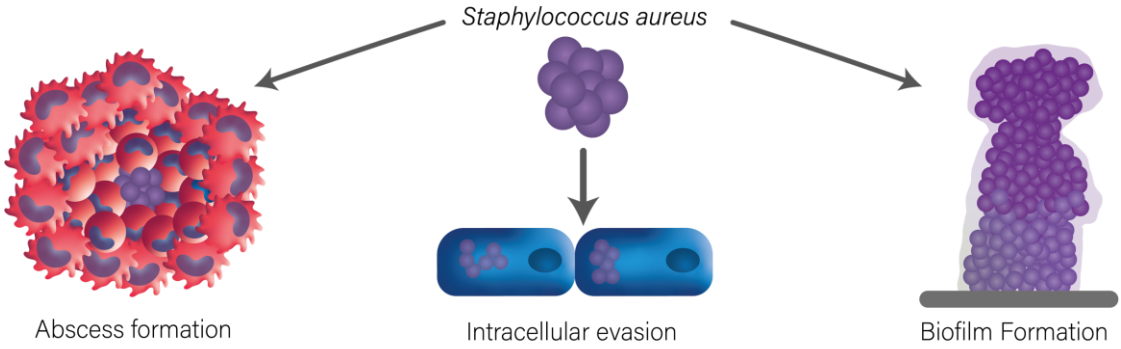

Figure 1.5: The several mechanisms of *S. aureus* immune evasion. A) abscess formation, here S. aureus utilises the host immune response to form a protective capsule with them at a core to persist and prevent phagocytosis via immune cells. B) Intracellular evasion tactics against immune cell phagocytosis or cellular invasion into neutrophils, macrophages and osteoblasts. C) Development of a complex biofilm on the surface of implants and necrotic tissue-protective by a matrix from desiccation and phagocytosis. Image adapted from Muthukrishnan et al. (2019).

1.5.2.1: Abscess Formation

Staphylococcus species can utilise abscess formation to their advantage to increase their pathogenicity; to invade and infect tissues and implants. An abscess is a dynamic mechanism that is regulated and controlled by both pathogens and the host. Here, the immune cells actively try to minimise and control the pathogen within the abscess by an influx of immune cells (reviewed in Muthukrishnan et al. 2019). *S. aureus*, however, can manipulate the influx of immune cells during an abscess development to their benefit as an inadvertent protective shield containing the bacteria safely within the centre (Masters et al. 2019). Within the centre surrounding the bacteria was a layer of necrotic neutrophils that were originally involved in phagocytose of the bacterial species, but ultimately failed to remove the pathogen (Ricciardi et al. 2018). These necrotic cells can also damage local cells and tissues (Ricciardi et al. 2018). Surrounding these necrotic cells are is a layer of viable neutrophils actively trying to, but ultimately failing to remove the pathogen and necrotic cells (Ricciardi et al. 2018). Within PJIs the presence of these cells and the development of abscesses can provide a link for the bacteria towards the implant and initiate the development of the bacterial biofilm.

1.5.2.2: Development of an *S. aureus* Related Biofilms

One of the most challenging aspects of treating PJIs is the ability of the microorganisms to develop sessile microbial communities called biofilms on the surface of the implant or the surrounding hard or connective tissue. The currently accepted definition of a biofilm is a sessile community of microbes attached to a surface that is embedded within an exo-polysaccharide matrix, known as the extracellular polymeric substance (EPS), that protects the microbes from the host responses and antibiotics (Garrett et al. 2008). These communities can develop some unique structures, such as pillar or mushroom-shaped constructs, along with intricate nutrient channels and development of these are dependent on the environment (Archer et al. 2011). The benefits of biofilms over free-swimming planktonic bacteria allow the bacterial community to withstand pH changes and nutrient deprivation, whilst also it provides protection against reactive oxygen species, biocides, desiccation, the host immune system and antimicrobial agents (Flemming and Wingender 2010; Petrova and Sauer 2012). As such, eradication of these biofilms is laborious often requiring surgical intervention.

Due to the complexity of these *S. aureus* biofilms, their formation occurs over many stages governed by different physical, chemical and biological processes. There are four generalised stages of biofilm formation: bacterial attachment, proliferation, maturation and detachment (Figure 1.6).

The first stage of developing a biofilm is the initial adhesion of the microbial species to the surface of the prosthesis or the surrounding necrotic connective tissue. When the implant is inserted within the patient, the implant surface is coated in ECM proteins, polysaccharides and other organic and inorganic particles which forms an absorptive layer also known as the conditioning layer (Davidson et al. 2019; Khoo et al. 2010). This provides the bacteria with a site for anchorage and nutrition to start the biofilm formation (Garrett et al. 2008; Petrova and Sauer 2012). Studies observing the bacterial attachment, using glass and plastic, have shown that this is a two-step process from initial reversible attachment to a more irreversible attachment after the bacterial species have been given time to the initial biofilm (Agladze et al. 2003; Mann et al. 2009; Merritt et al. 2007). However, for the bacteria,

getting to the implant surface or tissue surface to start forming the biofilm, is a complex and trying process. Multiple physical forces are used or combated by the bacteria to get to the surface for attachment, these include Brownian motion, hydrodynamic forces, van der Waals forces, hydrophobic interactions, electrostatic charges and gravitational forces (Katsikogianni and Missirlis 2004; Kostakioti et al. 2013).

S. aureus utilises MSCRAMMS amongst other cell-wall anchoring proteins to form complexes with the surface to shift it from reversible to irreversible attachment. Once irreversibly adhered the bacteria start forming microcolonies, which eventually matures and start forming into mushroom or tower-like structures whilst simultaneously producing EPS, containing DNA, polysaccharides and a variety of other proteins vital for survival (Garrett et al. 2008; Hoiby et al. 2010; 2011; McConoughey et al. 2014 The EPS allows the planktonic bacteria to develop a completely different lifestyle; the matrix immobilises the bacterial cells within proximity to each other, forming cell-cell interactions termed a synergist microcolony (Flemming and Wingender 2010). The EPS provides protection from the host immune system, whilst allowing resistance against antimicrobial agents and protects the biofilm against desiccation. This is a particularly important aspect due to microorganisms experience high levels of water stress (Flemming et al. 2016; Morawietz et al. 2006). Protection from desiccation is achieved by retention of water within the EPS, by hydrated polymers whilst a top of the matrix slightly hardens forming a barrier against evaporation (Flemming et al. 2016). The EPS can capture nutrients, gases and molecules from the substratum (the area that the biofilm has grown on) or the local environment (Flemming et al. 2016). Once matured, parts of the biofilm are detached allowing the bacterial species to disperse into the host's localised environment for further colonisation and infection. This aspect is vital for bacterial survival, the transmission of disease and biological dispersal (Kaplan 2010).

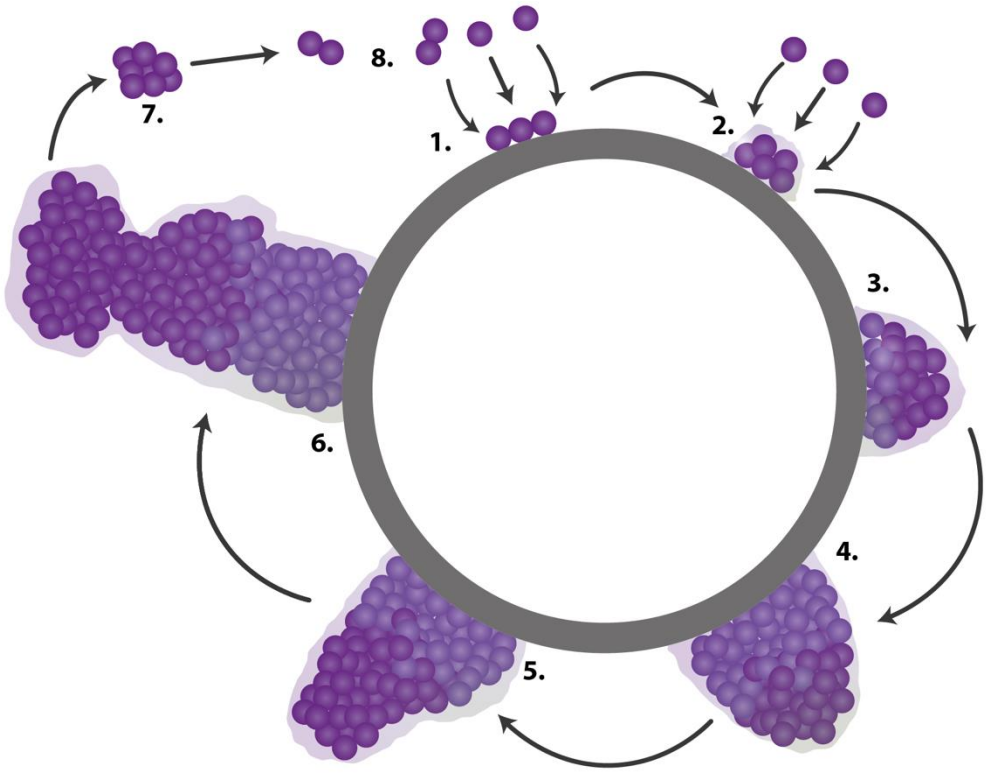

Figure 1.6: Development of an *S. aureus* biofilm. 1) The initial adhesion of planktonic *S. aureus* species, that binds and anchor themselves to the conditioning layer on the surface of the implant or tissue. 2) Once the bacteria have bound and are irreversibly attached, they start forming microcolonies, whilst simultaneously producing EPS containing DNA, polysaccharides and a variety of other proteins vital for survival. The microcolony allows additional binding sites of planktonic bacterial species and thus allow maturation of the microcolony. 3, 4 & 5) The microcolony undergoes proliferation, aided by surrounding EPS which protects the microcolonies, from desiccation, whilst simultaneously capturing nutrients, gases and molecules within the microenvironment, vital for the bacterial species survival and maturation of the biofilm. 6) Mature biofilms can be formed as pillar or mushroom-shaped constructs, along with intricate nutrient channels. 7 & 8) Following maturation, parts of the biofilm are detached allowing the bacterial species to disperse planktonically into the host's localised environment for further colonisation and infection. Image adapted from (Hoiby et al. 2011) and Moormeier and Bayles (2017).

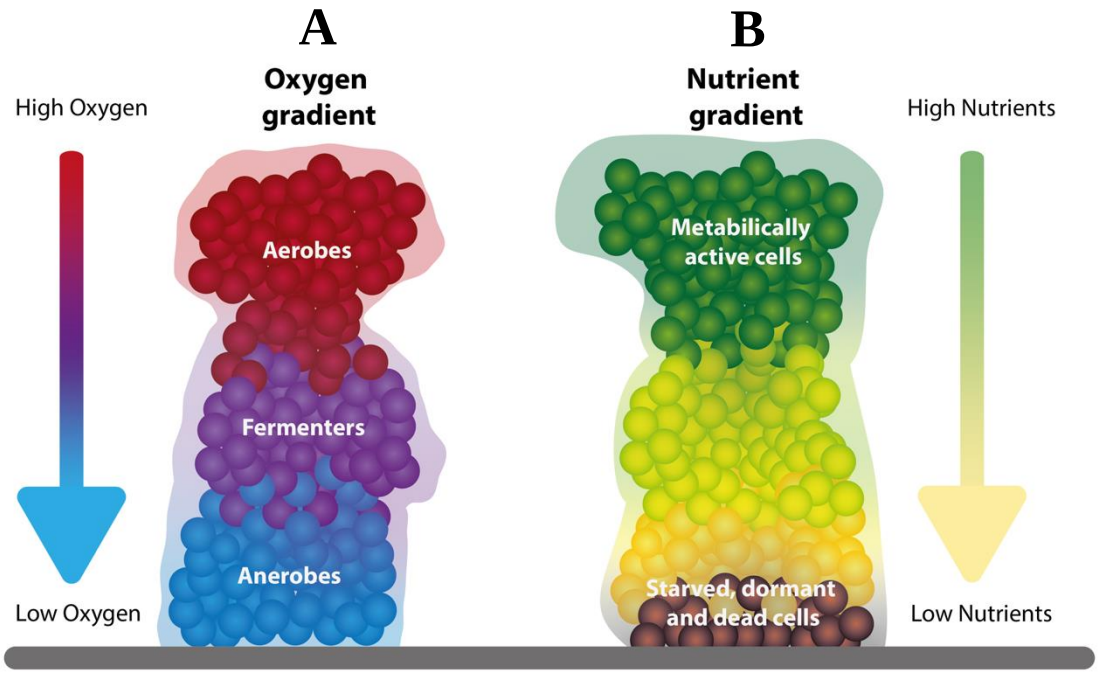

Figure 1.7: Oxygen and nutrient gradients within *S aureus* biofilms. Within a mature biofilm, there is a complex nutrient and oxygen gradient that gives rise to heterogeneous populations of *S. aureus*. A) Oxygen gradients are formed when the *S. aureus* species in the top layer of the biofilm are actively respiring, thus reducing the oxygen concentration, which alters the phenotype of microorganisms towards facultative anaerobic species deeper within the biofilm. B) Nutrient gradients are formed when the top layer of bacterial species within the biofilm actively consume the majority of the nutrients, required for metabolism. As the nutrients are depleted the bacterial cells towards the substratum are starved resulting in them undergoing growth inhibition, become dormant or undergo cell death. Figure adapted from Flemming et al. (2016).

Due to the complexity of the environment within a biofilm, the nutrient, chemical and physiological conditions throughout the biofilm are not consistent. As such, heterogeneity is observed and this is seen regardless of the biofilm is monomicrobial or polymicrobial. Heterogeneity can present itself as chemical, structural or biological gradients, altering and changing the phenotype of bacterial species throughout a single biofilm that would not be seen to the same extent in planktonic species (Stewart and Franklin 2008).

Oxygen is the most studied gradient within biofilms and the amount of oxygen typically differs for different species biofilms. However, typically as oxygen passes through the biofilm, it gradually depletes due to bacterial cells in the top layer actively respiring reducing

the oxygen concentration, this alters the phenotype of microorganisms to facultative anaerobic species the deeper within the biofilm (Figure 1.7A; Stewart and Franklin 2008). This variation and the effects caused by oxygen concentrations have been seen in *S. aureus* biofilms. *Staphylococcus aureus* are gram-positive facultative anaerobes in the presence of oxygen. These types of bacteria will grow aerobically, however, in the absence of oxygen, they will grow fermentatively (Ribeiro et al. 2012; Stewart and Franklin 2008). Becker et al. (2001) showed *S. aureus* biofilms upregulated different genes encoding for fermentation or glycolysis, possibly due to the amount of oxygen present throughout the biofilm. Similarly, nutrient gradients also have effects on the biofilm, especially within aerobic oligotrophic biofilms. Here, nutrients are consumed by microorganisms on the upper surface of the biofilm and gradually is reduced through the biofilm, this causes cells towards the substratum to be starved, resulting in them undergoing growth inhibition, dormant status or cell death (Figure 1.7B; Flemming et al. 2016).

Quorum sensing (QS) or bacterial cell-to-cell signalling allows bacteria to regulate their biofilm communities to their environment, their cell population densities and provide changes to their spatial arrangement, aid in bacterial attachment and dispersal (Bodelon et al. 2016; Donlan 2002). QS and their regulated genes allow bacteria to undergo a variety of processes, including bioluminescence, antibiotic production, controlling virulence factor secretions, cell differentiation, stress tolerance, biofilm production and competence (Bassler and Losick 2006; Bodelon et al. 2016). Bacterial can control these variables via production, secretion and detection of small extracellular signalling molecules, also called autoinducers (Papenfort and Bassler 2016). As the population increases, so do the production of autoinducers. When a certain concentration threshold is reached, the bacteria start to detect the autoinducers and start altering their population and gene expression (Bassler and Losick 2006).

1.5.2.3: Bacterial Evasion of Immune Cells

Blood circulating neutrophils are released from circulation and are attracted towards the pathogen via chemotaxis. *S. aureus* can interfere with this neutrophil chemotaxis through the secretion of phenol-soluble modulins (PSMs), chemotaxis inhibitory proteins of *S.*

aureus, formyl peptide receptors-like 1 inhibitor and its homologue formyl peptide receptors-like 1 inhibitor-like; and superantigen-like proteins (SSLs; reviewed in Thammavongsa et al. 2015). These PSM can interfere with the biological functions of a variety of neutrophils and can stimulate cytokines by neutrophils through activation of formyl peptide receptor-2 on the cell surface (Thammavongsa et al. 2015). CHIPS bind to specifically human formyl peptide receptor-1 and C5a receptors on human neutrophils (de Haas et al. 2004; Postma et al. 2004). These complement proteins are vital in the innate immune response and the bacteria can interfere with these to prevent the activation and subsequent downstream cascade initiate by the pathway. The *Staphylococcus* complement inhibitor (SCIN) inhibits C3 convertase and its subsequent cleavage of the complement C3 protein into C3a and C3b, which can be used as opsonisation markers or chemoattractants for phagocytes (Gros et al. 2008). The formyl peptide receptors-like 1 inhibitor and its homologue blocks both formyl peptide receptor-1 and formyl peptide receptor-2 (Prat et al. 2009; Thammavongsa et al. 2015). The SSLs are secretory proteins with a similarity to the *Staphylococcus* superantigens. *In vitro* studies have shown that SSL5 interfere with the binding of neutrophils on P-selectin and the P-selectin glycoprotein ligand-1, which affect the cells' adhesion and rolling capabilities (Bestebroer et al. 2007). SSL5 can also affect the activation of neutrophils by binding to the glycosylated N-termini of the g protein-coupled receptors required for chemokine and anaphylatoxin-mediated activation (Thammavongsa et al. 2015). SSL3 binds to toll-like receptor 2 on macrophages and inhibits TNFα and prevents these cells from recognising the bacteria (Yokoyama et al. 2012).

1.5.2.4: Bacterial Evasion of Phagocytosis and Intracellular Survival

S. aureus bacteria can also survive and escape the phagocytosis process by blocking lysozyme or peptide binding to surface envelope via lysis- or alanyl-phosphatidylglycerol synthesis, peptidoglycan acetylation and D-alaylation of teichoic acids. They can survive the bactericidal compounds via staphyloxanthin (Thammavongsa et al. 2015). Alkyl hydroperoxide reductase can provide bacteria protection from hydrogen peroxide, whilst flavohemoglobin can detoxify nitric oxide (Cosgrove et al. 2007; Richardson et al. 2008). The bacteria can also induce cell lysis using leukocidins via β-barrel pore-forming toxins (β-PFT), which are soluble monomers which when bound to cell surface receptors develop into pore structures that pierce the lipid-bilayer (Heuck et al. 2001). HLgAB γ-haemolysis is one such

leukocidin that can bind to the chemokine receptors: CCR2, CXCR1 and CXCR2 and induce lysis in human red blood cells, neutrophils, monocytes and macrophages (Malachowa and DeLeo 2011; Spaan et al. 2014). Leukocidins ED has been shown to induce lysis in DCs, T-lymphocytes and macrophages, as it binds to the chemokine receptors CCR5, CXCR1 and CXCR2 (Alonzo et al. 2013; Reyes-Robles et al. 2013). Macrophages derived from human monocytes and infected with *S. aureus* were able to survive phagocytosis and resided within vacuoles, with no signs of apoptosis or necrosis for up to 72 h after which they lysed the cell and escaped (Kubica et al. 2008). *S. aureus* that lack key surface cell wall adhesins such as α-toxins and protein A were killed by macrophage phagocytosis (Kubica et al. 2008).

S. aureus can also evade the immune response by residing intracellularly within immune and bone marrow cells as 'Trojan horses'. *In vitro* and *in vivo* assessment showed that *S. aureus* was able to reside within PMN. This survival is possibly achieved by the bacteria's ability to residing within PMN vacuoles-like macropinosomes and by limiting PMN towards the infection site aided in host defence, whereas increasing PMN in infection sites decreased the mice survival and increased pathogenicity (Gresham et al. 2000). Studies have shown that *S. aureus* is also able to internalise within osteoblasts and osteocytes *in vivo* within an osteomyelitis patient (Bosse et al. 2005). Osteocytes have also been seen to actively internalise bacteria, where Yang et al. (2018a) has shown that *in vitro* analysis of osteoblastic differentiated human osteocytes with internalised *S. aureus* had been highly active compared to their uninfected counterparts, along with internal SVC development, indicating the bacteria's move towards a more quiescent state. The same study showed that *ex vivo* patient derived cancellous bone samples that were infected with *S. aureus* also induced osteocyte intracellular internalisation. These internalised bacterial species were surrounding by an EPS-glycocalyx and has been seen within other studies observing the same phenomenon within chick calvaria and tibial osteoblasts (Reilly et al. 2000). This provides a protective barrier around the bacteria utilising this EPS-glycocalyx matrix, from both antibiotics, immune cells and provides attachments to the mineral bone and implants for biofilm production (Bosse et al. 2005). Bacterial species that have been internalised within osteoblasts can also alter their function by increasing the production of IL-6 and IL-1β used for osteoclastogenesis (Bost et al. 1999; Marriott et al. 2002). Theories suggest that the SCV seen by Yang et al. (2018a), is a form of *S. aureus* phenotype switching within

internalised cells to remain dormant evading the immune cell response, whilst it forms a large colony of SCV to enable increase success in dissemination and reinfection (Garzoni and Kelley 2011; Tuchscherr et al. 2011).

1.6: Preclinical *In Vitro, In Vivo* and *Ex Vivo* Models for Prosthetic Joint Infections

Majority of the research that has been undertaken to understand the process of PJI and osteomyelitis is via the use of laboratory-based models, in conjunction with patient-derived data. Understanding the process that leads to bacterial-induced bone destruction is multifaceted so having model systems that can in some part replicate whole or parts of the infection process on cells and tissues of the bone can in some way could provide answers of the disease progression and be able to develop novel strategies to counteract and resolve the infection. To develop a new model system it is vital to understand the strengths and limitations of previous models and these can include knowledge gained from either *in vitro*, *in vivo* and *ex vivo* model systems. Indeed in considering the strengths and limitations of any model system there two simple aphorisms: "humans are definitely no 70kg mice" (Leist and Hartung 2013) and "all models are wrong, but some are useful" as stated by George Box (Box 1976).

1.6.1: *In Vitro* Models

In vitro models are very simplistic, they are meant to represent the multicellular bone marrow complex using a single or a combination of two cells within a culture system. The benefit of these models is that they can be cultured within an environment that can be manipulated to achieve and model different cellular responses. *In vitro* cultures using both primary and cell lines have been invaluable in understanding osteoclast development, osteoblast mineral production, MSC signal pathways, immune cell response to bacterial induce products and a variety of bone marrow cell responses to *S. aureus,* as previously described. However, these models do not consider the complex cellular interactions or the spatial arrangement of different cells within cell niches that are seen *in situ*.

In more recent years, to address these limitations, novel 3D *in vitro* culture techniques have been developed, to enable unique *in vivo* like cell-cell interactions and spatial arrangements between one or two cell types within a specialised support matrix and the information gained from these models has been invaluable and has shed light on a variety of process involved in bone repair. Vazquez et al. (2014), showed that it is possible to form *in vitro* co-cultures of osteocytes MLO-Y4 cell lines embedded deep within a Type I collagen gel and osteoblast MC3T3-E1(14) or MG63 cell lines layered on near the surface of the gel, to replicate the cortical and endosteum later of bone. These cells were viable after 7 days, displayed *in vivo* phenotypes and were bioactive; able to induce transcriptions for pro-mineralisation related genes for osteocalcin, RunX2, type I collagen and alkaline phosphatase activity during culture. When subjected to mechanical load osteocytes increased prostaglandin E2 gene expression and when stimulated with BMP-2 MG63 cells increased Type I collagen gene expression. This study demonstrated that two different cell types from two completely different species can co-exist and respond to cellular, mechanical and chemical cues bio-actively as they would *in situ*.

Spheroid 3D *in vitro* co-cultures, have been able to show unique interactions between MSCs and endothelial cells. Co-cultures of umbilical vein endothelial cells with human bone marrow MSCs, have shown that endothelial cells regulate MSCs towards an osteogenic linage by elevating Wnt and BMP signalling (Saleh et al. 2011). Specific signalling pathways linked to angiogenesis and endothelial cell migration could be inhibited, with platelet-derived growth factors specifically found to have a profound effect on developing uncoordinated endothelial cells vascular network organisation and cellular migration (Marshall et al. 2018). Marshall et al. (2018) utilised spheroid cultures of pre-differentiated MSCs directed towards chondrogenic and osteogenic linages and co-culture both linages together with endothelial cells. The presence of the endothelial cells affected the distribution of osteogenic and chondrogenic cells. Spheroids with just osteogenic and chondrogenic cells showed similar morphology found in high cartilage areas of bone, with a lateral separation of the two cells. However, when both linages are combined with endothelial cells the morphology changed to induce a central core region containing a mixture of all cell types with an outer region composed of mainly osteogenic cells. Therefore, these studies highlight the importance of cell culture within a 3D environment as

the cell responses vastly change compared to their standard 2D counterparts. Such models are limited and cannot sustain the large variety of cells typically found in the bone marrow and they cannot replicate the variety of interactions between the multitude of cells or to the ECM.

1.6.2: *In Vivo* Models

I*n vivo* models have their advantages over *in vitro* cell culture models in that they can have a multitude of cells, with the complex cell-to-cell and cell-ECM interactions intact but are subject to the host systemic influences that can manipulate results. Such *in vivo* models can utilise a variety of animal species and specifically for bone infections studies have used a variety of mammals including dogs, rodents and rabbits though there has been no universally standard reference model developed for PJIs (Bernthal et al. 2010; Craig et al. 2005; de Mesy Bentley et al. 2017; Petty et al. 1985; Pribaz et al. 2012). Through these *in vivo* studies our understanding of PJI and osteomyelitis has expanded, such as understanding that *S. aureus* is capable of *in vivo* cell internalisation of osteoblasts, osteocytes and leukocytes (Bosse et al. 2005; Tuchscherr et al. 2011), or the understanding that these bacteria utilise the canalicular network of the cortical bone (de Mesy Bentley et al. 2017). Such models require large numbers of animals with often one animal representing one experiment, in the case of (de Mesy Bentley et al. 2017) a total of 30 mice were used, 10 per experiment. In a study by Craig et al. (2005) where rabbits were used to develop a knee model used to study the influences of biomaterial infections, 42 different knees were used with each knee representing one experiment. This clearly shows that the number of animals used within these studies is expansive and as such, there is an ethical implication on such studies. Recently, *in vivo* live bioluminescence imaging has been used to investigate bacterial infections associated with the implantation of a variety of biomaterials, in 12-week old male C57BL/6 wild-type mice or in mice that were deficient in IL-1β or Toll-like receptor-2, both of which are vital in the immune response (Bernthal et al. 2011; Bernthal et al. 2010). The model utilised bioluminescent *S. aureus* which was accurately used to replicate bacterial burden in real-time as the pathogen spread. This model has the potential to follow the spread of infection within a live animal without euthanising a large number of animals; although strict regulations on the handling of animals along with systemic influences or

changes in physiological responses due to fear or fright during experimental procedures can have a profound effect on the data obtained (Abubakar et al. 2016; Smith et al. 2010; Stavrakis et al. 2013).

1.6.3: *Ex Vivo* Models

Ex vivo models can provide some of the benefits seen in both *in vivo* and *in vitro* models. They can preserve the cellular diversity within the skeletal system encased within a natural ECM which are found within *in vivo* models. They also allow direct access to the tissue so the cells can be controlled and manipulated during culture with reagents and other cells, a benefit of *in vitro* models. This enables researchers to manipulate and control these models by either analysing key biological, cellular, or mechanical factors that can be assessed independently within a 3D space (Abubakar et al. 2016; Cramer et al. 2021; Sloan et al. 2013; Takai et al. 2004). Thus, the *ex vivo* model bridges strengths brought from both *in vitro* and *in vivo* models whilst also answering the ethical parameters laid out by the NC3Rs program (Prescott and Lidster 2017). This program was developed to reduce, reuse and refine the number of animals used in medical experiments (Prescott and Lidster 2017). *In vivo* models utilise vast numbers of animal hosts for experimental repeats whilst *ex vivo* models significantly reduces the number of animals by utilising multiple experiments to be carried out from tissues from a single animal independently from each other (Roberts et al. 2013). As shown in Figure 1.8 there have been a variety of *ex vivo* models developed that include: long bone models, limb bone models, calvaria models, femoral head models, organotypic slice models and bone core models (Chagin et al. 2010; Curtin et al. 2012; Ehnert et al. 2020; Madsen et al. 2011; Marino et al. 2016; Mohammad et al. 2008; Ohshiba et al. 2003; Smith et al. 2014a; Smith et al. 2014b; Smith et al. 2010; Srinivasaiah et al. 2019; Swarup et al. 2018). These *ex vivo* models have been designed for the analysis of understanding the events that cause conditions such as: periodontitis, inflammatory bone destruction and osteoarthritis, (Madsen et al. 2011; Roberts et al. 2013; Sloan et al. 2013) or the analysis of key skeletal events such as understanding the mechanisms of skeletal development, growth, matrix turnover, endochondral ossification, dentinogenesis and elucidating the effects of mechanical loading (el Haj et al. 1990; Houston et al. 2016; Kanczler et al. 2012; Kluter et al.

2020; Madsen et al. 2011; Mohammad et al. 2008; Sloan et al. 1998; Smith et al. 2014a; Smith et al. 2014b; Srinivasaiah et al. 2019).

In the case of investigating the interaction of the bone marrow microenvironment with the mineral tissue in orthopaedic infections, no satisfactory *ex vivo* model exists. The majority of *ex vivo* bone models either remove or retain very little bone marrow. As such, *ex vivo* bone models tend to overlook the importance of the bone marrow cell populations on key bone events such as bone formation or resorption, focusing instead on the mineral tissue and the cells found on or within the mineral surface including; osteocytes, osteoblasts, lining cells and osteoclasts. These models do not consider the impact and role that local immune cell populations or specialised cellular niches play in orthopaedic conditions, and for a model to be suitable for implant orthopaedic infections certain key parameters must be in place. Firstly, the bone marrow must be retained, to ensure that the local immune cell populations that play key roles in initiating or resolving inflammation and play key roles in PJI are present. Secondly, the model must provide multiple samples from one whole tissue, thereby limiting the number of animals used. Thirdly, the model should be physiologically relevant to hip and knee implant-associated infections, therefore a model should utilise either the femur or the tibia. Finally, the model should have easy access to the bone marrow cavity to allow for easy nutrient and growth factor delivery and provide ease of infecting the bone marrow space.

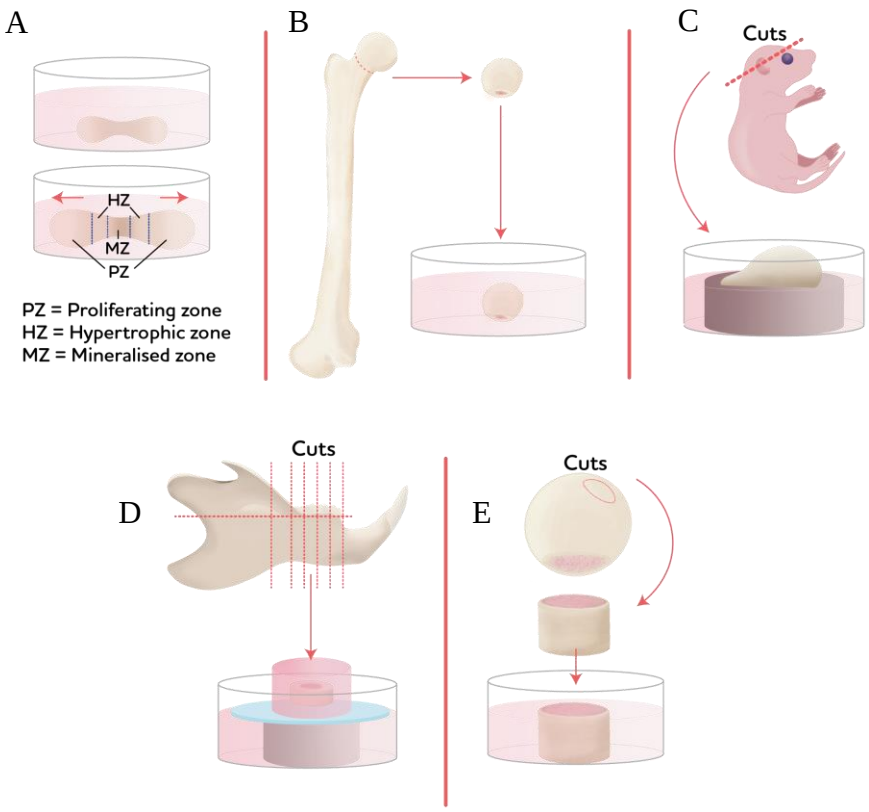

Figure 1.8: Current *ex vivo* bone models. A) Long bone and limb cultures, B) Femoral head models, C) Calvarial models, D) slice models and E) Bone core models. Image adapted and created from information provided from Ehnert et al. (2020), utilising models originally published by Chagin et al. (2010); Curtin et al. (2012); Ehnert et al. (2020); Madsen et al. (2011); Marino et al. (2016); Mohammad et al. (2008); Ohshiba et al. (2003); Roberts et al. (2013); Sloan et al. (1998); Sloan et al. (2013); Smith et al. (2014a); Smith et al. (2014b); Smith et al. (2010); Srinivasaiah et al. (2019); Swarup et al. (2018).

1.6.3.1: Long bone/ limb cultures

The use of long bone and limb cultures have been developed to observe key cellular events during early bone development, including the role and behaviour of stem cells, linear bone growth, chondrogenesis, hypertrophic ossification, endochondral ossification and ECM mineralisation (Figure 1.8A; Chagin et al. 2010; Kanczler et al. 2012; Smith et al. 2014a,b; Houston et al. 2016; Abubakar et al. 2019). This method of culturing was suggested by Thesingh and Burger (1983), where metatarsals from immature 12-17-day-old Swiss albino mouse embryos, specifically the three middle metatarsals of the feet, were removed and cultured and was used in understanding the process of endochondral ossification and bone growth. This model has since been translated to long bones of chick embryos (Garbieri et al. 2021; Kanczler et al. 2012; Smith et al. 2014a; Smith et al. 2014b) and mice (Houston et al. 2016; Kunimoto et al. 2016). The main advantage of these cultures is that the whole bone organ is explanted and cultured within a controlled and manipulated environment. This provides the total cellular diversity, extracellular structures and niche to be retained, as they would *in situ*. These models can also be manipulated further with the addition of hydrogel scaffolds inserted within the bone shaft itself, as a hydrogel spacer and to support skeletal growth from the bone and within the hydrogel. These hydrogel scaffolds can be loaded with growth factors such as VEGF, BMP-2 and TGF-β3 and cells such as Stro-1 enriched human BMSCs (Smith et al. 2014a; Smith et al. 2014b). By controlling the release of growth factors with or without cells, in-depth analysis can be made on BMSC multilineage differentiation within the local bone marrow environment. The addition of BMP-2 highlighted increase mineralisation into the hydrogel scaffolds indicated by extensive deposition of collagen fibrils and osteoid matrix, whereas VEGF increases migration of cells into the gels and hydrogels with BMSCs and TGF-β3 increased the proliferation of chondrocytes-like cells (Smith et al. 2014a; Smith et al. 2014b).

These long bone and limb models and the ability to manipulate them with external treatments can provide insights into rare conditions, that are difficult to model effectively. These models have been used to model catch-up growth that occurs in children after exposure to glucocorticoid steroids. Here, the growth velocity rises exponentially following the termination of steroid treatment, thereby giving a mismatch of bone size between the target aimed size and the actual size due to steroids ability to enhance the proliferation

capacity of chondrocytes (Chagin et al. 2010). External treatments of dexamethasone on metatarsals showed inhibition of bone growth via chondrocyte proliferation and differentiation, which was subsequently initiated once treatment was terminated thus, modelling the effects of the catch-up growth phenomenon (Chagin et al. 2010).

The use of immature animal derived neonatal and embryonic tissues has advantages since they can be cultured long term, which can range from as little as 72 h (Houston et al. 2016) to several months (Chagin et al. 2010). The use of such models, though extensive in their culture period, have issues in that immature and developing bone lack complete mineralisation of the tissue and maturation of immune cells make such studies unsuitable and unrepresentative for most clinical studies. This is especially the case for modelling osteomyelitis, which is associated with mature bones rather than developmental bones, thus, making this model unsuitable despite its advantages.

1.6.3.2: Femoral head

Femoral head models, as the name suggests, utilises extracted femoral heads that can be cultured within culture media for several hours to weeks (Figure 1.8B; Madsen et al. 2011; Swarup et al. 2018). Similar to long bone and limb models, external supplementation of cytokines can be used to model osteoarthritis cartilage degradation, by simulating catabolic or anabolic conditions, allowing analysis of loss or formation of collagen in a controlled environment (Madsen et al. 2011). These femoral heads can be obtained from mice (Madsen et al. 2011) or from discarded bovine samples sourced from abattoirs or human patient samples following total hip replacement (Swarup et al. 2018). The use of human tissues provides a more representative model to the clinical situation. The culture of the femoral heads can either be simple by submerging the tissue within culture media (Madsen et al. 2011), or complex within an enclosed perfusion bioreactor with media supplied through the vasculature (Swarup et al. 2018). In human femoral heads, cell viability following perfusion was increased compared to non-perfused tissue when viability was analysed using a live/dead Hoechst and Calcein stain. By utilising the tissues natural vascular system of the femoral head to distribute nutrients to the cells deep within the model has advantages in that no further modification needs to be done to the model to supply cells with nutrients. However, a limitation of this model was short term culture period, which

was restricted to 12 h – 24 h (Swarup et al. 2018). This is possibly due to fact that the femoral head is a highly cartilage rich tissue and have very little natural vasculature, which limits the distribution of nutrients to the whole tissue, therefore limiting the potential of utilising this model for understanding osteomyelitis or PJIs. Typically, during total hip or knee replacement surgeries, these sites of high cartilage on the femur, such as the femoral head or the lateral and medial condyles are removed, thus limiting their use as a PJI model.

1.6.3.3: Calvaria models

Rodent neonatal calvaria has also be used to assess bone metabolism, development and repair (Figure 1.8C). These models can also be influenced by externally supplementing the culture media with various treatments including parathyroid hormone, dexamethasone, BMPs, endothelin-1, dickkopf-1, statins and proteasome inhibitors, to observe the effects on bone formation (Bringhurst and Potts 1981; Clines et al. 2007; Garrett et al. 2003; Mohammad et al. 2008; Mundy et al. 1999; Yin et al. 2003). An additional benefit of calvarial models is that studies have utilised them as a co-culture model by addition of cancer cells to model bone metastasis and its role in osteolysis. Co-cultures can include human breast cancer (MCF-7 or MDA-MB-231) or prostate tumour cell lines (LnCap clone FGC or PC-3; Ohshiba et al. 2003; Curtin et al. 2012) . These studies highlight that the presence of the cancer cell lines significantly increased cyclooxygenases-2 induced prostaglandin E2 synthesis and RANKL in osteoblasts thus increasing subsequent osteoclastic bone resorption by significant increased osteoclastic numbers. The ability to introduce externally sourced cells and model their effects to induce osteolysis is a clear strength of this model. In the case of modelling bacterial-induced osteolysis/osteomyelitis, the reduced size of bone marrow space in the calvaria, which is extensive in long bones, reduces the ability to model the pro-and anti-inflammatory immune cell response on inducing osteolysis against the presence of the bacteria.

1.6.3.4: *Ex vivo* slice models

The examples above all use whole tissue samples and thus the number of samples available from each animal is limited. To overcome this, the use organotypic slice models (Figure 1.8D) can be utilised. These models utilise slices of whole tissues, that can be cultured independently from each other under different experimental conditions, thereby extending

the use of the original tissue into multiple experiments. Tissue slices can be as as thin as 300 µm (Srinivasaiah et al. 2019) to several mm thick (Roberts et al. 2013; Sloan et al. 1998; Sloan and Smith 1999; Sloan et al. 2013; Smith et al. 2010). Rodent tissues has been utilised from the femur (Srinivasaiah et al. 2019), the mandible (Smith et al. 2010) and tooth (Roberts et al. 2013; Sloan et al. 1998; Sloan and Smith 1999). Femur slices from 4-day old postnatal Sprague-Dawley rats have been used to investigate cellular transitions of osteogenic and chondrogenic cells performing endochondral ossification, whilst being viable in culture for up to 15-22 days (Srinivasaiah et al. 2019). This model did have extensive bone marrow following sectioning at 0 days, however by 15 – 22 days in culture there was a significant lack of cells in the bone marrow cavity with large portions of the bone marrow fragmented and missing. However, this bone marrow cavity was not extensively analysed for the presence or maintenance of the various immune cells which play an active role in the bone remodelling process (Srinivasaiah et al. 2019).

The tooth slice model utilised incisor tissue slices from 28-day-old Wistar rats which were embedded within a semi-solid agar termed Trowell-type cultures, suspended at a liquid/air interphase for up to 7 to 14 days (Sloan et al. 1998; Sloan and Smith 1999). Here the authors observed preservation of the tooth architecture with an intact dentine-pulp complex along with analysis of active odontoblast secreted ECM. This model has continued to investigate TGFβ stimulation of odontoblasts (Sloan and Smith 1999), pulp responses to the presence of dental materials (Murray et al. 2000), the pulp response to heat and light-curing of dental materials (Lynch et al. 2018), pulpal infection by *Streptococcus anginosus* or *Enterococcus faecalis* (Nishio Ayre et al. 2018). This model has been adapted using human teeth and has been utilised in observing the effects of TGF-β1 response in the dental-pulp complex and surrounding cells (Dobie et al. 2002; Farges et al. 2003; Melin et al. 2000).

The mandible slice model has also been used to investigate the processes involved in periodontal inflammation and associated bone destruction (Sloan et al. 2013; Smith et al. 2010). This model similarly utilises the Trowell-type culture system and allows the culture of tissues for up to 21 days with good viability and architecture of the surrounding tissues and cells, along with maintenance of bone matrix proteins and observations of osteoclasts (Sloan et al. 2013; Smith et al. 2010). This model has been adapted to induce a pro-

inflammatory condition following supplementation with bacterial lipopolysaccharide, with observations on periodontal ligament immune cell populations and osteoclast numbers along with secretions of pro-inflammatory cytokines (Sloan et al. 2013). The mandible slice model has also shown that the addition of supplements such as TNFα, M-CSF and RANKL stimulated or maintained numbers of resident immune cells such as monocytes, macrophages and neutrophils, along with osteoclasts after culture within the periodontal ligament (Sloan et al. 2013). The model was further adapted to include the microinjection of dental pulp progenitor cells into the mandible using a microneedle. The study showed that these cells were viable, proliferated after culture and migrated to interact with the dentine, resulting in morphological changes (Colombo et al. 2015).

1.6.3.5: Bone shaft and bone core models

Bone shaft and bone core models (Figure 1.8E) have proved useful to explore the impact of mechanical loading. Bones experience a variety of different mechanical stimuli at variable intensities that can alter the response of the local bone microenvironment such as perfusion and compression strains (Cramer et al. 2021). To model, the impact of these stains on the local mechanosensory osteocyte cells and the effects on mineralisation and resorption, bone shaft and bone core models have been utilised. Bone shaft models tend to use small animals such as chicks and rats (Cheng et al. 1994; Dallas et al. 1993; Davidson et al. 2012; Lozupone et al. 1996; Rawlinson et al. 1995). Bone core models tend to utilise bone samples from larger animal species such as bovine, ovine, porcine, rabbit and canine and have also been used from human tissues (Birmingham et al. 2016; Chan et al. 2009; Davies et al. 2006; el Haj et al. 1990; Elson et al. 2015; Endres et al. 2009; Hao et al. 2013; Kluter et al. 2020; Mann et al. 2006; Meyer et al. 2016; Rawlinson et al. 1991; Richards et al. 2007; Rupin et al. 2010; Schnieders et al. 2013; Simpson et al. 2009; Takai et al. 2004; Vivanco et al. 2013).

Individual perfusion systems have been deployed to generate a load on the local bone cell microenvironment via fluid flow using a peristaltic pump to circulate tissue culture media through the tissue. This provides cells deep within the bone tissue with nutrients, waste removal and shear stress, thus reducing the risk of nutrient deficiency and waste build-up (Cramer et al. 2021; Davidson et al. 2012). The use of perfusions system alone has been demonstrated to significantly improve osteocyte numbers and viability in Sprague–Dawley

rat femoral shafts and bone cores from 3-month-old calves for up to 2 weeks in culture, when compared to static cultures (Chan et al. 2009; Davidson et al. 2012). Typically, the use of modelling osteocyte mechanosensory responses to load, requires removal of the local bone marrow microenvironment, leaving behind or artificially seeding extracted osteoblasts to observe the direct interaction on the osteocytes or the mineralisation and osteoid formation by osteoblasts lining the cortical bone (Chan et al. 2009). Similarly, observation of the interaction of osteoblasts osteoid formation and osteocyte signalling without the bone marrow microenvironment have been utilised in hydrostatic pressure models by Takai et al. (2004) and perfusion and compression models by Rawlinson et al. (1991). The trabecular bovine metatarsal bone core model by Takai et al. (2004) also showed improved osteocyte viability and increased osteoid deposition following loading over 22 days of culture. When utilising a combination of perfusion and compression stimulus on trabecular canine bone cores there was an increase in prostaglandin E2 and prostacyclin response from osteocytes and osteoblast cells within the cortical bone (Rawlinson et al. 1991). Comparable results were shown in rat ulna bone shaft models, which were stimulated using high-load dynamic strains, resulting in increased prostaglandin E2, prostaglandin I2 and glucose 6-phosphate dehydrogenase from cortical bone osteocytes and osteoblast cells (Cheng et al. 1994; Rawlinson et al. 1991; Rawlinson et al. 1995). The upregulation of prostaglandin E2 following loading has been shown to induce bone mineralisation within *ex vivo* models along with increased calcium deposition from *in vitro* rat marrow stromal cells that were seeded onto titanium mesh scaffolds and subjected to perfusion culture (Bancroft et al. 2002; Chan et al. 2009). Bone cores utilising the ZetOS^{TM} bioreactor, a culture system that houses a dynamic bioreactor with a peristaltic pump and tissue culture chamber, is used to induce physiological and mechanical loads and signals on bone samples for up to 28 days (David et al. 2008; Endres et al. 2009). The effect of this ZetOS^{TM} culture system on bone core models has shown improved osteocyte viability along with increased osteoid deposition, mineralisation and trabecular bone thickening when compared to unloaded samples from bovine or human bone samples (Endres et al. 2009; Mann et al. 2006; Richards et al. 2007; Schnieders et al. 2013). Osteoblast activity was also improved with this system with significant increases in Runx2 and osteocalcin expression along with an increase in alkaline phosphatase activity (David et al. 2008). There are very few studies regarding mechanical loading and bone resorption, currently only (David et al. 2008) has reported that mechanical

loading on bone cores showed no osteoclast resorption activity was enhanced by the ZetOS™ system. Since the majority of the implant-associated infections mainly occur in the femoral shaft, bone core models are not often a suitable substitute to model orthopaedic infections, simply because cores are often taken from joints such as the femoral head or lateral medial condyles which also contain trabecular bone along with cartilage, which are removed during TKA and THA and replaced with synthetic replacements (Elson et al. 2015; Hao et al. 2013; Marsh and Newman 2021). There are currently no studies utilising bone core models on the effects of bacterial infections on bone resorption or formation, with or without mechanical stimulus. The use of rodent femoral or tibial bone shaft models may be a suitable model to adapt for understanding hip and knee PJIs.

The lack of bone marrow in such studies above limits key interactions other bone marrow cells may play in inducing bone mineralisation or resorption. As such, maintaining the immune cell populations along with HSCs and BMSCs within their cellular niches whilst preserving the cellular heterogeneity of the bone marrow cavity, would allow researchers to model the effects of the BMU, immune cell populations and mechanical stimuli within a 3D environment. Trabecular bone cores cultures in a bioreactor that were stimulated with perfusion and low magnitude high-frequency vibrations, induced BMSCs osteogenesis when these cores were subjected to both vibrations and fluid shear stress when compared to fluid flow or static only controls (Birmingham et al. 2015). This shows the importance of retaining premature undifferentiated cells such as BMSCs found in the bone marrow cavity, rather than removing the bone marrow cavity and relying on the results obtained from mature differentiated cells such as osteoblasts and osteocytes, as key.

Overall, these models provide the potential in developing a novel *ex vivo* model that can be used to understand the processes involved within PJI and osteomyelitis infections. One challenge of most of these models has been the inability to culture and maintain the bone marrow for prolonged culture periods, and this is vital if we are to understand the interaction of the bone marrow microenvironment on the development of bacterial-induced osteolysis. The development of such a model can provide the reproducibility and manipulative environment seen within *in vitro* models whilst simultaneously provide the

multiple cell types seen within *in vivo* models, whilst also adhering to the NC3Rs ethos to reduce, refine and replace *in vivo* animal models where possible.

1.7: Aims and Objectives

Currently, there is no adequate model to investigate the mechanism leading to bacterial-induced osteolysis. The femur is considered more clinically representative for use as a *ex vivo* models as it is the site of the knee and hip implants and subsequent infections. Therefore, this Thesis aims to:

- Develop a novel *ex vivo* femur model and characterise the cell composition with the intention that it may be used to study mechanisms of infection, leading to implant-associated osteolysis.
- Investigate the cellular responses following supplementation of known pro-osteoclastogenic factors on the local immune cell population.
- Establish a co-culture with a known osteolytic species and assess bacterial attachment within the bone marrow cavity.
- Evaluate the inflammatory cellular response to the presence of the bacterial and their virulence factors following infection.

This Thesis would ultimately aim to establish an infection model to investigate the cellular responses by bacteria associated with PJI and osteolysis, such *Staphylococcus aureus* so that it can be used to develop antimicrobials. Furthermore, this model would have the potential to investigate cellular responses of other pro-inflammatory conditions that lead to localised bone destructions.

Chapter 2:
Development of an *Ex Vivo* Femoral Slice Model

2.1: Introduction

The interaction between the bone, the host immune response and bacteria in leading to pathological tissue destruction is poorly understood. As discussed within the General Introduction (Chapter 1), *Staphylococcus. aureus* (*S. aureus*) species have been identified as the main colonisers, where they can either bind to the implant (leading to septic osteolysis conditions) or form attachment directly to the bone and the bone marrow stroma (leading to osteomyelitis cases). If left untreated, bacteria grow and can develop into mature biofilms (Kavanagh et al. 2018b; Yang et al. 2018a). Once colonised, the bacteria can directly alter the bone remodelling unit, inhibiting osteoblast bone formation, increasing osteoclastogenesis and bone resorption (Cao et al. 2017; Ren et al. 2017a; Ren et al. 2017b; Trouillet-Assant et al. 2015). To understand the cellular and signalling details of this process, a model system is required that can replicate and explore these complex interactions with the bone marrow stroma and bacterial species.

In vitro studies have been used to study bacterial interaction within mammalian cells. As an example, Claro et al. (2011) and Widaa et al. (2012) looked at the effect of *Staphylococcus* protein A (SpA) on mouse clonal MC3T3-E1 pre osteoblastic cells lines. Newman wild type *S. aureus* species specifically expressing SpA were fixed in formalin and added to the cell lines; this was to ensure that the bacterial species do not compete with the cells over nutrients in the culture media. Both studies compared uninfected controls and Newman *S. aureus*-deficient in SpA, which showed a significant reduction in gene expression of collagen type I, osteopontin, osteonectin, osteocalcin and a reduction in mineralisation, as measured by calcium and alkaline phosphatase levels. Such *in vitro* models are valuable in understanding complex interactions and downstream signalling mechanisms in a environment that can be controlled, but they lack the spatial arrangement of native tissues. Adult stem cells are located *in vivo* within a specific niche, where stimulating factors determine their differentiation fate (Ferraro et al. 2010). In the case of bone marrow, haematopoietic stem cells (HSCs) are located near the sinusoidal blood vessels in a perivascular niche in contact with perivascular bone marrow mesenchymal stromal cells (MSCs) and sinusoidal endothelial cells (To et al. 2011). Using specific gene markers of *Ctnnal* (an a-catulin gene) and *Hoxb5* (coding homeobox b5), it is possible to specifically target the location of these HSCs, with over 80 % located near these vessels (Crane et al.

2017). There is also an endothelial HSC niche located near osteoblasts on the endosteal surface of the bone (Ferraro et al. 2010). These cells when nearby, allow maintenance of HSCs with cytokines including G-CSF, thrombopoietin, angiopoietin 1 and CXCL12 (Calvi and Link 2015). It has been proposed that these two niches have distinct roles, with the perivascular niche playing a more active role in renewing the hemopoietic cells, while the endosteal niches are quiescent, only becoming active when the need arises (Boulais and Frenette 2015; Ferraro et al. 2010). However, this observation has been disputed with evidence suggesting sinusoid HSCs also have quiescent populations (Acar et al. 2015). This specifically highlights that such *in vitro* cultures lose such key cellular behaviours found *in vivo* when such cells are isolated and cultured away from their natural environment. Besides, *in vitro* models are unable to develop a complex extracellular matrix (ECM), a dynamic scaffold secreted by cells for their adhesion, differentiation and proliferation, whilst forming structural support to tissues (Gentili and Cancedda 2009).

An alternative to *in vitro* models are *in vivo* models, which do have a defined ECM and contain these established cell niches and cells in their respective microenvironments. However, such models predominantly use mice and as outlined in a review by Mestas and Hughes (2004), mice do have variable differences in immunology compared to humans, with increased lymphocyte and reduce neutrophil percentages. This is important to consider, particularly during developing early infections models. Polymorphonuclear leukocytes, especially neutrophils and macrophages, are the main responders following infection. These cells, as mentioned previously, play key roles in phagocytosis, or NETosis, of bacterial species, dead cells and debris during acute inflammation. As such, the process of the innate immune response may differ in murine model systems, compared to human studies. Researchers must be careful in interpreting data from such *in vivo* animal models as their observed responses are not always directly translatable to human physiology and have additional systemic influences that may not be otherwise seen; skewing results. Although most *in vivo* models give information on cellular expressions, responses and behaviour *in situ,* this is lost during *in vitro* cultures and there is an increasing push to reduce *in vivo* models. The NC3Rs program was developed to reduce, reuse and refine the number of animals used in medical experiments (Prescott and Lidster 2017). Such *in vivo* models use a

single animal per experiment and therefore, utilise a vast number of animals to achieve experimental repeat.

This has led to the development of *ex vivo* model systems as a compromise between *in vitro* and *in vivo* models. These models maintain the complex specific spatial arrangement of cells within their niche *in situ,* whilst being able to directly alter and manipulate the localised environment directly. This manipulation can also provide easy access to the bone marrow space for the addition of cells and supplements, which can initiate an immune or cellular response that can be controlled. Furthermore, the spatial arrangement of the cells within *ex vivo* models are similar to their *in vivo* counterparts, so that they can remain in their localised cellular niche, without the tissue being subjected to systemic influences.

There are many forms of *ex vivo* models. These can be synthetically developed to use biomaterials, such as collagen and hyaluronan scaffolds, to support the co-culture of osteoblasts and *S. aureus* species. Results show that in a three-dimensional (3D) space, MC3T3-E1 pre-osteoblastic mouse cell lines following infection with mildly fixed SpA specific *S. aureus* species, resulted in significant expression of extracellular alkaline phosphatase, calcium deposition and mineralisation following infection (Kavanagh et al. 2018a). Though synthetic models provide a 3D space, they again lack the multiple cells types needed to study complex cellular interactions found *in vivo*.

A mammalian *ex vivo* murine femoral head model has been established for the study of interactions between chondrocytes, osteoblast and osteoclasts cells, within a closed compartment similar to their *in situ* formation (Madsen et al. 2011). Within the model it was possible to create culture conditions to induce either a catabolic and anabolic response; successfully monitoring proteoglycan levels as biomarkers indicating increased bone resorption and cartilage degradation or cartilage formation. This shows that such *ex vivo* models can provide information between different tissues and diseases that are unable to be accurately replicated during *in vitro* cultures.

Ex vivo models have the advantage of maximising the use of the obtained tissue, from one single animal in a variety of different experiments. Here tissues are sectioned into thin slices

and cultured in a variety of different culture methods. These can either be on mechanical support, on a porous filter paper with an embedding matrix, such as an agarose gel (Sloan et al. 2013; Smith et al. 2010) or without (Garrett 2003) or submerged within culture media (Madsen et al. 2011; Roberts et al. 2013; Sloan et al. 1998). These tissue slices can all be independent, can be used under different experimental conditions and have been used for prolonged cultures over several days (Sloan et al. 2013; Smith et al. 2010). Whilst successes have been achieved in the development of a mandible tissue slice model, this model contains tissue such as the periodontal ligament, dentine pulp along with a small, thin amount of bone marrow (Smith et al. 2010). Furthermore, long bones such as the femur are formed from the mesoderm, which is in contrast to the neuroectoderm and neural crest cells which forms the mandible during foetal development (Aghaloo et al. 2010). As such, there are differences between the behaviour of bone cells in the bone marrow in both locations. Investigations into the stem cells derived from the mesoderm and neuroectoderm have found that these cells have 'positional memory' which selectively recruits cells from their own embryonic lineage when the cells are grafted at sites opposite of their original developmental source (Leucht et al. 2008). Here, osteoprogenitor cells that were transplanted from the mandible into a fractured tibia or tibial cells into a fractured mandible. The tibial cells continued to express Hox-positive genes (*Hoxa11*) in the mandible which is typically Hox-negative (lacking the *Hoxa11* gene), however they lacked the differential capability into osteoblasts but instead formed a cartilaginous callus. When the Hox-negative neural crest cells were transplanted into the Hox-positive tibia there was a genetic switch, with the Hox-negative mandibular cells expressing *Hoxa11* gene, along with increased osteogenic capacity (Leucht et al. 2008). MSCs have a form of epigenetic memory resulting in bone marrow-derived MSCs having a stronger pro-osteogenic and reduced adipogenic differential potential and vice versa for adipose-tissue derived MSCs, however chondrogenic differential potential was the same for both cells (Xu et al. 2017). The number of functional osteoclasts in the mandible marrow are greater compared to long bones. Under hormonal treatment with 1,25 dihydroxy vitamin D_3 and parathyroid long bones generated more osteoclasts compared to the mandible (Chaichanasakul et al. 2014). The mandible has demonstrated a higher collagen content, with lower mature crosslinks and with increased mineralisation, compared to long bones (Aghaloo et al. 2010). Due to these variations in bone marrow cell functions between these tissues, it is more preferable to

develop a model in the femur, as these factors can potentially influence bacterial and cell behaviour

Against this background, there is a need to develop an *ex vivo* model which will enable the better study of osteolytic or osteomyelitis infections within the bone marrow cavity. To achieve this, the current Chapter aimed to identify the viability of bone marrow cells within a femoral shaft cultured *ex vivo*. Following the successes of the culture of mandible tissue slices, femoral tissue slices were cultured at either at the base of a culture well surrounded by culture media or at a liquid/air interface. Cell viability was assessed, measuring apoptosis and necrosis. The persistence of neutrophils, MSCs, monocytes, macrophages and osteoclasts were assessed in a chosen culture method. Collectively, these results will be taken forward and optimised in the subsequent Chapter, preparing for studies involving bacterial co-cultures.

2.2: Material and Methods

2.2.1: Extraction and Obtaining the Semi-Cylindrical Femoral Slices

All long bones used in the following experiments were from 21-28-day old Wistar rats, freshly sacrificed using CO_2 asphyxiation. Femurs were dissected using a sterile scalpel and sterilised by dipping in 70 % ethanol (ThermoFisher Scientific, Loughborough, United Kingdom) for 5 s and immediately washed in phosphate-buffered saline (PBS) (Dulbecco A) (ThermoFisher Scientific,). Washed femurs were placed in culture media containing Gibco™ alpha Minimum Essential Medium (αMEM) media (ThermoFisher Scientific), supplemented with 10 % heat-inactivated foetal bovine serum (HI FBS) (Gibco™ South America origin, ThermoFisher Scientific), 1 % L-ascorbic acid 2-phosphate sesquimagnesium salt hydrate (Sigma-Aldrich, Poole, United Kingdom) and 1 % antibiotic antimycotic solution (Sigma-Aldrich); all cooled on a bed of ice.

Using a Buehler IsoMet diamond-edged 102 mm rotary blade (Buehler, Illinois, USA) that had been previously sterilised with 70 % ethanol and cooled while in use with PBS, the femoral head and lateral and medial condyles from the femurs were removed. The resulting ~4-6 mm femoral shaft was bisected along the sagittal plane down the centre, using the diamond-edged blade, into two further ~2-3 mm rods with a diameter between ~0.5-1 mm. These bisected sections were further sectioned transversely along the centre of the femoral shaft. This resulted in a total of four semi-cylindrical femoral slices for each femur with a bone marrow cavity retained for experimentation (Figure 2.1).

2.2.2: Removal of the Positive Control Tissues

Immunohistochemical positive control tissues were dissected from the same Wistar rats used to obtain the femurs, (listed in Table 2.1). Using sterile scalpels and forceps, femurs, heart, lungs, testes, brain, kidney and spleens were removed and immediately fixed in 10 % formalin for 24 h. Following fixation tissues were processed and sectioned, as described in Section 2.5.

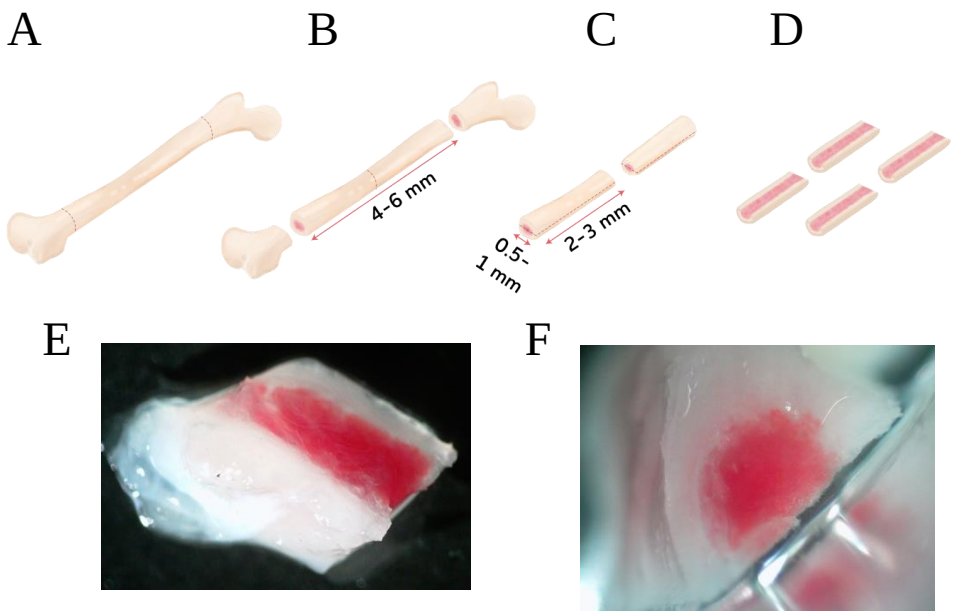

Figure 2.1: Schematic diagram of obtaining rat semi-cylindrical femoral slices.
Femurs were dissected from 21-28-day old Wistar rats. A) Femurs were removed and cut (along the red line) using a diamond-edged saw to remove the femoral head and lateral and medial condyles. B) The ~4-6 mm femoral shaft was bisected in the middle at around ~2-3 mm. C) The bisected femoral shafts were sectioned sagittally down the formal shaft. D) This resulted in two further halves from each bisected shaft totalling 4 semi-cylindrical slices at ~0.5-1 x ~2-3 mm dimensions per femur (totalling eight per animal). E) representing a live image of the sagittal plane of the femoral slice and F) representing a live image of the transverse plane of the femoral slice.

2.2.3: Culture of *ex vivo* Semi-Cylindrical Femoral Slices

Bisected semi-cylindrical slices were immediately transferred into individual wells of a 12-well culture plate (Starstedt, Leicester, United Kingdom), containing 1 mL αMEM culture media supplemented with 10 % HI FBS, 1 % of L-ascorbic acid 2-phosphate sesquimagnesium salt hydrate at 100 µM concentration and 1 % antibiotic antimycotic solution. Tissues were left to stabilise to the culture media for 10-20 min within a sterile, humidified incubator at 37^{o}C, 5 % CO_2. Two culture arrangements for the culture of the femoral slice were used; either via immersion within culture media termed base-type culture (Section 2.2.3.1) or at liquid-air interface suspended above culture media termed a Trowell-type culture (Section 2.2.3.2).

2.2.3.1: Culture of ex vivo Femoral Slices Within Culture Media (Base-Type Cultures)

Femoral slices were submerged in individual wells of a 6-well culture plate (Starstedt) containing 3 mL basal culture media (αMEM media, supplemented with 10 % HI FBS, 1 % L-ascorbic acid 2-phosphate and 1 % antibiotic antimycotic solution, 100×, Figure 2.2A). Tissues were incubated at 37^{o}C, 5 % CO_2 for either 24 h and 48 h. Uncultured femoral slices served as 0 h controls and were immediately fixed (Section 2.2.6).

2.2.3.2: Culture of ex vivo Femoral Slices at the Liquid-Air Interface (Trowel-Type Cultures)

To individual wells of a 6-well culture plate, 3 mL of basal culture media was added. A silicon support ring (35mm high sterile micro-insert, Thistle Scientific, Glasgow, United Kingdom) was placed into the media. A Merck™ 0.45 µm Pore Size MF-Millipore™ mixed cellulose ester membranes with a grid (Merck Millipore, Gillingham, United Kingdom) was laid over the support ring, with edges falling into the surrounding media.

Meanwhile, a 1 % (weight/volume) agarose solution was prepared. 1 g of TopVision™ low melting point agarose (ThermoFisher Scientific) was added to 50 mL of pure αMEM and heated to 50 ^{o}C, to make a 2 % (weight/volume) solution. 10 mL of 2 % dissolved agarose was mixed with 10 mL of αMEM media containing 20 % HI FBS, 2 % L-ascorbic acid 2-phosphate and 2 % antibiotic antimycotic solution. The solutions were vortexed and 3 mL was added to individual wells of a 12-well culture plate (Starstedt). The agarose was cooled within the culture plate for 5-10 min, after which individual femoral slices were submerged within each gel separately, orientated with the periosteum and cortical bone facing towards the base of the culture plate and the exposed sagittal cut bone marrow facing upwards (Figure 2.2B). The agarose embedded femoral slices were left to completely solidify for a further 5-10 min. The agarose plugs containing the femoral slices were removed and placed onto the cellulose membrane support (described above) and cultured for 24 h and 48 h at 37 ^{o}C, 5 % CO_2. Two 0 h uncultured controls were also included; femoral slices that were embedded in agarose gel for 5-10 min and then removed from the agarose gel prior to fixing,

the second control consisted of unembedded slices that were immediately fixed (Section 2.2.6).

2.2.3.3: Culture of Hydrogen Peroxide Treated Trowell-type Cultured Positive Control Slice to Induce Necrosis

Culture media and agarose gel for Trowell type culture were prepared as described in section 2.2.3.2. To induce necrosis in the tissue slice 500 µM of 60 % weight/volume hydrogen peroxide (H_2O_2, ThermoFisher Scientific) was added to the culture media. Tissue slices were left to incubate for 48 h, before the agarose plug was carefully removed from the surface of the femoral slice. The femoral slice was slowly extracted using sterile forceps and the remaining culture media and agarose plugs were collected and combined before storage at -80 ^{o}C. This sample was used as a positive control for the LDH assay.

2.2.3.4: Sample Collection and Storage

Following culture, slices in base-type cultures were carefully removed using sterile forceps and media was collected and stored at -80 ^{o}C for additional experiments. For Trowell-type cultures, the top surface of the agarose plug was carefully removed to expose the femoral slice using sterile forceps. The femoral slice was slowly lifted using sterile forceps and the remaining culture media and agarose plugs were collected and combined before storage at -80 ^{o}C.

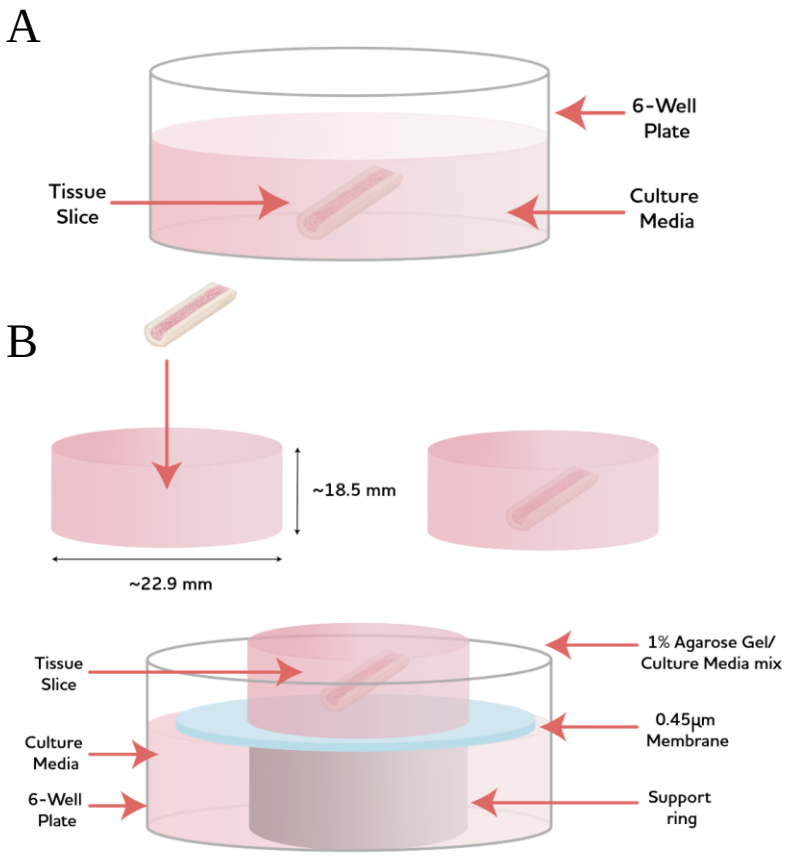

Figure 2.2: Schematic diagram of culturing semi-cylindrical femoral slices.
Semi-cylindrical femoral slices were either culture as A) Base-type culture where the tissue was submerged at a bottom of a 6-well plate within culture media or B) Trowell-type culture embedded into 1 % (w/v) low melting point agarose, containing αMEM media supplemented with 10 % HI FBS, 1 % L-ascorbic acid 2-phosphate and 1 % antibiotic antimycotic solution (100×). The embedded semi-cylindrical slice was then cultured at a liquid/air interface above culture media.

2.2.4: Detection of Necrosis Using the Colorimetric Lactate Dehydrogenase Assay

Lactate dehydrogenase (LDH) is an enzyme present within all cells. When the plasma membrane of the cell is damaged, LDH is released into the surrounding extracellular environment, which can be quantified to provide a measure of necrosis. Accumulation of the enzyme in culture media following *ex vivo* culture, as described above, was detected using the Pierce™ LDH Cytotoxicity Assay Kit (ThermoFisher Scientific). The principle of the assay is based on the ability of the LDH to reduce nicotinamide adenine dinucleotide $(NAD)^+$ to NADH, using H^+ released during the oxidation of lactate to pyruvate. Diaphorase, a catalyst that uses hydrogen from NADH (converting it back to NAD^+) to convert the

tetrazolium salt to a red formazan dye. The dye is read at an absorbance at 490 nm and is proportional to the amount of LDH released.

Tissue culture media harvested in Section 2.2.3.4 and the positive control from Section 2.2.3.3 was defrosted at room temperature. 50 µL of culture media along with 50 µL of the positive control samples were added in triplicate to individual wells of a 96-well culture plate (Starstedt) and was mixed with 50 µL of reaction buffer from the assay. The culture plate was left to incubate in the dark, at room temperature, for 30 min. where a colour change occurred within the wells containing the media to a deep red. Following incubation, 50 µL of LDH stop solution was added to each sample to terminate the reaction. This colour change was quantified using a Fluorostar Omega Spectrometer (BMG Labtech Ltd, Aylesbury, United Kingdom) measuring absorbance at 490 and 680 nm. To assess LDH activity, 680 nm absorbance value (background signal from the spectrometer) was subtracted from 490 nm absorbance value. The percentage cytotoxicity was calculated using the manufacturer's instructions, where the test sample is divided by the positive control (representing the maximum possible LDH release) and multiplied by 100 to obtain a percentage.

2.2.5: Tissue Decalcification, Processing and Sectioning

2.2.5.1: Fixation and Decalcification

Immediately following culture, femoral slices extracted from either the culture media or agarose gel were fixed in 5 mL of 10 % formalin for 24 h. Slices were then removed and demineralised using 20 mL of 14 % ethylenediaminetetraacetic acid (EDTA) tetrasodium salt hydrate (Sigma Aldrich), pH 7.4, at 4 ^{o}C for 1 week, with gentle agitation.

2.2.5.2: Automated Processing of Semi-Cylindrical Femoral Slices

Following demineralisation, femoral slices were transferred into biopsy tissue processing bags (Cellpath Ltd, Newtown, United Kingdom), to prevent direct damage of exposed bone marrow during processing. These biopsy bags were then transferred into labelled biopsy

cassettes and washed in gently running tap water for 20-30 min, to remove residual EDTA tetrasodium salt. The cassettes were then transferred into 10 % formalin solution for 10 min and then immediately loaded into the Leica ASP300s Automated Tissue Processor (Leica Biosystems, Milton Keynes, United Kingdom), for embedding within paraffin wax overnight. During processing, each cassette was passed through 70 % and 90 % ethanol for 1 h each, respectively. Each cassette was further washed for 4x 110 min in 100 % ethanol. Cassettes were washed with xylene for 2x 135 min and a final wash in xylene for 110 min. Each cassette was then submerged into 2x 135 min washes of molten paraffin wax at 60 – 65 ^{o}C. Once processed, tissue sections were transferred to a Leica FG1150H modular tissue embedding centre (Leica Biosystems), where femoral slices were embedded into a paraffin block. A biopsy mould was filled with paraffin wax. Here, the femoral slice was oriented with the transverse plane of the femoral shaft, the part that connected to either the femoral head or lateral and medial condyles depending on the region of the femoral shaft used, facing downwards towards the base of the mould. A labelled biopsy cassette was attached to the mould and left to solidify on a cold plate for 20 min. The solidified paraffin blocks were removed from the mould ready for sectioning.

2.2.5.3: Sectioning of Femoral Slices

Paraffin-embedded femoral slices were sectioned using the Shandon Finesse Me^{+} Microtome (ThermoFisher Scientific). Tissue sections were cut at 5 µm, floated onto a water bath for 2 min at 40 ^{o}C and mounted onto glass slides. Slides were placed in an incubator at 60 ^{o}C for 45 min to increase adherence of the Section to the glass surface and then stored in a dust-free environment until required.

2.2.6: Haematoxylin and Eosin Staining

Haematoxylin and eosin (H&E) staining was achieved using an automated H&E Staining Machine (Shandon Linistain, ThermoFisher Scientific) via the haematoxylin regressive method. Tissue sections, mounted onto poly-L-lysine adhesion glass slides (ThermoFisher Scientific), were reheated to 60 ^{o}C to increase adherence of the tissue section to the glass slide. Each slide was deparaffinised by xylene washes (3x2 min each). The excess xylene was

removed through a sequence of washes in graded ethanol at 100 % 2x2 min, 70 % 1x2 min and rehydrated in water for 2 min. The slides were stained in Harris Haematoxylin (Cellpath Ltd) for 4x2 min and the residual haematoxylin was removed from the sections with 5 % acetic acid dissolved in 70 % ethanol for 2 min. After washing with tap water, the slides were blued in Scott's tap water for 2 min and plain tap water for 2 min. Sections were then stained with eosin Y (ThermoFisher Scientific) for 2 min, before being further washed in tap water for 2 min and dehydrated through graded ethanol (ethanol at 70 % for 2 min, 100 % 2x2 min and xylene 3x 2 min). Stained slides were removed from the processer and within a laminar flow hood, covered in DPX mounting medium (Cellpath Ltd.), covered with coverslips and left to air dry overnight.

2.2.7: Osteoclast Staining

Osteoclasts were stained using a tartrate resistant acid phosphatase (TRAP) kit (Sigma-Aldrich), following the manufacturer's instructions. The principle of the assay relies on the detection of an acid phosphatase isoenzyme which, unlike acid phosphatases found in many other cell types, is enzymatically active in the presence of tartrate. This isoenzyme was considered specific to the large multi-nucleated osteoclasts, but has also been identified present in macrophages, which can be regarded as mono-nucleated precursor cells (Raisanen et al. 2005). Histological staining involves the hydrolysis of naphthol AS_BI phosphate by acid phosphatases (in acidic conditions) to release Naphthol AS-BI, which couples immediately with fast garnet GBC forming insoluble maroon dye deposits at sites of activity. The addition of tartrate to the solution and identification of multi-nucleated cells can be used to specifically stain for osteoclasts.

First, distilled water was preheated to 37 ^{o}C. Then in a separate container, 1 mL of fast garnet GBC base solution was mixed with 1 mL of sodium nitrite solution and left to stand for 2 min, forming the diazotized fast garnet GBC solution. To 45 mL of preheated distilled water, 1 mL of diazotized fast garnet GBC solution, 500 µL of Naphthol AS-BI phosphate solution and 2 mL of acetate solution was added. To one solution, 1 mL of tartrate solution was added (used to specifically stain osteoclasts) and in the other tartrate was omitted (staining all acid phosphatase leukocytes cells).

Tissue mounted onto Superfrost™ Plus Adhesion Slides (ThermoFisher Scientific) were deparaffinised in xylene for 3x5 min each and rehydrated in graded alcohols at 100 %, 75 % and 50 % for 3x5 min each, before being rinsed in distilled water for 5 min. Slides were removed and placed in a solution containing tartrate. Additional slides with serial sections of the same sample were also placed in the tartrate omitted solution. Both solutions were incubated at 37 ^{o}C for 1 h in the dark. All slides were then counterstained using Gill's hematoxylin and rinsed in tap water to blue the nuclei. Sections were mounted using VectaMount® AQ mounting media (Vector Laboratories, Peterborough, United Kingdom), before being visualised by light microscopy and imaged (Section 2.2.10).

2.2.8: Immunohistochemistry Analysis of Specific Immune, Apoptotic and Necrotic Antibodies

Tissue immunohistochemistry (IHC) was carried using the VECTASTAIN® Elite® ABC HRSP Kit (Peroxidase, Rabbit IgG, Vector Laboratories), according to the manufacturer's instructions. Tissue sections, mounted onto Superfrost™ Plus Adhesion Slides (ThermoFisher Scientific), were heated in the oven at 60 ^{o}C for 45 min. Slides were deparaffinised for 3x5 min in xylene and rehydrated in 3x5 min in graded ethanol (ThermoFisher Scientific) at 100 %, 75 % and 50 %, before being rinsed in distilled water for 5 min. Rehydrated slides were placed within a humidified chamber containing distilled water, to prevent tissue sections from drying out. A circle was drawn around each Section using a hydrophobic liquid blocker pen (Vector Laboratories), to help contain all reagents used over the tissue sections. For endogenous peroxidases that are similar in structure to the enzyme used, they may cause a reaction to the substrate used later, giving false positive staining. These peroxidases are normal in tissues and to quench their activity, sections were treated with 0.3 % hydrogen peroxide in 40 % methanol mixed with Tris Buffered Saline (TBS) for 15 min.

The sections were washed in tris buffered saline (TBS) for 3x5 min each. For antibodies that require access to intracellular antigen targets, tissue sections were permeabilised, with 0.1 % Triton X-100 (Sigma-Aldrich) in TBS for 5 min (Table 2.1) and washed 3x5 min with TBS. Tissue sections requiring antigen retrieval were immersed in 10 mM citric acid at pH 6, heated at 100 ^{o}C in a water bath, for 20 min; and then left to cool within the citric acid for a

further 20 min. The sections were then blocked using 1 % normal goat serum in TBS for 1 h at room temperature. For removal of any endogenous biotin, biotin receptor and avidin binding sites that naturally occur within the tissue, an avidin and biotin blocking kit (Vector Laboratories) was used. To each tissue section, 50 µL of avidin D solution was applied for 15 min before being washed in TBS for 5 min, after which 50 µL of biotin solution was applied over each Section for 15 min, before being washed in TBS for 3x5 min.

Tissues were then incubated with primary antibodies at specified concentrations (Table 2.1) overnight at 4 ^{o}C. Negative controls were carried out on tissues where the primary antibody was replaced with TBS or isotype control antibody was used, instead of the primary antibody (Table 2.2). Both controls were incubated overnight at 4 ^{o}C. Tissue sections were washed in TBS 3x for 5 min. An appropriate secondary antibody (Table 2.3) was applied for 30 min at room temperature and washed in TBS (3x5 min). To each section, the avidin and enzyme-linked biotin peroxidase complex from the ABC kit was applied for an additional 30 min. Tissue sections were washed in TBS for 3x5 min.

The immunoreaction was visualised with either Nova Red Peroxidase (HRSP) Substrate Kit (Vector Laboratories) or 3,3'-diaminobenzidine (DAB) Peroxidase (HRSP) Substrate Kit (Vector Laboratories) (Table 2.1), both solutions were made up following the manufacturer's instructions. Nova red complex was incubated for 30 s on tissue sections to achieve the desired staining. Alternatively, the DAB complex was added over tissues and incubated for 30 s. Staining was terminated via immersion of sections in tap water for 5 min. Gill's haematoxylin (Sigma Aldrich) counterstain was applied for 10-30 s onto the tissue sections before the excess stain was removed within tap water for 5 min. Tissue sections were dehydrated through graded ethanol and washed twice in xylene, before mounting each Section with DPX mounting medium and covering with a coverslip. Sections were imaged as described in Section 2.2.10.

Antibody	Cells stained	Antibody Source	Code	Isotype	Source/ species reactivity	Dilution	Positive control	Chromogen substrate detection system	Antigen retrieval	Permeabilisation
CD14	Monocytes/Macrophages	Abcam, Cambridge, United Kingdom	Ab203294	IgG	Rabbit polyclonal	1:100	Rat lung tissue	Nova red	Citric acid pH 6 100 °C	NA
CD68 [ED1]	Monocytes/Macrophages/ Osteoclasts	Abcam	Ab31630	IgG	Mouse monoclonal	1:100	Rat lung tissue	Nova red	Citric acid pH 6 100 °C	NA
Neutrophil elastase	Neutrophils	Abcam	Ab21595	IgG	Rabbit polyclonal	1:100	Rat bone marrow	DAB	Citric acid pH 6 100 °C	Triton x-100 0.3 % in TBS
LDH	Necrotising cells	Abcam	Ab203285	IgG	Rabbit polyclonal	1:100-1:500	Rat testis	DAB	NA	NA
CD90/ Thy1	Mesenchymal stromal cells	Abcam	Ab225	IgG1	Mouse monoclonal	1:100	Rat brain tissue	Nova red	NA	NA
CD73	Mesenchymal stromal cells	Abcam	Ab175396	IgG	Rabbit polyclonal	1:50–1:100	Unable to obtain	DAB	NA	NA
CD105 [8A1]	Mesenchymal stromal cells	Abcam	Ab230925	IgG2b	Mouse monoclonal	10ug/mL	Rat Spleen tissue	DAB	Citric acid pH 6 100 °C	NA
Cleaved-caspase-3 (Asp 175)	Apoptotic cells	Cell Signalling Technologies, London, United Kingdom	9661	IgG	Rabbit polyclonal	1:200	Rat testes	DAB	Citric acid pH 6 100 °C	NA
BAX [E63]	Apoptotic cells	Abcam	Ab32503	IgG	Rabbit monoclonal	1:250	Rat kidney	DAB	Citric acid pH 6 100 °C	NA

Table 2.1: Immunohistochemistry primary antibodies.

Antibody	Source of Antibody	Code
Normal rabbit immunoglobulin	Peprotech, London, United Kingdom	500-P00
IgG1 mouse monoclonal	Abcam	ab170190
IgG2b mouse monoclonal	Abcam	ab170192

Table 2.2: Immunohistochemistry IgG isotype control antibodies.

Secondary antibody	Source of Antibody	Code
Biotinylated goat anti-rabbit IgG secondary antibody	Vector Laboratories	PK-6101
Biotinylated horse anti-mouse IgG secondary antibody rat absorbed	Vector Laboratories	BA- 2001

Table 2.3: Immunohistochemistry IgG secondary antibodies.

2.2.9: Imaging

Stained tissue sections were examined using an Olympus AX70 Fluorescent Microscope (Olympus Corporation, Tokyo, Japan) and imaged using the PAX-it Image Analysis Software (PAX-it, Villa Park, USA). Five brightfield images for H&E and IHC treated tissue slides of the bone marrow were obtained at x600 or x400 magnification respectively.

2.2.10: Image Analysis

Analysis of images was carried out using ImageJ application (U.S. National Institutes of Health, Bethesda, USA). For H&E sections, all haematoxylin stained nuclei within the bone marrow cavity were counted in an area of approximately 10,000 μm^2 for each image and repeated five times for each tissue section. The average of all five images was obtained.

For IHC stained sections, five semi-random 50x50 μm^2 area boxes were applied over areas of positive antibody-specific stained cells in the bone marrow cavity and positive and negative stained cells were counted at x400 magnification (Figure 2.3). Positive stained cells

for each of the 5 images per tissue section were totalled together and averaged for each time point, for each repeat. Total positive and negative cell counts were totalled together for each of the 5 images per tissue section and averaged for each time point, for each repeat. Using both counts a percentage of positively stained cell remaining at each timepoint was calculated. Each percentage count for each image was averaged for each time point, for each repeat.

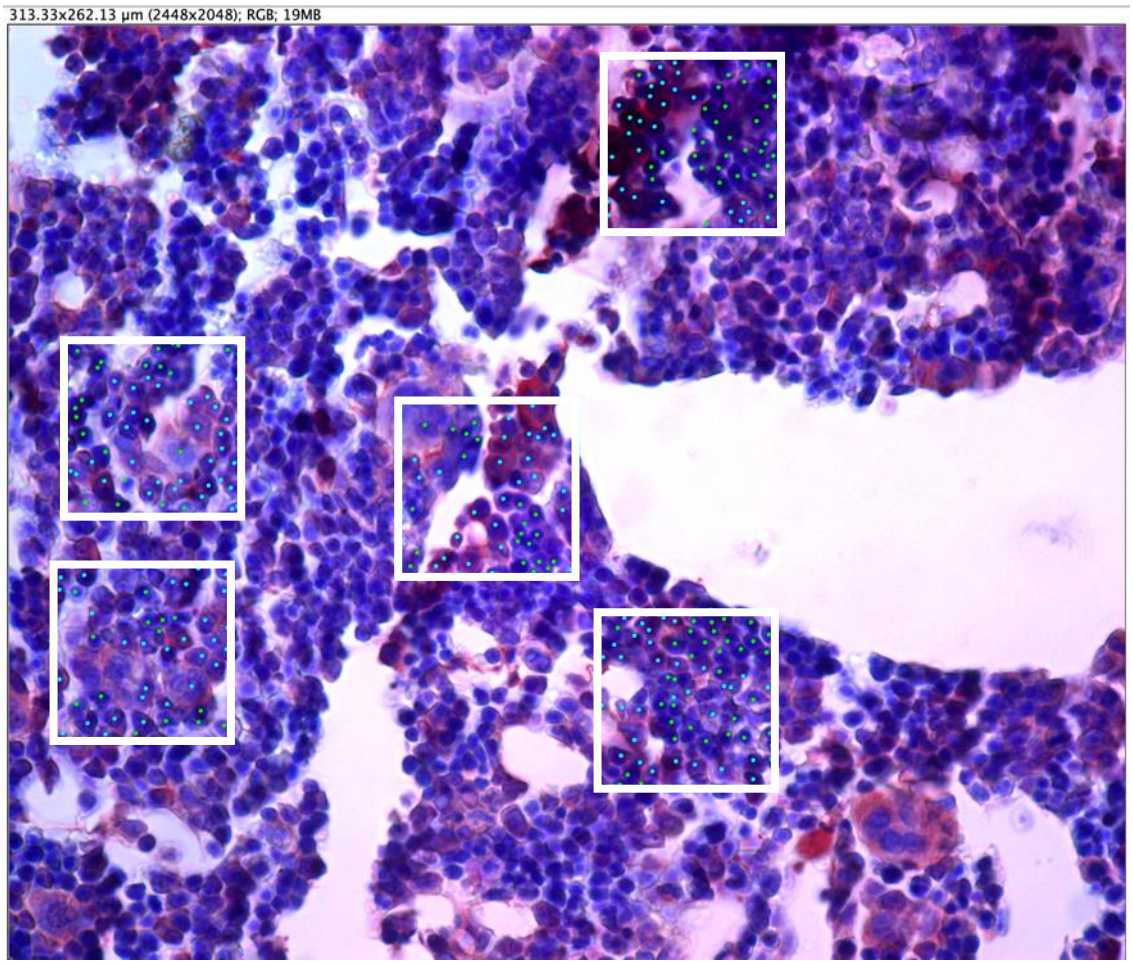

Figure 2.3: Cell counts for immunohistochemistry images within the ImageJ software.
Five semi-random boxes of 2500 µm^2 areas were applied over a single x400 magnification image. Five x400 images were taken for each antibody stain for each timepoint, all five images had positive and negative cells counted. Cells counted for each image were totalled and averaged and a percentage count was tabulated.

2.2.11: Statistical Analysis

All experiments described above were performed in triplicate on a minimum of three separate occasions. Statistical analysis was performed using Graphpad Prism, Version 8.00 (Graphpad Software, San Diego, USA). One-way analysis of variance (ANOVA) with Tukey's post-test was used to identify significant differences in data across groups for one independent variable. A two-way ANOVA with Tukey's post-test Holm-Sidak's post-test was used to determine differences in data with two or more independent variables. Significance was determined at $*P < 0.05$, $**P < 0.01$, $***P < 0.001$, $****P < 0.0001$.

2.3: Results

2.3.1: Histomorphology Evaluation of Bone Marrow Cells Using H&E of Trowell and Base-Type Cultures

Histological H&E stained tissue sections from Trowell-type cultures and base-type cultures are displayed in Figures 2.4A-F and 2.5A-F, respectively. There was a high density of nuclei stained bone marrow cells within the bone marrow cavity, in femoral slices termed '0 h', that were either agarose embedded (Figure 2.4 A&B) or not embedded (Figure 2.5 A&B), following sectioning via the bone saw and directly fixed. There were cuboidal and elongated cells lining the endosteum towards the edge of the cortical bone (Figure 2.4B and 2.5B). Large, megakaryocyte-like cells were also seen throughout the bone marrow (Figure 2.4B and 2.5B). Megakaryocytes derived from haematopoietic stem cells (HSCs), have a similar appearance to osteoclasts, though they lobed nucleus which appears as multinucleated in histological samples and are typically large cells up to 50 -100 µm in size, although they lack the osteoclast ruffled border and are not $TRAP^+$ (Jawad et al. 2016). The location of these cells vary, megakaryocytes are located within the bone marrow and osteoclasts are located adjacent to hard tissue. There was also the presence of adipose-like vacuole deposits, identifiable as distinct areas of non-staining vacuoles. The cortical bone contained lacunae, defined by small pore-like gaps containing one or two cells. These cells within the lacunae had an elongated morphology, typical of osteocytes. There were also large pockets of self-contained bone marrow, within the cortical tissue.

Following 24 h in Trowell-type culture, the changes in the bone marrow morphology were noticeable (Figures 2.4C&D). There were fewer stained nuclei cells compared to 0 h controls. The remaining bone marrow cells were spread and diffused throughout the bone marrow cavity, with a large concentration of cells lining the exposed bone marrow. There was a reduction in the size of the adipose-like vacuoles, with the majority seen at the exposed bone marrow (Figure 2.4D). There was a loss of the elongated and cuboidal cells lining the cortical tissue (Figure 2.4D). There was also a loss of the megakaryocyte cells in the bone marrow. There was apparent shrinkage of the bone marrow cavity, this was indicated by the visible gap between the cortical bone and the bone marrow space (Figure 2.4D). Within

the cortical bone, there was the presence of lacunae with nuclei stained osteocyte-like cells, similar to 0 h.

Following 48 h of Trowell-type culture, the bone marrow cavity underwent further loss of cells, along with shrinkage of the soft bone marrow tissue (Figures 2.4E&F). There were large pockets of densely packed nuclei stained cells. In contrast, there were large areas of bone marrow with little or no cells. There was still some presence of adipose-like vacuoles (Figure 2.4E). There was still the presence of stained osteocyte-like cells embedded within cortical bone

Base-type cultures following 24 h also showed a reduction of cells within the bone marrow cavity, similar to Trowell-type cultures (Figure 2.5C&D). The base-type cultures had fewer cells remaining in the bone marrow soft tissue, unlike Trowell-type cultures. The only area of a visible dense layer of cells was towards the lining of the exposed bone marrow. There was a reduced presence of adipose-like cells and tissue within the bone marrow, with few seen towards the edge of the exposed bone marrow. Towards the endosteum, there was also a loss of elongated and cuboidal cells, similar to Trowell-type cultures. There was also a loss of megakaryocytes. There was apparent bone marrow shrinkage, clearly shown by a visible gap between both the cortical and trabecular bone and the bone marrow cavity. The lacunae in the cortical bone showed nuclei stained osteocyte-like cells.

Following 48 h, base-type culture slices showed further loss of cells, with little or few nuclei stained cells spread throughout within the the bone marrow cavity (Figure 2.5E&F). There was damage to the underlying matrix, with gaps visible throughout the cavity. There was no presence of adipose tissues or megakaryocytes. The cortical structure, however, did retain the osteocyte-like cells within their lacunae.

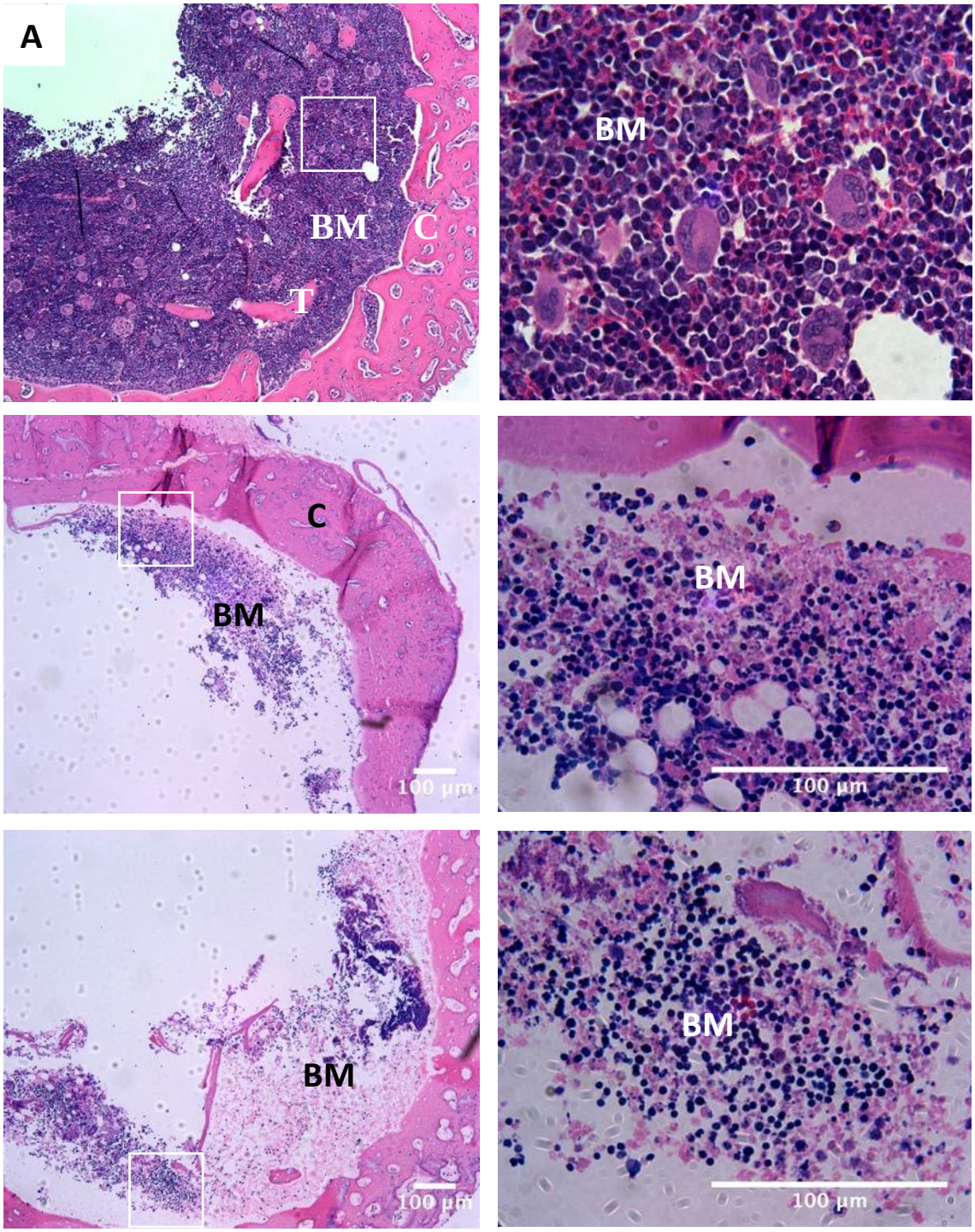

Figure 2.4: Haematoxylin and eosin-stained femoral slices of Trowell-type cultures.
Representative images of low (x100) and high (x600) magnification of haematoxylin and eosin-stained femoral slices of Trowell-type cultures at 0 h (A and B), 24 h (C and D) and 48 h (E and F). Images show structures of the bone and soft marrow tissue, with pink eosin staining the cortical (C) and trabecular (T) bone, along with haematoxylin stained bone marrow (BM) cell nuclei. Within the bone marrow, adipose-like vacuoles (A) and megakaryocytes (M) can be seen. White boxes display an area of ~20, 000 μm^2 area used for x600 magnification images.

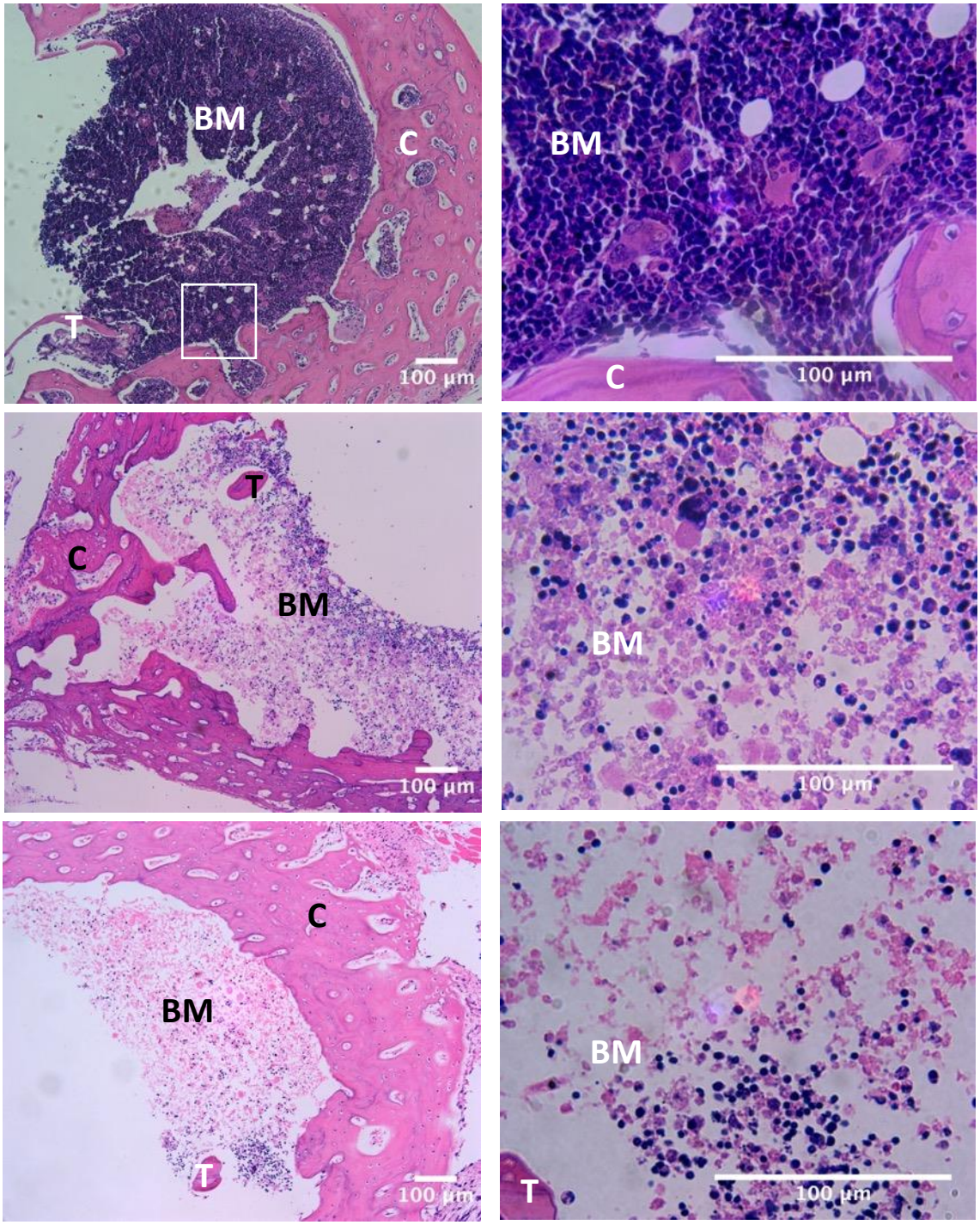

Figure 2.5: Haematoxylin and eosin-stained femoral slices of base-type cultures.
Representative images of low (x100) and high (x600) magnification haematoxylin and eosin-stained femoral slices of base-type cultures at 0 h (A and B), 24 h (C and D) and 48 h (E and F). Images show structures of the bone and soft tissue with pink eosin staining the cortical (C) and trabecular (T) bone. Haematoxylin stained bone marrow (BM) cells nuclei. Within the bone marrow, adipose-like vacuoles (A) and megakaryocytes (M) can be seen. White boxes display an area of ~20, 000 μm^2 area used for x600 magnification images.

2.3.2: Cellular Nuclear Counts of Bone Marrow Cells

Cells were counted within a 10,000 μm^2 area and compared between all timepoints and cultures system; and percentage loss were calculated against cell numbers in 0 h controls (Figure2.6 A&B).

Cell counts for 0 h uncultured control, showed an mean of 354 cells. The process of agarose embedding did not compromise the number of cells, with 0 h Trowell-type culture that had been agarose embedded showed a mean of 321 cells.

Base-type cultures at 24 h, showed a significant decrease in mean cell numbers to 63 cells ($P < 0.001$) when compared to 0 h uncultured controls (Figure 2.6A). The mean percentage loss of cells was 82 % which was significant ($P < 0.001$) compared to 0 h controls (Figure 2.6B). After 48 h the mean number of was 53 cells, which was non-significant compared to 24 h ($P > 0.05$) but was significant when compared to 0 h uncultured controls ($P < 0.0001$, Figure 2.6A). The mean percentage loss of cells was 85 % which was significant when compared to 0 h uncultured controls ($P < 0.0001$, Figure 2.6B).

Trowell-type cultures at 24 h, showed a significant decrease in mean cell numbers to 170 cells when compared to 0 h uncultured controls ($P < 0.0001$) and 0 h Trowell-culture (agarose embedded) controls ($P < 0.0001$, Figure 2.6A). This was significantly higher compared to 24 h base-type cultures ($P < 0.0001$). The mean percentage loss of cells was 47 % which was significant compared 0 h Trowell-culture (agarose embedded) controls ($P < 0.0001$, Figure 2.6B). This was significantly increased compared to 24 h base-type cultures ($P < 0.0001$). After 48 h the mean number of Trowell-type culture of cells was 127 cells, which was significantly decreased compared to 24 h ($P < 0.01$), 0 h uncultured controls ($P < 0.0001$) and 0 h Trowell-culture controls ($P < 0.0001$, Figure 2.6A). This was significantly higher compared to 48 h base-type cultures ($P < 0.05$). The mean percentage loss of cells was 67 % which was significantly increased when compared to 24 h culture ($P < 0.01$) and 0 h Trowell-culture ($P < 0.0001$, Figure 2.6B). This was significantly increased compared to 48 h base-type cultures ($P < 0.01$).

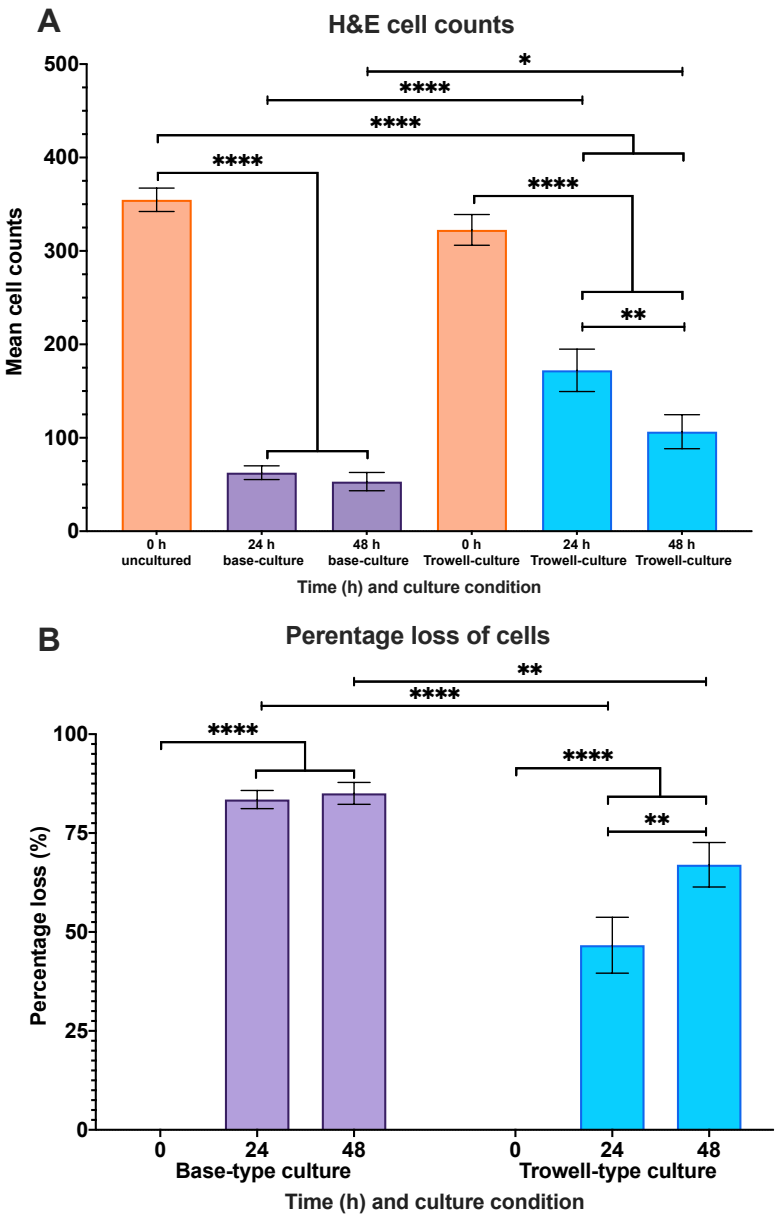

Figure 2.6: Total cell counts and percentage loss of cells from haematoxylin and eosin stained slices for base- and Trowell-type cultures. Graphs A) mean cell counts and B) mean percentage loss of cells following base-type and Trowell-type cultures over 48 h, compared to uncultured 0 h controls. Trowell-type cultures show significantly higher levels of cell counts and reduced percentage loss of cells compared to base-type cultures. Graphs represent error bars for 0 h and 24 h Trowell-type cultures (n=4), 0 h uncultured, 48 h base-type culture and 48 h Trowell-type culture (n=5) and 24 h base-type culture (n=7). Significance within groups determined via one-way ANOVA. Significance between groups determined via two-way ANOVA with Tukey post-hoc test. Error bars represent mean ±S.E.M, **P<0.05, **P < 0.01, ***P < 0.001 and ****P < 0.0001*.

2.3.3: External Cells Within the Culture Media or Agarose Gel

Cells were observed in the surrounding growth media or agarose gel in both culture systems at 24 h and 48 h (Figure 2.7). Base-type cultures showed suspended cells within the culture media at 24 h and 48 h (Figure 2.7 A and B) along with cells attached to the base of the culture plate after 48 h (Figure 2.7B). Trowell-type cultures also showed cells suspended in the surrounding agarose gel following 24 h and 48 h in culture (Figure 2.7 C, D & E).

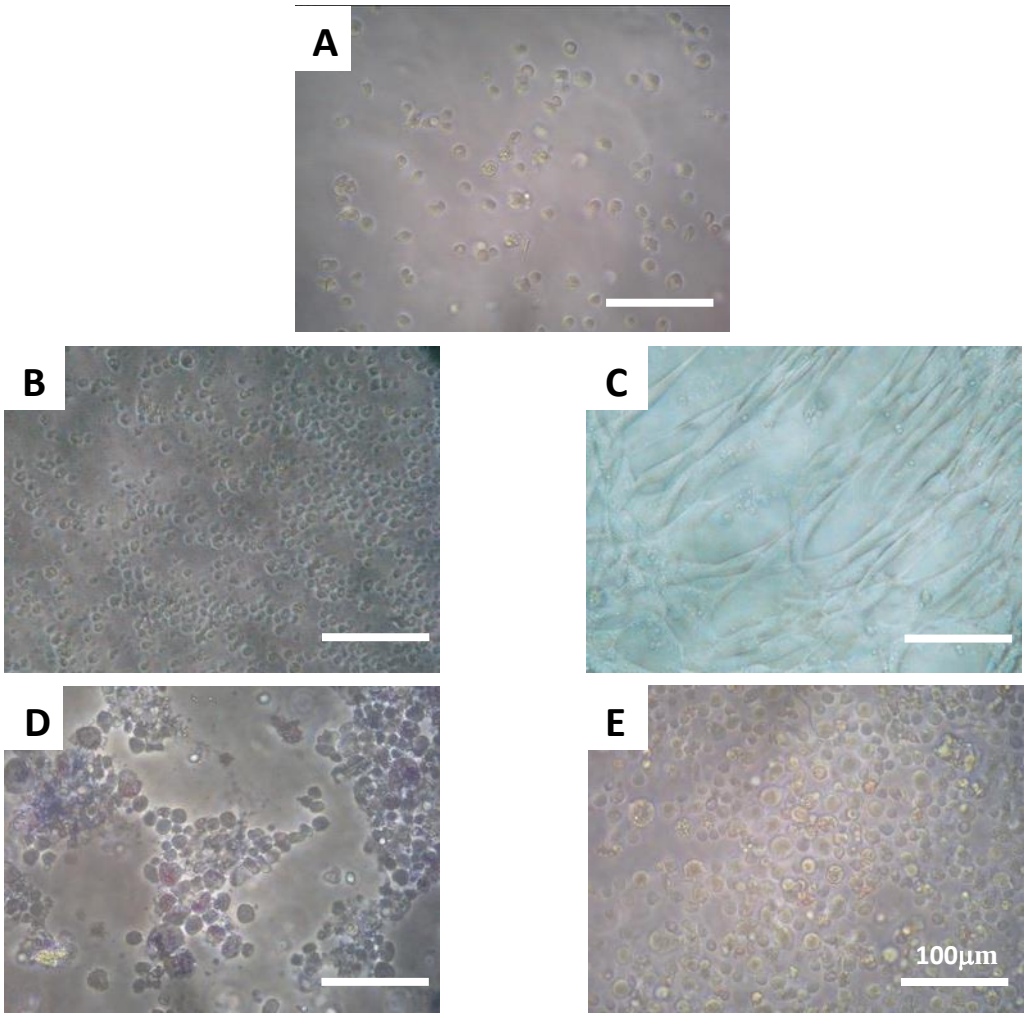

Figure 2.7: Cellular explants from base- and Trowell-type cultures. Representative images of cellular explants in base-type culture media at 24 h (A) and 48 h (B and C) along with images of explants within the agarose gel from Trowell-type cultures at 24 h (D) and 48 h (E and F) at x200 magnification. Base-type cultures show both suspension cells (A and B) and adhered cells to the base of the culture plate (C). Trowell-type cultures show cells suspended within the agarose gel (D, E and F).

2.3.4: Cellular Necrosis Analysis of Base and Trowell-Type Cultures

2.3.4.1: Immunohistochemistry Analysis of LDH localisation for Base- and Trowell-Type Cultures

Both base and Trowell-type cultured tissue sections were stained with LDH antibody (Figure 2.8 and 2.9) over 48 h and cells were counted within a 12.5 mm^2 area. Both cultures show significant cell loss of bone marrow cells and LDH stained cells over 48 h in culture. Trowell-type cultures had a significantly lower number of LDH stained cells at 24 h and 48 h in relation to the total bone marrow cells when compared to base-type cultures.

Both culture systems used the same 0 h uncultured femoral slices as controls, as all slices were obtained from a single animal per repeat. These controls were obtained via direct sectioning of the tissue using the bone saw and fixed immediately. At 0 h. the mean number of bone marrow cells was 391 cells, from which 83 cells were positive for LDH. (Figures 2.8A, 2.9A and 2.10A&B). The mean percentage of cells remaining that were stained positive for LDH was 38 % (Figure 2.10C).

Tissue slices cultured at a base-type culture at 24 h showed a significantly lower number of bone marrow cells, showing a mean of 128 cells when compared to 0 h controls ($P < 0.0001$, Figure 2.8B and 2.10B). The mean number of LDH stained cells at this 24 h was 54 cells, which was significantly lower compared to 0 h controls ($P < 0.01$, Figure 2.8B and 2.10A). The mean percentage of cells remaining that were stained positive for LDH at 24 h was 74 % which was significantly elevated when compared to 0 h controls ($P < 0.0001$, Figure 2.10C). Following 48 h of culture, there was a non-significant decrease for bone marrow cells showing a mean of 88 cells ($P > 0.05$, Figure 2.8C and 2.10B). The mean number of LDH positive stained cells significantly decreased to 31 cells compared to 24 h base-type cultures ($P < 0.05$, Figure 2.8C and 2.10A). The mean percentage of cells remaining that were stained positive for LDH at 48 h was 33 % and was significantly decreased when compared to 0 h controls ($P < 0.01$) and 24 h base-type cultures ($P < 0.05$, Figure 2.10C).

Tissue slices cultured at a Trowell-type culture at 24 h showed a significantly lower number of bone marrow cells representing a mean of 121 cells when compared to 0 h controls ($P <$

0.0001, Figure 2.9B and 2.10B). There was no significant difference in the mean number of bone marrow cells at 24 h between either culture system (*P > 0.05*). The mean number of LDH stained cells at 24 h was 15 cells, which was significantly lower compared to 0 h controls (*P < 0.0001,* Figure 2.9B and 2.10A). The mean percentage of cells remaining that were stained positive for LDH at 24 h was 11 % which was not significant when compared to 0 h controls (*P > 0.05*) and 24 h base-type culture samples, (*P > 0.05*, Figure 2.10C). Following 48 h of culture, there was a non-significant decrease for bone marrow cells showing a mean of 80 cells when compared to 24 h Trowell-type cultured samples (*P > 0.05*, Figure 2.9C and 2.10B). There was no significant difference in the mean number of bone marrow cells at 48 h between either culture system (*P > 0.05*). The mean number of LDH positive stained cells at 48 h was 16 cells and was non-significant compared to 24 h Trowell-type cultures (*P < 0.05*, Figure 2.8C and 2.10A). There was a significantly lower number of cells stained positive for LDH in Trowell-type cultures when compared to 24 h base-type culture samples (*P < 0.0001,* Figure 2.10B). The mean percentage of cells remaining that were stained positive for LDH was 23 % and was significantly higher when compared to 24 h Trowell-type cultures and no significant difference was seen when compared to 0 h controls (*P > 0.05*, Figure 2.10C). When compared to 48 h base-type cultures there was significantly lower percentage of cells stained positive for LDH in the Trowell-type culture (*P < 0.05*, Figure 2.10C).

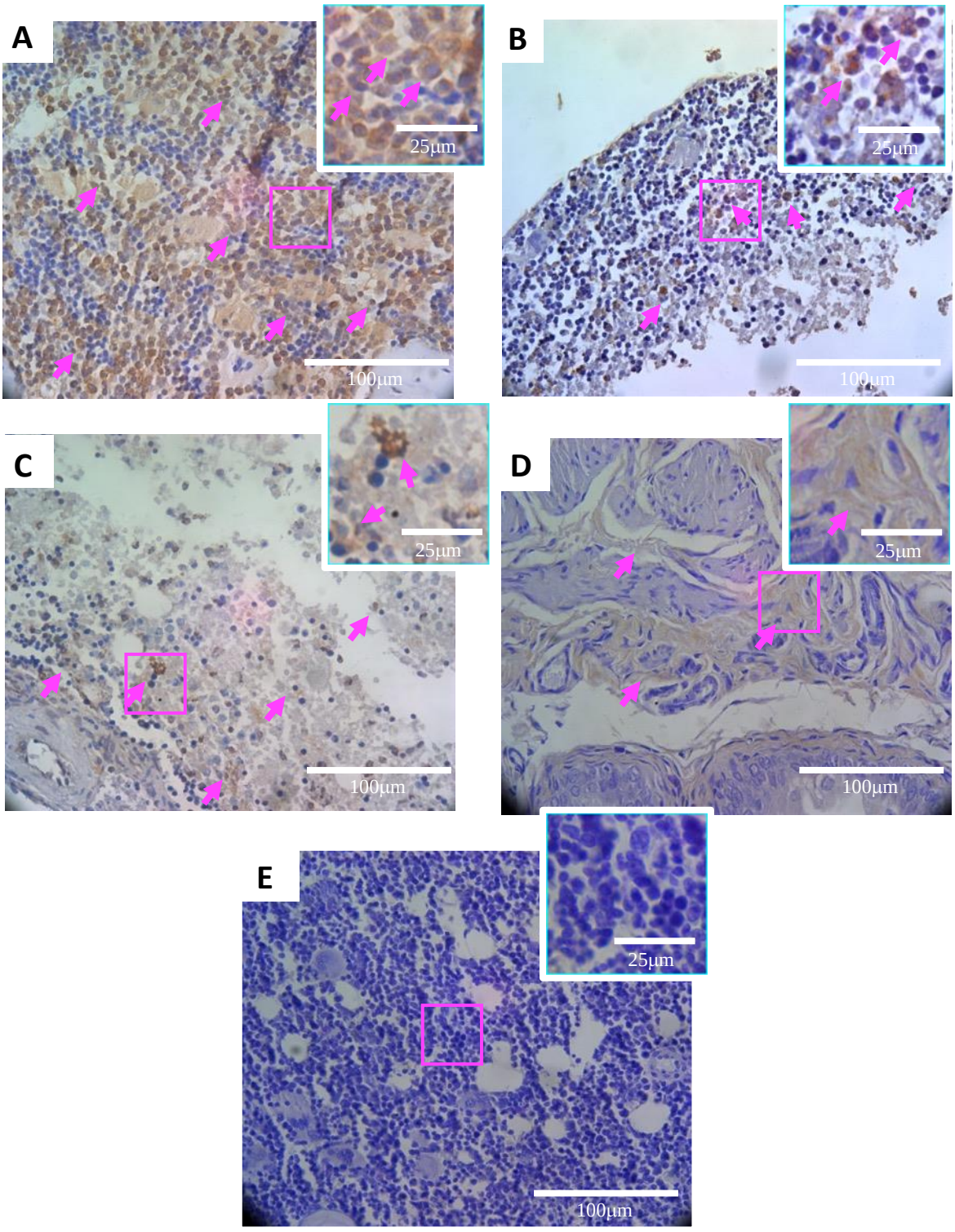

Figure 2.8: Base-type cultures stained for LDH. Representative images of immunohistochemistry staining for LDH-labelled antibodies within the bone marrow of base-type cultures. A) 0 h uncultured controls, B) 24 h cultures, C) 48 h cultures, D) rat testes positive control, and E) negative control by omitting the primary antibody and staining only the secondary antibody. Images indicating reduced LDH staining over 48 h. Images show 50 µm boxes display magnified areas of the bone marrow with positive cell labelling (examples indicated by arrows).

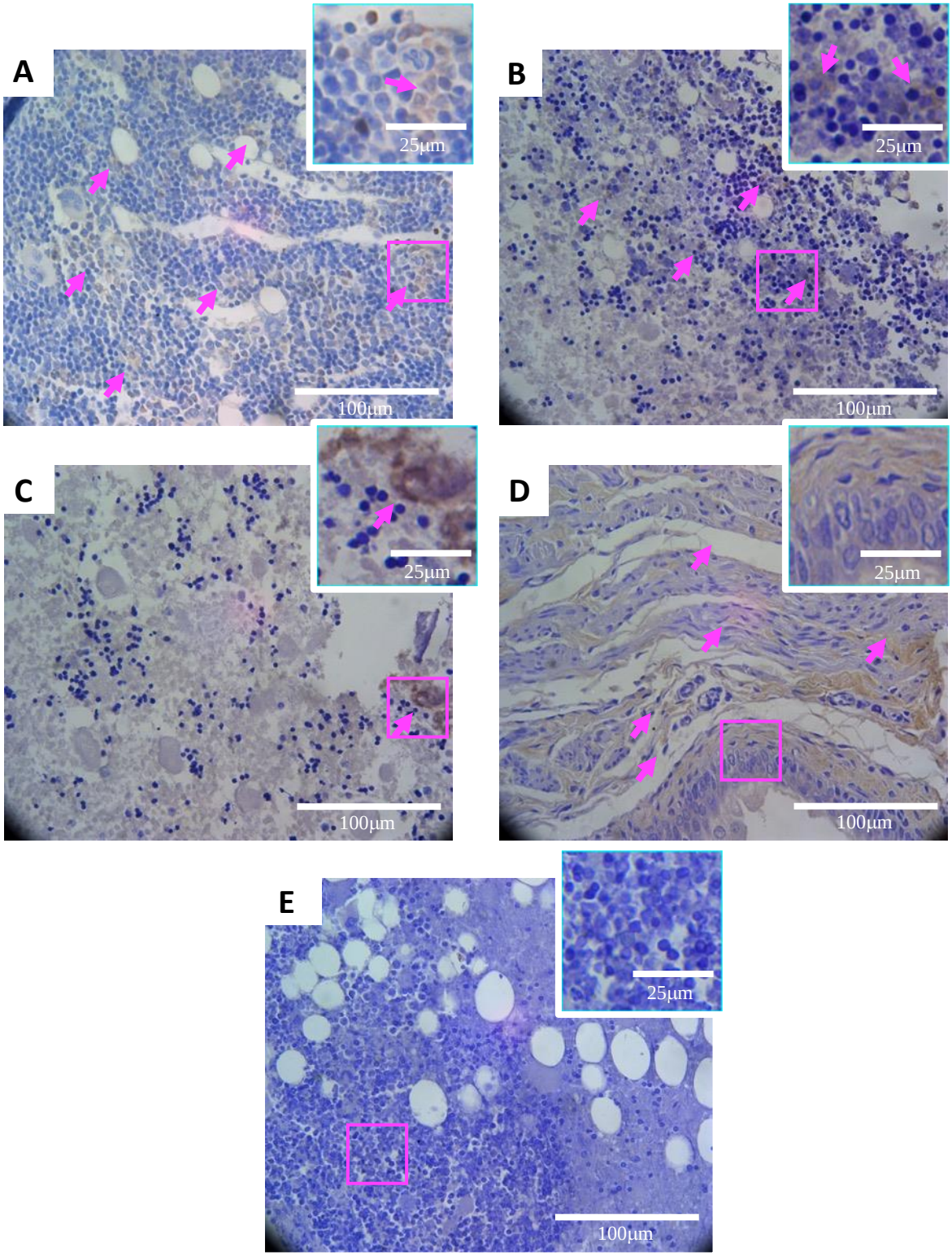

Figure 2.9: Trowell-type cultures stained for LDH. Representative images of immunohistochemistry staining for LDH-labelled antibodies within the bone marrow of Trowell-type cultures. A) 0 h uncultured controls, B) 24 h cultures, C) 48 h cultures, D) rat testes positive control and E) negative control by omitting the primary antibody and staining only the secondary antibody. Images indicating lower LDH staining over 48 h. Images show 50 µm boxes display magnified areas of the bone marrow with positive cell labelling (examples indicated by arrows).

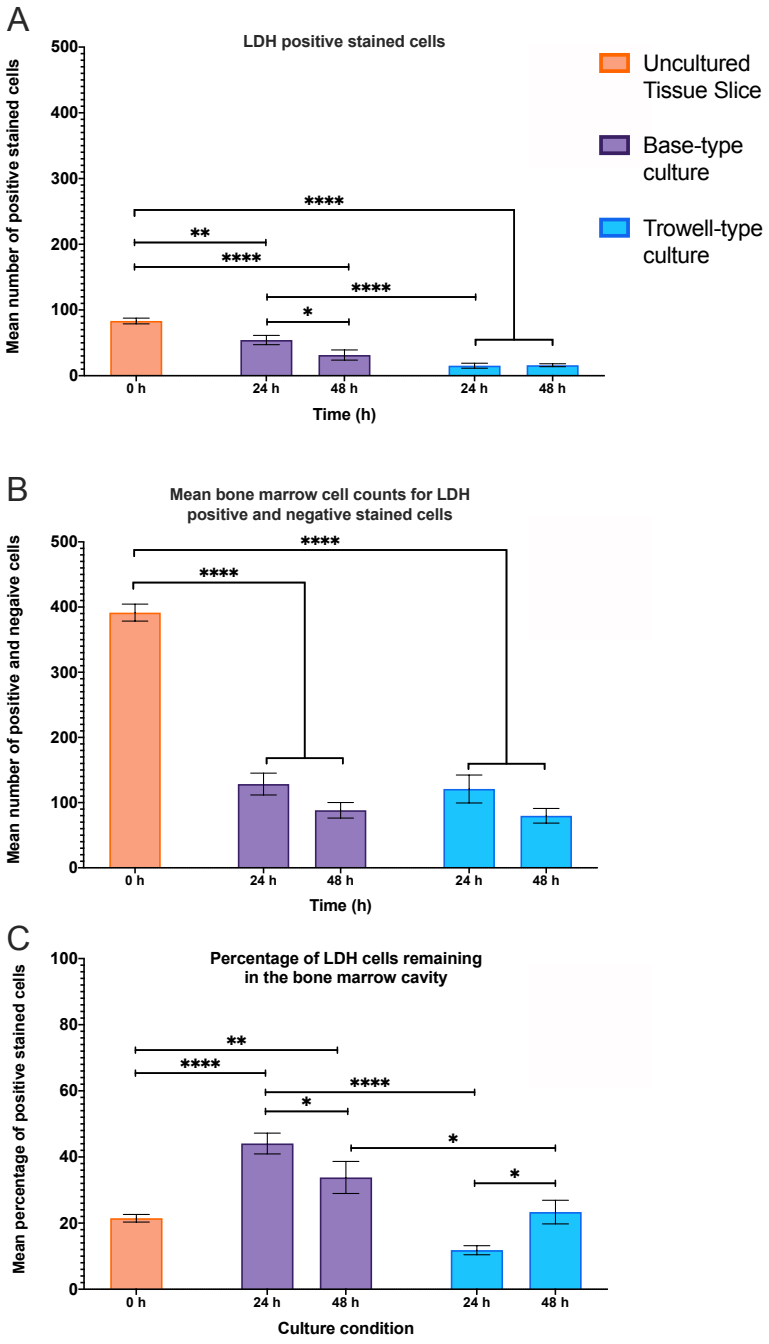

Figure 2.10: LDH stained cells in base and Trowell-type cultures. Immunohistochemical analysis for LDH-labelled antibodies within the bone marrow for 0 h uncultured controls, 24 h and 48 h Base-type cultures and Trowell-type cultures. Graph A) showing data for mean cell counts for LDH positive stained cells. Graph B) shows mean cell counts for both LDH positive and negative stained cells. Graph C) showing the percentage of LDH positive stained cells remaining in the bone marrow cavity. Base-type cultures showed significant mean number and percentage of LDH positive cells at 24 h compared to Trowell-type cultures. Trowell-type cultures show lower levels of LDH staining in relation to mean bone marrow cells. Mean bone marrow cell counts show significant loss of cells over 48 h of culture. Significance within groups determined via one-way ANOVA and between groups determined via two-way ANOVA with Tukey post-hoc test. Error bars represent mean ±S.E.M (N=3), **P<0.05, **P < 0.01 and ****P < 0.0001*.

2.3.4.2: LDH Absorbance and Percentage Cytotoxicity Following Culture With Base- and Trowell-Type Cultures

To analyse LDH release from necrotising cells the surrounding culture media was analysed via an LDH colourimetric assay. The LDH absorbance and the corresponding percentage cytotoxicity calculations are graphed in Figure 2.11 A&B).

The mean LDH absorbance at 0 h for unculture controls was low, corresponding to a mean 7% cytotoxicity. When compared to samples treated with 500 µM of 60 % weight/volume H_20_2 both the mean absorbance and percentage cytotoxicity were significantly lower at 0 h (*P < 0.0001*).

Base-type cultures at 24 h showed significantly elevated mean LDH absorbance levels (*P < 0.0001*) when compared to 0 h uncultured controls. When compared to with 500 µM 60 % weight/volume H_20_2 positive control there was no significance between 24 h base-type culture and the positive control (*P > 0.05*). The mean percentage cytotoxicity was 107 % which was significantly elevated when compared to 0 h controls (*P < 0.0001*). When compared to with 500 µM 60 % weight/volume H_20_2 positive control there was no significance between 24 h base-type culture and the positive control (*P > 0.05*). Base-type cultures at 48 h showed slightly lower mean LDH absorbance levels which were non-significant when compared to 24 h base-type cultures (*P > 0.05*) although levels were still significantly elevated compared to 0 h uncultured controls (*P < 0.0001*). When compared to with 500 µM 60 % weight/volume H_20_2 positive control there was no significance between 48 h base-type culture and the positive control (*P > 0.05*). The mean percentage cytotoxicity was 85 % which was non-significant compared to 24 h base-type cultures (*P > 0.05*) but was significantly elevated when compared to 0 h controls (*P < 0.0001*). When compared to with 500 µM 60 % weight/volume H_20_2 positive control there was no significance between 48 h base-type cultures and the positive control (*P > 0.05*).

Trowell-type cultures, tissue sections that were embedded within the agarose plug and immediately removed (termed 0 h Trowell-type culture), showed significantly low mean LDH

absorbance values along with low mean LDH cytotoxicity at 7 %, when compared to the samples treated with 500 µM of 60 % weight/volume H_2O_2 (*P < 0.0001*, Figure 2.11 A&B).

At 24 h there was a non-significant (*P > 0.05*) increase in mean LDH absorbance when compared to 0 h Trowell-type cultures and was significantly lower compared to the 500 µM 60 % weight/volume positive controls (*P < 0.0001*, Figure 2.11A). When compared to 24 h base-type cultures there was significantly lower LDH absorbance for Trowell-type cultures (*P < 0.0001*). The mean LDH percentage cytotoxicity at 24 h Trowell-type culture was 13 % and was non-significant when compared to 0 h Trowell-type culture control (*P > 0.05*, Figure 2.11B). When compared to 24 h base-type cultures there was significantly lower LDH percentage cytotoxicity for Trowell-type cultures (*P < 0.0001*).

At 48 h there was a non-significant increase in mean LDH absorbance when compared to 24 h Trowell-type cultures (*P > 0.05* Figure 2.11A). However, there was a significant increase in LDH absorbance when compared to 0 h Trowell-type cultures (*P < 0.05*) and was significantly lower compared to the 500 µM 60 % weight/volume positive controls (*P < 0.0001*, Figure 2.11A). When compared to 48 h base-type cultures there was significantly lower LDH absorbance for 48 h Trowell-type cultures (*P < 0.0001*). The mean LDH percentage cytotoxicity at 48 h Trowell-type culture was 26 % and was non-significant when compared to 0 h Trowell-type culture control or 24 h Trowell-type culture (*P > 0.05*, Figure 2.11B). However, percentage cytotoxicity was significantly lower compared to the LDH positive controls (*P < 0.0001*, Figure 2.11B). When compared to 48 h base-type cultures there was significantly lower LDH percentage cytotoxicity for Trowell-type cultures (*P < 0.0001*).

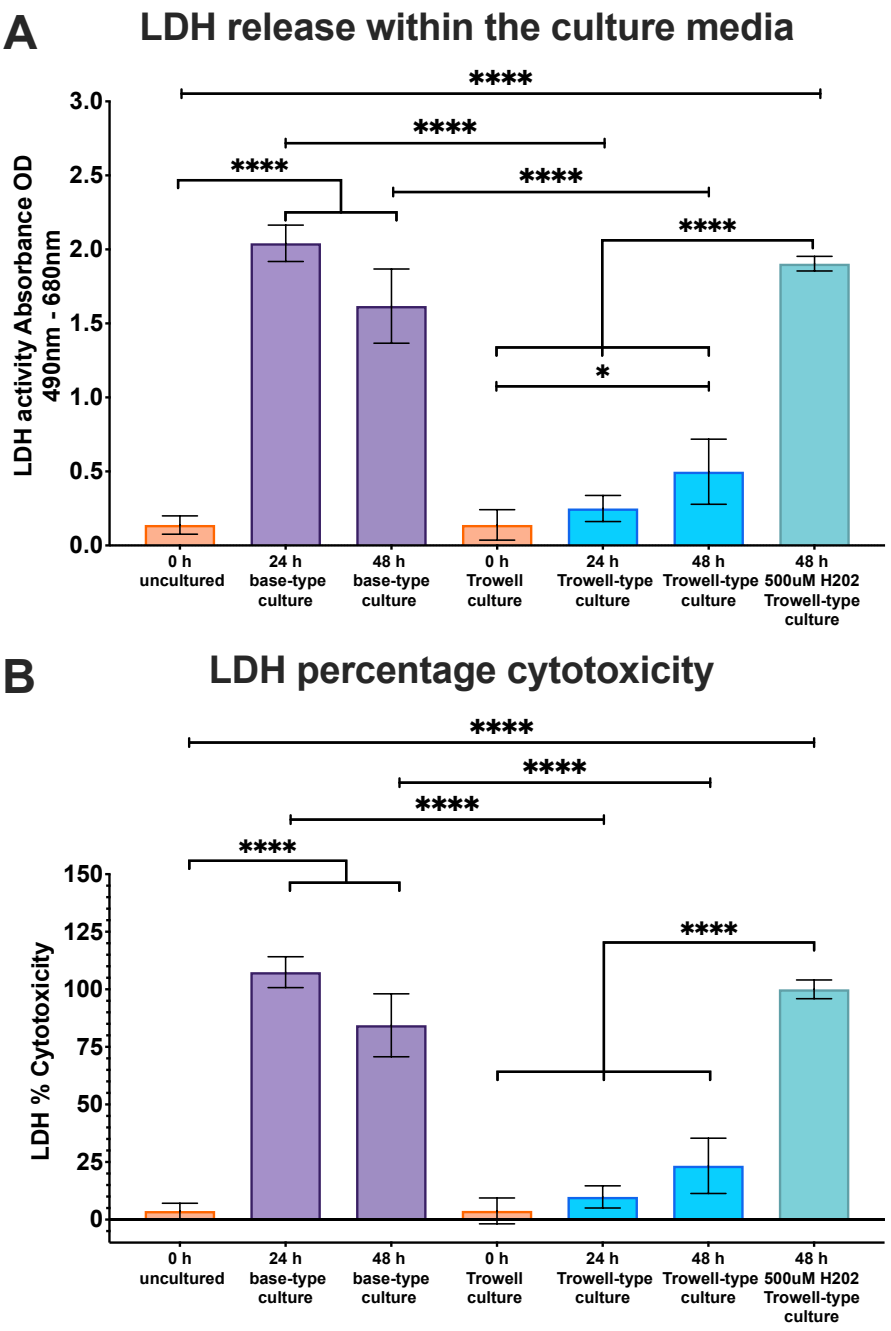

Figure 2.11: Necrosis analysis of LDH extracellular release following culture of Base- and Trowell-type cultures. Mean LDH release and percentage cytotoxicity was analysed over 0 h, 24 h and 48 h in both Trowell- and Base- type cultures. Graph A) shows the mean absorbance of extracellular LDH that has been released into surrounding culture media. Graph B) shows the mean percentage cytotoxicity of LDH for each culture method. Both graphs indicate significant increase in LDH extracellular release and percentage cytotoxicity for base-type cultures, compared to controls and Trowell-type cultures. Graphs show data for 0 h agarose embedded, 24 h and 48 h Trowell-type cultures (n=4) along with 0 h uncultured, 24 h and 48 h base-type cultures and 500 µM of 60 % weight/volume H_2O_2 (n=3). Significance between groups determined via two-way ANOVA with Tukey post-hoc test. Error bars represent mean ±S.E.M , **P<0.05 and ****P < 0.0001*.

2.3.5: Analysis of Apoptosis Cell Localisation Within Base- and Trowell-Type Culture Systems

Apoptosis localisation using immunohistochemistry was assessed in both culture systems within a 12.5 mm^2 area. Two markers of apoptosis were analysed, an early marker (cleaved caspase-3) and a late maker (BAX). The same 0 h uncultured control histology sections were used for both culture systems.

2.3.5.1: Analysis of Cleaved Caspase-3 Immunohistochemistry Localisation

Cleaved caspase-3 analysis showed low immuno-localised staining indicating reduced early apoptosis for both culture systems. At 0 h. the mean number of bone marrow cells was 401 cells, from which 66 cells were positive for cleaved caspase-3. (Figures 2.12A, 2.13A and 2.14A&B). The mean percentage of cells remaining that were stained positive for cleaved caspase-3 was 16 % (Figures 2.14C).

Tissue slices cultured at a base-type culture at 24 h showed a significantly lower number of bone marrow cells, showing a mean of 161 cells when compared to 0 h controls (*P < 0.0001*, Figure 2.12B and 2.14B). The mean number of cleaved caspase-3 stained cells at this 24 h was 32 cells, which was significantly decreased compared to 0 h controls (*P < 0.05*, Figure 2.12B and 2.14A). The mean percentage of cells remaining that were stained positive for cleaved caspase 3 was 20 %, this was non-significant when compared to 0 h controls (*P >0.05*, Figure 2.14C). Following 48 h of culture, there was a non-significant decrease for bone marrow cells showing a mean of 103 cells when compared to 24 h base-type cultures (*P > 0.05*, Figure 2.12C and 2.14B). The mean number of cleaved caspase-3 positive stained cells non-significantly decreased to 22 cells compared to 24 h base-type cultures (*P > 0.05*, Figure 2.12C and 2.14A). The mean percentage of cells remaining that were stained positive for cleaved caspase 3 was 29 % and was significantly increased when compared to 0 h controls (*P < 0.05*) and non-significantly increased compared to 24 h base-type cultures (*P > 0.05*, Figure 2.14C).

Tissue slices cultured at a Trowell-type culture at 24 h showed a significantly lower number of bone marrow cells representing a mean of 133 cells when compared to 0 h controls (*P < 0.0001*, Figure 2.13B and 2.14B). The mean number of cleaved caspase-3 stained cells at 24

h was 20 cells, which was significantly lower compared to 0 h controls (*P < 0.001,* Figure 2.13B and 2.14A). The mean percentage of cells remaining that were stained positive for cleaved caspase 3 at 24 h was 13 % and was non-significant when compared to 0 h controls (*P > 0.05*, Figure 2.14C). Following 48 h of culture, there was a non-significant decrease for bone marrow cells showing a mean of 84 cells when compared to 24 h Trowell-type cultured samples (*P > 0.05*, Figure 2.13C and 2.14B). The mean number of cleaved caspase-3 positive stained cells at 48 h was 7 cells and was non-significant compared to 24 h Trowell-type cultures (*P < 0.05*, Figure 2.13C and 2.14A). The mean percentage of cells remaining that were stained positive for cleaved caspase 3 was 7.4 % and was non-significantly lower when compared to 24 h Trowell-type cultures (*P > 0.05*) and 0 h controls (*P < 0.0001*, Figure 2.14C).

There was no significant difference in the mean number of bone marrow cells at either 24 h or 48 h between either culture system (*P > 0.05*). There was no significant difference in the mean number of cells stained positive for cleaved caspase-3 in either culture system at 24 h or 48 h (*P > 0.05*). There was no significant difference in the percentage number of cells stained positive for cleaved caspase-3 in either culture system at 24 h (*P > 0.05*) but showed a significant difference at 48 h (*P < 0.01*).

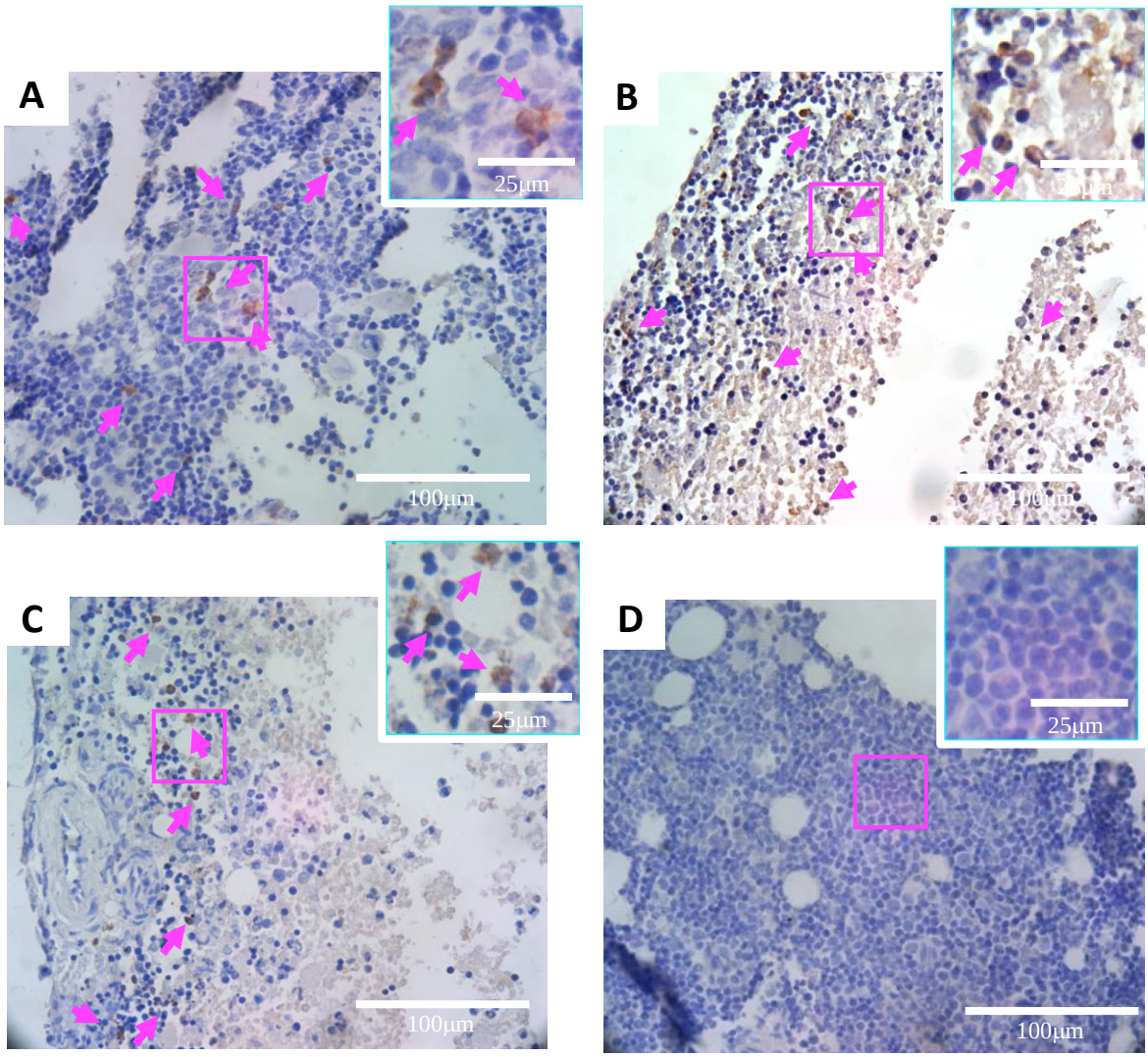

Figure 2.12: Base-type cultures stained for cleaved caspase-3. Immunohistochemistry staining for cleaved caspase-3 labelled antibodies within the bone marrow of base-type cultures. A) 0 h uncultured controls, B) 24 h cultures, C) 48 h cultures and D) a negative control by omitting the primary antibody and staining only the secondary antibody. Images show a reduction in cleaved caspase-3 positive staining over 48 h. 50 µm boxes display magnified areas of the bone marrow with positive cell labelling (examples indicated by arrows).

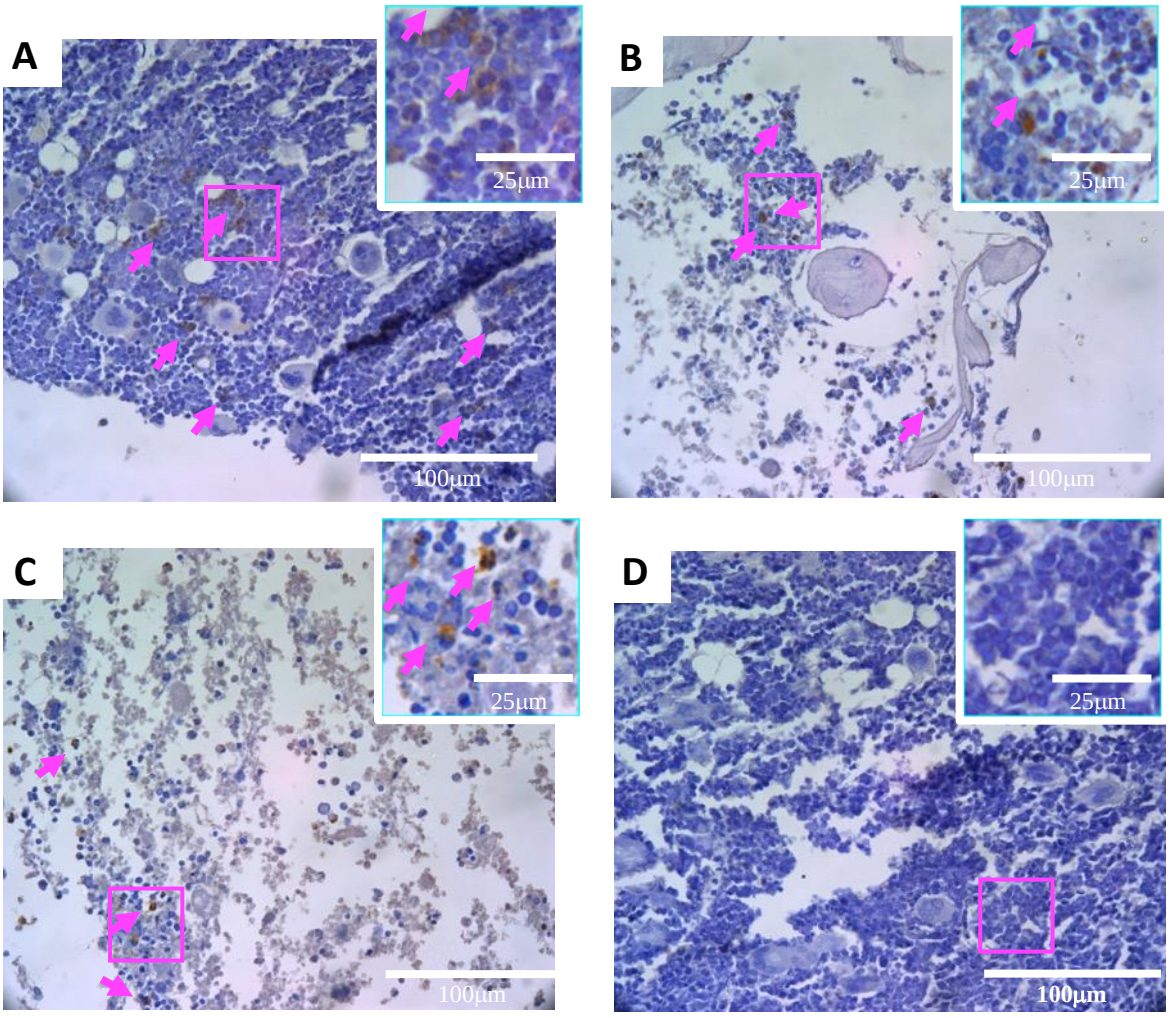

Figure 2.13: Trowell--type cultures stained for cleaved caspase-3. Immunohistochemistry staining for cleaved caspase-3 labelled antibodies within the bone marrow of Trowell-type cultures. A) 0 h uncultured controls, B) 24 h cultures, C) 48 h cultures and D) a negative control by omitting the primary antibody and staining only the secondary antibody. Images show a reduction in cleaved caspase-3 positive staining over 48 h. 50 µm boxes display magnified areas of the bone marrow with positive cell labelling (examples indicated by arrows).

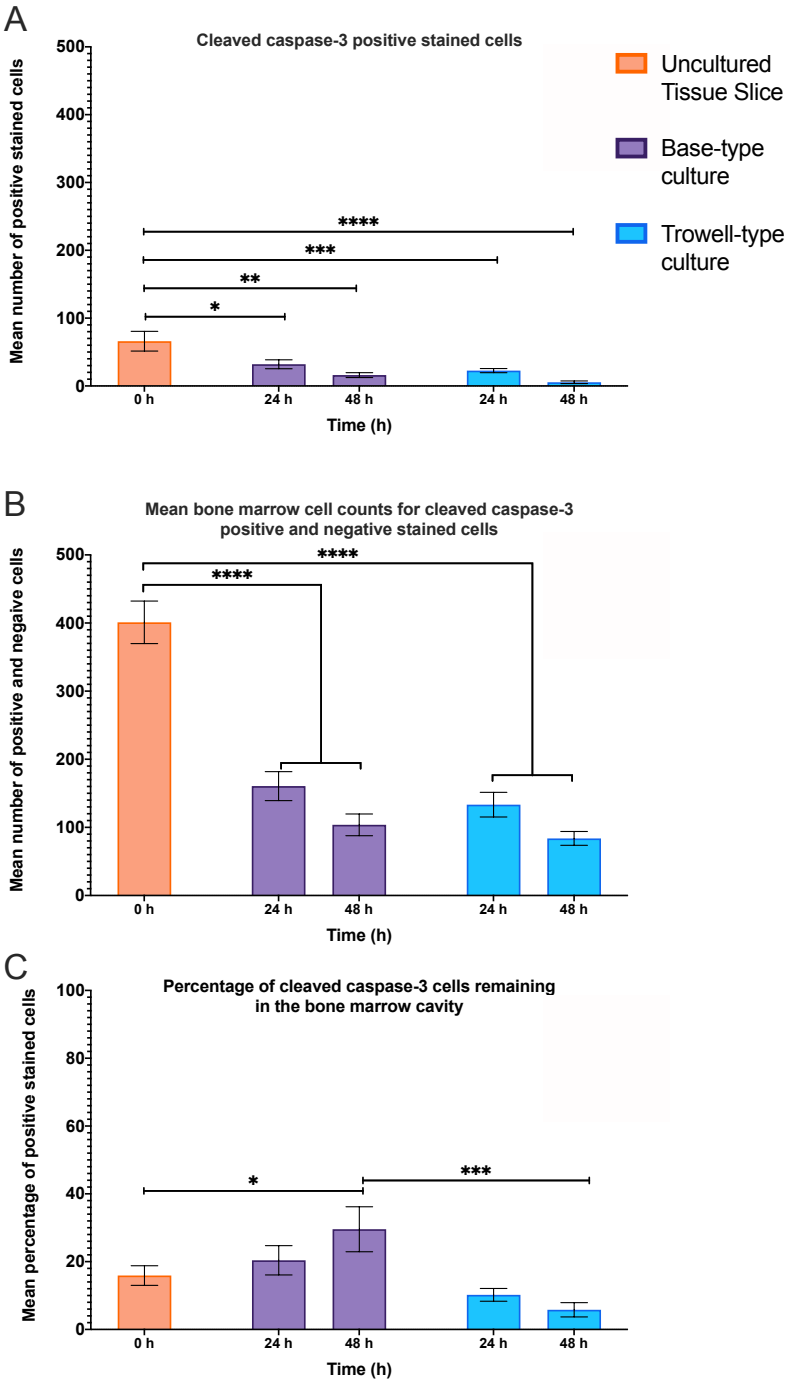

Figure 2.14: Cleaved caspase-3 stained cells in base and Trowell-type cultures. Immunohistochemical analysis for cleaved caspase-3 labelled antibodies within the bone marrow for 0 h uncultured controls, 24 h and 48 h Base-type cultures and Trowell-type cultures. Graph A) showing data for mean cell counts for cleaved caspase-3 positive stained cells. Graph B) shows mean cell counts for both cleaved caspase-3 positive and negative stained cells. Graph C) showing the mean percentage of cleaved caspase-3 positive stained cells remaining in the bone marrow cavity. Both culture systems show a loss of both bone marrow cells and cleaved caspase-3 stained cells following 24 h and 48 h in culture. There was no difference in the number of cleaved caspase-3 stained cells between either culture systems at 24 h or 48 h. Percentage of stained cells were higher for base-type cultures at 48 h than Trowell-type cultures. Significance within groups determined via one-way ANOVA and between groups determined via two-way ANOVA with Tukey post-hoc test. Error bars represent mean ±S.E.M (N=3), *****P < 0.0001*.

2.3.5.2: Analysis of BAX Immunohistochemistry Localisation

In comparison to cleaved caspase-3, there was higher immunolocalisation of BAX, indicating an increase in cells actively undergoing or concluding the apoptotic process. At 0 h. the mean number of bone marrow cells was 375 cells, from which 311 cells were positive for BAX. (Figures 2.15A, 2.16A and 2.17A&B). The mean percentage of cells remaining that were stained positive for BAX was 84 % (Figures 2.17C).

Tissue slices cultured at a base-type culture at 24 h showed a significantly lower number of bone marrow cells, showing a mean of 131 cells when compared to 0 h controls (*P < 0.0001*, Figure 2.15B and 2.17B). The mean number of BAX stained cells at this 24 h was 56 cells, which was significantly decreased compared to 0 h controls (*P < 0.0001*, Figure 2.15B and 2.17A). The mean percentage of cells remaining that were stained positive for BAX was 47 %, this was significantly decreased when compared to 0 h controls (*P < 0.0001*, Figure 2.17C). Following 48 h of culture, there was a non-significant decrease for bone marrow cells showing a mean of 112 cells when compared to 24 h base-type cultures (*P > 0.05*, Figure 2.15C and 2.17B). The mean number of BAX positive stained cells non-significantly decreased to 54 cells compared to 24 h base-type cultures (*P > 0.05*, Figure 2.15C and 2.17A). The mean percentage of cells remaining that were stained positive for cleaved caspase 3 was 50 % and was significantly decreased when compared to 0 h controls (*P < 0.0001*) and non-significantly increased compared to 24 h base-type cultures (*P > 0.05*, Figure 2.17C).

Tissue slices cultured at a Trowell-type culture at 24 h showed a significantly lower number of bone marrow cells representing a mean of 143 cells when compared to 0 h controls (*P < 0.0001*, Figure 2.16B and 2.17B). The mean number of BAX stained cells at 24 h was 68 cells, which was significantly decreased when compared to 0 h controls (*P < 0.0001,* Figure 2.16B and 2.17A). The mean percentage of cells remaining that were stained positive for BAX at 24 h was significantly decreased to 48 % and when compared to 0 h controls (*P < 0.0001*, Figure 2.17C). Following 48 h of culture, there was a non-significant decrease for bone marrow cells showing a mean of 80 cells when compared to 24 h Trowell-type cultured samples (*P > 0.05*, Figure 2.16C and 2.17B). The mean number of BAX positive stained cells

at 48 h was 40 cells and was non-significant compared to 24 h Trowell-type cultures ($P < 0.05$, Figure 2.16C and 2.17A). The mean percentage of cells remaining that were stained positive for BAX was 57 % and was non-significantly higher when compared to 24 h Trowell-type cultures ($P > 0.05$) and significantly lower when compared to 0 h controls ($P < 0.0001$, Figure 2.17C).

There was no significant difference in the mean number of bone marrow cells at either 24 h or 48 h between either culture system ($P > 0.05$). There was no significant difference in the mean number of cells stained positive for BAX in either culture system at 24 h or 48 h ($P > 0.05$). There was no significant difference in the percentage number of cells stained positive for BAX in either culture system at 24 h or 48 h ($P > 0.05$).

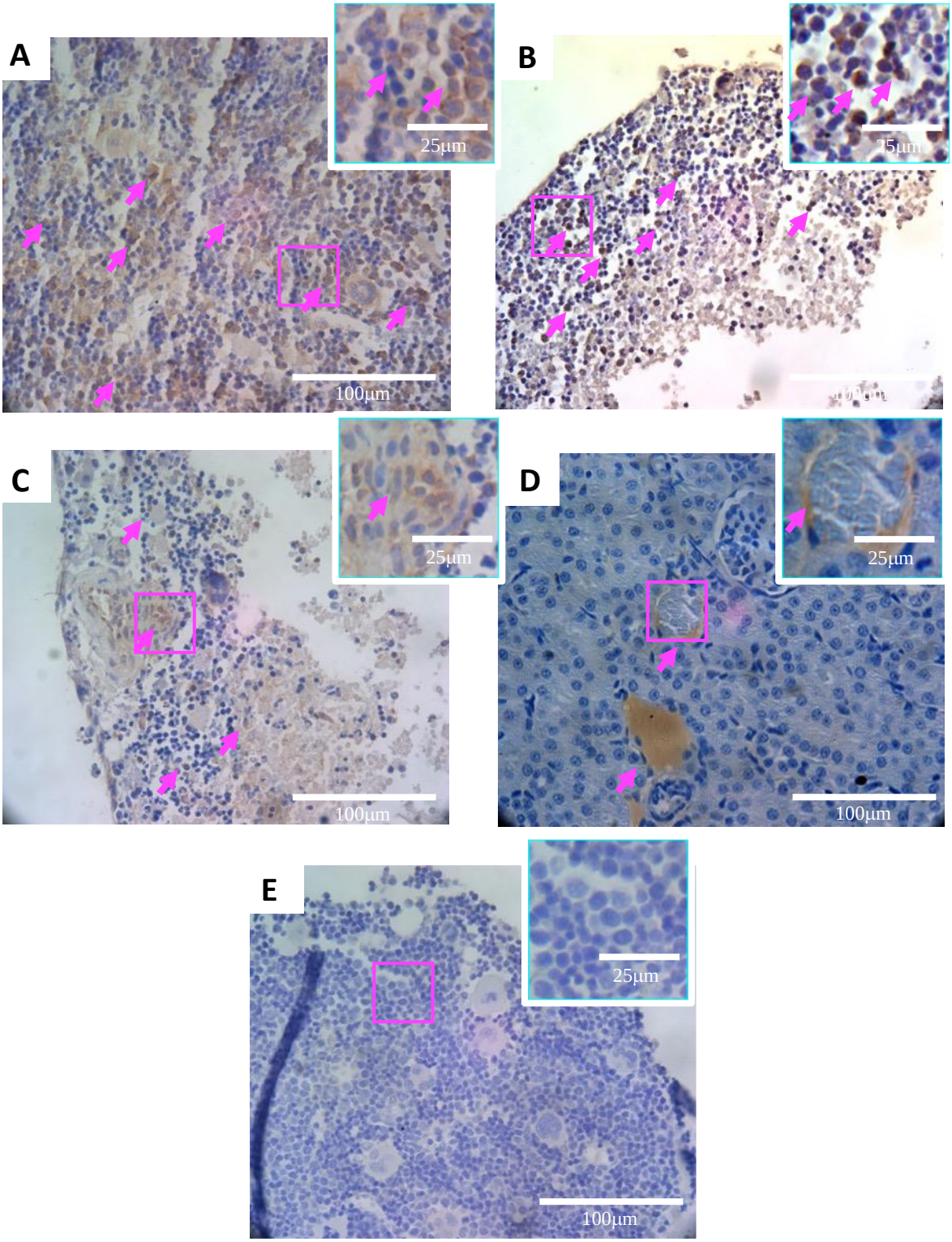

Figure 2.15: Base-type cultures stained for BAX. Immunohistochemistry staining for BAX labelled antibodies within the bone marrow of base-type cultures. A) 0 h uncultured controls, B) 24 h cultures, C) 48 h cultures, D) rat kidney positive control and E) negative control by omitting the primary antibody and staining only the secondary antibody. Images show a reduction in BAX positive staining over 48 h. 50 µm boxes display magnified areas of the bone marrow with positive cell labelling (examples indicated by arrows).

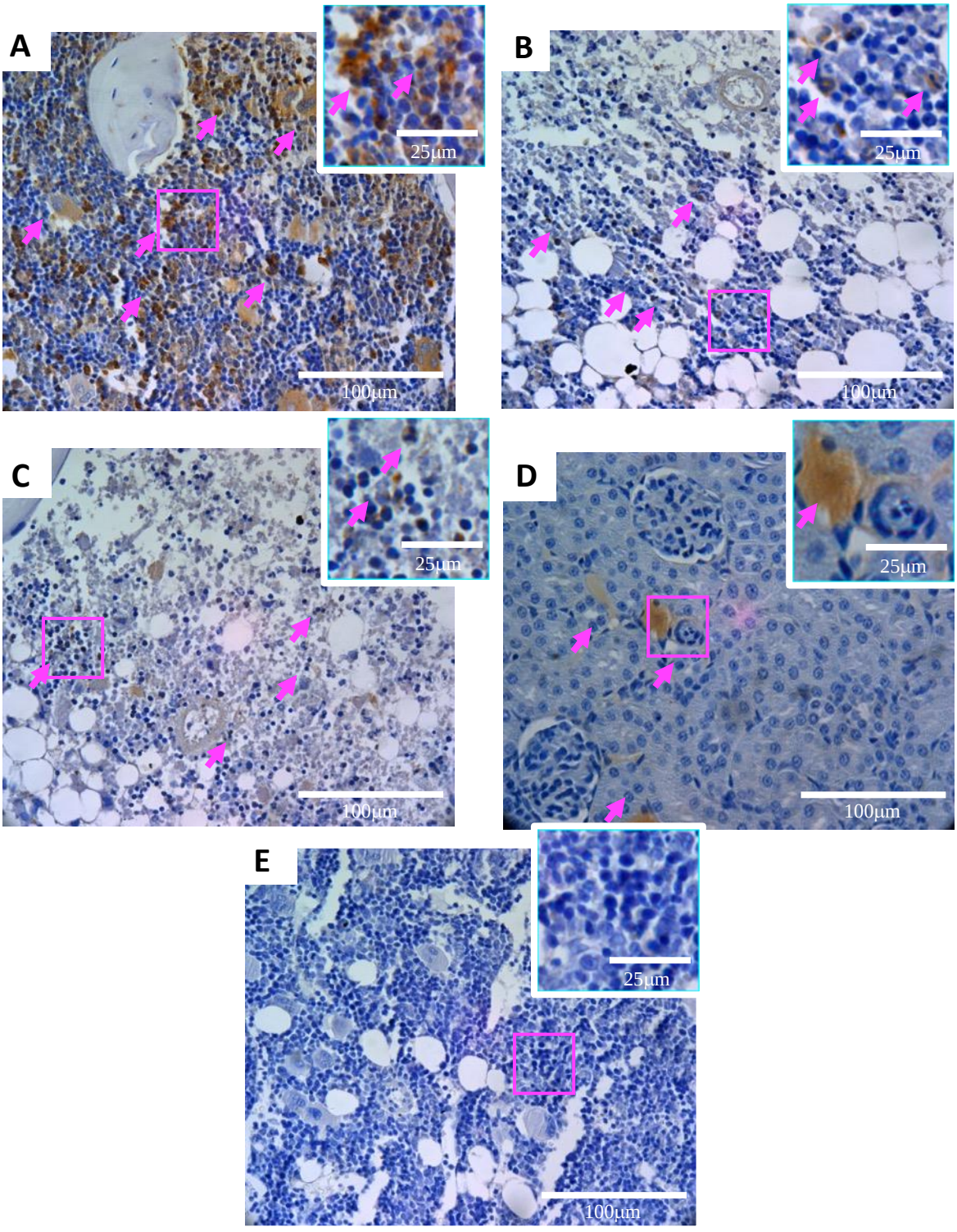

Figure 2.16: Trowell-type culture stained for BAX. Immunohistochemistry staining for BAX labelled antibodies within the bone marrow from Trowell-type cultures. A) 0 h uncultured controls, B) 24 h cultures, C) 48 h cultures, D) rat kidney positive control and E) negative control by omitting the primary antibody and staining only the secondary antibody Images show a reduction in BAX positive staining over 48 h. 50 µm boxes display magnified areas of the bone marrow with positive cell labelling (examples indicated by arrows

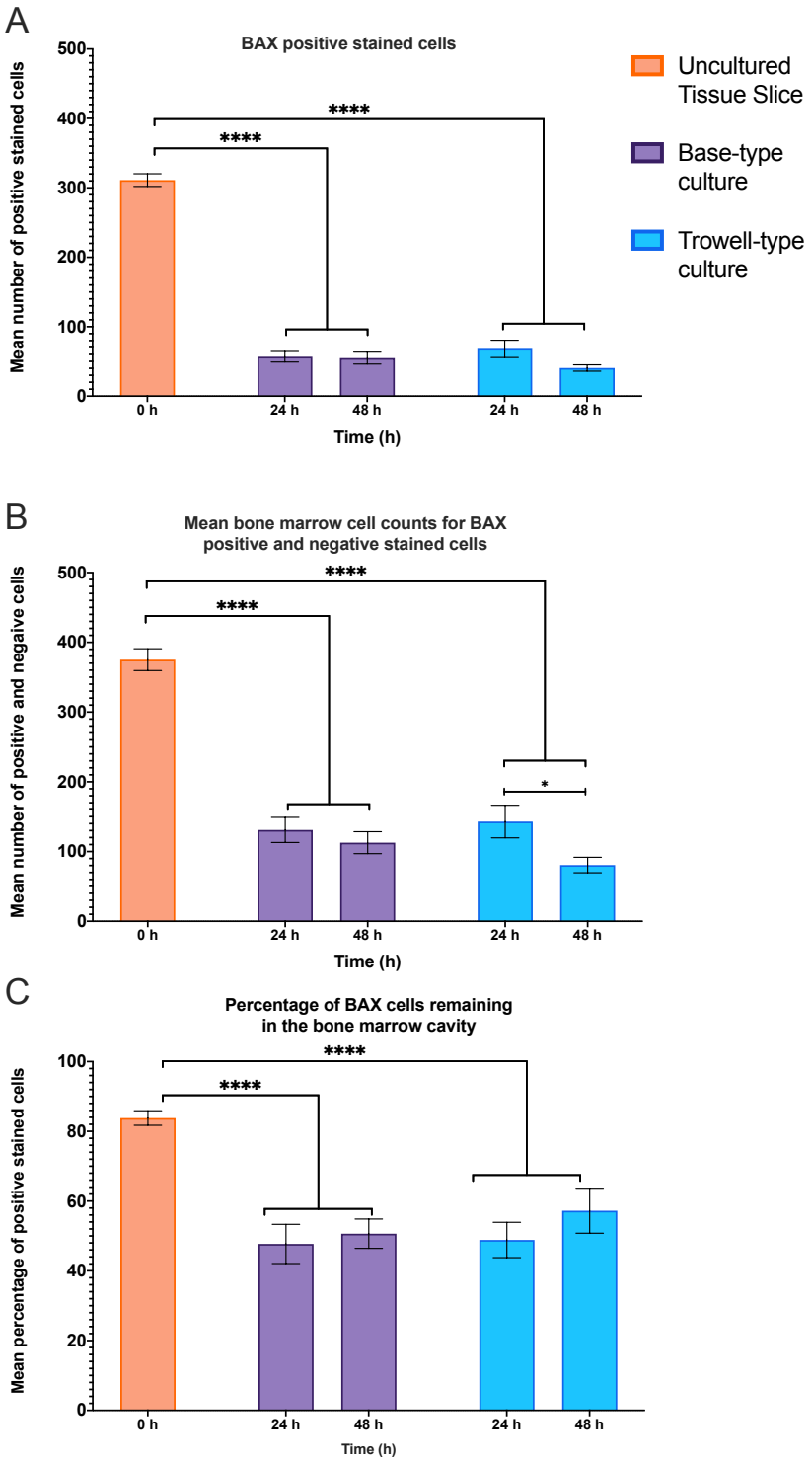

Figure 2.17: BAX stained cells in base and Trowell-type cultures. Immunohistochemical analysis for BAX-labelled antibodies within the bone marrow for 0 h uncultured controls, 24 h and 48 h Base-type cultures and Trowell-type cultures. Graph A) showing data for mean cell counts for BAX positive stained cells. Graph B) shows mean cell counts for both BAX positive and negative stained cells. Graph C) showing the mean percentage of BAX positive stained cells remaining in the bone marrow cavity. Both culture systems show a loss of both bone marrow cells and BAX stained cells following 24 h and 48 h in culture. There was no difference in the number or percentage of BAX stained cells between either culture systems at 24 h or 48 h. Significance within groups determined via one-way ANOVA and between groups determined via two-way ANOVA with Tukey post-hoc test. Error bars represent mean ±S.E.M (N=3), ** $P < 0.05$* and *****$P < 0.0001$*.

2.3.6: Immunohistochemical Detection of Bone Marrow Immune Cells Within the Trowell-Type Cultures Over 48 h

Due to reduced levels of necrosis and significantly improved cell number of bone marrow cells during Trowell-type cultures when compared to base-type cultures, the Trowell-type cultures were taken forward for detection of immune cells and mesenchymal stromal cells.

2.3.6.1: Immunohistochemical Detection of CD14 Cells

Immuno-detection of immune cells targeting monocytes were undertaken in Trowell-type cultures over 48 h, using the CD14 myeloid cell marker, within a 12.5 mm^2 area. At 0 h. the mean number of bone marrow cells was 349 cells, from which 192 cells were positive for CD14 (Figures 2.18A and 2.22A&B). The mean percentage of cells remaining that were stained positive for CD14 at 0 h was 54 % (Figure 2.22C). At 24 h there was a significant decrease in the number of bone marrow cells representing a mean of 107 cells when compared to 0 h controls (*P < 0.0001*, Figure 2.18B and 2.22B). The mean number of CD14 stained cells at 24 h was 60 cells, which was significantly decreased when compared to 0 h controls (*P < 0.0001,* Figure 2.18B and 2.22A). The mean percentage of cells remaining that were stained positive for CD14 at 24 h was 51 % and was non-significant when compared to 0 h uncultured controls (*P > 0.05*, Figure 2.22C). Following 48 h of culture, there was a non-significant decrease for bone marrow cells showing a mean of 82 cells when compared to 24 h Trowell-type cultured samples (*P > 0.05*, Figure 2.18C and 2.22B). The mean number of CD14 positive stained cells at 48 h non-significantly decreased to 47 cells when compared to 24 h cultures (*P > 0.05*, Figure 2.18C and 2.22A). The mean percentage of cells remaining that were stained positive for CD14 at 48 h was non-significantly increased to 59 % when compared to 0 h uncultured control or 24 h (*P > 0.05*, Figure 2.22C).

2.3.6.2: Immunohistochemical Detection of CD68 Cells.

Trowell-type cultured tissue sections were stained using the pan monocyte, macrophage and osteoclast marker, CD68 within a 12.5 mm^2 area. At 0 h. the mean number of bone marrow cells was 251 cells, from which 15 cells were positive for CD68 (Figures 2.19A and

2.22A&B). The mean percentage of cells remaining that were stained positive for CD68 at 0 h was 9 % (Figure 2.22C). Here, there was clear immunolocalisation within the bone marrow cavity, with both small cells and large multinucleated osteoclast-like cells could be observed near the cortical or trabecular hard tissue, though when compared to CD14 cells, the number of stained CD68 cells was reduced (Figure 2.19A). At 24 h there was a significant decrease in the number of bone marrow cells representing a mean of 85 cells when compared to 0 h controls (*P < 0.0001*, Figure 2.18B and 2.22B). The mean number of CD68 stained cells at 24 h was 20 cells, which was non-significantly increased when compared to 0 h controls (*P > 0.05,* Figure 2.19B and 2.22A). The mean percentage of cells remaining that were stained positive for CD68 at 24 h was significantly increased to 20 % when compared to 0 h uncultured controls (*P < 0.05*, Figure 2.22C). Following 48 h of culture, there was a non-significant increase for bone marrow cells showing a mean of 98 cells when compared to 24 h Trowell-type cultured samples (*P > 0.05*, Figure 2.19C and 2.22B). The mean number of CD68 positive stained cells at 48 h non-significantly increased to 30 cells when compared to 24 h cultures (*P > 0.05*, Figure 2.19C and 2.22A). The mean percentage of cells remaining that were stained positive for CD68 at 48 h was non-significantly higher at 26 % when compared to 24 h (*P > 0.05*) and significantly higher compared to 0 h controls (*P < 0.001*, Figure 2.22C).

Specific cellular counts for large multinucleated CD68 positive cells with more than three nuclei were very few. At 0 h uncultured controls only 2 large multinucleated CD68 positive cells were seen (Figure 2.19A and 2.22A). The mean percentage of multinucleated cells remaining that were stained positive for CD68 at 0 h was 3 % (Figure 2.22C). At 24 h the mean number of CD68 multinucleated cells was decreased to 1 cell, this was non-significant when compared to 0 h controls (*P > 0.05*, Figure 2.19B and 2.22A). The mean percentage of multinucleated cells remaining that were stained positive for CD68 at 24 h was 3 %, this was non-significant when compared to 0 h controls (*P > 0.05*, Figure 2.22C). At 48 h the number of positive CD68 multinucleated cells were maintained at 1 cell, this was non-significant when compared to 0 h and 24 h samples (*P > 0.*05, Figure 2.19C and 2.22A). The mean percentage of multinucleated cells remaining that were stained positive for CD68 at 48 h was non-significantly lower at 1 %, when compared to 24 h and 0 h controls (*P > 0.05*, Figure 2.22C).

2.3.6.3: Detection of Trap Positive Multinucleated Osteoclast-Like Cells

TRAP analysis was used to observe large multinucleated osteoclasts within the tissue sections per 12.5 mm^2 area. Cellular counts for TRAP stained tissues concur with CD68 results. Large multinucleated osteoclast-like cells were attached towards the cortical or trabecular tissue at a high number (although significantly lower than the positive control, $P < 0.01$), the mean number of TRAP positive cells was 5 cells at 0 h (Figure 2.20 A&E). These results were similar to CD68 stained cells, where large multinucleated cells were completely lost following 24 h and 48 h culture with no positive stained cells observed (Figures 2.20B, C & E).

2.3.6.4: Immunohistochemical Detection of Neutrophils

Immuno-detection of neutrophils was undertaken in Trowell-type cultures over 48 h, using the neutrophil elastase cell marker, within a 12.5 mm^2 area. At 0 h. the mean number of bone marrow cells was 459 cells, from which 296 cells were positive for neutrophil elastase (Figures 2.21A and 2.22A&B). The mean percentage of cells remaining that were stained positive for neutrophil elastase at 0 h was 65 % (Figure 2.22C). Following 24 h and 48 h in culture, there was a large amount of background staining observed, not present in 0 h uncultured controls (Figure 2.21 B&C). At 24 h there was a significant decrease in the number of bone marrow cells representing a mean of 179 cells when compared to 0 h controls ($P < 0.0001$, Figure 2.21B and 2.22B). The mean number of neutrophil elastase stained cells at 24 h was 89 cells, which was significantly decreased when compared to 0 h controls ($P < 0.0001$, Figure 2.21B and 2.22A). The mean percentage of cells remaining that were stained positive for neutrophil elastase at 24 h was non-significantly lower at 49 % when compared to 0 h uncultured controls ($P > 0.05$, Figure 2.22C). Following 48 h of culture, there was a significant decrease for bone marrow cells showing a mean of 92 cells when compared to 24 h Trowell-type cultured samples ($P < 0.05$, Figure 2.21C and 2.22B). The mean number of neutrophil elastase positive stained cells at 48 h significantly decreased to 33 cells when compared to 24 h cultures ($P > 0.001$, Figure 2.21C and 2.22A). The mean

percentage of cells remaining that were stained positive for neutrophil elastase at 48 h was significantly lower at 40 % when compared to 24 h ($P < 0.05$) and 0 h controls ($P < 0.001$, Figure 2.22C).

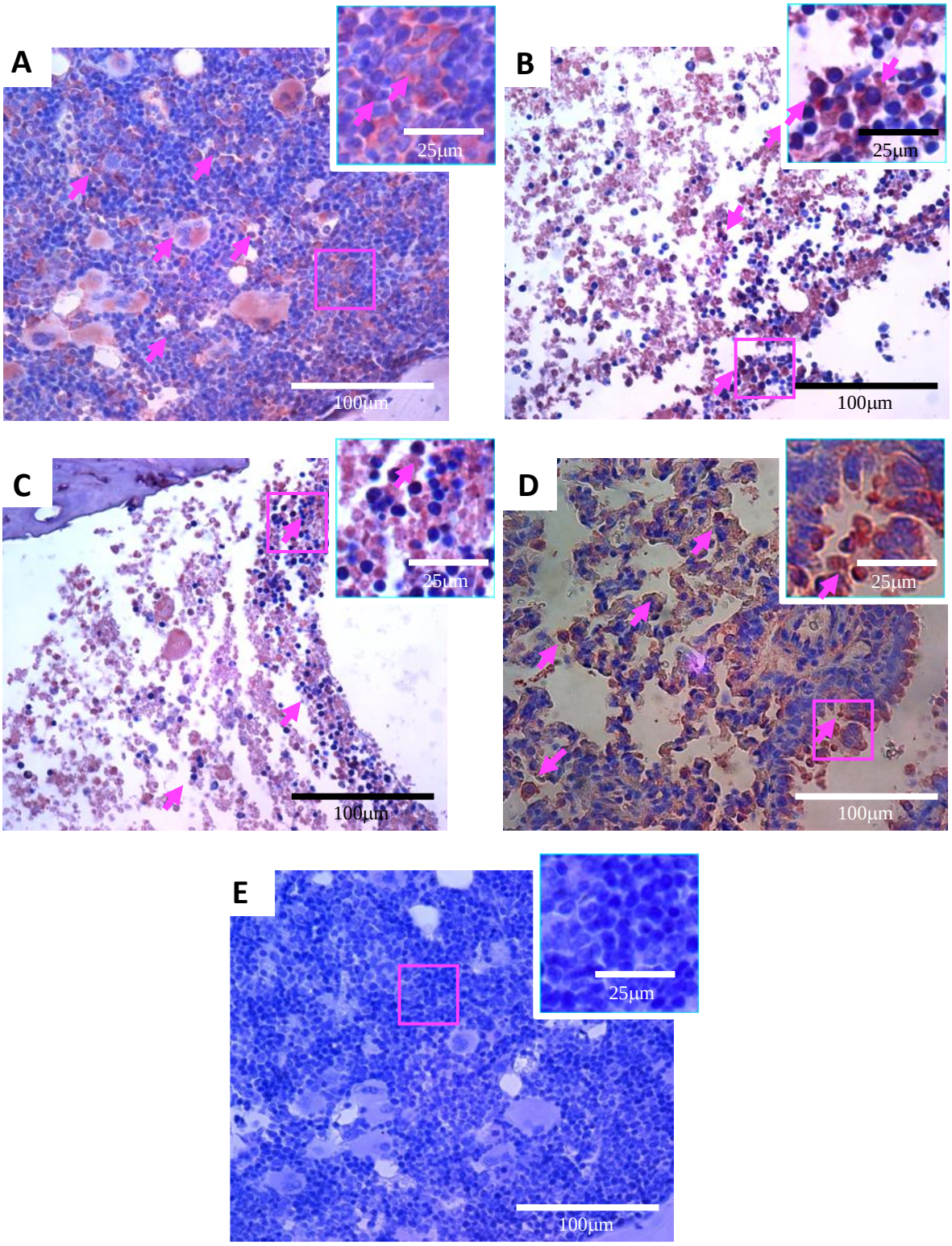

Figure 2.18: Trowell-type cultures stained for CD14. Representative images of immunohistochemistry stained $CD14^{+}$ labelled monocytes and macrophages within the bone marrow from Trowell-type cultures (examples indicated by arrows). A) 0 h uncultured controls, B) 24 h cultures, C) 48 h cultures, D) lung positive control and E) negative control by omitting the primary antibody and staining only the secondary antibody.

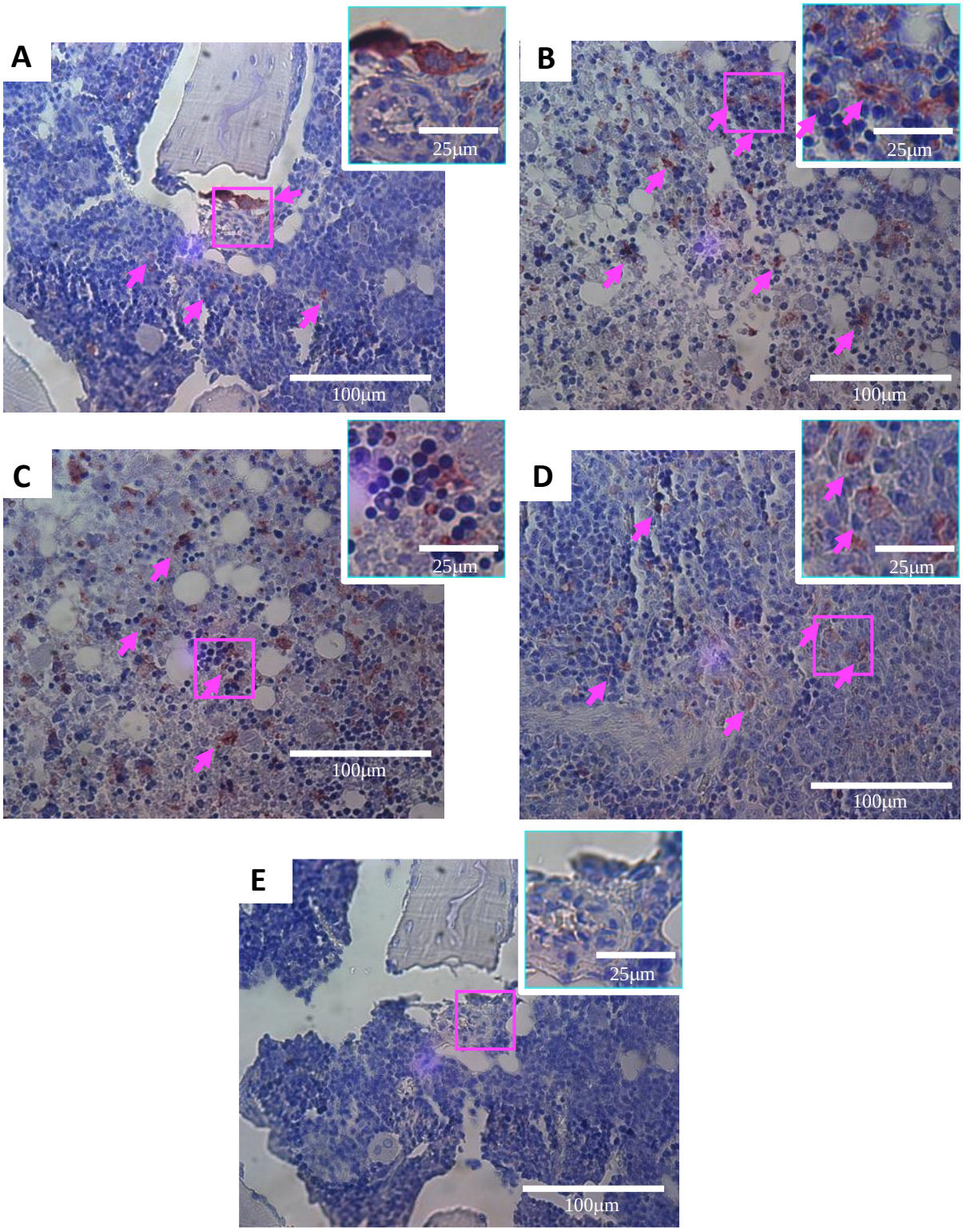

Figure 2.19: Trowell-type cultures stained with CD68. Representative images of immunohistochemistry stained CD68⁺ labelled cells within the bone and the bone marrow from Trowell-type cultures (examples indicated by arrows). A) 0 h uncultured controls, B) 24 h cultures, C) 48 h cultures, D) spleen positive control and E) negative control by omitting the primary antibody and staining only the secondary antibody.

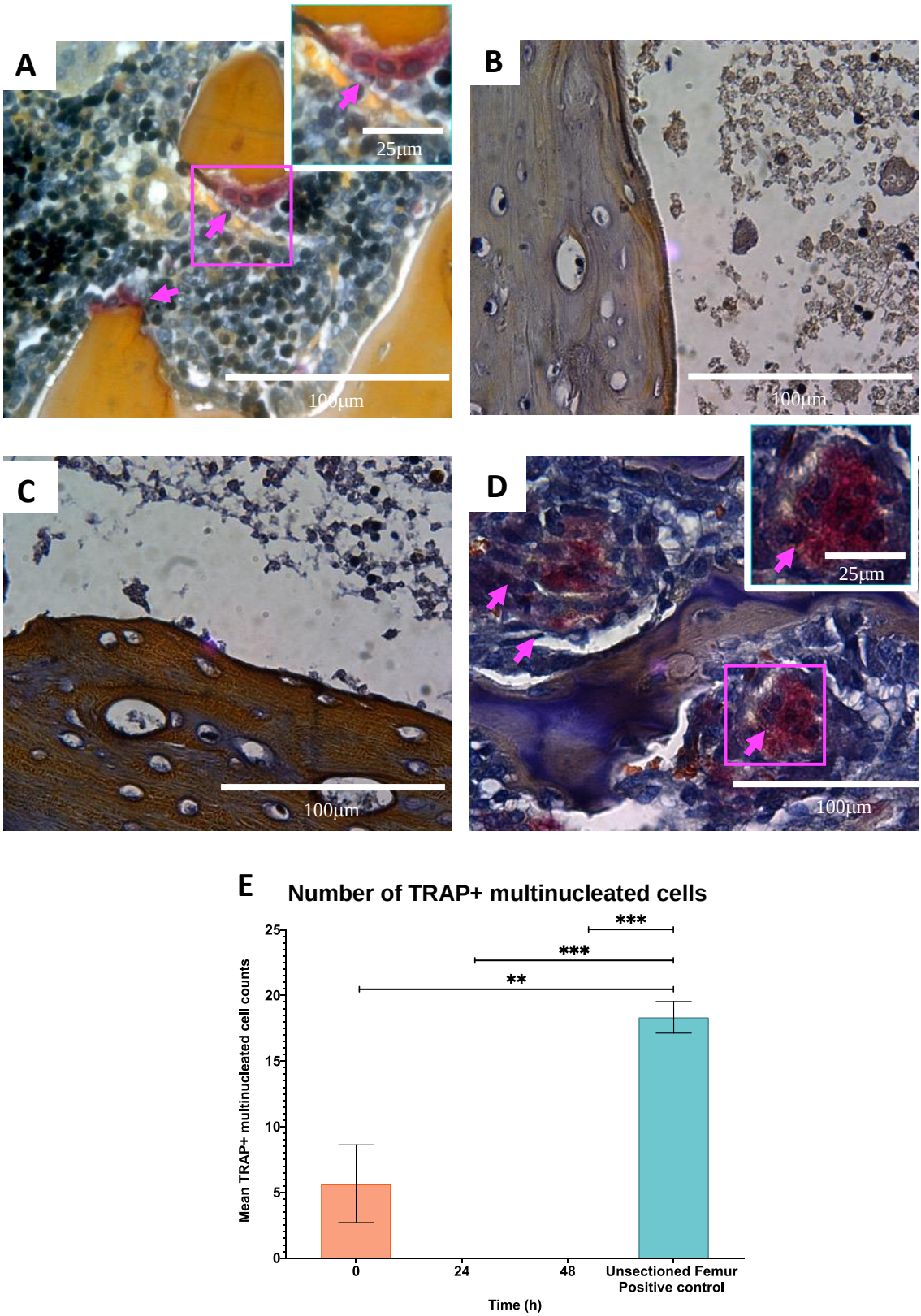

Figure 2.20: Trowell-type cultures stained for tartrate-resistant acid phosphatase positive osteoclasts. Representative images of TRAP$^+$ stained cells within the cortical bone and the bone marrow from Trowell-type cultures (examples indicated by arrows). A) 0 h uncultured controls, B) 24 h cultures, C) 48 h cultures, D) whole unsectioned femur positive control and E) mean cell counts of IHC images of TRAP$^+$ labelled cells. Graph and images show a reduction in TRAP$^+$ staining over 48 h. Significance within groups determined via one-way ANOVA. Error bars represent mean ±S.E.M (n=3), ** $P < 0.01$ and ***$P < 0.001$.

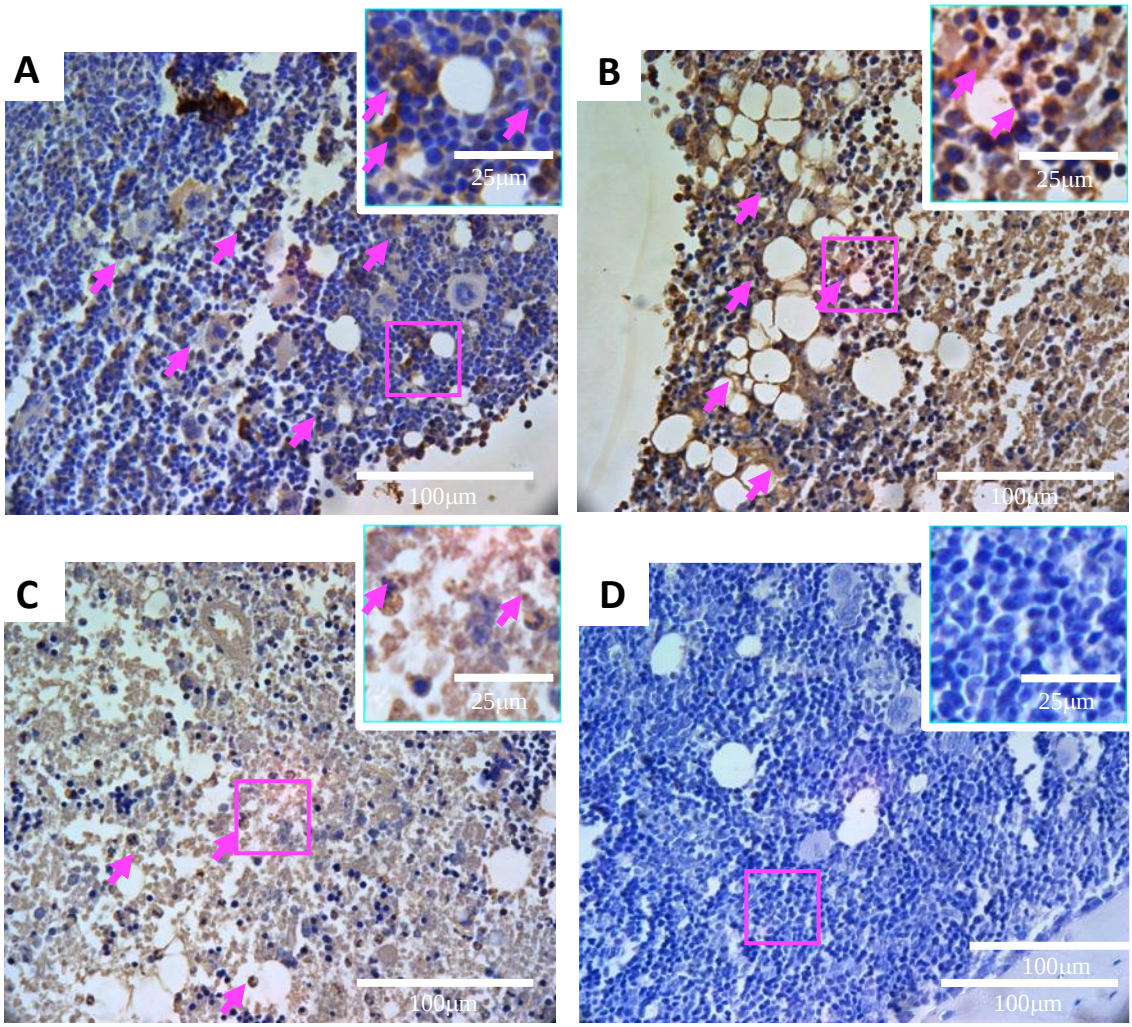

Figure 2.21: Trowell-type cultures stained with neutrophil elastase. Representative images of immunohistochemistry stained neutrophil cells with neutrophil elastase antibody within the bone marrow from Trowell-type cultures (examples indicated by arrows). A) 0 h uncultured controls, B) 24 h cultures, C) 48 h cultures and D) negative control by omitting the primary antibody and staining only the secondary antibody control.

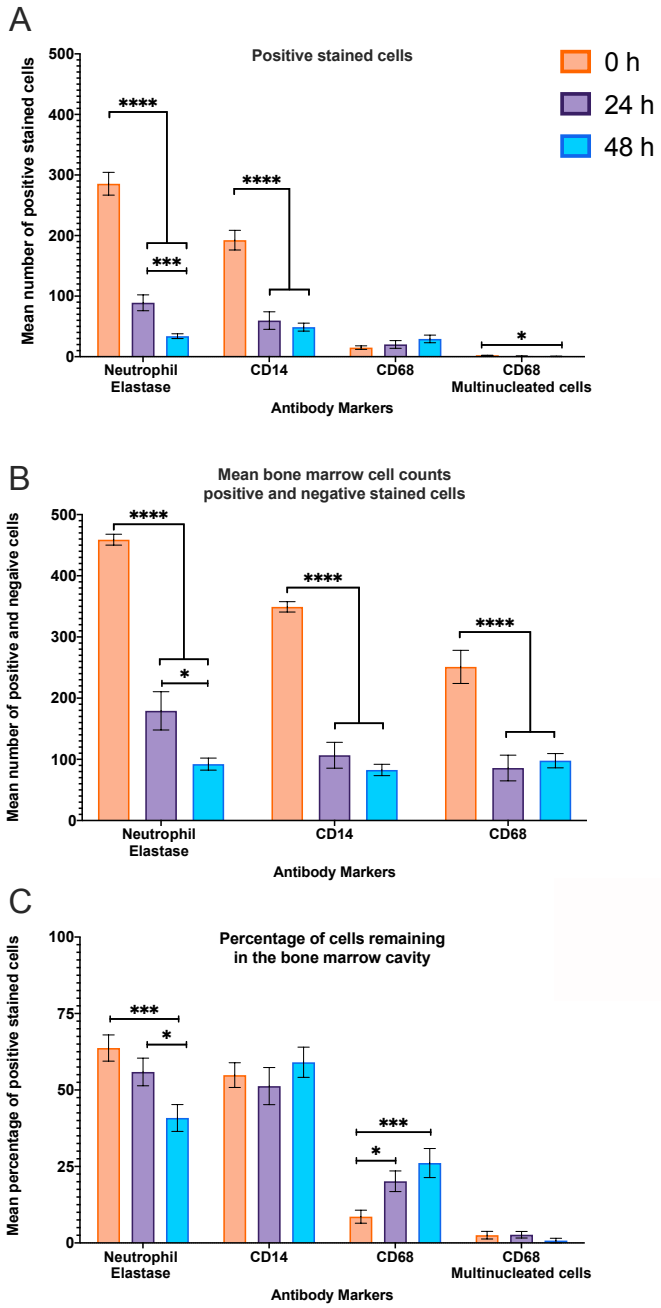

Figure 2.22: Immunolocalisation of immune cells in Trowell-type cultures. Immunolocalisation of Trowell-type cultures stained with markers to identify neutrophils (neutrophil elastase), myeloid precursors including monocytes and macrophages (CD14), macrophages and multinucleated osteoclast-like cells (CD68). Graph A) showing data for mean cell counts for positive stained cells. Graph B) shows mean cell counts for both positive and negative stained cells. Graph C) showing the mean percentage of positive stained cells remaining in the bone marrow cavity. Graphs show mean bone marrow cell loss over 48 h in culture. There was loss of cells stained for neutrophil elastase, CD14 and multinucleated CD68 stained cells over 48 h in culture. There was maintenance of CD68 stained cells over 48 h. Percentage analysis show maintenance of CD14 cells despite loss of positive stained cell numbers along with increase in CD68 cells over 48 h. Significance within groups determined via one-way ANOVA with Tukey post-hoc test. Error bars represent mean ±S.E.M (n=3), *$P < 0.05$, **$P < 0.01$, ***$P < 0.001$ and ****$P < 0.0001$

2.3.7: Immunohistochemical Detection of Bone Marrow Multipotent Mesenchymal Stromal Cell Markers Within the Trowell-Type Culture Over 48 h.

To identify mesenchymal stromal cells, immunohistochemical localisation of CD73, CD90 and CD105 was undertaken in Trowell-type cultures within a 12.5 mm^2 area. At 0 h. the mean number of bone marrow cells was 341 cells, from which 244 cells were positive for CD72 (Figures 2.23A and 2.26A&B). The mean percentage of cells remaining that were stained positive for CD73 at 0 h was 71 % (Figure 2.26C). At 24 h there was a significant decrease in the number of bone marrow cells representing a mean of 116 cells when compared to 0 h controls (*P < 0.0001*, Figure 2.23B and 2.26B). The mean number of CD73 stained cells at 24 h was 98 cells, which was significantly decreased compared to 0 h controls (*P > 0.05,* Figure 2.23B and 2.26A). The mean percentage of cells remaining that were stained positive for CD73 at 24 h was non-significantly increased to 81 % when compared to 0 h controls (*P > 0.05*, Figure 2.26C). At 48 h, there was a non-significant decrease for bone marrow cells showing a mean of 91 cells when compared to 24 h cultured samples (*P > 0.05*, Figure 2.19C and 2.22B). The mean number of CD73 positive stained cells at 48 h non-significant decrease to 78 cells when compared to 24 h cultures (*P > 0.05*, Figure 2.23C and 2.26A). The mean percentage of cells remaining that were stained positive for CD73 cells at 48 h was non-significant at 83 % when compared to 24 h or 0 h controls (*P > 0.05*, Figure 2.26C). This indicates that though the numbers of CD73 stained cells are reduced during culture, compared to the rest of the cells in the bone marrow, these cells are one of the main cell markers remaining over 48 h.

Similar immunolocalisation was observed for CD105 stained cells with higher levels of staining seen over 48 h. At 0 h. the mean number of bone marrow cells was 357 cells, from which 227 cells were positive for CD105 (Figures 2.24A and 2.26A&B). The mean percentage of cells remaining that were stained positive for CD105 at 0 h was 64 % (Figure 2.26C). At 24 h there was a significant decrease in the number of bone marrow cells representing a mean of 145 cells when compared to 0 h controls (*P < 0.0001*, Figure 2.24B and 2.26B). The mean number of CD105 stained cells at 24 h was 37 cells, which was significantly decreased when compared to 0 h controls (*P > 0.05,* Figure 2.24B and 2.26A). The mean percentage of cells remaining that were stained positive for CD105 at 24 h was significantly decreased to 37 % when compared to 0 h controls (*P < 0.001*, Figure 2.26C). At 48 h, there was a

significant decrease for bone marrow cells showing a mean of 92 cells when compared to 24 h cultured samples (*P < 0.05*, Figure 2.24C and 2.26B). The mean number of CD105 positive stained cells at 48 h was non-significantly decreased to 31 cells when compared to 24 h cultures (*P > 0.05*, Figure 2.24C and 2.26A). The mean percentage of cells remaining that were stained positive for CD105 at 48 h was non-significant at 35 % when compared to 24 h (*P > 0.05*) and was significantly lower compared to 0 h controls (*P < 0.001*, Figure 2.26C). Although the number of CD105 cells reduced over 48 h this was consistent with the loss of bone marrow cells during culture, approximately 40-50 % of these cells remained during culture.

CD90 immuno-detection at 0 h showed very little to no staining in multiple tissue sections. At 0 h. the mean number of bone marrow cells was 342 cells, from which 16 cells were positive for CD90 (Figures 2.25A and 2.26A&B). The mean percentage of cells remaining that were stained positive for CD90 at 0 h was 8 % (Figure 2.26C). At 24 h there was a significant decrease in the number of bone marrow cells representing a mean of 141 cells when compared to 0 h controls (*P < 0.0001*, Figure 2.25B and 2.26B). The mean number of CD90 stained cells at 24 h non-significantly increased to 26 cells, when compared to 0 h controls (*P > 0.05,* Figure 2.25B and 2.26A). The mean percentage of cells remaining that were stained positive for CD90 at 24 h was non-significantly increased to 20 % when compared to 0 h controls (*P > 0.05*, Figure 2.26C). At 48 h, there was a non-significant decrease for bone marrow cells showing a mean of 77 cells when compared to 24 h cultured samples (*P > 0.05*, Figure 2.25C and 2.26B). The mean number of CD90 positive stained cells at 48 h was maintained at 21 cells when compared to 24 h cultures (*P > 0.05*, Figure 2.25C and 2.26A). The mean percentage of cells remaining that were stained positive for CD90 at 48 h was non-significantly higher at 25 % when compared to 24 h and 0 h controls (*P > 0.05*, Figure 2.26C).

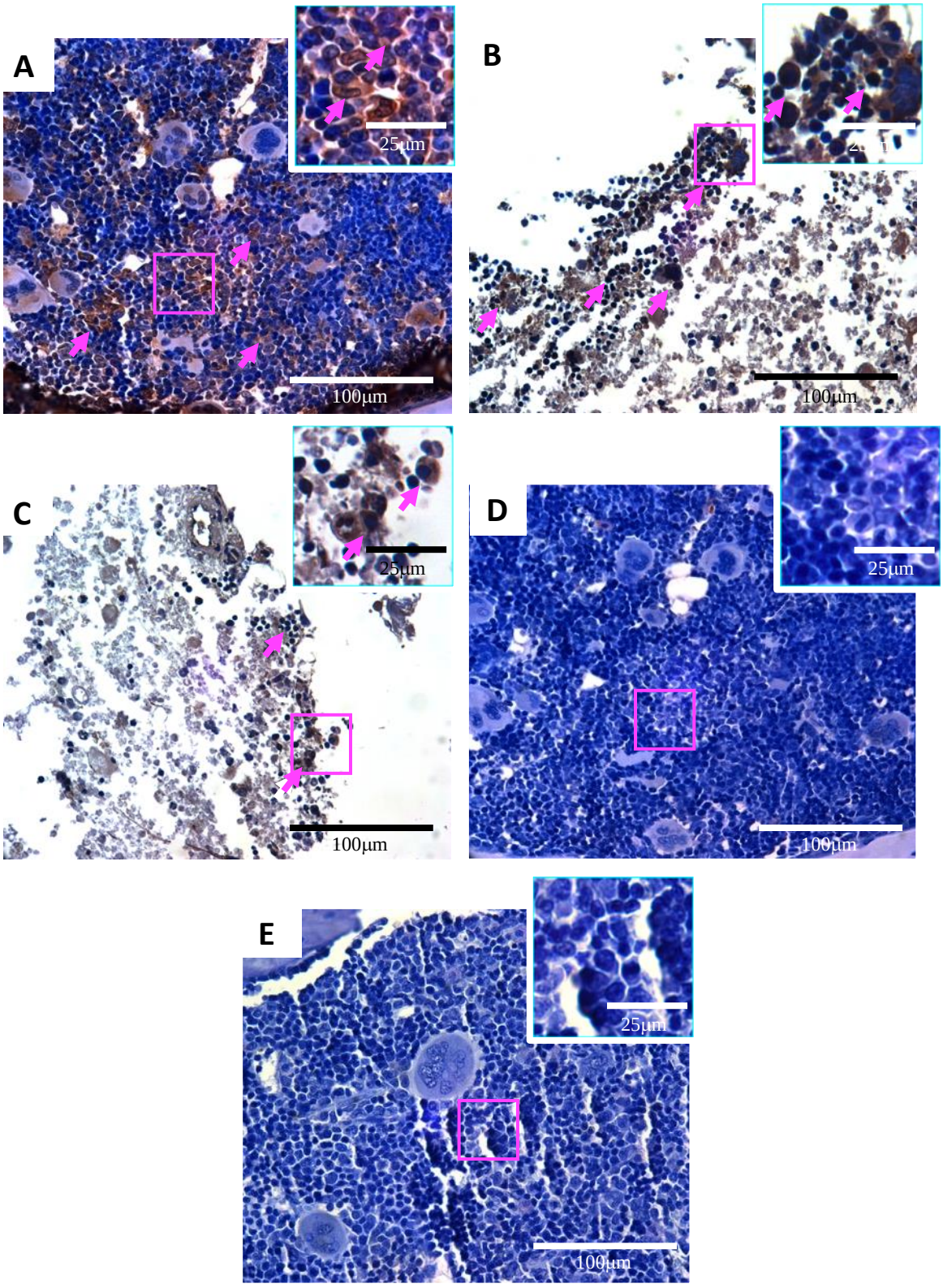

Figure 2.23: Trowell-type cultures stained with CD73. Representative images of immunohistochemistry stained CD73 labelled cells within the bone marrow from Trowell-type cultures (examples indicated by arrows). A) 0 h uncultured controls, B) 24 h cultures, C) 48 h cultures, D) negative control by omitting the primary antibody and staining only the secondary antibody and E) omission of the primary antibody and replacing with IgG polyclonal antibody.

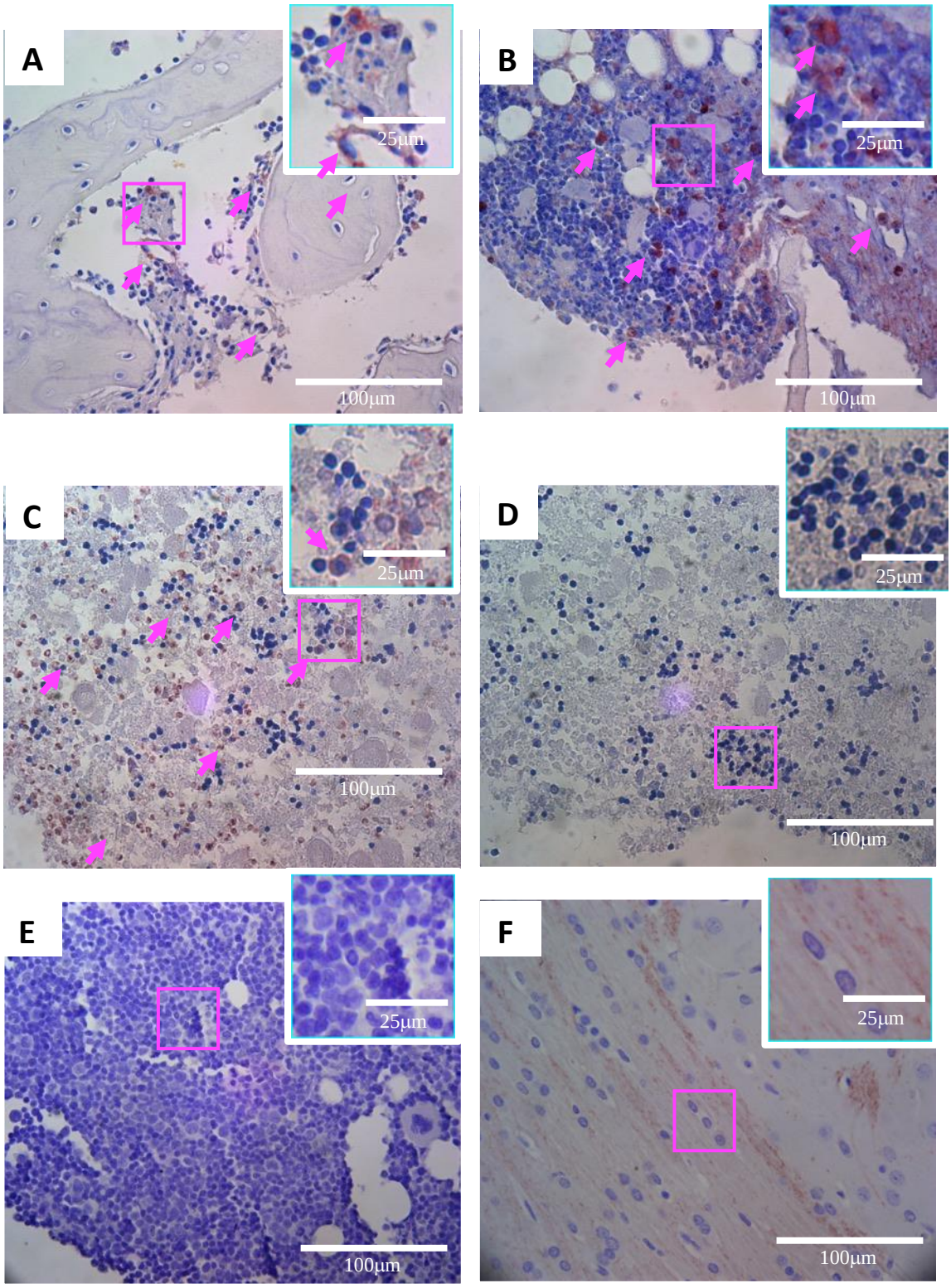

Figure 2.24: Trowell-type cultures stained for CD90. Representative images of immunohistochemistry stained CD90 labelled cells within the bone marrow from Trowell-type cultures (examples indicated by arrows). A) 0 h uncultured controls, B) 24 h cultures, C) 48 h cultures, D) negative control by omitting the primary antibody and staining only the secondary antibody, E) IgG1 isotype control and F) Rat brain positive control with high levels of CD90 staining.

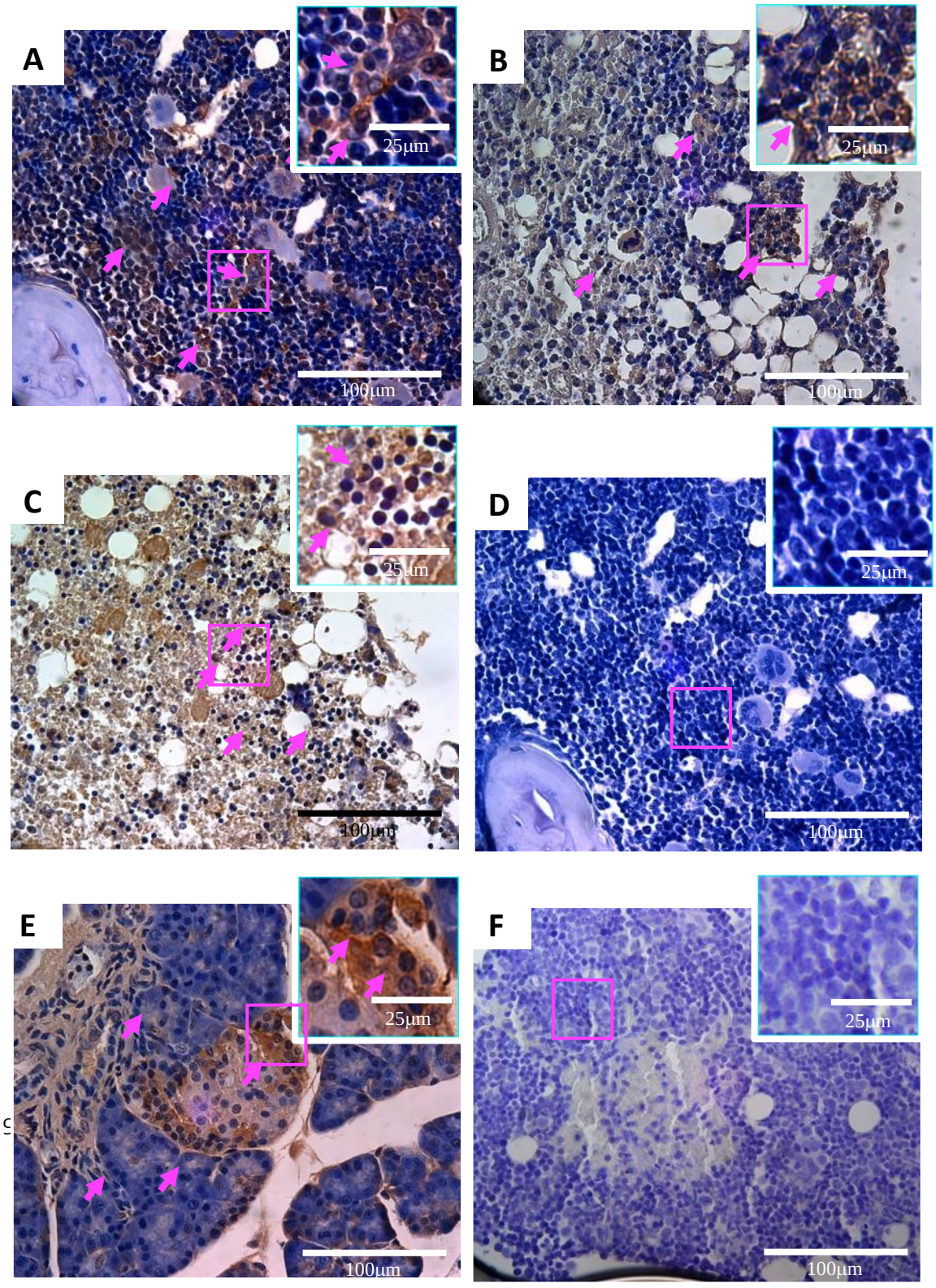

Figure 2.25: Trowell-type cultures stained for CD105. Representative images of immunohistochemistry stained CD105 labelled cells within the bone marrow from Trowell-type cultures (examples indicated by arrows). A) 0 h uncultured controls, B) 24 h cultures, C) 48 h cultures, D) negative control by omitting the primary antibody and staining only the secondary antibody, E) rat spleen positive control tissue showing high levels of CD105 staining and F) IgG2b isotype control.

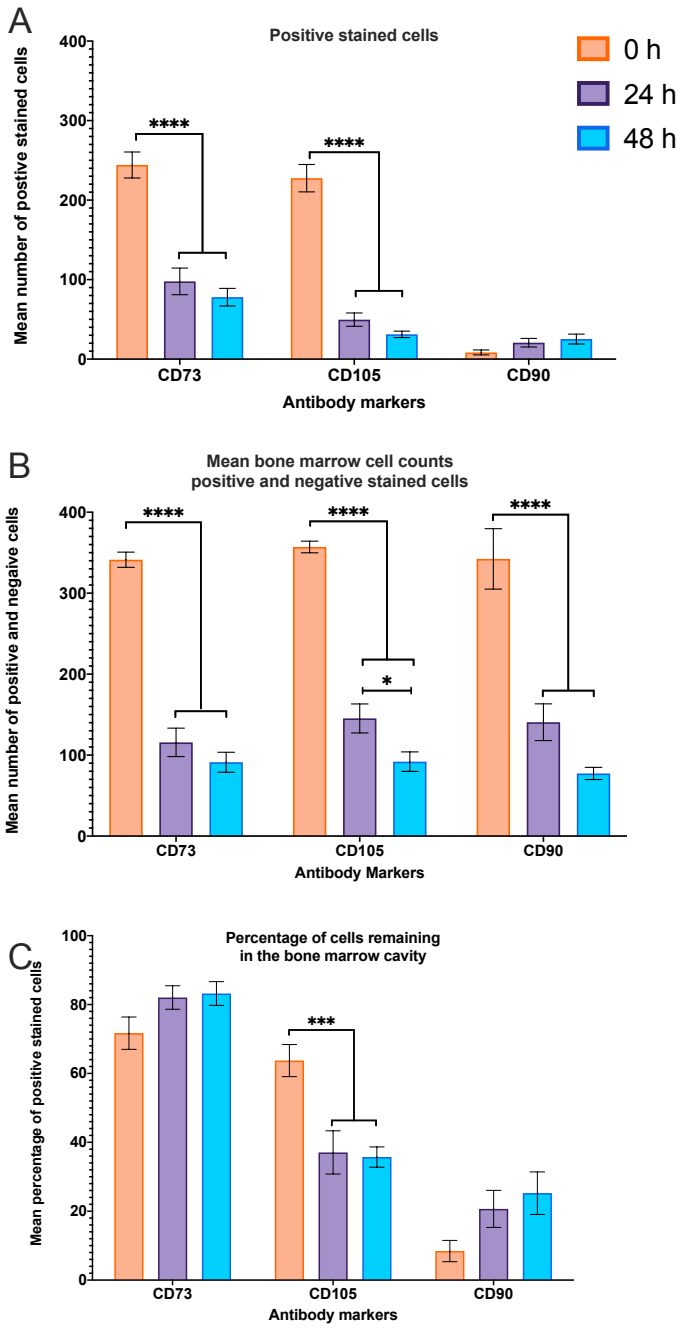

Figure 2.26: MSC cell markers immunolocalization within Trowell-type cultures. Analysis of cells stained with three mesenchymal stromal cells markers; CD73, CD105 and CD90 for tissue sections from Trowell-type cultures over 48 h. Graph A) mean positive stained cells. Graph B) mean bone marrow cell counts for IHC positive and negative stained cells. Graph C) showing the mean percentage of positive stained cells remaining in the bone marrow cavity. Graph shows a loss of mean bone marrow cells over 48 h in culture. Immunolocalisation shows a loss of CD105 and CD73 cells over 48 hrs with maintenance for CD90 cells. Percentage of stained cells indicate maintenance of CD73 and CD90 cell markers over 48 h. Significance within groups determined via one-way ANOVA with Tukey post-hoc test. Error bars represent mean ±S.E.M (n=3), ** P < 0.05*, **** P < 0.001* and ***** P < 0.0001.*

2.4: Discussion

This Chapter has highlighted the challenges and limitations of developing an *ex vivo* slice model. Significant cell loss was seen in femoral slices cultured at either a liquid/air interphase, here defined as Trowell-type cultures, or within basal culture media, defined as base-type cultures. Analysis of viability using apoptosis and necrosis markers indicated that Trowell-type cultures had significant lower synthesis of both markers. A detailed analysis of the cell populations within Trowell-type cultures indicated that there was a significant loss in neutrophil elastase, CD14, CD105 and CD73 cell markers, due to an unsuitable culture environment to support such cell populations.

During the preparation of the slices using the bone saw, there is a clear presence of initial trauma-induced to the bone marrow with increased localisation of both apoptotic and necrotic markers in the cells. Necrosis is not a controlled process and involves the loss of the cell membrane integrity along with inducing inflammation (Fink and Cookson 2005). Apoptosis, involves a controlled process that induces nuclear fragmentation, cell shrinkage and apoptotic bodies that avoids causing inflammation (Fink and Cookson 2005). The osteocytes in the cortical bone are exposed and the bone marrow tissue is compromised following sectioning. Osteocytes play a key role following trauma-induced to the bone providing biochemical and physical signals, such as an increase in osteopontin to recruit a variety of MSC derived cells whilst some undergo apoptosis and recruit osteoclasts, initiating bone resorption and remodelling (Choy et al. 2020).

Further analysis of necrosis following sectioning of the bone at 0 h indicated increase immunolocalisation of the LDH enzyme with little LDH leakage into the surrounding culture media or agarose gel, when compared to the positive control. LDH is a cellular enzyme that is present in all cells and is released when the plasma membrane is compromised (Chan et al. 2013). This indicates that the cellular membrane of these cells has started to become compromised possibly due to the process of sectioning, thus allowing for staining of the internal LDH within the cell which has not yet leached out of the cell as indicated by the assay. Typically during necrosis, there is swelling and rupture of the internal organelles along with the breakdown of the integrity of the plasma membrane, thus causing leakage of cellular components into the bone marrow microenvironment (Chan et al. 2013).

Following 24 h and 48 h of cells cultured within the base of the culture-plate had a significant increase in LDH leakage into the surrounding culture media. There was also increased LDH immunolocalisation within the bone marrow cavity. This indicates that there is active and continual necrosis of the bone marrow microenvironment during culture within the base-type cultures. Trowell-type cultures had significantly lower levels of LDH release than their base-type cultured counterparts. Although, both culture models showed increased levels of LDH release and subsequent reduction of immunolocalisation of LDH within the cells after 24 h and 48 h compared to 0 h controls, though Trowell-type cultures showed no significant elevation of LDH leakage unlike base cultures at 24 h and 48 h. Femoral slices cultured as a base-type culture during the first 24 h had elevated extracellular LDH leakage, similar to levels seen within the positive control when compared to 0 h controls and 24 h in Trowell-type cultures and levels were maintained during 48 h. Together this indicates that sectioning of the femur induced in part some initial necrotic trauma to the bone marrow cells, which is prolonged during base-type cultures but were reduced in Trowell-type cultures. This would suggest that the addition of the agarose gel provides support and nutrients to the encased cells, whilst it reduces the amount of stress placed upon the cells and maintains their viability and membrane integrity, indicating that the initial necrosis seen is not continued or specifically caused by the prolonged culture within a liquid/air interface.

Similarly, analysis of two pro-apoptotic markers; BAX, a BLC-2 family apoptotic promotor and caspase-3 via cleavage, an enzyme that is vital for initiating and inducing apoptosis via both intrinsic and extrinsic apoptotic pathways, showed an increase in BAX cellular localisation, compared to cleaved caspase-3 during culture (Deng et al. 2017; Dolka et al. 2016). During the first 24 h, there was a significant decrease observed in cleaved caspase-3 positive cells in total cell numbers for both base or Trowell-type cultures when compared to controls, with levels later maintained by 48 h. Interestingly, there was no significance in the percentage of cleaved caspase-3 stained cells for Trowell-type culture, with percentage levels decreasing over 48 h, although for base-type cultures there was a significant increase in cleaved caspase-3 percentage stained cells by 48 h. BAX analysis, indicated that there was a significant decrease in total numbers or percentages of positively labelled cells following culture for 24 h in both base- and Trowell-type cultures and were maintained by

48 h in culture. Trowell-type cultures at 48 h the number of BAX cells was significantly reduced compared to 24 h. Overall, there was a higher numbers and percentages of BAX-stained cells, compared to cleaved caspase-3 stained cells in both base and trowel-type cultures at 0 h and 24 h. It is highly possible that this initial increase in apoptosis at 0 h cultures, can be attributed to the sectioning process. `It is also highly possible this can be caused by culture conditions and there was no way to delineate the cause during optimisation of the model. The initial increase of apoptosis at 0 h regardless of the cause, indicates that these stresses are only temporary for the Trowell-type culture within the first 24 h where there is a reduction in apoptosis, possibly due to the availability of nutrients from the surrounding agarose gel and culture media. As a consequence of the cell culture, tissues or cells subjected to external culture conditions such as nutrient gradients and waste by-products can limit their survival capabilities (Arden and Betenbaugh 2006). It is possible that sectioning of the tissue caused some trauma to the bone marrow cell that together with the culture environment, impacted the viability of the cells within the bone marrow cavity, by committing the cells down either an apoptotic or necrotic pathway.

Analysis of the total bone marrow cells within both base- and Trowell-type culture systems following 24 h and 48 h, showed a reduction in cellular numbers compared to uncultured 0 h controls. The local bone marrow environment following direct sectioning showed large cell numbers of bone marrow cells. Analysis of H&E stained sections, indicated high numbers, showing a mean of ~1773.8 cells per 10,000 μm^2 at 0 h for uncultured controls and 1613 cells per 10,000 μm^2 at 0 h Trowell-type culture, respectively. This model at 0 h showed a high presence of various bone marrow cells, including, megakaryocytes, osteoblasts, lining cells, a variety of leukocytes, adipose-like vacuoles. During the first 24 h in culture, the morphology of the bone marrow cavity displayed substantial changes to the bone marrow architecture. There was evidence of tissue shrinkage in both culture systems, whereby the bone marrow had pulled away from the cortical bone interface with the presence of large gaps within the matrix after 24 h, which was not present at 0 h. There was a high number of cells localised towards the edge of the bone marrow that was exposed towards the agarose gel or the culture medium. There was also the presence of cells within the agarose gel and culture media for both culture systems. By 48 h, both base-type cultures and Trowell-type cultures had no significance in cell numbers compared to 24 h. Analysis of

the morphology of the bone marrow indicated increased areas devoid of cells on average for both cultures, therefore the decision was made to terminate the culture period at 48 h. This reduction in time of culture was consistent with previous *ex vivo* models which managed to maintain a culture for up to 48 h total for the tooth slice model and up to 7 days and 21 days for the mandible model (Colombo et al. 2015; Nishio Ayre et al. 2018; Roberts et al. 2013; Sloan et al. 2013; Smith et al. 2010).

The percentage loss of cells for Trowell-type culture was significantly lower compared to base-type cultures at 24 h, though there was no difference in loss of cells by 48 h. In comparison, the mandible model, cultured as a Trowell-type culture showed an average of 100 cells per 100 x 100 μm^2 at 0 h and then 60 cells per 100 x 100 μm^2 following 7 days in culture, a 40 % loss, within the periodontal ligament (Sloan et al. 2013). This shows that the femoral slice model had cells that were rapidly lost by 48 h even though there was a higher initial number of cells at 0 h when compared to the mandible model due to the difference in density and size of bone marrow between the two tissues. However, the data that is obtained from this model is comparable to observations found in a similar *ex vivo* femoral slice model by Srinivasaiah et al. (2019). Here, Sprague Dawley rat femurs were embedded into 2.5 % agarose before being sectioned into 300-400 µm slices. Unlike the semi-cylindrical femoral slice presented in this chapter, the authors managed to culture the 300 µm femoral slices for up to 15 days at air-liquid interphase. Histological images from the study by Srinivasaiah et al. (2019) suggests that there was rapid bone marrow cell loss in the femoral shaft, similar to the results presented within this chapter although no total cell counts or percentage loss analysis were carried out authors. No IHC analysis of bone marrow immune cells or viability analysis was undertaken by the authors. This rapid cellular loss could be in part due to the initiation of early bone fracture healing along with a possible increase in matrix-degrading proteins and pro-inflammatory cytokines initiating mobilisation of cells, though these markers were not tested in this model.

Overall, both culture systems induced significant loss of cells within the bone marrow. Although, the Trowell-type culture system had a lower number of cells lost from the bone marrow cavity, along with significantly reduced LDH expression and immunolocalisation when compared to Base-type cultures. Therefore, of the two culture systems the Trowell-

type culture was considered to be a better model system. This model was used to characterise these remaining cells within bone marrow during culture. Following 24 h of culture, the cells that were remaining within the bone marrow were mainly cells showing markers for monocytes, macrophages and MSCs, the latter of which were more in abundance than immune cells. The neutrophils and multinucleated osteoclasts started to decline, though their percentage of positively labelled cells remained non-significant. Analysis of IHC stained cells following 48 h in Trowell-type culture, showed no significant differences in the number or percentage of cells stained positive for CD14, CD68 or neutrophil elastase, compared to 0 h or 24 h in Trowell-type culture. Percentage analysis of these immune cells indicated approximately 30 - 40 % of neutrophils, 50 % of CD14 and 25 % of CD68 stained cells. There was no presence of TRAP stained osteoclasts, though CD68 analysis did indicate few large multinucleated cells. By 48 h, there was a higher number of MSCs cell markers when compared to 0 h and 48 h controls. There was a higher number of MSC cell markers CD73 and CD105 when compared to immune cell markers . This indicates that the main cells that are retained during cultures are possibly MSCs, with lower numbers of immune cells. One possible explanation of this can be that these immune cells are migrating out of the tissue slice or differentiating due to an increase in pro-inflammatory cytokine or chemokine synthesis, though these proteins were not assessed within this model.

Neutrophils numbers significantly decreased over 48 h, but had no significant reduction in percentages normalised cells over 48 h compared to controls, although there was intense background staining of neutrophil elastase. Typically, within tissues neutrophils have a very short lifespan surviving for 24 h and 48 h in culture and only 8 h-12 h in circulation (Mayadas et al. 2014; Navegantes et al. 2017). Following injury, polymorphonuclear neutrophils are primed and activated following binding to TNFα and IL-1 (Bhatia et al. 2006). These cells are involved in phagocytosis and production of reactive oxygen species, in addition to the release of proteolytic enzymes such as neutrophil elastase (Bhatia et al. 2006). Elastase levels have been upregulated in studies following femoral nailing in patients with acute femoral fractures (Giannoudis et al. 1999). These elastases effects can be broad with effects ranging from degradation of the ECM and connective tissue molecules, such as proteoglycans, collagens and elastin (Peters et al. 1994). In patients that had surgery for

tissue debridement following osteomyelitis, elevated neutrophil elastase levels at 57 % after 2-4 days post-operation were observed, which reduced 25 % after 9-11 days (Peters et al. 1994). Peripheral blood from patients following major trauma to the long bones or pelvis showed that neutrophil elastase levels were released 2 -4 days following trauma, with levels becoming variable depending on the severity of the injury (Bhatia et al. 2006).

Belaaouaj et al. (1998) reported that mice lacking in neutrophil elastase and infected with *E. coli* and *Klebsiella pneumonia,* two gram-negative bacterial species are more susceptible to sepsis and death, compared to their wild type counterparts. This was due to the three-fold difference in the spread of the bacterial species to the bloodstream and subsequently to major organs in the neutrophil elastase-deficient mice than the wild type. Neutrophil mobilisation and numbers were similar in both species along with their ability to recruit other immune cells, although mice lacking in neutrophil elastase had less bactericidal activity. Following gram-positive *Staphylococcus aureus* (*S. aureus*) infection mortality was greater in wild type than deficient mice, due to the inability of the neutrophils in eradicating *S. aureus*. It is presumed that the wild type mice resulted in a greater degree of surrounding tissue damage via the neutrophil elastase than the deficient mice. This suggests that neutrophil elastases have an active role in antimicrobial activity, however, it is very much species-dependent. In rheumatoid arthritis, inflammatory diseases neutrophil elastase has been seen to increase the release of chemokines and cytokines including; TNFα, IL-8, IFN-γ and granulocyte macrophage-colony stimulating factor (GM-CSF, Muley et al 2016). The addition of neutrophil elastase within the *in vivo* mice knee joint model induced leukocyte extravasation and increased fluid flow through vessels, whilst subsequently increasing leukocyte rolling and adhesion on the synovial venules until the joint became hyperaemic (Muley et al. 2016). All this suggests that the increase in background neutrophil elastase seen within the *ex vivo* femoral model is unsurprising and may play an active role in ECM degradation and the subsequent migration of cells out of the bone marrow into the surrounding agarose seen during 24 h and 48 h in culture.

As mentioned previously, monocytes, macrophages and osteoclasts are vital during septic osteolysis or osteomyelitis. Using CD14 and CD68 cell markers, there was a high percentage of CD14 normalised myeloid cells and low numbers of CD68 labelled monocytes,

macrophages or osteoclasts retained in the bone marrow cavity. There was complete abolition of osteoclasts during cultures, with little to no multinucleated cells retained during 48 h of culture. In contrast, the 300 µm femoral slice model by Srinivasaiah et al. (2019) showed an increase in percentage osteoclasts in the diaphysis region of the femoral shaft increasing from ~1 % per $6x10^6$ μm^2 at day 0 to ~5 % per $6x10^6$ μm^2. Osteoclasts are a key player during septic loosening due to the dysregulation of resorption and formation. Osteoclasts and macrophages are notoriously difficult to culture requiring supplementation of the cytokines macrophage colony-stimulating factor (M-CSF) and the receptor activator the nuclear kappa-B ligand (RANKL). The addition of these cytokines can drive the bone cell populations to differentiate into osteoclast-like cells (Costa-Rodrigues et al. 2011; Marino et al. 2014). TNFα plays a key role in osteoclastogenesis and macrophages phagocytosis activity (Luo et al. 2018). There is a possibility that there is an increase in TNFα following sectioning to the bone marrow and the lack of multinucleated osteoclast-like cells shows that these pro-inflammatory cytokines are not sufficient alone to maintain osteoclasts in this model. Within the *ex vivo* mandible model, supplementation with M-CSF and RANKL was used to maintain osteoclast-like cells during culture (Sloan et al. 2013). Therefore, there is a need to further supplement our model with both M-CSF and RANKL to maintain both macrophages and osteoclasts.

A limitation of this model is the lack of an active blood supply, therefore, it is not possible for a full haematoma to form, though there was the presence of bone marrow shrinkage, dysregulation and possible degradation of the surrounding ECM in both culture systems. The bone marrow ECM environment mainly consists of collagen types I, III, IV and V, laminin, glycosaminoglycans, proteoglycans, fibronectin, thrombospondin and vitronectin (Janowska-Wieczorek et al. 2000). The degradation of the surrounding ECM seen in the model could be due to the role of matrix metalloproteinases (MMPs). These MMPs are zinc-dependent proteolytic enzymes that play active roles in the degradation of the ECM and the basement membranes (Yu and Han 2006). These MMPs, tend to occur at low levels, though they have been known to be upregulated during inflammation, tissue remodelling, wound healing and cancer progression (Shirvaikar et al. 2012).

The addition of the sagittal sectioning through the bone marrow cavity to form a semi-cylindrical femoral slice can have interesting connotations. The tooth slice model by Nishio Ayre et al. (2018); Roberts et al. (2013); Sloan and Smith (1999) utilise the traditional transverse disc sectioning. These authors found that the dental-pulp matrix was more stable in culture with little degradation, unlike the current femur model, which had increased degradation during culture. An explanation of this could be in part due to the structure of the dentine and its association with the soft pulpal matrix. The structure of the dentine to the dental pulp is multifaceted though it is comprised of a network of collagen type I and III, along with proteoglycans and glycoproteins forming an anchored, stable and structured support matrix (Sloan 2015). Although there is a similarity in the orientation of structures in the femur compared to the tooth, with bone marrow extending into the osteoblast/ line cell layer, which in turn lays next to the osteoid and mature cortical bone. These osteoblasts within long bones differentiate as osteocytes and embed themselves into the cortical bone, they do not provide any structural support.

Overall, this Chapter has laid out the foundation to develop and optimise a novel bone marrow *ex vivo* model system. The current maximum culture period was only possible for 48 h for two different culture systems. Trowell-type cultures were chosen due to improved viability, though this model did still exhibit significant cell loss over 48 h, when compared to base-type culture the loss was significantly lower. Cells that were retained during these cultures displayed cell surface markers that identify MSCs, neutrophils, monocytes and macrophages, although majority of these cell markers were reduced over 48 h in Trowell-type culture. There was a lack of osteoclasts retained during culture, which are responsible for inducing bone resorption following the presence of a bacterial pathogen around an implant and thus have key roles in septic osteolysis and osteomyelitis. As such, the next step within the model is to improve the viability and numbers of the two key osteoclast precursor immune cells monocytes and macrophages along with maintenance of osteoclast number with the addition of cytokines of M-CSF and RANKL.

Chapter 3:
Manipulation of the Femoral Slice Model with Pro-Osteoclastic Cytokines and Injection of Bone Marrow Cells

Chapter 3.1: Introduction

Chapter 2 demonstrated the potential to culture cells in the bone marrow within an *ex vivo* environment for a short-term culture period. Many of the bone marrow osteoclast cell precursors, the monocytes and macrophages, were present, while the osteoclasts themselves, which play key roles in implant induced osteolysis, were non-existent in 24 h and 48 h cultures. This is not that surprising considering these cells require a very delicate environment for culture and maintenance. To try and maintain these osteoclast precursors within the *ex vivo* model, further refinement of the culture environment was undertaken. However, due to the lack of information on maintaining these cells within a three-dimensional *ex vivo* environment, it is pertinent to look towards *in vitro* and *in vivo* studies on how to maintain these cells within the culture.

Two key cytokines have been shown to play a key role in the regulation, maintenance and support of monocyte/macrophage precursors and their subsequent differentiation into osteoclasts. These two cytokines include the receptor activator the nuclear factor kappa B ligand (RANKL) and the macrophage colony stimulating factor (M-CSF). The addition of M-CSF and RANKL to osteoclast precursors has helped facilitate the understanding of pathological bone resorption or pathological bone mineralisation. One of the early studies that helped display the importance of M-CSF on osteoclast differentiation was via analysis of osteopetrosis mutant mouse ('op/op' mouse) *in vivo* model. Here, mice were genetically altered to induce the condition of osteopetrosis, where bone mineralisation was pathologically increased and had a subsequent reduction in osteoclast precursors. Within this model, low osteoclast numbers were formed, due to a defect in the gene coding for M-CSF production (Yoshida et al. 1990). RANKL is vital to initiate osteoclast differentiation, function and survival. Genetically modified mice, with RANK, knocked out, had increased defects in bone resorption and were to develop functional osteoclasts (Dougall et al. 1999). Additionally, genetically modified RANKL knock-out mice had impaired osteoclastogenesis and bone remodelling with pathologically increased mineralisation (Xiong et al. 2011).

Within the current model developed within this Thesis, where there was a lack of osteoclasts, although there was a considerable percentage of monocytes and macrophages, the addition of M-CSF and RANKL to the model was considered a logical approach. However,

there is a clear need to know the optimal effective concentration range of these cytokines, as various studies have shown variability in the optimal dosage used within experimentations. High concentrations of M-CSF (100 ng/mL) and RANKL (50 ng/mL) have been utilised to induce osteoclast differentiation from murine bone marrow isolated from 6-week-old tsA58 transgenic mice (Takeshita et al. 2000). *In vitro* mice spleen ST2 cell lines were differentiated into multinucleated osteoclast-like cells in a dose-dependent manner with RANKL at 10 or 30 ng/mL along with 10 ng/mL M-CSF (Simonet et al. 1997). A similar study that used a slightly higher concentration of both M-CSF (20 ng/mL) and RANKL (50 ng/mL), were sufficient in inducing around 200 osteoclast-like cells, from male 5-week-old mice femur and tibial bone marrow cells (Shiratori et al. 2018). Together, these studies highlight that protocols vary with no set parameters or criteria in place to standardise the culture method to induce differentiation and formation of multinucleated osteoclast-like cells *in vitro*, with different papers utilising different concentrations of cytokines.

In the case of the current *ex vivo* femoral slice model, the addition of the agarose plug surrounding the femoral slice could be a potential barrier for adequate penetration of the cytokine into the bone marrow. Lacey et al. (1998), has shown that for murine bone marrow derived cells cultured in semi-solid agar, similar to the current *ex vivo model*, the addition of 30 ng/mL M-CSF and 20 ng/mL RANKL over 144 h, induced a greater number of osteoclasts then M-CSF alone. This shows that these two cytokines are capable of penetrating through a semi-solid agar whilst stimulating and differentiating cells embedded within. This provides a good basis for the current model, where osteoclast numbers are low and the addition of these cytokines within the culture media and to the agarose plug could be sufficient in inducing osteoclasts. This is supported by studies that developed an *ex vivo* mandible model, which was stimulated with either 30 or 60 ng/mL RANKL along with 10 or 20 ng/mL M-CSF within a Trowell-type culture and was able to maintain a population of TRAP-positive multinucleated osteoclast-like cells over 14 days in culture, although the numbers were low at 1 cell per 100 μm^2 area (Sloan et al. 2013). Collectively, these studies show that there is great variability in the concentrations of cytokines used to obtain osteoclast-like cells within the culture. Therefore, there will be a need to optimise these concentrations within the current model.

As mentioned previously, osteoclasts are fundamentally important for the development of septic osteolysis in PJI and osteomyelitis conditions. I*n vitro* studies from Claro et al. (2011) demonstrated that the binding of *Staphylococcus* protein A (SpA) on mouse clonal MC3T3-E1 pre-osteoblastic cell lines induces increased expression and secretion of RANKL compared to uninfected controls and SpA negative mutant *Staphylococcus aureus (S. aureus)*. Osteoprotegerin (OPG), a natural inhibitor to RANKL prevented bone resorption, whilst relatively high in uninfected controls was significantly lower in infected osteoblasts. Similar results have been shown for human osteoblast cell lines incubated with conditioned media collected from methicillin-resistant or susceptible *S. aureus* biofilm, over 14 days in culture. Results showed a significant increase in RANKL production, along with no increase in OPG when compared to non-infected controls (Sanchez et al. 2013). The presence of *S. aureus* in either planktonic form or within a biofilm can increase RANKL production and increase bone resorption. *In vitro* studies by Ren et al. (2017a; 2017b) on Raw 264.7 monocyte and macrophage cell lines infected with either live *S. aureus* or isolated SpA, increased the differentiation of osteoclast precursors to mature osteoclast-like cells. Both live and heat-inactivated *S. aureus,* along with *S. aureus* conditioned media without the bacteria, significantly induced the differentiation and formation of osteoclast-like cells and increased these cells' resorption activities. The addition of SpA alone or with RANKL significantly increased the formation of osteoclast-like cells and their resorption activity compared to cells stimulated with RANKL alone. Trouillet-Assant et al. (2015) showed that direct infection and internalisation of primary murine bone marrow osteoclast precursor cells, with three different *S. aureus* species (methicillin and gentamicin-susceptible *S. aureus* strain ACTC number 8325-4*,* a mutant species negative for the fibronectin-binding protein DU5883 and an ATCC 6850 *S. aureus* type strain), increased the proinflammatory cytokine production of infected precursors. The addition of these cytokines to uninfected mature osteoclasts enhanced the cells resorptive capabilities, whilst also increasing the osteoclastogenesis of uninfected precursors. Together these studies highlight the co-synergistic effect that bacterial infections have for inducing osteoclasts into an active resorptive state. It is vital to try and maintain these osteoclast-like cells within the *ex vivo* femoral slice model, before the addition of bacteria to observe the resorptive effect the addition of bacteria can have within a controlled three-dimensional environment.

This current Chapter aimed to maintain or differentiate already present osteoclast precursors or mature osteoclast-like cell populations. This was done by supplementing the femoral slice with two different concentrations of M-CSF and RANKL externally in the culture media and internally directly within the bone marrow. Monocytes, macrophage and osteoclast cell survival and maintenance was analysed. Additionally, mixed tibial bone marrow cells were also injected into the bone marrow cavity along with M-CSF and RANKL to try and increase the local bone marrow population and reduce cell loss over 48 h.

3.2: Material and Methods

3.2.1: Extraction of Rodent Tibial Bone Marrow Cells

Primary bone marrow cells were harvested from tibias dissected from freshly sacrificed male 21-28 day-old Wistar rats. Tibias were sterilised in 70 % ethanol for 5 s and washed immediately in phosphate buffered saline (PBS) (ThermoFisher Scientific, Loughborough, United Kingdom) and washed in alpha Minimum Essential Medium (αMEM) containing 10 % HI FBS (ThermoFisher Scientific), 1 % L-ascorbic acid 2-phosphate (Sigma-Aldrich, Poole, United Kingdom) and 1 % antibiotic antimycotic solution (Sigma-Aldrich), all cooled on a bed of ice.

Using a 70 % ethanol sterilised diamond-edged rotary blade, cooled while in use with PBS, the tibias, lateral and medial condyles, the lateral and medial malleolus and the adjoining fibula, were removed. The resulting tibial shaft was placed in αMEM media with 10 % HI FBS, 1 % of L-ascorbic acid 2-phosphate at 100 µM concentration and 1 % antibiotic antimycotic solution. Using a 21-gauge BD precision glide syringe needle filled with PBS, the bone marrow from the tibias was flushed out. To minimise any cross-reactivity between different animals, only the tibias from each animal were pooled together and reintroduced back into the femur of that same animal. Each animal was considered a separate experimental repeat. Cells were spun at 438 x g for 5 min using the ThermoFisher Heraeus Labofuge 400 centrifuge (ThermoFisher). The supernatants were removed and the resulting cell pellets were washed in αMEM. Cells were re-spun at 438 x g for 5 min and the supernatant was removed. The resulting pellets were resuspended in 1 mL of ACK lysis buffer, to lyse resident erythrocytes, (Gibco, ThermoFisher Scientific) for 5 min at 37 ^{o}C. Cells were spun at 95 x g for 5 min and the supernatants were removed. The resulting cell pellets were washed in 1 mL αMEM containing 10 % HI FBS, 1 % L-ascorbic acid 2-phosphate and 1 % antibiotic antimycotic solution and filtered through a 70 µm cell strainer. Cells were then either used for *in vitro* culture to isolate osteoclast precursors (Section 3.2.6) or *ex vivo* microinjection into the bone marrow cavity of femoral slices (Section 3.2.2.3).

3.2.2: Culture of *ex vivo* Femoral Slices

3.2.2.1: Extraction and Obtaining of Semi-Cylindrical Femoral Slices

The process to obtain four 2 mm semi-cylindrical femoral shafts was the same as previously described in Section 2.2.1. These Semi-cylindrical femoral slices were embedded into 1 % agarose and culture media gel and cultured at a liquid air/interphase using the Trowell-type culture, as previously described in Section 2.2.3.2. Culture media and agarose gel was supplemented with either 20 ng/mL M-CSF and 30 ng/mL RANKL or 40 ng/mL M-CSF and 60 ng/mL RANKL. Femoral slices were left in culture for 24 h or 48 h within a sterile humidified incubator at 37^{o}C, 5 % CO_2. Uncultured femoral slices served as 0 h controls and were immediately fixed.

3.2.2.3: Microinjection of Tibial Mixed Bone Marrow into the *ex vivo* Femoral Slices.

As previously described in Sections 2.2.3.2 and 3.2.2, femurs were sectioned using a rotary diamond edge bone saw in semi-cylindrical femoral halves. Femurs from the left and right side of the animal provided contralateral experimental samples, with one femur microinjected with tibia bone marrow cells and the other injected with basal media alone. Extracted bone marrow cells from the tibia were counted and 10,000 cells per 1 µL were injected into the bone marrow cavity. In order to maintain cells within a relatively localised region of the tissue, cells and media were injected approximately 1 mm deep into the centre of the bone marrow cavity of the exposed femoral shaft, using a 10 µL SGE gas-tight syringe with a 26-gauge bevel tip needle (Sigma-Aldrich). A control slice was injected with basal culture media containing 10 % HI FBS, 1 % L-ascorbic acid 2-phosphate and 1 % antibiotic antimycotic solution, along with 30 ng/mL RANKL and 20 ng/mL M-CSF. These femoral slices were stored within a covered 6-well culture plate containing 500 µL of αMEM, to prevent tissue dehydration, for 10 min before agarose embedding. Femoral slices were cultured using the Trowell-type culture method previously described in Section 2.2.3.2, for either 24 or 48 h in a sterile humidified incubator at 37^{o}C, 5 % CO_2. Uncultured femoral slices served as 0 h controls and were immediately fixed.

Tissue samples were collected for Trowell-type cultures as previously described in Section 2.2.3.4. Following extraction of the femoral slice for tissue processing, the remaining agarose plug was combined with basal culture media before storage at -80 ^{o}C.

As previously described in Section 2.2.5.1, the extracted femoral slices was fixed in 10 % formalin prior to decalcification in 14 % EDTA tetrasodium salt hydrate (pH 7.4) (Sigma Aldrich) for 1 week, before being embedded into paraffin wax, sectioned at 5 µm and mounted onto glass slides.

3.2.3: Detection of Necrosis Using a Colourimetric Lactate Dehydrogenase Assay

To detect necrosis via analysis of Lactate Dehydrogenase (LDH) in the cell culture media and agarose gel, a LDH assay was carried out using the Pierce™ LDH Cytotoxicity Assay Kit (ThermoFisher Scientific), as previously described in Section 2.2.4.

3.2.4: *In Vitro* Culture of Osteoclast Precursors with M-CSF and RANKL supplementation

Cells were seeded onto glass cover slides placed into individual wells of a 24-well plate at a density of 1 x 10^5 cells/well. Cells were cultured in αMEM containing 10 % HI FBS, and 1 % Antibiotic Antimycotic Solution along with 20 ng/mL of M-CSF for 48 h within a sterile, humidified incubator at 37 ^{o}C, 5 % CO2. After 48 h, non-adhered cells were then removed. The remaining adherent cells were washed in 3x in 5 mL of ice-cold PBS before being cultured in 10 % HI FBS, and 1 % Antibiotic Antimycotic Solution with or without supplementation with M-CSF and RANKL at various concentration ranges at; 20 ng/mL M-CSF and 30 ng/mL RANKL, 40 ng/mL M-CSF and 60 ng/mL RANKL, and 100 ng/mL M-CSF and 100 ng/mL RANKL. Cells were cultured for up to 7 days, with half the media changed every 48 h to replenish the cytokines. Controls were cultured with 10 % HI FBS, and 1 % Antibiotic Antimycotic Solution with the addition of no cytokine supplementation. Following culture, cell culture media was removed and cells were fixed with 10 % formalin solution for 24 h at 4 ^{o}C before staining with a tartrate resistant acid phosphatase, leukocyte (TRAP) Kit (Sigma-Aldrich).

3.2.4: *In Vitro* and *Ex vivo* Osteoclast staining

Osteoclast staining was achieved using a TRAP kit and reagents were prepared, as previously described in Section 2.2.7. The TRAP solution was made up using heated distilled water at 37 ^{o}C, to which diazotized fast garnet GBC solution, naphthol AS-BI phosphate solution, acetate and tartrate were all added. A control solution that omitted the tartrate was also prepared.

In vitro cultures with the addition of M-CSF and RANKL at different concentrations or the addition of microinjected bone marrow cells were stained for the presence of osteoclast-like cells after 7 days of culture. To individual wells of the 24-well plate, 1 mL of TRAP solution was added and left to incubate for 1 h at 37 ^{o}C. After which TRAP solution was removed, and nuclei were counterstained using Gills haematoxylin solution for 5 min, before being washed rinsed in tap water for 5 min to blue the nuclei. Cells were imaged at X 100 magnification using the Olympus AX70 Fluorescent Microscope (Olympus Corporation, Tokyo, Japan) and the number of large multi-nucleated with 3 or more nuclei were counted and tabulated.

Ex vivo femoral slices with the addition of M-CSF and RANKL at different concentrations or the addition of microinjected bone marrow cells were stained for the presence of osteoclast-like cells. Tissue sections mounted onto glass slides were deparaffinised first with xylene and then rehydrated through graded ethanol at 100 %, 75 % and 50 %, before being rinsed in distilled water. Slides were removed and placed in a TRAP solution that contained or omitted the tartrate. Tissue sections were incubated in the dark at 37 ^{o}C for 1 h. Sections were counterstained using Gill's haematoxylin and rinsed in tap water to blue the nuclei. Tissue sections were covered with a VectaMount® AQ mounting media (Vector Laboratories, Peterborough, United Kingdom) before being covered with a coverslip. Tissue sections were visualised by light microscopy and imaged.

3.2.5: Haematoxylin and Eosin Staining

Haematoxylin and Eosin staining was carried out on the 5 µm cut tissue sections mounted onto glass slides as previously detailed in Section 2.2.6.

3.2.6: Immunohistochemistry Analysis of Specific Immune, Apoptotic and Necrotic Antibodies

Immunohistochemistry (IHC) staining was carried using the VECTASTAIN® Elite® ABC HRSP Kit (Peroxidase, Rabbit IgG, Vector Laboratories), according to the manufacturer's instructions, for cleaved caspase-3, BAX, CD14 and CD68 antibodies as previously described in Section 2.2.8.

3.2.7: Imaging and Image Analysis

Imaging and image analysis were carried out, as previously detailed in Sections 2.2.9 and 2.2.10, using an Olympus AX70 Fluorescent Microscope. Analysis of images was carried out using the Image J application (U.S. National Institutes of Health, Bethesda, USA). Cell counts for H&E stained sections were counted in an area of 10 mm^2 per image and this was repeated to obtain five separate images. From these five counts, an average was obtained. Using these cell counts, a percentage loss of cells over 48 h were calculated.

Immunohistochemistry stained images, captured at X 400 magnification, were counted by applying five 50 x 50 um^2 area boxes over regions containing a high proportion of cells and bone marrow tissue and all the positively labelled cells and non-labelled cells were counted separately. Cell counts for each of the 5 images per Section were totalled together and averaged for counts within each time point. A percentage of stained cells was calculated using the total number of positively labelled cells against the total number of all cells (labelled and non-labelled cells) for each of the 5 images and an average was obtained.

3.2.8: Statistical Analysis

Statistical analysis was carried using Graphpad Prism version 8.00. One-way ANOVA with Tukey's post-test was used to identify significant differences in data across groups for one independent variable. A two-way ANOVA with Tukey's post-test was used to determine differences in data with two or more independent variables. Statistical significance was determined at *$P < 0.05$, **$P < 0.01$, ***$P < 0.001$, ****$P < 0.0001$.

3.3: Results

This Chapter investigated the further development of the femoral slice model by supplementation with cytokines that promote monocyte survival and osteoclast differentiation. Three different concentrations of M-CSF and RANKL were analysed *in vitro* before being used within the *ex vivo* model. The first series of results reported on the supplementation of the surrounding culture media and agarose gel with two different concentrations of M-CSF and RANKL; identifying the optimal concentration within an *ex vivo* environment. Data in the analysis of this first Section uses data for the Trowell-type cultures from Chapter 2 as a no cytokine control, which was done around the same time as the work presented in this chapter. The results presented then continue to develop the femoral slice model, where the optimally identified cytokine concentrations were injected within the bone marrow cavity, along with mixed bone marrow cells derived from the tibial long bones, to assess if this aids cell survival further.

3.3.1: Bone Marrow Cells Induce Osteoclast-like Cell Formation in the Presence of M-CSF and RANKL.

To induce osteoclast-like cells from mixed bone marrow cells, cells were stimulated with various concentration combinations of M-CSF and RANKL *in vitro* for up to 7 days and cells were counted in a area of $4.68x10^6$ μm^2. Cells supplemented without any cytokines for 7 days had a mean of 18.7 cells (Figure 3.1 A&E). Cells supplemented with 20 ng/mL M-CSF and 30 ng/mL RANKL induced a significantly increased number of multinucleated osteoclast-like cells at 7 days to a mean of 53.7 cells (Figure 3.1 B&E) when compared to either; control no M-CSF and RANKL supplementation ($P < 0.0001$, Figure 3.1 A&E), supplementations with 40 ng/mL M-CSF and 60 ng/mL RANKL ($P < 0.0001$, Figure 3.1 C&E) and supplementations with 100 ng/mL M-CSF and 100 ng/mL RANKL ($P < 0.0001$, Figure 3.1 D&E). Cells supplemented with 40 ng/mL M-CSF and 60 ng/mL RANKL had a mean of 23.5 cells (Figure 3.1 C&E). Cells supplemented with 100 ng/mL M-CSF and 100 ng/mL RANKL had a mean of 19.6 cells (Figure 3.1 D&E).

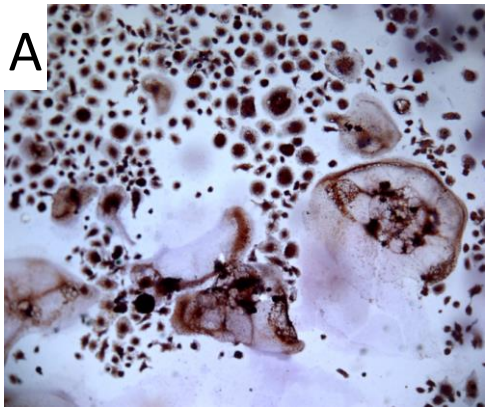

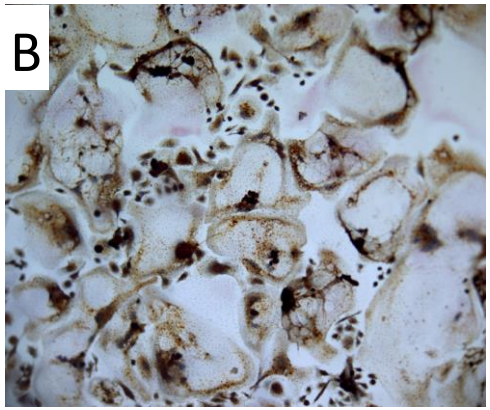

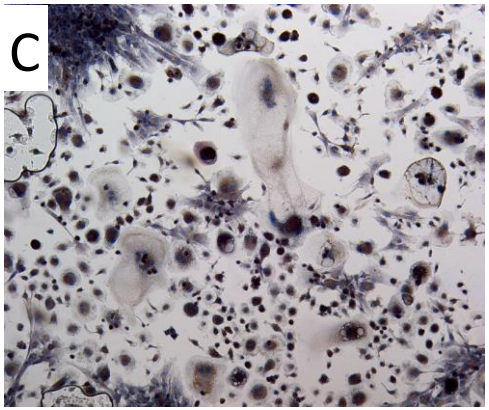

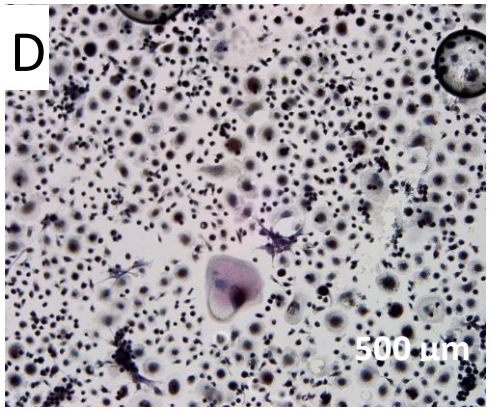

Control no M-CSF or RANKL | **20 ng/mL M-CSF 30 ng/mL RANKL** | **40 ng/mL M-CSF 60 ng/mL RANKL** | **100 ng/mL M-CSF 100 ng/mL RANKL**

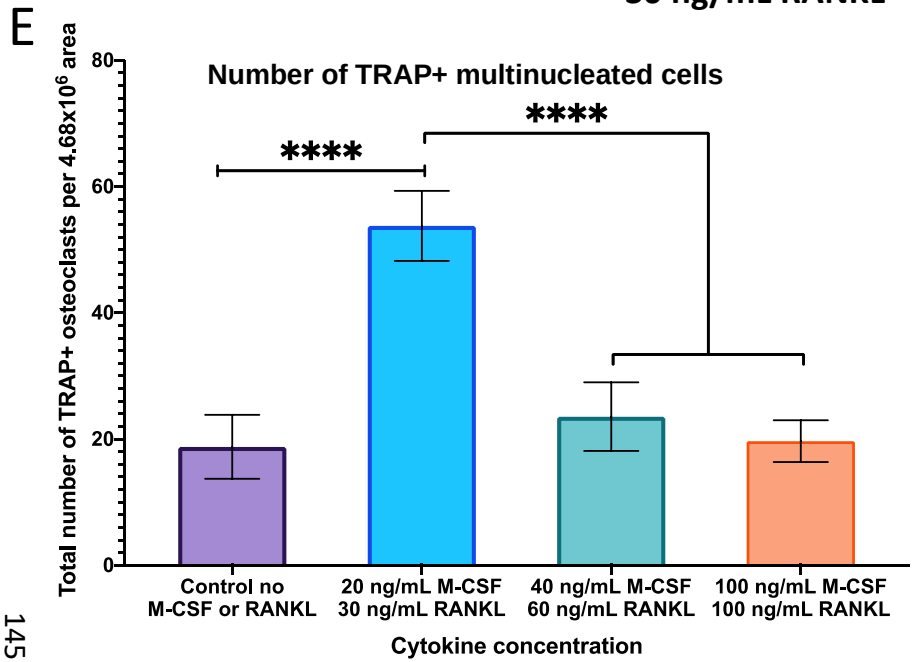

Figures 3.1: Differentiation potential of bone marrow-derived cells into mature osteoclast-like cells following the addition of M-CSF and RANKL. Images A-H show images of differentiated cells into mature osteoclast-like cells after 7 days in culture. Cells were cultured in either; A) no M-CSF and RANKL, B) with 20 ng/mL of M-CSF and 30 ng/mL of RANKL, C) with 40 ng/mL of M-CSF and 60 ng/mL of RANKL and D) with 100 ng/mL of M-CSF and 100 ng/mL of RANKL. Graph E) shows the differentiation efficiency of bone marrow-derived cells into $TRAP^+$ osteoclast-like cells with or without the presence of M-CSF and RANKL at 7 days respectively. Significance between groups determined via two-way ANOVA with Tukey post-hoc test. Error bars represent mean ±S.E.M (n=3) **P < 0.05, **P < 0.01 and **** P < 0.001*.

3.3.2: Nuclear Cellular Counts of the Bone Marrow Following M-CSF and RANKL Supplementation

3.3.2a: Nuclear Cellular Counts of the Bone Marrow Following M-CSF and RANKL Supplementation Within the Surrounding Culture Media.

To assess the number of cells retained during culture in the femoral slice, following supplementation with M-CSF and RANKL, cellular nuclear counts (Figure 3.2A) and percentage loss of cells (Figure 3.2B) was calculated within a 10,000 μm^2 area. Statistical analysis was compared within each culture group and between groups at 0 h, 24 h and 48 h of culture. Slices supplemented with either 20 ng/mL M-CSF and 30 ng/mL RANKL or 40 ng/mL M-CSF / 60 ng/mL RANKL, were compared to 0 h uncultured control femoral slices.

For tissue slices supplemented with 20 ng/mL M-CSF and 30 ng/mL RANKL, cell counts for 0 h uncultured controls, showed a mean of 294 cells. After 24 h there was a significant decrease in the mean number of cells to 112 cells ($P < 0.0001$). The mean percentage loss of cells after 24 h was 62 % which was significant compared to 0 h controls ($P < 0.001$). At 48 h the mean number of cells was significantly decreased to 57 cells when compared to 24 h samples ($P < 0.05$) and 0 h controls ($P < 0.0001$). The mean percentage loss of cells was 81 % which was significant when compared to 24 h samples ($P < 0.01$) and 0 h controls ($P < 0.0001$).

Tissue slices that were supplemented with 40 ng/mL M-CSF and 60 ng/mL RANKL cell counts for 0 h uncultured controls, showed a mean of 295 cells. After 24 h there was a significant decrease in the mean number of cells to 105 cells ($P < 0.0001$). The mean percentage loss of cells after 24 h was 65 % which was significant compared to 0 h controls ($P < 0.001$). At 48 h the mean number of cells were non-significantly decreased to 66 cells when compared to 24 h samples ($P > 0.05$) and significantly reduced compared to 0 h controls ($P < 0.0001$). The mean percentage loss of cells was 78 % which was non-significant when compared to 24 h samples ($P > 0.05$) and significant compared to 0 h controls ($P < 0.0001$).

There was no significant difference between cell counts and percentage loss of cells (*P > 0.05*) at 0 h, 24 or 48 h, when compared to unsupplemented slices to slices supplemented with either 20 ng/mL M-CSF and 30 ng/mL RANKL or 40 ng/mL M-CSF and 60 ng/mL RANKL.

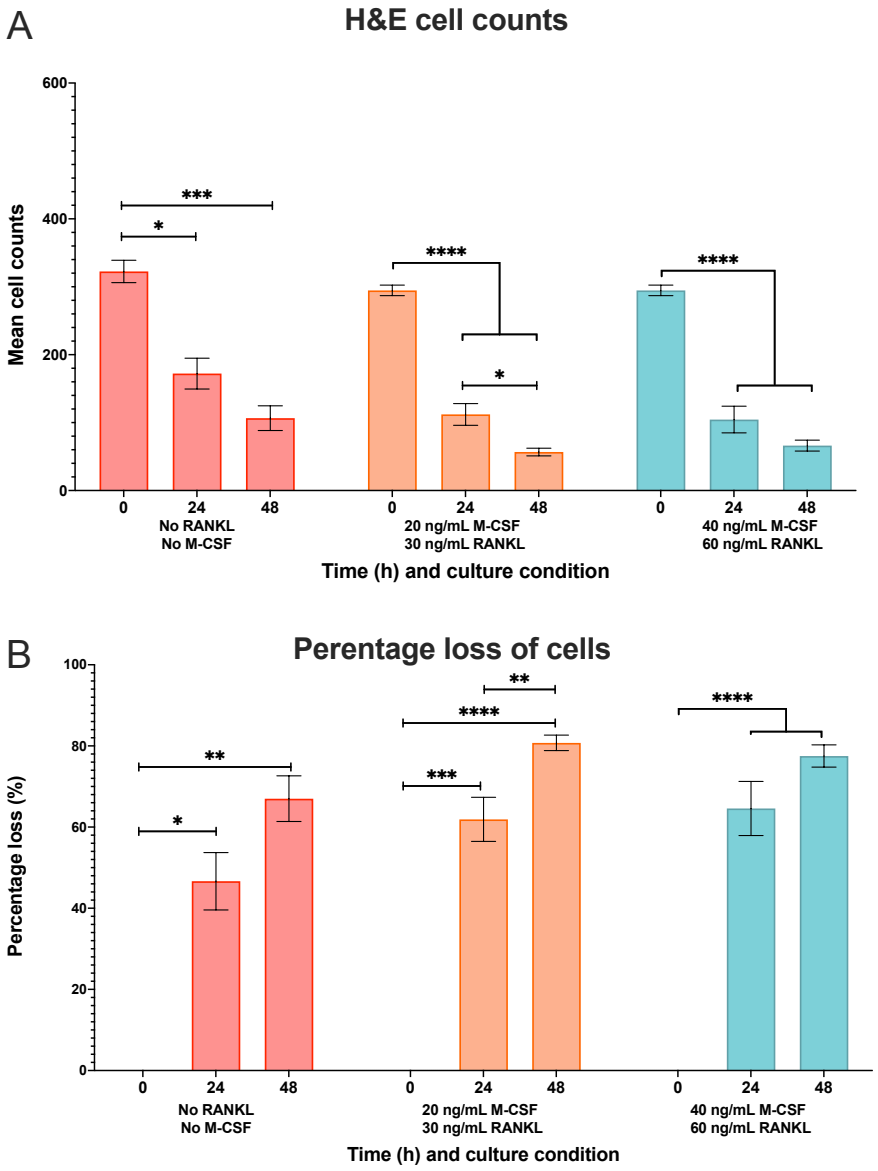

Figure 3.2: Total cell counts and percentage loss following culture with M-CSF and RANKL. Graphs A) mean cell counts and B) mean percentage loss of cells, following the supplementation of cytokines added to surrounding culture media at two different concentrations at 20 ng/mL M-CSF and 30 ng/mL RANKL or 40 ng/mL M-CSF / 60 ng/mL RANKL, when compared to no cytokine supplemented samples. Graphs show cell loss over 48 h for all culture conditions. Significance within groups determined via one-way ANOVA and between groups via two-way ANOVA with Tukey post-hoc test. Error bars represent mean ±S.E.M for M-CSF and RANKL 0 h (n=4), 24 h (n=4) and 48 h (n=5), 20 ng/mL M-CSF and 30 ng/mL RANKL supplementation 0 h (n=3), 24 h (n=6) and 48 h (n=5) and 40 ng/mL M-CSF / 60 ng/mL RANKL supplementation 0 h (n=4), 24 h (n=5) and 48 h (n=5) *$P < 0.05$, ** $P < 0.001$, ***$P < 0.001$ and ****$P < 0.0001$.

3.3.2b: Cellular Counts for Femoral Slices Supplemented With M-CSF and RANKL With Microinjection of Mixed Tibial Bone Marrow Cells

Femoral slices microinjected with mixed tibial bone marrow cells were also analysed for the total nuclear cell counts (Figure 3.3 A) and percentage loss of cells (Figure 3.3 B), within a 10,000 μm^2 area. These slices were supplemented with 20 ng/mL M-CSF and 30 ng/mL RANKL in the surrounding basal and agarose culture media and with the αMEM media used to microinject the cells into the bone marrow cavity. Cultures were analysed at 0 h, 24 h and 48 h. Two controls were used as a comparison: the first was femoral slices injected only with αMEM culture media, with 20 ng/mL M-CSF and 30 ng/mL RANKL, without any tibial bone marrow cells along with the same cytokines added to the basal culture media and agarose. An additional control was the culture of the femoral slice in the presence of 20 ng/mL M-CSF and 30 ng/mL RANKL in the agar but without any injection.

For tissue slices that were supplemented with 20 ng/mL M-CSF and 30 ng/mL RANKL, cell counts for 0 h uncultured controls, showed a mean of 294 cells. After 24 h there was a significant decrease in the mean number of cells to 112 cells ($P < 0.0001$). The mean percentage loss of cells after 24 h was 62 % which was significant compared to 0 h controls ($P < 0.001$). At 48 h the mean number of cells was significantly decreased to 57 cells when compared to 24 h samples ($P < 0.05$) and 0 h controls ($P < 0.0001$). The mean percentage loss of cells was 81 % which was significant when compared to 24 h samples ($P < 0.01$) and 0 h controls ($P < 0.0001$).

Femoral slices microinjected with mixed tibial bone marrow cells containing 20 ng/mL M-CSF and 30 ng/mL RANKL and incubated with culture media supplemented with 20 ng/mL M-CSF and 30 ng/mL RANKL had a mean of 505.5 cells at 0 h, this was a significant increase in the number of cells at the beginning of culture compared to no injection slices supplemented with M-CSF and RANKL ($P < 0.0001$). After 24 h the mean number of cells within the bone marrow was 358 cells and this was not significant compared to 0 h controls ($P > 0.05$). The mean percentage loss of cells after 24 h was low at 29 % which was non-significant compared to 0 h controls ($P < 0.001$). Microinjected cultures with tibial bone marrow cells at 24 h demonstrated a significant improvement in the number of cells, when compared to 24 h no injection slices supplemented with M-CSF and RANKL ($P < 0.01$). After

48 h the mean number of cells within the bone marrow was 246 cells this was not significant compared to 24 h cultures (*P > 0.05*), however this was significantly decreased compared to 0 h controls (*P < 0.05*). The mean percentage loss of cells after 48 h was 51 % which was significant compared to 24 h cultures (*P < 0.05*) and 0 h controls (*P < 0.01*). When comparing microinjected cultures with tibial bone marrow cells to no injection M-CSF and RANKL supplemented slices, there was a very significant increase in cells at 48 h for microinjected tibial bone marrow slices (*P < 0.01*).

3.3.2c: Cellular Counts for Femoral Slices Supplemented With M-CSF and RANKL Without Microinjection of Mixed Tibial Bone Marrow Cells

Analysis was also carried out on femoral slices injected with αMEM containing 20 ng/mL M-CSF and 30 ng/mL RANKL without any tibial bone marrow cells and had the surrounding culture media supplemented with 20 ng/mL M-CSF and 30 ng/mL RANKL . At 0 h, the mean number of cells was 419 this was not significant when compared to no injection control slices with M-CSF and RANKL (*P > 0.05*) even though the mean number of cells was higher. There was a non-significant decrease in cell numbers, when compared to microinjected slices with tibial bone marrow cells at 0 h (*P > 0.05*).

After 24 h the mean number of cells within the bone marrow was 234 cells and this was significant compared to 0 h controls (*P < 0.05*). This was also non-significant when compared to no injection controls and tibial bone marrow microinjected slices (*P > 0.05*). The mean percentage loss of cells after 24 h was 44 % which was significant compared to 0 h controls (*P < 0.05*). The percentage loss of cells was significantly reduced when compared to tibial bone marrow microinjected slices (*P < 0.0001*) and non-significant when compared to no injection controls (*P > 0.05*). At 48 h the mean number of cells within the bone marrow was 211 cells and this was significant compared to 0 h controls (*P < 0.05*) but not when compared to 24 h samples (*P > 0.05*). This was significantly increased when compared to 48 h no injection controls (*P < 0.05*) and was not significant when compared to 48 h tibial bone marrow microinjected slices (*P > 0.05*). The mean percentage loss of cells after 24 h was 50 % which was significant compared to 0 h controls (*P < 0.01*) but not when compared to 24 h samples (*P > 0.05*). The percentage loss of cells was significantly reduced when compared

to 48 h no injection controls ($P < 0.01$) and non-significant when compared to 48 h tibial bone marrow microinjected slices ($P > 0.05$).

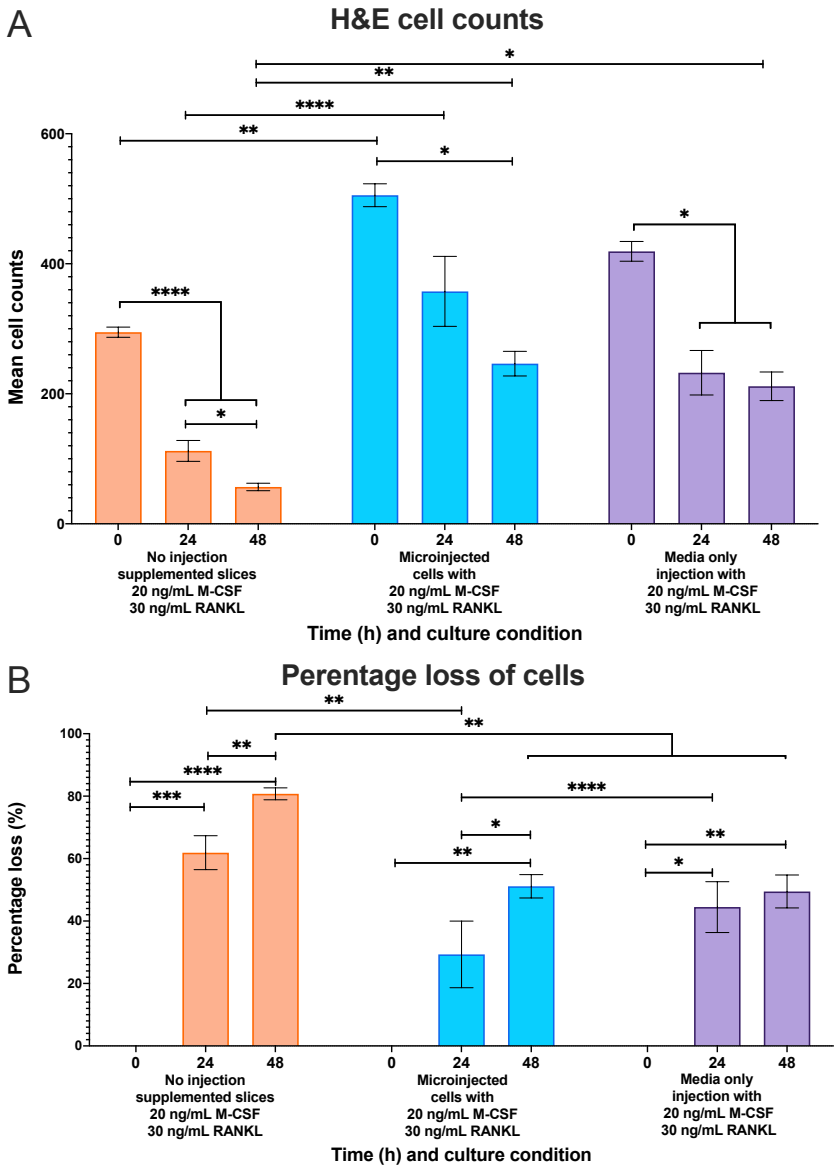

Figure 3.3: Total cell counts and percentage loss following microinjection and supplementation with M-CSF and RANKL. Graphs A) the mean cell counts and B) mean percentage loss of cells slices supplemented with 20 ng/mL M-CSF and 30 ng/mL RANKL in the surrounding culture media and within the bone marrow cavity with or without mixed tibial bone marrow cells. Graphs indicate that microinjection of both cells and media increase cell counts and reduce percentage loss of cells over 48 h. Microinjected data was compared 20 ng/mL M-CSF and 30 ng/mL RANKL supplemented slices to surrounding culture media without any microinjection from Figure 3.2. Graphs show cell loss over 48 h for all culture conditions. Significance within groups determined via one-way ANOVA and between groups via two-way ANOVA with Tukey post-hoc test. Error bars represent mean ±S.E.M for 20 ng/mL M-CSF and 30 ng/mL RANKL supplementation 0 h (n=3), 24 h (n=6) and 48 h (n=5), injection of tibial cells and M-CSF and RANKL 0 h, 24 h and 48 h (n=3) and media only injection with M-CSF and RANKL 0 h, 24 h and 48 h (n=3). *$P < 0.05$, ** $P < 0.01$, *** $P < 0.001$ and ****$P < 0.0001$.

3.3.3: Cellular Viability

3.3.3a: Cellular Necrosis of Extracellular LDH Release From Slices Supplemented With M-CSF and RANKL

Extracellular LDH released from cells during culture was quantified using a colourimetric assay. Results are shown in Figure 3.4A as absorbance or in Figure 3.4B as average percentage cytotoxicity.

Femoral slices supplemented with 20 ng/mL M-CSF and 30 ng/mL RANKL showed a significant increase in mean absorbance of LDH released from cells at 24 h when compared to 0 h uncultured controls ($P < 0.001$). When compared to samples without any M-CSF and RANKL there was a significant increase in absorbance with samples with the addition of M-CSF and RANKL ($P < 0.01$). The percentage cytotoxicity at 24 h was 50 % which was significantly increased when compared to 0 h controls ($P < 0.0001$). When compared to samples without any M-CSF and RANKL at 24 h there was a significant increase in percentage cytotoxicity ($P < 0.01$). After 48 h there was a non-significant increase in LDH absorbance when compared to 24 h samples ($P > 0.05$) and was significant compared to 0 h controls ($P < 0.001$). Comparison to 48 h samples without M-CSF and RANKL showed a significant increase in LDH release ($P < 0.05$). The percentage cytotoxicity at 48 h was 58 % which was significantly increased when compared to 0 h controls ($P < 0.0001$) and non-significant when compared to 24 h samples ($P > 0.05$). Comparison to 48 h samples without M-CSF and RANKL showed a significant increase in LDH percentage cytotoxicity ($P < 0.05$). All samples demonstrated significant lower LDH activity when compared to the positive control ($P < 0.0001$).

Femoral slices supplemented with 40 ng/mL M-CSF / 60 ng/mL RANKL showed a significant increase in mean absorbance of LDH released from cells at 24 h when compared to 0 h uncultured controls ($P < 0.01$). When compared to samples supplemented 20 ng/mL M-CSF and 30 ng/mL RANKL at 24 h there was no significant difference in absorbance ($P > 0.05$). When compared to samples without any M-CSF and RANKL there was a significant increase in absorbance with samples with the addition of M-CSF and RANKL ($P < 0.01$). The percentage cytotoxicity at 24 h was 45 % which was significantly increased when compared

to 0 h controls (*P < 0.001*). When compared to samples supplemented 20 ng/mL M-CSF and 30 ng/mL RANKL at 24 h there was no significant difference in percentage cytotoxicity (*P > 0.05*). When compared to samples without any M-CSF and RANKL at 24 h there was a significant increase in percentage cytotoxicity (*P < 0.01*). After 48 h there was a slight non-significant increase in LDH absorbance when compared to 24 h samples (*P > 0.05*) and was significant compared to 0 h controls (*P < 0.001*). When compared to samples supplemented 20 ng/mL M-CSF and 30 ng/mL RANKL or without M-CSF and RANKL at 48 h there was no significant difference in absorbance (*P > 0.05*). The percentage cytotoxicity at 48 h was 50 % which was significantly increased when compared to 0 h controls (*P < 0.001*) and non-significant when compared to 24 h samples (*P > 0.05*). When compared to samples supplemented 20 ng/mL M-CSF and 30 ng/mL RANKL or without M-CSF and RANKL at 48 h there was no significant difference in absorbance (*P > 0.05*). All samples demonstrated significant lower LDH activity when compared to the positive control (*P < 0.0001*).

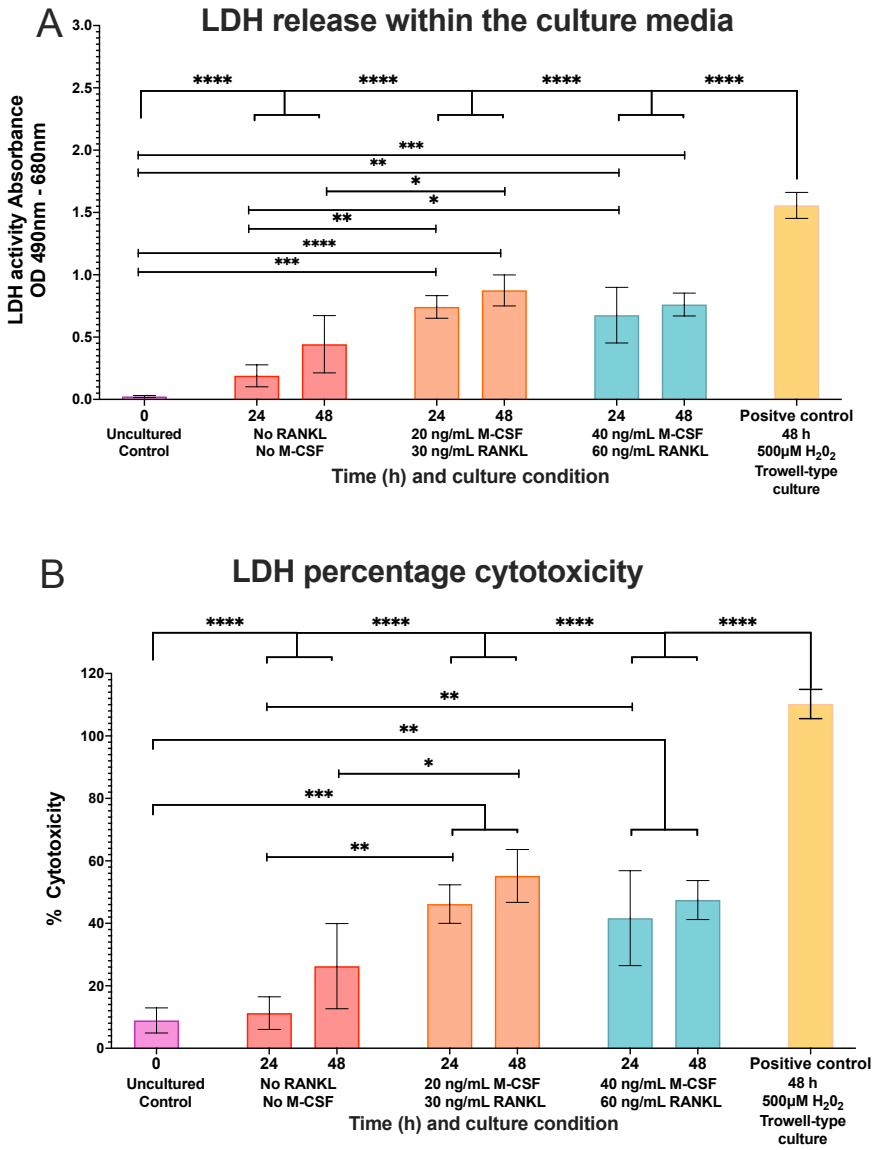

Figure 3.4: Extracellular LDH analysis following culture with M-CSF and RANKL. Graphs indicating A) LDH release and B) percentage cytotoxicity of tissue slices following supplementation of two different concentrations of cytokines at 20 ng/mL M-CSF and 30 ng/mL RANKL or 40 ng/mL M-CSF / 60 ng/mL RANKL into the surrounding culture media, when compared to no cytokine supplemented samples. Data for control no M-CSF and RANKL obtained from Figure 2.11. Graphs show an increase in LDH and cytotoxicity of supplemented slices over 48 h. Significance within groups determined via one-way ANOVA and between groups via two-way ANOVA with Tukey post-hoc test. Error bars represent mean ±S.E.M for uncultured control 0 h (n=4), no M-CSF and RANKL 24 h (n=4) and 48 h (n=4), 20 ng/mL M-CSF and 30 ng/mL RANKL supplementation 24 h (n=5) and 48 h (n=4), 40 ng/mL M-CSF / 60 ng/mL RANKL supplementation 24 h (n=4) and 48 h (n=4). *$P < 0.05$, ** $P < 0.01$, ***$P < 0.001$ and ****$P < 0.0001$.

3.3.3b: Extracellular LDH Analysis of Slices Supplemented With M-CSF and RANKL and Injected With Tibial Mixed Bone Marrow Cells.

Extracellular LDH activity for microinjected samples with or without mixed tibial bone marrow cells is shown in Figure 3.5A for absorbance and Figure 3.5B for percentage cytotoxicity. Following microinjection with mixed tibial bone marrow cells supplemented with 20 ng/mL M-CSF and 30 ng/mL RANKL, LDH absorbance was low at 0 h and was non-significant compared to 0 h no M-CSF and RANKL uncultured samples ($P > 0.05$). The percentage cytotoxicity at 0 h with a mean of 0 %, was non-significant compared to 0 h no M-CSF and RANKL uncultured samples ($P > 0.05$). At 24 h there was no significant change in absorbance when compared to 0 h for microinjected samples ($P > 0.05$). When compared to 24 h no injection and 20 ng/mL M-CSF and 30 ng/mL RANKL supplemented slices, there was a significant decrease in LDH release for microinjected samples ($P < 0.01$). At 24 h there was a non-significant increase in percentage cytotoxicity to a mean of 4 % when compared to 0 h microinjected samples ($P > 0.05$). When compared to 24 h no injection and 20 ng/mL M-CSF and 30 ng/mL RANKL supplemented slices, there was a significant decrease in percentage cytotoxicity by 46 % for microinjected samples ($P < 0.0001$). At 48 h there was a non-significant decrease in absorbance when compared to 24 h and 0 h microinjected samples ($P > 0.05$). When compared to 48 h no injection and 20 ng/mL M-CSF and 30 ng/mL RANKL supplemented slices, there was a significant decrease in LDH release for microinjected samples ($P < 0.01$). At 48 h there was a non-significant decrease in percentage cytotoxicity to a mean of 0 % when compared to 24 h and 0 h microinjected samples ($P > 0.05$). When compared to 48 h no injection and 20 ng/mL M-CSF and 30 ng/mL RANKL supplemented slices, there was a significant decrease in percentage cytotoxicity by 58 % for microinjected samples ($P < 0.0001$). All microinjected samples were significantly lower when compared to the positive control ($P < 0.0001$).

3.3.3c: Extracellular LDH Analysis of Slices Supplemented With M-CSF and RANKL and Without Injection With Tibial Mixed Bone Marrow Cells.

LDH activity for slices injected with αMEM media supplemented with 20 ng/mL M-CSF and 30 ng/mL RANKL, had a similarly reduced level of LDH absorbance which was also low at 0 h and was non-significant compared to 0 h no M-CSF and RANKL uncultured samples and 0 h

microinjected samples with cells and supplements (*P > 0.05*). The percentage cytotoxicity at 0 h with a mean of 3 %, was non-significant compared to 0 h no M-CSF and RANKL uncultured samples and 0 h microinjected samples with cells and supplements (*P > 0.05*). At 24 h there was no significant change in absorbance when compared to 0 h for microinjected samples (*P > 0.05*). When compared to 24 h no injection and 20 ng/mL M-CSF and 30 ng/mL RANKL supplemented slices, there was a significant decrease in LDH release for microinjected samples (*P < 0.01*). There was no significant difference in LDH release when compared to 24 h microinjected samples with cells and supplements (*P > 0.05*). At 24 h there was a non-significant decrease in percentage cytotoxicity to a mean of 2 % when compared to 0 h microinjected samples (*P > 0.05*). When compared to 24 h no injection and 20 ng/mL M-CSF and 30 ng/mL RANKL supplemented slices, there was a significant decrease in percentage cytotoxicity by 48 % for media only microinjected samples (*P < 0.0001*). There was no significant difference in percentage cytotoxicity when compared to 24 h microinjected samples with cells and supplements (*P > 0.05*). At 48 h there was a non-significant increase in absorbance when compared to 24 h and 0 h media only microinjected samples (*P > 0.05*). When compared to 48 h no injection and 20 ng/mL M-CSF and 30 ng/mL RANKL supplemented slices, there was a significant decrease in LDH release for microinjected samples (*P < 0.01*). There was no significant difference in LDH release when compared to 48 h microinjected samples with cells and supplements (*P > 0.05*). At 48 h there was a non-significant increase in percentage cytotoxicity to a mean of 5 % when compared to 24 h and 0 h microinjected samples (*P > 0.05*). When compared to 48 h no injection and 20 ng/mL M-CSF and 30 ng/mL RANKL supplemented slices, there was a significant decrease in percentage cytotoxicity by 53 % for microinjected samples (*P < 0.0001*). There was no significant difference in percentage cytotoxicity when compared to 48 h microinjected samples with cells and supplements (*P > 0.05*). All microinjected samples were significantly lower when compared to the positive control (*P < 0.0001*).

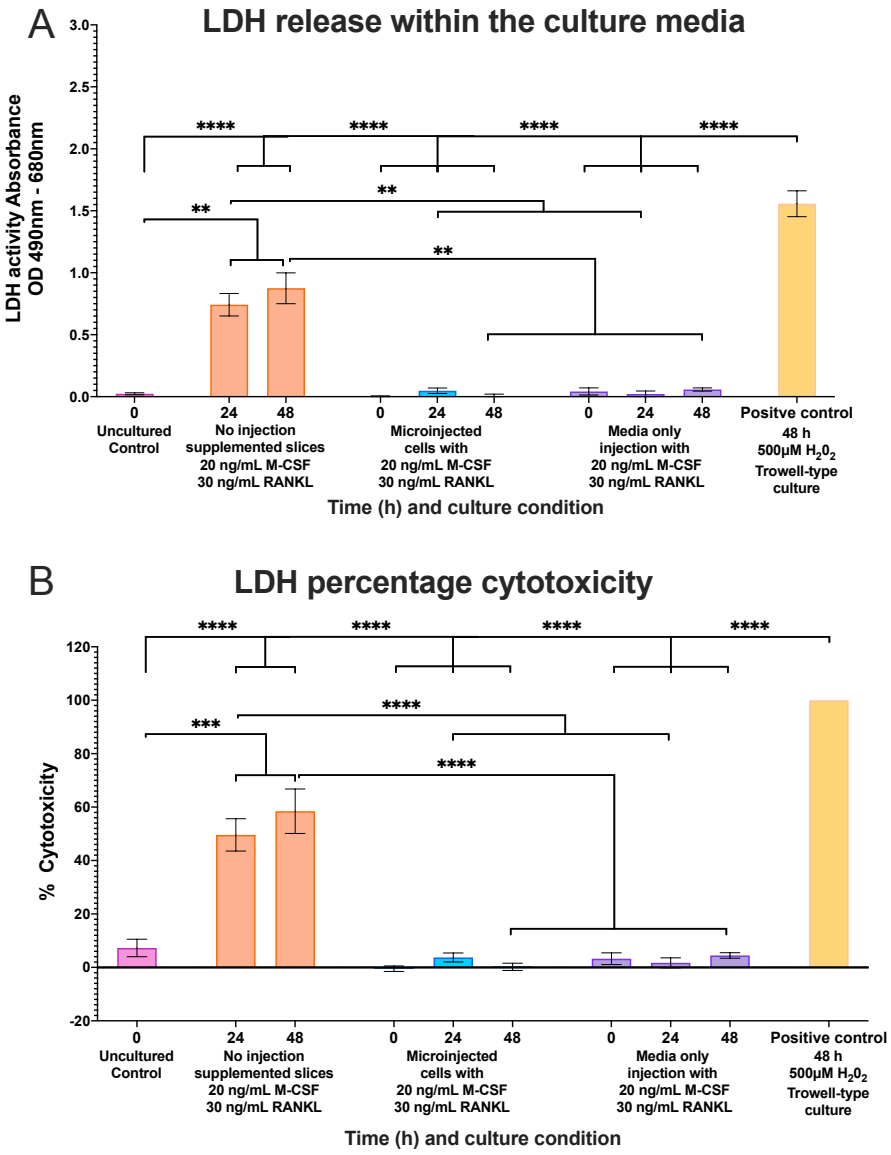

Figure 3.5: Extracellular LDH analysis following microinjection and culture with M-CSF and RANKL. Graphs indicating A) LDH release and B) percentage cytotoxicity of tissue slices following Trowell-type cultures supplemented with 20 ng/mL M-CSF and 30 ng/mL RANKL in the surrounding culture media and within the bone marrow cavity with or without mixed tibial bone marrow cells. Graphs show that microinjection of the bone marrow cavity with culture media with or without cells has very low LDH release and cytotoxicity on the cells. Significance within groups determined via one-way ANOVA and between groups via two-way ANOVA with Tukey post-hoc test. Error bars represent mean ±S.E.M for uncultured control 0 h (n=4), 20 ng/mL M-CSF and 30 ng/mL RANKL supplementation 24 h (n=5) and 48 h (n=4), injection of tibial cells and M-CSF and RANKL 0 h (n=5), 24 h and 48 h (n=3) and media only injection with M-CSF and RANKL 0 h (n=5), 24 h and 48 h (n=3). *$P < 0.05$, ** $P < 0.01$ and ****$P < 0.0001$.

3.3.4: Analysis of Apoptosis Cell Localisation Within Slices Supplemented With M-CSF and RANKL

The number of cleaved caspase-3 and BAX cell and percentage localised immunostaining was analysed within slices supplemented with M-CSF and RANKL within a 12.5 mm^2 area.

3.3.4a: Analysis of Cleaved Caspase-3 Immunohistochemistry Localisation In M-CSF and RANKL Supplemented Femoral Slices

Cleaved caspase-3 analysis at 0 h showed the mean number of bone marrow cells at 401 cells, from which 66 cells were positive for cleaved caspase-3 which represented a 15 % positive staining (Figures 3.6A,B&C and Supplementary Figure 4A).

Following 24 h culture with 20 ng/mL M-CSF and 30 ng/mL RANKL, there was a significant decrease in the number of bone marrow cells representing a mean of 187 cells when compared to 0 h controls (*P < 0.001,* Figure 3.6B and Supplementary Figure 4B). There was a non-significant decrease (*P < 0.05*) in the mean number of positively stained cleaved caspase 3 cells to 53 cells when compared to 0 h controls (Figure 3.6A and Supplementary Figure 4B). When compared to 24 h slices without M-CSF and RANKL supplementation there was a significant increase in the number of cleaved caspase 3 cells for supplemented slices (*P < 0.05*). At 24 h the mean percentage of cells remaining that were stained positive cleaved caspase 3 significantly increased to 30 % (*P < 0.05*, Figure 3.6C). When compared to 24 h slices without M-CSF and RANKL supplementation there was a significant increase in the percentage of cleaved caspase 3 cells for supplemented slices (*P < 0.01*). At 48 h in culture there was a significant decrease in the number of mean bone marrow cells to 90 cells when compared to 24 h samples (*P < 0.01,* Figure 3.6B and Supplementary Figure 4C). At 48 h there was a non-significant decrease in the mean number of positively stained cells for cleaved caspase 3 to 31 cells when compared to 24 h samples and a significant decrease when compared to 0 h controls (*P > 0.05*, Figure 3.6A and Supplementary Figure 4C). When compared to 48 h slices without M-CSF and RANKL supplementation there was a non-significant increase in the number of cleaved caspase 3 cells for supplemented slices (*P > 0.05*). At 48 h the mean percentage of cells remaining that were stained positive cleaved caspase 3 was non-significantly increased to 40 % localisation (*P > 0.05*, Figure 3.6C). When

compared to 48 h slices without M-CSF and RANKL supplementation there was a significant increase in the percentage of cleaved caspase 3 cells for supplemented slices (*P < 0.001*).

Following 24 h culture with 40 ng/mL M-CSF and 60 ng/mL RANKL, there was a significant decrease in the number of bone marrow cells representing a mean of 207 cells when compared to 0 h controls (*P < 0.01,* Figure 3.6A and Supplementary Figure 4D). Following 24 h culture with 40 ng/mL M-CSF / 60 ng/mL RANKL, there was a non-significant decrease (*P > 0.05*) in the mean number of positively stained cleaved caspase 3 cells to 39 cells when compared to 0 h controls (Figure 3.6A and Supplementary Figure 4D). There was a non-significant decrease in the mean number of cleaved caspase 3 cells when compared to slices supplemented with 20 ng/mL M-CSF and 30 ng/mL RANKL at 24 h (*P > 0.05*), and a non-significant increase when compared to 24 h slices without M-CSF and RANKL supplementation (*P > 0.05*). At 24 h the mean percentage of cells remaining that were stained positive cleaved caspase 3 was non-significant at 23 % when compared to 0 h controls (*P > 0.05*, Figure 3.6C). This percentage was non-significant when compared to slices supplemented with 20 ng/mL M-CSF and 30 ng/mL RANKL at 24 h (*P > 0.05*) or slices without M-CSF and RANKL supplementation at 24 h (*P > 0.05*). At 48 h in culture there was maintenance in the number of mean bone marrow cells to 212 cells when compared to 24 h samples (*P < 0.01,* Figure 3.6B and Supplementary Figure 4E). This was significantly increased compared to no RANKL and M-CSF supplemented slices (*P < 0.05*). At 48 h there was a non-significant increase in the number of positively stained cleaved caspase 3 cells to a mean of 57 cells when compared to 24 h samples and a non-significant decrease when compared to 0 h controls (*P > 0.05*, Figure 3.6A and Supplementary Figure 4E). When compared to 48 h slices without M-CSF and RANKL supplementation there was a significant increase in the number of cleaved caspase 3 cells for supplemented slices (*P < 0.001*). There was no significant difference in cleaved caspase -3 labelled cells when compared to 48 h slices supplemented with 20 ng/mL M-CSF and 30 ng/mL RANKL (*P > 0.05*) although mean cell numbers were increased for slices supplemented with 40 ng/mL M-CSF / 60 ng/mL RANKL. At 48 h the mean percentage of cells remaining that were stained positive cleaved caspase 3 significantly increased to 48 % localisation (*P < 0.05*, Figure 3.6C). There were no significant differences in the mean percentage when compared to slices supplemented with 20 ng/mL M-CSF and 30 ng/mL RANKL at 24 h (*P > 0.05*), although there was a significant

increase when compared to 24 h slices without M-CSF and RANKL supplementation (*P < 0.0001*).

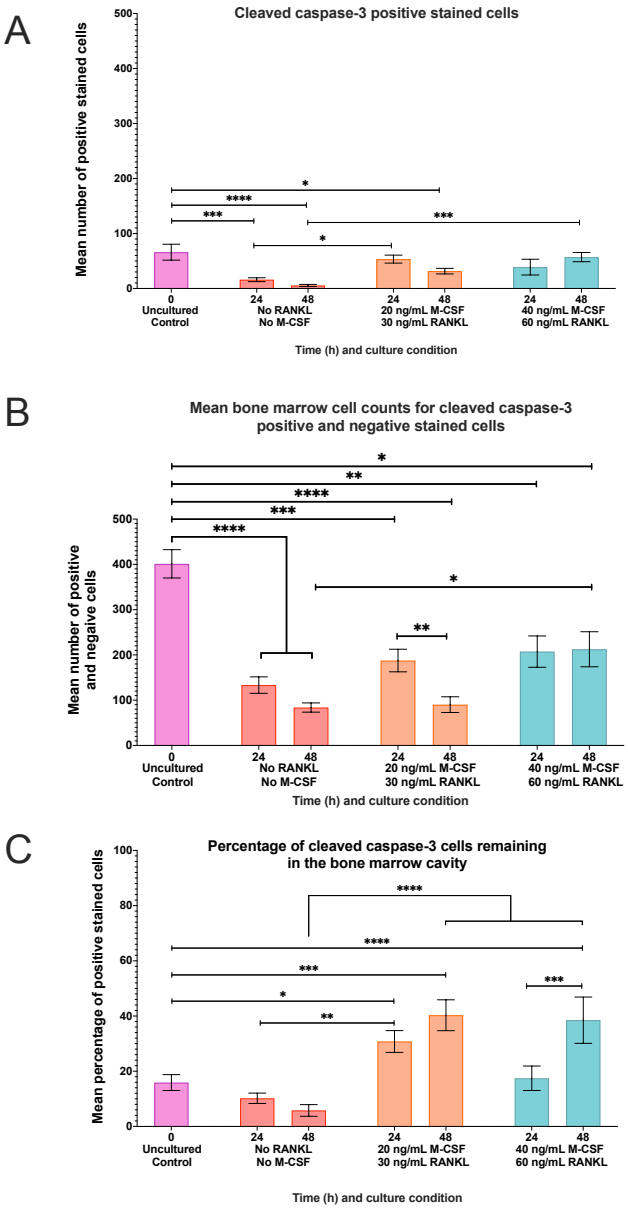

Figure 3.6: Cleaved caspase-3 analysis following culture with M-CSF and RANKL. Immunohistochemical analysis for cleaved caspase-3 labelled cells for slices supplemented with either 20 ng/mL M-CSF and 30 ng/mL RANKL or 40 ng/mL M-CSF and 60 ng/mL RANKL and compared to no cytokine supplemented samples. A) Graph showing data for mean cell counts for cleaved caspase-3 positive stained cells. B) Graph shows mean cell counts for both cleaved caspase-3 positive and negative stained cells. Graph C) showing the mean percentage of cleaved caspase-3 positive stained cells remaining in the bone marrow cavity. Data for 0 h uncultured controls and no M-CSF and RANKL supplemented slices obtained from Figures 2.17. Graphs show loss of bone marrow cells during culture for all culture conditions. Supplemented slices show low number of cleaved-caspase-3 stained comparable to controls. Percentage analysis show increase inpositive stained cells for supplemented slices. Significance within groups determined via one-way ANOVA and between groups via two-way ANOVA with Tukey post-hoc test. Error bars represent mean ±S.E.M (n=3), **P < 0.05, ** P < 0.01, *** P < 0.001 and ****P < 0.0001.*

3.3.4b: Analysis of Cleaved Caspase-3 Immunohistochemistry Localisation in Slices Injected With M-CSF and RANKL With Or Without Mixed Tibial Bone Marrow Cells.

For slices microinjected with mixed tibial bone marrow cells supplemented with 20 ng/mL M-CSF and 30 ng/mL RANKL at 0 h showed a mean of 419 bone marrow cells of which a mean of 20 cells was positive for cleaved caspase-3 (Figure 3.7A&B, Supplementary Figure 5A). When compared to 0 h no M-CSF and RANKL samples, microinjected slices had a significantly lower number of cleaved caspase-3 positive cells ($P < 0.01$). The mean percentage of cells remaining that were stained positive for cleaved caspase-3 at 0 h was low at 5 % and was non-significant when compared to 0 h no M-CSF and RANKL uncultured samples ($P > 0.05$, Figure 3.7C). Following 24 h culture, there was a significant decrease in the number of bone marrow cells representing a mean of 132 cells when compared to 0 h controls ($P > 0.0001$, Figure 3.7B and Supplementary Figure 5B). At 24 h the mean number of cleaved caspase 3 stained cells was non-significant maintaining at 20 cells when compared to 0 h microinjected controls ($P > 0.05$) and 24 h no injection only supplemented slices with 20 ng/mL M-CSF and 30 ng/mL RANKL samples ($P > 0.05$, Figure 3.7A and Supplementary Figure 5B). The mean percentage of cells remaining that were stained positive for cleaved caspase-3 at 24 h was significantly increased to 20 % when compared to 0 h microinjected controls ($P < 0.05$, Figure 3.7C). This was not significant when compared to 24 h no injection only supplemented slices with 20 ng/mL M-CSF and 30 ng/mL RANKL samples ($P > 0.05$). Following 48 h culture, the maintenance in the number of bone marrow cells represented a mean of 134 cells when compared to 24 h samples ($P < 0.05$, Figure 3.7B and Supplementary Figure 5C). At 48 h in culture, the mean number of cleaved caspase 3 stained cells was non-significantly increased to 36 cells when compared to 0 h microinjected controls ($P > 0.05$) and non-significant when compared to 48 h no injection only supplemented slices with 20 ng/mL M-CSF and 30 ng/mL RANKL samples ($P > 0.05$, Figure 3.7A and Supplementary Figure 5C). The mean percentage of cells remaining that were stained positive for cleaved caspase-3 at 48 h was significantly increased to 31 % when compared to 24 h microinjected samples ($P < 0.05$) and 0 h microinjected controls ($P < 0.0001$, Figure 3.7B). This percentage was not significant when compared to 24 h no injection only supplemented slices with 20 ng/mL M-CSF and 30 ng/mL RANKL samples ($P > 0.05$).

For slices injected with αMEM media supplemented with 20 ng/mL M-CSF and 30 ng/mL RANKL at 0 h showed a mean of 356 bone marrow cells of which a mean of 27 cells was positive for cleaved caspase-3 (Figure 3.7A&B, Supplementary Figure 5D). When compared to 0 h no M-CSF and RANKL samples, αMEM media microinjected slices had a significantly lower number of cleaved caspase-3 positive cells (*P < 0.01*) and were not significant compared to slices microinjected with mixed tibial bone marrow cells supplemented with 20 ng/mL M-CSF and 30 ng/mL RANKL (*P > 0.05*). The mean percentage of cells remaining that were stained positive for cleaved caspase-3 at 0 h was low at 8 %. This percentage was not significant when compared to 0 h no injection only supplemented slices with 20 ng/mL M-CSF and 30 ng/mL RANKL samples and 0 h slices microinjected with mixed tibial bone marrow cells (*P > 0.05*, Figure 3.7C). Following 24 h culture, there was a significant decrease in the number of bone marrow cells representing a mean of 160 cells when compared to 0 h controls (*P > 0.0001*, Figure 3.7B and Supplementary Figure 5E). At 24 h the mean number of cleaved caspase 3 stained cells was non-significantly increased to 29 cells when compared to 0 h media only injected samples (*P > 0.05*), 24 h no M-CSF and RANKL samples (*P > 0.05*) and microinjected with mixed tibial bone marrow cells supplemented with 20 ng/mL M-CSF and 30 ng/mL RANKL (*P > 0.05,* Figure 3.7A and Supplementary Figure 5E). The mean percentage of cells remaining that were stained positive for cleaved caspase-3 at 24 h was non-significantly increased to 17 % when compared to 0 h media only injected controls (*P > 0.05*, Figure 3.7C). This percentage was not significant when compared to 0 h no injection only supplemented slices with 20 ng/mL M-CSF and 30 ng/mL RANKL samples and 0 h slices microinjected with mixed tibial bone marrow cells (*P > 0.05*). Following 48 h culture, there was a significant decrease in the number of bone marrow cells representing a mean of 74 cells when compared to 24 h samples (*P > 0.05*, Figure 3.7B and Supplementary Figure 5F). At 48 h the mean number of cleaved caspase 3 stained cells was non-significantly decreased to 11 cells when compared to 24 h media only injected (*P < 0.05*) and non-significant when compared to 48 h no M-CSF and RANKL samples (*P > 0.05*) and 48 h microinjected with mixed tibial bone marrow cells supplemented with 20 ng/mL M-CSF and 30 ng/mL RANKL (*P > 0.05,* Figure 3.7A and Supplementary Figure 5F). The mean percentage of cells remaining that were stained positive for cleaved caspase-3 at 48 h was non-significantly decreased to 13 % when compared to 0 h and 24 h media only injected samples (*P > 0.05*, Figure 3.7C). This percentage was significantly reduced when compared to 48 h no injection only

supplemented slices with 20 ng/mL M-CSF and 30 ng/mL RANKL samples (*P < 0.001*) and 48 h slices microinjected with mixed tibial bone marrow cells (*P < 0.01*).

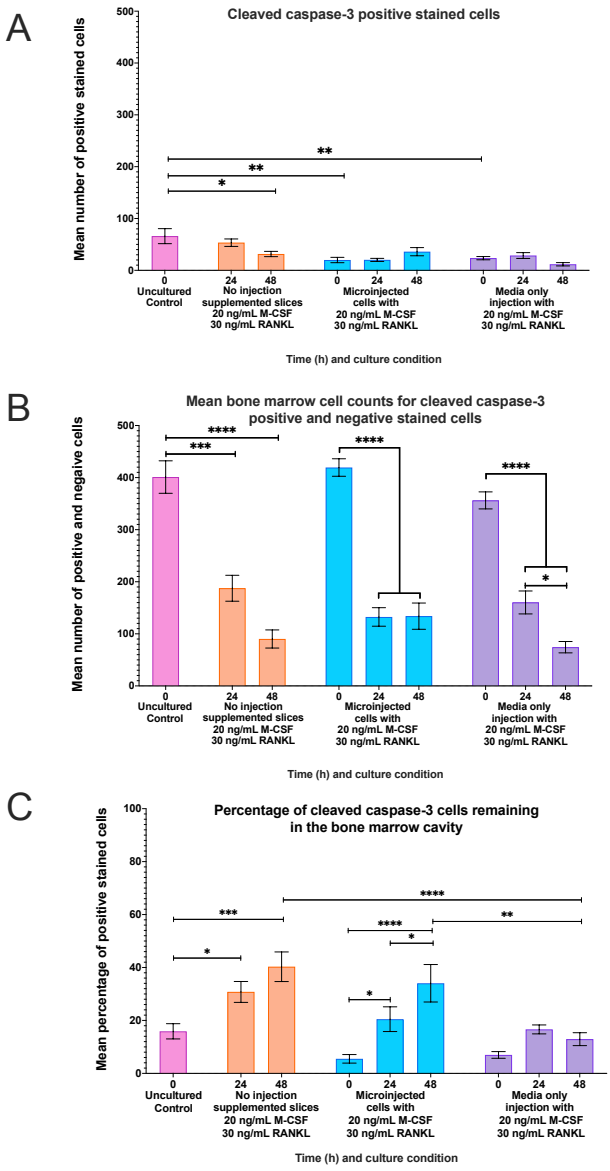

Figure 3.7: Cleaved caspase-3 analysis following microinjection and culture with M-CSF and RANKL. Immunohistochemical analysis for cleaved caspase-3 labelled cells for slices supplemented with 20 ng/mL M-CSF and 30 ng/mL RANKL in both the culture media and injected within the bone marrow cavity along with or without mixed tibial bone marrow cells. Trowell-type cultures supplemented with 20 ng/mL M-CSF and 30 ng/mL RANKL and no microinjection from Figure 3.6 was used as a control. Graph A) showing data for mean cell counts for cleaved caspase-3 positive stained cells. Graph B) showing mean cell counts for both cleaved caspase-3 positive and negative stained cells. Graph C) showing the mean percentage of cleaved caspase-3 positive stained cells remaining in the bone marrow cavity. Graphs shows loss of bone marrow cells along with reduced levels of cleaved caspase-3 stained cells for both microinjected slices over 48 h. Percentage of stained cells remaining show increase cleaved caspase-3 for tibial bone marrow injected samples over 48 h. Significance within groups determined via one-way ANOVA and between groups via two-way ANOVA with Tukey post-hoc test. Error bars represent mean ±S.E.M (n=3), **P < 0.05, ** P < 0.01, *** P < 0.001 and ****P < 0.0001.*

3.3.4d: Analysis of BAX Immunohistochemistry Localisation in M-CSF and RANKL Supplemented Femoral Slices

BAX analysis at 0 h showed the mean number of bone marrow cells at 375 cells, from which 311 cells were positive for BAX, corresponding to 84 % of positive stained cells (Figures 3.8A,B&C and Supplementary Figure 6A).

Following 24 h culture with 20 ng/mL M-CSF and 30 ng/mL RANKL, there was a significant decrease in the number of bone marrow cells representing a mean of 157 cells when compared to 0 h controls (*P < 0.0001,* Figure 3.8B and Supplementary Figure 6B). There was a significant decrease (*P < 0.05*) in the mean number of positively stained BAX cells to 74 cells when compared to 0 h controls (Figure 3.8A and Supplementary Figure 6B). When compared to 24 h slices without M-CSF and RANKL supplementation there was no significant difference for BAX-stained cells (*P > 0.05*). At 24 h the mean percentage of cells remaining that were stained positive for BAX significantly decreased to 48 % (*P < 0.0001*, Figure 3.8C). When compared to 24 h slices without M-CSF and RANKL supplementation there was no significance in percentage of BAX cells for supplemented slices (*P > 0.05*). At 48 h in culture there was a significant decrease in the number of mean bone marrow cells to 91 cells when compared to 24 h samples (*P < 0.05,* Figure 3.8B and Supplementary Figure 6C). At 48 h there was a non-significant decrease (*P > 0.05*) in the mean number of positively stained cells for BAX to 50 cells when compared to 24 h samples and a significant decrease when compared to 0 h controls (*P < 0.0001*, Figure 3.8A and Supplementary Figure 6C). When compared to 48 h slices without M-CSF and RANKL supplementation there was no significant difference for BAX-stained cells (*P > 0.05*). At 48 h the mean percentage of cells remaining that were stained positive for BAX non-significantly increased to 56 % localisation when compared to 24 h samples (*P > 0.05*, Figure 3.8C). When compared to 48 h slices without M-CSF and RANKL supplementation there was no significant differences in the percentage of BAX cells for supplemented slices (*P > 0.05*).

Following 24 h culture with 40 ng/mL M-CSF and 60 ng/mL RANKL, there was a significant decrease in the number of bone marrow cells representing a mean of 191 cells when compared to 0 h controls (*P < 0.01,* Figure 3.8A and Supplementary Figure 6D). At 24 h culture with 40 ng/mL M-CSF / 60 ng/mL RANKL, there was a significant decrease (*P < 0.05*)

in the mean number of positively stained BAX cells to 74 cells when compared to 0 h controls (Figure 3.8A and Supplementary Figure 6D). There was a no significant differences in the mean number of BAX-stained cells when compared to slices supplemented with 20 ng/mL M-CSF and 30 ng/mL RANKL at 24 h (*P > 0.05*), or 24 h slices without M-CSF and RANKL supplementation (*P > 0.05*). At 24 h the mean percentage of cells remaining that were stained positive for BAX significantly decreased to 47 % (*P < 0.0001*, Figure 3.8C). There was a no significant differences in the mean percentage of BAX-stained cells when compared to slices supplemented with 20 ng/mL M-CSF and 30 ng/mL RANKL at 24 h (*P > 0.05*), or 24 h slices without M-CSF and RANKL supplementation (*P > 0.05*). At 48 h in culture there was a non-significant decrease in the number of mean bone marrow cells to 106 cells when compared to 24 h samples (*P > 0.05,* Figure 3.8B and Supplementary Figure 6E). This was significantly increased compared to no RANKL and M-CSF supplemented slices (*P < 0.05*). At 48 h there was a non-significant decrease (*P > 0.05*) in the mean number of positively stained cells for BAX to 49 cells when compared to 24 h samples and a significant decrease when compared to 0 h controls (*P < 0.0001*, Figure 3.8A and Supplementary Figure 6E). There was a no significant differences in the mean number of BAX-stained cells when compared to slices supplemented with 20 ng/mL M-CSF and 30 ng/mL RANKL at 24 h (*P > 0.05*), or 24 h slices without M-CSF and RANKL supplementation (*P > 0.05*). At 48 h the mean percentage of cells remaining that were stained positive for BAX non-significantly increased to 56 % localisation when compared to 24 h samples (*P > 0.05*, Figure 3.8C). There was a no significant differences in the mean percentage of BAX-stained cells when compared to slices supplemented with 20 ng/mL M-CSF and 30 ng/mL RANKL at 24 h (*P > 0.05*), or 24 h slices without M-CSF and RANKL supplementation (*P > 0.05*).

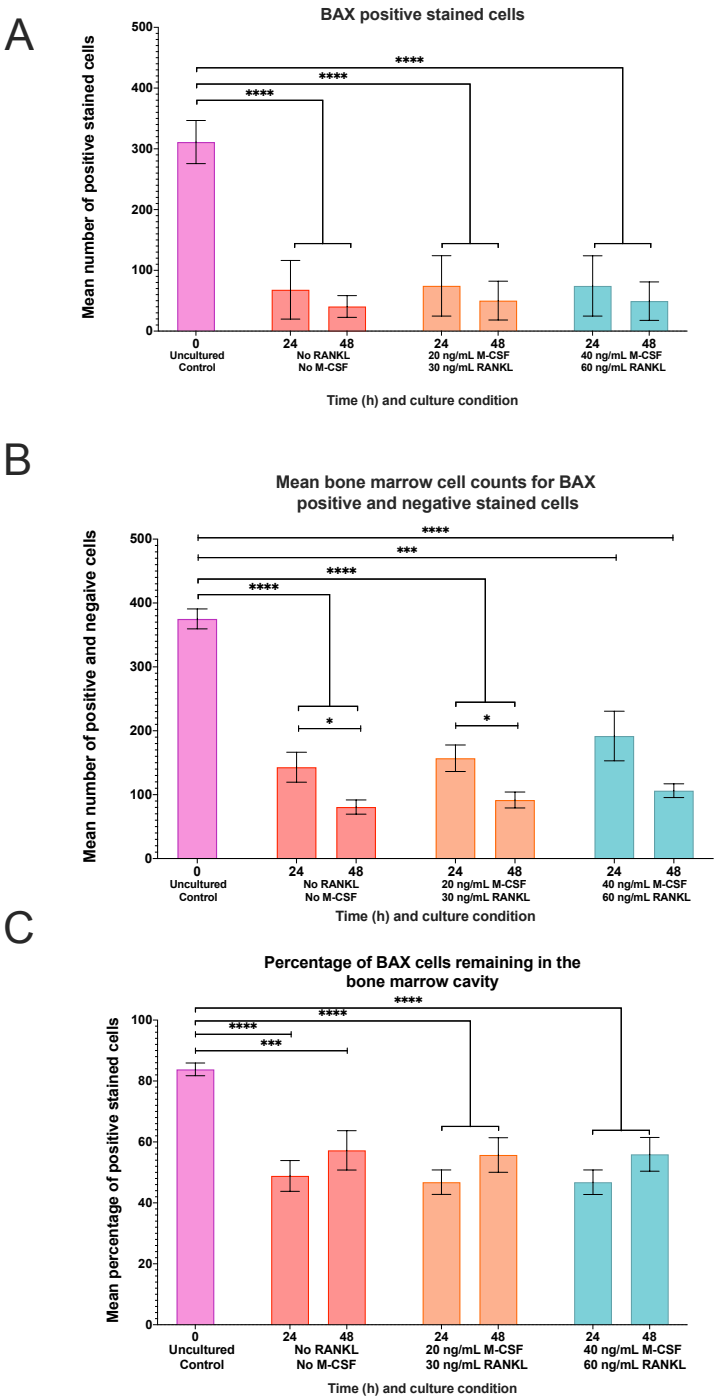

Figure 3.8: BAX analysis following culture with M-CSF and RANKL. Immunohistochemical analysis for BAX-labelled antibodies for slices supplemented with either 20 ng/mL M-CSF and 30 ng/mL RANKL or 40 ng/mL M-CSF and 60 ng/mL RANKL and compared to no cytokine supplemented samples. A) Graph showing data for mean cell counts for BAX positive stained cells. B) Graph shows mean cell counts for both BAX positive and negative stained cells. Graph C) showing the percentage of LDH positive stained cells remaining in the bone marrow cavity. Data for 0 h uncultured controls and no M-CSF and RANKL supplemented slices obtained from Figure 2.17. Graphs show no significance in numbers or percentage of BAX-stained cells for slices with or without M-CSF and RANKL at 24 h or 48 h. All cultures show a loss of both bone marrow cells and BAX-stained cells following 24 h and 48 h in culture. Significance within groups determined via one-way ANOVA and between groups via two-way ANOVA with Tukey post-hoc test. Error bars represent mean ±S.E.M (n=3), *$* P < 0.05$, ***$P < 0.001$ and ****$P < 0.0001$.

3.3.4e: Analysis of BAX Immunohistochemistry Localisation in Slices Injected With Or Without M-CSF and RANKL With Mixed Tibial Bone Marrow Cells.

For slices microinjected with mixed tibial bone marrow cells supplemented with 20 ng/mL M-CSF and 30 ng/mL RANKL at 0 h showed a mean of 314 bone marrow cells of which a mean of 141 cells was positive for BAX (Figure 3.9A&B, Supplementary Figure 5A). When compared to 0 h no M-CSF and RANKL samples, Bax stained cells for microinjected slices were significantly reduced when compared to 0 h no injection no M-CSF and RANKL uncultured controls (*P < 0.0001*). The mean percentage of cells remaining that were stained positive for BAX at 0 h was low at 43 %, this was significantly reduced when compared to 0 h no injection no M-CSF and RANKL uncultured controls (*P < 0.0001*, Figure 3.9C). Following 24 h culture, there was a significant decrease in the number of bone marrow cells representing a mean of 119 cells when compared to 0 h controls (*P > 0.0001*, Figure 3.9B and Supplementary Figure 5B). At 24 h the mean number of BAX-stained cells significantly decreased to 27 cells when compared to 0 h microinjected controls (*P < 0.0001*, Figure 3.9A and Supplementary Figure 7B). This was significantly reduced when compared to 24 h no injection only supplemented slices with 20 ng/mL M-CSF and 30 ng/mL RANKL samples (*P < 0.01*). The mean percentage of cells remaining that were stained positive for BAX at 24 h was significantly increased to 25 % when compared to 0 h microinjected controls (*P < 0.01*), this was significantly reduced when compared to 0 h no injection only supplemented slices with 20 ng/mL M-CSF and 30 ng/mL RANKL samples (*P < 0.0001,* Figure 3.9C). Following 48 h culture, there was maintenance in the number of bone marrow cells represented a mean of 124 cells when compared to 24 h samples (*P < 0.05*, Figure 3.9B and Supplementary Figure 5C). Following 48 h in culture, the mean number of BAX-stained cells was non-significantly increased to 17 cells when compared to 24 h microinjected controls (*P > 0.05*, Figure 3.9A and Supplementary Figure 7C). This was not significant when compared to 48 h no injection only supplemented slices with 20 ng/mL M-CSF and 30 ng/mL RANKL samples (*P > 0.05*). The mean percentage of cells remaining that were stained positive for BAX at 48 h non-significantly increased to 24 % when compared to 24 h microinjected samples (*P > 0.05*, Figure 3.9C). This percentage was significantly decreased when compared to 48 h no injection only supplemented slices with 20 ng/mL M-CSF and 30 ng/mL RANKL samples (*P < 0.0001*).

For slices injected with αMEM media supplemented with 20 ng/mL M-CSF and 30 ng/mL RANKL at 0 h showed a mean of 307 bone marrow cells of which a mean of 133 cells was positive for BAX (Figure 3.9A&B, Supplementary Figure 5D). When compared to 0 h no M-CSF and RANKL samples, αMEM media microinjected slices had a significantly reduced number of BAX-stained cells (*P < 0.0001*) and this was not significant when compared to slices microinjected with mixed tibial bone marrow cells supplemented with 20 ng/mL M-CSF and 30 ng/mL RANKL (*P > 0.05*). The mean percentage of cells remaining that were stained positive for BAX at 0 h was 45 %. This percentage was significant when compared to 0 h no injection no M-CSF and RANKL uncultured controls (*P < 0.0001*) and was non-significant when compared 0 h slices microinjected with mixed tibial bone marrow cells (*P > 0.05*, Figure 3.9C). Following 24 h culture, there was a significant decrease in the number of bone marrow cells representing a mean of 142 cells when compared to 0 h controls (*P > 0.001*, Figure 3.9B and Supplementary Figure 5E). At 24 h the mean number of BAX-stained cells was significantly decreased to 37 cells when compared to 0 h αMEM media only injected controls (*P < 0.0001*, Figure 3.9A and Supplementary Figure 7E). This was not significant when compared to 24 h no injection only supplemented slices with 20 ng/mL M-CSF and 30 ng/mL RANKL cultured samples and 24 h slices microinjected with mixed tibial bone marrow cells (*P > 0.05*). The mean percentage of cells remaining that were stained positive for BAX at 24 h was significantly decreased to 27 % when compared to 0 h αMEM media only injected controls (*P < 0.01*, Figure 3.9C). This percentage was significant when compared to 0 h no injection uncultured controls (*P < 0.01*) and 0 h slices microinjected with mixed tibial bone marrow cells (*P < 0.01*). Following 48 h culture, there was a significant decrease in the number of bone marrow cells representing a mean of 74 cells when compared to 24 h samples (*P > 0.05*, Figure 3.9B and Supplementary Figure 5F). Following 48 h in culture, the mean number of BAX-stained cells was non-significantly decreased to 18 cells when compared to 24 h media only injected samples (*P > 0.05*) and this was significant compared to 0 h αMEM media only injection controls (*P < 0.0001*, Figure 3.9A and Supplementary Figure 7F). This was not significant when compared to 48 h no injection only supplemented slices with 20 ng/mL M-CSF and 30 ng/mL RANKL samples and 48 h slices microinjected with mixed tibial bone marrow cells (*P > 0.05*). The mean percentage of cells remaining that were stained positive for BAX at 48 h was non-significantly decreased to 22 % when compared to 24 h αMEM media only injected samples (*P > 0.05*, Figure 3.9C). This

percentage was significantly reduced when compared to 48 h no injection only supplemented slices with 20 ng/mL M-CSF and 30 ng/mL RANKL samples ($P < 0.001$) and non-significant when compared to 48 h slices microinjected with mixed tibial bone marrow cells ($P > 0.05$).

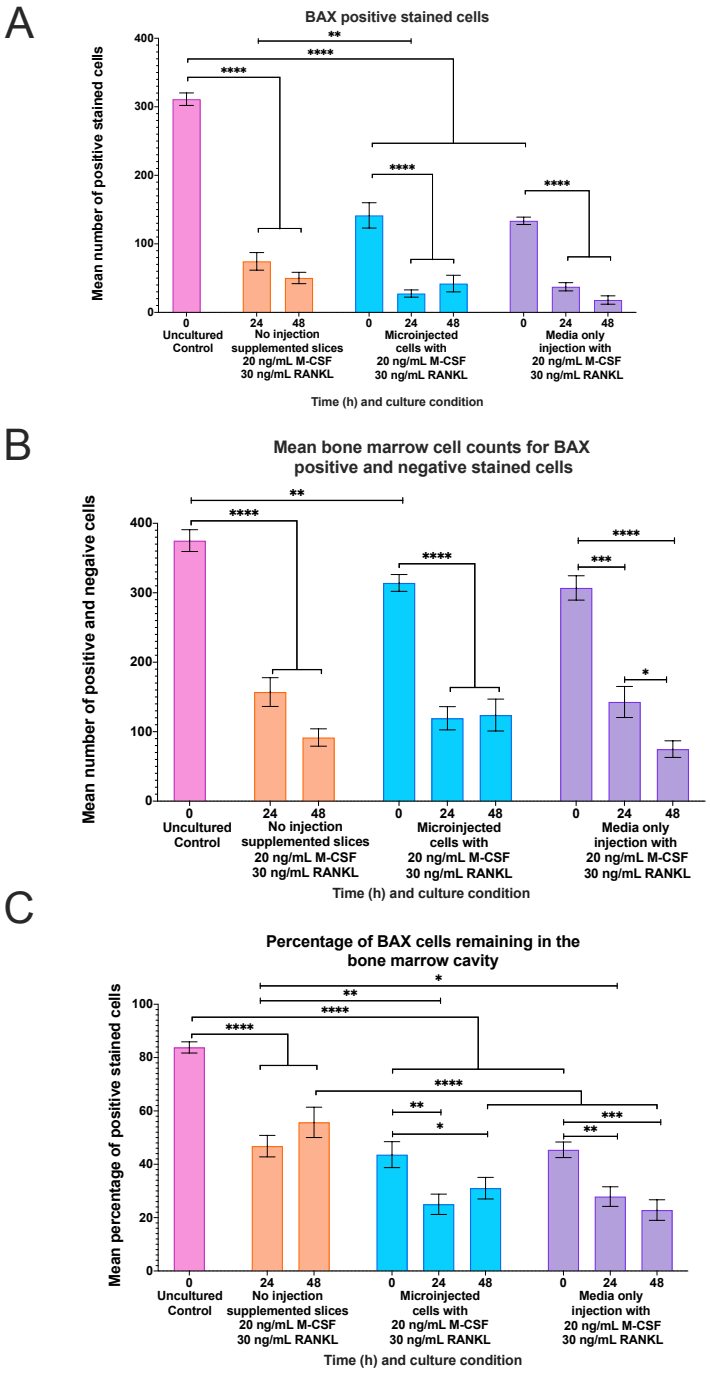

Figure 3.9: BAX analysis following microinjection and culture with M-CSF and RANKL Immunohistochemical analysis for BAX-labelled antibodies for slices supplemented with 20 ng/mL M-CSF and 30 ng/mL RANKL in both the culture media and injected within the bone marrow cavity along with or without mixed tibial bone marrow cells. Graph A) Graph showing data for mean cell counts for BAX positive stained cells. Graph B) Graph shows mean cell counts for both BAX positive and negative stained cells. Graph C) showing the percentage of LDH positive stained cells remaining in the bone marrow cavity. Graphs show no difference in BAX-stained cells at 24 h or 48 h for slices with or without microinjection of media or cells. All cultures show a loss of both bone marrow cells and BAX-stained cells following 24 h and 48 h in culture. Trowell-type cultures supplemented with 20 ng/mL M-CSF and 30 ng/mL RANKL and no microinjection from Figure 3.8 was used as a control. Significance within groups determined via one-way ANOVA and between groups via two-way ANOVA with Tukey post-hoc test. Error bars represent mean ±S.E.M (n=3), **P < 0.05, ** P < 0.01, *** P < 0.001 and ****P < 0.0001.*

3.3.5: Immunohistochemical Detection of Bone Marrow Monocytes, Macrophages and Osteoclasts Following Supplementations With M-CSF and RANKL.

3.3.5a: Immunohistochemical Detection of Monocytes and Macrophages Using CD14 Localisation in M-CSF and RANKL Supplemented Femoral Slices

Immuno-detection of CD14 myeloid cells were undertaken in slices supplemented with M-CSF and RANKL over 48 h, average number and percentages were calculated within a 12.5 mm^2 area (Figure 3.10 A&B). At 0 h for uncultured controls, the mean number of bone marrow cells at 349 cells, from which there was a mean of 192 cells positive for CD14 which represented 54 % of positively labelled cells (Figure 3.10 A,B&C, Supplementary Figure 8A).

Following 24 h culture with 20 ng/mL M-CSF and 30 ng/mL RANKL, there was a significant decrease in the number of bone marrow cells representing a mean of 144 cells when compared to 0 h controls (*P < 0.0001,* Figure 3.10B and Supplementary Figure 8B). At 24 h culture with 20 ng/mL M-CSF and 30 ng/mL RANKL, there was a significant decrease in the mean number of positively stained CD14 cells to 52 cells when compared to 0 h controls (*P < 0.0001*, Figure 3.10A and Supplementary Figure 8B). When compared to 24 h slices without M-CSF and RANKL supplementation there was no significance in the number of CD14 cells (*P > 0.05*). At 24 h the mean percentage of cells remaining that were stained positive for CD14 significantly decreased to 34 % (*P < 0.05*, Figure 3.10C). When compared to 24 h slices without M-CSF and RANKL supplementation there was no significance in the percentage of CD14 cells for supplemented slices (*P > 0.05*). At 48 h in culture there was a significant decrease in the number of mean bone marrow cells to 87 cells when compared to 24 h samples (*P < 0.05,* Figure 3.10B and Supplementary Figure 8C). At 48 h there was a non-significant decrease in the mean number of positively stained cells for CD14 to 33 cells when compared to 24 h samples (*P < 0.05*) and a significant decrease when compared to 0 h controls (*P < 0.0001*, Figure 3.10A and Supplementary Figure 8C). When compared to 48 h slices without M-CSF and RANKL supplementation there was no significance in the number of CD14 cells (*P > 0.05*). At 48 h the mean percentage of cells remaining that were stained positive for CD14 non-significantly increased to 37 % when compared to 24 h samples (*P > 0.05*, Figure 3.10C). When compared to 48 h slices without M-CSF and RANKL supplementation there were no significant differences in the percentage of CD14 cells for

supplemented slices even though the overall mean was lower for supplemented slices (*P > 0.05*).

Following 24 h culture with 40 ng/mL M-CSF and 60 ng/mL RANKL, there was a significant decrease in the number of bone marrow cells representing a mean of 191 cells when compared to 0 h controls (*P < 0.0001,* Figure 3.10B and Supplementary Figure 8D). At 24 h culture there was a significant decrease (*P < 0.0001*) in the mean number of positively stained CD14 cells to 25 cells when compared to 0 h controls (Figure 3.10A and Supplementary Figure 8D). This was not significant in the mean number of CD14 stained cells when compared to slices supplemented with 20 ng/mL M-CSF and 30 ng/mL RANKL at 24 h (*P > 0.05*), or 24 h slices without M-CSF and RANKL supplementation (*P > 0.05*). At 24 h the mean percentage of cells remaining that were stained positive for CD14 significantly decreased to 17 % (*P < 0.0001*, Figure 3.10C). This mean percentage of CD14 stained cells was not significant when compared to slices supplemented with 20 ng/mL M-CSF and 30 ng/mL RANKL at 24 h (*P > 0.05*), or 24 h slices without M-CSF and RANKL supplementation (*P > 0.05*). At 48 h in culture there was a non-significant decrease in the number of mean bone marrow cells to 109 cells when compared to 24 h samples (*P > 0.05,* Figure 3.10B and Supplementary Figure 8E). At 48 h there was a non-significant increase (*P > 0.05*) in the mean number of positively stained cells for CD14 to 33 cells when compared to 24 h samples and a significant decrease when compared to 0 h controls (*P > 0.0001*, Figure 3.10A and Supplementary Figure 8E). The mean number of CD14 stained cells was not significant when compared to slices supplemented with 20 ng/mL M-CSF and 30 ng/mL RANKL at 24 h (*P > 0.05*), or 24 h slices without M-CSF and RANKL supplementation (*P > 0.05*). At 48 h the mean percentage of cells remaining that were stained positive for CD14 significantly increased to 34 % when compared to 24 h samples (*P < 0.05*, Figure 3.10C). The mean percentage of CD14 stained cells was not significant when compared to slices supplemented with 20 ng/mL M-CSF and 30 ng/mL RANKL at 24 h (*P > 0.05*), or 24 h slices without M-CSF and RANKL supplementation (*P > 0.05*).

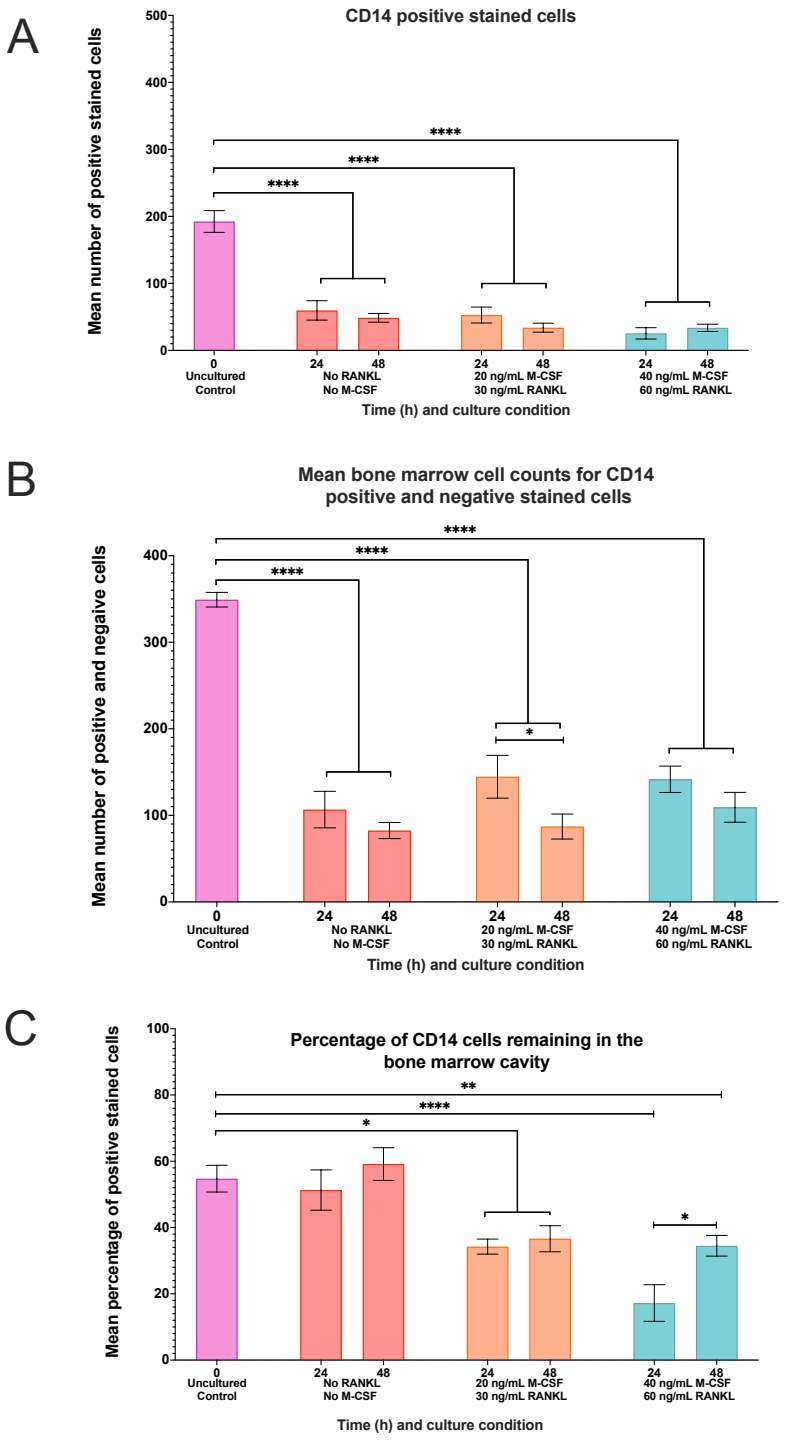

Figure 3.10: CD14 analysis following culture with M-CSF and RANKL. Immunohistochemical analysis for CD14 analysis for slices supplemented with either 20 ng/mL M-CSF and 30 ng/mL RANKL or 40 ng/mL M-CSF and 60 ng/mL RANKL and compared to no cytokine supplemented samples. Graph A) showing data for mean cell counts for CD14 positive stained cells. Graph B) showing mean cell counts for both CD14 positive and negative stained cells. Graph C) showing the percentage of CD14 positive stained cells remaining in the bone marrow cavity. Data for 0 h uncultured controls and no M-CSF and RANKL supplemented slices obtained from Figures 2.22. Graphs show no significance in CD14 stained cells for slices with or without M-CSF and RANKL. All cultures show a loss of both bone marrow cells and CD14-stained cells following 24 h and 48 h in culture. Significance within groups determined via one-way ANOVA and between groups via two-way ANOVA with Tukey post-hoc test. Error bars represent mean ±S.E.M (n=3), $*P < 0.05$, $** P < 0.01$ and $****P < 0.0001$.

3.3.5b: Immunohistochemical Detection of Monocytes and Macrophages Using $CD14^+$ Localisation in Slices Injected With M-CSF and RANKL With Or Without Mixed Tibial Bone Marrow Cells.

Immuno-detection of CD14 stained cells for myeloid cells was undertaken in slices microinjection with either; mixed tibial bone marrow cells supplemented with 20 ng/mL M-CSF and 30 ng/mL RANKL or αMEM media injection supplemented with 20 ng/mL M-CSF and 30 ng/mL RANKL, the average number of stained cell and percentages localisation were calculated within a 12.5 mm^2 area.

For slices microinjected with mixed tibial bone marrow cells supplemented with 20 ng/mL M-CSF and 30 ng/mL RANKL at 0 h showed a mean of 318 bone marrow cells of which a mean of 150 cells was positive for CD14 (Figure 3.11A&B, Supplementary Figure 9A). This was non-significantly reduced when compared to CD14 stained slices for 0 h no injection no M-CSF and RANKL uncultured controls (*P > 0.05*). The mean percentage of cells remaining that were stained positive for CD14 at 0 h was 48 %, this was non-significant when compared to 0 h no injection no M-CSF and RANKL uncultured controls (*P > 0.05*, Figure 3.11C). Following 24 h culture, there was a significant decrease in the number of bone marrow cells representing a mean of 148 cells when compared to 0 h controls (*P < 0.0001*, Figure 3.11B and Supplementary Figure 9B). At 24 h the mean number of CD14 stained cells significantly decreased to 53 cells when compared to 0 h microinjected controls (*P < 0.05*, Figure 3.11A and Supplementary Figure 9B). This was non-significant when compared to 24 h no injection only supplemented slices with 20 ng/mL M-CSF and 30 ng/mL RANKL samples (*P > 0.05*). The mean percentage of cells remaining that were stained positive for CD14 at 24 h significantly decreased to 30 % when compared to 0 h microinjected controls (*P < 0.01*), this was non-significant when compared to 24 h no injection only supplemented slices with 20 ng/mL M-CSF and 30 ng/mL RANKL samples (*P > 0.05,* Figure 3.11C). Following 48 h culture, there was non-significant decrease in the number of bone marrow cells represented a mean of 111 cells when compared to 24 h samples (*P > 0.05*, Figure 3.11B and Supplementary Figure 9C). At 48 h, the mean number of CD14 stained cells was non-significantly increased to 38 cells when compared to 24 h microinjected controls (*P > 0.05*, Figure 3.11A and Supplementary Figure 9C). This was non-significant when compared to 48 h no injection only supplemented slices with 20 ng/mL M-CSF and 30 ng/mL RANKL samples (*P > 0.05*).

The mean percentage of cells remaining that were stained positive for CD14 at 48 h significantly increased to 54 % when compared to 24 h microinjected samples (*P < 0.01*, Figure 3.11C). This percentage was non-significant when compared to 48 h no injection only supplemented slices with 20 ng/mL M-CSF and 30 ng/mL RANKL samples (*P < 0.0001*).

For slices injected with αMEM media supplemented with 20 ng/mL M-CSF and 30 ng/mL RANKL at 0 h showed a mean of 333 bone marrow cells of which a mean of 121 cells were positive for CD14 (Figure 3.11A&B, Supplementary Figure 9D). When compared to 0 h no M-CSF and RANKL samples, αMEM media microinjected slices had a significantly reduced number of CD14 stained cells (*P < 0.0001*) and was non-significant when compared to slices microinjected with mixed tibial bone marrow cells supplemented with 20 ng/mL M-CSF and 30 ng/mL RANKL (*P > 0.05*). The mean percentage of cells remaining that were stained positive for CD14 at 0 h was 41 % (Figure 3.11C). This percentage was non-significantly lower when compared to 0 h no injection no M-CSF and RANKL uncultured controls (*P > 0.05*) and 0 h slices microinjected with mixed tibial bone marrow cells (*P > 0.05*, Figure 3.11C). Following 24 h culture, there was a significant decrease in the number of bone marrow cells representing a mean of 140 cells when compared to 0 h controls (*P < 0.001*, Figure 3.11B and Supplementary Figure 9E). At 24 h the mean number of CD14 stained cells was significantly decreased to 58 cells when compared to 0 h αMEM media only injected controls (*P < 0.001*, Figure 3.11A and Supplementary Figure 9E). This was not significant when compared to 24 h no injection only supplemented slices with 20 ng/mL M-CSF and 30 ng/mL RANKL cultured samples (*P > 0.05*) and 24 h slices microinjected with mixed tibial bone marrow cells (*P > 0.05*). The mean percentage of cells remaining that were stained positive for CD14 at 24 h was maintained at 42 % when compared to 0 h αMEM media only injected controls (*P < 0.01*, Figure 3.11C). This percentage was not significant when compared to 0 h no injection only supplemented slices with 20 ng/mL M-CSF and 30 ng/mL RANKL samples (*P > 0.05*) and 0 h slices microinjected with mixed tibial bone marrow cells (*P > 0.05*). Following 48 h in culture, there was a significant decrease in the number of bone marrow cells representing a mean of 63 cells when compared to 24 h samples (*P < 0.05*, Figure 3.11B and Supplementary Figure 9F). The mean number of CD14 stained cells at 48 h was significantly decreased to 16 cells when compared to 24 h αMEM media only injected samples (*P < 0.05*) and 0 h controls (*P < 0.0001*, Figure 3.11A and Supplementary Figure 9F).

This was not significant when compared to 48 h no injection only supplemented slices with 20 ng/mL M-CSF and 30 ng/mL RANKL samples ($P > 0.05$) and 48 h slices microinjected with mixed tibial bone marrow cells ($P > 0.05$). The mean percentage of cells remaining that were stained positive for CD14 at 48 h was non-significantly decreased to 24 % when compared to 24 h αMEM media only injected samples ($P > 0.05$) and 0 h controls ($P > 0.05$, Figure 3.11C). This percentage was not significant when compared to 48 h no injection only supplemented slices with 20 ng/mL M-CSF and 30 ng/mL RANKL samples ($P > 0.05$) and significant when compared to 48 h slices microinjected with mixed tibial bone marrow cells ($P < 0.001$).

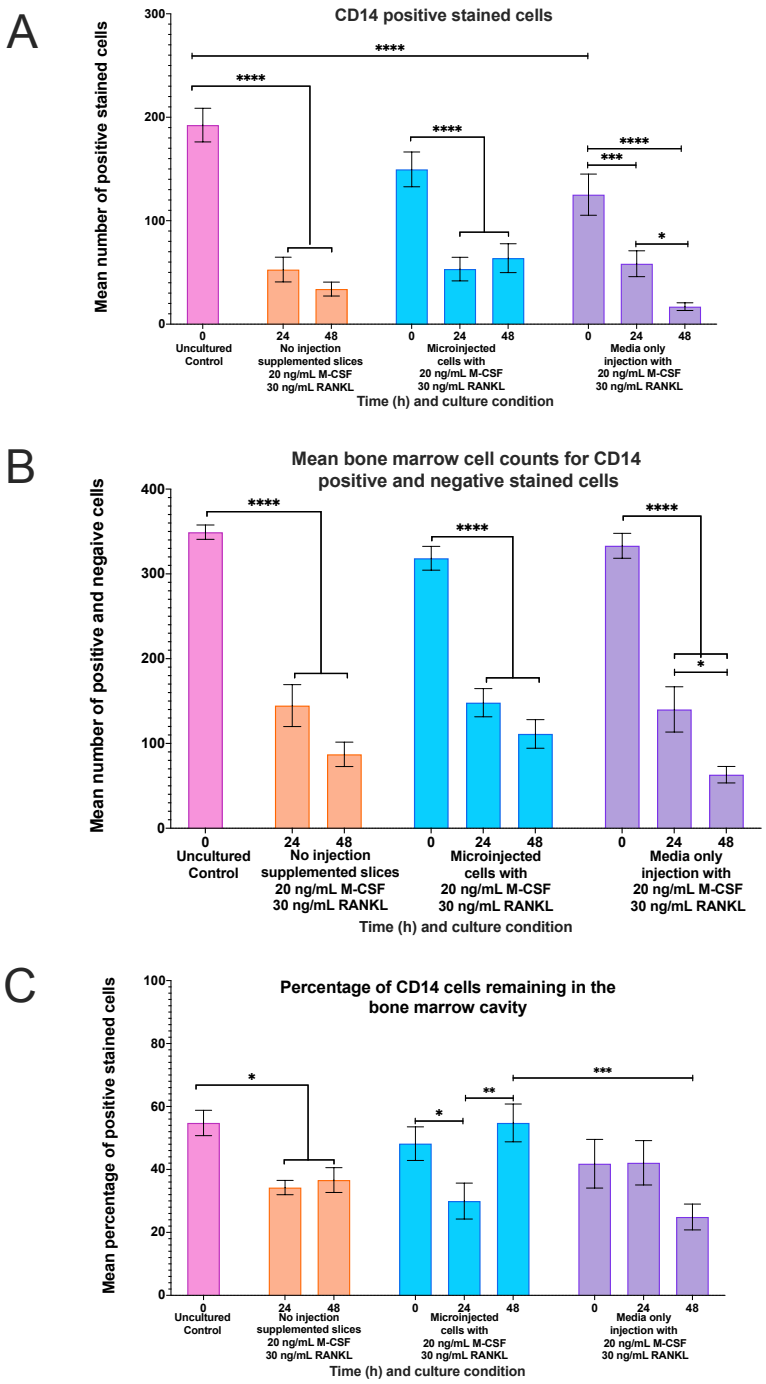

Figure 3.11: CD14 analysis following microinjection and culture with M-CSF and RANKL. Immunohistochemical analysis for CD14 analysis for slices supplemented with 20 ng/mL M-CSF and 30 ng/mL RANKL in both the culture media and injected within the bone marrow cavity along with or without mixed tibial bone marrow cells. Trowell-type cultures supplemented with 20 ng/mL M-CSF and 30 ng/mL RANKL without microinjection from Figure 3.10 was used as a control. Graph A) data for mean cell counts for CD14 positive stained cells. Graph B) shows mean cell counts for both CD14 positive and negative stained cells. Graph C) showing the percentage of CD14 positive stained cells remaining in the bone marrow cavity. Graphs shows loss of bone marrow cells and CD14 stained cells over 48 h. Percentage analysis show maintenance in stained cells for tibial injected slices over 48 h. Significance within groups determined via one-way ANOVA and between groups via two-way ANOVA with Tukey post-hoc test. Error bars represent mean ±S.E.M (n=3), $*P < 0.05$ and $****P < 0.0001$.

3.3.5d: Immunohistochemical Detection of Monocytes and Macrophages Using CD68 Localisation in M-CSF and RANKL Supplemented Femoral Slices

Immuno-detection of CD68 monocytes, macrophages or osteoclasts were undertaken in slices supplemented with M-CSF and RANKL over 48 h, average number and percentages were calculated within a 12.5 mm^2 area (Figure 3.12 A&B). At 0 h for uncultured controls, the mean number of bone marrow cells at 251 cells, from which there was a mean of 15 cells positive for CD68 which represented 8.5 % of positively labelled cells (Figure 3.12 A,B&C Supplementary Figure 10A).

Following 24 h in culture with 20 ng/mL M-CSF and 30 ng/mL RANKL, there was a significant decrease in the number of bone marrow cells representing a mean of 105 cells when compared to 0 h controls (*P < 0.01,* Figure 3.12B and Supplementary Figure 10B). Following 24 h in culture with 20 ng/mL M-CSF and 30 ng/mL RANKL, there was no significant difference in the mean number of positively stained CD68 cells maintained at 18 cells when compared to 0 h controls (*P > 0.05*, Figure 3.12A and Supplementary Figure 10B). When compared to 24 h slices without M-CSF and RANKL supplementation there was no significance in the number of CD68 cells (*P > 0.05*). At 24 h the mean percentage of cells remaining that were stained positive for CD68 significantly increased to 20 % compared to 0 h uncultured controls (*P < 0.05*, Figure 3.12E). When compared to 24 h slices without M-CSF and RANKL supplementation there was no significance in the percentage of CD68 cells for supplemented slices (*P > 0.05*). At 48 h in culture there was a non-significant decrease in the number of mean bone marrow cells to 87 cells when compared to 24 h samples (*P > 0.05,* Figure 3.12B and Supplementary Figure 10C). At 48 h there was a non-significant increase in the mean number of positively stained cells for CD68 to 19 cells when compared to 24 h samples (*P > 0.05*) and 0 h controls (*P > 0.05*, Figure 3.12A and Supplementary Figure 10C). When compared to 48 h slices without M-CSF and RANKL supplementation there was no significance in the number of CD68 cells (*P > 0.05*). At 48 h the mean percentage of cells remaining that were stained positive for CD68 non-significantly increased to 33 % when compared to 24 h samples (*P > 0.05*, Figure 3.12E). When compared to 48 h slices without M-CSF and RANKL supplementation there were no significant differences in the percentage of CD68 cells for supplemented slices (*P > 0.05*).

Following 24 h in culture with 40 ng/mL M-CSF and 60 ng/mL RANKL, there was a significant decrease in the number of bone marrow cells representing a mean of 137 cells when compared to 0 h controls (*P < 0.05,* Figure 3.12B and Supplementary Figure 10D). At 24 h , there was a non-significant increase in the mean number of positively stained CD68 cells to 22 cells when compared to 0 h controls (*P > 0.05*, Figure 3.12A and Supplementary Figure 10D). This was not significant when compared to slices supplemented with 20 ng/mL M-CSF and 30 ng/mL RANKL at 24 h (*P > 0.05*) or 24 h slices without M-CSF and RANKL supplementation (*P > 0.05*). At 24 h the mean percentage of cells remaining that were stained positive for CD68 non-significantly increased to 17 % (*P > 0.05*, Figure 3.12E). This mean percentage of CD68 stained cells was not significant when compared to slices supplemented with 20 ng/mL M-CSF and 30 ng/mL RANKL at 24 h (*P > 0.05*), or 24 h slices without M-CSF and RANKL supplementation (*P > 0.05*). At 48 h in culture there was a non-significant decrease in the number of mean bone marrow cells to 97 cells when compared to 24 h samples (*P > 0.05,* Figure 3.12B and Supplementary Figure 10E). At 48 h there was a non-significant decrease in the mean number of positively stained cells for CD68 to 14 cells when compared to 24 h samples (*P > 0.05*) and 0 h controls (*P > 0.05*, Figure 3.11A and Supplementary Figure 10E). The mean number of CD68 stained cells was not significant when compared to slices supplemented with 20 ng/mL M-CSF and 30 ng/mL RANKL at 24 h (*P > 0.05*) or 24 h slices without M-CSF and RANKL supplementation (*P > 0.05*). At 48 h the mean percentage of cells remaining that were stained positive for CD68 non-significantly decreased to 13 % when compared to 24 h samples (*P > 0.05*, Figure 3.12E). The mean percentage of CD68 stained cells were significantly reduced when compared to slices supplemented with 20 ng/mL M-CSF and 30 ng/mL RANKL at 24 h (*P < 0.0001*), or 24 h slices without M-CSF and RANKL supplementation (*P < 0.05*).

3.3.5e: Immunohistochemical Detection of CD68 Positive Multinucleated Osteoclast-Like Cells in M-CSF and RANKL Supplemented Femoral Slices.

Cellular counts for large multinucleated (3 or more nuclei) typical for osteoclast-like cells were also analysed with CD68 positive cells within a 12.5 mm^2 area. At 0 h for uncultured controls, there were very few cells within the femoral slice showing a mean of 2 cells. The mean percentage of positive multinucleated CD68 cells (Figure 3.12C and C).

Following 24 h culture with 20 ng/mL M-CSF and 30 ng/mL RANKL, there was a non-significant decrease in the number of multinucleated CD68 cells with a mean of 1 cell when compared to 0 h controls (*P > 0.05*, Figure 3.12C and Supplementary Figure 11B). This was non-significant when compared to no M-CSF and RANKL 24 h samples (*P > 0.05*). The mean percentage of multinucleated cells remaining that were stained positive for CD68 was similarly low at 24 h with a mean of 2 % (Figure 3.12D). This percentage was non-significant when compared to 0 h controls (*P > 0.05*) and when compared to no M-CSF and RANKL 24 h samples (*P > 0.05*). Following 48 h, there was a non-significant increase in the number of multinucleated CD68 cells to a mean of 2 cells when compared to 0 h controls and 24 h samples (*P > 0.05*, Supplementary Figure 11C). This was non-significant when compared to no M-CSF and RANKL 24 h samples (*P > 0.05*). The mean percentage of multinucleated cells remaining that were stained positive for CD68 at 48 h showed a significant increase to a mean of 7 % when compared to 24 h samples (*P < 0.05*) and non-significant compared to 0 h controls (*P > 0.05*). This percentage was significant when compared to no M-CSF and RANKL 24 h samples (*P < 0.01*).

Following 24 h culture with 40 ng/mL M-CSF / 60 ng/mL RANKL, there was a non-significant decrease in the number of multinucleated CD68 cells with a mean of 1 cell when compared to 0 h controls (*P > 0.05*, Figure 3.12C and Supplementary Figure 11D). This was non-significant when compared to no M-CSF and RANKL 24 h samples (*P > 0.05*) and slices cultured with 20 ng/mL M-CSF and 30 ng/mL RANKL samples (*P > 0.05*). The mean percentage of multinucleated cells remaining that were stained positive for CD68 was low at 24 h with a mean of 1 % (Figure 3.12D). This percentage was non-significant when compared to 0 h controls (*P > 0.05*), no M-CSF and RANKL 24 h samples (*P > 0.05*) and 20 ng/mL M-CSF and 30 ng/mL RANKL samples (*P > 0.05*). Following 48 h, there was a non-significant decrease in the number of multinucleated CD68 cells to a mean of 0 cells when compared to 0 h controls and 24 h samples (*P > 0.05*, Supplementary Figure 11C). This was non-significant when compared to no M-CSF and RANKL 24 h samples (*P > 0.05*) and 20 ng/mL M-CSF and 30 ng/mL RANKL samples (*P > 0.05*). The mean percentage of multinucleated cells remaining that were stained positive for CD68 at 48 h showed a non-significant decrease to a mean of 2 % when compared to 24 h samples (*P < 0.05*) and 0 h

controls ($P > 0.05$). This percentage was non-significant when compared to 48 h no M-CSF and RANKL 24 h samples ($P > 0.05$) and significant when compared to 48 h 20 ng/mL M-CSF and 30 ng/mL RANKL samples ($P < 0.01$).

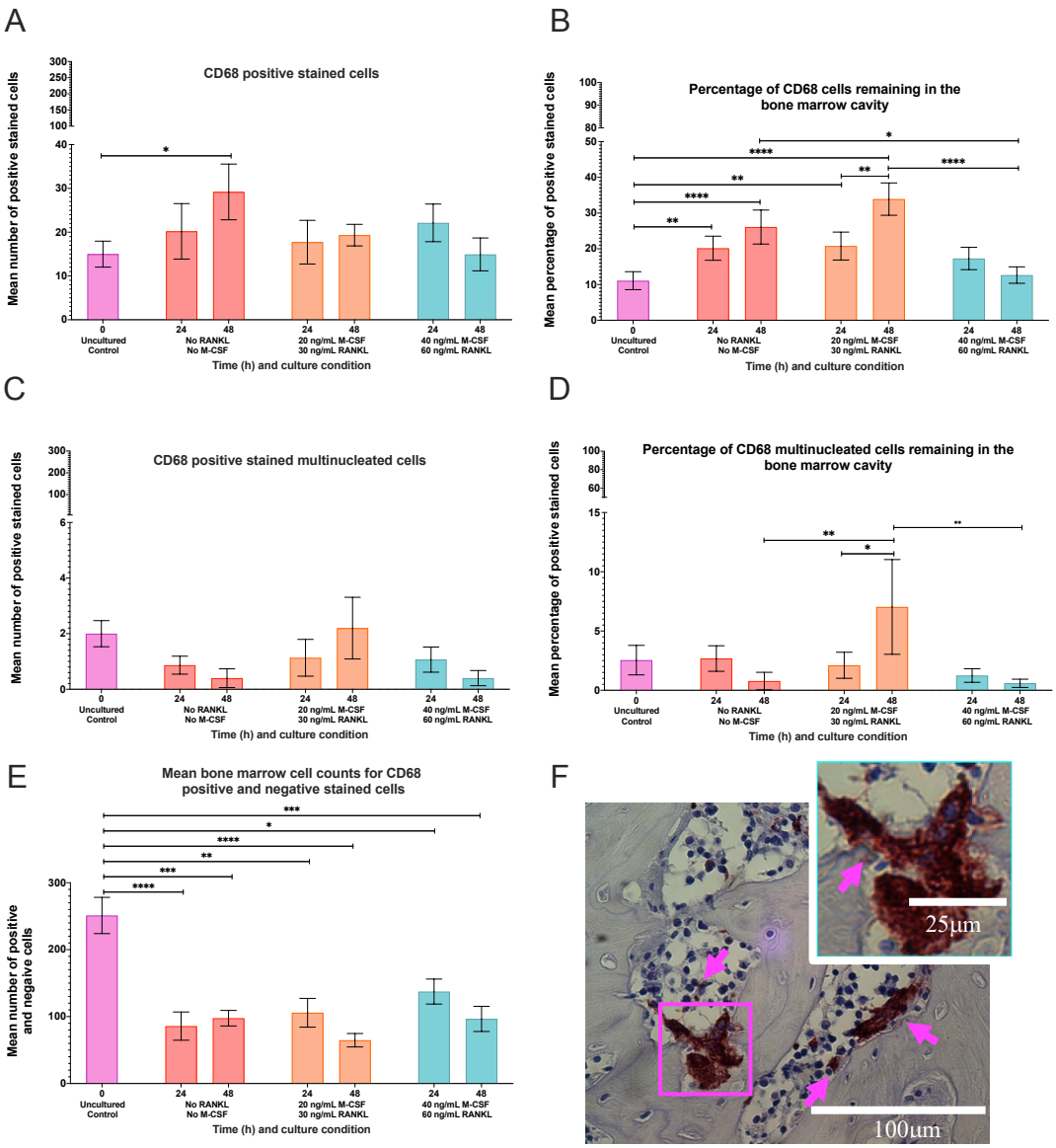

Figure 3.12: CD68 analysis following culture with M-CSF and RANKL. Immunohistochemical analysis for CD68 labelled cells for slices supplemented with either 20 ng/mL M-CSF and 30 ng/mL RANKL or 40 ng/mL M-CSF and 60 ng/mL RANKL and compared to no cytokine supplemented samples. Graphs show (A) mean CD68 stained cell counts, (B) mean percentage of CD68 stained cells remaining, (C) mean CD68 stained multinucleated osteoclast-like cell counts with three or more cell nuclei, (D) mean percentage of CD68 stained multinucleated osteoclast-like cells and (E) mean cell counts for both CD68 positive and negative stained cells. Image F) shows a representative image of a CD68 positive multinucleated cell embedded within the cortical bone at 0 h. Data for 0 h uncultured controls and no M-CSF and RANKL supplemented slices obtained from Figures 2.22. Graphs show maintenance in CD68 cells for slices with and without M-CSF and RANKL over 48 h. All cultures show a loss of both bone marrow cells following 24 h and 48 h in culture. Graphs for multinucleated CD68 labelled cells show maintenance over 48 h for all culture conditions, with 20 ng/mL M-CSF and 30 ng/mL RANKL slices at 48 h showing significant increase in cells. Significance within groups determined via one-way ANOVA and between groups via two-way ANOVA with Tukey post-hoc test. Error bars represent mean ±S.E.M (n=3), *$P < 0.05$, ** $P < 0.01$, *** $P < 0.001$ and ****$P < 0.0001$.

3.3.5f: Immunohistochemical Detection of Monocytes and Macrophages using CD68 Localisation in Slices Injected With M-CSF and RANKL With Or Without Mixed Tibial Bone Marrow Cells.

Immuno-detection of CD68 stained cells for myeloid cells was undertaken in slices microinjection with either; mixed tibial bone marrow cells supplemented with 20 ng/mL M-CSF and 30 ng/mL RANKL or αMEM media injection supplemented with 20 ng/mL M-CSF and 30 ng/mL RANKL, the average number of stained cell and percentages localisation were calculated within a 12.5 mm^2 area.

For slices microinjected with mixed tibial bone marrow cells supplemented with 20 ng/mL M-CSF and 30 ng/mL RANKL at 0 h showed a mean of 355 bone marrow cells of which a mean of 15 cells was positive for CD14 (Figure 3.13A&B, Supplementary Figure 12A). This was non-significantly higher for CD68 stained slices when compared to 0 h no injection and no M-CSF and RANKL uncultured controls (*P > 0.05*). The mean percentage of cells remaining that were stained positive for CD68 at 0 h was 4 %, this was non-significant when compared to 0 h no injection and no M-CSF and RANKL uncultured controls (*P > 0.05*, Figure 3.13E). Following 24 h culture, there was a significant decrease in the number of bone marrow cells representing a mean of 169 cells when compared to 0 h controls (*P < 0.001*, Figure 3.13B and Supplementary Figure 12B). At 24 h the mean number of CD68 stained cells significantly increased to 31 cells when compared to 0 h microinjected controls (*P < 0.05*, Figure 3.13A and Supplementary Figure 12B). This was non-significant when compared to 24 h no injection only supplemented slices with 20 ng/mL M-CSF and 30 ng/mL RANKL (*P > 0.05*). The mean percentage of cells remaining that were stained positive for CD68 at 24 h significantly increased to 29 % when compared to 0 h microinjected controls (*P < 0.001*), this was non-significant when compared to 24 h no injection only supplemented slices with 20 ng/mL M-CSF and 30 ng/mL RANKL samples (*P > 0.05,* Figure 3.13E). Following 48 h culture, there was non-significant decrease in the number of bone marrow cells represented a mean of 122 cells when compared to 24 h samples (*P > 0.05*, Figure 3.13B and Supplementary Figure 12C). At 48 h, the mean number of CD68 stained cells was significantly increased to 52 cells when compared to 24 h microinjected controls (*P < 0.01*, Figure 3.13A and Supplementary Figure 12C). This was significant when compared to 48 h no injection only supplemented slices with 20 ng/mL M-CSF and 30 ng/mL RANKL (*P <*

0.0001). The mean percentage of cells remaining that were stained positive for CD68 at 48 h significantly increased to 35 % when compared to 24 h microinjected samples (*P < 0.05*, Figure 3.13E). This percentage was not significant when compared to 48 h no injection only supplemented slices with 20 ng/mL M-CSF and 30 ng/mL RANKL samples (*P > 0.05*).

For slices injected with αMEM media supplemented with 20 ng/mL M-CSF and 30 ng/mL RANKL at 0 h showed a mean of 286 bone marrow cells of which a mean of 7 cells were positive for CD68 (Figure 3.13A&B, Supplementary Figure 12D). When compared to 0 h no injection and no M-CSF and RANKL uncultured controls, αMEM media microinjected slices had a non-significantly reduced number of CD68 stained cells (*P > 0.05*) and was non-significant to slices microinjected with mixed tibial bone marrow cells supplemented with 20 ng/mL M-CSF and 30 ng/mL RANKL (*P > 0.05*). The mean percentage of cells remaining that were stained positive for CD68 at 0 h was very low at 2 %. This percentage was non-significantly lower when compared to 0 h no injection and no M-CSF and RANKL uncultured controls (*P > 0.05*) and 0 h slices microinjected with mixed tibial bone marrow cells (*P > 0.05*, Figure 3.13E). Following 24 h culture, there was a significant decrease in the number of bone marrow cells representing a mean of 134 cells when compared to 0 h controls (*P < 0.001*, Figure 3.13B and Supplementary Figure 12E). At 24 h the mean number of CD68 stained cells non-significantly increased to 21 cells when compared to 0 h αMEM media only injected controls (*P > 0.05*, Figure 3.13A and Supplementary Figure 12E). This was not significant when compared to 24 h no injection only supplemented slices with 20 ng/mL M-CSF and 30 ng/mL RANKL cultured samples (*P > 0.05*) and 24 h slices microinjected with mixed tibial bone marrow cells (*P > 0.05*). The mean mean percentage of cells remaining that were stained positive for CD68 at 24 h was significantly increased at 21 % when compared to 0 h αMEM media only injected controls (*P < 0.001*, Figure 3.13E). This percentage was not significant when compared to 0 h no injection only supplemented slices with 20 ng/mL M-CSF and 30 ng/mL RANKL samples (*P > 0.05*) and 0 h slices microinjected with mixed tibial bone marrow cells (*P > 0.05*). Following 48 h in culture, there was a non-significant decrease in the number of bone marrow cells representing a mean of 67 cells when compared to 24 h samples (*P > 0.05*, Figure 3.13B and Supplementary Figure 12F). The mean number of CD68 stained cells at 48 h was non-significantly decreased to 15 cells when compared to 24 h αMEM media only injected samples (*P > 0.05*) and 0 h controls (*P >*

0.05, Figure 3.13A and Supplementary Figure 12F). This was not significant when compared to 48 h no injection only supplemented slices with 20 ng/mL M-CSF and 30 ng/mL RANKL samples (*P > 0.05*) and significantly lower compared to 48 h slices microinjected with mixed tibial bone marrow cells (*P < 0.0001*). The mean percentage of cells remaining that were stained positive for CD68 at 48 h was maintained at 23 % when compared to 24 h αMEM media only injected samples (*P > 0.05*) and significant compared to 0 h controls (*P < 0.0001*, Figure 3.13E). This percentage was not significant when compared to 48 h no injection only supplemented slices with 20 ng/mL M-CSF and 30 ng/mL RANKL samples (*P > 0.05*) and significant when compared to 48 h slices microinjected with mixed tibial bone marrow cells (*P < 0.001*).

3.3.5g: Immunohistochemical Detection of CD68 Positive Multinucleated Osteoclast-Like Cell Localisation in Slices Injected With M-CSF and RANKL With Or Without Mixed Tibial Bone Marrow Cells.

CD68 positive multinucleated cells showed a steady decline following injection with mixed tibial bone marrow cells supplemented with 20 ng/mL M-CSF and 30 ng/mL RANKL. 0 h cultures showed a mean of 1.5 CD68 multinucleated cells Figure 3.13C and Supplementary Figure 14A). This was non-significant when compared to 0 h no injection and no M-CSF and RANKL uncultured controls (*P > 0.05*). The mean percentage of multinucleated cells remaining that were stained positive for CD68 at 0 h were 1 %, this was non-significant when compared to 0 h no injection and no M-CSF and RANKL uncultured controls (*P > 0.05*, Figure 3.13D). At 24 h the mean number of multinucleated CD68 cells non-significantly decreased to 0.2 cells when compared to 0 h microinjected controls (*P > 0.05*, Figure 3.13C and Supplementary Figure 14B). This was non-significant when compared to 24 h no injection supplemented slices with 20 ng/mL M-CSF and 30 ng/mL RANKL (*P > 0.05*). The mean percentage of multinucleated cells remaining that were stained positive for CD68 at 24 h was non-significantly decreased to 0 % when compared to 0 h microinjected controls (*P > 0.05*), this was non-significant when compared to 24 h no injection only supplemented slices with 20 ng/mL M-CSF and 30 ng/mL RANKL samples (*P > 0.05,* Figure 3.13D). Following 48 h in culture, there were no multinucleated CD68 cells remaining showing a mean of 0 cells when compared to 24 h microinjected controls (*P > 0.05*, Figure 3.13C and Supplementary Figure 14C). This was non-significant when compared to 48 h no injection only

supplemented slices with 20 ng/mL M-CSF and 30 ng/mL RANKL (*P > 0.05*). The mean percentage of multinucleated cells remaining that were stained positive for CD68 at 48 h was also 0 % and was non-significant when compared to 24 h microinjected samples (*P > 0.05*, Figure 3.13D). This percentage was significant when compared to 48 h no injection only supplemented slices with 20 ng/mL M-CSF and 30 ng/mL RANKL samples (*P < 0.01*).

For slices injected with αMEM media injection supplemented with 20 ng/mL M-CSF and 30 ng/mL RANKL, there was a maintenance in multinucleated cells between 0 h and 24 h, however, these cells were lost by 48 h. At 0 h, the mean number of positive multinucleated cells was 1 (Figure 3.13C, Supplementary Figure 14D). This was not significant when compared to 0 h no injection and no M-CSF and RANKL uncultured controls (*P > 0.05*) and to slices microinjected with mixed tibial bone marrow cells supplemented with 20 ng/mL M-CSF and 30 ng/mL RANKL (*P > 0.05*). The mean percentage of multinucleated cells remaining that were stained positive for CD68 for CD68 at 0 h was very low at 0.2 %. This percentage was non-significantly lower when compared to 0 h no injection and no M-CSF and RANKL uncultured controls (*P > 0.05*) and 0 h slices microinjected with mixed tibial bone marrow cells (*P > 0.05*, Figure 3.13D). At 24 h the mean number of multinucleated CD68 stained cells were maintained at 1 cell when compared to 0 h αMEM media only injected controls (*P > 0.05*, Figure 3.13C and Supplementary Figure 14E). This was not significant when compared to 24 h no injection only supplemented slices with 20 ng/mL M-CSF and 30 ng/mL RANKL cultured samples (*P > 0.05*) and 24 h slices microinjected with mixed tibial bone marrow cells (*P > 0.05*). The mean percentage of multinucleated cells remaining that were stained positive for CD68 at 24 h was also maintained at 0.3 % when compared to 0 h αMEM media only injected controls (*P > 0.05*, Figure 3.13D). This percentage was not significant when compared to 0 h no injection only supplemented slices with 20 ng/mL M-CSF and 30 ng/mL RANKL samples (*P > 0.05*) and 0 h slices microinjected with mixed tibial bone marrow cells (*P > 0.05*). Following 48 h in culture, there were no multinucleated CD68 cells remaining showing a mean of 0 cells when compared to 24 h αMEM media only injected samples (*P > 0.05*, Figure 3.13C and Supplementary Figure 14F). This was not significant when compared to 24 h no injection only supplemented slices with 20 ng/mL M-CSF and 30 ng/mL RANKL cultured samples (*P > 0.05*) and 24 h slices microinjected with mixed tibial bone marrow cells (*P > 0.05*). The mean percentage of multinucleated cells remaining that were stained

positive for CD68 at 48 h was also 0 % and was non-significant when compared to 24 h αMEM media only injected samples (*P > 0.05*, Figure 3.13D). This percentage was significant when compared to 48 h no injection only supplemented slices with 20 ng/mL M-CSF and 30 ng/mL RANKL samples (*P < 0.01*) and was not significant when compared 48 h slices microinjected with mixed tibial bone marrow cells (*P > 0.05*).

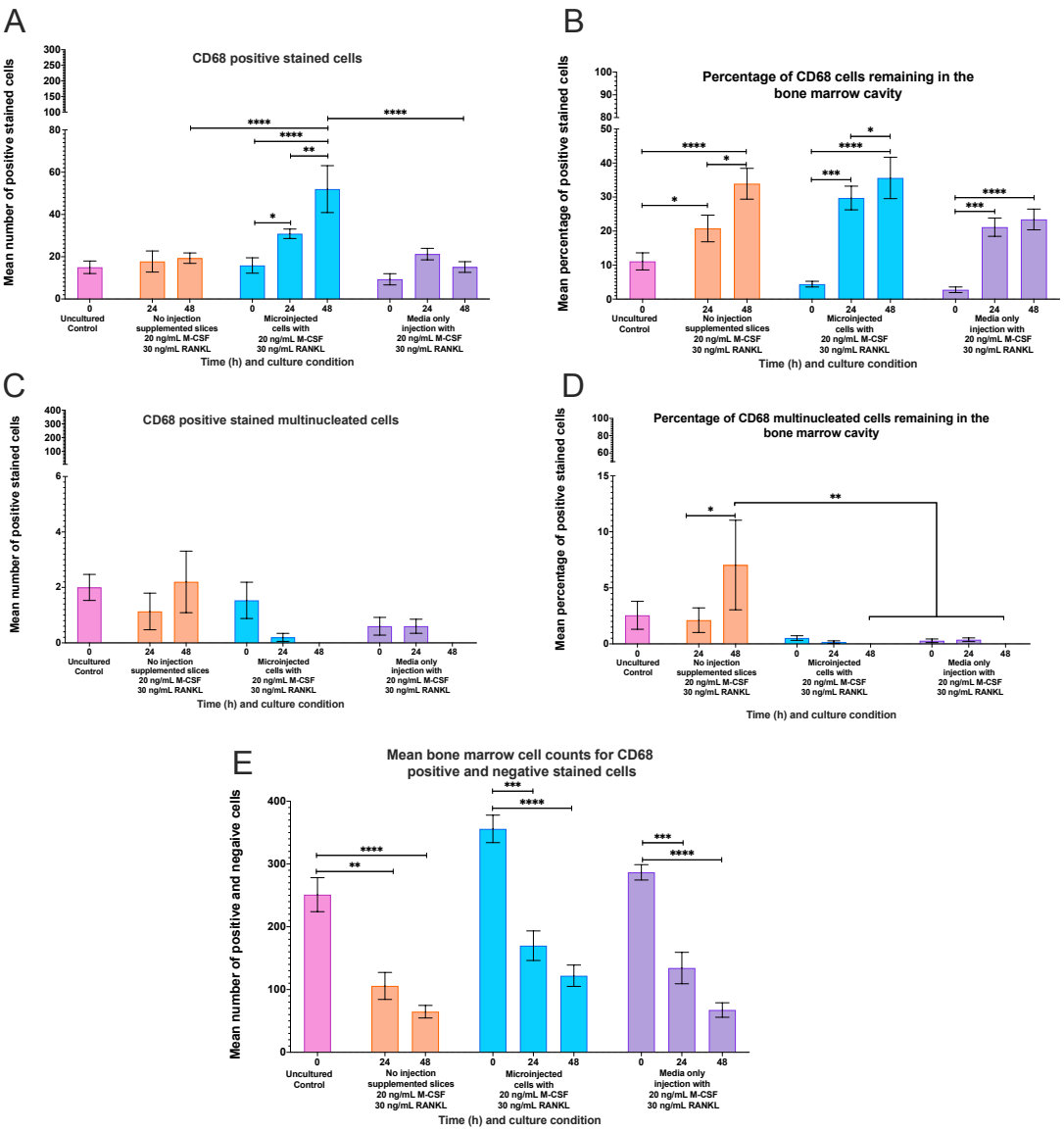

Figure 3.13: CD68 analysis following microinjection and culture with M-CSF and RANKL. Immunohistochemical analysis for CD68 labelled cells for slices supplemented with 20 ng/mL M-CSF and 30 ng/mL RANKL in both the culture media and injected within the bone marrow cavity along with or without mixed tibial bone marrow cells. Trowell-type cultures supplemented with 20 ng/mL M-CSF and 30 ng/mL RANKL and no microinjection from Figure 3.11 was used as a control. Graphs show (A) mean CD68 stained cell counts, (B) mean percentage of CD68 stained cells remaining, (C) mean CD68 stained multinucleated osteoclast-like cell counts with three or more cell nuclei, (D) mean percentage of CD68 stained multinucleated osteoclast-like cells and (E) mean cell counts for both CD68 positive and negative stained cells. Graph shows significant increase of CD68 cells counts over 48 h with injection of tibial cells. Graph shows loss of bone marrow cells over 48 h. Graph show few multinucleated cells for injected slices compared to no injected slices. Significance within groups determined via one-way ANOVA and between groups via two-way ANOVA with Tukey post-hoc test. Error bars represent mean ±S.E.M (n=3), *$P < 0.05$, **$P < 0.01$, *** $P < 0.001$ and ****$P < 0.0001$.

3.4: Discussion

The results of the current Chapter aimed to further support cell survival of monocytes and osteoclasts within the femoral slice model first by supplementing the surrounding culture media with M-CSF and RANKL and then microinjecting media containing M-CSF and RANKL with or without mixed tibial bone marrow cells directly into the bone marrow cavity. *In vitro* analysis of M-CSF and RANKL highlighted cytokine concentrations of 20 ng/mL M-CSF and 30 ng/mL RANKL was significant in inducing a high number of osteoclast cells. Within the *ex vivo* slice model two different concentrations of M-CSF and RANKL were used based on *in vitro* data 20 ng/mL M-CSF and 30 ng/mL RANKL or a higher double concentrated 40 ng/mL M-CSF and 60 ng/mL RANKL. The addition of cytokines at either concentration to the surrounding bone marrow media, induced no significant difference in CD14 or CD68 cells during 48 h in culture when compared to unsupplemented controls. Slices supplemented with 20 ng/mL M-CSF and 30 ng/mL RANKL induced a significant percentage number of multinucleated CD68 cells at 48 h. The microinjection of mixed bone marrow cells along with 20 ng/mL M-CSF and 30 ng/mL RANKL directly into the bone marrow cavity, along with the same concentration of cytokines added to the surrounding agarose gel and culture media, did not induce significant increases in CD14 cells after 48 h when compared to media only injection control. CD68 cells did significantly increase after 48 h when compared to media only injection controls, although multinucleated cells were unable to be supported. Although all culture systems with or without the inclusion of microinjected of cytokines showed a significant loss in cells over 48 h; there was a significant reduction in cell loss of ~30 % at 24 h and 48 h in injected slices. This reduction in cell loss corresponded with a reduction in necrosis and apoptosis following injection of cells and media. This is an improvement to the model, and although it does not mitigate the loss of cells, it does highlight that this model can be manipulated further to reduce the limitations seen in the previous chapter.

To determine if the addition of M-CSF and RANKL would induce osteoclast-like cells from myeloid precursors. *In vitro* differentiation analysis was performed from primary rodent bone marrow cells with the addition of M-CSF and RANKL at variable concentrations. This *in* vitro optimisation was to standardise the concentration ranges of cytokines that would be appropriate within the *ex vivo* model system. Studies have shown that there is a lack of

standardisation of these two cytokines with researchers utilising a different range of concentrations for each study to obtain multinucleated osteoclast-like cells (Chen et al. 2008; Hodge et al. 2011; Marino et al. 2014; Shiratori et al. 2018; Takeshita et al. 2000). Utilising work from previous researchers including Lacey et al. (1998); Shiratori et al. (2018); Sloan et al. (2013); Takeshita et al. (2000), three different cytokine concentrations were compared, a low concentration at 20 ng/mL M-CSF and 30 ng/mL RANKL, a semi-low concentration at 40 ng/mL M-CSF and 60 ng/mL RANKL, a high concentration at 100 ng/mL M-CSF and 100 ng/mL RANKL and control was used with no M-CSF or RANKL. The *in vitro* analysis highlighted that only the addition of 20 ng/mL M-CSF and 30 ng/mL RANKL induced a significant increase in $TRAP^+$ multinucleated osteoclasts after 7 days in culture, with the other two concentrations having no significant changes compared to no cytokine controls. This is comparable to data by Chen et al. (2008) 30 ng/mL M-CSF to 10 ng/mL RANKL induced ~40 $TRAP^+$ multinucleated osteoclast-like cells after 7 days in culture from RAW 246.7 murine cell-lines. Shiratori et al. (2018) demonstrated that primary bone marrow macrophages from male ddY mice induced ~200 $TRAP^+$ multinucleated osteoclast-like cells using 20 ng/mL M-CSF and 50 ng/mL RANKL and at a similar cell seeding density of 1.5 x105 cells/mL. Luo et al. (2018) showed that using bone marrow macrophages isolated from C57BL/6 mice induced ~35 $TRAP^+$ multinucleated osteoclast-like cells with the addition of using 30 ng/mL M-CSF and 50 ng/mL RANKL. This is comparable to the levels seen within this study at 40 ng/mL M-CSF and 60 ng/mL RANKL, though the concentrations used within this chapter were 10 ng/mL higher than the study by Luo et al. (2018). Studies using osteoclast precursors isolated from human umbilical cord blood at $4x10^4$ –10^5 cells/mL show inhibition of osteoclast resorption activity under high concentrations of M-CSF. The data obtained in this chapter suggests that higher doses of M-CSF prevented osteoclast formation in a dose-dependent manner.

Within the *ex vivo* model 20 ng/mL M-CSF and 30 ng/mL RANKL was added to the culture media. Due to the complexity of the bone marrow microenvironment with the risk of the cytokines not reaching the bone marrow cavity effectively the double concentration of M-CSF and RANKL was also added to the culture environment, even though *in vitro* analysis did not yield significant osteoclast-like cells.

The data presented in this chapter highlights that there was no significant difference in the numbers and percentage of CD14 and CD68 myeloid cells over 48 h following cytokine supplementation compared to control. The addition of cytokines decreased the percentage of $CD14^+$ myeloid cells over 48 h. The injection of cytokines into the bone marrow cavity decreased the numbers of CD14 myeloid cells over 48 h. Unsurprisingly the addition of bone marrow cells with cytokines into the bone marrow cavity increase the percentage of $CD14^+$ and $CD68^+$ myeloid cells at 48 h.

M-CSF has previously been shown to induce hematopoietic stem cells (HSC) down a myeloid linage fate rather than a granular fate. This is proposed to occur by inducing the gene *PU.1* within HSC within the presence of M-CSF, although this was seen *in vivo* over 2 weeks, which is something that would not be possible to occur in the current model (Mossadegh-Keller et al. 2013). *PU.1* has been shown to bind to the promotor gene coding for the M-CSF receptor (M-CSFR) and upregulating the promotion of the M-CSFR on the surface of monocytic cells. Abolishment of *PU.1* has shown a decrease in M-CSFR promotor within monocytic cells (Zhang et al. 1994). The possible reason as to why there was no significant difference in CD14 or CD68 numbers for either unsupplemented or externally supplemented slices at 24 or 48 h could simply be due to the presence of naturally occurring M-CSF within the bone marrow cavity. M-CSF is secreted by bone marrow mesenchymal stromal cells (MSCs) and their lineage cells osteoblasts and osteocytes; naturally, these cells induce elevated M-CSF levels following fracture healing as seen within *in vivo* BALB/c mice models and within serum and hematomas of patients following long bone fractures (Kon et al. 2001; Kottstorfer et al. 2013; Sarahrudi et al. 2010). It is hypothesised by Sarahrudi et al. (2010) that these elevations in both the serum and haematoma M-CSF may be required for early osteoclast formation during the first two weeks post-fracture soft callous formation. This is supported by data of high numbers and percentages of MSC markers seen towards the traumatised exposed surface of the bone marrow. This indicates that MSCs are actively being recruited to sites of trauma possibly due to an increased expression of the monocytic chemotactic protein (MCP)-3 (also known as CCL7) which can be used by MSCs as a chemoattractant and can be upregulated during the first 48 h following fractures in mice (Ishikawa et al. 2014). Therefore, this high presence of MSCs towards the site of bone marrow trauma along with damage to the periosteum and endosteum may naturally influence the secretion of M-CSF

in the surrounding area ready to prime CD14 and CD68 monocytes/macrophages to undergo osteoclast differentiation.

In addition to the added M-CSF, the model was also supplemented with RANKL within the culture media and agarose gel or the bone marrow cavity via microinjection. This was added to maintain osteoclast precursors and osteoclast cell populations that were lost during culture in unsupplemented slices. The analysis was carried out using CD68 cells that were multinucleated, fused polykarons that are maturing to osteoclasts or fully mature osteoclasts, distinguished via size and location toward the cortical bone, along with TRAP staining.

Statistical analysis showed no significant difference in the numbers of multinucleated CD68 cells supplemented with M-CSF and RANKL for 24 or 48 h compared to unsupplemented controls. General trends show that the mean multinucleated CD68 cell and percentage numbers tended to decrease steadily over 48 h for all culture conditions; except for slices supplemented with 20 ng/mL M-CSF and 30 ng/mL RANKL, without any microinjection which increased numbers of CD68 cells between 24 h and 48 h. TRAP staining showed no staining at all for any of the culture groups at 24 or 48 h. Typically, as shown with the *in vitro* analysis osteoclast formation can take up to 7 days to differentiate monocytes/macrophages into mature osteoclasts. Therefore, the limited time of culture of 48 h would not be sufficient to differentiate tissue resident macrophages or monocytes into osteoclasts with the presence of M-CSF and RANKL. Another possibility for the reduction in osteoclast-like cells at 24 h and 48 h for higher concentrated cytokine combination and cytokines injected within the bone marrow cavity, is due to a possible increase in osteoprotegerin (OPG) secretion in response to increased local or surrounding levels of RANKL, however, OPG levels were not studied in this model. This is supported by Kottstorfer et al. (2014), where following fractures in patients there were elevated levels of OPG within the first 24 h in fracture hematomas then in serum but were together elevated compared to healthy controls. The authors found that soluble RANKL levels were elevated within the fracture hematoma then the serum but were together elevated compared to healthy controls. Kon et al. (2001) Mice with tibial fractures induced increased OPG levels along with RANKL levels after 24 h, with OPG levels reduced by 72 h. This supports the idea that areas of bone marrow that were

injected with RANKL or had elevated levels of culture RANKL possibly induce elevated expression of OPG to prevent early bone resorption.

Within the Trowell-type model after 24 h in culture, a dense number of cells were at the periphery of the exposed bone marrow, this is possibly in response to low nutrient and oxygen gradients within the bone marrow cavity during culture. Static 3D tissue cultured scaffolds tend to form nutrient gradients, due to a lack of active transport to the centre of tissues, providing adequate nutrients to the surface of the scaffold, then the cells retained within the scaffold (Brindley et al. 2011) Oxygen cannot adequately diffuse through the tissue, where passive diffusion can only occur in 150-200 μm thick sections, which in this model would consist of the outermost layer of bone marrow (Brindley et al. 2011). This is demonstrated by Volkmer et al. (2008) who showed that within the centre of static 3D cultures there is increased hypoxia due to lack of oxygen diffusion which is reduced in dynamic 3D cultures. These nutrient and oxygen gradients may explain why apoptosis and LDH are high for samples without microinjection of media and cells within the bone marrow and why LDH (though not apoptosis) might be reduced in injected slices as the addition of media can provide nutrients and oxygen within the centre of the tissue within the first 24 h of culture.

Both the removal and injection of cells into the bone marrow microenvironment can cause a variety of disruptions to the local cellular environment vital for their survival. High shear stress cells can lyse cells if the applied fluid force exceeds the cells lysing capacity, which is the tolerance of the cell membrane when compressional force is applied, forces that exceed this results in damage and rupture of the cell membrane (Mardikar and Niranjan 2000). Though, the process of microinjection can have a profound impact on the bone cells response to mechanotransduction, where various mechanical stimuli are converted to biochemical responses that help regulate cell function. These can involve biochemical signals where growth factors and chemokines bind to appropriate receptors to influence cell behaviour (as previously mentioned). However, these additional physical cues can positively/negatively influence cell behaviour within the local cell environment. Oscillatory fluid flow has been shown to positively induce bone remodelling and prevent osteoclastogenesis by inhibiting RANKL production and increasing OPG synthesis on ST-2

murine bone marrow stromal cells (Kim et al. 2006a). This potential decrease in RANKL was negated by the addition of RANKL in the culture media. Studies have also shown that fluid shear stress on osteoblasts and osteocytes increase levels of nitric oxide, prostaglandin E2 and I2, transforming growth factor β, intracellular free calcium and cyclic adenosine monophosphate (reviewed in Gurkan and Akkus 2008). Osteoclasts and pre-osteoclasts precursors are also sensitive to fluid shear stress due to their proximity to endosteal surface and secrete autocrine factors such as nitric oxide, prostaglandin E2 and I2 all of which regulate resorption activity (McAllister et al. 2000). The presence of fluid shear stress may be beneficial to stimulate osteoprogenitors to migrate to sites that require mineralisation (Gurkan and Akkus 2008).

Whilst, preparing tibial bone marrow cells for microinjection, the cells were dislodged from the local ECM via media injection through either a 25-gauge or 21-gauge syringe needle. The resulting cell suspension was subjected to centrifugal force to pellet the cells which were further resuspended in culture media., Next, cells were passed through 21-gauge and then 25- gauge needles to achieve a single cell suspension after which the cells were again centrifuged and resuspended in culture media via pipetting. Finally, this cell suspension was injected into the bone marrow cavity using a 26-gauge microneedle. As a consequence of this treatment, both the cell suspension and the femoral bone marrow cavity cells would have been subjected to various fluid forces which can induce hydrodynamic shear stress. Flushing cells through narrow gauge needles could influence their cell viability, though studies have shown that subjecting MSC to the fluid force generated by 20 to 30-gauge needles had minimal effect on apoptosis, necrosis and cell numbers (Walker et al. 2010). The effects of these fluid forces can potentially have a variety of effects in these *ex vivo* models, thus influencing the results seen on the reduction of osteoclastic numbers following microinjection. Analysis of fluid forces on bone marrow MSCs have shown an increase in cell numbers along with an upregulation of pro-osteogenic genes including, bone sialoprotein, osteocalcin and osteonectin for these cells isolated from rodent or human sources, along with a decrease in adipogenic gene expression for lipoprotein lipase (Kreke et al. 2005). This suggests that beneficially fluid forces induce osteogenic differentiation of MSCs whilst suppressing adipogenic differentiation. The authors suggest that this is due to an increase in AP-1 which binds to promoter regions of many osteoblast genes, including

alkaline phosphatase, collagen type I and osteocalcin (Kreke et al. 2005; Kreke et al. 2008). Additionally, when hydrostatic pressure was constantly applied on osteoclast precursors this decreased osteoclast differentiation (Rubin et al. 1997). This suggests that these forces do have an active role in terminating osteoclast activity in favour of more osteogenic responses. The addition of fluid forces can also aid other cells and provide beneficial effects to hematopoietic cells and leukocytes, that are naturally exposed to high levels of shear stress especially within the vasculature which they utilise for cellular detachment and migration (Brindley et al. 2011). However, in vitro assessment of shear stress on leukocytes suggested that forces exceeding 60 NM^{-2} for 10 min or more lysed 25 % of cells, suggesting that forces that allow for detachment when removed from their normal cellular environment can cause a negative effect on the cells (Brindley et al. 2011). This is possibly due to the removal of vital signalling cascades *in vitro* that are induced *in vivo* within the vasculature or with the ECM via macromolecules, growth factors and integrins vital for cell survival.

The results of this chapter highlight the continual challenges presented in developing an *ex vivo* bone model. Microinjection of tibial bone marrow cells into the femoral bone marrow cavity along with 20 ng/mL M-CSF and 30 ng/mL RANKL managed to increase the number of cells over the first 24 h. There was a significant increase in the percentage of CD14 cells over 48 h and significantly increase in CD68 myeloid cell populations over 48 h. Due to the higher number of cells after microinjection along with increased maintenance of CD14 and CD68 myeloid cells that play key roles in osteolysis within the bone marrow cavity it was important to observe the effects of these cells in a co-culture environment with a known osteolytic inducing bacterium, *S. aureus*. This can provide valuable data on the ratio of pro-and anti-inflammatory cytokine release which can influence osteoclastogenesis and osteoclastic activity leading to pathological bone loss following infection.

Chapter 4:
Co-culture of the Femoral Slice Model with *Staphylococcus aureus*

4.1: Introduction

The two main colonising species in prosthetic joint infections (PJI) and osteomyelitis implant infections are typically *Staphylococcus aureus* (*S. aureus*) and *Staphylococcus epidermidis* (*S. epidermidis*) (Bemer et al. 2014; Lange et al. 2016; Phillips et al. 2006). These bacterial species often cause inflammation of the local bone marrow environment along with an influx of pro-inflammatory cytokines, resulting in prolonged pathological bone loss, apoptosis or necrosis (Missiakas and Winstel 2020). Sites of tissue apoptosis or necrosis, allow bacterial species to spread, colonise and progress into the bone marrow cavity and towards the implant or hard tissue. The development of the *ex vivo* femoral slice model in previous Chapters provides a system to model the inflammatory cellular response to the presence of the bacterial species and their virulence factors following infection.

Clinical studies tend to focus more on the diagnostic aspects of the infection, whilst developing methods to differentiate between aseptic and septic osteolysis for implant-associated infections. There has been increasing use of analysing synovial fluid for upregulation of various biomarkers for detecting the presence of bacterial infection following total hip replacements (THR) and total knee arthroplasties (TKR). The synovial fluid is a typically clear fluid that maintains the joint health and provides lubrication, however, during infection and/or inflammation the fluid can become cloudy along with an increase in leucocytes and additional pro-inflammatory markers that can be used for analysis (Block and Genzen 2020). Here, clinicians can easily extract synovial fluid around the prosthesis and run a wide spectrum of diagnostic tests, including white blood cell (WBC) counts, upregulation of a-defensins, C-reactive protein, erythrocyte sedimentation rate (ESR) and examples of various interleukins (IL) (Bingham et al. 2014; Deirmengian et al. 2010; Deirmengian et al. 2014b; Elgeidi et al. 2014). Use of these synovial fluid biomarkers extracted from patients with either aseptic or septic osteolysis has shown significant elevations in pro-inflammatory cytokines, especially Interleukin- 1 beta (IL-1β), Interleukin-6 (IL-6) and Tumour Necrosis Factor alpha (TNFα) along with significant elevations of anti-inflammatory cytokines, Interleukin-4 (IL-4) and Interleukin-10 (IL-10; Di Cesare et al. 2005; Bauer et al. 2019; Froschen et al. 2020) . Such diagnostic clinical studies do not observe the effect these makers have on the local host environment, focusing mainly on these biomarker expressions alone.

The use of pro-inflammatory cytokines to analyse their effects on local bone marrow cell populations *in vitro* and *in vivo* models are limited due to a variety of factors. Firstly, *in vitro* models are excellent in providing a culture environment that can be controlled and manipulated, but are limited by the number of cells that can be cultured (Roberts et al. 2013). Research using *in vitro* models only provides a snapshot of the effect of these pro-inflammatory cytokines on the cell type that is being studied. *In vitro* models lack the specialised cell niches that occurs *in situ* or the complex cell-to-cell interactions formed with other cells that reside in the bone marrow cavity. In contrast, *in vivo* models do maintain specialised cell niches and complex cell-to-cell interactions. *In vivo* models are subjected to various emotions and systemic influences that can skew results and thus provide less reliable data (Cramer et al. 2021; Roberts et al. 2013; Smith et al. 2014a).

Few studies have been developed to assess the effects of *S. aureus* within an *ex vivo* environment, especially a model that retains an ECM and immune cells. It is known that the upregulation of the pro-inflammatory cytokines within the bone marrow microenvironment causes dysregulation of the bone remodelling unit, with an increase in markers that can influence osteoclastogenesis that includes, IL-1β, IL-6, TNFα, macrophage-colony stimulating factor (M-CSF) and receptor activator of the nuclear factor kappa B (NF-κB) ligand (RANKL), along with an inhibited expression of osteoprotegerin (OPG, Marriott et al. 2004; Bottner et al. 2007; Sanchez et al. 2013; Josse et al. 2015). The increase of pro-inflammatory cytokines causes a downregulation of anti-inflammatory cytokines, following infection. Biofilm formation leads to persistent inflammation and influx of immune cells in the local environment resulting in increased damage to surrounding bone marrow. Inhibition of the osteoblastic bone formation has been observed following infection with *S. aureus*, with *In vitro* studies showing a decrease in alkaline phosphatase activity, osteopontin, osteocalcin and osteonectin in the presence of *Staphylococcus* protein A (Claro et al. 2011; Jin et al. 2013; Widaa et al. 2012).

In developing this co-culture model, *S. aureus* was chosen as the infective agent due to its role as a primary coloniser in both PJI and osteomyelitis. The model must be representative

of the clinical scenario and be comparable to other *in vivo* clinical and research studies. Firstly, an analysis must be taken of the viability and attachment of the infective organism within the bone marrow cavity. Secondly, the pro-inflammatory and anti-inflammatory cellular response must be assessed to observe any differences in either the innate or adaptive immune response following infection. Successes in both would allow further modification of the model to understand and develop antimicrobials for *S. aureus* implant-associated infections.

4.2: Materials and methods

4.2.1: Microorganism Culture

Two *Staphylococcus aureus* type strains were used for all experiments; NCTC 7791 and NCTC 6571 (Public Health England, Salisbury, United Kingdom). NCTC 6571 is commonly known as the Oxford strain and NCTC 7791 is a strain originally isolated from an osteomyelitis patient. Bacterial strains were subcultured onto Oxoid tryptone soya agar (TSA) plates (ThermoFisher Scientific, Loughborough, United Kingdom) incubated at 37 ^{o}C, 5 % CO_2 for 24 h, before experimentation.

4.2.2 Bacteria Enumeration of Viable Colony Forming Units (CFU)

To determine the optimal number of CFU needed to infect the femoral slice, a calibration curve using the Miles and Misra viable drop count method was used (Miles et al. 1938). An individual colony, from either of the two strains, was inoculated within 10 mL of Oxoid brain heart infusion (BHI) ThermoFisher Scientific) bacterial culture broth and was incubated overnight for 15 h within an aerobic incubator at 37 ^{o}C and 5 % CO_2 until the bacterial cultured BHI reached the exponential phase of growth. Following overnight incubation, the turbidity of the bacterial BHI culture was diluted using sterile BHI to six different absorbance optical density (OD) values at 0.22, 0.13, 0.09, 0.08, 0.07 and 0.05, using a 0D600 DiluPhotometer spectrophotometer (Implen INC, Westlake Village, USA). The spectrophotometer was standardised at 600 nm using sterile BHI without bacteria, which acted as a blank. Following absorbance readings at; 0.22, 0.13, 0.09, 0.08, 0.07 or 0.05, 20 µL of bacterial suspension for each absorbance was aliquoted and added to 180 µL of PBS within an individual well of a 96-well plate. This bacterial PBS suspension was serially diluted at a ratio of 1:10 from 10^8 to 10^1 CFU/mL and two 10 mL drops of each dilution were added to TSA plates and incubated overnight within an aerobic incubator at 37 ^{o}C and 5 % CO_2. Following overnight incubation, colonies were grown from each droplet until they were sufficient in number to count individually using ImageJ (U.S. National Institutes of Health, Bethesda, USA), the average of these counts was used to back-calculate the original dilution factor to determine the original CFU/mL. A standard curve was generated against the OD values to determine the accurate bacterial inoculation rates for subsequent experiments.

4.2.3: Bacterial Growth Curves in Tissue Culture Conditions and Bacterial Culture Media

To determine the optimal growth for each bacterial strain within tissue culture media, three different culture media compositions were compared, adapted from Roberts et al. (2013). The first culture media was αMEM media (ThermoFisher Scientific) supplemented with 10 % heat-inactivated foetal bovine serum (HI FBS, Gibco™ South America origin, ThermoFisher Scientific), L-Ascorbic acid 2-phosphate sesquimagnesium salt hydrate (Sigma-Aldrich, Poole, United Kingdom), along with 20 ng/mL M-CSF (Peprotech, London, United Kingdom) and 30 ng/mL RANKL (Peprotech). The second culture media was αMEM supplemented with 10 % FBS, 1 % L-ascorbic acid 2-phosphate, 10 % BHI, 20 ng/mL M-CSF and 30 ng/mL RANKL. BHI was used as a positive control for bacterial growth.

A single bacterial colony was inoculated from overnight cultures of individual TSA plates, colonised with either NCTC 6571 or NCTC 7791 bacterial strains and added to 10 mL of pure BHI solution and incubated overnight within an aerobic incubator at 37 ^{o}C and 5 % CO_2. Overnight culture media for both strains had turbidity determined and adjusted to absorbance OD_{600} reading at 0.08-0.10, which represented 10^8 CFU/mL for both stains. Bacterial suspensions were then serially diluted in αMEM to 10^4 CFU/mL and were centrifuged at 438 x g for 3 min using the ThermoFisher Heraeus Labofuge 400 centrifuge (ThermoFisher) and resuspended in αMEM. A final serial dilution to 10^2 CFU/mL was made in either αMEM supplemented with 10 % FBS, 1 % L-ascorbic acid 2-phosphate, 20 ng/mL M-CSF and 30 ng/mL RANKL, or in αMEM supplemented with 10 % FBS, 1 % L-ascorbic acid 2-phosphate, 10 % BHI, 20 ng/mL M-CSF and 30 ng/mL RANKL. For the universal BHI control, both strains were serially diluted from 10^8 CFU/mL to 10^2 CFU/mL in pure sterile BHI solution only. To individual wells of a 96-well culture plate (Starstedt, Leicester, United Kingdom) bacterial suspensions at 10^2 CFU/mL, were pipetted at 100 µL. A blank control to measure background absorbance of the culture media was used with either sterile BHI or αMEM supplemented with 10 % FBS, 1 % L-ascorbic acid 2-phosphate at 100 µM concentration, 20 ng/mL M-CSF and 30 ng/mL RANKL. The remaining bacterial suspensions were aliquoted at 5 mL within individual universal tubes ready for cell viability staining, described in Section 4.2.4. The 96-well culture plate was incubated for 24 h at 37 ^{o}C and 5 % CO_2 within a Fluorostar Omega Spectrometer (BMG Labtech Ltd, Aylesbury, United Kingdom) and

absorbance was read automatically every h at 550nm. Readings were blank corrected and readings tabulated.

4.2.4 Viability Staining of Bacterial Strains

To assess bacterial viability during culture, a Live/Dead *Bac*Light Bacterial Viability Kit (ThermoFisher Scientific) was used, following the manufacturer's instructions. Bacterial cells were stained with green fluorescent acid stain SYTO9 and the red fluorescent acid stain propidium iodide. SYTO9 labelled all bacteria including those with and without intact membranes. However, propidium iodide only stains bacteria with damaged membranes and when used together the percentage of live (SYTO9) to damaged/dead cells (propidium iodide) can be quantified.

The assay used overnight cultures of bacterial suspensions grown in different culture media, described in Section 4.2.2. Bacterial suspensions that were initially incubated within an aerobic incubator at 37 ^{o}C and 5 % CO_2, were aliquoted at 50 µL, at 0 h, 6 h, 19 h and 24 h into sterile 1.5 mL microcentrifuge tubes (Starlabs, Milton Keynes, United Kingdom). The bacterial Live/Dead stain mix was prepared according to the manufacturers' instructions at a 1:1 v/v ratio by combining 5 µL of a vial containing live stain mixture (1.67 mM of SYTO 9 dye 1.67 mM of propidium iodide), to 5 µL of a vial containing the dead stain mixture (1.67 mM of SYTO 9 dye, 18.3 mM of propidium iodide). The Live/Dead solution was vortexed and 1 µL was added to 50 µL bacterial suspensions, before being vortexed and incubated devoid of any light for 15 min at room temperature. Following incubation, 5 µL of stained bacterial suspension was added to poly-lysine glass slides (ThermoFisher Scientific) and was secured by a coverslip. Slides were immediately imaged using an Olympus AX70 Fluorescent Microscope (Olympus Corporation, Tokyo, Japan), using x200 magnification. Images were analysed using ImageJ, where the green and red channels per image were separated and the total and percentage cell counts for each channel were quantified and tabulated.

4.2.5: Co-Culture of the Femoral Slice Model

To elucidate bacterial attachment, immune cell response and subsequent pro-inflammatory and anti-inflammatory effects of the bacterial species within the bone marrow microenvironment, both bacterial strains were co-cultured live within the *ex vivo* femoral slice model. Femurs were extracted from freshly sacrificed 21-28 day-old Wistar rats and sectioned into semi-cylindrical femoral slices as previously described in Sections 2.2.1 and 3.2.2. Semi-cylindrical slices were microinjected with extracted mixed tibial bone marrow cells along with 20 ng/mL of M-CSF and 30 ng/mL of RANKL as previously described in section 3.2.1 and 3.2.2.3. Semi-cylindrical femoral slices were embedded into 1 % agarose and culture media gel and cultured at a liquid air/interphase using the Trowell-type culture with culture media and agarose gel supplemented with 20 ng/mL M-CSF and 30 ng/mL RANKL as previously described in section 3.2.2.1.

4.2.5.3: Infection of *ex vivo* Semi-Cylindrical Femoral Slices

Overnight bacterial inoculations grown within BHI were vortexed and adjusted to give OD between 0.08-0.1. Controls of heat-inactivated bacterial suspensions were prepared from overnight bacteria suspensions grown in BHI, with both *S. aureus* strains heated in the water bath at 80 ^{O}C for 30 min. Both viable and heat-inactivated bacteria suspensions were individually diluted down to 10^2 CFU/mL in of αMEM containing 10 % HI FBS, 1 % L-ascorbic acid 2-phosphate, supplemented with 20 ng/mL M-CSF and 30 ng/mL RANKL. 3 mL of basal media with bacterial suspensions were added to individual wells of a 6-well culture plate, containing a support ring and 0.45 µm membrane. The 1 % w/v agarose gel was infected by first diluting both viable and heat-inactivated bacteria suspensions to 10^4 CFU/mL using basal media containing double the concentration of supplements (20 % FBS and 2 % L-ascorbic acid 2-phosphate and 40 ng/mL M-CSF and 60 ng/mL RANKL). Following this, 1.5 mL of basal culture media with 10^4 CFU/mL of diluted heat-inactivated or viable bacterial suspensions were added to 1.5 mL of αMEM, combined with 2 % agarose and mixed at a 1:1 ratio within individual wells of a 12-well culture plate, and left to cool for 10 min. To individual wells of a 12-well culture plate, containing the 3 mL of the 1 % agarose gel and viable bacteria suspension, femoral slices were embedded and left to cool to form an agarose plug for 10 min. The solidified infected plug was laid over the 0.45 µm membrane

and femoral slices were left to culture for;6 h, 19 h and 24 h within a sterile humidified incubator at 37 ^{o}C, 5 % CO_2 and uncultured femoral slice served as 0 h controls and were immediately fixed in 10 % formalin solution (ThermoFisher Scientific). Non-infected slices were used as a non-infection control.

4.2.5.4: Sample Collection and Storage

Sample collection for infected or non-infected Trowell-type cultures was conducted, as previously described in Section 2.2.3.4. Following removal of the femoral slices from the agarose gel, the remaining gel and culture media was combined and stored at -80 ^{o}C. Femoral slices were then fixed in 10 % formalin prior to decalcification in 14 % EDTA tetrasodium salt hydrate (pH 7.4) (Sigma Aldrich) for 1 week, before being embedded into paraffin wax, sectioned at 5 µm and mounted onto glass slides, as previously described in Section 2.2.3.4.

4.2.6: Detection of Necrosis Using a Colourimetric Lactate Dehydrogenase Assay

Lactate Dehydrogenase (LDH) necrosis activity was assessed following infection using the Pierce LDH Cytotoxicity Assay Kit (ThermoFisher Scientific) was carried out as previously described in Section 2.2.4

4.2.7: Haematoxylin and Eosin Staining

Automated H&E staining was carried out, as previously detailed in Section 2.2.6.

4.2.8: Identification of Secreted Pro-Inflammatory and Anti-Inflammatory Cytokines Using Enzyme-Linked Immunosorbent Assay (ELISA)

Basal media collected at 0 h, 6 h, 19 h and 24 h, were assessed for levels of pro-inflammatory cytokines (TNFα, IL-6 and IL-1β) or anti-inflammatory cytokines (IL-4 and Il-10). Pro-inflammatory cytokines were assessed using the Rat Mini ABTS ELISA Development Kit (Peprotech) and ABTS ELISA Buffer Kit (Peprotech), following the manufacturer's

instructions. Anti-inflammatory cytokines were assessed using the Rat DuoSet ELISA Development System (R&D Systems, Abingdon, United Kingdom) and DuoSet Ancillary Reagent Kit (R&D Systems), according to the manufacturer's instructions.

The capture antibody, an antibody that is raised against the antigen of interest, was reconstituted to 100 ug/mL in either double-distilled water (ddH_2O) or PBS, filtered through 0.2 μM syringe filters depending on the source of Kit used, before being diluted to working concentrations in 10 mL of PBS, specifics shown in Table 3.1. To each well of an ELISA 96-well culture plate, 100 μL of the capture antibody was added and left to incubate overnight at room temperature. Following incubation, each well was aspirated and washed four times using 200 μL of wash buffer containing 1 % Tween-20 in PBS for Peprotech ELISA Kits or 0.05 % Tween-20 in PBS for R&D Systems ELISA Kits, followed by gentle tapping onto clean absorbent paper towels. The plate was blocked using a blocking buffer containing 1 % BSA in PBS and 300 μL was added to each well and left to incubate overnight at 4 ^{o}C. Plates were then aspirated and washed 4x in wash buffer from the Kit. Standards were added to the ELISA plate and were either reconstituted to 0.2 μM filtered ddH_2O (Peprotech) or 0.2 μM filtered reagent diluent (R&D Systems), to the volumes shown in Table 3.1. Standards were serial diluted to ranges shown for each cytokine (Table 3.1), in reagent diluent and 100 μL was added to individual wells of the ELISA plate, after which in the remaining wells, basal culture media samples were added to the ELISA plate. Basal media and agarose plug from the co-culture of femoral slice model (Section 4.2.5) were defrosted and homogenised by vortex to break up large pieces of agarose gel and were again subjected to further homogenisation by pipette action to detect the levels of cytokines captured within both the agarose gel and basal media. Samples and blank basal media were centrifuged at 1218 x g for 5 min at room temperature using the ThermoFisher Heraeus Labofuge 400 centrifuge and supernatants were either diluted down or remained undiluted, depending on the cytokine Kit used, as stated in Table 3.1. Aliquots of 100 μL were added to individual wells of the ELISA culture plate, not containing the standard solutions. Basal αMEM containing 10 % HI FBS, 1 % L-ascorbic acid 2-phosphate, 20 ng/mL M-CSF and 30 ng/mL RANKL, was used as a blank and 100 μL were also added to individual wells of the ELISA culture plate.

Samples, standards and blanks were incubated overnight at 4°C. Following incubation, each well was aspirated and washed 4x in 200 μL of wash buffer.

The detection antibody was reconstituted in either 0.2 μM filtered ddH_2O (Peprotech) or reagent diluent (R&D Systems) and diluted further in 10 mL using a diluent to the concertation shown in Table 3.1. 100 μL was added to each individual wells of the ELISA plate and incubated overnight at 4°C. Once incubated, each well was aspirated and washed 4x in wash buffer. Following washing, avidin horseradish peroxidase (HRP) conjugate was diluted in 10 mL of diluent to concentrations shown in Table 3.1 for each cytokine; and 100 μL was added to each individual wells of the ELISA culture plate. The culture plate was then incubated at room temperature for 30 min, following which, wells were aspirated and washed 4x in 200 μL of wash buffer.

Once washed, a liquid substrate was applied to each well, resulting in a colour change, with the intensity of the colour change representing the increased synthesis of the cytokine and is quantified using a Fluorostar Omega Spectrometer. The protocol following the addition of the substrate differed for each ELISA Kit. For Peprotech ELISA Kits, 100 μL of ABTS liquid substrate was applied to each individual well and absorbance read using the Spectrometer at 490 nm and 680 nm, every 90 s for 30 min. Wavelength correction was applied via subtraction of 490 nm reading from 680 nm.

For R&D ELISA Kits, 100 μL of substrate solution of a 1:1 mixture of hydrogen peroxide and tetramethylbenzidine, was applied to each individual well and left to incubate for 20 min at room temperature in the dark. A 50 μL stop solution containing sulphuric acid was added to each individual well. The 96-well plate was then read using the Spectrometer at an absorbance of 540 nm and 570 nm, with wavelength correction applied via the subtraction of 540 nm reading from 570 nm.

Cytokine	ELISA kit	Product code	Capture antibody reconstitution (100 ug/mL)	Capture antibody concentration used	Standard reconstitution	Standard concentration used	Sample dilution	Detection antibody reconstitution	Detection antibody working concentration	Detection antibody concentration used	HRP concertation dilution (10 mL)
TNFα	Peprotech	900-M73	210 µL ddH_20	1 ug/mL	1000 µL ddH_20	31.25 - 3000 pg/mL	1:10 in diluent	110 µL ddH_20	100 ug/mL	0.5 ug/mL	1:2000
IL-1β	Peprotech	900-M91	410 µL ddH_20	1 ug/mL	1000 µL ddH_20	62.5 - 4000 pg/mL	1:15 in diluent	110 µL ddH_20	100 ug/mL	0.5 ug/mL	1:2000
IL-6	Peprotech	900-M86	250 µL ddH_20	1 ug/mL	1000 µL ddH_20	46.825 - 2000 pg/mL	No dilution used	60 µL ddH_20	100 ug/mL	0.25 ug/mL	1:2000
IL-4	R&D systems	DY504	1000 µL PBS	2 ug/mL	500 µL of reagent diluent	15.6 - 31000 pg/mL	No dilution used	1000 µL of reagent diluent	200 ug/mL	of 200 ng/mL	1:200
IL-10	R&D systems	DY522	500 µL PBS	4 ug/mL	500 µL of reagent diluent	62.5 - 4000 pg/mL	No dilution used	1000 µL of reagent diluent	300 ug/mL	300 ng/mL supplemented with 2 % heat inactivated normal goat serum	1:40

Table 3.1: ELISA kit reagents, antibodies, standards and horseradish peroxidase (HRP) concentrations.

4.2.9: Modified Gram Stain on Histological Tissue Sections to Identify Attached Bacteria Within the *ex vivo* Model

To improve the contrast between the Gram-positive bacterium and the tissue within the femoral slice, a modified Gram stain was used as described by Becerra et al. (2016). This method utilises a saffron alcoholic solution (VWR, Pennsylvania, United States), which is a mixture of saffron pistil mixed into < 5 % absolute ethanol and < 95 % methanol solution, that is used following conventional Gram staining technique. As previously detailed in Section 3.2.6, tissue slices following co-culture were demineralised using EDTA, paraffin-embedded and sectioned at 5 µm onto glass super frost slides. To enable tissue sections to be Gram stained, slides were deparaffinised three times in xylene washes for 5 min each and washed 3x in graded ethanol at 100 %, 75 % and 50 % for 5 min each, before being submerged in distilled water for a minimum of 5 min. All steps were performed at room temperature. Rehydrated slides were then stained with crystal violet solution for 30 s, before being rinsed in running tap water. Slides were flooded with iodine solution for 10 s and sections were rinsed in running tap water. Sections were then covered in acetone for 5 s, before immediately being rinsed in running tap water. Sections were counterstained in 5 s of safranin and rinsed in running tap water. Sections were dehydrated in 2x washes of 95 % and 100 % ethanol for 2 min each, before being submerged in alcoholic saffron (VWR) for 5 min, after which a final 100 % ethanol wash was undertaken on the sections for 2 min. Sections were passed through xylene for 2 min, before mounting each section with DPX mounting medium and covering with a coverslip. Slides were visualised using the Olympus AX70 Fluorescent Microscope.

Two positive control tissues were used and treated the same as above. The first was rat lung tissues infected with NCTC 6571. Rat lungs were extracted at the same time as the femurs from 15-21-day-old Wistar Rats and placed into αMEM in an incubator for 1 h at 37 ^{o}C and 5 % CO_2 to acclimatise to the culture environment. Overnight NCTC 6571 bacteria cultures within BHI were vortexed and adjusted to give OD between 0.08-0.1. Bacterial suspensions were diluted down to 10^2 CFU/mL in αMEM containing 10 % HI FBS, within individual wells of a 6-well culture plate. The lung tissue was removed from the incubator and placed within the tissue culture media containing the diluted bacterial suspension and cultured for 24 h at

37 ^{o}C and 5 % CO_2. Following culture, the lung tissue was removed and fixed in 10 % formalin solution for 24 h before being processed into paraffin wax using Leica ASP300s Automated Tissue Processor (Leica Biosystems, Milton Keynes, United Kingdom), embedded into biopsy moulds and section using Shandon Finesse Me^{+} Microtome (ThermoFisher Scientific) onto glass slides as described in Sections 2.2.5.2 and 2.2.5.3, respectively.

The second positive control was the isolation of TSA grown NCTC 6571 colony, which was mixed into a drop of phosphate buffered saline and spread over a glass slide. The slide was then air-dried and stained.

4.2.10: Scanning Electron Microscopy

Scanning electron microscopy (SEM) was carried out on 5 µm tissue slices. Tissue slices were deparaffinised with xylene, 3x5 min, washed in graded ethanol at 100 % 3x5 min each, before being left to air-dry overnight. The air-dried samples were sputter-coated with gold and imaged on a VAGA SEM system (Tescan, Brno, Czech Republic), at 5-10 kV. Images were taken using ATLAS software. Images were then pseudo-coloured using Adobe Photoshop 2020 (Adobe Inc., California, USA). Photoshop utilises a non-destructive approach to photo manipulation. The original black and white SEM image is retained as a separate image layer. Each layer exists separate from other layers, if a layer is added on top of another layer the underlying layer is never manipulated or touched. In Photoshop a colour image layer was applied on top of the original image layer as a layer mask. This layer mask can be selectively coloured using a range of solid colours and a layer blend mode is applied to blend the top colour layer to the image layer underneath. This allows the solid colours to become transparent allowing the original image to be visualised with the appearance of being coloured. This process can be reversed anytime without manipulating the original image.
S. aureus bacterial species were identified by their cocci appearance, with diameters of 0.5 - 1.5 µm and form grape-like bunches, positively matched structures were pseudo-coloured purple (Ribeiro et al. 2012). Bone marrow cells were identified and pseudo-coloured red. These cells were identified by larger size and their cell surface characteristics, immature cells have a smoother cell surface, whilst mature monocytes and macrophage cells tend to have ruffles on their cell surface and other mature lymphocytes tend to have a microvilli-like

structure on their cell surface (Soligo et al. 1985). Mineral bone was pseudo-coloured yellow, whilst the slide background showing no tissue or cellular structures were pseudo-coloured teal.

4.2.11: Dual Labelled Immunohistochemistry for Apoptosis, Necrosis and Immune Cell Markers Along With *Staphylococcus Aureus* Protein A

Using the protocol previously described in Section 2.2.8, immunohistochemistry (IHC) staining was utilised for dual labelling of markers for bacteria and apoptosis/necrosis markers to observe potential colocalization. Following co-culture in Section 4.2.5, demineralised paraffin-embedded femoral sections of 5µm were deparaffinised in 3x5 min washes of xylene and rehydrated using graded ethanol 100 – 70 % for 5 min each. Slides were rinsed in ddH_2O for 5 min and were surrounded by a hydrophobic barrier using an ImmEdge Hydrophobic Barrier pap pen (Vector Laboratories, Peterborough, United Kingdom). The tissues sections were then quenched with 0.3 % hydrogen peroxide in 40 % methanol in Tris Buffered Saline (TBS) for 15 min. Slides were washed 3x times in TBS for 5 min, before undergoing antigen retrieval with citric acid (pH 6) for 20 min, heated at 100 ^{o}C in a water bath. The sections were then blocked using 1 % normal goat serum in TBS for 1 h at room temperature. Sections were blocked for avidin and biotin using the Avidin/Biotin Blocking Kit (Vector Laboratories), following the manufacturer's protocol. 50 µL of Avidin D solution was applied to each Section for 15 min and washed in TBS for 5 min, after which 50 µL of biotin solution was applied for 15 min and further washed in TBS for 5 min. Once washed, tissue sections were incubated with primary antibodies at specific concentrations for Bax, cleaved caspase 3, LDH, CD14 and CD68 (Table 2.1), overnight at 4 ^{o}C. Controls were applied on separate tissue sections as either isotype control antibodies (Table 2.2), or with primary antibody exclusion with TBS alone and incubated at either 1 h at room temperature or overnight at 4 ^{o}C.

Tissue sections were washed in TBS twice for 5 min. A biotinylated goat anti-rabbit IgG secondary antibody (Vector Laboratories) was applied over the tissue sections for 30 min at room temperature. Tissue sections were then washed three times in TBS for 5 min followed by the addition of 10 µL of avidin/biotin complex reagent from the kit for 30 min at room

temperature. Tissue sections were washed in TBS 3x5 min. DAB Peroxidase (HRP) Substrate Kit was used (Vector Laboratories), as previously described (Section 2.2.8), to visualise the location of the antibody chromogens. This was achieved by the addition of DAB complex over tissue sections for 30 s. The reaction was stopped by immersing sections in ddH_2O for 5 min.

Tissues were blocked again in 1 % normal goat serum in TBS for 1 h at room temperature, to prevent non-specific antibody binding to tissue or Fc receptors. Tissue sections were blocked for avidin and biotin using the Avidin/Biotin Blocking Kit, as previously described. Sections were washed and incubated with anti-*Staphylococcus aureus* antibody [704] (ab37644; Abcam, Cambridge, United Kingdom), overnight at 4 ^{o}C. Sections were washed in TBS 3x and biotinylated goat anti-mouse (rat preabsorbed) IgG secondary antibody (Vector Laboratories) was applied for 30 min. Tissue sections were further washed 3x in TBS for 5 min each and ABC reagent was applied for 30 min at room temperature. Following incubation, tissue sections were labelled with Nova Red Peroxidase (HRP) Substrate Kit, as previously described in Section 2.2.8. Nova red complex was incubated on tissue sections for 30 s, until the desired staining was achieved and terminated via immersion of sections in tap water for 5 min. Tissues were counterstained with haematoxylin for 10-30 s, before being blued in running tap water for 5 min. This blueing step converts the soluble purplish colour of the haematoxylin in the nucleus to a more insoluble permeant blue colour, this is caused by the pH of the tap water. Tissues were dehydrated in graded ethanol 70 – 100 % for 5 min each and passed through three washes of xylene for 5 min each. Tissue sections were mounted with DPX, applied with a coverslip and examined.

4.2.12: Imaging and Image Analysis

Imaging and image analysis were carried out, as previously detailed in Sections 2.2.9 and 2.2.10, using an Olympus AX70 Fluorescent Microscope. Analysis of images was carried out using the Image J application (National Institute of Health website). Cell counts for H&E stained sections were counted in an area of 10,000 um^2 per image and this was repeated to obtain five separate images. From these five counts, an average was obtained. Using these cell counts, a percentage loss of cells over 48 h were calculated.

4.2.13: Statistical Analysis

Statistical analysis was carried using Graphpad Prism version 8.00. One-way ANOVA with Tukey's post-test was used to identify significant differences in data across groups for one independent variable. A two-way ANOVA with Tukey's post-test was used to determine differences in data with two or more independent variables. Statistical significance was determined at $*P < 0.05$, $**P < 0.01$, $***P < 0.001$, $****P < 0.0001$.

4.3: Results

4.3.1: Bacteria Enumeration of *Staphylococcus aureus*

To ensure that bacterial cultures for all future experiments were standardised to a set CFU/mL, viable plate counts were used, using the Miles and Misra method. Using a linear standard curve, both *S. aureus* type strains at an initial absorbance OD of 0.1 gives a starting population of approximately 10^8 CFU/mL (Figure 4.1 A&B). For all future experiments, the overnight bacterial cultures were read at 0.1 before experimentation, as it gave an ~10^8 CFU/mL and therefore, can be used to standardise the dilution factor of CFU/mL required for each experimentation.

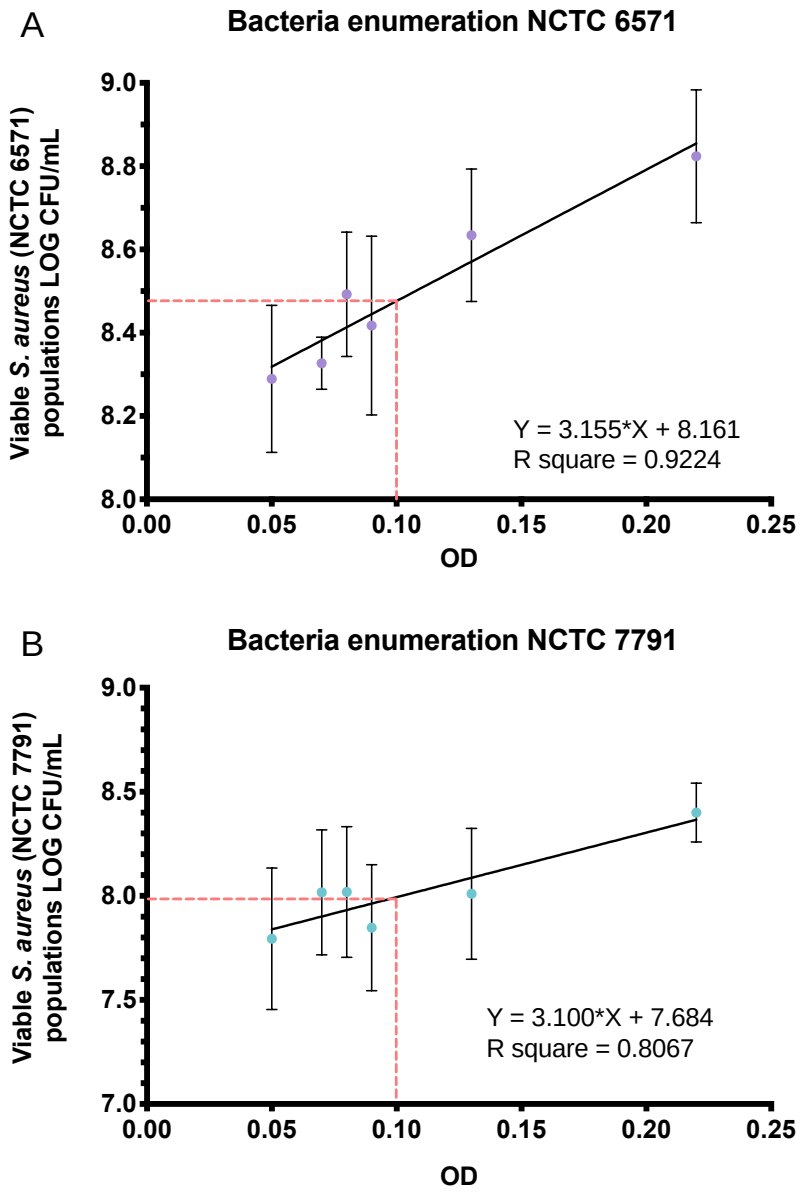

Figure 4.1: Bacterial enumeration standard curve. Graph A) bacterial enumeration for Oxford *S. aureus* 6571. Graph B) bacterial enumeration for 7791 clinical *S. aureus.* Colony counts at different serial dilution concentration from different OD600 reading. The number of colonies was multiplied by the dilution factor to give the concentration of CFU/mL in the original sample for that OD600. The dilution factor of 5 was used showing individual countable CFU. Line indicates LOG10 CFU/mL for OD600 for 0.1. Error bars represent mean ± SD (n=3).

4.3.2: The Growth of *Staphylococcus aureus* Under Standard Culture Conditions in Various Basal Culture Media.

The growth of the bacteria within different culture conditions all showed typical growth characteristics for lag, exponential, stationary and death phases for the bacteria. Bacterial growth for both type strains was slightly reduced when cultured in the presence of 20 % BHI in αMEM, supplemented with 10 % FBS, 1 % L-ascorbic acid 2-phosphate, 10 % BHI, 20 ng/mL M-CSF and 30 ng/mL RANKL but, demonstrated similar typical growth characteristics similar to BHI controls. There was a ~45 - 50 % reduction of growth in cultures that did not contain BHI which also showed typical growth characteristics for lag, exponential, stationary and death growth phases for the bacteria (Figure 4.2 A and B).

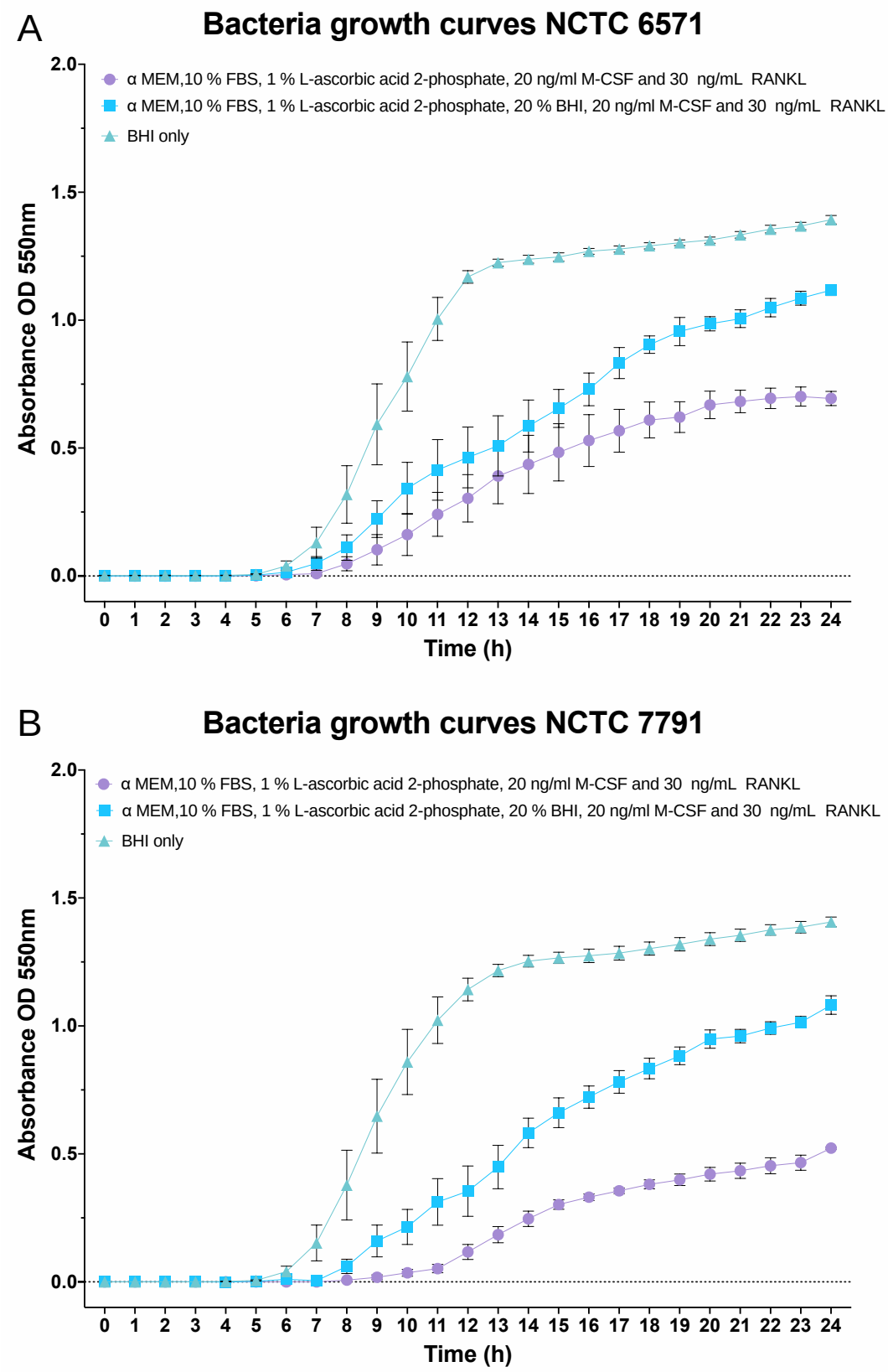

Figure 4.2: Absorbance of bacterial suspensions grown in different mammalian and bacterial culture media. Media of pure BHI and a-MEM with M-CSF and RANKL along with and without 20 % BHI broth, over 24 h incubation in 5 % CO_2 at 37 °C. Graph A) NCTC 6571 *S. aureus* type strain and Graph B) NCTC 7791 type strain. Error bars represent mean ± SEM (n=3).

4.3.3: The Viability of *Staphylococcus aureus* Under Standard Culture Conditions in Various Basal Culture Media.

Bacterial live/dead analysis for NCTC 6571 and NCTC 7791 *S. aureus* type strains over 24 hrs are shown in Figures 4.3 and 4.4, respectively.

4.3.3.1: The Viability of *Staphylococcus aureus* Grown in BHI Bacterial Broth Culture Media Alone.

Following culture within pure BHI, there were few viable cell counts at 2 h for both NCTC 6571 and NCTC 7791 strains, representing a mean of 315 and 22 cells respectively (Figures 4.3Ai, 4.3Bi, 4.4Ai and 4.4Bi). Percentage cell counts for viable bacteria at 2 h represented a mean of 47 % for NCTC 6571 and 60 % for NCTC 7791, respectively (Figures 4.3Aii and 4.4Aii). By 6 h, there was a non-significant decrease in the mean numbers of both NCTC 6571 and NCTC 7791 viable strains which had a mean of 31 and 20 cells, respectively, when compared to 0 h ($P > 0.05$; Figures 4.3Ai, 4.3Bii, 4.4Ai and 4.4Bii). There were no significant differences in the mean numbers of both NCTC 6571 and NCTC 7791 viable strains which had a mean of 49 % and 64 %, respectively when compared to 0 h ($P > 0.05$; Figures 4.3Ai, 4.3Bii, 4.4Ai and 4.4Bii). At 19 h there was a significant increase in the mean numbers of both NCTC 6571 and NCTC 7791 viable strains which had a mean of 6614 and 8070 cells, respectively, when compared to 0 h and 6 h ($P < 0.0001$; Figures 4.3Ai, 4.3Biii, 4.4Ai and 4.4Biii). The mean percentages of viable NCTC 6571 bacteria had a mean of 91 % and were significant when compared to 0 h ($P < 0.001$) and 6 h ($P < 0.01$; Figures 4.3Aii). The mean percentages of viable NCTC 7791 bacteria had a mean of 91 % and were non-significant when compared to 0 h and 6 h ($P > 0.05$; Figures 4.4Aii). At 24 h there was a significant decrease in the mean numbers of both NCTC 6571 and NCTC 7791 viable strains which had a mean of 4702 ($P < 0.0001$) and 5291 ($P < 0.01$) cells, respectively when compared to 19 h (Figures 4.3Ai, 4.3Biv, 4.4Ai and 4.4Biv). At 24 h there was a non-significant increase in the mean percentage of both NCTC 6571 and NCTC 7791 viable strains which had a mean of 95 % and 92 %, respectively, when compared to 19 h ($P > 0.05;$ Figures 4.3Ai, 4.3Biv, 4.4Ai and 4.4Biv).

Following culture within pure BHI, there were few non-viable cell counts at 2 h for both NCTC 6571 and NCTC 7791 strains, representing a mean of 409 and 11 cells respectively (Figures 4.3Ai and 4.4Ai). Percentage cell counts for non-viable bacteria at 2 h represented a mean of 46 % for NCTC 6571 and 40 % for NCTC 7791, respectively (Figures 4.3Aii and 4.4Aii). By 6 h, there was a non-significant in the mean numbers of both NCTC 6571 and NCTC 7791 non-viable strains which had a mean of 21 and 37 cells, respectively, when compared to 0 h ($P > 0.05$; Figures 4.3Ai and 4.4Ai). There was a non-significant decrease in the mean numbers of both NCTC 6571 and NCTC 7791 non-viable strains which had a mean of 40 % and 36 %, respectively, when compared to 0 h ($P > 0.05$; Figures 4.3Aii and 4.4Aii). At 19 h there was a non-significant increase in the mean numbers of both NCTC 6571 and NCTC 7791 non-viable strains which had a mean of 879 and 2683 cells, respectively, when compared to 0 h and 6 h ($P > 0.05$; Figures 4.3Ai and 4.4Ai). The mean percentages of non-viable NCTC 6571 bacteria had a mean of 9 % and was significant when compared to 0 h ($P < 0.05$) and 6 h ($P < 0.05$; Figures 4.3Aii). The mean percentages of non-viable NCTC 7791 bacteria had a mean of 13 % and was non-significant when compared to 0 h and 6 h ($P > 0.05$; Figures 4.4Aii). At 24 h there was a non-significant decrease in the mean numbers of both NCTC 6571 and NCTC 7791 non-viable strains which had a mean of 296 and 611, respectively, when compared to 19 h ($P > 0.05$; Figures 4.3Ai and 4.4Ai). At 24 h there was a non-significant decrease in the mean percentage of both NCTC 6571 and NCTC 7791 non-viable strains which had a mean of 5 % and 8 %, respectively when compared to 19 h ($P > 0.05$; Figures 4.3Ai and 4.4Ai).

4.3.3.2: The Viability of Staphylococcus aureus Grown in Tissue Culture Media Supplemented with 20 % BHI Bacterial Broth Culture Media.

Following culture within αMEM, 10% BHI, 1 % L-ascorbic acid 2-phosphate at 100 µM concentration, 20 ng/mL M-CSF and 30 ng/mL RANKL, there were few viable cell counts at 2 h for both NCTC 6571 and NCTC 7791 strains, representing a mean of 54 and 106 cells respectively (Figures 4.3Aiii, 4.3Bv, 4.4Aiii and 4.4Bv). Percentage cell counts for viable bacteria at 2 h represented a mean of 58 % for NCTC 6571 and 57 % for NCTC 7791, respectively (Figures 4.3Aiv and 4.4Aiv). By 6 h, there was a non-significant decrease in the

mean numbers of both viable NCTC 6571 and NCTC 7791 strains which had a mean of 18 and 123 cells, respectively, when compared to 0 h (*P > 0.05*; Figures 4.3Aiv, 4.3Bvi, 4.4Aiv and 4.4Bvi). There were no significant differences in the mean numbers of both viable NCTC 6571 and NCTC 7791 strains which had a mean of 49 % and 61 %, respectively when compared to 0 h (*P > 0.05*; Figures 4.3Aiv and 4.4Aiv). At 19 h there was a significant increase in the mean numbers of both viable NCTC 6571 and NCTC 7791 strains which had a mean of 2674 and 2204 cells, respectively, when compared to 0 h and 6 h (*P < 0.0001*; Figures 4.3Aiii, 4.3Bvii, 4.4Aiii and 4.4Bvii). The mean percentages of viable NCTC 6571 bacteria had a mean of 78 % and was significant when compared to 6 h (*P < 0.01*; Figures 4.3Aiii). The mean percentages of viable NCTC 7791 bacteria had a mean of 71 % and was non-significant when compared to 6 h (*P > 0.05*; Figures 4.4Aii). At 24 h there was a significant decrease in the mean numbers of viable NCTC 6571 bacteria which had a mean of 1877 (*P < 0.01*) when compared to 19 h (Figures 4.3Aiii, 4.3Bviii). At 24 h there was a non-significant increase in the mean numbers of viable NCTC 7791 bacteria which had a mean of 2790 (*P > 0.05*) when compared to 19 h (Figures 4.4Aiii, 4.4Bviii). At 24 h there was no significant difference in the mean percentage of both viable NCTC 6571 and NCTC 7791 strains which had a mean of 89 % and 67 %, respectively when compared to 19 h (*P > 0.05;* Figures 4.3Aiv and 4.4Aiv).

Following culture within αMEM, 10% BHI, 1% L-ascorbic acid 2-phosphate at 100 µM, 20 ng/mL M-CSF and 30 ng/mL RANKL, there were few non-viable cell counts at 2 h for both NCTC 6571 and NCTC 7791 strains, representing a mean of 20 and 17 cells respectively (Figures 4.3Aiii and 4.4Aiii). Percentage cell counts for non-viable bacteria at 2 h represented a mean of 31 % for NCTC 6571 and 32 % for NCTC 7791, respectively (Figures 4.3Aiv and 4.4Aiv). By 6 h, there was no significant differences in the mean numbers of both NCTC 6571 and NCTC 7791 non-viable strains which had a mean of 16 and 31 cells, respectively, when compared to 0 h (*P > 0.05*; Figures 4.3Aiii and 4.4Aiii). There was a non-significant increase in the mean numbers of both NCTC 6571 and NCTC 7791 non-viable strains which had a mean of 51 % and 38 %, respectively when compared to 0 h (*P > 0.05*; Figures 4.3Aiv and 4.4Aiv). At 19 h there was a non-significant increase in the mean numbers of non-viable NCTC 6571 bacteria to a mean of 1265 (*P > 0.*05) and a significant increase in the mean numbers of non-viable NCTC 7791 bacteria to a mean of 1118 cells (*P < 0.0001*) when compared to 0 h and 6 h (Figures 4.3Aiii and 4.4Aiii). The mean percentages of non-

viable NCTC 6571 bacteria had a mean of 22 % and was significant when compared to 6 h (*P < 0.01*; Figures 4.3Aiv). The mean percentages of non-viable NCTC 7791 bacteria had a mean of 28 % and was non-significant when compared to 6 h (*P > 0.05*; Figures 4.4Aiv). At 24 h there was a non-significant decrease in the mean numbers of both non-viable NCTC 6571 and NCTC 7791 strains which had a mean of 255 and 457, respectively, when compared to 19 h (*P > 0.*05; Figures 4.3Aiii and 4.4Aiii). At 24 h there was no significant in the mean percentage of both NCTC 6571 and NCTC 7791 non-viable strains which had a mean of 10 % and 33 %, respectively when compared to 19 h (*P > 0.05*; Figures 4.3Ai and 4.4Ai).

4.3.3.3: The Viability of *Staphylococcus aureus* Grown in Tissue Culture Media Without Supplementation with BHI Bacterial Broth Culture Media.

Following culture within αMEM, 1 % L-ascorbic acid 2-phosphate at 100 µM concentration, 20 ng/mL M-CSF and 30 ng/mL RANKL, there were few viable cell counts at 2 h for both NCTC 6571 and NCTC 7791 strains, representing a mean of 73 and 41 cells respectively (Figures 4.3Av, 4.3Bix, 4.4Av and 4.4Bix). Percentage cell counts for viable bacteria at 2 h represented a mean of 66 % for NCTC 6571 and 49 % for NCTC 7791, respectively (Figures 4.3Avi and 4.4Avi). By 6 h, there was no significance in the mean numbers of both viable NCTC 6571 and NCTC 7791 strains which had a mean of 60 and 138 cells, respectively, when compared to 0 h (*P > 0.05*; Figures 4.3Av, 4.3Bx 4.4Av and 4.4Bx). There were no significant differences in the mean percentages of both NCTC 6571 and NCTC 7791 viable strains at 6 h which had a mean of 61 % and 61 %, respectively when compared to 0 h (*P > 0.05*; Figures 4.3Avi and 4.4Avi). At 19 h there was a significant increase in the mean viable numbers of both NCTC 6571 and NCTC 7791 strains which had a mean of 1910 and 2205 cells, respectively, when compared to 0 h and 6 h (*P < 0.0001*; Figures 4.3Av, 4.3Bxi, 4.4Av and 4.4Bxi). There was a non-significant increase in the mean percentages of both NCTC 6571 and NCTC 7791 viable strains at 19 h to 76 % and 72 %, respectively, when compared to 0 h and 6 h (*P > 0.05*; Figures 4.3Avi and 4.4Avi). At 24 h there was a non-significant increase in the mean viable numbers of both NCTC 6571 and NCTC 7791 strains to 2167 and 2790 cells respectively when compared to 19 h (*P > 0.05*; Figures 4.3Av, 4.3Bxii, 4.4Av and 4.4Bxii). There was a slight non-significant decrease in mean percentages of both NCTC 6571 and

NCTC 7791 viable strains at 24 h to 68 % and 67 %, respectively, when compared to 0 h and 6 h (*P > 0.05*; Figures 4.3Avi and 4.4Avi).

Following culture within αMEM, 10% BHI, 1 % L-ascorbic acid 2-phosphate at 100 µM concentration, 20 ng/mL M-CSF and 30 ng/mL RANKL, there were few non-viable cell counts at 2 h for both NCTC 6571 and NCTC 7791 strains, representing a mean of 55 and 17 cells respectively (Figures 4.3Av and 4.4Av). Percentage cell counts for non-viable bacteria at 2 h represented a mean of 34 % for NCTC 6571 and 32 % for NCTC 7791, respectively (Figures 4.3Avi and 4.4Avi). By 6 h, there were no significant differences in the mean numbers of both NCTC 6571 and NCTC 7791 non-viable strains which had a mean of 34 and 31 cells, respectively, when compared to 0 h (*P > 0.05*; Figures 4.3Av and 4.4Av). There was no significance in the mean numbers of both NCTC 6571 and NCTC 7791 non-viable strains which had a mean of 28 % and 39 %, respectively, when compared to 0 h (*P > 0.05*; Figures 4.3Avi and 4.4Avi). At 19 h there was a non-significant increase in the mean numbers of non-viable bacteria for NCTC 6571 to a mean of 531 (*P > 0.05*) and a significant increase in the mean numbers of non-viable bacteria for NCTC 7791 to a mean of 1118 cells (*P < 0.0001*) when compared to their respective 0 h and 6 h time points (Figures 4.3Av and 4.4Av). At 19 h there was a non-significant decrease in the mean percentage of both NCTC 6571 and NCTC 7791 non-viable strains which had a mean of 24 % and 29 %, respectively when compared to 19 h (*P > 0.05*; Figures 4.3Ai and 4.4Ai). At 24 h there was a non-significant increase in the mean numbers of non-viable bacteria for both NCTC 6571 and NCTC 7791 strains which had a mean of 913 and 1429, respectively, when compared to 19 h (*P > 0.05*; Figures 4.3Av and 4.4Av). At 24 h there was a non-significant increase in the mean percentage of both NCTC 6571 and NCTC 7791 non-viable strains to a mean of 32 % and 33 %, respectively, when compared to 19 h (*P > 0.05*; Figures 4.3Ai and 4.4Ai).

.

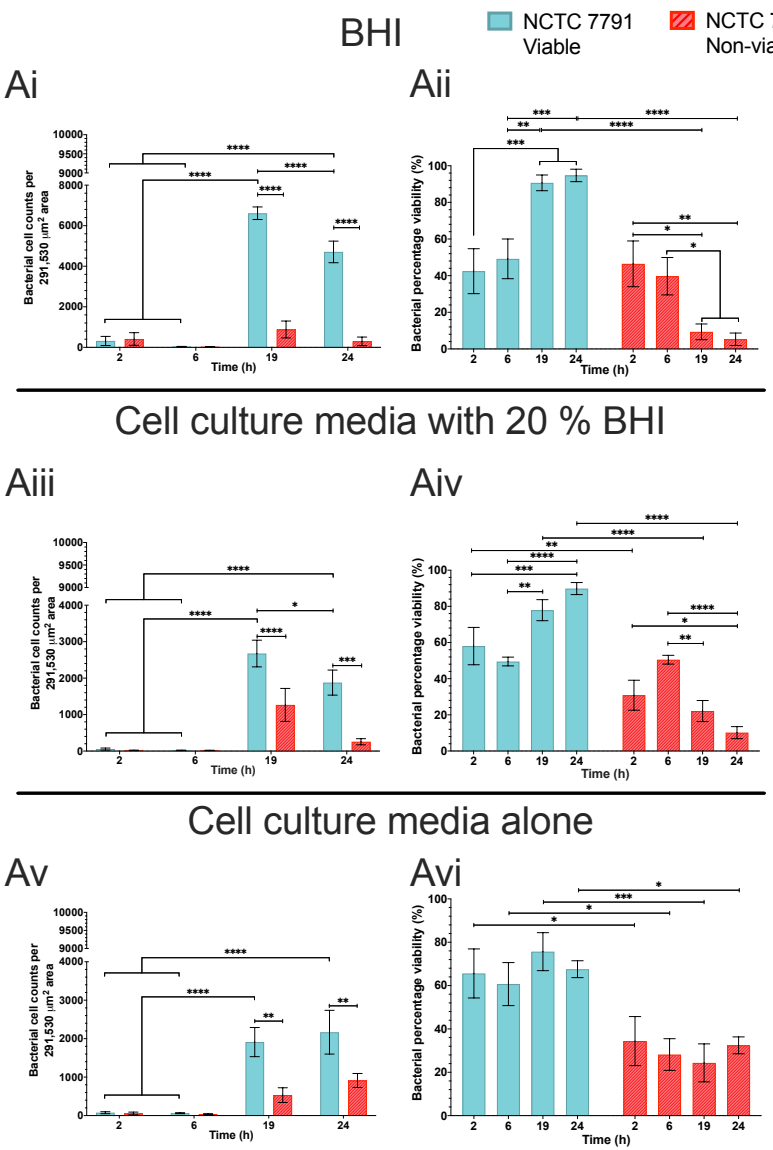

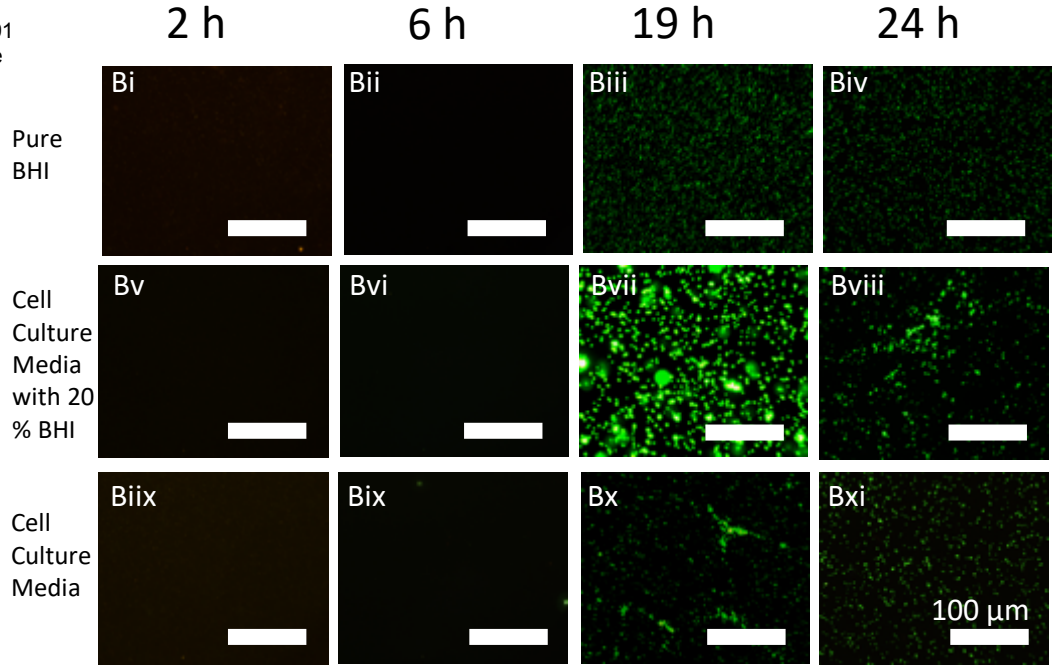

Figure 4.3: Viability analysis of NCTC 6571 over 24 h in different culture media. Viability analysis of NCTC 6571 bacterial species grown in different culture media. Graphs show Mean cell counts (Ai, Aiii & Av), mean percentage viability (Aii, Aiv & Avi), and images show viable (green-stained) and non-viable (red-stained) bacterial images over 2 h, 6 h, 19 h and 24 h. Culture media include; pure BHI broth (Ai, Aii & Bv-viii) αMEM, 20 % BHI, 10 % L-ascorbic acid 2-phosphate, 20 ng/mL M-CSF and 30 ng/mL RANKL (Aiii, Aiv & Biix-xi) αMEM, 10 % L-ascorbic acid 2-phosphate, 20 ng/mL M-CSF and 30 ng/mL RANKL (Av, Avi & Biix-Bxi). Data shows that all culture media supported bacterial growth, although culture media without BHI had reduced bacterial growth. Significance within groups determined via one-way ANOVA and between groups determined via two-way ANOVA with Tukey post-hoc test. Error bars represent mean ±S.E.M (n=3), **P<0.05, **P < 0.01, ***P < 0.001 and ****P < 0.0001*.

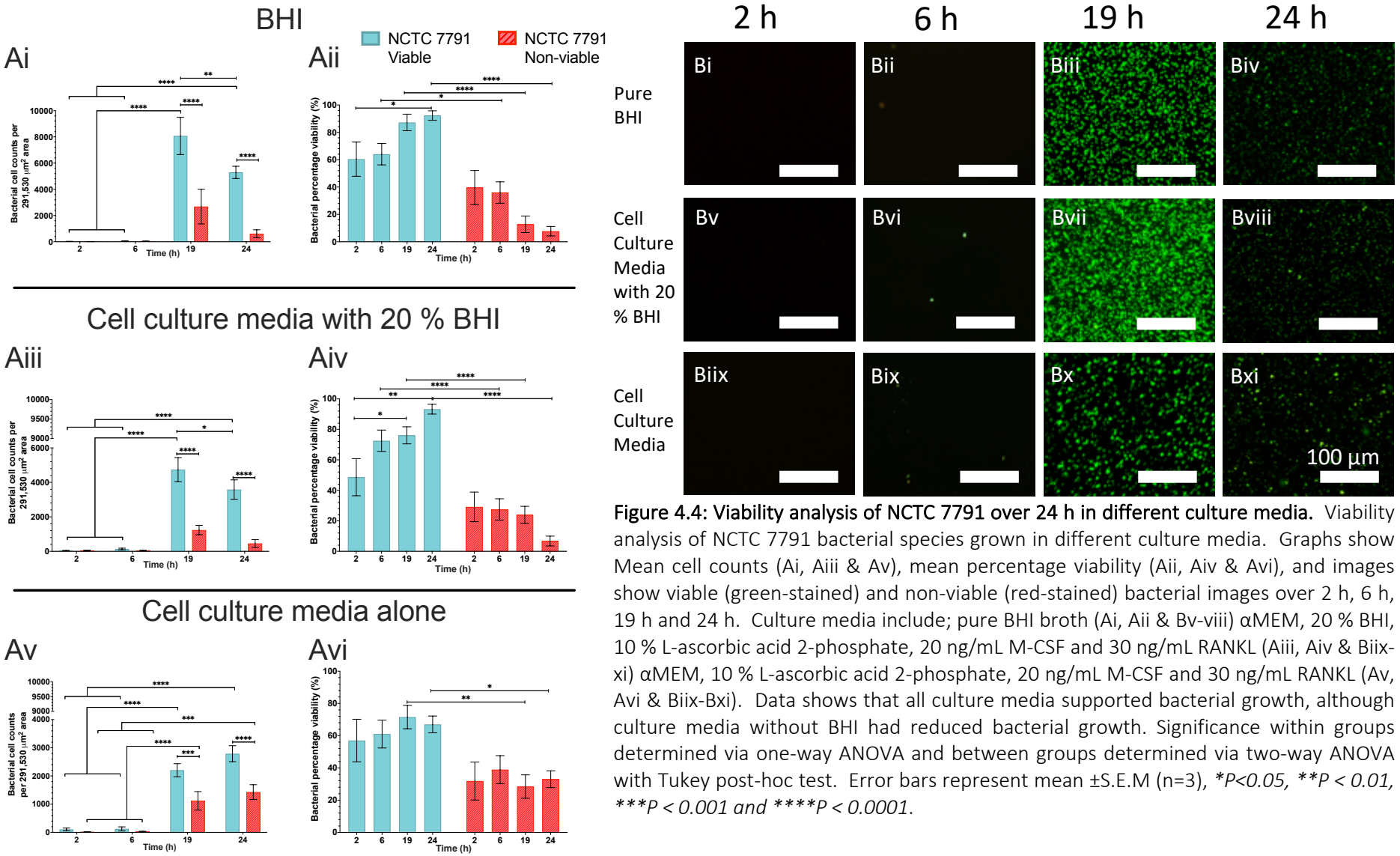

Figure 4.4: Viability analysis of NCTC 7791 over 24 h in different culture media. Viability analysis of NCTC 7791 bacterial species grown in different culture media. Graphs show Mean cell counts (Ai, Aiii & Av), mean percentage viability (Aii, Aiv & Avi), and images show viable (green-stained) and non-viable (red-stained) bacterial images over 2 h, 6 h, 19 h and 24 h. Culture media include; pure BHI broth (Ai, Aii & Bv-viii) αMEM, 20 % BHI, 10 % L-ascorbic acid 2-phosphate, 20 ng/mL M-CSF and 30 ng/mL RANKL (Aiii, Aiv & Biix-xi) αMEM, 10 % L-ascorbic acid 2-phosphate, 20 ng/mL M-CSF and 30 ng/mL RANKL (Av, Avi & Biix-Bxi). Data shows that all culture media supported bacterial growth, although culture media without BHI had reduced bacterial growth. Significance within groups determined via one-way ANOVA and between groups determined via two-way ANOVA with Tukey post-hoc test. Error bars represent mean ±S.E.M (n=3), **P<0.05, **P < 0.01, ***P < 0.001 and ****P < 0.0001*.

4.3.4: Modified Gram-Stain of the Co-Cultured Femoral Slice Model

Histological sections of tissues co-cultured with bacterial species were stained with modified gram stain to identify *S. aureus* type strains, NCTC 6571 and NCTC 7791, within the femoral slice model. Slices co-cultured with NCTC 6571 did not show any bacterial attachment following 0 or 6 h (Figures 4.5A and B). After 19 h, cocci-shaped bacteria in grape-like aggregates were seen within the bone marrow cavity (Figure 4.5C). After 24 h, a high density of cocci-shaped bacteria was seen throughout the bone marrow cavity (Figure 4.5D pink arrows).

Similarly, slices co-cultured with NCTC 7791 did not show any bacterial attachment following 0 or 6 h (Figures 4.6A and B). After 19 h cocci-shaped bacteria were seen within the bone marrow cavity (Figure 4.6C). After 24 h, high density of cocci shaped bacteria was seen throughout the bone marrow cavity (Figure 4.6D) and a large-scale biofilm was seen attached to the periosteum surrounding the cortical bone in one of the tissue samples (Figure 4.6E).

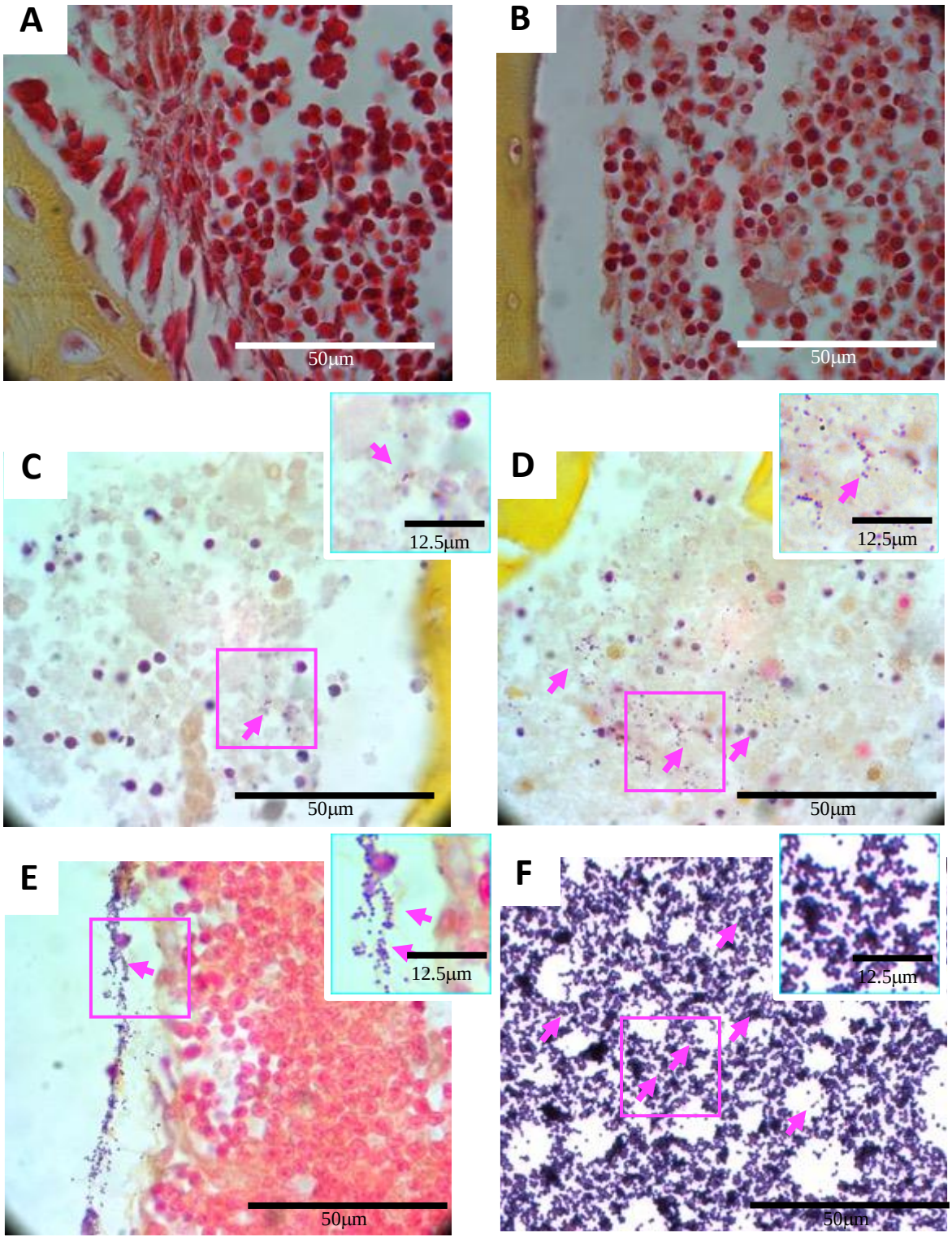

Figure 4.5: Modified gram staining of NCTC 6571-infected slices. NCTC 6571 *S. aureus* infection was analysed using modified gram staining within tissue sections following Trowell-type culture at x100 magnification, showing attachment of bacterial species in the bone marrow. Images A) 0 h control, B) 6 h culture, C) 19 h culture, D) 24 h culture E) Rat lung infected with NCTC 6571 positive control tissue and F) direct staining of overnight gram-positive NCTC 6571 *S. aureus* strain. Arrows indicate the presence of positive cocci-shaped *S. aureus* species within the tissue.

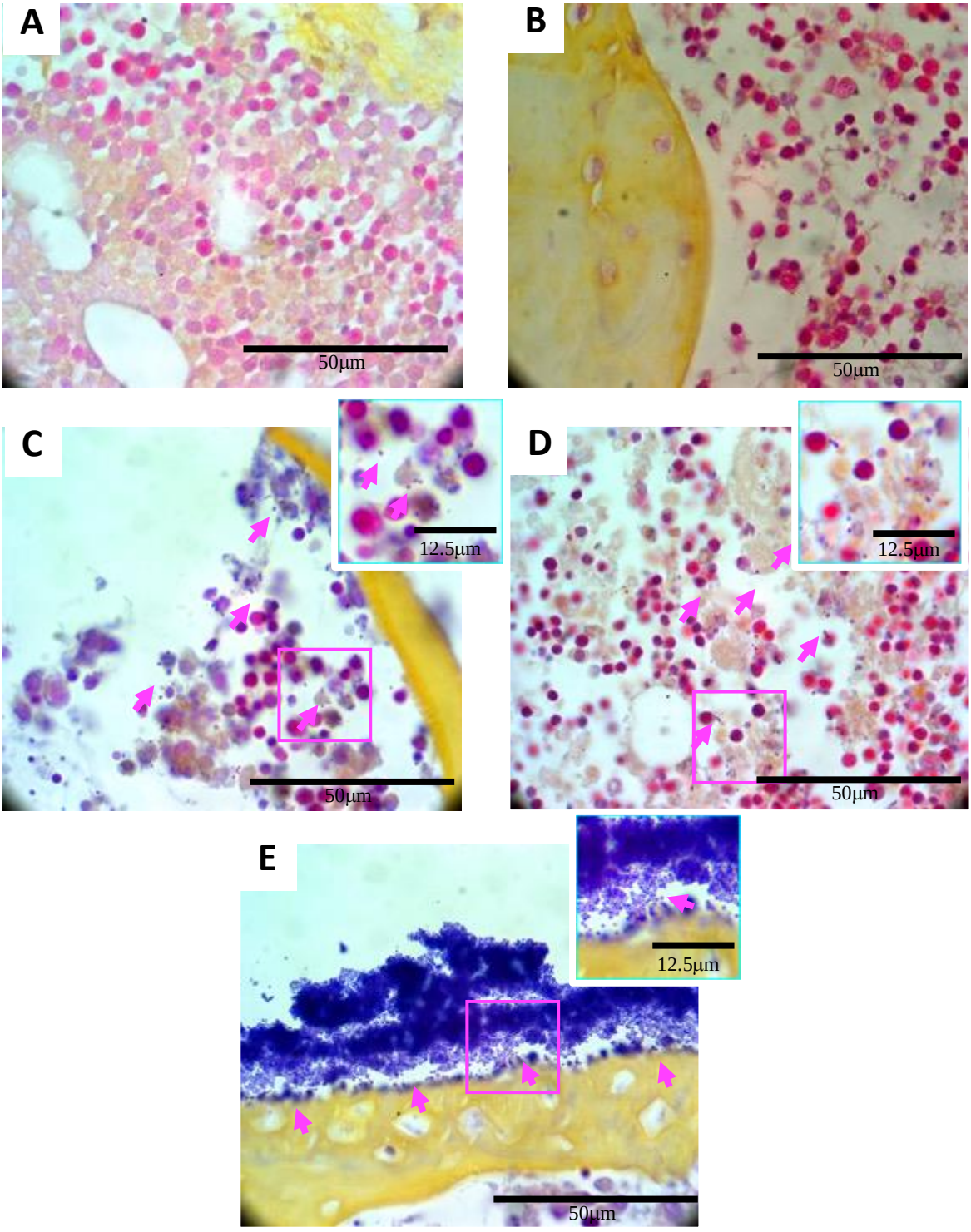

Figure 4.6: Modified gram staining of NCTC 7791-infected slices. NCTC 7791 *S. aureus* infection was analysed using modified gram staining in tissue sections following Trowell-type culture at x100 magnification, showing attachment of bacterial species in the bone marrow. Images A) 0 h control, B) 6 h culture, C) 19 h culture, both D) and E) 24 h culture. Arrows indicate the presence of positive *S. aureus* species within the tissue.

4.3.5: Scanning Electron Microscopy of the Co-Cultured Femoral Slice Model

Co-cultured tissue sections with both *S. aureus* type strains, NCTC 6571 and NCTC 7791, were imaged at 24 h using Scanning Electron Microscopy. Images show small bacterial colonies of NCTC 6571 *S. aureus* co-culture slices within the bone marrow cavity with leukocyte-type cells nearby (Figure 4.7A). A large-scale biofilm was seen attached to the periosteum surrounding the cortical bone in NCTC 7791 *S. aureus* infected slices (Figure 4.7B).

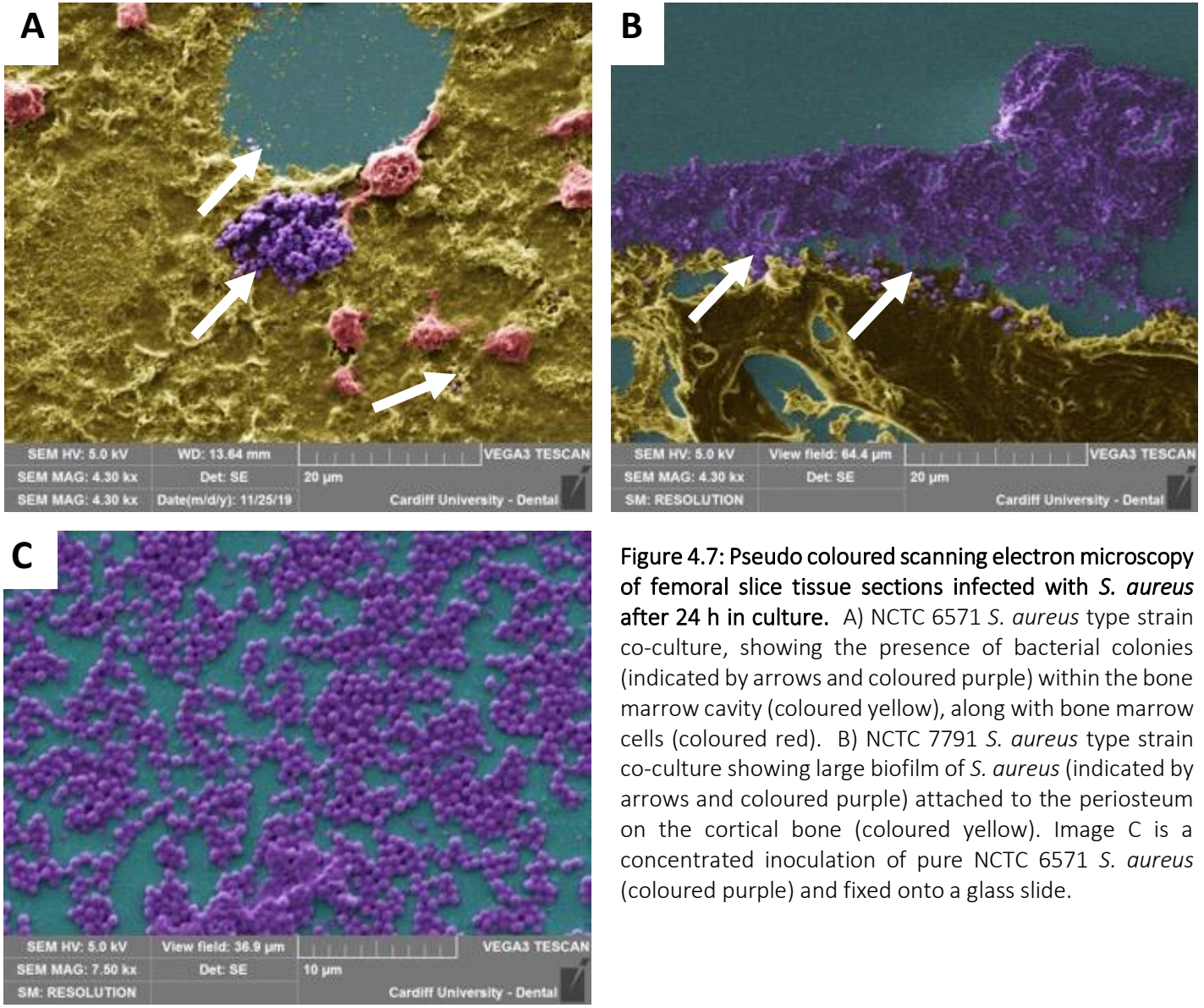

Figure 4.7: Pseudo coloured scanning electron microscopy of femoral slice tissue sections infected with *S. aureus* after 24 h in culture. A) NCTC 6571 *S. aureus* type strain co-culture, showing the presence of bacterial colonies (indicated by arrows and coloured purple) within the bone marrow cavity (coloured yellow), along with bone marrow cells (coloured red). B) NCTC 7791 *S. aureus* type strain co-culture showing large biofilm of *S. aureus* (indicated by arrows and coloured purple) attached to the periosteum on the cortical bone (coloured yellow). Image C is a concentrated inoculation of pure NCTC 6571 *S. aureus* (coloured purple) and fixed onto a glass slide.

4.3.6: Total Bone Marrow Cell Counts and Percentage Loss of Cells Following Infection With NCTC 6571 and NCTC 7791

To assess the number of bone marrow cells retained during the 24 h culture within the femoral slice following infection with *S. aureus*, NCTC 6571 and NCTC 7791, both mean cell counts (Figure 4.8A) and mean percentage loss of cells (Figure 4.8B) were calculated within a 10,000 μm^2 area. Statistical analysis was compared within each culture group and between groups at 0 h, 6 h, 19 h and 24 h of culture.

Samples without infection at 0 h showed an mean cell count of 488 cells. At 6 h the mean cell counts non-significantly increased to 515 cells ($P > 0.05$) when compared to 0 h. At 6 h the mean percentage loss of cells non-significantly decreased to -6 % ($P > 0.05$) when compared to 0 h. At 19 h the mean cell counts significantly decreased to 359 cells ($P < 0.05$) when compared to 6 h. At 19 h the mean percentage loss of cells significantly increased to 27 % ($P < 0.01$) when compared to 0 h and 6 h timepoints. At 24 h the mean cell counts non-significantly increased to 417 cells ($P > 0.05$) when compared to 19 h. At 24 h the mean percentage loss of cells non-significantly decreased to 15 % ($P > 0.05$) when compared to 0 h and 6 h timepoints.

Samples infected with NCTC 6571 at 0 h showed a mean cell count of 505 cells. At 6 h the mean cell counts non-significantly increased to 554 cells ($P > 0.05$) when compared to 0 h. At 6 h the mean percentage loss of cells non-significantly decreased to -9 % ($P > 0.05$) when compared to 0 h. At 19 h the mean cell counts significantly decreased to 244 cells ($P < 0.0001$) when compared to 6 h. At 19 h the mean percentage loss of cells significantly increased to 77 % ($P < 0.0001$) when compared to 0 h and 6 h timepoints. At 24 h the mean cell counts non-significantly decreased to 118 cells ($P > 0.05$) when compared to 19 h. At 24 h the mean percentage loss of cells was maintained at 77 % ($P > 0.05$) when compared to 19 h. Compared to non-infected controls there was a significant difference at 24 h for mean cell counts ($P < 0.0001$) and at 19 h and 24 h for percentage loss ($P < 0.0001$).

Samples infected with NCTC 7791 at 0 h showed a mean cell count of 609 cells. At 6 h the mean cell counts non-significantly decreased to 597 cells ($P > 0.05$) when compared to 0 h.

At 6 h the mean percentage cell counts non-significantly increased to 2 % (*P > 0.05*) when compared to 0 h. At 19 h the mean cell counts significantly decreased to 210 cells (*P < 0.0001*) when compared to 6 h. At 19 h the mean percentage cell counts significantly increased to 66 % (*P < 0.0001*) when compared to 0 h and 6 h timepoints. At 24 h the mean cell counts were maintained at 208 cells, this was non-significant when compared to 19 h (*P > 0.05*). At 24 h the mean percentage cell counts were maintained at 66 % (*P > 0.05*) when compared to 19 h. Compared to NCTC 6571 there was no significant difference *P > 0.05*) at either 0 h, 6 h, 19 h or 24 h timepoints for either the mean cell counts or mean percentage loss of cells. Compared to non-infected controls there was a significant difference at 19 h and 24 h for mean cell counts (*P < 0.05*) and at 19 h and 24 h for the mean percentage loss of cell (*P < 0.0001*).

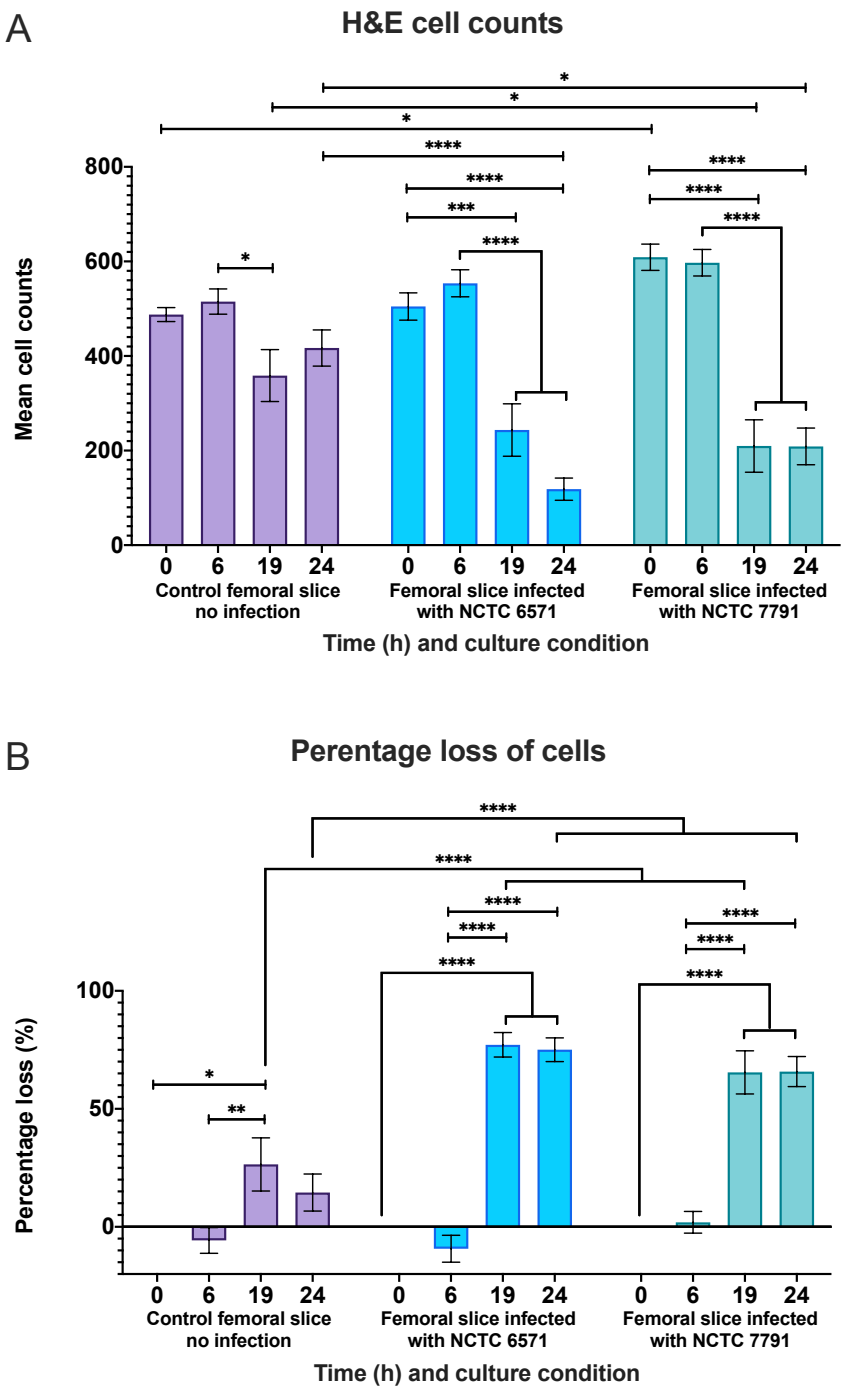

Figure 4.8: Mean cell counts and percentage loss following Trowell-type cultures supplemented with M-CSF and RANKL with and without co-culture of *S. aureus strains*, NCTC 6571 and NCTC 7791. Graph A) the mean cell counts and Graph B) the mean percentage loss of cells for slices without bacterial species and slices infected with NCTC 6571 or NCTC 7791. Graphs show a reduction if cell counts following infection, which is not seen in controls. Significance within groups determined via one-way ANOVA. Significance between groups determined via two-way ANOVA with Tukey post-hoc test. Error bars represent mean ±S.E.M (n=3), **P<0.05, **P < 0.01, ***P < 0.001 and ****P < 0.0001*.

4.3.7: Apoptosis Cell Viability Analysis Following *Staphylococcal Aureus* Dual-Labelling Immunohistochemistry

4.3.7.1: BAX Cell Viability Analysis

To assess the level of apoptosis using BAX labelled cells were analysed in the bone marrow cavity of tissue slices infected with *S. aureus* type strains, NCTC 6571 and NCTC 7791 over 24 h, within a 12.5 mm^2 area.

Tissue slices not infected with either strain of *S. aureus*, at 0 h showed a mean of 434 bone marrow cells of which 190 cells were stained positive for BAX (Figures 4.9A and 4.10A&B). The mean percentage of cells remaining that were stained positive for BAX was 43.2 % (Figure 4.10C). The mean number of bone marrow cells at 24 h significantly decreased to 116 cells (*P < 0.0001*, Figures 4.9B and 4.10B). The mean number of cells stained positive for BAX at 24 h decreased significantly to 40 cells (*P < 0.01*) when compared to 0 h (Figure 4.9B and 4.10A). The mean percentage of cells remaining that were stained positive for BAX after 24 h was 38.6 %, this was non-significant (*P > 0.05*) when compared to 0 h (Figure 4.10C).

Tissue slices infected with *S. aureus* NCTC 6571, at 0 h showed a mean of 511 bone marrow cells of which 320 cells were stained positive for BAX (Figures 4.9C and 4.10A). The mean bone marrow cell counts were non-significantly elevated for slices infected with NCTC 6571 compared to uninfected control (*P > 0.05*). The mean number of BAX-stained cells were significantly elevated when compared to 0 h non-infected controls (*P < 0.01*). The mean percentage of cells remaining that were stained positive for BAX at 0 h was 65 % (Figure 4.10C), this was significant when compared to 0 h non-infected controls (*P < 0.05*). The mean number of bone marrow cells at 24 h significantly decreased to 206 cells (*P < 0.0001*, Figures 4.9C and 4.10B). The mean bone marrow cell counts were significantly elevated for slices infected with NCTC 6571 compared to non-infected control (*P <0.05*). The mean number of cells staining positive for BAX decreased significantly to 172 cells at 24 h (*P < 0.01*) when compared to 0 h cultures (Figure 4.9D and 4.10A). This was significantly elevated when compared to 24 h non-infected controls (*P < 0.001*). The mean percentage of cells remaining

that were stained positive for BAX after 24 h increased non-significantly to 77.7 % (*P > 0.05*) when compared to 0 h (Figure 4.10C). This percentage was significant when compared to 24 h non-infected controls (*P < 0.0001*).

Tissue slices infected with *S. aureus* NCTC 7791, at 0 h showed a mean of 372 bone marrow cells of which 265 cells were stained positive for BAX (Figures 4.9E and 4.10A&B). The mean bone marrow cell counts were significantly reduced for slices infected with NCTC 6571 compared to slices infected with NCTC 7791 (*P <0.001*). The mean number of BAX-stained cells were bon-significant when compared to 0 h non-infected controls (*P > 0.05*) and 0 h NCTC 6571 samples (*P > 0.05*). The mean percentage of cells remaining that were stained positive for BAX at 0 h was 70.9 %, which was significantly elevated when compared to 0 h non-infected controls (*P < 0.0001*) and was non-significant when compared to 0 h NCTC 6571 samples (*P > 0.05*, Figure 4.10C). The mean number of bone marrow cells at 24 h significantly decreased to 184 cells (*P < 0.0001*, Figures 4.9F and 4.10B). The mean number of cells staining positive for BAX decreased significantly to 147 cells at 24 h (*P < 0.05*) when compared to 0 h cultures (Figures 4.9F and 4.10A). This was increased significantly when compared to 24 h non-infected controls (*P < 0.05*) and was non-significant compared to 24 h NCTC 6571 samples (*P > 0.05*). The mean percentage of cells remaining that were stained positive for BAX after 24 h increased non-significantly to 80.3 % (*P > 0.05*) when compared to 0 h (Figure 4.10C). This percentage was significant when compared to 24 h non-infected controls (*P < 0.0001*) and was non-significant compared to 24 h NCTC 6571 samples (*P > 0.05*).

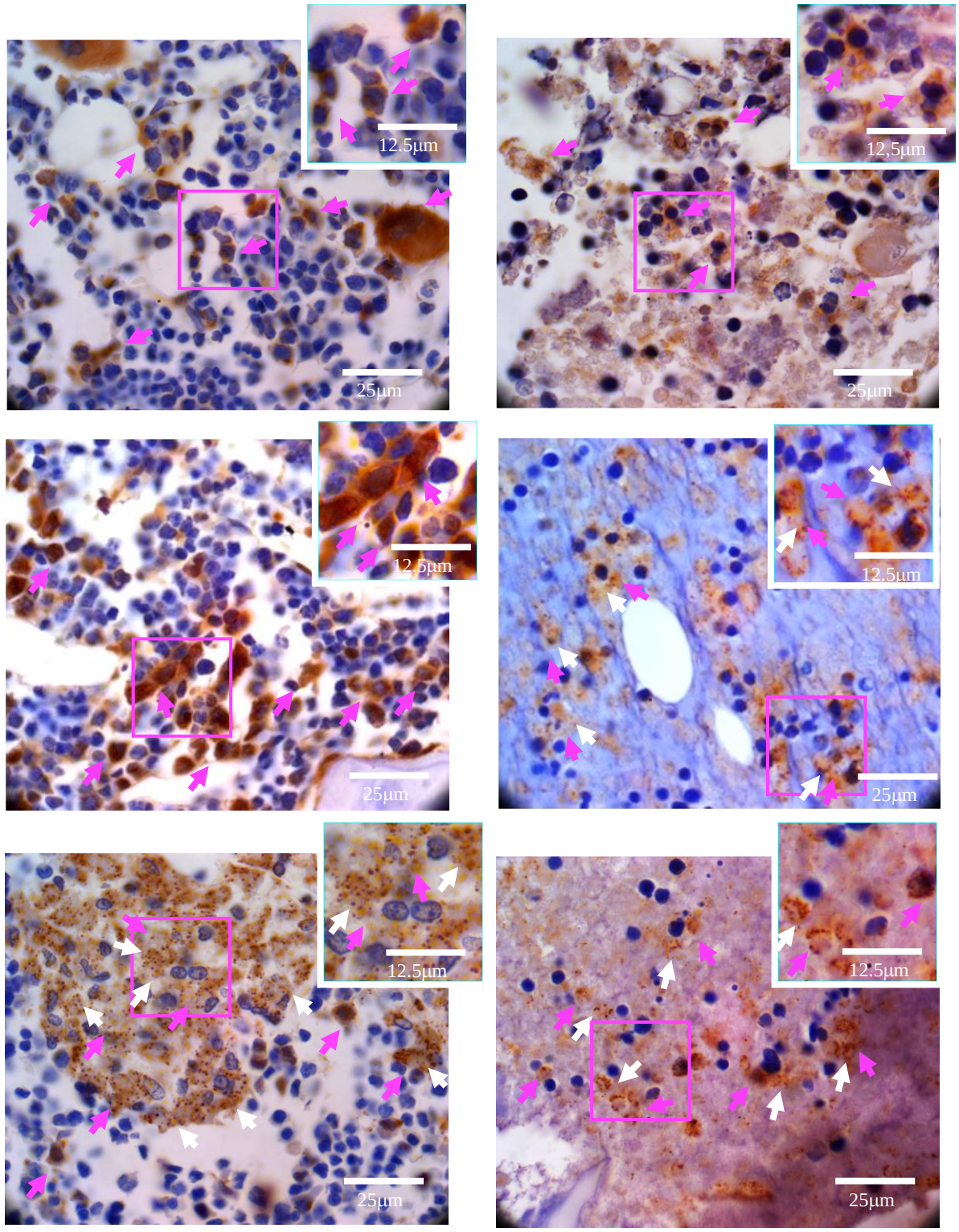

Figure 4.9: Co-culture of Staphylococcus aureus infected tissue slices stained for BAX. Representative images of immunohistochemistry staining for BAX-labelled antibodies (BAX positive cells stained as brown indicated with pink arrows) within the bone marrow of Trowell-type cultures following infection with *Staphylococcus aureus* bacterial species (bacterial species stained as red indicated with white arrows). Control non-infected tissue slices at A) 0 h and B) 24 h. NCTC 6571 infected slices at C) 0 h and D) 24 h. NCTC 6571 infected slices at D) 0 h and E) 24 h. 12.5 µm boxes display magnified areas of the bone marrow with both positive LDH cells and bacterial cells labelled.

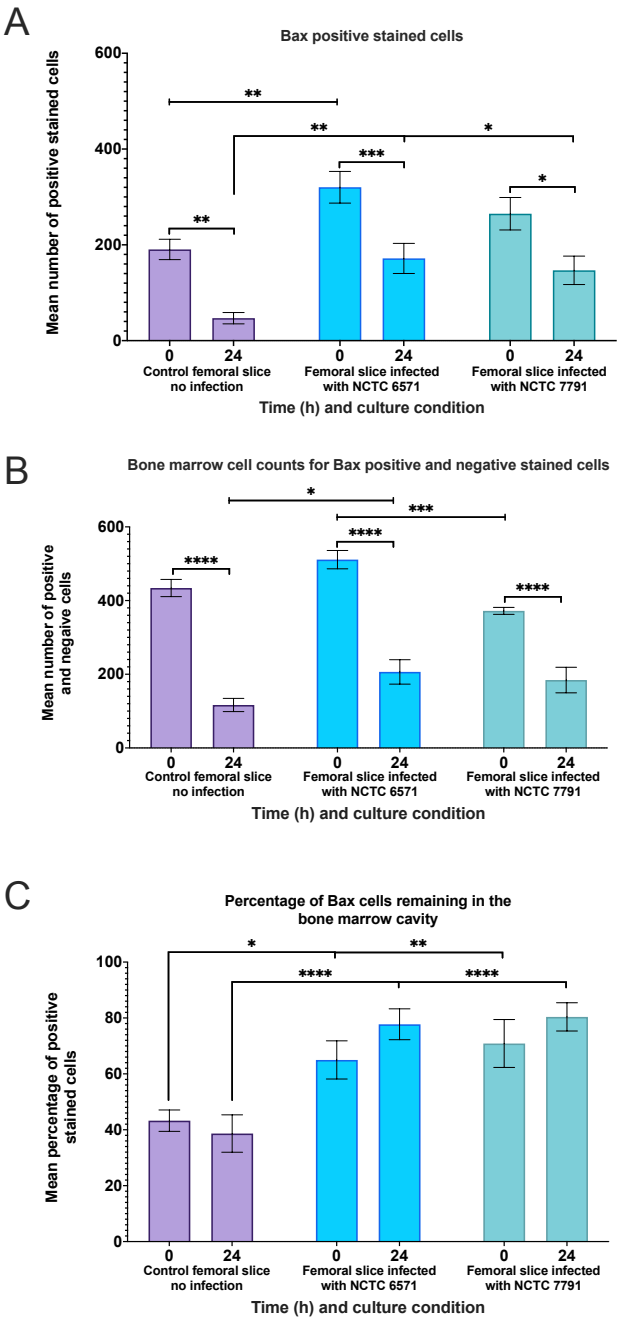

Figure 4.10: BAX analysis following microinjection and culture with M-CSF and RANKL. Semi-quantitative analysis for BAX labelled cells within the bone marrow of Trowell-type cultures supplemented with 20 ng/mL M-CSF and 30 ng/mL RANKL and infected with *S. aureus strains*, NCTC 6571 and NCTC 7791. Graph A) Graph showing data for mean cell counts for BAX positive stained cells. Graph B) Graph shows mean cell counts for both BAX positive and negative stained cells. Graph C) showing the mean percentage of BAX positive stained cells remaining in the bone marrow cavity. Infected slices showed a significantly higher number of mean cells counts for infected slices and a significantly higher percentage counts for BAX after 24 h compared to non-infected samples. Significance within groups determined via one-way ANOVA. Significance between groups determined via two-way ANOVA with Tukey post-hoc test. Error bars represent mean ±S.E.M (n=3), **P<0.05, **P < 0.01, ***P < 0.001 and ****P < 0.0001*.

4.3.7.2: Cleaved Caspase 3 Cell Viability Analysis

Analysis of cleaved caspase-3 apoptosis for slices infected with *S. aureus* type strains, NCTC 6571 and NCTC 7791 over 24 h, were calculated within a 12.5 mm^2 area.

Tissue slices not infected with either strain of *S. aureus*, at 0 h showed a mean of 497 bone marrow cells of which 40 cells were stained positive for cleaved caspase-3 (Figures 4.11A and 4.12A&B). The mean percentage of cells remaining that were stained positive for cleaved caspase 3 was 8 % (Figure 4.12C). The mean number of bone marrow cells at 24 h significantly decreased to 157 cells (*P < 0.0001*, Figures 4.11B and 4.12B). The mean number of cells stained positive for cleaved caspase-3 at 24 were maintained at 40 cells (*P < 0.05*) when compared to 0 h controls (Figure 4.11B and 4.12A). The mean percentage of cells remaining that were stained positive for cleaved caspase 3 increased after 24 h to 25.6 %, this was non-significant (*P > 0.05*) when compared to 0 h (Figure 4.12C).

Tissue slices infected with *S. aureus* NCTC 6571, at 0 h showed a mean of 468 bone marrow cells of which 343 cells were stained positive for cleaved caspase-3 (Figures 4.11C and 4.12A). The mean number of cleaved caspase-3-stained cells were significantly elevated when compared to 0 h non-infected controls (*P < 0.0001*). The mean percentage of cells remaining that were stained positive for cleaved caspase 3 was 74.2 % which was significantly elevated when compared to 0 h non-infected controls (*P < 0.0001*, Figure 4.12C). The mean number of bone marrow cells at 24 h significantly decreased to 185 cells (*P < 0.0001*, Figures 4.11C and 4.12B). The mean number of cells staining positive for cleaved caspase-3 decreased significantly to 69 cells at 24 h (*P < 0.0001*) when compared to 0 h cultures (Figure 4.11D and 4.12A). This was non-significant when compared to 24 h non-infected controls (*P > 0.05*). The mean percentage of cells remaining that were stained positive for cleaved caspase 3 after 24 h decreased significantly to 49.7 % (*P < 0.0001*) when compared to 0 h and was significant when compared to 24 h non-infected controls (*P < 0.0001*, Figure 4.12C).

Tissue slices infected with *S. aureus* NCTC 7791, at 0 h showed a mean of 485 bone marrow cells of which 226 cells were stained positive for cleaved caspase-3 (Figures 4.11E and 4.12A&B). The mean number of cleaved caspase-3 stained cells were significantly elevated

when compared to 0 h non-infected controls (*P < 0.001*) and was significant when compared to 0 h NCTC 6571 samples (*P < 0.05*). The mean percentage of cells remaining that were stained positive for cleaved caspase 3 at 0 h was 43.5 % (Figure 4.12C). This percentage was significantly elevated when compared to 0 h non-infected controls (*P < 0.001*) and was significant when compared to 0 h NCTC 6571 samples (*P < 0.01*). The mean number of bone marrow cells at 24 h significantly decreased to 216 cells (*P < 0.0001*, Figures 4.11F and 4.12B). The mean number of cells staining positive for cleaved caspase-3 decreased non-significantly to 154 cells (*P > 0.05*) compared to 0 h cultures (Figures 4.11F and 4.12A). This was increased significantly when compared to 24 h non-infected controls (*P < 0.05*) and was non-significant compared to 24 h NCTC 6571 samples (*P > 0.05*). The mean percentage of cells remaining that were stained positive for cleaved caspase 3 after 24 h increased significantly to 73.6 % (*P < 0.01*) when compared to 0 h (Figure 4.12C). This percentage was significant when compared to 24 h non-infected controls (*P < 0.0001*) and was significant compared to 24 h NCTC 6571 samples (*P < 0.05*).

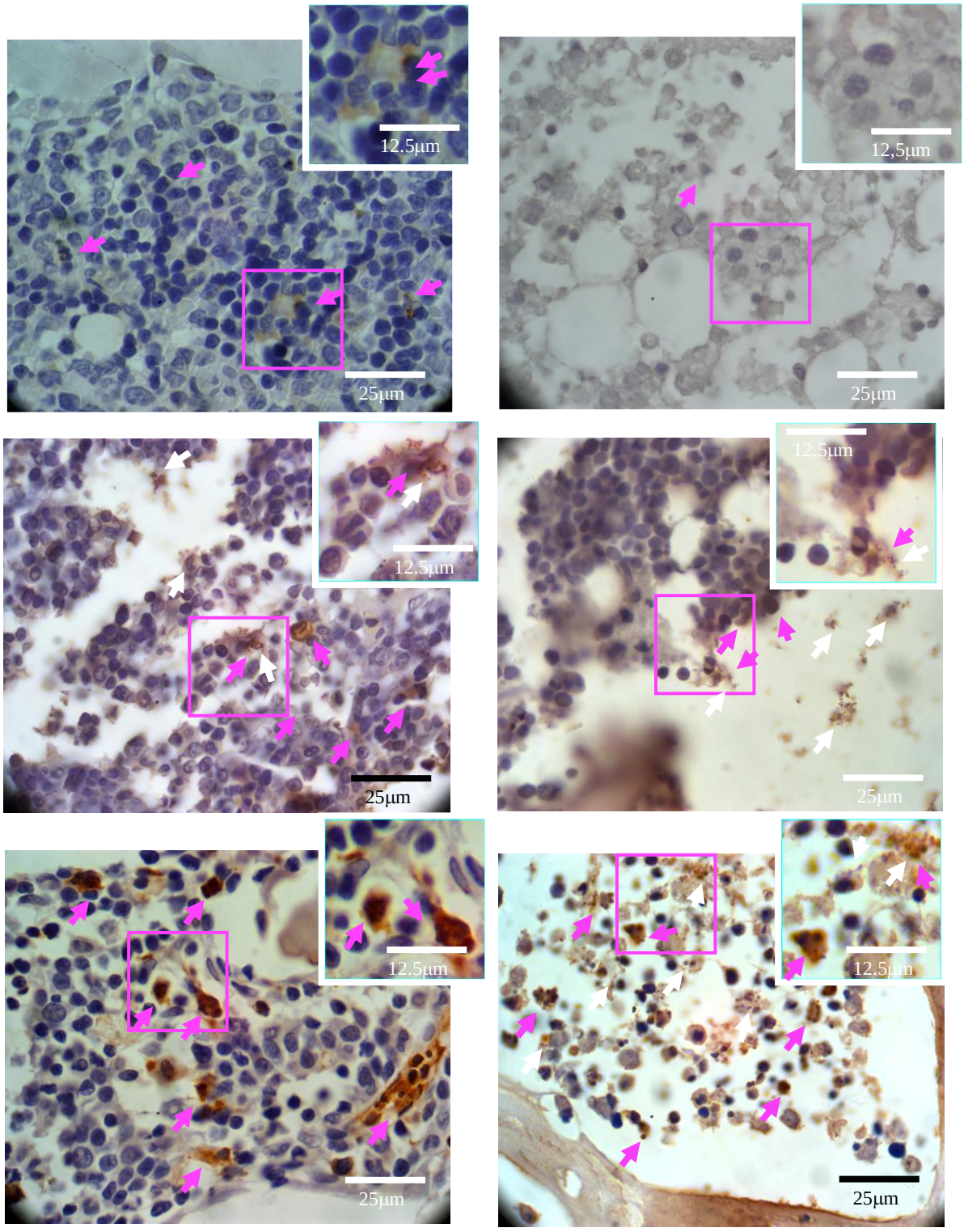

Figure 4.11: Co-culture of Staphylococcus aureus infected tissue slices stained for cleaved caspase 3. Representative images of immunohistochemistry staining for cleaved caspase 3 -labelled antibodies (cleaved caspase 3 positive cells stained as brown indicated with pink arrows) within the bone marrow of Trowell-type cultures following infection with *Staphylococcus aureus* bacterial species (bacterial species stained as red indicated with white arrows). Control non-infected tissue slices at A) 0 h and B) 24 h. NCTC 6571 infected slices at C) 0 h and D) 24 h. NCTC 6571 infected slices at D) 0 h and E) 24 h. 12.5 µm boxes display magnified areas of the bone marrow with both positive cleaved caspase 3 cells and bacterial cells labelled.

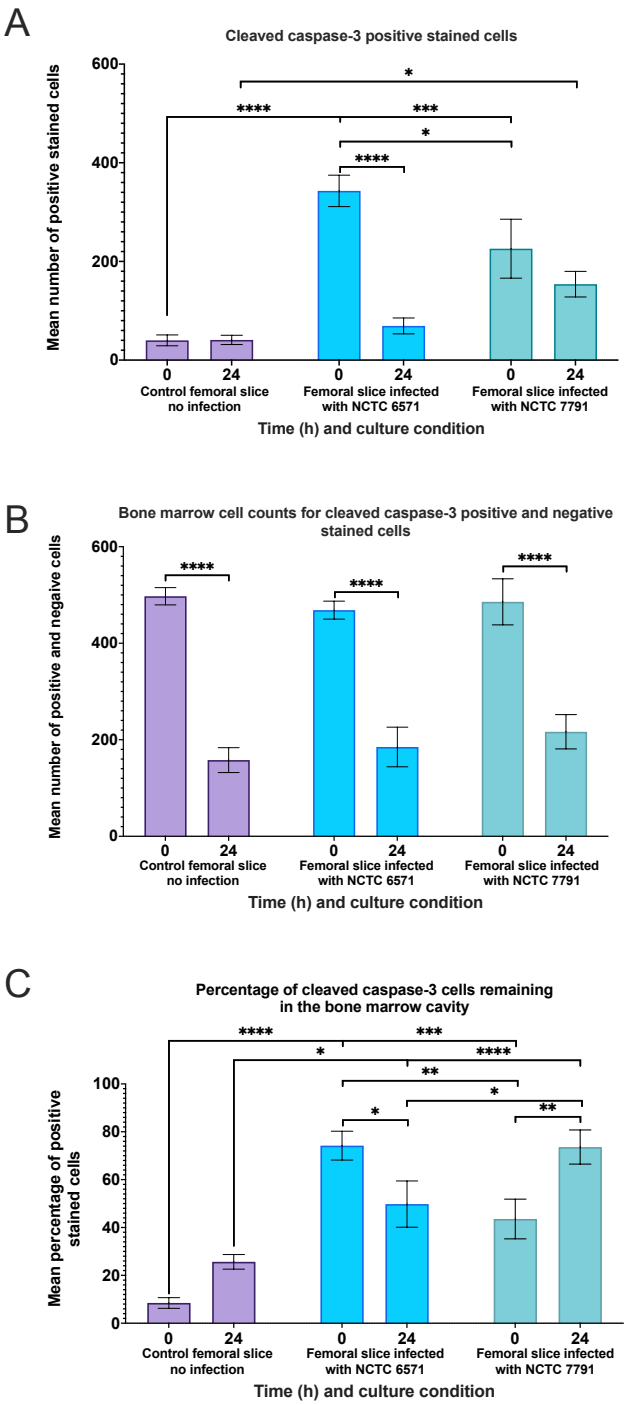

Figure 4.12: Cleaved caspase 3 analysis following microinjection and culture with M-CSF and RANKL. Semi-quantitative analysis for cleaved caspase 3 labelled cells within the bone marrow of Trowell-type cultures supplemented with 20 ng/mL M-CSF and 30 ng/mL RANKL and infected with *S. aureus strains*, NCTC 6571 and NCTC 7791 Graph A) showing data for mean cell counts for cleaved caspase-3 positive stained cells. Graph B) showing mean cell counts for both cleaved caspase-3 positive and negative stained cells. Graph C) showing the mean percentage of cleaved caspase-3 positive stained cells remaining in the bone marrow cavity. Infected slices showed a significantly higher number of mean cells counts for infected slices and a significantly higher percentage counts after 24 h compared to non-infected samples. Significance within groups determined via one-way ANOVA. Significance between groups determined via two-way ANOVA with Tukey post-hoc test. Error bars represent mean ±S.E.M (n=3), **P<0.05, **P < 0.01, ***P < 0.001 and ****P < 0.0001*.

4.3.8: Necrosis Cell Viability Analysis Following *Staphylococcal Aureus* Infection

4.3.8.1: Lactate Dehydrogenase Immunohistochemistry Necrosis Analysis

Analysis of LDH stained cells to identify necrosis within slices infected with *S. aureus* type strains, NCTC 6571 and NCTC 7791 over 24 h, were calculated within a 12.5 mm^2 area.

Tissue slices not infected with either strain of *S. aureus*, at 0 h showed a mean of 322 bone marrow cells of which 70 cells were stained positive for LDH (Figures 4.13A and 4.14A&B). The mean percentage of cells remaining that were stained positive for LDH was 21 % (Figure 4.14C). The mean number of bone marrow cells at 24 h significantly decreased to 212 cells ($P < 0.05$, Figures 4.13B and 4.14B). The mean number of cells stained positive for LDH at 24 non-significantly decreased to 19 cells ($P < 0.05$) when compared to 0 h controls (Figure 4.13B and 4.14A). The mean percentage of cells remaining that were stained positive for LDH after 24 h was 20 %, this was non-significant ($P > 0.05$) when compared to 0 h.

Tissue slices infected with *S. aureus* NCTC 6571, at 0 h showed a mean of 406 bone marrow cells of which 314 cells were stained positive for LDH (Figures 4.13C and 4.14A). The mean number of LDH-stained cells were significantly elevated when compared to 0 h non-infected controls ($P < 0.0001$). The mean percentage of cells remaining that were stained positive for LDH was 77 %, which was significantly elevated when compared to 0 h non-infected controls ($P < 0.0001$, Figure 4.14C). The mean number of bone marrow cells at 24 h significantly decreased to 59 cells ($P < 0.0001$, Figures 4.13C and 4.14B). The mean bone marrow cells at 24 h were significantly reduced when infected with NCTC 6571 when compared to no infection control slices at 24 h ($P < 0.001$). The mean number of cells staining positive for LDH decreased significantly to 24 cells at 24 h ($P < 0.0001$) when compared to 0 h cultures (Figure 4.13D and 4.14A). This was non-significant when compared to 24 h non-infected controls ($P > 0.05$). The mean percentage of cells remaining that were stained positive for LDH after 24 h decreased significantly to 42 % ($P < 0.0001$) when compared to 0 h and was also significant when compared to 24 h non-infected controls ($P < 0.05$, Figure 4.13C). Both 0 h and 24 h showed presence of bacteria in areas of dense LDH staining (Figures 4.13 A&B).

Tissue slices infected with *S. aureus* NCTC 7791, at 0 h showed a mean of 450 bone marrow cells of which 253 cells were stained positive for LDH (Figures 4.13E and 4.14A&B). The mean bone marrow cells at 0 h were significantly increased when infected with NCTC 7791 when compared to no infection control slices at 0 h ($P < 0.01$). The mean number of LDH stained cells were significantly elevated when compared to 0 h non-infected controls ($P < 0.0001$) and was non-significant when compared to 0 h NCTC 6571 samples ($P > 0.05$). The mean percentage of cells remaining that were stained positive for LDH at 0 h was 57.6 % (Figure 4.13C). This was significantly elevated when compared to 0 h non-infected controls ($P < 0.0001$) but was non-significant when compared to 0 h NCTC 6571 samples ($P > 0.05$). The mean number of bone marrow cells at 24 h significantly decreased to 146 cells ($P < 0.0001$, Figures 4.13F and 4.14B). The mean number of cells staining positive for LDH decreased significantly to 89 cells ($P < 0.0001$) when compared to 0 h cultures (Figures 4.13F and 4.14A). This was significant when compared to 24 h non-infected controls ($P < 0.001$) and 24 h NCTC 6571 samples ($P < 0.01$). The mean percentage of cells remaining that were stained positive for LDH after 24 h increased non-significantly to 68.6 % ($P > 0.05$) when compared to 0 h and was significant when compared to 24 h non-infected controls ($P < 0.001$) and 24 h NCTC 6571 samples ($P < 0.01$, Figure 4.13C). Both 0 h and 24 h showed presence of bacteria in areas of dense LDH staining (Figures 4.13 A&B).

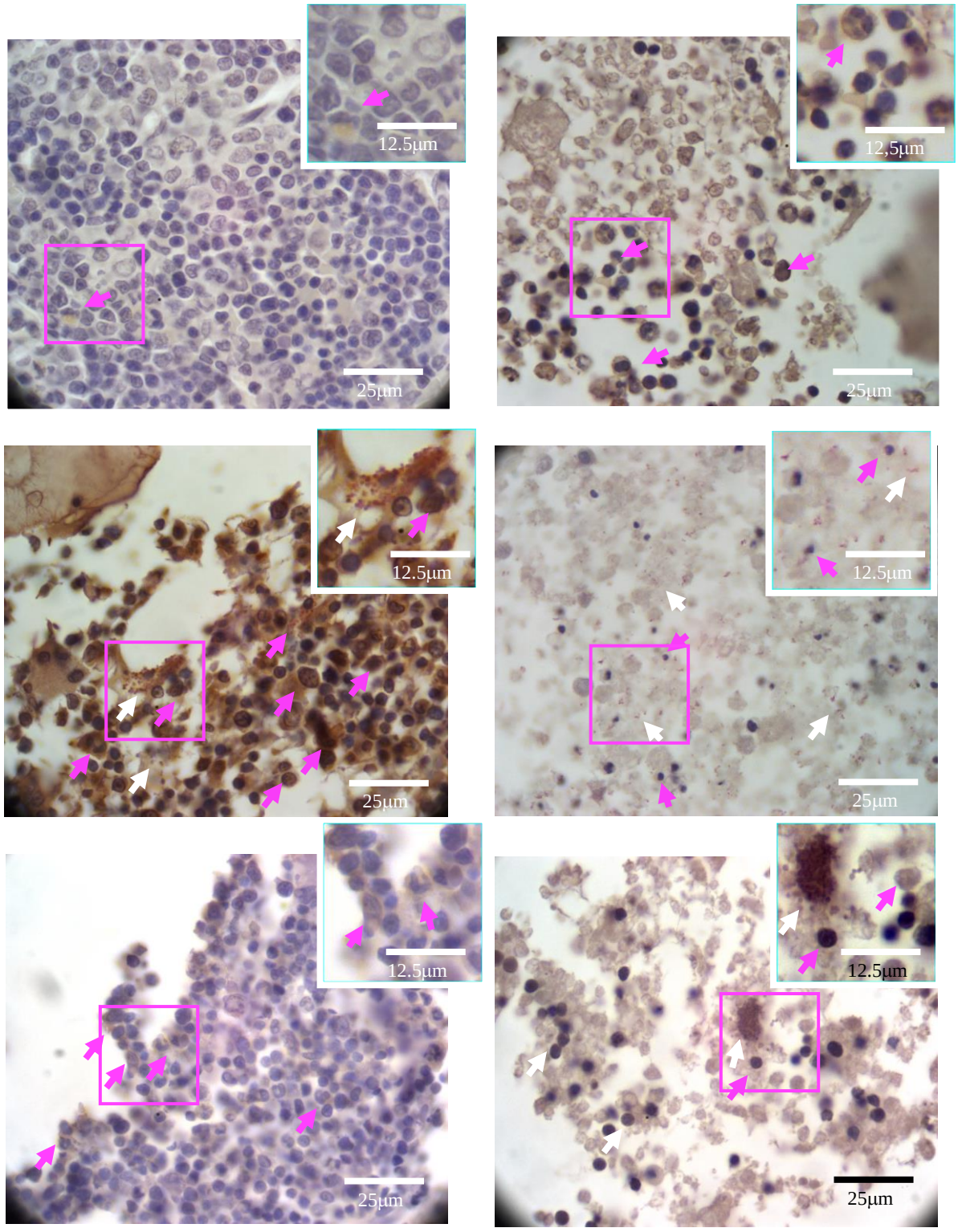

Figure 4.13: Co-culture of Staphylococcus aureus infected tissue slices stained for LDH. Representative images of immunohistochemistry staining for LDH-labelled antibodies (LDH positive cells stained as brown indicated with pink arrows) within the bone marrow of Trowell-type cultures following infection with *Staphylococcus aureus* bacterial species (bacterial species stained as red indicated with white arrows). Control non-infected tissue slices at A) 0 h and B) 24 h. NCTC 6571 infected slices at C) 0 h and D) 24 h. NCTC 7791 infected slices at D) 0 h and E) 24 h. 12.5 µm boxes display magnified areas of the bone marrow with both positive LDH cells and bacterial cells labelled.

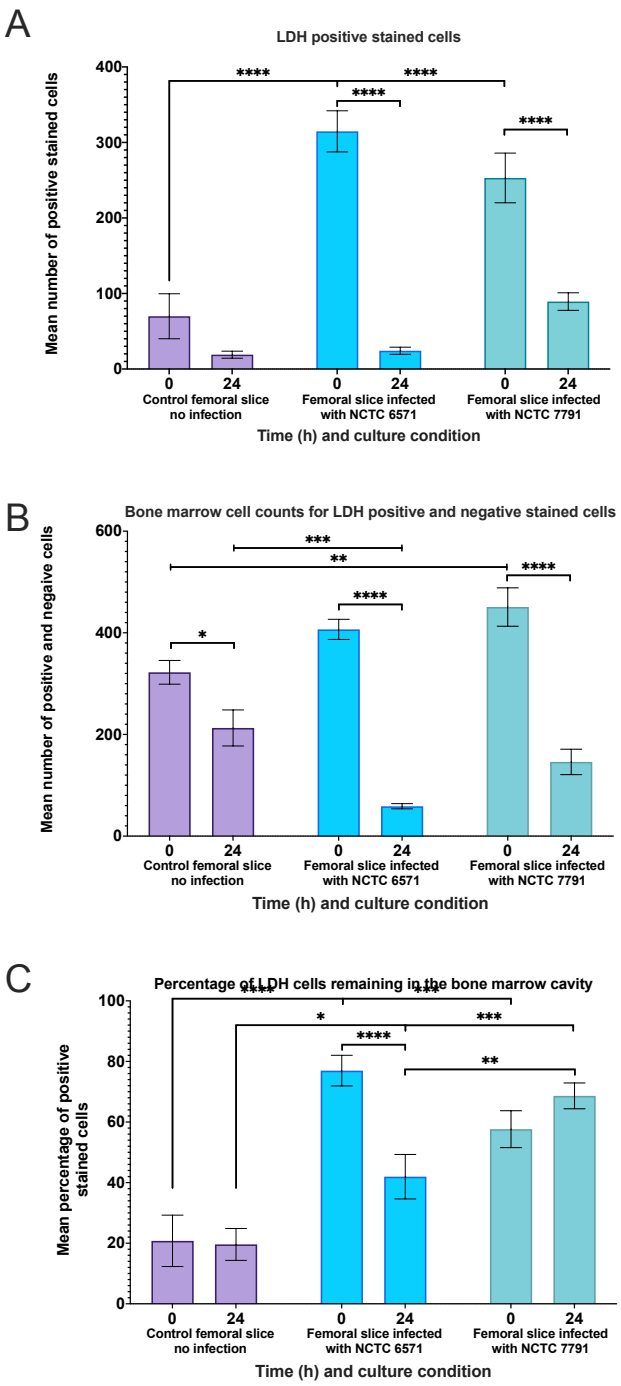

Figure 4.14: LDH analysis following microinjection and culture with M-CSF and RANKL. Semi-quantitative analysis for LDH labelled cells within the bone marrow of Trowell-type cultures supplemented with 20 ng/mL M-CSF and 30 ng/mL RANKL and infected with *S. aureus strains*, NCTC 6571 and NCTC 7791 Graph A) showing data for mean cell counts for LDH positive stained cells. Graph B) showing mean cell counts for both LDH positive and negative stained cells. Graph C) showing the percentage of LDH positive stained cells remaining in the bone marrow cavity. Infected slices showed a significantly higher number of mean cells counts at 0 h. There was a significantly higher percentage of LDH cells remaining after 24 h when compared to control non-infected samples. Significance within groups determined via one-way ANOVA. Significance between groups determined via two-way ANOVA with Tukey post-hoc test. Error bars represent mean ±S.E.M (n=3), **P<0.05, **P < 0.01, ***P < 0.001 and ****P < 0.0001*.

4.3.8.2: Detection Of Necrosis Using A Colourimetric Lactate Dehydrogenase Assay in Femoral Slices Co-Culture With *Staphylococcus aureus*

LDH analysis was carried out following co-culture of tissue slices with *S. aureus* type strains, NCTC 6571 and NCTC 7791 over 24 h, are shown in Figures 4.15A for absorbance and Figure 4.15B for percentage cytotoxicity. Samples without infection or heat-inactivated samples showed no significant difference ($P > 0.05$) in LDH absorbance activity or parentage cytotoxicity at 0 h,6 h, 19 h or 24 h timepoints.

When samples were infected with NCTC 6571 type strain, there was no significant difference ($P > 0.05$) in either LDH absorbance activity or percentage cytotoxicity between 0 h and 6 h. By 19 h, there was a 58 % significant increase ($P < 0.001$) in LDH activity compared to 6 h, which was non-significantly ($P > 0.05$) reduced by 24 h. Both 19 h and 24 h showed no significant difference ($P > 0.05$) in percentage cytotoxicity, compared to the positive control. When compared to non-infected controls or heat-inactivated samples, only 19 h NCTC 6571-infected samples showed a significant increase for LDH absorbance ($P < 0.05$) and percentage cytotoxicity ($P < 0.01$).

When samples were infected with NCTC 7791 type strain, there was no significant difference ($P > 0.05$) in either LDH absorbance activity or percentage cytotoxicity between 0 h and 6 h. By 19 h, there was a significant increase ($P < 0.05$) in LDH absorbance activity and a significant ($P < 0.05$) 48 % cytotoxicity, when compared to 6 h. Both LDH absorbance and was percentage cytotoxicity non-significantly ($P > 0.05$) reduced slightly by 24 h. When compared to NCTC 6571-Infected samples or heat-inactivated samples, there was no significant difference ($P > 0.05$) in either LDH absorbance or percentage cytotoxicity for 0 h,6 h, 19 h or 24 h samples. When compared to the positive control, only 0 h,6 h, 19 h and 24 h 7791 NCTC samples were significantly reduced for LDH absorbance ($P < 0.0001$).

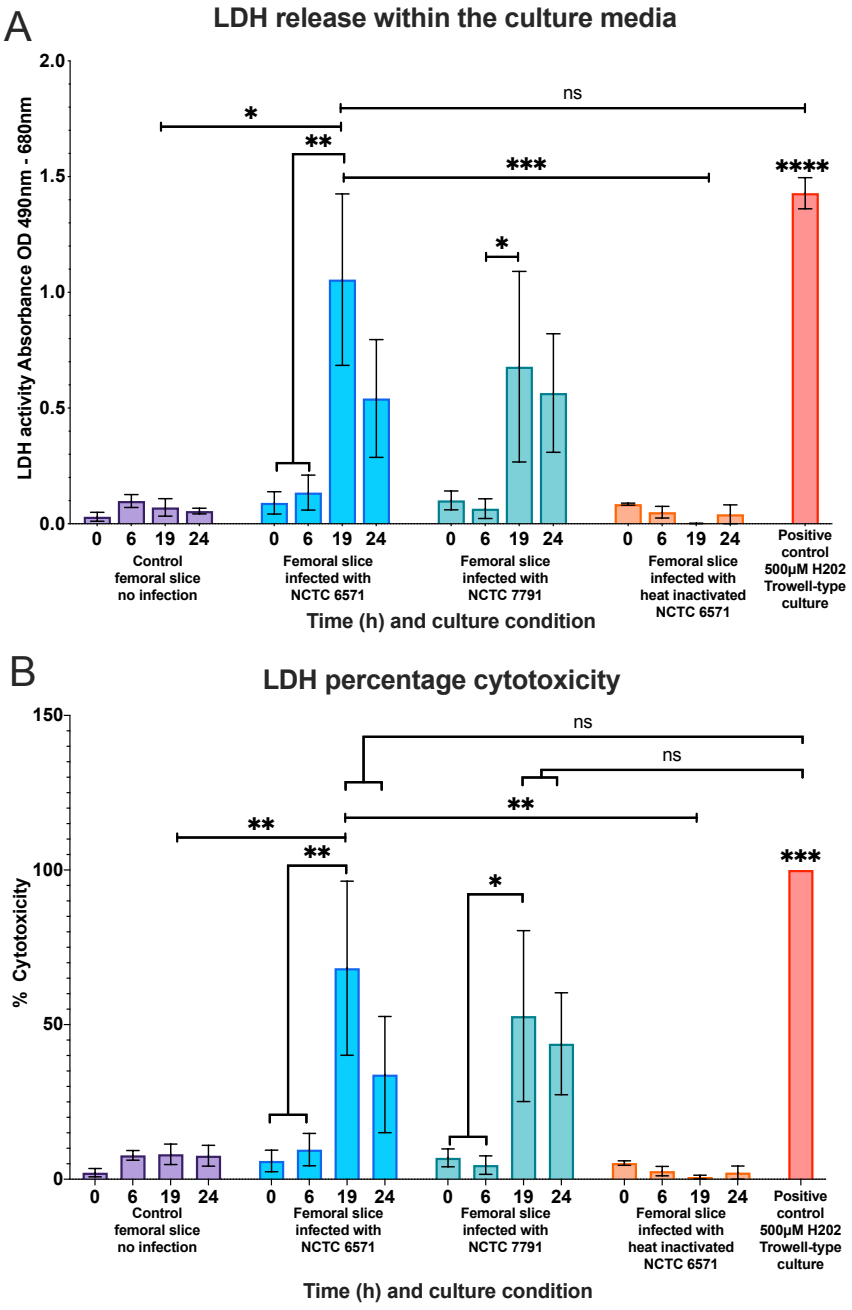

Figure 4.15: LDH activity following supplementation with M-CSF and RANKL and co-culture of *S. aureus strains* NCTC 6571 and NCTC 7791. Graphs indicate Graph A) absorbance and Graph B) percentage cytotoxicity. A significant increase was seen in LDH absorbance and percentage cytotoxicity after 19 h for both infected samples. Graphs shows that infected samples have increased LDH release and percentage cytotoxicity at 19 h and 24 h following infection. Significance within groups determined via one-way ANOVA. Significance between groups determined via two-way ANOVA with Tukey post-hoc test. Error bars represent mean ±S.E.M (n=6), *$P<0.05$, ** $P<0.01$, ***$P<0.001$ and ****$P< 0.0001$

4.3.9: Pro-Inflammatory Cytokine Secretion

4.3.9.1: Interleukin-1 Beta

IL-1β protein release analysis that was carried out following co-culture of tissue slices with *S. aureus* type strains, NCTC 6571 and NCTC 7791 over 24 h, are shown in Figures 4.16. Samples without infection showed no significant difference ($P > 0.05$) in IL-1β activity between 0 h and 6 h, showing an average of 43 pg/mL and 74 pg/mL, respectively. By 19 h, IL-1β non-significantly increased ($P > 0.05$) to an average of 300 pg/mL, with levels maintained to 283 pg/mL by 24 h.

When samples were infected with NCTC 6571 type strain, no significant difference ($P > 0.05$) in IL-1β protein release between 0 h and 6 h, showing an average of 47 pg/mL and 153 pg/mL respectively. By 19 h there was a significant increase in IL-1β protein release average at 724 pg/mL, but was non-significantly ($P > 0.05$) reduced by 24 h to an average of 331 pg/ mL. When compared to non-infected control samples, there was no significant difference ($P > 0.05$) in IL-1β synthesis for 0 h, 6, 19 h or 24 h samples. When compared to heat-inactivated NCTC 6571 and 7791-infected samples, only 19 h NCTC 6571-infected samples and 19 h heat-inactivated samples showed significance ($P < 0.01$).

When samples were infected with NCTC 7791 type strain, there was again little by no significant difference ($P > 0.05$) in IL-1β protein release between 0 h and 6 h, showing an average of 88 pg/mL and 149 pg/mL, respectively. By 19 h, there was a significant increase ($P < 0.01$) in IL-1β protein release showing an average of 742 pg/mL, which non-significantly ($P > 0.05$) increased to an average of 919 pg/ mL by 24 h. When compared to non-infected control samples, there was no significant difference ($P > 0.05$) IL-1β synthesis for 0 h, 6 or 19 h samples, with only the 24 h samples showed a significant difference in IL-1β synthesis ($P < 0.01$). When compared to heat-inactivated NCTC 7791-infected samples, only 19 h ($P < 0.01$) and 24 h ($P < 0.001$) NCTC 7791-infected samples showed significance.

Samples infected with heat-inactivated NCTC 6571 and 7791 showed no significant difference ($P > 0.05$) in IL-1β activity between 0 h, 6, 19 h and 24 h.

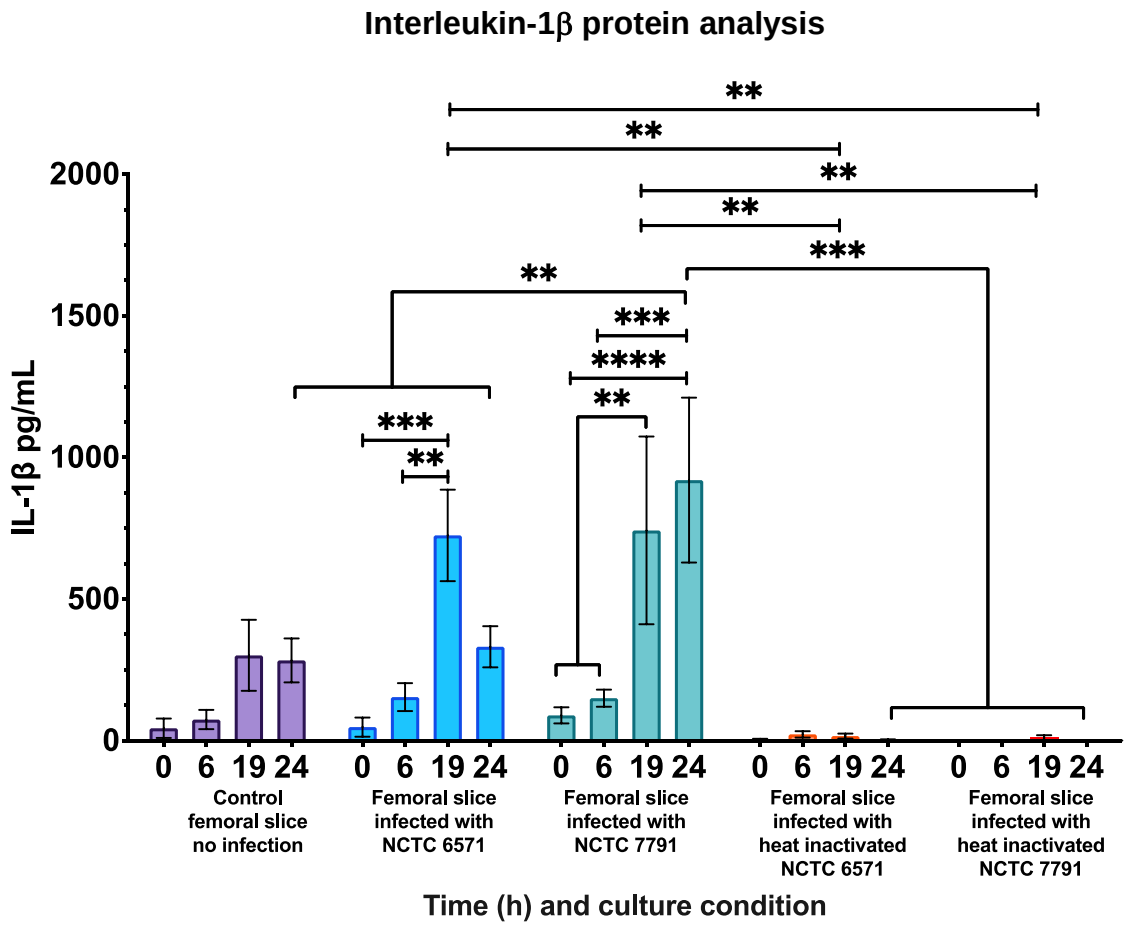

Figure 4.16: IL-1β protein analysis following Trowell-type cultures supplemented with M-CSF and RANKL with and without co-culture of *S. aureus strains*, NCTC 6571 and NCTC 7791. Graph shows IL-1β analysis with or without infection with *S. aureus* bacterial species over 24 h. Following infection there was a significant increase in IL-1β synthesis at 19 h. NCTC 7791-infected samples had a increased levels of protein release after 24 h. Little to no synthesis was seen in non-infected controls or heat-inactivated samples. Significance within groups determined via one-way ANOVA. Significance between groups determined via two-way ANOVA with Tukey post-hoc test. Error bars represent mean ±S.E.M n=6 for control, NCTC 6571 and NCTC 7791 infected samples and n=3 for heat-inactivated NCTC 6571 and heat-inactivated NCTC 7791 infected samples, *$P<0.05$, ** $P<0.01$, ***$P<0.001$ and ****$P< 0.0001$

4.3.9.2: Interleukin-6

IL-6 protein release analysis that was carried out following co-culture of tissue slices with *S. aureus* type strains, NCTC 6571 and NCTC 7791 over 24 h, are shown in Figures 4.17. Samples without infection showed no significant difference ($P > 0.05$) in IL-6 activity between 0 h and 6 h, with an average of 43 pg/mL and 74 pg/mL, respectively. However, there was a slight non-significant decrease ($P > 0.05$) after 19 h to an average of 8 pg/mL, but increased non-significantly ($P > 0.05$) to 28 pg/mL by 24 h.

When samples were infected with NCTC 6571 type strain, there was no significant difference ($P > 0.05$) in IL-6 protein release between 0 h and 6 h, showing an average of 11 pg/mL and 16 pg/mL, respectively. By 19 h there was a significant increase ($P < 0.0001$) in IL-6 protein release, showing an average of 273 pg/mL, which non-significantly ($P > 0.05$) reduced to an average of 157 pg/ mL by 24 h. When compared to non-infected controls or heat-inactivated NCTC 6571-infected samples, only 19 h samples showed a significant difference in IL-6 synthesis ($P < 0.001$).

When samples were infected with NCTC 7791 type strain, there was no significant difference ($P > 0.05$) in IL-6 protein release between 0 h and 6 h, showing an average of 45 pg/mL and 4 pg/mL, respectively. By 19 h, there was a non-significant increase ($P > 0.05$) in IL-6 protein release showing an average of 113 pg/mL, which was non-significantly ($P > 0.05$) reduced to an average of 162 pg/mL by 24 h. When compared to non-infected controls or heat-inactivated NCTC 7791 samples, there was no significant difference ($P > 0.05$) in IL-6 synthesis for 0 h, 6, 19 h or 24 h samples. When compared to NCTC 6571-infected samples, there was only a significant difference ($P < 0.05$) in IL-6 synthesis for 19 h samples.

Samples infected with heat-inactivated NCTC 6571 showed no significant difference ($P > 0.05$) in IL-6 activity between 0 h and 6 h, with an average of 0 pg/mL and 13 pg/mL, respectively. However, there was a non-significant change in IL-6 synthesis ($P > 0.05$) after 19 h, there was an increase in levels showing an average of 74 pg/mL. By 24 h IL-6 levels were not significantly ($P > 0.05$) reduced to 43 pg/mL, when compared to 0 h, 6 or 19 h.

Samples infected with heat-inactivated NCTC 7791 showed no significant difference ($P > 0.05$) in IL-6 activity between 0 h and 6 h, with little IL-6 levels of 15 pg/mL and 0 pg/mL respectively. However, there was a non-significant change in IL-6 synthesis ($P > 0.05$) after 19 h, there was an increase in levels averaging at 59 pg/mL. By 24 h, IL-6 levels continued to increase, though this was not significant ($P > 0.05$) to 120 pg/mL when compared to 0 h, 6 or 19 h.

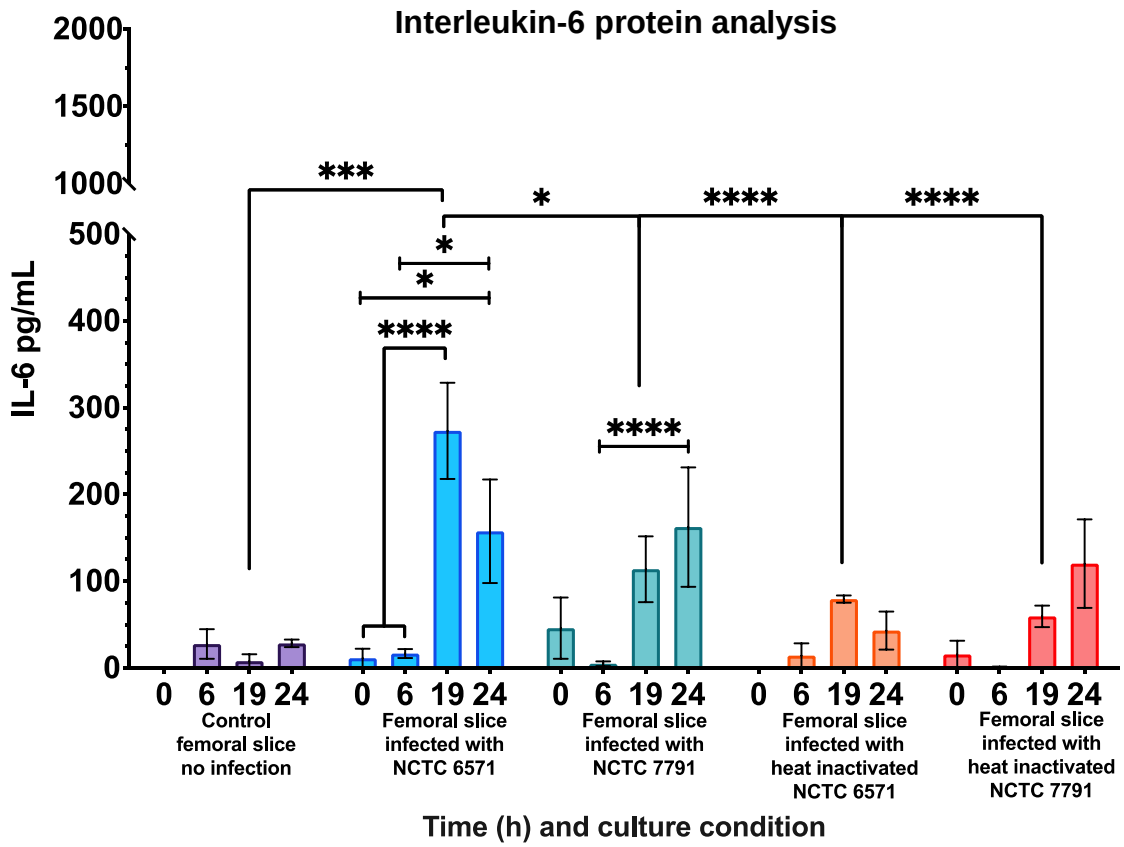

Figure 4.17: IL-6 protein analysis following Trowell-type cultures supplemented with M-CSF and RANKL with and without co-culture of *S. aureus strains*, NCTC 6571 and NCTC 7791. Graph shows IL-6 analysis with or without infection with *S. aureus* bacterial species over 24 h. Following infection there was a significant increase in IL-6 synthesis at 19 h for NCTC 6571-infected samples, with NCTC 7791-infected samples showing only significant levels of protein release after 24 h. Little to no synthesis was seen in non-infected controls or heat-inactivated samples. Significance within groups determined via one-way ANOVA. Significance between groups determined via two-way ANOVA with Tukey post-hoc test. Error bars represent mean ±S.E.M n=6 for control, NCTC 6571 and NCTC 7791 infected samples and n=3 for heat-inactivated NCTC 6571 and heat-inactivated NCTC 7791 infected samples, *$P<0.05$, ***$P<0.001$ and ****$P< 0.0001$

4.3.9.3: Tumor Necrosis Factor-Alpha

TNFα protein release analysis that was carried out following co-culture of tissue slices with *S. aureus* type strains, NCTC 6571 and NCTC 7791 over 24 h, are shown in Figures 4.18. Samples without infection showed no TNFα protein release at 0 h, 6, 19 h or 24 h, with an average of 0 pg/mL for all time points.

When samples were infected with NCTC 6571 type strain, there was no significant difference (*P > 0.05*) in TNFα protein release between 0 h and 6 h, with no detectable levels for either time point, showing an average of 0 pg/mL. By 19 h, there was a non-significant increase (*P > 0.05*) in TNFα protein release showing an average of 150 pg/mL, which was reduced non-significantly (*P > 0.05*) to an average of 15 pg/ mL by 24 h. When compared to non-infected controls or heat-inactivated NCTC 6571 samples, there was no significant difference (*P > 0.05*) TNFα synthesis for 0 h, 6, 19 h or 24 h samples.

When samples were infected with NCTC 7791 type strain, there was no expression in TNFα protein release between 0 h and 6 h, showing 0 pg/mL. By 19 h, there was a non-significant increase (*P > 0.05*) in TNFα protein release showing an average of 166 pg/mL, which increased significantly (*P < 0.0001*) to an average of 537 pg/ mL by 24 h. When compared to non-infected controls samples, there was no significant difference (*P > 0.05*) in TNFα synthesis for 0 h, 6 or 19 h and significance was only seen between the 24 h samples (*P < 0.0001*). When compared to NCTC 6571-infected samples, there was only a significant difference (*P < 0.0001*) in TNFα synthesis between the 24 h samples. When compared to heat-inactivated NCTC 7791-infected samples, there was no significant difference (*P > 0.05*) TNFα synthesis for 0 h, 6 or 19, significance was only seen between the 24 h samples (*P < 0.0001*).

Samples infected with heat-inactivated NCTC 6571 showed no significant difference (*P > 0.05*) in TNFα activity between 0 h and 6 h, with an average of 0 pg/mL and 11 pg/mL, respectively. By 19 h, TNFα levels declined to 2 pg/mL and this was not significant (*P < 0.05*) and reduced, to 0 pg/mL by 24 h. Samples infected with heat-inactivated NCTC 7791 showed no TNFα protein release at 0 h, 6, 19 h or 24 h.

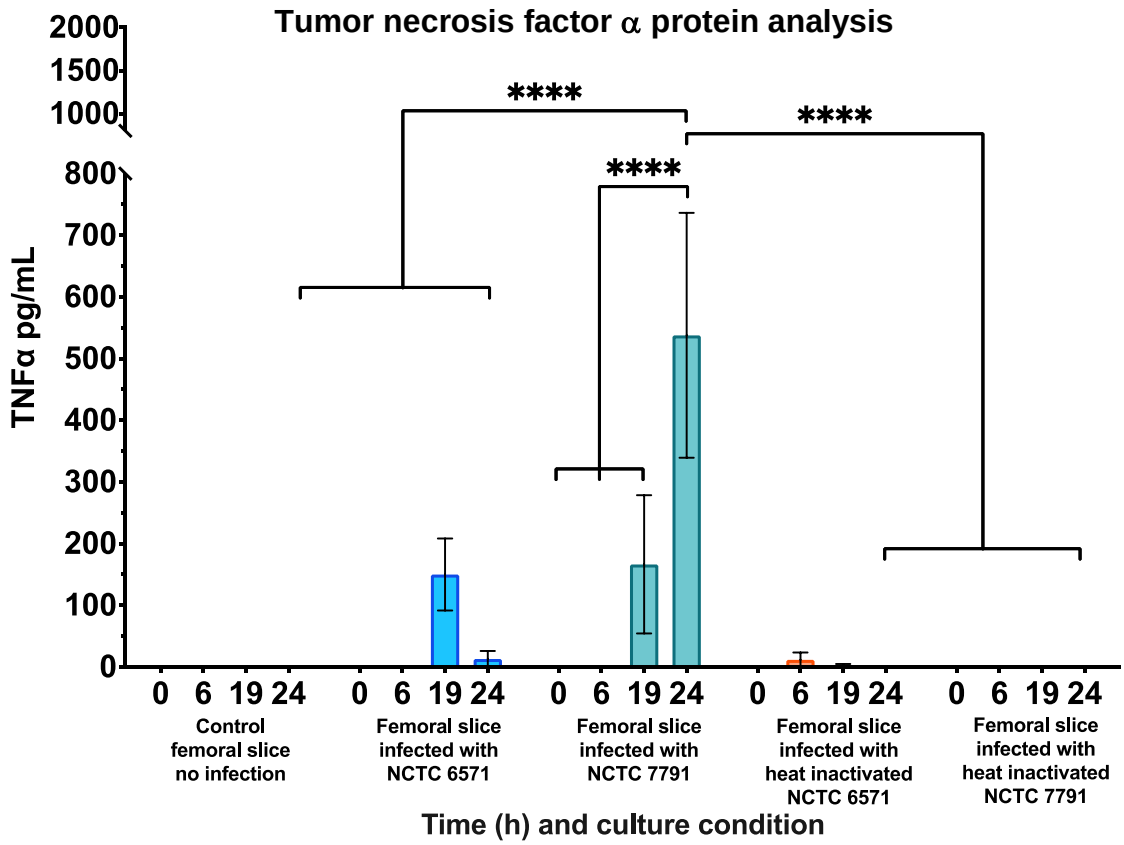

Figure 4.18: TNFα protein analysis following Trowell-type cultures supplemented with M-CSF and RANKL with and without co-culture of *S. aureus strains*, NCTC 6571 and NCTC 7791. Graph shows TNFα analysis with or without infection with *S. aureus* bacterial species over 24 h. Following infection there was a significant increase in TNFα synthesis after 19 h for NCTC 6571-infected samples, with NCTC 7791-infected samples only showing significant levels of protein release after 24 h. Little to no protein release was seen in non-infected controls or heat-inactivated samples. Significance within groups determined via one-way ANOVA. Significance between groups determined via two-way ANOVA with Tukey post-hoc test. Error bars represent mean ±S.E.M n=6 for control, NCTC 6571 and NCTC 7791 infected samples and n=3 for heat-inactivated NCTC 6571 and heat-inactivated NCTC 7791 infected samples, ****$P< 0.0001$

4.3.10: Anti-Inflammatory Cytokine Release

4.3.10.1: Interleukin-10

IL-10 protein release analysis that was carried out following co-culture of tissue slices with *S. aureus* type strains, NCTC 6571 and NCTC 7791 over 24 h, are shown in Figures 4.19. Samples without infection showed no IL-10 protein release at 0 h, 6, 19 h or 24 h.

When samples were infected with NCTC 6571 type strain, there was no significant difference ($P > 0.05$) in IL-10 synthesis between 0 h and 6 h, though there was a steady increase in synthesis showing 13 pg/mL and 22 pg/mL respectively. By 19 h, there was a non-significant increase ($P > 0.05$) in IL-10 protein release showing an average of 29 pg/mL, which steadily increased to an average of 31 pg/ mL by 24 h, although this was determined to be non-significant ($P > 0.05$). When compared to non-infected controls samples or heat-inactivated NCTC 6571, there was no significant difference ($P > 0.05$) IL-10 synthesis for 0 h, 6, 19 h or 24 h samples.

When samples were infected with NCTC 7791 type strain, there was no significant difference ($P > 0.05$) in IL-10 synthesis between 0 h and 6 h, although there was a steady increase in synthesis showing 14 pg/mL and 15 pg/mL, respectively. By 19 h, there was a non-significant increase ($P > 0.05$) in IL-10 protein release showing an average of 23 pg/mL, which increased non-significantly ($P > 0.05$) to an average of 48 pg/ mL by 24 h. When compared to non-infected controls samples, there was no significant difference ($P > 0.05$) IL-10 synthesis for 0 h, 6 or 19 h, significance ($P < 0.05$) was only seen between the 24 h samples. When compared to heat-inactivated NCTC 7791-infected samples, there were no significant differences ($P > 0.05$) in IL-10 synthesis for 0 h, 6, 19 h or 24 h samples.

Samples infected with heat-inactivated NCTC 6571 or NCTC 7791 showed no significant difference ($P > 0.05$) in IL-10 activity between 0 h, 6, 19 h or 24 h.

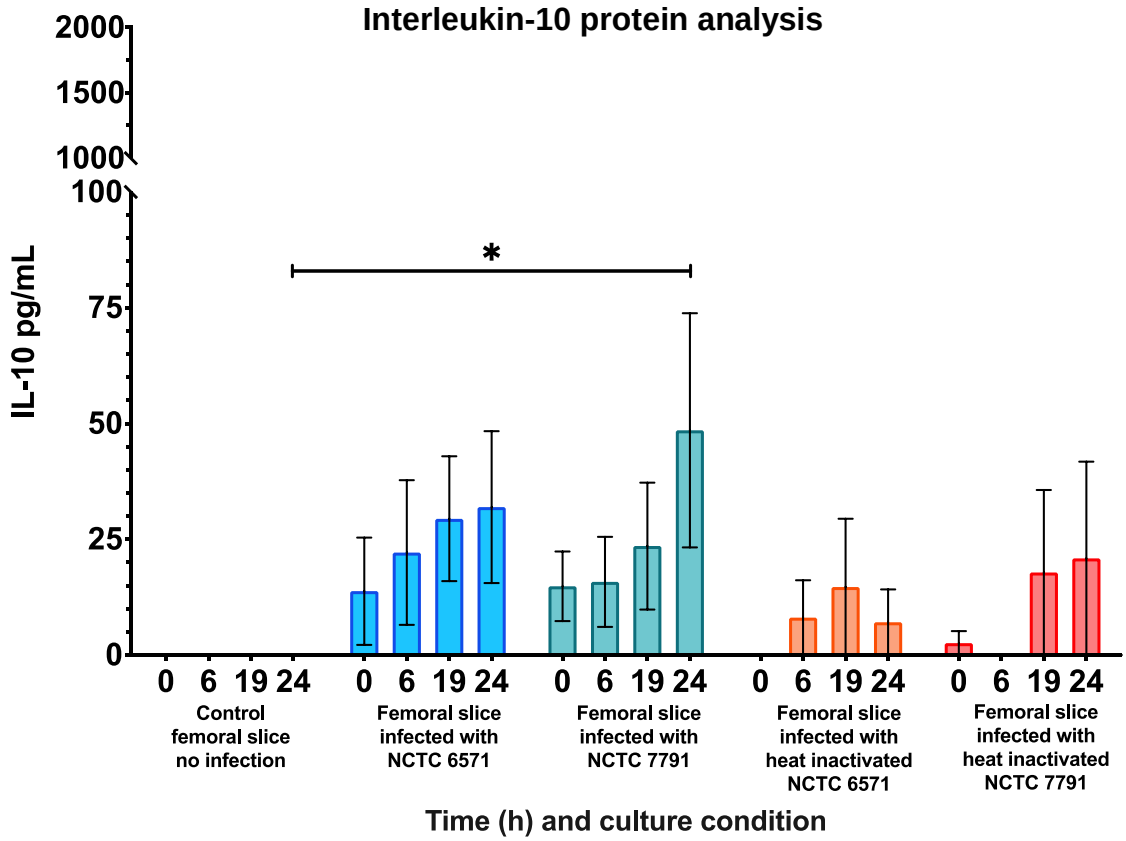

Figure 4.19: IL-10 protein analysis following Trowell-type cultures supplemented with M-CSF and RANKL with and without co-culture of *S. aureus strains*, NCTC 6571 and NCTC 7791. Graph shows IL-10 analysis with or without infection with *S. aureus* bacterial species over 24 h. Following infection there was a non-significant steady increase in IL-10 synthesis over 24 h for NCTC 6571 and NCTC 7791-infected samples. No protein release was seen in non-infected controls, but similar levels of protein release to infected samples were seen for heat-inactivated samples. Significance within groups determined via one-way ANOVA. Significance between groups determined via two-way ANOVA with Tukey post-hoc test. Error bars represent mean ±S.E.M n=6 for control, NCTC 6571 and NCTC 7791 infected samples and n=3 for heat-inactivated NCTC 6571 and heat-inactivated NCTC 7791 infected samples, *$P< 0.05$.

4.3.10.2: Interleukin-4

IL-4 protein release analysis that was carried out following co-culture of tissue slices with *S. aureus* type strains, NCTC 6571 and NCTC 7791 over 24 h, are shown in Figures 4.20. Samples without infection showed no IL-4 protein release at 0 h, 6, 19 h or 24 h.

When samples were infected with NCTC 6571 type strain, there was no significant difference ($P > 0.05$) in IL-4 synthesis between 0 h and 6 h, showing 2 pg/mL and 5 pg/mL, respectively. By 19 h, there was a significant increase ($P < 0.0001$) in IL-4 protein release showing an average of 35 pg/mL, which was non-significantly ($P > 0.05$) reduced slightly to an average of 30 pg/ mL by 24 h. When compared to non-infected controls samples, there was only a significant difference ($P > 0.05$) in IL-4 synthesis between the 19 h ($P < 0.001$) and 24 h samples ($P < 0.01$). When compared to heat-inactivated NCTC 6571-infected samples, there was only s significant difference ($P > 0.05$) in IL-4 synthesis between the two 19 h ($P < 0.01$) and 24 h samples ($P < 0.05$).

When samples were infected with NCTC 7791 type strain, there was no significant difference ($P > 0.05$) in IL-4 synthesis between 0 h and 6 h, showing an average of 4 pg/mL and 3 pg/mL, respectively. By 19 h, there was a non-significant increase ($P > 0.05$) in IL-4 protein release showing an average of 14 pg/mL, which was non-significantly ($P > 0.05$) increased to an average of 19 h pg/ mL by 24 h. When compared to non-infected controls or heat-inactivated NCTC 7791 samples, there was no significant difference ($P > 0.05$) IL-4 synthesis for 0 h, 6, 19 h or 24 h samples. When compared to NCTC 6571-infected samples, only the 24 h samples showed significance ($P < 0.05$).

Samples infected with heat-inactivated NCTC 6571 or heat-inactivated NCTC 7791 showed no significant difference ($P > 0.05$) in IL-4 activity between 0 h, 6, 19 h and 24 h.

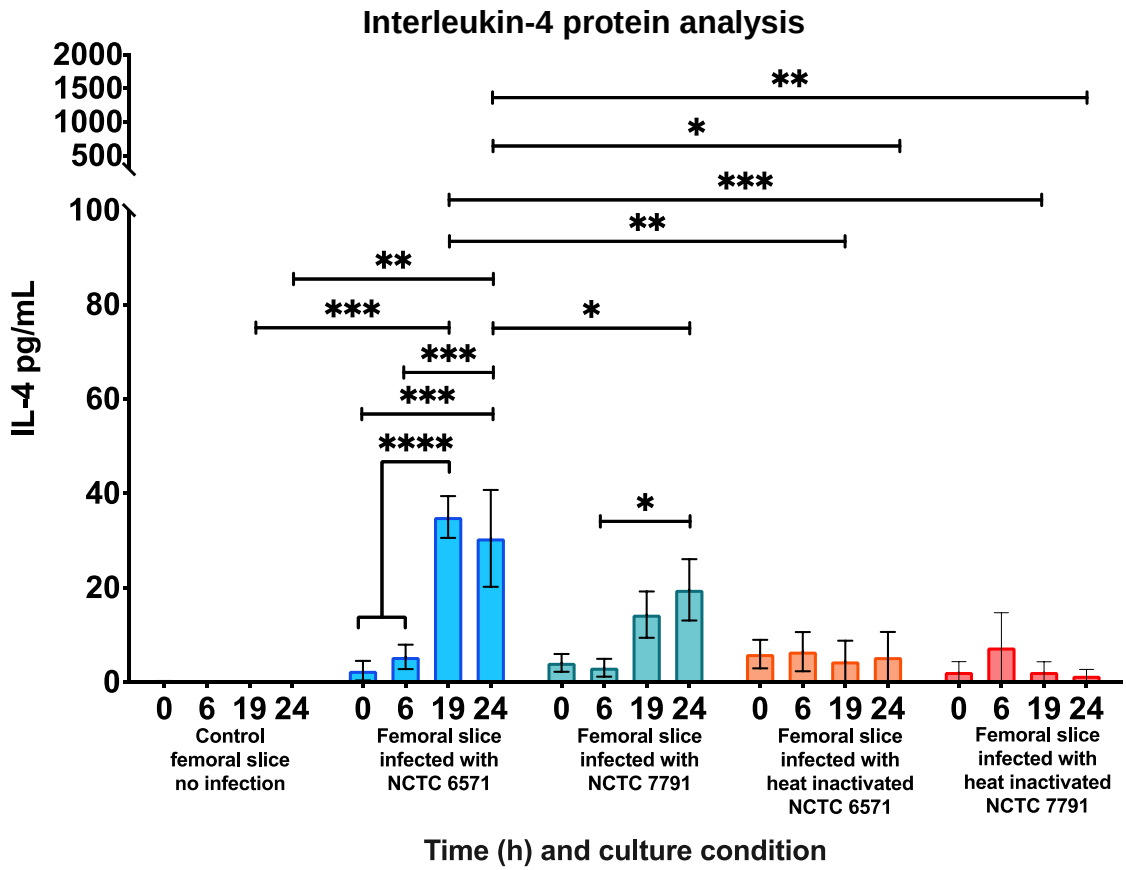

Figure 4.20: IL-4 protein analysis following Trowell-type cultures supplemented with M-CSF and RANKL with and without co-culture of *S. aureus strains*, NCTC 6571 and NCTC 7791. Graph shows IL-4 analysis with or without infection with *S. aureus* bacterial species over 24 h. The graph shows a significant increase in IL-4 levels at 19 h and 24 h for NCTC 6571-infected samples. There was a steady increase in IL-4 levels for NCTC 7791-infected samples, with only 24 h showing significance. No protein release was seen in non-infected controls, but low protein release was seen for heat-inactivated samples. Significance within groups determined via one-way ANOVA. Significance between groups determined via two-way ANOVA with Tukey post-hoc test. Error bars represent mean ±S.E.M n=6 for control, NCTC 6571 and NCTC 7791 infected samples and n=3 for heat-inactivated NCTC 6571 and heat-inactivated NCTC 7791 infected samples, * $P < 0.05$, ** $P < 0.01$, *** $P < 0.001$ and **** $P < 0.0001$.

4.3.11: Immune cell analysis

4.3.11.1: CD14 Bone Marrow Immunohistochemistry Localisation Following Infection With NCTC 6571 and NCTC 7791

Analysis of CD14 positive immune cells for slices infected with *S. aureus* type strains, NCTC 6571 and NCTC 7791 over 24 h, were calculated within a 12.5 mm^2 area.

Tissue slices not infected with either strain of *S. aureus*, at 0 h showed a mean of 489 bone marrow cells of which 343 cells were stained positive for CD14 (Figures 4.21A&B). The mean percentage of cells remaining that were stained positive for CD14 was 72 % (Figure 4.21C). The mean number of bone marrow cells at 24 h significantly decreased to 111 cells (*P < 0.0001*, Figures 4.21B). The mean number of cells stained positive for CD14 at 24 were significantly decreased to 69 cells (*P < 0.001*) when compared to 0 h controls (Figure 4.21A). The mean percentage of cells remaining that were stained positive for CD14 after 24 h was 56 %, this was non-significant (*P > 0.05*) when compared to 0 h. (Figure 4.21C)

Tissue slices infected with *S. aureus* NCTC 6571, at 0 h showed a mean of 379 bone marrow cells of which 347 cells were stained positive for CD14 (Figures 4.21A). The mean number of CD14-stained cells were significantly decreased when compared to 0 h non-infected controls (*P < 0.01*). The mean percentage of cells remaining that were stained positive for CD14 was 91 %, this was non-significantly elevated when compared to 0 h non-infected controls (*P > 0.05*, Figure 4.21C). The mean number of bone marrow cells at 24 h significantly decreased to 78 cells (*P < 0.0001*, Figures 4.21B). The mean number of cells stained positive for CD14 significantly decreased to 52 cells at 24 h (*P < 0.0001*) when compared to 0 h cultures (Figure 4.21A). This was non-significant when compared to 24 h non-infected controls (*P > 0.05*). The mean percentage of cells remaining that were stained positive for CD14 after 24 h decreased significantly to 71 % (*P < 0.05*) when compared to 0 h (Figure 4.21C). This was non-significant when compared to 24 h non-infected controls (*P > 0.05*).

Tissue slices infected with *S. aureus* NCTC 7791, at 0 h showed a mean of 385 bone marrow cells of which 226 cells were stained positive for CD14 (Figures 4.21A&B). The mean number

of bone marrow cells were significantly decreased when compared to 0 h non-infected controls (*P < 0.01*). The mean number of CD14-stained cells were significantly elevated when compared to 0 h non-infected controls (*P < 0.0001*) and was non-significant when compared to 0 h NCTC 6571 samples (*P > 0.05*). The percentage of cells remaining that were stained positive for CD14 at 0 h was 91 %, this was non-significant when compared to 0 h non-infected controls (*P > 0.05*) and 0 h NCTC 6571 samples (*P > 0.05*, Figure 4.21C). The mean number of bone marrow cells at 24 h significantly decreased to 163 cells (*P < 0.0001*, Figures 4.21B). The mean number of bone marrow cells were significantly increased at 24 h when compared to compared to 24 h NCTC 6571 samples (*P < 0.01*). The mean number of cells stained positive for CD14 decreased significantly to 87 cells (*P < 0.0001*) compared to 0 h cultures (Figures 4.21A). This was non-significant when compared to 24 h non-infected controls (*P > 0.05*) and 24 h NCTC 6571 samples (*P > 0.05*). The mean percentage of cells remaining that were stained positive for CD14 after 24 h decreased non-significantly to 73 % (*P > 0.05*) when compared to 0 h (Figure 4.21C). This percentage was not significant when compared to 24 h non-infected controls (*P > 0.05*) and 24 h NCTC 6571 samples (*P > 0.05*).

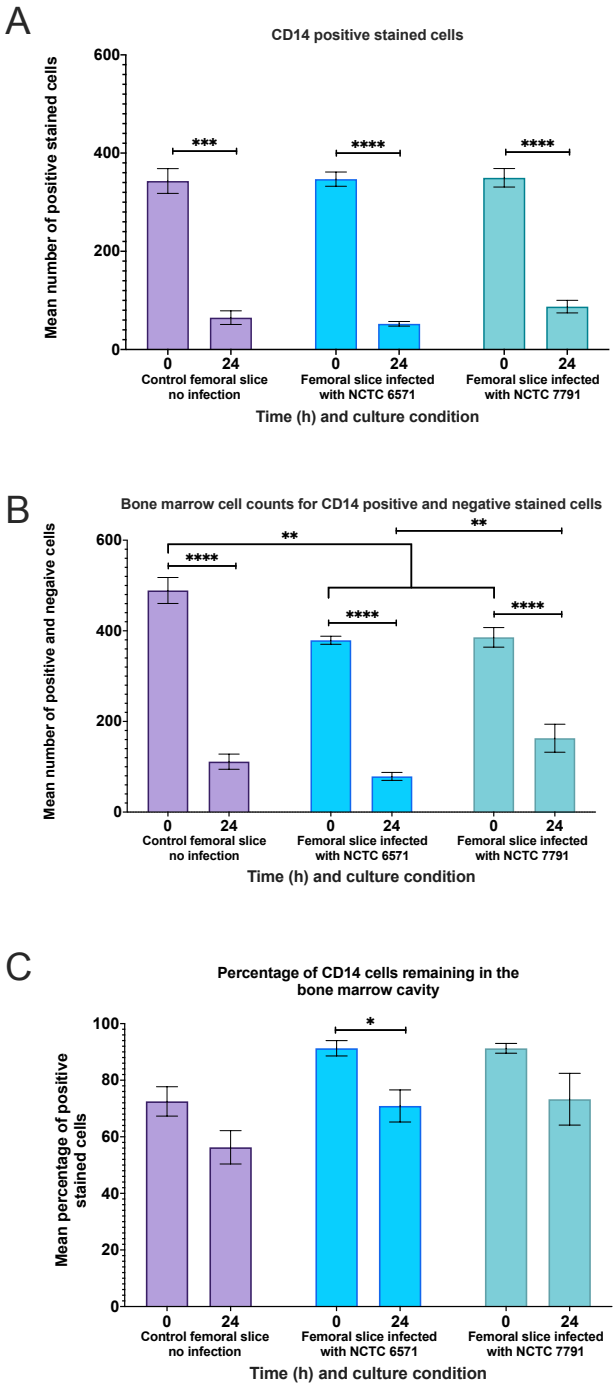

Figure 4.21 CD14 analysis following *S. aureus* infection and culture with M-CSF and RANKL. Semi-quantitative analysis for CD14 labelled cells within the bone marrow of Trowell-type cultures supplemented with 20 ng/mL M-CSF and 30 ng/mL RANKL and infected with *S. aureus strains*, NCTC 6571 and NCTC 7791 Graph A) showing data for mean cell counts for CD14 positive stained cells. Graph B) showing mean cell counts for both CD14 positive and negative stained cells. Graph C) showing the percentage of CD14 positive stained cells remaining in the bone marrow cavity. Infected slices showed a significantly higher number of total cells counts for infected slices and a significantly higher percentage counts at 0 h compared to control non-infected samples. By 24 h, cell counts for infected samples drop to levels seen in control with percentage counts remain high for infected samples. Significance within groups determined via one-way ANOVA. Significance between groups determined via two-way ANOVA with Tukey post-hoc test. Error bars represent mean ±S.E.M (n=3), **P<0.05, **P < 0.01, ***P < 0.001 and ****P < 0.0001*.

4.3.11.2: CD68 Bone Marrow Immunohistochemistry Localisation Following Infection With NCTC 6571 and NCTC 7791

Analysis of CD68 positive immune cells for slices infected with *S. aureus* type strains, NCTC 6571 and NCTC 7791 over 24 h, were calculated within a 12.5 mm^2 area.

Tissue slices not infected with either strain of *S. aureus*, at 0 h showed a mean of 362 bone marrow cells of which a mean of 35 cells were stained positive for CD68 (Figures 4.22A&E). The mean percentage of cells remaining that were stained positive for CD68 was 9.5 % (Figure 4.22B). The mean number of bone marrow cells at 24 h significantly decreased to 111 cells (*P < 0.0001*, Figures 4.22E). The mean number of cells stained positive for CD68 at 24 non-significantly increased to 20 cells (*P < 0.001*) when compared to 0 h controls (Figure 4.22A). The mean percentage of cells remaining that were stained positive for CD68 after 24 h non-significantly increased to 19 % (*P > 0.05*) when compared to 0 h (Figure 4.22B).

Tissue slices infected with *S. aureus* NCTC 6571, at 0 h showed a mean of 271 bone marrow cells of which a mean of 37 cells were stained positive for CD68 (Figures 4.22A&E). The mean number of bone marrow cells was significant when compared to 0 h non-infected controls (*P < 0.01*). The mean number of CD68-stained cells were significantly elevated when compared to 0 h non-infected controls (*P < 0.01*). The mean percentage of cells remaining that were stained positive for CD68 was 15 %, this was not significant when compared to 0 h non-infected controls (*P > 0.05*, Figure 4.22B). The mean number of bone marrow cells at 24 h significantly decreased to 63 cells (*P < 0.0001*, Figures 4.22E). The mean number of cells stained positive for CD68 non-significantly decreased to 20 cells at 24 h (*P > 0.05*) when compared to 0 h cultures (Figure 4.22A). This was non-significant when compared to 24 h non-infected controls (*P > 0.05*). The mean percentage of cells remaining that were stained positive for CD68 after 24 h increased significantly to 35 % (*P < 0.001*) when compared to 0 h (Figure 4.22B). This percentage was significant when compared to 24 h non-infected controls (*P < 0.01*).

Tissue slices infected with *S. aureus* NCTC 7791, at 0 h showed a mean of 224 bone marrow cells of which a mean of 8 cells were stained positive for CD68 (Figures 4.22A&E). The mean number of bone marrow cells was significant when compared to 0 h non-infected controls

(*P < 0.001*) and was non-significant when compared to 0 h NCTC 6571 samples (*P > 0.05*). The mean number of CD68-stained cells at 0 h were significantly elevated when compared to 0 h non-infected controls (*P < 0.0001*) and was non-significant when compared to 0 h NCTC 6571 samples (*P > 0.05*). The mean percentage of cells remaining that were stained positive for CD68 at 0 h was 8 %, this was not significant when compared to 0 h non-infected controls (*P > 0.05*) and 0 h NCTC 6571 samples (*P > 0.05*, Figure 4.22B). The mean number of bone marrow cells at 24 h non-significantly decreased to 180 cells (*P > 0.05*, Figures 4.22E). The mean number of bone marrow cells were significantly increased at 24 h when compared to compared to 24 h NCTC 6571 samples (*P < 0.01*). The mean number of cells stained positive for CD68 non-significantly increased to 23 cells (*P > 0.05*) compared to 0 h cultures (Figures 4.22A). This was non-significant when compared to 24 h non-infected controls (*P > 0.05*) and 24 h NCTC 6571 samples (*P > 0.05*). The mean percentage of cells remaining that were stained positive for CD68 after 24 h increased non-significantly to 21 % (*P > 0.05*) when compared to 0 h (Figure 4.22B). This was not significant when compared to 24 h non-infected controls (*P > 0.05*) and was significantly decreased when compared to 24 h NCTC 6571 samples (*P < 0.05*).

4.3.11.3: Multinucleated CD68 Bone Marrow Immunohistochemistry Localisation Following Infection With NCTC 6571 and NCTC 7791

To assess the level of multinucleated CD68 osteoclast-like cells within the bone marrow cavity following *S. aureus* infection over 24 h, both mean cell and percentage counts (Figure 4.22C&D) for CD68 positive cells containing 3 or more nuclei and located adjacent to the cortical bone were analysed within a 12.5 mm^2 area.

Tissue slices not infected with either strain of *S. aureus*, at 0 h, the mean number of multinucleated cells stained positive for CD68 was low at 2 cells (Figure 4.22C). The mean percentage of multinucleated cells remaining that were stained positive for CD68 was 1 % (Figure 4.22D). After 24 h the number of multinucleated cells stained positive for CD68 was significantly decreased to a mean of 0 cells which (*P < 0.05*) when compared to 0 h (Figure 4.22C). The mean percentage of multinucleated cells remaining that were stained positive for CD68 at 24 h was maintained at 1 %, (*P > 0.05*) when compared to 0 h (Figure 4.22D).

Tissue slices infected with *S. aureus* NCTC 6571, at 0 h multinucleated cells stained positive for CD68 showed a mean of 1 cell (Figure 4.22C). This was not significant when compared to 0 h non-infected controls (*P > 0.05*). The mean percentage of multinucleated cells remaining that were stained positive for CD68 was 2 % and was non-significant when compared to 0 h non-infected controls (*P > 0.05*, Figure 4.22D). At 24 h the mean number of multinucleated cells staining positive for CD68 increased non-significantly to 7 cells (*P > 0.05*) when compared to 0 h cultures (Figure 4.22C). This was non-significant when compared to 24 h non-infected controls (*P > 0.05*). The mean percentage of multinucleated cells remaining that were stained positive for CD68 after 24 h increased non-significantly to 6 % (*P > 0.05*) when compared to 0 h 6571 infected slices and 24 h non-infected controls (*P > 0.05*, Figure 4.22D).

Tissue slices infected with *S. aureus* NCTC 7791, at 0 h multinucleated cells stained positive for CD68 was 3 cells (Figure 4.22C). This was not significant when compared to 0 h non-infected controls (*P > 0.05*) but was significantly increased when compared to 0 h NCTC 6571 samples (*P < 0.001*). The mean percentage of multinucleated cells remaining that were stained positive for CD68 at 0 h was 4 % and was not significant when compared to 0 h non-infected controls (*P > 0.05*) and 0 h NCTC 6571 samples (*P > 0.05*, Figure 4.22D). At 24 h, the mean number of multinucleated cells staining positive for CD68 significantly decreased to 1 cell (*P < 0.05*) compared to 0 h cultures (Figure 4.22C). This was non-significant when compared to 24 h non-infected controls (*P > 0.05*) and 24 h NCTC 6571 samples (*P > 0.05*). The mean percentage of multinucleated cells remaining that were stained positive for CD68 after 24 h decreased non-significantly to 2 % (*P > 0.05*) when compared to 0 h 7791 infected samples, 24 h non-infected controls (*P > 0.05*) and 24 h NCTC 6571 infected samples (Figure 4.22D).

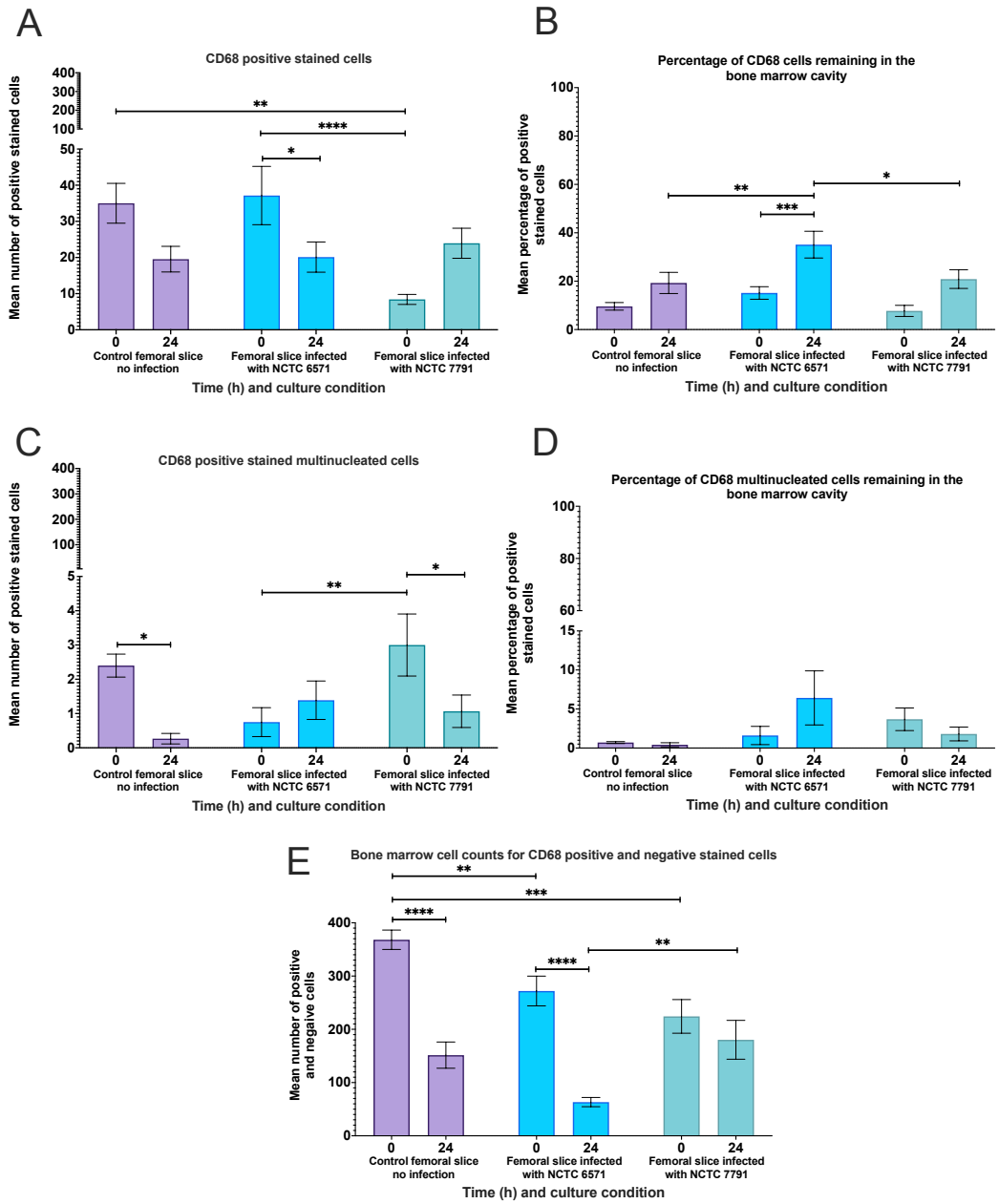

Figure 4.22 CD68 analysis following *S. aureus* infection and culture with M-CSF and RANKL. Semi-quantitative analysis for CD68 labelled cells within the bone marrow of Trowell-type cultures supplemented with 20 ng/mL M-CSF and 30 ng/mL RANKL and infected with *S. aureus strains*, NCTC 6571 and NCTC 7791. Graphs show (A) mean CD68 stained cell counts, (B) mean percentage of CD68 stained cells remaining, (C) mean CD68 stained multinucleated osteoclast-like cell counts, (D) mean percentage of CD68 stained multinucleated osteoclast-like cells and (E) mean cell counts for both CD68 positive and negative stained cells. Infected slices showed a higher number of total cells counts at 0 h compared to non-infected samples. By 24 h, cell counts for infected samples drop to levels seen in control, with percentage counts remaining high for NCTC 6571 infected samples. Infected slices show no significant difference in multinucleated cells compared to control non-infected samples at either 0 h or 24 h. Significance within groups determined via one-way ANOVA. Significance between groups determined via two-way ANOVA with Tukey post-hoc test. Error bars represent mean ±S.E.M (n=3), *$P < 0.05$, *** $P < 0.001$ and ****$P < 0.0001$.

4.4: Discussion

This chapter aimed to assess whether the femoral slice model could be successfully infected with bacterial strains to induce a pro-inflammatory response. The data presented within this chapter shows successful colonisation of the *S. aureus* bacteria within the femoral slice along with an increase in pro-inflammatory cytokines along with increased cell death following infection. However, simulating a true *in vivo* response using the current *ex vivo* models is difficult. Culture time was limited to 24 h and had to rely on the already present population of immune cells housed within the bone marrow cavity. There is no active blood supply therefore there cannot be migration of circulating monocytes and macrophages to site the of infection.

In this model, two different, yet relevant *S. aureus* type strains were chosen for analysis, NCTC 6571 and NCTC 7791. NCTC 6571, is commonly known as the oxford strain and the second NCTC 7791, which was originally isolated from an osteomyelitis patient. NCTC 6571 was first used by Heatley (1944) to develop an infectious standardised control, to observe the effects and susceptibility of penicillin as an antibiotic against clinically isolated Staphylococcus species. Since then it has been commonly used as a reference control species for antibiotic susceptibility testing in laboratory-based setting (Kearns et al. 2006). This is possibly caused by the continual subculturing of NCTC 6571 within a controlled laboratory environment, that is devoid of a hostile environment that it would have typically encountered *in vivo*. As a result, the bacterial species is proposed to have mutated and evolved to reduce certain cell wall adhesins (CWA) and virulence factors on its cell surface that it would have relied on for survival in a hostile *in vivo* environment, making it potentially less pathogenic and more susceptible to host immune responses and antibiotic than its clinical counterparts. In contrast, NCTC 7791 would have theoretically had all the CWA and virulence proteins it had produced to maintain its survival within the hostile *in vivo* environment.

This chapter has shown that *S. aureus* bacterial species could be successfully cultured in mammalian tissue culture media without the need for additional bacterial broth solution. Though culturing bacterial populations within culture media without bacterial broth did inhibit the growth of the bacterial species over 24 h compared to BHI supplemented

counterparts, characteristic bacterial growth phases could be seen during culture and majority of the bacterial cell populations were viable, with little death observed. This reduction of growth within the culture media without BHI is unsurprising, BHI helps promote the growth of the bacterial species and increase expression of virulence factors along with fatty acid chains on *S. aureus* surface, enabling improved colonisation (Sen et al. 2016). This enabled the co-culture of *S. aureus* within the *ex vivo* model without further modifications to the culture media. This provides analysis of the interactions of the bacterial species and any associated virulence factors on the bone marrow microenvironment, without any additional unintentional interference from the BHI on the local host cell populations.

Following bacterial co-culture, histological analysis revealed gram-positive cocci within the bone marrow cavity and around the edge of the cortical periosteum. By 19 h and 24 h, the bacterial presence was more pronounced within the bone marrow cavity and surrounding periosteum. No observable difference was seen of bacterial attachment within the bone marrow cavity between either type strains. Both species significantly reduced total bone marrow cell numbers including CD14 and CD68 immune cell populations following 24 h, although percentages of these immune cells remained high following infection.

It is known that *S. aureus* induced bone loss within PJIs and osteomyelitis is not only due to the direct action of the bacteria lysing the bone cells, but via a more indirect action by stimulating the bone marrow microenvironment to synthesise and secrete pro-inflammatory cytokines leading to the dysregulation of the bone remodelling unit and subsequent pathological implant osteolysis. of all the pro-inflammatory cytokines TNFα, IL-1 and IL-6 are considered the most important due to their direct interaction in inducing osteoclastogenesis of mature osteoclasts and the cells role bone resorption and are often seen within high levels within patients suspected of PJI (Deirmengian et al. 2010; Deirmengian et al. 2014a; Deirmengian et al. 2014b; Di Cesare et al. 2005; Froschen et al. 2020; Garcia-Alvarez et al. 2009; Vicenti et al. 2019). Within this chapter, following infection with both *S. aureus* type strains, TNFα, IL-1 and IL-6 cytokines levels were increased after 19 h and 24 h of culture, similar to the above *in vivo* studies. This increase in these pro-inflammatory cytokines can occur either as a direct response to the presence of the bacteria by monocytes and macrophages to induce a pro-inflammatory environment and to recruit

HSCs, monocytes, macrophages, neutrophils, natural killer cells and T–lymphocytes (Arango Duque and Descoteaux 2014; De Filippo et al. 2013; Lukacs et al. 1995; Moser et al. 1990; Wright et al. 2002). Typically these cells induce these cytokines either as an autocrine action system causing an effect on cells that secrete these cytokines, by an endocrine action system, by affecting cells that are at a distance or by a paracrine action system by affecting cells that are adjacent to the cytokine secreting cell (Zhang and An 2007). Within this model, percentage levels of CD14 and CD68 myeloid cells, which include monocytes and macrophages, were elevated following infection. Therefore, it is possible the increase in immune cells is responsible for the elevations in TNFα, IL-1β and IL-6 following infection.

In this model there was a significant increase in necrosis and apoptosis within the bone marrow cavity. As a consequence of this increase in cell death, there is a possibility that the increase in these cytokines detected in the *ex vivo* model could be attributed to increased levels of cellular debris and lysed intracellular contents caused by apoptosis and necrosis or other cell mechanisms following infection. One such additional mechanism is pyroptosis, a pro-inflammatory form of cell death that is caused by a result of microbial infections (Bergsbaken et al. 2009). This process is characterised by the activation of caspase-1 after inflammasome assembly increasing levels of LDH and the formation of IL-1β and IL-18 into their mature forms (Accarias et al. 2015; Bergsbaken et al. 2009). These intracellular contents are then secreted via the formation of small pores in the plasma membrane which progresses to cell lysis. (Accarias et al. 2015; Bergsbaken et al. 2009). An additional cell death mechanism that can be invoked following infection is necroptosis. Necroptosis is a form of programmed cell necrosis which is activated by the binding of specific ligands to either TNF receptor, Interferon receptor and toll-like receptors, resulting in pore formation causing leakage of intracellular contents. Cells that have undergone necroptosis are less readily phagocytoses and cleared by macrophages due to the high levels of CD47 in these cells (Gerlach et al. 2020). These mechanisms have both been seen to be invoked following infection with *S. aureus* (Accarias et al. 2015; Kitur et al. 2016). The fact that the presence of infections induces these mechanisms that can either increases levels of IL-1β via pyroptosis or the presence of cell debris and intracellular contents which can following increased cell death also explain the pro- and anti-inflammatory results seen following

infection of the model. TNFα can be seen as either membrane-bound or soluble (Ardestani et al. 2013), and IL-1β can also be found intracellularly within microvesicles, lysosomes and exosomes which can be shed or secreted out of the cells (Lopez-Castejon and Brough 2011).

TNFα has previously shown to induce M-CSF and RANKL expression in MSCs, osteoblasts and osteocytes (Hofbauer et al. 1999; Kitaura et al. 2004; Kitaura et al. 2005). The cytokines can also increase the M-CSF receptor and RANK expression on the surface of osteoclast precursors and plays a key role in osteoclastogenesis in a RANK/RANKL dependent and independent manner (Kobayashi et al. 2000; Komine et al. 2001; Luo et al. 2018; Yao et al. 2006). TNFα has also been shown to induce up-regulation of MMP-9, a collagen type IV degrading gelatinase, within osteoclast during RANKL induced osteoclastogenesis and bone resorption (Logar et al. 2007; Sundaram et al. 2007). Studies have shown osteoblasts and rat bone marrow derived MSCs are able to synthesis MMP-9 production in the presence of TNFα, suggesting that these mineralising cells are able to play key roles within pathological bone destruction (Ben David et al. 2008; Kaneko et al. 2001). Marazzi et al. (2018) in contrast reported no change in MMP-9 levels within the synovial fluid of PJI patients compared to non-infected controls, though no additional studies have looked in to MMP-9 synthesis in patients suspected for PJI. IL-1β plays key roles in initiating both bone formation and bone resorption (Lee et al. 2010; Ruscitti et al. 2015). IL-1β is dependent on RANK/RANKL to induce osteoclastogenesis and stimulates RANKL production in osteoblasts (Hofbauer et al. 1999; Lee et al. 2010). IL-1β can also play roles on MMP production and studies on rat bone marrow derived MSCs were able to induce MMP-9 following IL-1β supplementation (Ben David et al. 2008). IL-1 and IL-6 stimulated primary osteoblastic cells from 5-day-old mouse calvaria showed increases in key bone ECM degrading MMPs, MMP-2 and MMP-9 (gelatinases), MMP-3 (stromelysin) and MMP-13 (Collagenases; Kusano et al. 1998). IL-6 and its membrane-bound or soluble receptors are synthesised from various bone marrow cells including; monocytes, macrophages, T-lymphocytes and B-lymphocytes (Garbers et al. 2015; Wolf et al. 2014). In bone resorption, IL-6 plays a key role in inducing osteoclastogenesis via RANKL whilst simultaneously increasing RANKL synthesis in osteoblasts and MSCs (Yoshitake et al. 2008) (Dayer and Choy 2010; Feng et al. 2017). Together this suggests that all three pro-inflammatory cytokines play additional roles in ECM

degradation apart from initiating osteoclastogenesis and M-CSF and RANKL production in MSCs and its lineages. Though the effects of pathological MMP induced ECM bone marrow degradation following *S. aureus* induced infections is unknown, further analysis of these proteins within the *ex vivo* model could potentially shed light on this understudied area.

Within this model there was some slight differences were observed between the two type-strains on protein release for IL-6, TNFα and IL-1β. NCTC 7791 infections showed a steady increase in all three cytokines over 24 h, whereas NCTC 6571 infections showed an increase at 19 h with a large reduction of all cytokines by 24 h. When analysing LDH release for samples infected with NCTC 6571 there was a large increase in LDH at 19 h that subsequently dropped by 24 h. The LDH and pro-inflammatory cytokines increase by 19 h for NCTC 6571 infections could be due to a large number of cells responding to the increase of serum LDH at 19 h, whereby the majority of cells are subsequently destroyed. This causes a reduction in cell numbers within the bone marrow cavity by 24 h and subsequently a reduction of the amount of pro-inflammatory cytokines those cells can produce. Another explanation could be that these pro-inflammatory cytokines are actively being used up by the remaining bone marrow cells between 19 h and 24 h.

The co-culture model showed elevations of both IL-4 and IL-10 anti-inflammatory cytokines at 19 h and 24 h post-infection, though levels remained low. It may, therefore, be possible that these two anti-inflammatory cytokines are either released via cell mediated secretion or via intracellular release following lysis of cells via apoptosis or necrosis. IL-4 and IL-10 are induced within pro-osteoclastic inflammatory environments (Okamoto and Takayanagi 2011). Both these cytokines inhibit osteoclastogenesis and are produced by regulatory T-lymphocytes (Tregs) and T-helper (Th) cells, specifically Th2 cells (Okamoto and Takayanagi 2011; Sasaki et al. 2000). In addition to T-lymphocytes, other immune cells can produce IL-10 including dendritic cells, B-lymphocytes, macrophages and monocytes (Couper et al. 2008; Gjertsson et al. 2002). IL-10 protects the bone marrow cells from a variety of toxic shock syndromes (Sasaki et al. 2000). *S. aureus* can utilise IL-10 by manipulating the inflammatory environment to suppress inflammation and allow persistence within the host (Leech et al. 2017). Tregs are activated when there is an upregulation of toll-like receptor (TLR)-2 ligands and thus producing IL-10 (Frodermann et al. 2011). *S. aureus* has been shown

to induce similar molecules on their cell surface to TLR2 ligand inhibiting T-lymphocyte activation and inducing apoptosis of antigen presenting cells (Chau et al. 2009). Frodermann et al. (2011) showed that the addition of staphylococcus peptidoglycan induced TLR2 signalling from different *S. aureus* strains on human peripheral blood monocytes and monocyte derived macrophages. The authors observed increases in pro-inflammatory cytokine production also increased IL-10 synthesis over 1000 pg/mL within 24 h, however, the authors did not see any IL-4 synthesis. Leech et al. (2017) showed that mice following peritoneal infection with *S. aureus* induced IL-10 production locally and systemically within the first 24 h post-infection. IL-10 knockout mice induced greater bacterial infections into a variety of organs after 24 h this was by systemic infection by utilising the bloodstream. The authors showed that a variety of pro-inflammatory cytokines including IL-1β and TNFα were downregulated between 24 h and 72 h post-infection specifically in wild-type mice. Sasaki et al. (2000) demonstrated that mice infected with *S. aureus* induced IL-4 and IL-10 gene expression within spleens, although protein release for the two cytokines was low. *In vitro* analysis on heat killed *S. aureus* infections on primary uninfected murine spleen and kidney cells induced high levels of genetic expression of IL-4 and IL-10, along with a reduction in IFNγ after 7 days in culture (Sasaki et al. 2000). The authors suggest that both these anti-inflammatory cytokines play a protective mechanism on cells via regulation of IFNγ following infection, this is especially apparent when anti-IL-10 and anti-IL4 antibodies were added *in vivo*, prevented clearance of *S. aureus* from the kidneys and increased the presence of IFNγ. This may imply that the presence of these two anti-inflammatory cytokines can also act as a protective mechanism on the local cell population against a pro-inflammatory environment induced by the presence of the bacteria. This observation may explain why for NCTC 6571-infected slices there a reduction was in IL-1β, TNFα and IL-6 between 19 h and 24 h, as specifically at those times there was a significant increase in IL-4 and IL-10 production. Therefore, it could be hypothesised that the production of both IL-4 and IL-10 following infection, could be caused by the bacteria binding to various immune cells to induce an anti-inflammatory environment to downregulate the pro-inflammatory cytokines allowing them to persist within the bone marrow cavity. Similarly, the presence of these cytokines may be secreted by resident host immune cells such as Th2 cells, to protect the local bone marrow microenvironment from the effects of the elevated levels of pro-inflammatory cytokines

secreted following infection, although further analysis needs to be carried out to confirm this hypothesis.

Within this model for NCTC 7791 strain infections, a large biofilm was observed around the periosteum for one particular bone slice at 24 h. In previous samples both type strains showed some attachment to the periosteum indicating early-stage biofilm formation, however, the presence of a mature-like biofilm within 24 h was surprising. It is currently unknown if the ratio of virulence proteins, CWA and MSCRAMMs between NCTC 6571 and NCTC 7791 differ. *S. aureus* biofilms occur commonly within clinical environments, as it allows the microbes to withstand pH changes, nutrient deprivation, protection from oxygen radicals, desiccation, the immune response and antimicrobial agents (Flemming and Wingender 2010; Petrova and Sauer 2012). It is, therefore, possible that since NCTC 7791 *S. aureus* was originally isolated from an osteomyelitis patient, the bacterial species are more susceptible to biofilm formation to protect the microorganisms from various host responses.

The results presented within this chapter has shown that following infection of the *ex vivo* model via two *S. aureus* type strains, there was localised bacterial presence within the bone marrow cavity along with attachment to the periosteum. This led to a loss of bone marrow cells, along with increased localised apoptosis and necrosis. There was an increase in immune cell percentages, which is typical of *in situ* infections within PJIs. There was an increase in pro-inflammatory cytokines TNFα, IL-1β and IL-6 the three key players in inflammatory osteoclastogenesis, suggesting an active and representative immune response seen *in vivo* following infection. However, further refinement of the model is required to increase the culture period along with more detailed analysis on gene expression and matrix biochemical analysis. This model does show the potential to further understand and elucidate the various mechanisms utilised by *S. aureus* in developing bacterial-induced osteolysis and develop novel antimicrobial compounds for treatment.

Chapter 5:
General Discussion and Future Work

This Thesis aimed to develop and characterise a novel *ex vivo* femoral slice model to understand the events leading to prosthetic joint infections (PJI), subsequent implant loosening and to facilitate the development of novel antimicrobials. Cell composition, cellular viability and metabolism were characterised in two different model culture systems that have previously demonstrated success: the *ex vivo* tooth slice model and the *ex vivo* mandible model (Roberts et al. 2013; Sloan et al. 1998; Sloan et al. 2013; Smith et al. 2010). Of the two culture systems, the Trowell-type culture system demonstrated higher levels of cell viability and was chosen to investigate the responses of the local immune cell population with the addition of pro-osteoclastogenic factors. Finally, the model was co-cultured with known osteolytic bacterial species, and their attachment within the bone marrow cavity was assessed whilst simultaneously evaluating the inflammatory cellular response.

Using around twenty-five 21 to 28-day-old Wistar Rats, 6-8 semi-cylindrical halves were obtained from the femoral shafts of each animal and used as individual samples in this research. Other tissues were also obtained from these same animals and were used for other research experiments within the group, thus adhering to the guidelines of the NC3Rs institute. The NC3Rs are a UK based scientific organisation dedicated to reducing, refining and replacing the use of animals in scientific research (Prescott and Lidster 2017). This model from the onset establishes two of the 3Rs, refinement and reduction.

Two different culture methods were investigated, first a base-type culture where the tissue slice was submerged in culture media towards the base of a culture plate. Secondly, a Trowell-type culture where the tissue slice is suspended within an agarose matrix at a liquid-air interface. Evaluations of both models indicated that the Trowell-type model had vastly improved cell maintenance within the bone marrow cavity, in terms of both viability and metabolism. The benefit of the Trowell-type model allows the use of liquid-gas interface and medium tissue interface which improves tissue access to oxygen whilst still permitting access to the nutrients from the culture media below (Gohbara et al. 2010). Oxygen availability is a crucial component in maintaining viable tissues, as it is a key requirement for metabolic processes and cellular functions. The reduced level of oxygen in and around cells can lead to hypoxia and the development of reactive oxygen intermediates (Utting et al. 2006). Oxygen is vital for many metabolic processes cells, most notably in the generation of

adenosine triphosphate (ATP) that is required for cellular functions (Abaci et al. 2010). Hypoxia occurs when oxygen is insufficiently consumed below normal levels, this leads to insufficient ATP production and subsequent reduction in metabolic activities (Abaci et al. 2010). However, *in vivo,* the bone marrow is considered a hypoxic environment, with an oxygen tension between 1-7 %. Possibly due to the high oxygen consumption required by hemopoietic stem cells (HSCs) and their lineages, usual culture conditions of 21 % oxygen is considered hyperoxic (Hung 2013; Morikawa and Takubo 2016). Studies on chondrocyte cultures within 3 % w/w agarose gels have observed optimal diffusion of oxygen throughout the gel, although after 24 h of culture, a hypoxic region was observed at the centre of the gel (Guaccio et al. 2008). Within the agarose gel of the Trowell-type culture, a similar observation was noted, though not analysed. At the centre of the gel a small area surrounding the bone had a slightly acidic pH after 24 h and 48 h of culture (identified using the phenol indicator of the culture medium) when compared to the rest of the gel that had a slightly alkaline pH (Supplementary Figure 18). This colour change is indicative of hypoxia, where the pH drops when oxygen is low, typically known as acidosis (Khacho et al. 2014).

The amount of oxygen supplied to cells within the femoral bone slice can affect their responses. HSC's hypoxic responses are mediated by hypoxia-inducible factors (HIFs) (Morikawa and Takubo 2016). HSCs respond to a hypoxic environment by inducing HIF-1a which subsequently reduces HSC proliferation and maintains the cells within a quiescent state (Eliasson et al. 2010). Furthermore, analysis *in vitro* and *in vivo* have shown that HSCs localise within hypoxic regions of the bone marrow (Parmar et al. 2007) and that monocytes respond to the oxygen gradient and migrate towards hypoxic environments (reviewed in (Bosco et al. 2008). Therefore, it would be reasonable to assume that the reduction in the HSC lineages (demonstrated within Chapter 2) is possibly due to not only a hypoxic environment around the bone slice, suppressing HSC proliferation capacity, but also due to a lack of key cytokines such as M-CSF and RANKL, that are required to maintain these cells. It is also possible that there is some active migration of these resident HSCs and their lineages out of the bone marrow cavity, however, this hypothesis was not tested. Within the femoral slice model, high levels of MSC markers were observed within the bone marrow cavity, thus indicating that these cells can be maintained during culture even within a hypoxic environment. Some studies have shown that a hypoxic environment can beneficially

affect bone marrow mesenchymal stromal cells (MSCs) proliferation, differentiation, migration and expression of chemokines (Tsai et al. 2012). Within the bone marrow, specialised stem cell niches exist between MSCs and HSCs. MSCs with osteoblasts synthesise HSC supporting factors, such as chemokine C-X-C motif ligand 12 (CXCL12), stem cell factor, osteopontin, angiopoietin-1 and vascular cell adhesion protein-1 (Morikawa and Takubo 2016; Parmar et al. 2007). Having a potential hypoxic environment around the tissue slice is indicative of an *in vivo* environment, along with the stem cell niche and the spatial organisation of the cells observed within the model.

To further refine the *ex vivo* femoral slice model, it was necessary to demonstrate that the model could be adapted and changed to replicate various pathological local bone marrow microenvironments. To simulate a pro-inflammatory environment, two key pro-osteoclastic cytokines were added to the culture media: macrophage colony-stimulating factor (M-CSF) and receptor activator of nuclear factor kappa B ligand (RANKL), to maintain resident HSCs, monocytes and macrophages populations and try to direct these cells towards an osteoclastic lineage.

Due to the significant loss of cells within the model after 48 h, it was not possible to investigate and follow the differentiation of these cells into mature osteoclasts. Osteoclast differentiation protocols typically require at least 4 -10 days to generate mature osteoclasts, depending on the origin of the cells, culture method, the concentration of cytokines used (Marino et al. 2014; Takeshita et al. 2000). A 144 h model system was examined but was unsuccessful due to the loss of almost all cells within the bone marrow cavity and therefore these longer-term osteoclast investigations could not occur. The addition of M-CSF and RANKL did not result in the differentiation of monocytes/macrophages into osteoclasts but did improve the maintenance and viability of both CD14 and CD68 cells over the 48 h in culture. This was not unsurprising as the presence of M-CSF has been shown to improve macrophage and myeloid cell proliferation and viability through pathways involving DAP12 adaptor protein and b-catenin (Otero et al. 2009). An attempt to add more osteoclasts into the slices was carried out by first culturing bone marrow monocytes and macrophages *in vitro* and secondly differentiating these cells in the presence of M-CSF and RANKL to form mature osteoclasts. However, it was not possible to remove the mature osteoclasts from

the culture plate and add them to the femoral slice model, as any attempt of osteoclast removal caused a significant increase in their cell death.

The addition of other cytokine supplements to monocytes and macrophages cultures, including interleukin (IL) -23, tumor necrosis factor-alpha (TNFα), IL-6 IL-1α, IL-1β, IL-8 and IL-17, can be used to stimulate osteoclast formation (Chen et al. 2008; Shiratori et al. 2018). These cytokines also play a major role in septic osteolysis and are often expressed in greater quantities during infection (Deirmengian et al. 2010; Deirmengian et al. 2014a; Deirmengian et al. 2014b; Di Cesare et al. 2005; Froschen et al. 2020; Garcia-Alvarez et al. 2009; Vicenti et al. 2019). Adding these cytokines to the femoral slice model to generate osteoclast numbers would have formed an artificial pro-inflammatory environment that would affect the local bone marrow microenvironment. This would have falsely skewed the pro-inflammatory data obtained following infection. Therefore, it would have been inappropriate to increase osteoclast numbers by the addition of these cytokines to model PJIs and osteomyelitis. This does not mean that these cytokines and additional chemokines cannot be added to the bone marrow microenvironment similar to the addition of M-CSF and RANKL to the femur slice model. Control of the microenvironment and formation of specific cell niches would allow for greater adaptability and functionality to model different aspects of implant-related conditions or pathological bone metabolic conditions. One such example of another pathological bone condition that the model can be used to study is rheumatoid arthritis that subsequently causes osteoporosis at the immediate subchondral bone and at joint margins near inflamed joints (Goldring and Gravallese 2000). Though this current femoral slice model removed the sites of high cartilage, the femoral head and the lateral and medial condyles, it can be adapted to retain this tissue to observe the effects of individual pro-inflammatory cytokines on the bone marrow, the mineral tissue and the chondrocytes. This would allow the pathological cartilage loss that typifies osteoarthritis, to be observed within a controlled environment. This model may also be adapted to assess bone mineralisation and subsequent pathological mineralisation using the pro-mineralisation supporting supplements of dexamethasone, b-glycerophosphate, prostaglandin E2 and vitamin D3 to maintain and differentiate between both the MSCs (that were retained in high abundance) and the osteoblasts (that were lost after 24 h) (Marino et al. 2014; Perpétuo et al. 2019).

With the addition of cytokines (M-CSF and RANKL) and micro-injected tibial bone marrow cells, the culture period was extended to 144 h to investigate if it was possible to prolonging the culture period. Results demonstrated an almost total loss of all cells within the femoral bone marrow cavity (Supplementary Figure 19) and it was concluded that this model, as is, couldn't be extended past the 48 h culture period. This is not unsurprising, Srinivasaiah et al. (2019) showed that *ex vivo* cultures of 300 µm femoral slices with intact and densely populated bone marrow cavity had very few bone marrow cells remaining after 7 days in culture. This implies that bone marrow cell loss within such *ex vivo* models is expected. This could be due to the bone marrow cavity experiencing high levels of apoptosis and necrosis directly after sectioning compromising their viability. Another explanation could be that there are high levels of mobilisation from cells outside of the bone marrow cavity, as it was evident that there was a migration of cells from the bone marrow into the agarose gel following culture. However, the exact processes of any possible cell mobilisation are currently untested in this model. Therefore, due to this rapid cell loss, the model culture period was limited to 48 h. This short culture period is one of the major limitations of this model where sufficient numbers of bone cells within the bone marrow could not be extended beyond 24 h. This 24 h culture period was nevertheless sufficient to observe the initial effects following bacterial infection and provides a basis to further refine and develop this model to extend the culture period beyond 24 h without significant loss of cells. The use of a 24 h culture period was broadly consistent with the findings of static models, where *ex vivo* bone tissues models tend to be viable for a maximum of 48 h (Abubakar et al. 2017). This is due to the highly mobile and dynamic cell population within the bone marrow, that is subjected to chemotaxis and mobilisation via chemokines and cytokines that are often increased following trauma. This is why *ex vivo* bone models limit their analysis on osteocytes, which are often easier to culture as they are protected within the mineral tissue and are non-motile, allowing for retention of these cells for prolonged culture periods (Bellido and Delgado-Calle 2020). This limited culture period for the femoral slice model contrasts with previous *ex vivo* models; the mandible slice model and the tooth slice model which could prolong the culture period up to 14-21 days. The tissue architecture for both models are vastly different due to the relationship of the dentine structure with the dental

pulp and the way they are anchored together which is not seen within the femoral bone marrow cavity (Sloan 2015; Sloan et al. 1998; Sloan et al. 2013; Smith et al. 2010).

Following the initial characterisation of the *ex vivo* model, *Staphylococcus aureus*, a known osteolytic species, was introduced to the model. The results indicated that the binding of the bacteria occurred within the bone marrow cavity to the ECM and bone marrow cells. One sample formed a large biofilm along the periosteum of the bone slice. This caused massive necrotic and apoptotic damage to cells adjacent to the bacterial populations and near bacterial virulence adhesion molecule Staphylococcus protein A. This demonstrates the potential of the model system to study biofilm attachment and subsequent cellular responses but wasn't observed in all cultures. The results presented in this Thesis did demonstrate that the model was able to instigate a possible innate immune response following infection, with an increase in pro-inflammatory cytokines TNFα, IL-1β and IL-6, which play key roles in osteoclastogenesis, and are all typically upregulated clinically in bacterial bone infections. However, this study did utilise bacterial type strains from the culture collections, NCTC 6571 and NCTC 7791. These type strains would behave differently than those isolated directly from patients, NCTC 6571 is a known reference strain susceptible to a variety of antibiotics (Seaman et al. 2004). NCTC 7791 was originally inoculated from an osteomyelitis patient, however, subsequent inoculation within culture plates would have caused evolutions and adaptations from its original inoculation. Typically, *in vivo*, the bacteria would have evolved mechanisms, adhesins and virulence factors to allow survival within a very hostile environment. Removing the species from that environment to a culture plate with nutrients readily available would have caused evolutions and loss of its mechanisms, adhesins and virulence factors that it originally needed to survive, making it a very different strain type from its original inoculation. The use of patient isolated bacterial species from infected implants would have provided a better option, as these bacterial species would have still had their defensive mechanisms upregulated and co-cultures of these species would provide a true representation of the methods used by the bacteria to evade and dysregulate the local bone marrow microenvironment.

The data obtained from this co-culture infection *ex vivo* model is promising, suggesting that a pro-inflammatory-like cytokine response can be modelled effectively following direct

infection, without infecting live animals and thus reducing ethical concerns. Further refinement to this model can be achieved by using bacterial conditioned media without bacterial species to observe the effect of virulence factor secreted by the bacteria on the local bone marrow populations, especially on, osteogenic differentiation, mineralisation and bone resorption. This model utilised heat-inactivated bacterial species and showed no pro-inflammatory and anti-inflammatory cytokine response, the process of heating to ~80 ^{o}C to damage the bacteria would have also subsequently damaged secreted virulence factors. Infection using non-Staphylococcal bacterial species, such as Streptococcus, Enterococcus, Propionibacterium, *Escherichia coli*, *P. aeruginosa*, *Serratia marcescens*, Proteus species, Klebsiella species, Acinetobacter, *Granulicatella advances*, *Finegoldia Magna, Cutibacterium acnes* and anaerobic species can provide novel insights of additional bacterial species, that are considered to be of low virulence within PJIs and osteomyelitis and observe their infective capabilities on the local immune cells. These species would be important to model, as currently with the use of antibiotics, their virulence is not considered to be a concern. With the age of antimicrobial resistance, these non-dominant players may become key players in orthopaedic bone infections.

One key aspect of PJI that this Thesis was unable to model, was the effect of implant-associated biofilms on the local bone marrow environment. One simple way that the model can be adapted to incorporate an implant biofilm would be the use of a small wire or disc made of orthopaedic implant material such as titanium alloys (Ti-6al-4v) or tantalum for the biofilm to attach and establish itself upon. This model could look at the effects of the presence of the biofilm on the local bone marrow microenvironment and bone remodelling unit. Additionally, the use of aged Wistar rats rather than young, 21-28-day-old rats could provide a different response following infection. Pietschmann et al. (2007) showed that aged 23-month-old, Sprague-Dawley rats had reduced cancellous bone mineral density, bone volume and trabecular number in the proximal tibia when compared to their 5-month-old counterparts. The authors demonstrated that osteoclast generation was reduced in aged rats and RANKL mRNA expression was also reduced. A future adaptation to this model could be to use different aged rats and provide mechanical load similar to the *in vitro* studies by Vazquez et al. (2014), to observe the role of biomechanics on the relationship of the bacteria, osteocytes, MSCs, lining cells and osteoblasts to induce matrix degradation and

osteolysis. Currently, the relationship between *S. aureus* and MSCs and their lineages in matrix metalloprotease (MMP) production is unknown. Thus, this model has the potential to investigate this MMP production along with other signalling cascades that can induce matrix degradation caused by host cell response following infection, especially since high numbers of MSCs were retained during culture.

Infected prosthetic joints are unresponsive to antibiotics mainly due to poor vascular supply and the formation of biofilms (Kuiper et al. 2013). Typical treatment for initial infections following surgery is irrigation and debridement of the implant site and the prostheses can be salvaged with oral antibiotics if the infection was caused by an avirulent microorganism (Azzam et al. 2010; Marculescu et al. 2006). Irrigation and debridement have an increased failure rate, with success varying in different studies due to various factors, including antibiotic treatment and durations, patient sample selection and microbiological findings (Azzam et al. 2010; Marculescu et al. 2006). Current surgical techniques include removal of the infected implant and replacement with a new implant and undergoing antibiotic treatment, termed one-stage exchange. An alternative option is the removal of the infected implant, which is replaced with a temporary antibiotic covered joint spacer, antibiotic treatment and then after a couple of weeks is given a new implant, termed a two-stage exchange (Zimmerli 2006). Success rates vary between 84 – 96 % total hip arthroplasty and 84 – 97 % of total knee arthroplasty and does not prevent recurrent infections (Aslam and Darouiche 2012). Therefore, there is a need for the development of novel antimicrobials. This model would allow potential therapeutic advancements such as understanding and developing bone cement that can exert antimicrobial properties, or analysing the effects of antimicrobial loaded exosomes or liposomes on bacterial infections, which currently is an exciting new avenue within bone research with a vast array of therapeutic potential (Anagnostakos 2017; Yang et al. 2018b). To study the antimicrobial properties of bone cement, the *ex vivo* model can be infected the same way as described in this Thesis for 12 h -24 h and then apply a novel bone cement loaded with antibiotics or an intermediatory carrier such as liposomes containing antibiotics to observe the numbers of bacterial populations directly after treatment and the effect on the local bone marrow to clear the pathogen effectively.

As discussed throughout this Thesis a major limitation of this model was subjecting the femoral tissue with increased trauma to form the semi-cylindrical femoral slices, compromising the viability of the local bone marrow cell population. An alternative to improve cell numbers is to not section the bone sagittally down the femoral shaft and form semi-cylindrical slices but instead form cylindrical femoral shaft discs. This method was initially tested preliminarily before the use of semi-cylindrical slices (Data not shown). Preliminary analysis of using femoral discs showed a loss of cells in the centre of the discs and a high density of cell numbers towards the edge of the disc. This suggested that nutrients were insufficient in penetrating through the bone marrow cavity causing a loss of cell viability or inducing a possible migration of cells towards areas of bone that had direct contact with the culture media. This is due to a lack of active transport to the centre of tissues, causing increased nutrients and oxygen to the surface of the tissue exposed to the culture media. The cells retained deep within the tissue which has lower nutrient and oxygen provided, thus forming nutrient and oxygen gradients (Brindley et al. 2011) which was why the semi-cylindrical slices were chosen over cylindrical slices for this model.

As mentioned previously, static *ex vivo* bone models tend to be viable for a maximum of 48 h, as shown within this Thesis (Abubakar et al. 2017). Although previous models using Trowell-type cultures have shown extended cultures for up to 7-21 days, this is wholly dependent on the structure of the tissue that is being modelled (Sloan and Smith 1999; Smith et al. 2010). If the structure is like the bone marrow which is highly motile this can be a challenge to retain for extended culture periods as demonstrated within this Thesis. Perfusion bioreactor systems are an attractive alternative for culturing bone tissues as the system can provide cells deep within the bone marrow with nutrients and allow adequate waste removal, which reduces the risk of nutrient and oxygen deficiency throughout the bone tissue and waste build-up (Cramer et al. 2021; Davidson et al. 2012). For future work on this model, perfusion bioreactor system should be used to improve cell maintenance and viability when compared to tissues cultured in non-perfused systems, by actively controlling the pH, temperature, nutrients and gases required by the bone marrow, along with improved cell culture media circulation (Abubakar et al. 2017; Swarup et al. 2018). The use of a rotating oxygen-diffusion system provides culture media directly to the tissue surface, which has demonstrated success in osteogenic studies in human, bovine and ovine tissue

models (Abubakar et al. 2017). This is due to the effects of fluid shear stress on improving the maintenance of osteoblasts and MSCs and their bone formation capabilities (Kreke et al. 2005; Mitra et al. 2017; Wang et al. 2003). As observed within this model, the addition of fluid into the bone marrow cavity impacted the cell metabolism of various immune cell populations, therefore any adaptations to this model must carefully consider the effects of such hydrodynamics on the local cellular environment.

The use of a perfusion bioreactor system has been typically used on bone core models that are devoid of any bone marrow, to keep osteoblasts and osteocytes viable for extensive culture periods (Chan et al. 2009; Davidson et al. 2012) any bone core models that try to retain bone marrow tend to be limited with previous studies showing culture periods at 3 h (Hu et al. 2015) or 12 h (Swarup et al. 2018). Therefore, the use of an *ex vivo* model that has been overly sectioned like the semi-cylindrical femoral slice used within this Thesis would be inappropriate. The addition of a fluid flow perfusion system on a tissue with the bone marrow overly exposed, would accelerate cell loss, as the bone marrow cells would leach out when culture media flows through the bone marrow cavity. To adapt the *ex vivo* bone model to minimise bone marrow exposure to the culture environment whilst keeping the bone marrow enclosed within the cortical bone and allowing waste products to be removed is a challenge. One possible adaptation for the future of this model would be to bisect the femur in half down the centre of the femoral shaft, with femoral head and lateral and medial condyles intact and embedding bisected femur in the agarose gel with the bone marrow exposed section of the slice facing upwards. Using this adapted tissue slice along with an enclosed perfusion bioreactor, the culture media could be directed through the vasculature of the femur via fluid flow using a peristaltic pump to circulate the tissue culture media through the tissue, in a similar method used by Swarup et al. (2018). This would allow the bone marrow to be retained within its own natural scaffold whilst having adequate nutrients and supplements provided through the blood vessels, thus potentially reducing the apoptosis and necrosis of the bone marrow cells as seen in this Thesis and potentially preserving the bone marrow cells beyond 48 h of culture.

Overall, this Thesis has demonstrated an *ex vivo* model system that can be used to investigate the relationship between bacterial species and the bone marrow

microenvironment within a controlled culture environment. The model was able to observe bacterial cellular adherence to the mineral tissue and ECM whilst initiating a pro-inflammatory immune response. This model was able to be manipulated and developed with the addition of pro-osteoclastic cytokines and additional bone marrow cells to investigate the cellular responses of these pro-osteoclastogenic factors on the local immune cell population. Although future work is needed to refine this model to minimise cell loss and improve the culture period. Together, this Thesis has provided an *ex vivo* model that has the potential to understand the processes involved during early orthopaedic infections and to develop and assess therapeutic interventions.

References

Abaci, H. E., Truitt, R., Luong, E., Drazer, G. and Gerecht, S. (2010). Adaptation to oxygen deprivation in cultures of human pluripotent stem cells, endothelial progenitor cells, and umbilical vein endothelial cells. *Am J Physiol Cell Physiol* **298:**C1527-1537.

Abubakar, A. A., Ibrahim, S. M., Ali, A. K., Handool, K. O., Khan, M. S., Noordin Mustapha, M., Azmi Ibrahim, T. *et al.* (2019). Postnatal ex vivo rat model for longitudinal bone growth investigations. *Animal Model Exp Med* **2:**34-43.

Abubakar, A. A., Noordin, M. M., Azmi, T. I., Kaka, U. and Loqman, M. Y. (2016). The use of rats and mice as animal models in ex vivo bone growth and development studies. *Bone Joint Res* **5:**610-618.

Abubakar, A. A., Noordin, M. M., Azmi, T. I., Kaka, U. and Loqman, M. Y. (2017). The use of rats and mice as animal models in ex vivo bone growth and development studies. *Bone & joint research* **5:**610-618.

Acar, M., Kocherlakota, K. S., Murphy, M. M., Peyer, J. G., Oguro, H., Inra, C. N., Jaiyeola, C. *et al.* (2015). Deep imaging of bone marrow shows non-dividing stem cells are mainly perisinusoidal. *Nature* **526:**126-130.

Accarias, S., Lugo-Villarino, G., Foucras, G., Neyrolles, O., Boullier, S. and Tabouret, G. (2015). Pyroptosis of resident macrophages differentially orchestrates inflammatory responses to Staphylococcus aureus in resistant and susceptible mice. *Eur J Immunol* **45:**794-806.

Adamopoulos, I. E. and Mellins, E. D. (2015). Alternative pathways of osteoclastogenesis in inflammatory arthritis. *Nat Rev Rheumatol* **11:**189-194.

Aggarwal, S., Ghilardi, N., Xie, M. H., de Sauvage, F. J. and Gurney, A. L. (2003). Interleukin-23 promotes a distinct CD4 T cell activation state characterized by the production of interleukin-17. *J Biol Chem* **278:**1910-1914.

Aghaloo, T. L., Chaichanasakul, T., Bezouglaia, O., Kang, B., Franco, R., Dry, S. M., Atti, E. *et al.* (2010). Osteogenic potential of mandibular vs. long-bone marrow stromal cells. *J Dent Res* **89:**1293-1298.

Agladze, K., Jackson, D. and Romeo, T. (2003). Periodicity of cell attachment patterns during Escherichia coli biofilm development. *J Bacteriol* **185:**5632-5638.

Al-Qtaitat, A. I. and Aldalaen, S. M. (2014). A review of non-collagenous proteins; their role in bone. *American Journal of Life Sciences* **2:**351-355.

Alonzo, F., 3rd, Kozhaya, L., Rawlings, S. A., Reyes-Robles, T., DuMont, A. L., Myszka, D. G., Landau, N. R. *et al.* (2013). CCR5 is a receptor for Staphylococcus aureus leukotoxin ED. *Nature* **493:**51-55.

Amanna, I. J., Carlson, N. E. and Slifka, M. K. (2007). Duration of humoral immunity to common viral and vaccine antigens. *N Engl J Med* **357:**1903-1915.

Amarasekara, D. S., Yun, H., Kim, S., Lee, N., Kim, H. and Rho, J. (2018). Regulation of Osteoclast Differentiation by Cytokine Networks. *Immune Netw* **18:**e8.

Anagnostakos, K. (2017). Therapeutic Use of Antibiotic-loaded Bone Cement in the Treatment of Hip and Knee Joint Infections. *J Bone Jt Infect* **2:**29-37.

Anagnostakos, K., Schmid, N. V., Kelm, J., Grun, U. and Jung, J. (2009). Classification of hip joint infections. *Int J Med Sci* **6:**227-233.

Arango Duque, G. and Descoteaux, A. (2014). Macrophage cytokines: involvement in immunity and infectious diseases. *Front Immunol* **5:**491.

Archer, N. K., Mazaitis, M. J., Costerton, J. W., Leid, J. G., Powers, M. E. and Shirtliff, M. E. (2011). Staphylococcus aureus biofilms: properties, regulation, and roles in human disease. *Virulence* **2:**445-459.

Arciola, C. R., Campoccia, D., Gamberini, S., Baldassarri, L. and Montanaro, L. (2005). Prevalence of cna, fnbA and fnbB adhesin genes among Staphylococcus aureus isolates from orthopedic infections associated to different types of implant. *FEMS Microbiol Lett* **246:**81-86.

Arciola, C. R., Visai, L., Testoni, F., Arciola, S., Campoccia, D., Speziale, P. and Montanaro, L. (2011). Concise survey of Staphylococcus aureus virulence factors that promote adhesion and damage to peri-implant tissues. *Int J Artif Organs* **34:**771-780.

Arden, N. and Betenbaugh, M. J. (2006). Regulating apoptosis in mammalian cell cultures. *Cytotechnology* **50:**77-92.

Ardestani, S., Li, B., Deskins, D. L., Wu, H., Massion, P. P. and Young, P. P. (2013). Membrane versus soluble isoforms of TNF-alpha exert opposing effects on tumor growth and survival of tumor-associated myeloid cells. *Cancer Res* **73:**3938-3950.

Aslam, S. and Darouiche, R. O. (2012). Prosthetic joint infections. *Curr Infect Dis Rep* **14:**551-557.

Athanasou, N. A. (2011). The osteoclast--what's new? *Skeletal Radiol* **40:**1137-1140.

Auffray, C., Sieweke, M. H. and Geissmann, F. (2009). Blood monocytes: development, heterogeneity, and relationship with dendritic cells. *Annu Rev Immunol* **27:**669-692.

Aujla, S. J., Dubin, P. J. and Kolls, J. K. (2007). Th17 cells and mucosal host defense. *Semin Immunol* **19:**377-382.

Avery, S. J., Ayre, W. N., Sloan, A. J. and Waddington, R. J. (2020). Interrogating the Osteogenic Potential of Implant Surfaces In Vitro: A Review of Current Assays. *Tissue Eng Part B Rev* **26:**217-229.

Axmann, R., Bohm, C., Kronke, G., Zwerina, J., Smolen, J. and Schett, G. (2009). Inhibition of interleukin-6 receptor directly blocks osteoclast formation in vitro and in vivo. *Arthritis Rheum* **60:**2747-2756.

Azzam, K. A., Seeley, M., Ghanem, E., Austin, M. S., Purtill, J. J. and Parvizi, J. (2010). Irrigation and debridement in the management of prosthetic joint infection: traditional indications revisited. *J Arthroplasty* **25:**1022-1027.

Bancroft, G. N., Sikavitsas, V. I., van den Dolder, J., Sheffield, T. L., Ambrose, C. G., Jansen, J. A. and Mikos, A. G. (2002). Fluid flow increases mineralized matrix deposition in 3D perfusion culture of marrow stromal osteoblasts in a dose-dependent manner. *Proc Natl Acad Sci U S A* **99:**12600-12605.

Barnes, T. C., Anderson, M. E. and Moots, R. J. (2011). The many faces of interleukin-6: the role of IL-6 in inflammation, vasculopathy, and fibrosis in systemic sclerosis. *Int J Rheumatol* **2011:**721608.

Bassler, B. L. and Losick, R. (2006). Bacterially speaking. *Cell* **125:**237-246.

Bauer, T. W., Bedair, H., Creech, J. D., Deirmengian, C., Eriksson, H., Fillingham, Y., Grigoryan, G. *et al.* (2019). Hip and Knee Section, Diagnosis, Laboratory Tests: Proceedings of International Consensus on Orthopedic Infections. *J Arthroplasty* **34:**S351-S359.

Becerra, S. C., Roy, D. C., Sanchez, C. J., Christy, R. J. and Burmeister, D. M. (2016). An optimized staining technique for the detection of Gram positive and Gram negative bacteria within tissue. *BMC Res Notes* **9:**216.

Beck-Nielsen, S. S., Mughal, Z., Haffner, D., Nilsson, O., Levtchenko, E., Ariceta, G., de Lucas Collantes, C. *et al.* (2019). FGF23 and its role in X-linked hypophosphatemia-related morbidity. *Orphanet J Rare Dis* **14:**58.

Becker, P., Hufnagle, W., Peters, G. and Herrmann, M. (2001). Detection of differential gene expression in biofilm-forming versus planktonic populations of Staphylococcus aureus using micro-representational-difference analysis. *Appl Environ Microbiol* **67:**2958-2965.

Belaaouaj, A., McCarthy, R., Baumann, M., Gao, Z., Ley, T. J., Abraham, S. N. and Shapiro, S. D. (1998). Mice lacking neutrophil elastase reveal impaired host defense against gram negative bacterial sepsis. *Nat Med* **4:**615-618.

Belge, K. U., Dayyani, F., Horelt, A., Siedlar, M., Frankenberger, M., Frankenberger, B., Espevik, T. *et al.* (2002). The proinflammatory CD14+CD16+DR++ monocytes are a major source of TNF. *J Immunol* **168:**3536-3542.

Bellido, T. and Delgado-Calle, J. (2020). Ex Vivo Organ Cultures as Models to Study Bone Biology. *JBMR Plus* **4**.

Bemer, P., Plouzeau, C., Tande, D., Leger, J., Giraudeau, B., Valentin, A. S., Jolivet-Gougeon, A. *et al.* (2014). Evaluation of 16S rRNA gene PCR sensitivity and specificity for diagnosis of prosthetic joint infection: a prospective multicenter cross-sectional study. *J Clin Microbiol* **52:**3583-3589.

Ben David, D., Reznick, A. Z., Srouji, S. and Livne, E. (2008). Exposure to pro-inflammatory cytokines upregulates MMP-9 synthesis by mesenchymal stem cells-derived osteoprogenitors. *Histochem Cell Biol* **129:**589-597.

Bennett, S. R., Carbone, F. R., Karamalis, F., Miller, J. F. and Heath, W. R. (1997). Induction of a CD8+ cytotoxic T lymphocyte response by cross-priming requires cognate CD4+ T cell help. *J Exp Med* **186:**65-70.

Bergsbaken, T., Fink, S. L. and Cookson, B. T. (2009). Pyroptosis: host cell death and inflammation. *Nat Rev Microbiol* **7:**99-109.

Bernthal, N. M., Pribaz, J. R., Stavrakis, A. I., Billi, F., Cho, J. S., Ramos, R. I., Francis, K. P. *et al.* (2011). Protective role of IL-1beta against post-arthroplasty Staphylococcus aureus infection. *J Orthop Res* **29:**1621-1626.

Bernthal, N. M., Stavrakis, A. I., Billi, F., Cho, J. S., Kremen, T. J., Simon, S. I., Cheung, A. L. *et al.* (2010). A mouse model of post-arthroplasty Staphylococcus aureus joint infection to evaluate in vivo the efficacy of antimicrobial implant coatings. *PLoS One* **5:**e12580.

Bertani, F. R., Mozetic, P., Fioramonti, M., Iuliani, M., Ribelli, G., Pantano, F., Santini, D. *et al.* (2017). Classification of M1/M2-polarized human macrophages by label-free hyperspectral reflectance confocal microscopy and multivariate analysis. *Sci Rep* **7:**8965.

Bestebroer, J., Poppelier, M. J., Ulfman, L. H., Lenting, P. J., Denis, C. V., van Kessel, K. P., van Strijp, J. A. *et al.* (2007). Staphylococcal superantigen-like 5 binds PSGL-1 and inhibits P-selectin-mediated neutrophil rolling. *Blood* **109:**2936-2943.

Beyth, S., Borovsky, Z., Mevorach, D., Liebergall, M., Gazit, Z., Aslan, H., Galun, E. *et al.* (2005). Human mesenchymal stem cells alter antigen-presenting cell maturation and induce T-cell unresponsiveness. *Blood* **105:**2214-2219.

Bhatia, R., Dent, C., Topley, N. and Pallister, I. (2006). Neutrophil priming for elastase release in adult blunt trauma patients. *J Trauma* **60:**590-596.

Bingham, J., Clarke, H., Spangehl, M., Schwartz, A., Beauchamp, C. and Goldberg, B. (2014). The alpha defensin-1 biomarker assay can be used to evaluate the potentially infected total joint arthroplasty. *Clin Orthop Relat Res* **472:**4006-4009.

Birmingham, E., Kreipke, T. C., Dolan, E. B., Coughlin, T. R., Owens, P., McNamara, L. M., Niebur, G. L. *et al.* (2015). Mechanical stimulation of bone marrow in situ induces bone formation in trabecular explants. *Ann Biomed Eng* **43:**1036-1050.

Birmingham, E., Niebur, G. L., McNamara, L. M. and McHugh, P. E. (2016). An Experimental and Computational Investigation of Bone Formation in Mechanically Loaded Trabecular Bone Explants. *Ann Biomed Eng* **44:**1191-1203.

Birt, M. C., Anderson, D. W., Bruce Toby, E. and Wang, J. (2017). Osteomyelitis: Recent advances in pathophysiology and therapeutic strategies. *J Orthop* **14:**45-52.

Block, D. R. and Genzen, J. R. (2020). Diagnostic body fluid testing. In: Clarke, W. and Marzinke, M.A. (eds.) *Contemporary Practice in Clinical Chemistry*. Academic Press, pp. 469-486.

Bodelon, G., Montes-Garcia, V., Lopez-Puente, V., Hill, E. H., Hamon, C., Sanz-Ortiz, M. N., Rodal-Cedeira, S. *et al.* (2016). Detection and imaging of quorum sensing in Pseudomonas aeruginosa biofilm communities by surface-enhanced resonance Raman scattering. *Nat Mater* **15:**1203-1211.

Bonewald, L. F. and Johnson, M. L. (2008). Osteocytes, mechanosensing and Wnt signaling. *Bone* **42:**606-615.

Bosco, M. C., Puppo, M., Blengio, F., Fraone, T., Cappello, P., Giovarelli, M. and Varesio, L. (2008). Monocytes and dendritic cells in a hypoxic environment: Spotlights on chemotaxis and migration. *Immunobiology* **213:**733-749.

Boskey, A. L. (2013). Bone composition: relationship to bone fragility and antiosteoporotic drug effects. *Bonekey Rep* **2:**447.

Bosse, M. J., Gruber, H. E. and Ramp, W. K. (2005). Internalization of bacteria by osteoblasts in a patient with recurrent, long-term osteomyelitis. A case report. *J Bone Joint Surg Am* **87:**1343-1347.

Bost, K. L., Ramp, W. K., Nicholson, N. C., Bento, J. L., Marriott, I. and Hudson, M. C. (1999). Staphylococcus aureus infection of mouse or human osteoblasts induces high levels of interleukin-6 and interleukin-12 production. *J Infect Dis* **180:**1912-1920.

Bottner, F., Wegner, A., Winkelmann, W., Becker, K., Erren, M. and Gotze, C. (2007). Interleukin-6, procalcitonin and TNF-alpha: markers of peri-prosthetic infection following total joint replacement. *J Bone Joint Surg Br* **89:**94-99.

Boulais, P. E. and Frenette, P. S. (2015). Making sense of hematopoietic stem cell niches. *Blood* **125:**2621-2629.

Box, G. E. P. (1976). Science and Statistics. *Journal of the American Statistical Association* **71:**791-799.

Boyce, B. F. and Xing, L. (2007). Biology of RANK, RANKL, and osteoprotegerin. *Arthritis Res Ther* **9 Suppl 1:**S1.

Boyce, B. F. and Xing, L. (2008). Functions of RANKL/RANK/OPG in bone modeling and remodeling. *Arch Biochem Biophys* **473:**139-146.

Boyle, W. J., Simonet, W. S. and Lacey, D. L. (2003). Osteoclast differentiation and activation. *Nature* **423:**337-342.

Brindley, D., Moorthy, K., Lee, J. H., Mason, C., Kim, H. W. and Wall, I. (2011). Bioprocess forces and their impact on cell behavior: implications for bone regeneration therapy. *J Tissue Eng* **2011:**620247.

Bringhurst, F. R. and Potts, J. T., Jr. (1981). Bone collagen synthesis in vitro: structure/activity relations among parathyroid hormone fragments and analogs. *Endocrinology* **108:**103-108.

Brinkmann, V., Reichard, U., Goosmann, C., Fauler, B., Uhlemann, Y., Weiss, D. S., Weinrauch, Y. *et al.* (2004). Neutrophil extracellular traps kill bacteria. *Science* **303:**1532-1535.

Brocker, C., Thompson, D., Matsumoto, A., Nebert, D. W. and Vasiliou, V. (2010). Evolutionary divergence and functions of the human interleukin (IL) gene family. *Hum Genomics* **5:**30-55.

Brouillette, E., Grondin, G., Shkreta, L., Lacasse, P. and Talbot, B. G. (2003). In vivo and in vitro demonstration that Staphylococcus aureus is an intracellular pathogen in the presence or absence of fibronectin-binding proteins. *Microbial pathogenesis* **35:**159-168.

Bucay, N., Sarosi, I., Dunstan, C. R., Morony, S., Tarpley, J., Capparelli, C., Scully, S. *et al.* (1998). osteoprotegerin-deficient mice develop early onset osteoporosis and arterial calcification. *Genes Dev* **12:**1260-1268.

Burr, D. B. and Akkus, O. (2014). Bone Morphology and Organization. In: Allen, D.B.B.R. (ed.) *Basic and Applied Bone Biology*. San Diego: Academic Press, pp. 3-25.

Calvi, L. M. and Link, D. C. (2015). The hematopoietic stem cell niche in homeostasis and disease. *Blood* **126:**2443-2451.

Cao, F., Zhou, W., Liu, G., Xia, T., Liu, M., Mi, B. and Liu, Y. (2017). Staphylococcus aureus peptidoglycan promotes osteoclastogenesis via TLR2-mediated activation of the NF-kappaB/NFATc1 signaling pathway. *Am J Transl Res* **9:**5022-5030.

Carli, A. V., Ross, F. P., Bhimani, S. J., Nodzo, S. R. and Bostrom, M. P. (2016). Developing a Clinically Representative Model of Periprosthetic Joint Infection. *J Bone Joint Surg Am* **98:**1666-1676.

Chagin, A. S., Karimian, E., Sundstrom, K., Eriksson, E. and Savendahl, L. (2010). Catch-up growth after dexamethasone withdrawal occurs in cultured postnatal rat metatarsal bones. *J Endocrinol* **204:**21-29.

Chaichanasakul, T., Kang, B., Bezouglaia, O., Aghaloo, T. L. and Tetradis, S. (2014). Diverse osteoclastogenesis of bone marrow from mandible versus long bone. *J Periodontol* **85:**829-836.

Chan, F. K., Moriwaki, K. and De Rosa, M. J. (2013). Detection of necrosis by release of lactate dehydrogenase activity. *Methods Mol Biol* **979:**65-70.

Chan, M. E., Lu, X. L., Huo, B., Baik, A. D., Chiang, V., Guldberg, R. E., Lu, H. H. *et al.* (2009). A Trabecular Bone Explant Model of Osteocyte-Osteoblast Co-Culture for Bone Mechanobiology. *Cell Mol Bioeng* **2:**405-415.

Chang, M. K., Raggatt, L. J., Alexander, K. A., Kuliwaba, J. S., Fazzalari, N. L., Schroder, K., Maylin, E. R. *et al.* (2008). Osteal tissue macrophages are intercalated throughout human and mouse bone lining tissues and regulate osteoblast function in vitro and in vivo. *J Immunol* **181:**1232-1244.

Chaplin, D. D. (2010). Overview of the immune response. *J Allergy Clin Immunol* **125:**S3-23.

Charles, J. F. and Nakamura, M. C. (2014). Bone and the innate immune system. *Curr Osteoporos Rep* **12:**1-8.

Chau, T. A., McCully, M. L., Brintnell, W., An, G., Kasper, K. J., Vines, E. D., Kubes, P. *et al.* (2009). Toll-like receptor 2 ligands on the staphylococcal cell wall downregulate superantigen-induced T cell activation and prevent toxic shock syndrome. *Nat Med* **15:**641-648.

Chen, G., Deng, C. and Li, Y. P. (2012). TGF-beta and BMP signaling in osteoblast differentiation and bone formation. *Int J Biol Sci* **8:**272-288.

Chen, L., Wei, X. Q., Evans, B., Jiang, W. and Aeschlimann, D. (2008). IL-23 promotes osteoclast formation by up-regulation of receptor activator of NF-kappaB (RANK) expression in myeloid precursor cells. *Eur J Immunol* **38:**2845-2854.

Cheng, M. Z., Zaman, G. and Lanyon, L. E. (1994). Estrogen enhances the stimulation of bone collagen synthesis by loading and exogenous prostacyclin, but not prostaglandin E2, in organ cultures of rat ulnae. *J Bone Miner Res* **9:**805-816.

Chiang, C. Y., Kyritsis, G., Graves, D. T. and Amar, S. (1999). Interleukin-1 and tumor necrosis factor activities partially account for calvarial bone resorption induced by local injection of lipopolysaccharide. *Infect Immun* **67:**4231-4236.

Choy, M. H. V., Wong, R. M. Y., Chow, S. K. H., Li, M. C., Chim, Y. N., Li, T. K., Ho, W. T. *et al.* (2020). How much do we know about the role of osteocytes in different phases of fracture healing? A systematic review. *J Orthop Translat* **21:**111-121.

Clarke, B. (2008). Normal bone anatomy and physiology. *Clin J Am Soc Nephrol* **3 Suppl 3:**S131-139.

Claro, T., Widaa, A., O'Seaghdha, M., Miajlovic, H., Foster, T. J., O'Brien, F. J. and Kerrigan, S. W. (2011). Staphylococcus aureus protein A binds to osteoblasts and triggers signals that weaken bone in osteomyelitis. *PLoS One* **6:**e18748.

Clines, G. A., Mohammad, K. S., Bao, Y., Stephens, O. W., Suva, L. J., Shaughnessy, J. D., Jr., Fox, J. W. *et al.* (2007). Dickkopf homolog 1 mediates endothelin-1-stimulated new bone formation. *Mol Endocrinol* **21:**486-498.

Cogen, A. L., Nizet, V. and Gallo, R. L. (2008). Skin microbiota: a source of disease or defence? *Br J Dermatol* **158:**442-455.

Colombo, J. S., Howard-Jones, R. A., Young, F. I., Waddington, R. J., Errington, R. J. and Sloan, A. J. (2015). A 3D ex vivo mandible slice system for longitudinal culturing of transplanted dental pulp progenitor cells. *Cytometry A* **87:**921-928.

Colotta, F., Re, F., Muzio, M., Bertini, R., Polentarutti, N., Sironi, M., Giri, J. G. *et al.* (1993). Interleukin-1 type II receptor: a decoy target for IL-1 that is regulated by IL-4. *Science* **261:**472-475.

Compton, J. T. and Lee, F. Y. (2014). A review of osteocyte function and the emerging importance of sclerostin. *J Bone Joint Surg Am* **96:**1659-1668.

Cosgrove, K., Coutts, G., Jonsson, I. M., Tarkowski, A., Kokai-Kun, J. F., Mond, J. J. and Foster, S. J. (2007). Catalase (KatA) and alkyl hydroperoxide reductase (AhpC) have compensatory roles in peroxide stress resistance and are required for survival, persistence, and nasal colonization in Staphylococcus aureus. *J Bacteriol* **189:**1025-1035.

Costa, A. G., Cremers, S., Rubin, M. R., McMahon, D. J., Sliney, J., Jr., Lazaretti-Castro, M., Silverberg, S. J. *et al.* (2011). Circulating sclerostin in disorders of parathyroid gland function. *J Clin Endocrinol Metab* **96:**3804-3810.

Costa-Rodrigues, J., Fernandes, A. and Fernandes, M. H. (2011). Spontaneous and induced osteoclastogenic behaviour of human peripheral blood mononuclear cells and their CD14(+) and CD14(-) cell fractions. *Cell Prolif* **44:**410-419.

Couper, K. N., Blount, D. G. and Riley, E. M. (2008). IL-10: the master regulator of immunity to infection. *J Immunol* **180:**5771-5777.

Cracknell, R. (2010). The ageing population: key issues for 2010 parliament [Online]. London UK: House of Commons Parliament. Available at: http://www.parliament.uk/documents/commons/lib/research/key_issues/Key-Issues-The-ageing-population2007.pdf [Accessed: 9th April].

Craig, M. R., Poelstra, K. A., Sherrell, J. C., Kwon, M. S., Belzile, E. L. and Brown, T. E. (2005). A novel total knee arthroplasty infection model in rabbits. *J Orthop Res* **23:**1100-1104.

Cramer, E. E. A., Ito, K. and Hofmann, S. (2021). Ex vivo Bone Models and Their Potential in Preclinical Evaluation. *Curr Osteoporos Rep* **19:**75-87.

Crane, G. M., Jeffery, E. and Morrison, S. J. (2017). Adult haematopoietic stem cell niches. *Nat Rev Immunol* **17:**573-590.

Currey, J. D. (2011). The structure and mechanics of bone. *Journal of Materials Science* **47:**41-54.

Curtin, P., Youm, H. and Salih, E. (2012). Three-dimensional cancer-bone metastasis model using ex-vivo co-cultures of live calvarial bones and cancer cells. *Biomaterials* **33:**1065-1078.

Dallas, S. L., Zaman, G., Pead, M. J. and Lanyon, L. E. (1993). Early strain-related changes in cultured embryonic chick tibiotarsi parallel those associated with adaptive modeling in vivo. *J Bone Miner Res* **8:**251-259.

Dapunt, U., Hansch, G. M. and Arciola, C. R. (2016). Innate Immune Response in Implant-Associated Infections: Neutrophils against Biofilms. *Materials (Basel)* **9:**387.

David, V., Guignandon, A., Martin, A., Malaval, L., Lafage-Proust, M. H., Rattner, A., Mann, V. *et al.* (2008). Ex Vivo bone formation in bovine trabecular bone cultured in a dynamic 3D bioreactor is enhanced by compressive mechanical strain. *Tissue Eng Part A* **14:**117-126.

Davidson, D. J., Spratt, D. and Liddle, A. D. (2019). Implant materials and prosthetic joint infection: the battle with the biofilm. *EFORT Open Rev* **4:**633-639.

Davidson, E. H., Reformat, D. D., Allori, A., Canizares, O., Janelle Wagner, I., Saadeh, P. B. and Warren, S. M. (2012). Flow perfusion maintains ex vivo bone viability: a novel model for bone biology research. *J Tissue Eng Regen Med* **6:**769-776.

Davies, C. M., Jones, D. B., Stoddart, M. J., Koller, K., Smith, E., Archer, C. W. and Richards, R. G. (2006). Mechanically loaded ex vivo bone culture system 'Zetos': systems and culture preparation. *Eur Cell Mater* **11:**57-75; discussion 75.

Davies, R. and Choy, E. (2014). Clinical experience of IL-6 blockade in rheumatic diseases - implications on IL-6 biology and disease pathogenesis. *Semin Immunol* **26:**97-104.

Dayer, J. M. and Choy, E. (2010). Therapeutic targets in rheumatoid arthritis: the interleukin-6 receptor. *Rheumatology (Oxford)* **49:**15-24.

De Benedetti, F., Rucci, N., Del Fattore, A., Peruzzi, B., Paro, R., Longo, M., Vivarelli, M. *et al.* (2006). Impaired skeletal development in interleukin-6-transgenic mice: a model for the impact of chronic inflammation on the growing skeletal system. *Arthritis Rheum* **54:**3551-3563.

De Filippo, K., Dudeck, A., Hasenberg, M., Nye, E., van Rooijen, N., Hartmann, K., Gunzer, M. *et al.* (2013). Mast cell and macrophage chemokines CXCL1/CXCL2 control the early stage of neutrophil recruitment during tissue inflammation. *Blood* **121:**4930-4937.

de Haas, C. J., Veldkamp, K. E., Peschel, A., Weerkamp, F., Van Wamel, W. J., Heezius, E. C., Poppelier, M. J. *et al.* (2004). Chemotaxis inhibitory protein of Staphylococcus aureus, a bacterial antiinflammatory agent. *J Exp Med* **199:**687-695.

de Mesy Bentley, K. L., Trombetta, R., Nishitani, K., Bello-Irizarry, S. N., Ninomiya, M., Zhang, L., Chung, H. L. *et al.* (2017). Evidence of Staphylococcus Aureus Deformation, Proliferation, and Migration in Canaliculi of Live Cortical Bone in Murine Models of Osteomyelitis. *J Bone Miner Res* **32:**985-990.

Deirmengian, C., Hallab, N., Tarabishy, A., Della Valle, C., Jacobs, J. J., Lonner, J. and Booth, R. E., Jr. (2010). Synovial fluid biomarkers for periprosthetic infection. *Clin Orthop Relat Res* **468:**2017-2023.

Deirmengian, C., Kardos, K., Kilmartin, P., Cameron, A., Schiller, K. and Parvizi, J. (2014a). Combined measurement of synovial fluid alpha-Defensin and C-reactive protein levels: highly accurate for diagnosing periprosthetic joint infection. *J Bone Joint Surg Am* **96:**1439-1445.

Deirmengian, C., Kardos, K., Kilmartin, P., Cameron, A., Schiller, K. and Parvizi, J. (2014b). Diagnosing periprosthetic joint infection: has the era of the biomarker arrived? *Clin Orthop Relat Res* **472:**3254-3262.

Del Arco, A. and Bertrand, M. L. (2013). The diagnosis of periprosthetic infection. *Open Orthop J* **7:**178-183.

Dempsey, K. E., Riggio, M. P., Lennon, A., Hannah, V. E., Ramage, G., Allan, D. and Bagg, J. (2007). Identification of bacteria on the surface of clinically infected and non-infected

prosthetic hip joints removed during revision arthroplasties by 16S rRNA gene sequencing and by microbiological culture. *Arthritis Res Ther* **9:**R46.

Deng, B., Jiang, H., Zeng, K., Liang, Y., Wu, Y. and Yang, Y. (2017). Removal from adherent culture contributes to apoptosis in human bone marrow mesenchymal stem cells. *Mol Med Rep* **15:**3499-3506.

Di Cesare, P. E., Chang, E., Preston, C. F. and Liu, C. J. (2005). Serum interleukin-6 as a marker of periprosthetic infection following total hip and knee arthroplasty. *J Bone Joint Surg Am* **87:**1921-1927.

Ding, J., Ghali, O., Lencel, P., Broux, O., Chauveau, C., Devedjian, J. C., Hardouin, P. *et al.* (2009). TNF-alpha and IL-1beta inhibit RUNX2 and collagen expression but increase alkaline phosphatase activity and mineralization in human mesenchymal stem cells. *Life Sci* **84:**499-504.

Dobie, K., Smith, G., Sloan, A. J. and Smith, A. J. (2002). Effects of alginate hydrogels and TGF-beta 1 on human dental pulp repair in vitro. *Connect Tissue Res* **43:**387-390.

Dolka, I., Krol, M. and Sapierzynski, R. (2016). Evaluation of apoptosis-associated protein (Bcl-2, Bax, cleaved caspase-3 and p53) expression in canine mammary tumors: An immunohistochemical and prognostic study. *Res Vet Sci* **105:**124-133.

Dominici, M., Le Blanc, K., Mueller, I., Slaper-Cortenbach, I., Marini, F., Krause, D., Deans, R. *et al.* (2006). Minimal criteria for defining multipotent mesenchymal stromal cells. The International Society for Cellular Therapy position statement. *Cytotherapy* **8:**315-317.

Donlan, R. M. (2002). Biofilms: microbial life on surfaces. *Emerg Infect Dis* **8:**881-890.

Dougall, W. C., Glaccum, M., Charrier, K., Rohrbach, K., Brasel, K., De Smedt, T., Daro, E. *et al.* (1999). RANK is essential for osteoclast and lymph node development. *Genes Dev* **13:**2412-2424.

Duplomb, L., Baud'huin, M., Charrier, C., Berreur, M., Trichet, V., Blanchard, F. and Heymann, D. (2008). Interleukin-6 inhibits receptor activator of nuclear factor kappaB ligand-induced osteoclastogenesis by diverting cells into the macrophage lineage: key role of Serine727 phosphorylation of signal transducer and activator of transcription 3. *Endocrinology* **149:**3688-3697.

Eash, K. J., Greenbaum, A. M., Gopalan, P. K. and Link, D. C. (2010). CXCR2 and CXCR4 antagonistically regulate neutrophil trafficking from murine bone marrow. *J Clin Invest* **120:**2423-2431.

Ehnert, S., Rinderknecht, H., Aspera-Werz, R. H., Haussling, V. and Nussler, A. K. (2020). Use of in vitro bone models to screen for altered bone metabolism, osteopathies, and fracture healing: challenges of complex models. *Arch Toxicol* **94:**3937-3958.

el Haj, A. J., Minter, S. L., Rawlinson, S. C., Suswillo, R. and Lanyon, L. E. (1990). Cellular responses to mechanical loading in vitro. *J Bone Miner Res* **5:**923-932.

Elgeidi, A., Elganainy, A. E., Abou Elkhier, N. and Rakha, S. (2014). Interleukin-6 and other inflammatory markers in diagnosis of periprosthetic joint infection. *Int Orthop* **38:**2591-2595.

Eliasson, P., Rehn, M., Hammar, P., Larsson, P., Sirenko, O., Flippin, L. A., Cammenga, J. *et al.* (2010). Hypoxia mediates low cell-cycle activity and increases the proportion of long-term-reconstituting hematopoietic stem cells during in vitro culture. *Exp Hematol* **38:**301-310 e302.

Elson, K. M., Fox, N., Tipper, J. L., Kirkham, J., Hall, R. M., Fisher, J. and Ingham, E. (2015). Non-destructive monitoring of viability in an ex vivo organ culture model of osteochondral tissue. *Eur Cell Mater* **29:**356-369; discussion 369.

Endres, S., Kratz, M., Wunsch, S. and Jones, D. B. (2009). Zetos: a culture loading system for trabecular bone. Investigation of different loading signal intensities on bovine bone cylinders. *J Musculoskelet Neuronal Interact* **9:**173-183.

Erices, A., Conget, P., Rojas, C. and Minguell, J. J. (2002). Gp130 activation by soluble interleukin-6 receptor/interleukin-6 enhances osteoblastic differentiation of human bone marrow-derived mesenchymal stem cells. *Exp Cell Res* **280:**24-32.

Eriksen, E. F. (2010). Cellular mechanisms of bone remodeling. *Rev Endocr Metab Disord* **11:**219-227.

Falugi, F., Kim, H. K., Missiakas, D. M. and Schneewind, O. (2013). Role of protein A in the evasion of host adaptive immune responses by Staphylococcus aureus. *mBio* **4:**e00575-00513.

Farges, J. C., Romeas, A., Melin, M., Pin, J. J., Lebecque, S., Lucchini, M., Bleicher, F. *et al.* (2003). TGF-beta1 induces accumulation of dendritic cells in the odontoblast layer. *J Dent Res* **82:**652-656.

Feng, W., Liu, H., Luo, T., Liu, D., Du, J., Sun, J., Wang, W. *et al.* (2017). Combination of IL-6 and sIL-6R differentially regulate varying levels of RANKL-induced osteoclastogenesis through NF-kappaB, ERK and JNK signaling pathways. *Sci Rep* **7:**41411.

Ferraro, F., Celso, C. L. and Scadden, D. (2010). Adult stem cels and their niches. *Adv Exp Med Biol* **695:**155-168.

Fingerle, G., Pforte, A., Passlick, B., Blumenstein, M., Strobel, M. and Zieglerheitbrock, H. W. L. (1993). The Novel Subset of Cd14+/Cd16+ Blood Monocytes Is Expanded in Sepsis Patients. *Blood* **82:**3170-3176.

Fink, B., Gebhard, A., Fuerst, M., Berger, I. and Schafer, P. (2013). High diagnostic value of synovial biopsy in periprosthetic joint infection of the hip. *Clin Orthop Relat Res* **471:**956-964.

Fink, S. L. and Cookson, B. T. (2005). Apoptosis, pyroptosis, and necrosis: mechanistic description of dead and dying eukaryotic cells. *Infect Immun* **73:**1907-1916.

Flemming, H. C. and Wingender, J. (2010). The biofilm matrix. *Nat Rev Microbiol* **8:**623-633.

Flemming, H. C., Wingender, J., Szewzyk, U., Steinberg, P., Rice, S. A. and Kjelleberg, S. (2016). Biofilms: an emergent form of bacterial life. *Nat Rev Microbiol* **14:**563-575.

Flurin, L., Greenwood-Quaintance, K. E. and Patel, R. (2019). Microbiology of polymicrobial prosthetic joint infection. *Diagn Microbiol Infect Dis* **94:**255-259.

Foster, T. J. (2004). The Staphylococcus aureus "superbug". *J Clin Invest* **114:**1693-1696.

Foster, T. J. (2016). The remarkably multifunctional fibronectin binding proteins of Staphylococcus aureus. *Eur J Clin Microbiol Infect Dis* **35:**1923-1931.

Foster, T. J., Geoghegan, J. A., Ganesh, V. K. and Hook, M. (2014). Adhesion, invasion and evasion: the many functions of the surface proteins of Staphylococcus aureus. *Nat Rev Microbiol* **12:**49-62.

Franceschi, R. T., Xiao, G., Jiang, D., Gopalakrishnan, R., Yang, S. and Reith, E. (2003). Multiple signaling pathways converge on the Cbfa1/Runx2 transcription factor to regulate osteoblast differentiation. *Connect Tissue Res* **44 Suppl 1:**109-116.

Franchimont, N., Lambert, C., Huynen, P., Ribbens, C., Relic, B., Chariot, A., Bours, V. *et al.* (2005). Interleukin-6 receptor shedding is enhanced by interleukin-1beta and tumor necrosis factor alpha and is partially mediated by tumor necrosis factor alpha-converting enzyme in osteoblast-like cells. *Arthritis Rheum* **52:**84-93.

Fratzl, P., Gupta, H. S., Paschalis, E. P. and Roschger, P. (2004). Structure and mechanical quality of the collagen–mineral nano-composite in bone. *J. Mater. Chem.* **14:**2115-2123.

Frodermann, V., Chau, T. A., Sayedyahossein, S., Toth, J. M., Heinrichs, D. E. and Madrenas, J. (2011). A modulatory interleukin-10 response to staphylococcal peptidoglycan prevents Th1/Th17 adaptive immunity to Staphylococcus aureus. *J Infect Dis* **204:**253-262.

Froschen, F. S., Schell, S., Schildberg, F. A., Klausing, A., Kohlhof, H., Gravius, S. and Randau, T. M. (2020). Analysis of synovial biomarkers with a multiplex protein microarray in patients with PJI undergoing revision arthroplasty of the hip or knee joint. *Arch Orthop Trauma Surg* **140:**1883-1890.

Fuchs, T. A., Abed, U., Goosmann, C., Hurwitz, R., Schulze, I., Wahn, V., Weinrauch, Y. *et al.* (2007). Novel cell death program leads to neutrophil extracellular traps. *J Cell Biol* **176:**231-241.

Gaida, M. M., Mayer, B., Stegmaier, S., Schirmacher, P., Wagner, C. and Hänsch, G. M. (2012). Polymorphonuclear Neutrophils in Osteomyelitis: Link to Osteoclast Generation and Bone Resorption. *European Journal of Inflammation* **10:**413-426.

Gaine, W., Ramamohan, N., Hussein, N., Hullin, M. and McCreath, S. (2000a). Wound infection in hip and knee arthroplasty. *Bone & Joint Journal* **82:**561-565.

Gaine, W. J., Ramamohan, N. A., Hussein, N. A., Hullin, M. G. and McCreath, S. W. (2000b). Wound infection in hip and knee arthroplasty. *J Bone Joint Surg Br* **82:**561-565.

Gallo, J., Kolar, M., Dendis, M., Loveckova, Y., Sauer, P., Zapletalova, J. and Koukalova, D. (2008). Culture and PCR analysis of joint fluid in the diagnosis of prosthetic joint infection. *New Microbiol* **31:**97-104.

Garbers, C., Aparicio-Siegmund, S. and Rose-John, S. (2015). The IL-6/gp130/STAT3 signaling axis: recent advances towards specific inhibition. *Curr Opin Immunol* **34:**75-82.

Garbieri, T. F., Martin, V., Santos, C. F., Gomes, P. S. and Fernandes, M. H. (2021). The Embryonic Chick Femur Organotypic Model as a Tool to Analyze the Angiotensin II Axis on Bone Tissue. *Pharmaceuticals (Basel)* **14**.

Garcia-Alvarez, F., Navarro-Zorraquino, M., Castro, A., Grasa, J. M., Pastor, C., Monzon, M., Martinez, A. *et al.* (2009). Effect of age on cytokine response in an experimental model of osteomyelitis. *Biogerontology* **10:**649-658.

Garlanda, C., Dinarello, C. A. and Mantovani, A. (2013). The interleukin-1 family: back to the future. *Immunity* **39:**1003-1018.

Garrett, I. R. (2003). Assessing Bone Formation Using Mouse Calvarial Organ Cultures. In: Helfrich, M.H. and Ralston, S.H. (eds.) *Bone Research Protocols*. Totowa, NJ: Humana Press, pp. 183-198.

Garrett, I. R., Chen, D., Gutierrez, G., Zhao, M., Escobedo, A., Rossini, G., Harris, S. E. *et al.* (2003). Selective inhibitors of the osteoblast proteasome stimulate bone formation in vivo and in vitro. *J Clin Invest* **111:**1771-1782.

Garrett, T. R., Bhakoo, M. and Zhang, Z. (2008). Bacterial adhesion and biofilms on surfaces. *Progress in Natural Science* **18:**1049-1056.

Garzoni, C. and Kelley, W. L. (2011). Return of the Trojan horse: intracellular phenotype switching and immune evasion by Staphylococcus aureus. *EMBO Mol Med* **3:**115-117.

Geipel, U. (2009). Pathogenic organisms in hip joint infections. *Int J Med Sci* **6:**234-240.

Geissmann, F., Jung, S. and Littman, D. R. (2003). Blood monocytes consist of two principal subsets with distinct migratory properties. *Immunity* **19:**71-82.

Gentili, C. and Cancedda, R. (2009). Cartilage and bone extracellular matrix. *Curr Pharm Des* **15:**1334-1348.

Gerlach, B. D., Marinello, M., Heinz, J., Rymut, N., Sansbury, B. E., Riley, C. O., Sadhu, S. *et al.* (2020). Resolvin D1 promotes the targeting and clearance of necroptotic cells. *Cell Death Differ* **27:**525-539.

Giannoudis, P. V., Smith, R. M., Bellamy, M. C., Morrison, J. F., Dickson, R. A. and Guillou, P. J. (1999). Stimulation of the inflammatory system by reamed and unreamed nailing of femoral fractures. An analysis of the second hit. *J Bone Joint Surg Br* **81:**356-361.

Gibon, E., Loi, F., Cordova, L. A., Pajarinen, J., Lin, T., Lu, L., Nabeshima, A. *et al.* (2016). Aging Affects Bone Marrow Macrophage Polarization: Relevance to Bone Healing. *Regen Eng Transl Med* **2:**98-104.

Gilbert, L., He, X., Farmer, P., Boden, S., Kozlowski, M., Rubin, J. and Nanes, M. S. (2000). Inhibition of osteoblast differentiation by tumor necrosis factor-alpha. *Endocrinology* **141:**3956-3964.

Gjertsson, I., Hultgren, O. H. and Tarkowski, A. (2002). Interleukin-10 ameliorates the outcome of Staphylococcus aureus arthritis by promoting bacterial clearance. *Clin Exp Immunol* **130:**409-414.

Gohbara, A., Katagiri, K., Sato, T., Kubota, Y., Kagechika, H., Araki, Y., Araki, Y. *et al.* (2010). In vitro murine spermatogenesis in an organ culture system. *Biol Reprod* **83:**261-267.

Goldring, S. R. and Gravallese, E. M. (2000). Mechanisms of bone loss in inflammatory arthritis: diagnosis and therapeutic implications. *Arthritis Res* **2:**33-37.

Gresham, H. D., Lowrance, J. H., Caver, T. E., Wilson, B. S., Cheung, A. L. and Lindberg, F. P. (2000). Survival of Staphylococcus aureus inside neutrophils contributes to infection. *J Immunol* **164:**3713-3722.

Gros, P., Milder, F. J. and Janssen, B. J. (2008). Complement driven by conformational changes. *Nat Rev Immunol* **8:**48-58.

Guaccio, A., Borselli, C., Oliviero, O. and Netti, P. A. (2008). Oxygen consumption of chondrocytes in agarose and collagen gels: a comparative analysis. *Biomaterials* **29:**1484-1493.

Gurkan, U. A. and Akkus, O. (2008). The mechanical environment of bone marrow: a review. *Ann Biomed Eng* **36:**1978-1991.

Hao, L., Yong, G. and Lu, L. (2013). Bone formation in rabbit cancellous bone explant culture model is enhanced by mechanical load. *Biomedical engineering online* **12:**1-15.

Hawkins, J., Kodali, S., Matsuka, Y. V., McNeil, L. K., Mininni, T., Scully, I. L., Vernachio, J. H. *et al.* (2012). A recombinant Clumping factor A containing vaccine induces functional antibodies to Staphylococcus aureus that are not observed after natural exposure. *Clinical and Vaccine Immunology* CVI. 00354-00312.

Heatley, N. G. (1944). A method for the assay of penicillin. *Biochem J* **38:**61-65.

Hedegaard, C. J., Krakauer, M., Bendtzen, K., Lund, H., Sellebjerg, F. and Nielsen, C. H. (2008). T helper cell type 1 (Th1), Th2 and Th17 responses to myelin basic protein and disease activity in multiple sclerosis. *Immunology* **125:**161-169.

Heinrich, P. C., Behrmann, I., Muller-Newen, G., Schaper, F. and Graeve, L. (1998). Interleukin-6-type cytokine signalling through the gp130/Jak/STAT pathway. *Biochem J* **334 (Pt 2):**297-314.

Henderson, B. and Nair, S. P. (2003). Hard labour: bacterial infection of the skeleton. *Trends Microbiol* **11:**570-577.

Heuck, A. P., Tweten, R. K. and Johnson, A. E. (2001). Beta-barrel pore-forming toxins: intriguing dimorphic proteins. *Biochemistry* **40:**9065-9073.

Hodge, J. M., Collier, F. M., Pavlos, N. J., Kirkland, M. A. and Nicholson, G. C. (2011). M-CSF potently augments RANKL-induced resorption activation in mature human osteoclasts. *PLoS One* **6:**e21462.

Hofbauer, L. C., Lacey, D. L., Dunstan, C. R., Spelsberg, T. C., Riggs, B. L. and Khosla, S. (1999). Interleukin-1beta and tumor necrosis factor-alpha, but not interleukin-6, stimulate osteoprotegerin ligand gene expression in human osteoblastic cells. *Bone* **25:**255-259.

Hoiby, N., Ciofu, O., Johansen, H. K., Song, Z. J., Moser, C., Jensen, P. O., Molin, S. *et al.* (2011). The clinical impact of bacterial biofilms. *Int J Oral Sci* **3:**55-65.

Hong, J. H., Hwang, E. S., McManus, M. T., Amsterdam, A., Tian, Y., Kalmukova, R., Mueller, E. *et al.* (2005). TAZ, a transcriptional modulator of mesenchymal stem cell differentiation. *Science* **309:**1074-1078.

Houston, D. A., Staines, K. A., MacRae, V. E. and Farquharson, C. (2016). Culture of Murine Embryonic Metatarsals: A Physiological Model of Endochondral Ossification. *J Vis Exp* 54978.

Hu, M., Tian, G. W., Gibbons, D. E., Jiao, J. and Qin, Y. X. (2015). Dynamic fluid flow induced mechanobiological modulation of in situ osteocyte calcium oscillations. *Arch Biochem Biophys* **579:**55-61.

Hughes, F. J., Turner, W., Belibasakis, G. and Martuscelli, G. (2006). Effects of growth factors and cytokines on osteoblast differentiation. *Periodontol 2000* **41:**48-72.

Hung, S.-C. (2013). Effects of hypoxic culture on bone marrow mesenchymal stem cells: From bench to bedside. *Formosan Journal of Surgery* **46:**35-38.

Ishikawa, M., Ito, H., Kitaori, T., Murata, K., Shibuya, H., Furu, M., Yoshitomi, H. *et al.* (2014). MCP/CCR2 signaling is essential for recruitment of mesenchymal progenitor cells during the early phase of fracture healing. *PLoS One* **9:**e104954.

Ishimi, Y., Miyaura, C., Jin, C. H., Akatsu, T., Abe, E., Nakamura, Y., Yamaguchi, A. *et al.* (1990). IL-6 is produced by osteoblasts and induces bone resorption. *J Immunol* **145:**3297-3303.

Jablonski, K. A., Amici, S. A., Webb, L. M., Ruiz-Rosado Jde, D., Popovich, P. G., Partida-Sanchez, S. and Guerau-de-Arellano, M. (2015). Novel Markers to Delineate Murine M1 and M2 Macrophages. *PLoS One* **10:**e0145342.

Janowska-Wieczorek, A., Matsuzaki, A. and L, A. M. (2000). The Hematopoietic Microenvironment: Matrix Metalloproteinases in the Hematopoietic Microenvironment. *Hematology* **4:**515-527.

Jawad, M. D., Go, R. S., Reichard, K. K. and Shi, M. (2016). Increased Multinucleated Megakaryocytes as an Isolated Finding in Bone Marrow: A Rare Finding and Its Clinical Significance. *Am J Clin Pathol* **146:**561-566.

Jiang, X. X., Zhang, Y., Liu, B., Zhang, S. X., Wu, Y., Yu, X. D. and Mao, N. (2005). Human mesenchymal stem cells inhibit differentiation and function of monocyte-derived dendritic cells. *Blood* **105:**4120-4126.

Jin, T., Zhu, Y. L., Li, J., Shi, J., He, X. Q., Ding, J. and Xu, Y. Q. (2013). Staphylococcal protein A, Panton-Valentine leukocidin and coagulase aggravate the bone loss and bone destruction in osteomyelitis. *Cell Physiol Biochem* **32:**322-333.

Josse, J., Velard, F. and Gangloff, S. C. (2015). Staphylococcus aureus vs. Osteoblast: Relationship and Consequences in Osteomyelitis. *Front Cell Infect Microbiol* **5:**85.

Kanczler, J. M., Smith, E. L., Roberts, C. A. and Oreffo, R. O. (2012). A novel approach for studying the temporal modulation of embryonic skeletal development using organotypic bone cultures and microcomputed tomography. *Tissue Eng Part C Methods* **18:**747-760.

Kaneko, M., Tomita, T., Nakase, T., Ohsawa, Y., Seki, H., Takeuchi, E., Takano, H. *et al.* (2001). Expression of proteinases and inflammatory cytokines in subchondral bone regions in the destructive joint of rheumatoid arthritis. *Rheumatology (Oxford)* **40:**247-255.

Kaneshiro, S., Ebina, K., Shi, K., Higuchi, C., Hirao, M., Okamoto, M., Koizumi, K. *et al.* (2014). IL-6 negatively regulates osteoblast differentiation through the SHP2/MEK2 and SHP2/Akt2 pathways in vitro. *J Bone Miner Metab* **32:**378-392.

Kapadia, B. H., Berg, R. A., Daley, J. A., Fritz, J., Bhave, A. and Mont, M. A. (2016). Periprosthetic joint infection. *The Lancet* **387:**386-394.

Kapellos, T. S., Bonaguro, L., Gemund, I., Reusch, N., Saglam, A., Hinkley, E. R. and Schultze, J. L. (2019). Human Monocyte Subsets and Phenotypes in Major Chronic Inflammatory Diseases. *Front Immunol* **10:**2035.

Kaplan, J. B. (2010). Biofilm dispersal: mechanisms, clinical implications, and potential therapeutic uses. *J Dent Res* **89:**205-218.

Katsikogianni, M. and Missirlis, Y. (2004). Concise review of mechanisms of bacterial adhesion to biomaterials and of techniques used in estimating bacteria-material interactions. *Eur Cell Mater* **8:**37-57.

Kavanagh, N., O'Brien, F. J. and Kerrigan, S. W. (2018a). Staphylococcus aureus protein A causes osteoblasts to hyper-mineralise in a 3D extra-cellular matrix environment. *PLoS One* **13:**e0198837.

Kavanagh, N., Ryan, E. J., Widaa, A., Sexton, G., Fennell, J., O'Rourke, S., Cahill, K. C. *et al.* (2018b). Staphylococcal Osteomyelitis: Disease Progression, Treatment Challenges, and Future Directions. *Clin Microbiol Rev* **31:**e00084-00017.

Kawane, T., Qin, X., Jiang, Q., Miyazaki, T., Komori, H., Yoshida, C. A., Matsuura-Kawata, V. *et al.* (2018). Runx2 is required for the proliferation of osteoblast progenitors and induces proliferation by regulating Fgfr2 and Fgfr3. *Sci Rep* **8:**13551.

Kawasaki, T. and Kawai, T. (2014). Toll-like receptor signaling pathways. *Front Immunol* **5:**461.

Kearns, A. M., Ganner, M. and Holmes, A. (2006). The 'Oxford Staphylococcus': a note of caution. *J Antimicrob Chemother* **58:**480-481.

Khacho, M., Tarabay, M., Patten, D., Khacho, P., MacLaurin, J. G., Guadagno, J., Bergeron, R. *et al.* (2014). Acidosis overrides oxygen deprivation to maintain mitochondrial function and cell survival. *Nat Commun* **5:**3550.

Khoo, X., O'Toole, G. A., Nair, S. A., Snyder, B. D., Kenan, D. J. and Grinstaff, M. W. (2010). Staphylococcus aureus resistance on titanium coated with multivalent PEGylated-peptides. *Biomaterials* **31:**9285-9292.

Kim, C. H., You, L., Yellowley, C. E. and Jacobs, C. R. (2006a). Oscillatory fluid flow-induced shear stress decreases osteoclastogenesis through RANKL and OPG signaling. *Bone* **39:**1043-1047.

Kim, H. K., De La Luz Sierra, M., Williams, C. K., Gulino, A. V. and Tosato, G. (2006b). G-CSF down-regulation of CXCR4 expression identified as a mechanism for mobilization of myeloid cells. *Blood* **108:**812-820.

Kim, J. H., Jin, H. M., Kim, K., Song, I., Youn, B. U., Matsuo, K. and Kim, N. (2009). The mechanism of osteoclast differentiation induced by IL-1. *J Immunol* **183:**1862-1870.

Kim, O. Y., Chae, J. S., Paik, J. K., Seo, H. S., Jang, Y., Cavaillon, J. M. and Lee, J. H. (2012). Effects of aging and menopause on serum interleukin-6 levels and peripheral blood mononuclear cell cytokine production in healthy nonobese women. *Age (Dordr)* **34:**415-425.

Kitaura, H., Sands, M. S., Aya, K., Zhou, P., Hirayama, T., Uthgenannt, B., Wei, S. *et al.* (2004). Marrow stromal cells and osteoclast precursors differentially contribute to TNF-alpha-induced osteoclastogenesis in vivo. *J Immunol* **173:**4838-4846.

Kitaura, H., Zhou, P., Kim, H. J., Novack, D. V., Ross, F. P. and Teitelbaum, S. L. (2005). M-CSF mediates TNF-induced inflammatory osteolysis. *J Clin Invest* **115:**3418-3427.

Kitur, K., Wachtel, S., Brown, A., Wickersham, M., Paulino, F., Penaloza, H. F., Soong, G. *et al.* (2016). Necroptosis Promotes Staphylococcus aureus Clearance by Inhibiting Excessive Inflammatory Signaling. *Cell Rep* **16:**2219-2230.

Kluter, T., Hassan, R., Rasch, A., Naujokat, H., Wang, F., Behrendt, P., Lippross, S. *et al.* (2020). An Ex Vivo Bone Defect Model to Evaluate Bone Substitutes and Associated Bone Regeneration Processes. *Tissue Eng Part C Methods* **26:**56-65.

Kobayashi, K., Takahashi, N., Jimi, E., Udagawa, N., Takami, M., Kotake, S., Nakagawa, N. *et al.* (2000). Tumor necrosis factor alpha stimulates osteoclast differentiation by a mechanism independent of the ODF/RANKL-RANK interaction. *J Exp Med* **191:**275-286.

Kobayashi, S. D. and DeLeo, F. R. (2013). Staphylococcus aureus protein A promotes immune suppression. *mBio* **4:**e00764-00713.

Kohler, A., De Filippo, K., Hasenberg, M., van den Brandt, C., Nye, E., Hosking, M. P., Lane, T. E. *et al.* (2011). G-CSF-mediated thrombopoietin release triggers neutrophil motility and mobilization from bone marrow via induction of Cxcr2 ligands. *Blood* **117:**4349-4357.

Komine, M., Kukita, A., Kukita, T., Ogata, Y., Hotokebuchi, T. and Kohashi, O. (2001). Tumor necrosis factor-alpha cooperates with receptor activator of nuclear factor kappaB ligand in generation of osteoclasts in stromal cell-depleted rat bone marrow cell culture. *Bone* **28:**474-483.

Komori, T., Yagi, H., Nomura, S., Yamaguchi, A., Sasaki, K., Deguchi, K., Shimizu, Y. *et al.* (1997). Targeted disruption of Cbfa1 results in a complete lack of bone formation owing to maturational arrest of osteoblasts. *Cell* **89:**755-764.

Kon, T., Cho, T. J., Aizawa, T., Yamazaki, M., Nooh, N., Graves, D., Gerstenfeld, L. C. *et al.* (2001). Expression of osteoprotegerin, receptor activator of NF-kappaB ligand (osteoprotegerin ligand) and related proinflammatory cytokines during fracture healing. *J Bone Miner Res* **16:**1004-1014.

Kostakioti, M., Hadjifrangiskou, M. and Hultgren, S. J. (2013). Bacterial biofilms: development, dispersal, and therapeutic strategies in the dawn of the postantibiotic era. *Cold Spring Harb Perspect Med* **3:**a010306.

Kottstorfer, J., Kaiser, G., Thomas, A., Gregori, M., Kecht, M., Domaszewski, F. and Sarahrudi, K. (2013). The influence of non-osteogenic factors on the expression of M-CSF and VEGF during fracture healing. *Injury* **44:**930-934.

Kottstorfer, J., Thomas, A., Gregori, M., Kecht, M., Kaiser, G., Eipeldauer, S. and Sarahrudi, K. (2014). Are OPG and RANKL involved in human fracture healing? *J Orthop Res* **32:**1557-1561.

Kreke, M. R., Huckle, W. R. and Goldstein, A. S. (2005). Fluid flow stimulates expression of osteopontin and bone sialoprotein by bone marrow stromal cells in a temporally dependent manner. *Bone* **36:**1047-1055.

Kreke, M. R., Sharp, L. A., Lee, Y. W. and Goldstein, A. S. (2008). Effect of intermittent shear stress on mechanotransductive signaling and osteoblastic differentiation of bone marrow stromal cells. *Tissue Eng Part A* **14:**529-537.

Kubica, M., Guzik, K., Koziel, J., Zarebski, M., Richter, W., Gajkowska, B., Golda, A. *et al.* (2008). A potential new pathway for Staphylococcus aureus dissemination: the silent survival of S. aureus phagocytosed by human monocyte-derived macrophages. *PLoS One* **3:**e1409.

Kuiper, J. W., Vos, S. J., Saouti, R., Vergroesen, D. A., Graat, H. C., Debets-Ossenkopp, Y. J., Peters, E. J. *et al.* (2013). Prosthetic joint-associated infections treated with DAIR (debridement, antibiotics, irrigation, and retention): analysis of risk factors and local antibiotic carriers in 91 patients. *Acta Orthop* **84:**380-386.

Kular, J., Tickner, J., Chim, S. M. and Xu, J. (2012). An overview of the regulation of bone remodelling at the cellular level. *Clin Biochem* **45:**863-873.

Kunimoto, T., Okubo, N., Minami, Y., Fujiwara, H., Hosokawa, T., Asada, M., Oda, R. *et al.* (2016). A PTH-responsive circadian clock operates in ex vivo mouse femur fracture healing site. *Sci Rep* **6:**22409.

Lacey, D. L., Timms, E., Tan, H. L., Kelley, M. J., Dunstan, C. R., Burgess, T., Elliott, R. *et al.* (1998). Osteoprotegerin ligand is a cytokine that regulates osteoclast differentiation and activation. *Cell* **93:**165-176.

Lam, J., Takeshita, S., Barker, J. E., Kanagawa, O., Ross, F. P. and Teitelbaum, S. L. (2000). TNF-alpha induces osteoclastogenesis by direct stimulation of macrophages exposed to permissive levels of RANK ligand. *J Clin Invest* **106:**1481-1488.

Lange, J., Troelsen, A. and Soballe, K. (2016). Chronic Periprosthetic Hip Joint Infection. A Retrospective, Observational Study on the Treatment Strategy and Prognosis in 130 Non-Selected Patients. *PLoS One* **11:**e0163457.

Langvatn, H., Lutro, O., Dale, H., Schrama, J. C., Hallan, G., Espehaug, B., Sjursen, H. *et al.* (2015). Bacterial and Hematological Findings in Infected Total Hip Arthroplasties in Norway Assessment of 278 Revisions Due to Infection in the Norwegian Arthroplasty Register. *Open Orthop J* **9:**445-449.

Lee, K. S., Kim, H. J., Li, Q. L., Chi, X. Z., Ueta, C., Komori, T., Wozney, J. M. *et al.* (2000). Runx2 is a common target of transforming growth factor beta1 and bone morphogenetic protein 2, and cooperation between Runx2 and Smad5 induces osteoblast-specific gene expression in the pluripotent mesenchymal precursor cell line C2C12. *Mol Cell Biol* **20:**8783-8792.

Lee, Y. M., Fujikado, N., Manaka, H., Yasuda, H. and Iwakura, Y. (2010). IL-1 plays an important role in the bone metabolism under physiological conditions. *Int Immunol* **22:**805-816.

Leech, J. M., Lacey, K. A., Mulcahy, M. E., Medina, E. and McLoughlin, R. M. (2017). IL-10 Plays Opposing Roles during Staphylococcus aureus Systemic and Localized Infections. *J Immunol* **198:**2352-2365.

Leist, M. and Hartung, T. (2013). Inflammatory findings on species extrapolations: humans are definitely no 70-kg mice. *Archives of toxicology* **87:**563-567.

Letwin, O., Harper, S. and Walport, M. (2016). Future of an ageing population [Online]. London, UK: Goverment Office for Science. Available at: https://www.gov.uk/government/publications/future-of-an-ageing-population [Accessed: 9th April].

Leucht, P., Kim, J. B., Amasha, R., James, A. W., Girod, S. and Helms, J. A. (2008). Embryonic origin and Hox status determine progenitor cell fate during adult bone regeneration. *Development* **135:**2845-2854.

Li, Z., Kong, K. and Qi, W. (2006). Osteoclast and its roles in calcium metabolism and bone development and remodeling. *Biochem Biophys Res Commun* **343:**345-350.

Libraty, D. H., Patkar, C. and Torres, B. (2012). Staphylococcus aureus reactivation osteomyelitis after 75 years. *N Engl J Med* **366:**481-482.

Logar, D. B., Komadina, R., Prezelj, J., Ostanek, B., Trost, Z. and Marc, J. (2007). Expression of bone resorption genes in osteoarthritis and in osteoporosis. *J Bone Miner Metab* **25:**219-225.

Lomaga, M. A., Yeh, W. C., Sarosi, I., Duncan, G. S., Furlonger, C., Ho, A., Morony, S. *et al.* (1999). TRAF6 deficiency results in osteopetrosis and defective interleukin-1, CD40, and LPS signaling. *Genes Dev* **13:**1015-1024.

Lopez-Castejon, G. and Brough, D. (2011). Understanding the mechanism of IL-1beta secretion. *Cytokine Growth Factor Rev* **22:**189-195.

Lozupone, E., Palumbo, C., Favia, A., Ferretti, M., Palazzini, S. and Cantatore, F. P. (1996). Intermittent compressive load stimulates osteogenesis and improves osteocyte viability in bones cultured "in vitro". *Clin Rheumatol* **15:**563-572.

Lukacs, N. W., Strieter, R. M., Elner, V., Evanoff, H. L., Burdick, M. D. and Kunkel, S. L. (1995). Production of chemokines, interleukin-8 and monocyte chemoattractant protein-1, during monocyte: endothelial cell interactions. *Blood* **86:**2767-2773.

Luo, G., Li, F., Li, X., Wang, Z. G. and Zhang, B. (2018). TNFalpha and RANKL promote osteoclastogenesis by upregulating RANK via the NFkappaB pathway. *Mol Med Rep* **17:**6605-6611.

Lynch, C. D., Roberts, J. L., Al-Shehri, A., Milward, P. J. and Sloan, A. J. (2018). An ex-vivo model to determine dental pulp responses to heat and light-curing of dental restorative materials. *J Dent* **79:**11-18.

Ma, Q. L., Zhao, L. Z., Liu, R. R., Jin, B. Q., Song, W., Wang, Y., Zhang, Y. S. *et al.* (2014). Improved implant osseointegration of a nanostructured titanium surface via mediation of macrophage polarization. *Biomaterials* **35:**9853-9867.

Mackie, E. J., Ahmed, Y. A., Tatarczuch, L., Chen, K. S. and Mirams, M. (2008). Endochondral ossification: how cartilage is converted into bone in the developing skeleton. *Int J Biochem Cell Biol* **40:**46-62.

Mackie, E. J., Tatarczuch, L. and Mirams, M. (2011). The skeleton: a multi-functional complex organ: the growth plate chondrocyte and endochondral ossification. *J Endocrinol* **211:**109-121.

Madsen, S. H., Goettrup, A. S., Thomsen, G., Christensen, S. T., Schultz, N., Henriksen, K., Bay-Jensen, A. C. *et al.* (2011). Characterization of an Ex vivo Femoral Head Model Assessed by Markers of Bone and Cartilage Turnover. *Cartilage* **2:**265-278.

Malachowa, N. and DeLeo, F. R. (2011). Staphylococcus aureus survival in human blood. *Virulence* **2:**567-569.

Mann, E. E., Rice, K. C., Boles, B. R., Endres, J. L., Ranjit, D., Chandramohan, L., Tsang, L. H. *et al.* (2009). Modulation of eDNA release and degradation affects Staphylococcus aureus biofilm maturation. *PLoS One* **4:**e5822.

Mann, V., Huber, C., Kogianni, G., Jones, D. and Noble, B. (2006). The influence of mechanical stimulation on osteocyte apoptosis and bone viability in human trabecular bone. *J Musculoskelet Neuronal Interact* **6:**408-417.

Marahleh, A., Kitaura, H., Ohori, F., Kishikawa, A., Ogawa, S., Shen, W. R., Qi, J. *et al.* (2019). TNF-alpha Directly Enhances Osteocyte RANKL Expression and Promotes Osteoclast Formation. *Front Immunol* **10:**2925.

Marazzi, M. G., Randelli, F., Brioschi, M., Drago, L., Romano, C. L., Banfi, G., Massaccesi, L. *et al.* (2018). Presepsin: A potential biomarker of PJI? A comparative analysis with known and new infection biomarkers. *Int J Immunopathol Pharmacol* **31:**394632017749356.

Marculescu, C. E., Berbari, E. F., Hanssen, A. D., Steckelberg, J. M., Harmsen, S. W., Mandrekar, J. N. and Osmon, D. R. (2006). Outcome of prosthetic joint infections treated with debridement and retention of components. *Clin Infect Dis* **42:**471-478.

Mardikar, S. H. and Niranjan, K. (2000). Observations on the shear damage to different animal cells in a concentric cylinder viscometer. *Biotechnol Bioeng* **68:**697-704.

Marino, S., Logan, J. G., Mellis, D. and Capulli, M. (2014). Generation and culture of osteoclasts. *Bonekey Rep* **3:**570.

Marino, S., Staines, K. A., Brown, G., Howard-Jones, R. A. and Adamczyk, M. (2016). Models of ex vivo explant cultures: applications in bone research. *Bonekey Rep* **5:**818.

Marriott, I., Gray, D. L., Tranguch, S. L., Fowler, V. G., Jr., Stryjewski, M., Scott Levin, L., Hudson, M. C. *et al.* (2004). Osteoblasts express the inflammatory cytokine interleukin-6 in a murine model of Staphylococcus aureus osteomyelitis and infected human bone tissue. *Am J Pathol* **164:**1399-1406.

Marriott, I., Hughes, F. M., Jr. and Bost, K. L. (2002). Bacterial infection of osteoblasts induces interleukin-1beta and interleukin-18 transcription but not protein synthesis. *J Interferon Cytokine Res* **22:**1049-1055.

Marsh, M. and Newman, S. (2021). Trends and developments in hip and knee arthroplasty technology. *J Rehabil Assist Technol Eng* **8:**2055668320952043.

Marshall, J., Barnes, A. and Genever, P. (2018). Analysis of the Intrinsic Self-Organising Properties of Mesenchymal Stromal Cells in Three-Dimensional Co-Culture Models with Endothelial Cells. *Bioengineering (Basel)* **5:**92.

Martin, T. J. and Sims, N. A. (2005). Osteoclast-derived activity in the coupling of bone formation to resorption. *Trends Mol Med* **11:**76-81.

Masters, E. A., Trombetta, R. P., de Mesy Bentley, K. L., Boyce, B. F., Gill, A. L., Gill, S. R., Nishitani, K. *et al.* (2019). Evolving concepts in bone infection: redefining "biofilm", "acute vs. chronic osteomyelitis", "the immune proteome" and "local antibiotic therapy". *Bone Res* **7:**20.

Matsunobu, T., Torigoe, K., Ishikawa, M., de Vega, S., Kulkarni, A. B., Iwamoto, Y. and Yamada, Y. (2009). Critical roles of the TGF-beta type I receptor ALK5 in perichondrial formation and function, cartilage integrity, and osteoblast differentiation during growth plate development. *Dev Biol* **332:**325-338.

Matsuo, K. and Irie, N. (2008). Osteoclast-osteoblast communication. *Arch Biochem Biophys* **473:**201-209.

Mavrogenis, A. F., Dimitriou, R., Parvizi, J. and Babis, G. C. (2009). Biology of implant osseointegration. *J Musculoskelet Neuronal Interact* **9:**61-71.

Mayadas, T. N., Cullere, X. and Lowell, C. A. (2014). The multifaceted functions of neutrophils. *Annu Rev Pathol* **9:**181-218.

McAllister, T. N., Du, T. and Frangos, J. A. (2000). Fluid shear stress stimulates prostaglandin and nitric oxide release in bone marrow-derived preosteoclast-like cells. *Biochem Biophys Res Commun* **270:**643-648.

McGrath-Morrow, S. A., Collaco, J. M., Detrick, B. and Lederman, H. M. (2016). Serum Interleukin-6 Levels and Pulmonary Function in Ataxia-Telangiectasia. *J Pediatr* **171:**256-261 e251.

McGregor, N. E., Murat, M., Elango, J., Poulton, I. J., Walker, E. C., Crimeen-Irwin, B., Ho, P. W. M. *et al.* (2019). IL-6 exhibits both cis- and trans-signaling in osteocytes and osteoblasts, but only trans-signaling promotes bone formation and osteoclastogenesis. *J Biol Chem* **294:**7850-7863.

McHugh, K. P., Hodivala-Dilke, K., Zheng, M.-H., Namba, N., Lam, J., Novack, D., Feng, X. *et al.* (2000). Mice lacking β3 integrins are osteosclerotic because of dysfunctional osteoclasts. *Journal of Clinical Investigation* **105:**433-440.

McKellop, H., Shen, F. w., Lu, B., Campbell, P. and Salovey, R. (1999). Development of an extremely wear-resistant ultra high molecular weight polythylene for total hip replacements. *Journal of Orthopaedic Research* **17:**157-167.

Melin, M., Joffre-Romeas, A., Farges, J. C., Couble, M. L., Magloire, H. and Bleicher, F. (2000). Effects of TGFbeta1 on dental pulp cells in cultured human tooth slices. *J Dent Res* **79:**1689-1696.

Merritt, J. H., Brothers, K. M., Kuchma, S. L. and O'Toole, G. A. (2007). SadC reciprocally influences biofilm formation and swarming motility via modulation of exopolysaccharide production and flagellar function. *J Bacteriol* **189:**8154-8164.

Mestas, J. and Hughes, C. C. (2004). Of mice and not men: differences between mouse and human immunology. *J Immunol* **172:**2731-2738.

Metzger, C. E. and Narayanan, S. A. (2019). The Role of Osteocytes in Inflammatory Bone Loss. *Front Endocrinol (Lausanne)* **10:**285.

Meyer, L. A., Johnson, M. G., Cullen, D. M., Vivanco, J. F., Blank, R. D., Ploeg, H. L. and Smith, E. L. (2016). Combined exposure to big endothelin-1 and mechanical loading in bovine sternal cores promotes osteogenesis. *Bone* **85:**115-122.

Miles, A. A., Misra, S. S. and Irwin, J. O. (1938). The estimation of the bactericidal power of the blood. *J Hyg (Lond)* **38:**732-749.

Mills, C. D., Kincaid, K., Alt, J. M., Heilman, M. J. and Hill, A. M. (2000). M-1/M-2 macrophages and the Th1/Th2 paradigm. *J Immunol* **164:**6166-6173.

Missiakas, D. and Winstel, V. (2020). Selective Host Cell Death by Staphylococcus aureus: A Strategy for Bacterial Persistence. *Front Immunol* **11:**621733.

Mitra, D., Whitehead, J., Yasui, O. W. and Leach, J. K. (2017). Bioreactor culture duration of engineered constructs influences bone formation by mesenchymal stem cells. *Biomaterials* **146:**29-39.

Mohammad, K. S., Chirgwin, J. M. and Guise, T. A. (2008). Assessing new bone formation in neonatal calvarial organ cultures. *Methods Mol Biol* **455:**37-50.

Montanaro, L., Arciola, C. R., Baldassarri, L. and Borsetti, E. (1999). Presence and expression of collagen adhesin gene (cna) and slime production in Staphylococcus aureus strains from orthopaedic prosthesis infections. *Biomaterials* **20:**1945-1949.

Moormeier, D. E. and Bayles, K. W. (2017). Staphylococcus aureus biofilm: a complex developmental organism. *Mol Microbiol* **104:**365-376.

Morawietz, L., Classen, R. A., Schroder, J. H., Dynybil, C., Perka, C., Skwara, A., Neidel, J. *et al.* (2006). Proposal for a histopathological consensus classification of the periprosthetic interface membrane. *J Clin Pathol* **59:**591-597.

Morikawa, T. and Takubo, K. (2016). Hypoxia regulates the hematopoietic stem cell niche. *Pflugers Arch* **468:**13-22.

Morris, J. L., Letson, H. L., Grant, A., Wilkinson, M., Hazratwala, K. and McEwen, P. (2019). Experimental model of peri-prosthetic infection of the knee caused by Staphylococcus aureus using biomaterials representative of modern TKA. *Biol Open* **8:**bio045203.

Moser, B., Clark-Lewis, I., Zwahlen, R. and Baggiolini, M. (1990). Neutrophil-activating properties of the melanoma growth-stimulatory activity. *J Exp Med* **171:**1797-1802.

Mossadegh-Keller, N., Sarrazin, S., Kandalla, P. K., Espinosa, L., Stanley, E. R., Nutt, S. L., Moore, J. *et al.* (2013). M-CSF instructs myeloid lineage fate in single haematopoietic stem cells. *Nature* **497:**239-243.

Muley, M. M., Reid, A. R., Botz, B., Bolcskei, K., Helyes, Z. and McDougall, J. J. (2016). Neutrophil elastase induces inflammation and pain in mouse knee joints via activation of proteinase-activated receptor-2. *Br J Pharmacol* **173:**766-777.

Mundy, G., Garrett, R., Harris, S., Chan, J., Chen, D., Rossini, G., Boyce, B. *et al.* (1999). Stimulation of bone formation in vitro and in rodents by statins. *Science* **286:**1946-1949.

Murray, P. E., Lumley, P. J., Ross, H. F. and Smith, A. J. (2000). Tooth slice organ culture for cytotoxicity assessment of dental materials. *Biomaterials* **21:**1711-1721.

Muthukrishnan, G., Masters, E. A., Daiss, J. L. and Schwarz, E. M. (2019). Mechanisms of Immune Evasion and Bone Tissue Colonization That Make Staphylococcus aureus the Primary Pathogen in Osteomyelitis. *Curr Osteoporos Rep* **17:**395-404.

Nakashima, K., Zhou, X., Kunkel, G., Zhang, Z., Deng, J. M., Behringer, R. R. and de Crombrugghe, B. (2002). The novel zinc finger-containing transcription factor osterix is required for osteoblast differentiation and bone formation. *Cell* **108:**17-29.

Nakashima, T., Hayashi, M., Fukunaga, T., Kurata, K., Oh-Hora, M., Feng, J. Q., Bonewald, L. F. *et al.* (2011). Evidence for osteocyte regulation of bone homeostasis through RANKL expression. *Nat Med* **17:**1231-1234.

Navegantes, K. C., de Souza Gomes, R., Pereira, P. A. T., Czaikoski, P. G., Azevedo, C. H. M. and Monteiro, M. C. (2017). Immune modulation of some autoimmune diseases: the critical role of macrophages and neutrophils in the innate and adaptive immunity. *J Transl Med* **15:**36.

Negishi-Koga, T. and Takayanagi, H. (2009). Ca2+-NFATc1 signaling is an essential axis of osteoclast differentiation. *Immunol Rev* **231:**241-256.

Nicholson, L. B. (2016). The immune system. *Essays Biochem* **60:**275-301.

Nishimura, R., Moriyama, K., Yasukawa, K., Mundy, G. R. and Yoneda, T. (1998). Combination of interleukin-6 and soluble interleukin-6 receptors induces differentiation and activation of JAK-STAT and MAP kinase pathways in MG-63 human osteoblastic cells. *J Bone Miner Res* **13:**777-785.

Nishio Ayre, W., Melling, G., Cuveillier, C., Natarajan, M., Roberts, J. L., Marsh, L. L., Lynch, C. D. *et al.* (2018). Enterococcus faecalis Demonstrates Pathogenicity through Increased Attachment in an Ex Vivo Polymicrobial Pulpal Infection. **86:**e00871-00817.

NJR. (2016). National Joint Registry for England, Wales, Northern Ireland and the Isle of Man, 13th Annual Report 2016. UK: National Joint Registry.

Novack, D. V. and Faccio, R. (2011). Osteoclast motility: putting the brakes on bone resorption. *Ageing Res Rev* **10:**54-61.

Novack, D. V. and Teitelbaum, S. L. (2008). The osteoclast: friend or foe? *Annu Rev Pathol* **3:**457-484.

Ohshiba, T., Miyaura, C. and Ito, A. (2003). Role of prostaglandin E produced by osteoblasts in osteolysis due to bone metastasis. *Biochemical and Biophysical Research Communications* **300:**957-964.

Okamoto, K. and Takayanagi, H. (2011). Regulation of bone by the adaptive immune system in arthritis. *Arthritis Res Ther* **13:**219.

Orelio, C., Haak, E., Peeters, M. and Dzierzak, E. (2008). Interleukin-1-mediated hematopoietic cell regulation in the aorta-gonad-mesonephros region of the mouse embryo. *Blood* **112:**4895-4904.

Osta, B., Benedetti, G. and Miossec, P. (2014). Classical and Paradoxical Effects of TNF-alpha on Bone Homeostasis. *Front Immunol* **5:**48.

Otero, K., Turnbull, I. R., Poliani, P. L., Vermi, W., Cerutti, E., Aoshi, T., Tassi, I. *et al.* (2009). Macrophage colony-stimulating factor induces the proliferation and survival of macrophages via a pathway involving DAP12 and beta-catenin. *Nat Immunol* **10:**734-743.

Otto, F., Thornell, A. P., Crompton, T., Denzel, A., Gilmour, K. C., Rosewell, I. R., Stamp, G. W. *et al.* (1997). Cbfa1, a candidate gene for cleidocranial dysplasia syndrome, is essential for osteoblast differentiation and bone development. *Cell* **89:**765-771.

Papenfort, K. and Bassler, B. L. (2016). Quorum sensing signal-response systems in Gram-negative bacteria. *Nat Rev Microbiol* **14:**576-588.

Parameswaran, N. and Patial, S. (2010). Tumor necrosis factor-alpha signaling in macrophages. *Crit Rev Eukaryot Gene Expr* **20:**87-103.

Park, J. H., Lee, N. K. and Lee, S. Y. (2017). Current Understanding of RANK Signaling in Osteoclast Differentiation and Maturation. *Mol Cells* **40:**706-713.

Park, N. (2020). Population Estimates for UK, England and Wales, Scotland and Northern Ireland: mid-2019 [Online]. UK: Office of National Statistics. Available at: https://www.ons.gov.uk/peoplepopulationandcommunity/populationandmigration/popu

lationestimates/bulletins/annualmidyearpopulationestimates/mid2019estimates [Accessed: 18th July].

Parkinson, I. H. and Fazzalari, N. L. (2013). Characterisation of trabecular bone structure.*Skeletal Aging and Osteoporosis*. Springer, pp. 31-51.

Parmar, K., Mauch, P., Vergilio, J. A., Sackstein, R. and Down, J. D. (2007). Distribution of hematopoietic stem cells in the bone marrow according to regional hypoxia. *Proc Natl Acad Sci U S A* **104:**5431-5436.

Peacock, S. J., Moore, C. E., Justice, A., Kantzanou, M., Story, L., Mackie, K., O'Neill, G. *et al.* (2002). Virulent combinations of adhesin and toxin genes in natural populations of Staphylococcus aureus. *Infect Immun* **70:**4987-4996.

Pearle, A. D., Scanzello, C. R., George, S., Mandl, L. A., DiCarlo, E. F., Peterson, M., Sculco, T. P. *et al.* (2007). Elevated high-sensitivity C-reactive protein levels are associated with local inflammatory findings in patients with osteoarthritis. *Osteoarthritis Cartilage* **15:**516-523.

Peroglio, M., Gremillard, L., Chevalier, J., Chazeau, L., Gauthier, C. and Hamaide, T. (2007). Toughening of bio-ceramics scaffolds by polymer coating. *Journal of the European Ceramic Society* **27:**2679-2685.

Perpétuo, I. P., Bourne, L. E. and Orriss, I. R. (2019). Isolation and Generation of Osteoblasts. In: Idris, A.I. (ed.) *Bone Research Protocols*. New York, NY: Springer New York, pp. 21-38.

Peters, K. M., Koberg, K., Rosendahl, T. and Haubeck, H. D. (1994). PMN elastase in bone and joint infections. *Int Orthop* **18:**352-355.

Petrova, O. E. and Sauer, K. (2012). Sticky situations: key components that control bacterial surface attachment. *J Bacteriol* **194:**2413-2425.

Petty, W., Spanier, S., Shuster, J. J. and Silverthorne, C. (1985). The influence of skeletal implants on incidence of infection. Experiments in a canine model. *J Bone Joint Surg Am* **67:**1236-1244.

Phillips, J. E., Crane, T. P., Noy, M., Elliott, T. S. and Grimer, R. J. (2006). The incidence of deep prosthetic infections in a specialist orthopaedic hospital: a 15-year prospective survey. *J Bone Joint Surg Br* **88:**943-948.

Pietschmann, P., Skalicky, M., Kneissel, M., Rauner, M., Hofbauer, G., Stupphann, D. and Viidik, A. (2007). Bone structure and metabolism in a rodent model of male senile osteoporosis. *Exp Gerontol* **42:**1099-1108.

Pilsczek, F. H., Salina, D., Poon, K. K., Fahey, C., Yipp, B. G., Sibley, C. D., Robbins, S. M. *et al.* (2010). A novel mechanism of rapid nuclear neutrophil extracellular trap formation in response to Staphylococcus aureus. *J Immunol* **185:**7413-7425.

Plecko, M., Sievert, C., Andermatt, D., Frigg, R., Kronen, P., Klein, K., Stubinger, S. *et al.* (2012). Osseointegration and biocompatibility of different metal implants--a comparative experimental investigation in sheep. *BMC Musculoskelet Disord* **13:**32.

Poole, K. E., van Bezooijen, R. L., Loveridge, N., Hamersma, H., Papapoulos, S. E., Lowik, C. W. and Reeve, J. (2005). Sclerostin is a delayed secreted product of osteocytes that inhibits bone formation. *FASEB J* **19:**1842-1844.

Postma, B., Poppelier, M. J., van Galen, J. C., Prossnitz, E. R., van Strijp, J. A., de Haas, C. J. and van Kessel, K. P. (2004). Chemotaxis inhibitory protein of Staphylococcus aureus binds specifically to the C5a and formylated peptide receptor. *J Immunol* **172:**6994-7001.

Prabhakara, R., Harro, J. M., Leid, J. G., Harris, M. and Shirtliff, M. E. (2011a). Murine immune response to a chronic Staphylococcus aureus biofilm infection. *Infect Immun* **79:**1789-1796.

Prabhakara, R., Harro, J. M., Leid, J. G., Keegan, A. D., Prior, M. L. and Shirtliff, M. E. (2011b). Suppression of the inflammatory immune response prevents the development of chronic biofilm infection due to methicillin-resistant Staphylococcus aureus. *Infect Immun* **79:**5010-5018.

Prat, C., Haas, P. J., Bestebroer, J., de Haas, C. J., van Strijp, J. A. and van Kessel, K. P. (2009). A homolog of formyl peptide receptor-like 1 (FPRL1) inhibitor from Staphylococcus aureus (FPRL1 inhibitory protein) that inhibits FPRL1 and FPR. *J Immunol* **183:**6569-6578.

Prescott, M. J. and Lidster, K. (2017). Improving quality of science through better animal welfare: the NC3Rs strategy. *Lab Anim (NY)* **46:**152-156.

Pribaz, J. R., Bernthal, N. M., Billi, F., Cho, J. S., Ramos, R. I., Guo, Y., Cheung, A. L. *et al.* (2012). Mouse model of chronic post-arthroplasty infection: noninvasive in vivo bioluminescence imaging to monitor bacterial burden for long-term study. *J Orthop Res* **30:**335-340.

Pulido, L., Ghanem, E., Joshi, A., Purtill, J. J. and Parvizi, J. (2008). Periprosthetic joint infection: the incidence, timing, and predisposing factors. *Clin Orthop Relat Res* **466:**1710-1715.

Rahman, M. S., Akhtar, N., Jamil, H. M., Banik, R. S. and Asaduzzaman, S. M. (2015). TGF-beta/BMP signaling and other molecular events: regulation of osteoblastogenesis and bone formation. *Bone Res* **3:**15005.

Raisanen, S. R., Alatalo, S. L., Ylipahkala, H., Halleen, J. M., Cassady, A. I., Hume, D. A. and Vaananen, H. K. (2005). Macrophages overexpressing tartrate-resistant acid phosphatase show altered profile of free radical production and enhanced capacity of bacterial killing. *Biochem Biophys Res Commun* **331:**120-126.

Rawlinson, S. C., el-Haj, A. J., Minter, S. L., Tavares, I. A., Bennett, A. and Lanyon, L. E. (1991). Loading-related increases in prostaglandin production in cores of adult canine cancellous bone in vitro: a role for prostacyclin in adaptive bone remodeling? *J Bone Miner Res* **6:**1345-1351.

Rawlinson, S. C., Mosley, J. R., Suswillo, R. F., Pitsillides, A. A. and Lanyon, L. E. (1995). Calvarial and limb bone cells in organ and monolayer culture do not show the same early responses to dynamic mechanical strain. *J Bone Miner Res* **10:**1225-1232.

Regnault, A., Lankar, D., Lacabanne, V., Rodriguez, A., Thery, C., Rescigno, M., Saito, T. *et al.* (1999). Fcgamma receptor-mediated induction of dendritic cell maturation and major histocompatibility complex class I-restricted antigen presentation after immune complex internalization. *J Exp Med* **189:**371-380.

Reilly, S. S., Hudson, M. C., Kellam, J. F. and Ramp, W. K. (2000). In vivo internalization of Staphylococcus aureus by embryonic chick osteoblasts. *Bone* **26:**63-70.

Ren, L. R., Wang, H., He, X. Q., Song, M. G., Chen, X. Q. and Xu, Y. Q. (2017a). Staphylococcus aureus Protein A induces osteoclastogenesis via the NFkappaB signaling pathway. *Mol Med Rep* **16:**6020-6028.

Ren, L. R., Wang, Z. H., Wang, H., He, X. Q., Song, M. G. and Xu, Y. Q. (2017b). Staphylococcus Aureus Induces Osteoclastogenesis via the NF-kappaB Signaling Pathway. *Med Sci Monit* **23:**4579-4590.

Reyes-Robles, T., Alonzo, F., 3rd, Kozhaya, L., Lacy, D. B., Unutmaz, D. and Torres, V. J. (2013). Staphylococcus aureus leukotoxin ED targets the chemokine receptors CXCR1 and CXCR2 to kill leukocytes and promote infection. *Cell Host Microbe* **14:**453-459.

Reznikov, N., Shahar, R. and Weiner, S. (2014). Bone hierarchical structure in three dimensions. *Acta Biomater* **10:**3815-3826.

Rho, J. Y., Kuhn-Spearing, L. and Zioupos, P. (1998). Mechanical properties and the hierarchical structure of bone. *Med Eng Phys* **20:**92-102.

Ribeiro, M., Monteiro, F. J. and Ferraz, M. P. (2012). Infection of orthopedic implants with emphasis on bacterial adhesion process and techniques used in studying bacterial-material interactions. *Biomatter* **2:**176-194.

Ricciardi, B. F., Muthukrishnan, G., Masters, E., Ninomiya, M., Lee, C. C. and Schwarz, E. M. (2018). Staphylococcus aureus Evasion of Host Immunity in the Setting of Prosthetic Joint Infection: Biofilm and Beyond. *Curr Rev Musculoskelet Med* **11:**389-400.

Richards, M. K., Liu, F., Iwasaki, H., Akashi, K. and Link, D. C. (2003). Pivotal role of granulocyte colony-stimulating factor in the development of progenitors in the common myeloid pathway. *Blood* **102:**3562-3568.

Richards, R. G., Simpson, A. E., Jaehn, K., Furlong, P. I. and Stoddart, M. J. (2007). Establishing a 3D ex vivo culture system for investigations of bone metabolism and biomaterial interactions. *ALTEX* **24 Spec No:**56-59.

Richardson, A. R., Libby, S. J. and Fang, F. C. (2008). A nitric oxide-inducible lactate dehydrogenase enables Staphylococcus aureus to resist innate immunity. *Science* **319:**1672-1676.

Rincon, M., Anguita, J., Nakamura, T., Fikrig, E. and Flavell, R. A. (1997). Interleukin (IL)-6 directs the differentiation of IL-4-producing CD4+ T cells. *J Exp Med* **185:**461-469.

Ritchie, R. O., Buehler, M. J. and Hansma, P. (2009). Plasticity and toughness in bone. *Physics Today* **62:**41-47.

Roberts, J. L., Maillard, J. Y., Waddington, R. J., Denyer, S. P., Lynch, C. D. and Sloan, A. J. (2013). Development of an ex vivo coculture system to model pulpal infection by Streptococcus anginosus group bacteria. *J Endod* **39:**49-56.

Robling, A. G., Bellido, T. and Turner, C. H. (2006). Mechanical stimulation in vivo reduces osteocyte expression of sclerostin. *J Musculoskelet Neuronal Interact* **6:**354.

Romano, M., Fanelli, G., Albany, C. J., Giganti, G. and Lombardi, G. (2019). Past, Present, and Future of Regulatory T Cell Therapy in Transplantation and Autoimmunity. *Front Immunol* **10:**43.

Rosales, C. (2018). Neutrophil: A Cell with Many Roles in Inflammation or Several Cell Types? *Front Physiol* **9:**113.

Rubin, J., Biskobing, D., Fan, X., Rubin, C., McLeod, K. and Taylor, W. R. (1997). Pressure regulates osteoclast formation and MCSF expression in marrow culture. *J Cell Physiol* **170:**81-87.

Rupin, F., Bossis, D., Vico, L., Peyrin, F., Raum, K., Laugier, P. and Saied, A. (2010). Adaptive remodeling of trabecular bone core cultured in 3-D bioreactor providing cyclic loading: an acoustic microscopy study. *Ultrasound Med Biol* **36:**999-1007.

Ruscitti, P., Cipriani, P., Carubbi, F., Liakouli, V., Zazzeroni, F., Di Benedetto, P., Berardicurti, O. *et al.* (2015). The role of IL-1beta in the bone loss during rheumatic diseases. *Mediators Inflamm* **2015:**782382.

Saleh, F. A., Whyte, M. and Genever, P. G. (2011). Effects of endothelial cells on human mesenchymal stem cell activity in a three-dimensional in vitro model. *Eur Cell Mater* **22:**242-257; discussion 257.

Sanchez, C. J., Jr., Ward, C. L., Romano, D. R., Hurtgen, B. J., Hardy, S. K., Woodbury, R. L., Trevino, A. V. *et al.* (2013). Staphylococcus aureus biofilms decrease osteoblast viability, inhibits osteogenic differentiation, and increases bone resorption in vitro. *BMC Musculoskelet Disord* **14:**187.

Sarahrudi, K., Mousavi, M., Thomas, A., Eipeldauer, S., Vecsei, V., Pietschmann, P. and Aharinejad, S. (2010). Elevated levels of macrophage colony-stimulating factor in human fracture healing. *J Orthop Res* **28:**671-676.

Sasaki, S., Nishikawa, S., Miura, T., Mizuki, M., Yamada, K., Madarame, H., Tagawa, Y. I. *et al.* (2000). Interleukin-4 and interleukin-10 are involved in host resistance to Staphylococcus aureus infection through regulation of gamma interferon. *Infect Immun* **68:**2424-2430.

Scheller, J., Chalaris, A., Schmidt-Arras, D. and Rose-John, S. (2011). The pro- and anti-inflammatory properties of the cytokine interleukin-6. *Biochim Biophys Acta* **1813:**878-888.

Schnieders, J., Gbureck, U., Germershaus, O., Kratz, M., Jones, D. B. and Kissel, T. (2013). Ex vivo human trabecular bone model for biocompatibility evaluation of calcium phosphate composites modified with spray dried biodegradable microspheres. *Adv Healthc Mater* **2:**1361-1369.

Scully, I. L., Timofeyeva, Y., Keeney, D., Matsuka, Y. V., Severina, E., McNeil, L. K., Nanra, J. *et al.* (2015). Demonstration of the preclinical correlate of protection for Staphylococcus aureus clumping factor A in a murine model of infection. *Vaccine* **33:**5452-5457.

Seaman, P., Day, M., Russell, A. D. and Ochs, D. (2004). Susceptibility of capsular Staphylococcus aureus strains to some antibiotics, triclosan and cationic biocides. *J Antimicrob Chemother* **54:**696-698.

Semerad, C. L., Christopher, M. J., Liu, F., Short, B., Simmons, P. J., Winkler, I., Levesque, J. P. *et al.* (2005). G-CSF potently inhibits osteoblast activity and CXCL12 mRNA expression in the bone marrow. *Blood* **106:**3020-3027.

Sen, S., Sirobhushanam, S., Johnson, S. R., Song, Y., Tefft, R., Gatto, C. and Wilkinson, B. J. (2016). Growth-Environment Dependent Modulation of Staphylococcus aureus Branched-Chain to Straight-Chain Fatty Acid Ratio and Incorporation of Unsaturated Fatty Acids. *PLoS One* **11:**e0165300.

Sendi, P., Rohrbach, M., Graber, P., Frei, R., Ochsner, P. E. and Zimmerli, W. (2006). Staphylococcus aureus small colony variants in prosthetic joint infection. *Clin Infect Dis* **43:**961-967.

Sha, Z. and Compans, R. W. (2000). Induction of CD4(+) T-cell-independent immunoglobulin responses by inactivated influenza virus. *J Virol* **74:**4999-5005.

Shiratori, T., Kyumoto-Nakamura, Y., Kukita, A., Uehara, N., Zhang, J., Koda, K., Kamiya, M. *et al.* (2018). IL-1beta Induces Pathologically Activated Osteoclasts Bearing Extremely High Levels of Resorbing Activity: A Possible Pathological Subpopulation of Osteoclasts, Accompanied by Suppressed Expression of Kindlin-3 and Talin-1. *J Immunol* **200:**218-228.

Shirvaikar, N., Marquez-Curtis, L. A. and Janowska-Wieczorek, A. (2012). Hematopoietic Stem Cell Mobilization and Homing after Transplantation: The Role of MMP-2, MMP-9, and MT1-MMP. *Biochem Res Int* **2012:**685267.

Shui, C., Spelsberg, T. C., Riggs, B. L. and Khosla, S. (2003). Changes in Runx2/Cbfa1 expression and activity during osteoblastic differentiation of human bone marrow stromal cells. *J Bone Miner Res* **18:**213-221.

Simonet, W. S., Lacey, D. L., Dunstan, C. R., Kelley, M., Chang, M. S., Luthy, R., Nguyen, H. Q. *et al.* (1997). Osteoprotegerin: a novel secreted protein involved in the regulation of bone density. *Cell* **89:**309-319.

Simpson, A. E., Stoddart, M. J., Davies, C. M., Jahn, K., Furlong, P. I., Gasser, J. A., Jones, D. B. *et al.* (2009). TGFbeta3 and loading increases osteocyte survival in human cancellous bone cultured ex vivo. *Cell Biochem Funct* **27:**23-29.

Sims, N. A. and Gooi, J. H. (2008). Bone remodeling: Multiple cellular interactions required for coupling of bone formation and resorption. *Semin Cell Dev Biol* **19:**444-451.

Sinha, K. M. and Zhou, X. (2013). Genetic and molecular control of osterix in skeletal formation. *J Cell Biochem* **114:**975-984.

Sloan, A. J. (2015). Biology of the Dentin-Pulp Complex. pp. 371-378.

Sloan, A. J., Shelton, R. M., Hann, A. C., Moxham, B. J. and Smith, A. J. (1998). An in vitro approach for the study of dentinogenesis by organ culture of the dentine-pulp complex from rat incisor teeth. *Arch Oral Biol* **43:**421-430.

Sloan, A. J. and Smith, A. J. (1999). Stimulation of the dentine-pulp complex of rat incisor teeth by transforming growth factor-beta isoforms 1-3 in vitro. *Arch Oral Biol* **44:**149-156.

Sloan, A. J., Taylor, S. Y., Smith, E. L., Roberts, J. L., Chen, L., Wei, X. Q. and Waddington, R. J. (2013). A novel ex vivo culture model for inflammatory bone destruction. *J Dent Res* **92:**728-734.

Smith, E. L., Kanczler, J. M., Gothard, D., Roberts, C. A., Wells, J. A., White, L. J., Qutachi, O. *et al.* (2014a). Evaluation of skeletal tissue repair, part 1: assessment of novel growth-

factor-releasing hydrogels in an ex vivo chick femur defect model. *Acta Biomater* **10:**4186-4196.

Smith, E. L., Kanczler, J. M., Gothard, D., Roberts, C. A., Wells, J. A., White, L. J., Qutachi, O. *et al.* (2014b). Evaluation of skeletal tissue repair, part 2: enhancement of skeletal tissue repair through dual-growth-factor-releasing hydrogels within an ex vivo chick femur defect model. *Acta Biomater* **10:**4197-4205.

Smith, E. L., Locke, M., Waddington, R. J. and Sloan, A. J. (2010). An ex vivo rodent mandible culture model for bone repair. *Tissue Eng Part C Methods* **16:**1287-1296.

Soligo, D., de Harven, E., Pozzoli, E., Nava, M. T., Polli, N. and Lambertenghi-Deliliers, G. (1985). Scanning electron microscope cytochemistry of blood cells. *Scan Electron Microsc* 817-825.

Souza-Fonseca-Guimaraes, F., Adib-Conquy, M. and Cavaillon, J. M. (2012). Natural killer (NK) cells in antibacterial innate immunity: angels or devils? *Mol Med* **18:**270-285.

Spaan, A. N., Vrieling, M., Wallet, P., Badiou, C., Reyes-Robles, T., Ohneck, E. A., Benito, Y. *et al.* (2014). The staphylococcal toxins gamma-haemolysin AB and CB differentially target phagocytes by employing specific chemokine receptors. *Nat Commun* **5:**5438.

Srinivasaiah, S., Musumeci, G., Mohan, T., Castrogiovanni, P., Absenger-Novak, M., Zefferer, U., Mostofi, S. *et al.* (2019). A 300 mum Organotypic Bone Slice Culture Model for Temporal Investigation of Endochondral Osteogenesis. *Tissue Eng Part C Methods* **25:**197-212.

Stavrakis, A. I., Niska, J. A., Loftin, A. H., Billi, F. and Bernthal, N. M. (2013). Understanding infection: a primer on animal models of periprosthetic joint infection. *ScientificWorldJournal* **2013:**925906.

Stewart, P. S. and Franklin, M. J. (2008). Physiological heterogeneity in biofilms. *Nat Rev Microbiol* **6:**199-210.

Stroh, P., Gunther, F., Meyle, E., Prior, B., Wagner, C. and Hansch, G. M. (2011). Host defence against Staphylococcus aureus biofilms by polymorphonuclear neutrophils: oxygen radical production but not phagocytosis depends on opsonisation with immunoglobulin G. *Immunobiology* **216:**351-357.

Su, P., Tian, Y., Yang, C., Ma, X., Wang, X., Pei, J. and Qian, A. (2018). Mesenchymal Stem Cell Migration during Bone Formation and Bone Diseases Therapy. *International journal of molecular sciences* **19:**2343.

Sugars, R. V., Milan, A. M., Brown, J. O., Waddington, R. J., Hall, R. C. and Embery, G. (2003). Molecular interaction of recombinant decorin and biglycan with type I collagen influences crystal growth. *Connect Tissue Res* **44 Suppl 1:**189-195.

Summers, C., Rankin, S. M., Condliffe, A. M., Singh, N., Peters, A. M. and Chilvers, E. R. (2010). Neutrophil kinetics in health and disease. *Trends Immunol* **31:**318-324.

Sundaram, K., Nishimura, R., Senn, J., Youssef, R. F., London, S. D. and Reddy, S. V. (2007). RANK ligand signaling modulates the matrix metalloproteinase-9 gene expression during osteoclast differentiation. *Exp Cell Res* **313:**168-178.

Swarup, A., Weidner, H., Duncan, R. and Nohe, A. (2018). The Preservation of Bone Cell Viability in a Human Femoral Head through a Perfusion Bioreactor. *Materials (Basel)* **11**.

Takai, E., Mauck, R. L., Hung, C. T. and Guo, X. E. (2004). Osteocyte viability and regulation of osteoblast function in a 3D trabecular bone explant under dynamic hydrostatic pressure. *J Bone Miner Res* **19:**1403-1410.

Takayanagi, H. (2005). Mechanistic insight into osteoclast differentiation in osteoimmunology. *J Mol Med (Berl)* **83:**170-179.

Takeshita, S., Kaji, K. and Kudo, A. (2000). Identification and characterization of the new osteoclast progenitor with macrophage phenotypes being able to differentiate into mature osteoclasts. *J Bone Miner Res* **15:**1477-1488.

Tande, A. J. and Patel, R. (2014). Prosthetic joint infection. *Clin Microbiol Rev* **27:**302-345.

Thammavongsa, V., Kim, H. K., Missiakas, D. and Schneewind, O. (2015). Staphylococcal manipulation of host immune responses. *Nat Rev Microbiol* **13:**529-543.

Thesingh, C. W. and Burger, E. H. (1983). The role of mesenchyme in embryonic long bones as early deposition site for osteoclast progenitor cells. *Dev Biol* **95:**429-438.

Titanji, K. (2017). Beyond Antibodies: B Cells and the OPG/RANK-RANKL Pathway in Health, Non-HIV Disease and HIV-Induced Bone Loss. *Front Immunol* **8:**1851.

To, L. B., Levesque, J. P. and Herbert, K. E. (2011). How I treat patients who mobilize hematopoietic stem cells poorly. *Blood* **118:**4530-4540.

Tokarski, A. T., Novack, T. A. and Parvizi, J. (2015). Is tantalum protective against infection in revision total hip arthroplasty? *Bone Joint J* **97-B:**45-49.

Tong, S. Y., Davis, J. S., Eichenberger, E., Holland, T. L. and Fowler, V. G., Jr. (2015). Staphylococcus aureus infections: epidemiology, pathophysiology, clinical manifestations, and management. *Clin Microbiol Rev* **28:**603-661.

Touaitahuata, H., Blangy, A. and Vives, V. (2014). Modulation of osteoclast differentiation and bone resorption by Rho GTPases. *Small GTPases* **5:**e28119.

Trouillet-Assant, S., Gallet, M., Nauroy, P., Rasigade, J. P., Flammier, S., Parroche, P., Marvel, J. *et al.* (2015). Dual impact of live Staphylococcus aureus on the osteoclast lineage, leading to increased bone resorption. *J Infect Dis* **211:**571-581.

Tsai, C. C., Yew, T. L., Yang, D. C., Huang, W. H. and Hung, S. C. (2012). Benefits of hypoxic culture on bone marrow multipotent stromal cells. *Am J Blood Res* **2:**148-159.

Tsukayama, D. T., Estrada, R. and Gustilo, R. B. (1996). Infection after total hip arthroplasty. A study of the treatment of one hundred and six infections. *J Bone Joint Surg Am* **78:**512-523.

Tu, X., Rhee, Y., Condon, K. W., Bivi, N., Allen, M. R., Dwyer, D., Stolina, M. *et al.* (2012). Sost downregulation and local Wnt signaling are required for the osteogenic response to mechanical loading. *Bone* **50:**209-217.

Tuchscherr, L., Medina, E., Hussain, M., Volker, W., Heitmann, V., Niemann, S., Holzinger, D. *et al.* (2011). Staphylococcus aureus phenotype switching: an effective bacterial strategy to escape host immune response and establish a chronic infection. *EMBO Mol Med* **3:**129-141.

Utting, J. C., Robins, S. P., Brandao-Burch, A., Orriss, I. R., Behar, J. and Arnett, T. R. (2006). Hypoxia inhibits the growth, differentiation and bone-forming capacity of rat osteoblasts. *Exp Cell Res* **312:**1693-1702.

Vaananen, H. K. and Laitala-Leinonen, T. (2008). Osteoclast lineage and function. *Arch Biochem Biophys* **473:**132-138.

Vaananen, H. K., Zhao, H., Mulari, M. and Halleen, J. M. (2000). The cell biology of osteoclast function. *J Cell Sci* **113 (Pt 3):**377-381.

Vazquez, M., Evans, B. A., Riccardi, D., Evans, S. L., Ralphs, J. R., Dillingham, C. M. and Mason, D. J. (2014). A new method to investigate how mechanical loading of osteocytes controls osteoblasts. *Front Endocrinol (Lausanne)* **5:**208.

Vazquez, V., Liang, X., Horndahl, J. K., Ganesh, V. K., Smeds, E., Foster, T. J. and Hook, M. (2011). Fibrinogen is a ligand for the Staphylococcus aureus microbial surface components recognizing adhesive matrix molecules (MSCRAMM) bone sialoprotein-binding protein (Bbp). *J Biol Chem* **286:**29797-29805.

Vermes, C., Jacobs, J. J., Zhang, J., Firneisz, G., Roebuck, K. A. and Glant, T. T. (2002). Shedding of the interleukin-6 (IL-6) receptor (gp80) determines the ability of IL-6 to induce gp130 phosphorylation in human osteoblasts. *J Biol Chem* **277:**16879-16887.

Vicenti, G., Bizzoca, D., Nappi, V., Pesce, V., Solarino, G., Carrozzo, M., Moretti, F. *et al.* (2019). Serum biomarkers in the diagnosis of periprosthetic joint infection: consolidated evidence and recent developments. *Eur Rev Med Pharmacol Sci* **23:**43-50.

Vivanco, J., Garcia, S., Ploeg, H. L., Alvarez, G., Cullen, D. and Smith, E. L. (2013). Apparent elastic modulus of ex vivo trabecular bovine bone increases with dynamic loading. *Proc Inst Mech Eng H* **227:**904-912.

Volkmer, E., Drosse, I., Otto, S., Stangelmayer, A., Stengele, M., Kallukalam, B. C., Mutschler, W. *et al.* (2008). Hypoxia in static and dynamic 3D culture systems for tissue engineering of bone. *Tissue Eng Part A* **14:**1331-1340.

Wagner, C., Kaksa, A., Muller, W., Denefleh, B., Heppert, V., Wentzensen, A. and Hansch, G. M. (2004). Polymorphonuclear neutrophils in posttraumatic osteomyelitis: cells recovered from the inflamed site lack chemotactic activity but generate superoxides. *Shock* **22:**108-115.

Walker, P. A., Jimenez, F., Gerber, M. H., Aroom, K. R., Shah, S. K., Harting, M. T., Gill, B. S. *et al.* (2010). Effect of needle diameter and flow rate on rat and human mesenchymal stromal cell characterization and viability. *Tissue Eng Part C Methods* **16:**989-997.

Walsh, M. C., Takegahara, N., Kim, H. and Choi, Y. (2018). Updating osteoimmunology: regulation of bone cells by innate and adaptive immunity. *Nat Rev Rheumatol* **14:**146-156.

Wang, Y., Uemura, T., Dong, J., Kojima, H., Tanaka, J. and Tateishi, T. (2003). Application of perfusion culture system improves in vitro and in vivo osteogenesis of bone marrow-derived osteoblastic cells in porous ceramic materials. *Tissue Eng* **9:**1205-1214.

Wang, Z., Tang, X., Xu, W., Cao, Z., Sun, L., Li, W., Li, Q. *et al.* (2013). The different immunoregulatory functions on dendritic cells between mesenchymal stem cells derived from bone marrow of patients with low-risk or high-risk myelodysplastic syndromes. *PLoS One* **8:**e57470.

Wei, S., Kitaura, H., Zhou, P., Ross, F. P. and Teitelbaum, S. L. (2005). IL-1 mediates TNF-induced osteoclastogenesis. *J Clin Invest* **115:**282-290.

Westendorf, J. J., Kahler, R. A. and Schroeder, T. M. (2004). Wnt signaling in osteoblasts and bone diseases. *Gene* **341:**19-39.

Widaa, A., Claro, T., Foster, T. J., O'Brien, F. J. and Kerrigan, S. W. (2012). Staphylococcus aureus protein A plays a critical role in mediating bone destruction and bone loss in osteomyelitis. *PLoS One* **7:**e40586.

Wijenayaka, A. R., Kogawa, M., Lim, H. P., Bonewald, L. F., Findlay, D. M. and Atkins, G. J. (2011). Sclerostin stimulates osteocyte support of osteoclast activity by a RANKL-dependent pathway. *PLoS One* **6:**e25900.

Williams, D. F. (2008). On the mechanisms of biocompatibility. *Biomaterials* **29:**2941-2953.

Wolf, J., Rose-John, S. and Garbers, C. (2014). Interleukin-6 and its receptors: a highly regulated and dynamic system. *Cytokine* **70:**11-20.

Wright, D. E., Bowman, E. P., Wagers, A. J., Butcher, E. C. and Weissman, I. L. (2002). Hematopoietic stem cells are uniquely selective in their migratory response to chemokines. *J Exp Med* **195:**1145-1154.

Wright, J. A. and Nair, S. P. (2010). Interaction of staphylococci with bone. *Int J Med Microbiol* **300:**193-204.

Xiong, J., Onal, M., Jilka, R. L., Weinstein, R. S., Manolagas, S. C. and O'Brien, C. A. (2011). Matrix-embedded cells control osteoclast formation. *Nat Med* **17:**1235-1241.

Xu, L., Liu, Y., Sun, Y., Wang, B., Xiong, Y., Lin, W., Wei, Q. *et al.* (2017). Tissue source determines the differentiation potentials of mesenchymal stem cells: a comparative study of human mesenchymal stem cells from bone marrow and adipose tissue. *Stem Cell Res Ther* **8:**275.

Yamamura, M., Yamada, Y., Momita, S., Kamihira, S. and Tomonaga, M. (1998). Circulating interleukin-6 levels are elevated in adult T-cell leukaemia/lymphoma patients and correlate with adverse clinical features and survival. *Br J Haematol* **100:**129-134.

Yamashita, T., Takahashi, N. and Udagawa, N. (2012). New roles of osteoblasts involved in osteoclast differentiation. *World J Orthop* **3:**175-181.

Yang, D., Wijenayaka, A. R., Solomon, L. B., Pederson, S. M., Findlay, D. M., Kidd, S. P. and Atkins, G. J. (2018a). Novel Insights into Staphylococcus aureus Deep Bone Infections: the Involvement of Osteocytes. *mBio* **9:**e00415-00418.

Yang, X., Shi, G., Guo, J., Wang, C. and He, Y. (2018b). Exosome-encapsulated antibiotic against intracellular infections of methicillin-resistant Staphylococcus aureus. *Int J Nanomedicine* **13:**8095-8104.

Yao, Z., Li, P., Zhang, Q., Schwarz, E. M., Keng, P., Arbini, A., Boyce, B. F. *et al.* (2006). Tumor necrosis factor-alpha increases circulating osteoclast precursor numbers by promoting their proliferation and differentiation in the bone marrow through up-regulation of c-Fms expression. *J Biol Chem* **281:**11846-11855.

Yao, Z., Xing, L., Qin, C., Schwarz, E. M. and Boyce, B. F. (2008). Osteoclast Precursor Interaction with Bone Matrix Induces Osteoclast Formation Directly by an Interleukin-1-mediated Autocrine Mechanism. *The Journal of Biological Chemistry* **283:**9917-9924.

Yi, P. H., Cross, M. B., Moric, M., Sporer, S. M., Berger, R. A. and Della Valle, C. J. (2014). The 2013 Frank Stinchfield Award: Diagnosis of infection in the early postoperative period after total hip arthroplasty. *Clin Orthop Relat Res* **472:**424-429.

Yin, J. J., Mohammad, K. S., Kakonen, S. M., Harris, S., Wu-Wong, J. R., Wessale, J. L., Padley, R. J. *et al.* (2003). A causal role for endothelin-1 in the pathogenesis of osteoblastic bone metastases. *Proc Natl Acad Sci U S A* **100:**10954-10959.

Ying, W., Cheruku, P. S., Bazer, F. W., Safe, S. H. and Zhou, B. (2013). Investigation of macrophage polarization using bone marrow derived macrophages. *J Vis Exp* 50323.

Yokoyama, R., Itoh, S., Kamoshida, G., Takii, T., Fujii, S., Tsuji, T. and Onozaki, K. (2012). Staphylococcal superantigen-like protein 3 binds to the Toll-like receptor 2 extracellular domain and inhibits cytokine production induced by Staphylococcus aureus, cell wall component, or lipopeptides in murine macrophages. *Infect Immun* **80:**2816-2825.

Yoshida, H., Hayashi, S., Kunisada, T., Ogawa, M., Nishikawa, S., Okamura, H., Sudo, T. *et al.* (1990). The murine mutation osteopetrosis is in the coding region of the macrophage colony stimulating factor gene. *Nature* **345:**442-444.

Yoshii, T., Magara, S., Miyai, D., Nishimura, H., Kuroki, E., Furudoi, S., Komori, T. *et al.* (2002). Local levels of interleukin-1beta, -4, -6 and tumor necrosis factor alpha in an experimental model of murine osteomyelitis due to staphylococcus aureus. *Cytokine* **19:**59-65.

Yoshitake, F., Itoh, S., Narita, H., Ishihara, K. and Ebisu, S. (2008). Interleukin-6 directly inhibits osteoclast differentiation by suppressing receptor activator of NF-kappaB signaling pathways. *J Biol Chem* **283:**11535-11540.

Young, M. F. (2003). Bone matrix proteins: their function, regulation, and relationship to osteoporosis. *Osteoporos Int* **14 Suppl 3:**S35-42.

Yu, X. F. and Han, Z. C. (2006). Matrix metalloproteinases in bone marrow: roles of gelatinases in physiological hematopoiesis and hematopoietic malignancies. *Histol Histopathol* **21:**519-531.

Zhang, D. E., Hetherington, C. J., Chen, H. M. and Tenen, D. G. (1994). The macrophage transcription factor PU.1 directs tissue-specific expression of the macrophage colony-stimulating factor receptor. *Mol Cell Biol* **14:**373-381.

Zhang, J. M. and An, J. (2007). Cytokines, inflammation, and pain. *Int Anesthesiol Clin* **45:**27-37.

Zhang, W., Ge, W., Li, C., You, S., Liao, L., Han, Q., Deng, W. *et al.* (2004). Effects of mesenchymal stem cells on differentiation, maturation, and function of human monocyte-derived dendritic cells. *Stem Cells Dev* **13:**263-271.

Zhang, Y., Khan, D., Delling, J. and Tobiasch, E. (2012). Mechanisms underlying the osteo- and adipo-differentiation of human mesenchymal stem cells. *ScientificWorldJournal* **2012:**793823.

Zimmerli, W. (2006). Prosthetic-joint-associated infections. *Best Practice & Research Clinical Rheumatology* **20:**1045-1063.

Zimmerli, W. and Moser, C. (2012). Pathogenesis and treatment concepts of orthopaedic biofilm infections. *FEMS Immunol Med Microbiol* **65:**158-168.

Zimmerli, W., Trampuz, A. and Ochsner, P. E. (2004). Prosthetic-joint infections. *N Engl J Med* **351:**1645-1654.

Appendix I

Supporting documentation for Chapter 3

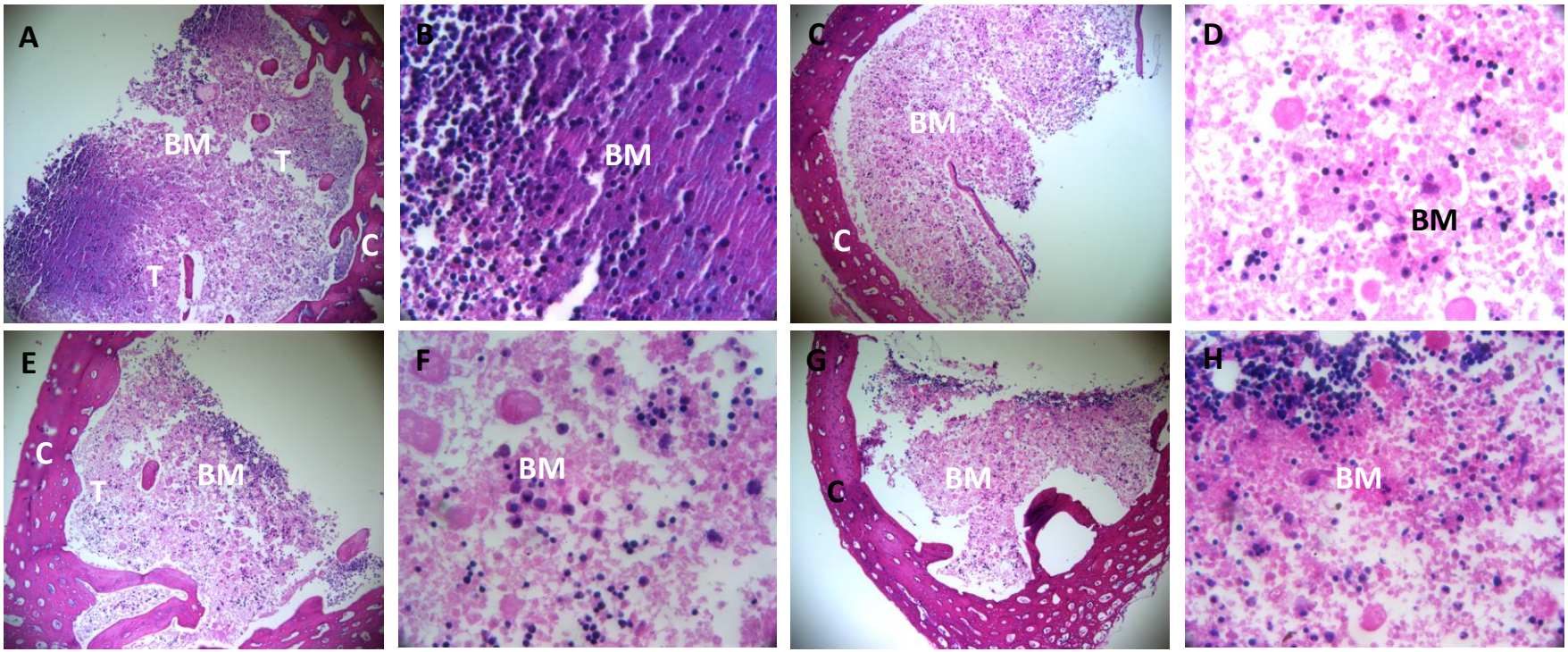

Supplementary Figure 1: Representative images at x100 and x600 magnification of haematoxylin and eosin stained tissue slices of Trowell-type cultures supplemented with either; 20 ng/mL M-CSF and 30 ng/mL RANKL over 24 h (A & B) and or 48 h (C & D) or with 40 ng/mL M-CSF and 60 ng/mL RANKL over 24 h (E & F) or 48 h (G & H). Images show the structure of the bone with pink eosin staining the cortical (C) and trabecular (T) bone along with haematoxylin stained bone marrow (BM) cell nuclei. White boxes display an area of ~20, 000 μm^2 area used for x600 magnification images. Scale bar equates to 100 μm^2 for both magnifications.

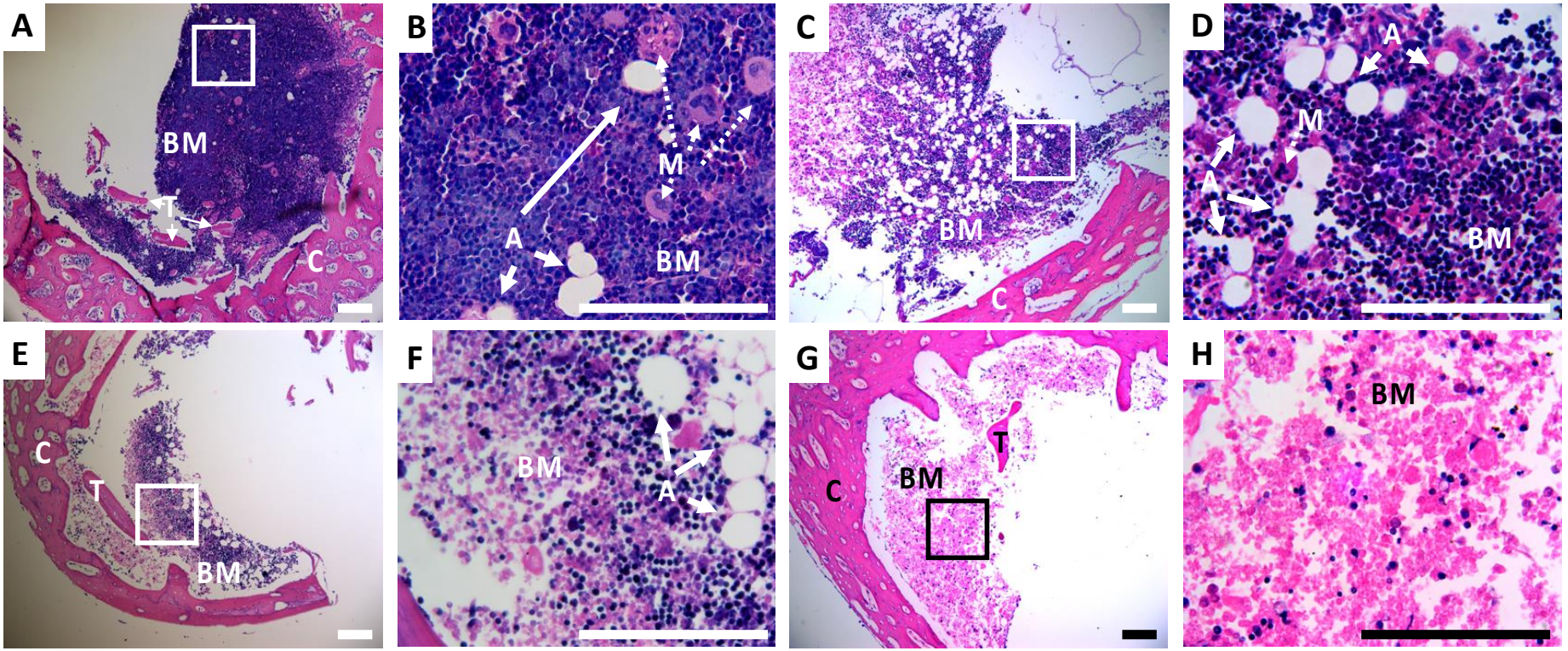

Supplementary Figure 2: Representative images of low (x100) and high (x600) magnification haematoxylin and eosin stained tissue slices of Trowell-type cultures microinjected with mixed bone marrow cells supplemented with 20 ng/mL M-CSF and 30 ng/mL RANKL over; 0 h (A and B), 24 h (C and D), 48 h (E and F) and 144 h (G and H). Images show structure of the bone with pink eosin staining the cortical (C) and trabecular (T) bone along with haematoxylin stained bone marrow (BM) cell nuclei. Within the bone marrow, adipose-like vacuoles (A) and megakaryocytes (M) can be seen. Scale bar equates to 100 μm^2 for both magnifications. Boxes display an area of ~20, 000 μm^2 area used for x600 magnification images.

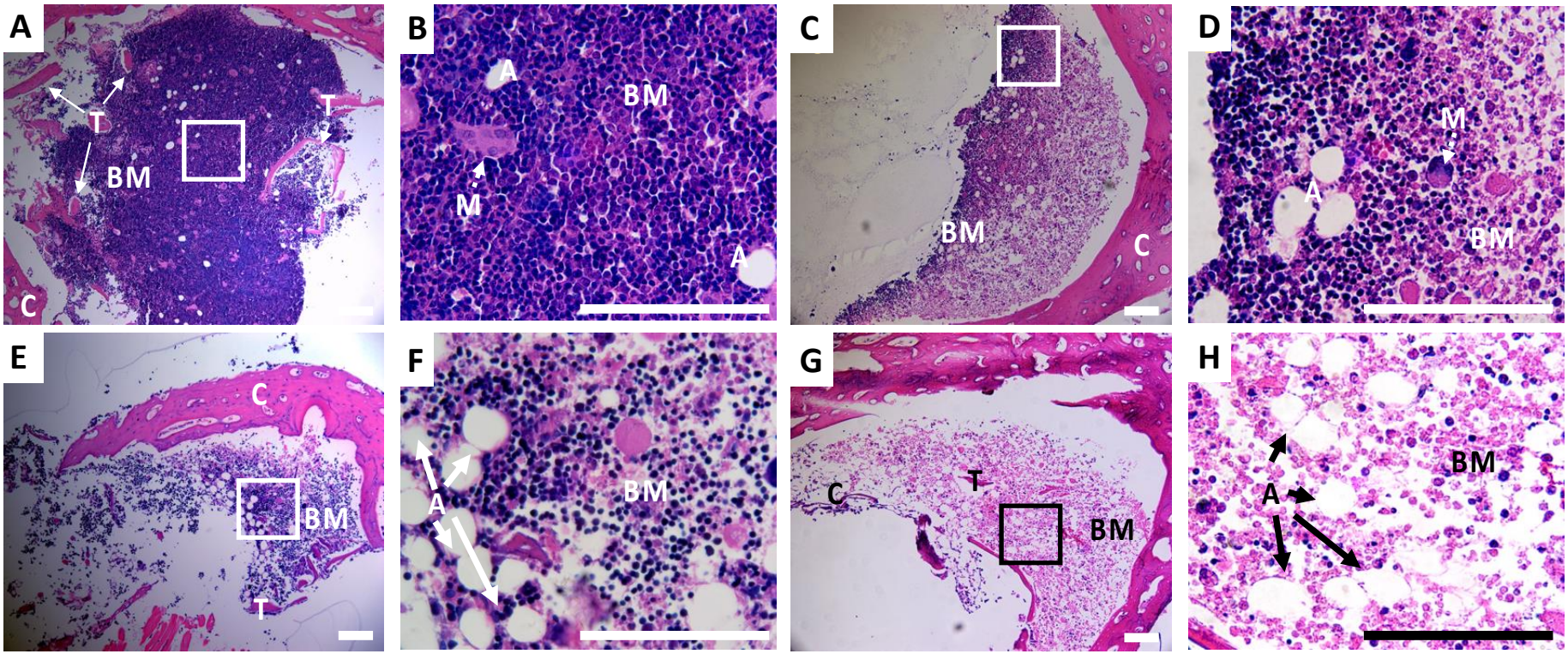

Supplementary Figure 3: Representative images of low (x100) and high (x600) magnification haematoxylin and eosin stained tissue slices of Trowell-type cultures microinjected with αMEM only supplemented with 20 ng/mL M-CSF and 30 ng/mL RANKL over; 0 h (A and B), 24 h (C and D), 48 h (E and F) and 144 h (G and H). Images show structure of the bone with pink eosin staining the cortical (C) and trabecular (T) bone along with haematoxylin stained bone marrow (BM) cell nuclei. Within the bone marrow, adipose-like vacuoles (A) and megakaryocytes (M) can be seen. Scale bar equates to 100 μm^2 for both magnifications. Boxes display an area of ~20, 000 μm^2 area used for x600 magnification images.

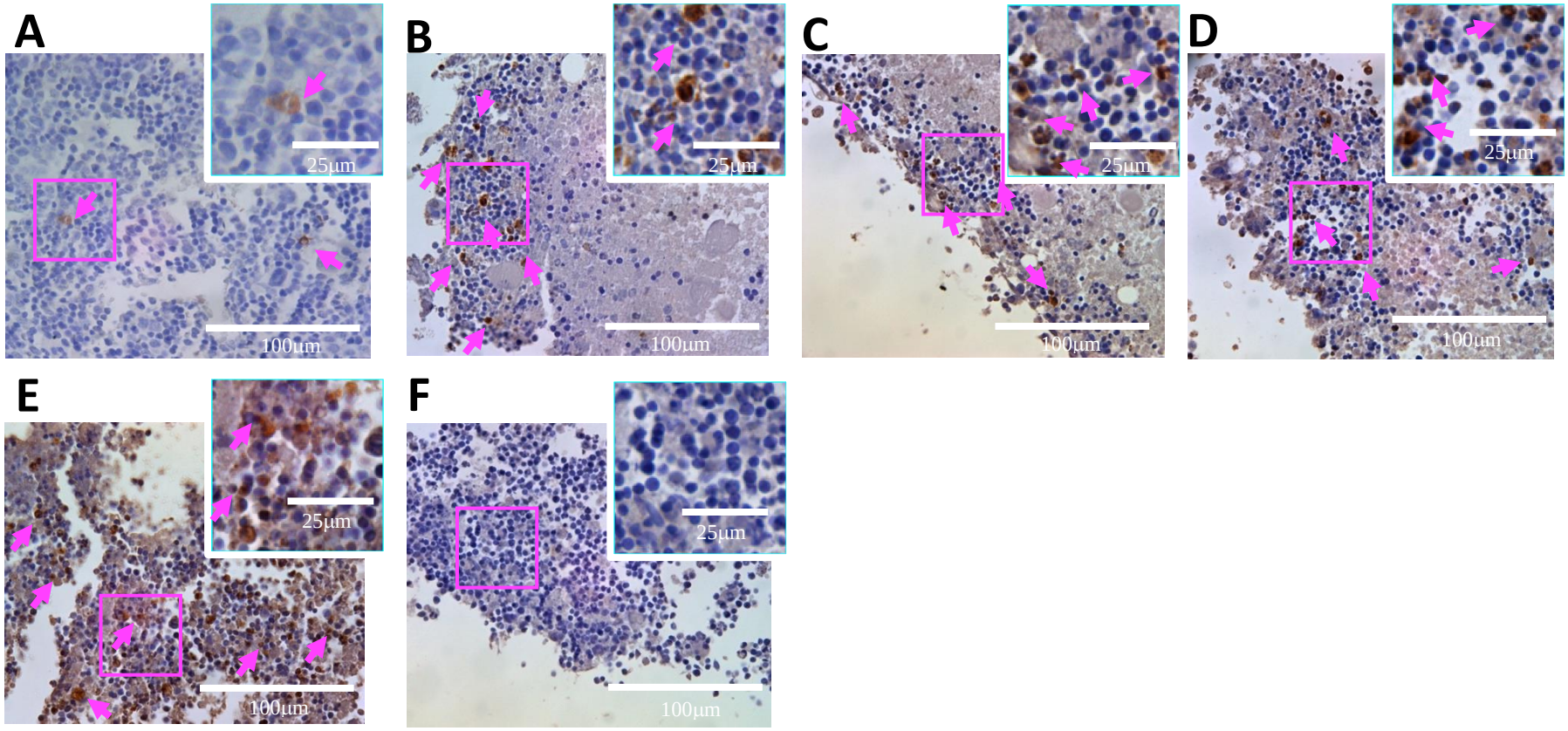

Supplementary Figure 4: Immunohistochemistry staining for cleaved caspase-3 labelled antibodies within the bone marrow of Trowell-type cultures supplemented with M-CSF and RANKL (examples indicated by arrows). 0 h uncultured controls (A), 20 ng/mL M-CSF and 30 ng/mL RANKL cultured at 24 h (B) or 48 h (C), 40 ng/mL M-CSF and 60 ng/mL RANKL cultured at 24 h (D) and 48 h (E) and a negative control by omitting the primary antibody and staining only the secondary antibody (F). Within images show 50 µm boxes display magnified areas of the bone marrow with positive cell labelling.

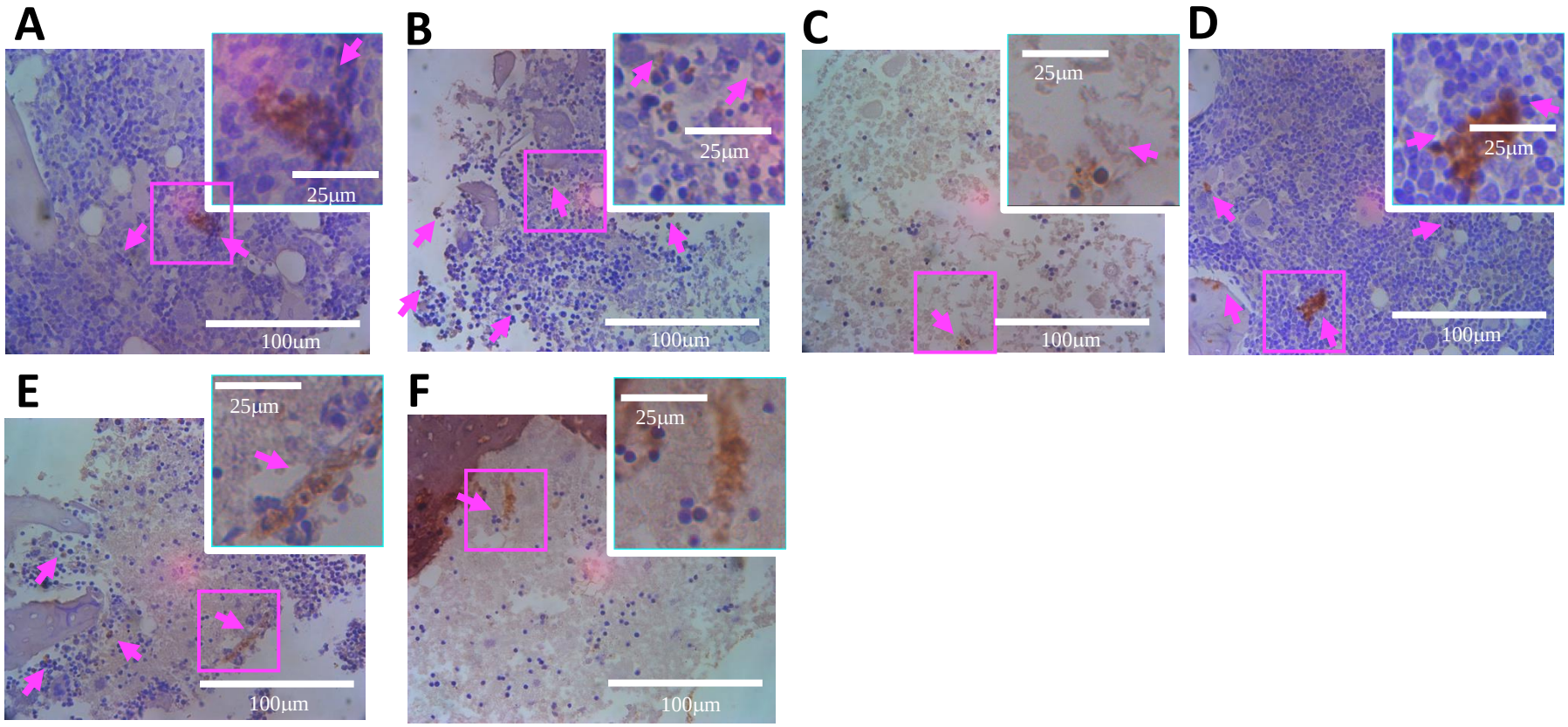

Supplementary Figure 5: Immunohistochemistry staining for cleaved caspase-3 labelled antibodies within the bone marrow Trowell-type cultured femoral slices microinjected with either mixed bone marrow cells (A-C) or αMEM sham injection (D-F) supplemented with 20 ng/mL M-CSF and 30 ng/mL RANKL over 48 h compared to uncultured 0 h controls (examples indicated by arrows). Images for mixed bone marrow microinjected slices for; 0 h (A), 24 h (B) and 48 h (C). Images for αMEM media only microinjected slices cultured at 0 h (D) 24 h (E) and 48 h (F). Within images show 50 µm boxes display magnified areas of the bone marrow with positive cell labelling.

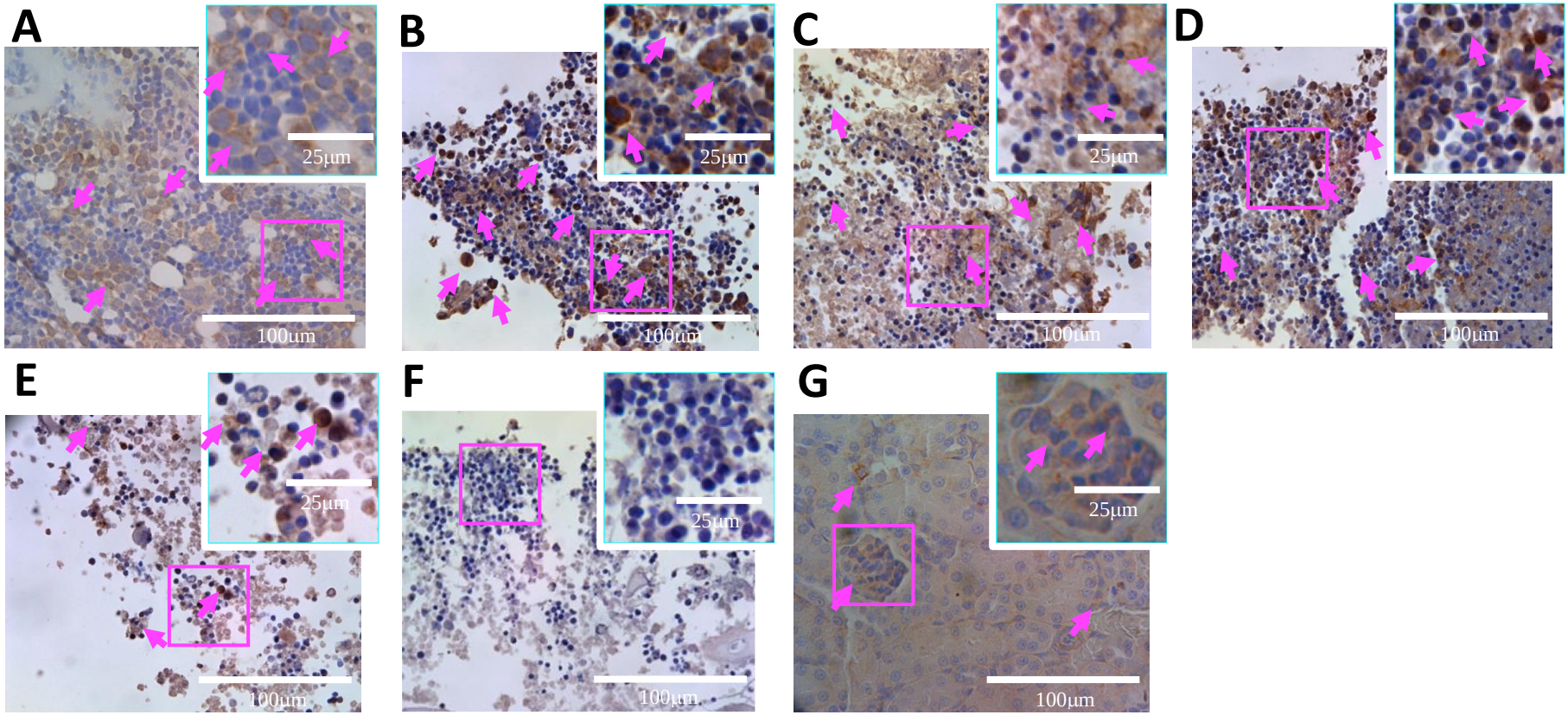

Supplementary Figure 6: Immunohistochemistry staining for BAX labelled antibodies within the bone marrow of Trowell-type cultures supplemented with M-CSF and RANKL (examples indicated by arrows). 0 h uncultured controls (A), 20 ng/mL M-CSF and 30 ng/mL RANKL cultured at 24 h (B) or 48 h (C), , 40 ng/mL M-CSF and 60 ng/mL RANKL cultured at 24 h (D) and 48 h (E), a negative control by omitting the primary antibody and staining only the secondary antibody (F) and (G) kidney positive control. Within images show 50 µm boxes display magnified areas of the bone marrow with positive cell labelling.

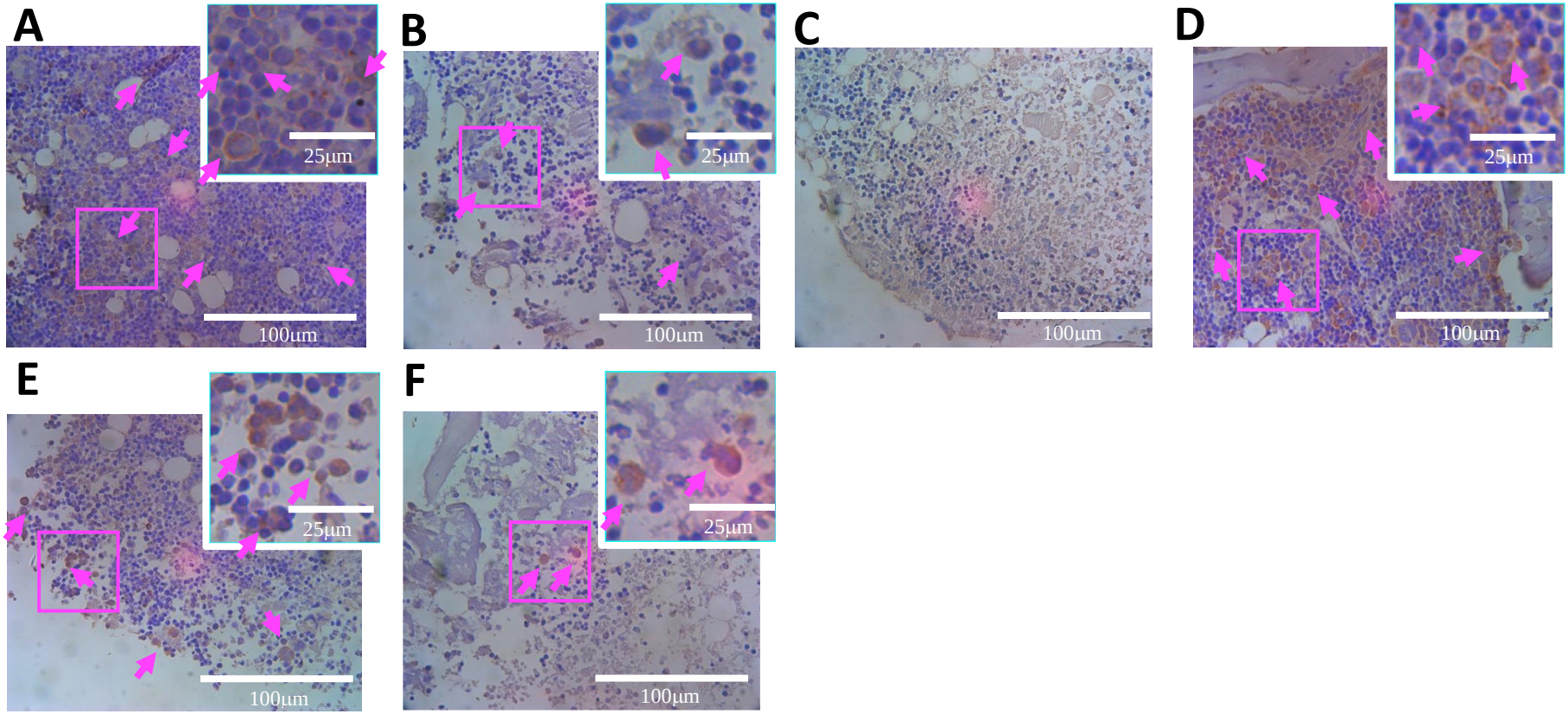

Supplementary Figure 7: Immunohistochemistry staining for BAX labelled antibodies within the bone marrow Trowell-type cultured femoral slices microinjected with either mixed bone marrow cells (A-C) or αMEM sham injection (D-F) supplemented with 20 ng/mL M-CSF and 30 ng/mL RANKL over 48 h compared to uncultured 0 h controls (examples indicated by arrows). Images for mixed bone marrow microinjected slices for; 0 h (A), 24 h (B) and 48 h (C). Images for αMEM media only microinjected slices cultured at 0 h (D) 24 h (E) and 48 h (F). Within images show 50 µm boxes display magnified areas of the bone marrow with positive cell labelling.

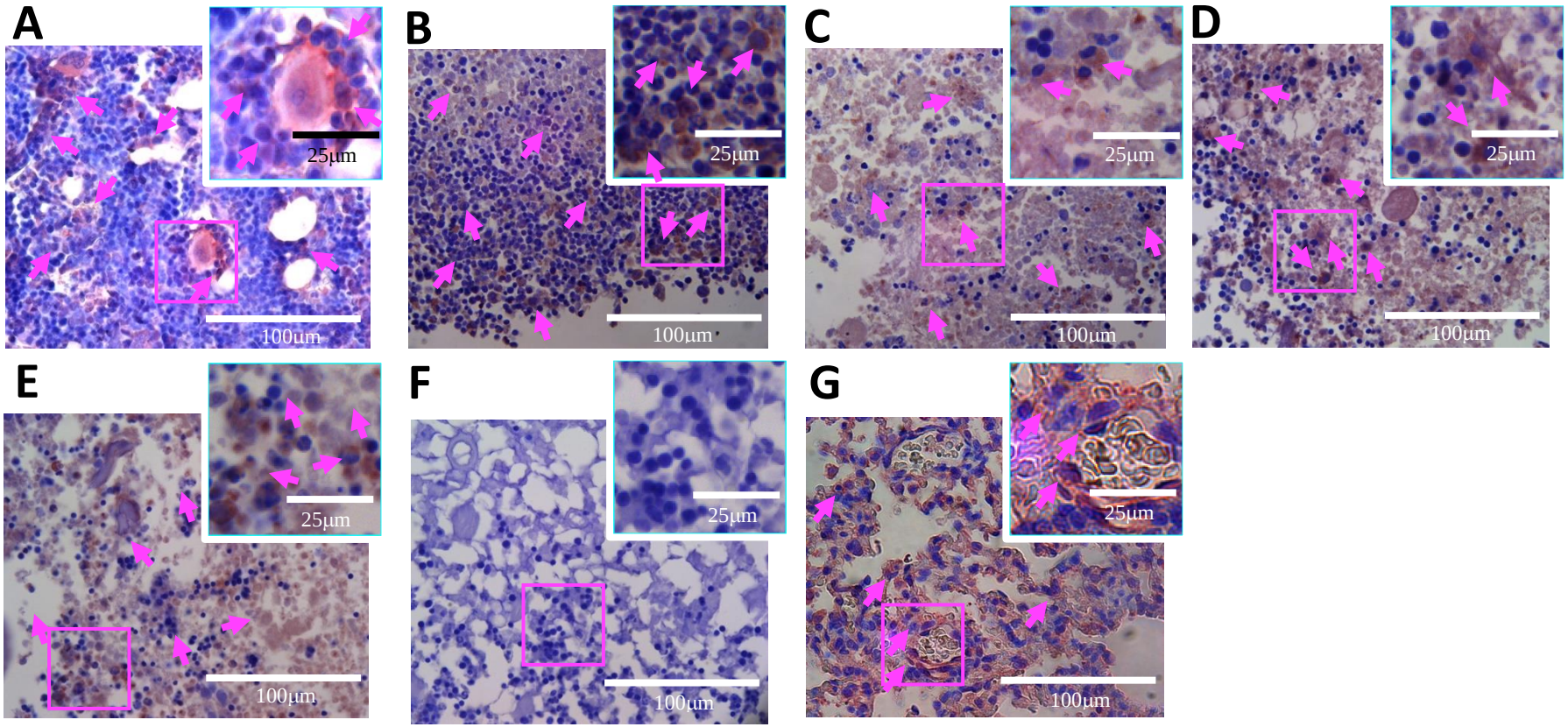

Supplementary Figure 8: Immunohistochemistry staining for $CD14^{+}$ labelled antibodies within the bone marrow of Trowell-type cultures supplemented with M-CSF and RANKL (examples indicated by arrows). 0 h uncultured controls (A), 20 ng/mL M-CSF and 30 ng/mL RANKL cultured at 24 h (B) or 48 h (C), , 40 ng/mL M-CSF and 60 ng/mL RANKL cultured at 24 h (D) and 48 h (E), a negative control by omitting the primary antibody and staining only the secondary antibody (F) and (G) rat lung positive control. Within images show 50 µm boxes display magnified areas of the bone marrow with positive cell labelling.

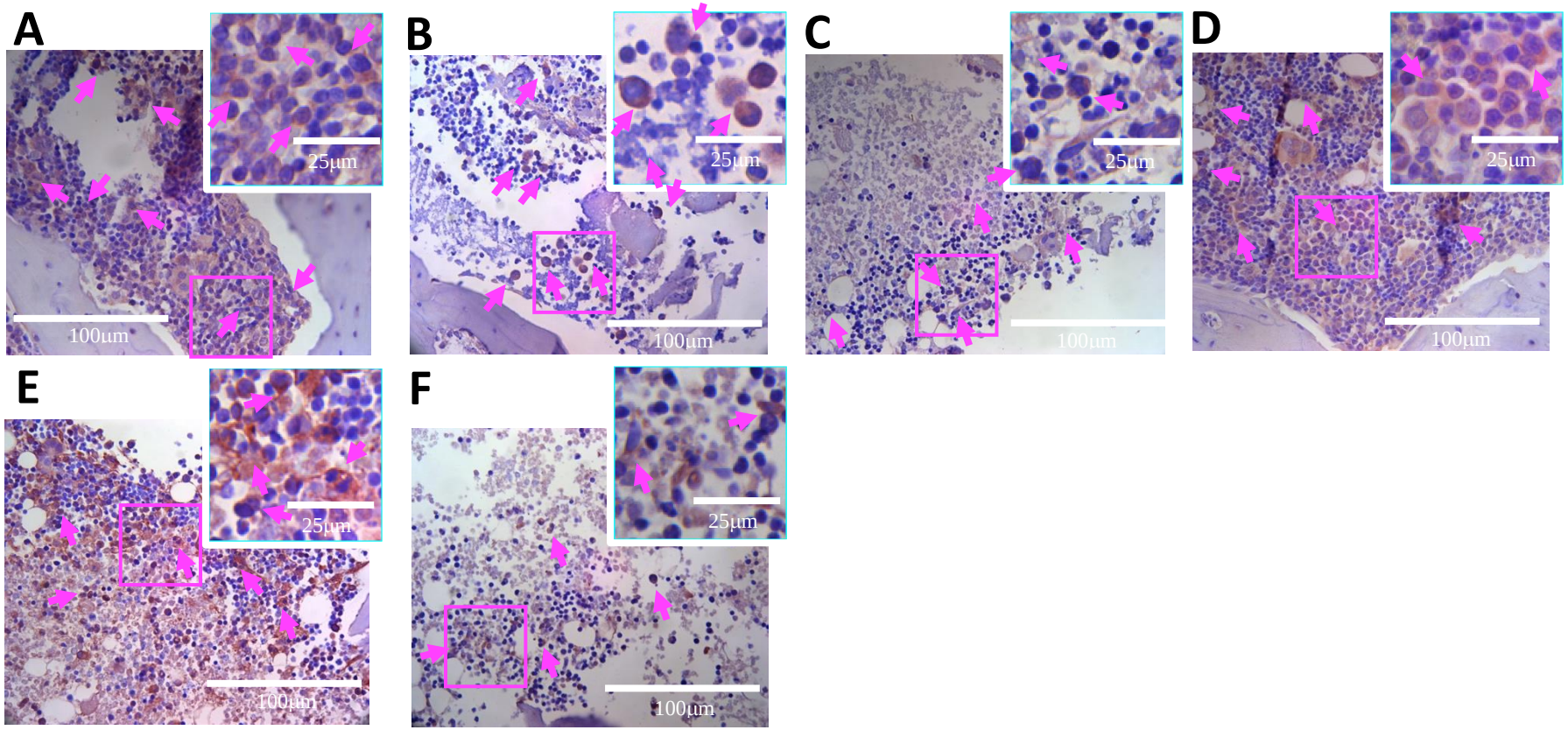

Supplementary Figure 9: Immunohistochemistry staining for $CD14^{+}$ labelled antibodies within the bone marrow Trowell-type cultured femoral slices microinjected with either mixed bone marrow cells (A-C) or αMEM sham injection (D-F) supplemented with 20 ng/mL M-CSF and 30 ng/mL RANKL over 48 h compared to uncultured 0 h controls (examples indicated by arrows). Images for mixed bone marrow microinjected slices for; 0 h (A), 24 h (B) and 48 h (C). Images for αMEM media only microinjected slices cultured at 0 h (D) 24 h (E) and 48 h (F). Within images show 50 µm boxes display magnified areas of the bone marrow with positive cell labelling.

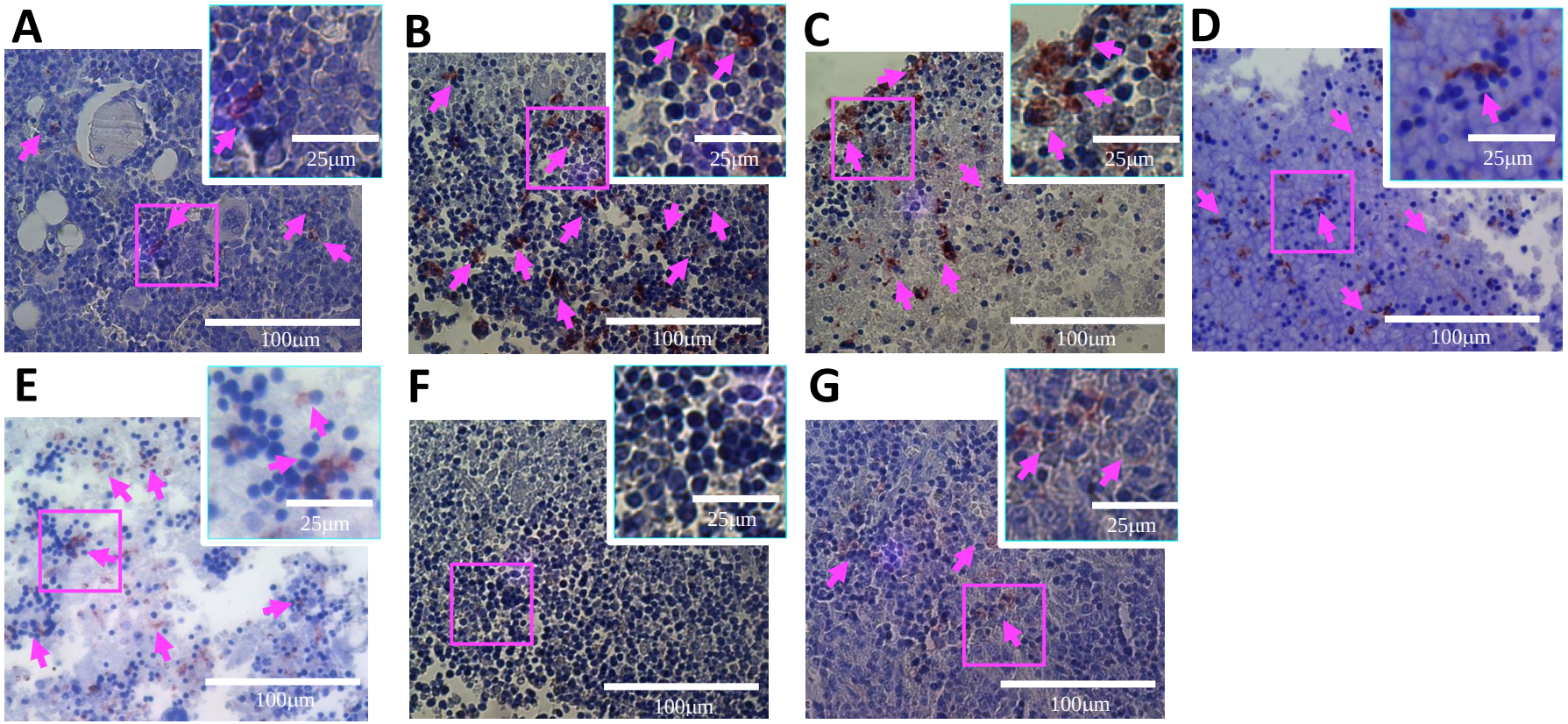

Supplementary Figure 10: Immunohistochemistry staining for CD68 labelled antibodies within the bone marrow of Trowell-type cultures supplemented with M-CSF and RANKL (examples indicated by arrows). 0 h uncultured controls (A), 20 ng/mL M-CSF and 30 ng/mL RANKL cultured at 24 h (B) or 48 h (C), , 40 ng/mL M-CSF and 60 ng/mL RANKL cultured at 24 h (D) and 48 h (E), a negative control by omitting the primary antibody and staining only the secondary antibody (F) and (G) rat spleen positive control. Within images show 50 µm boxes display magnified areas of the bone marrow with positive cell labelling

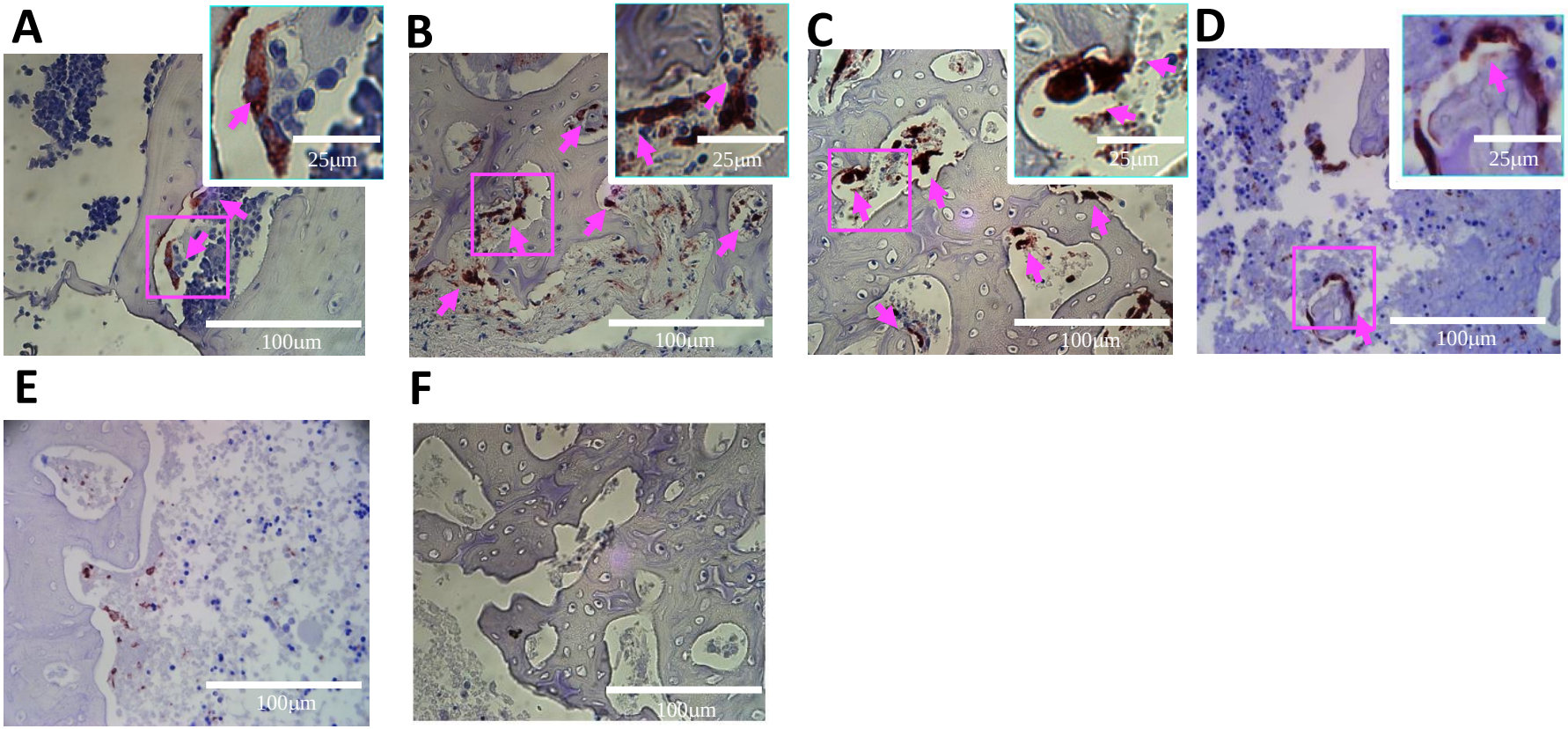

Supplementary Figure 11: Immunohistochemistry staining for CD68 labelled antibodies within the bone marrow of Trowell-type cultures supplemented with M-CSF and RANKL specifically for multinucleated premature or mature osteoclast-like cells (examples indicated by arrows). 0 h uncultured controls (A), 20 ng/mL M-CSF and 30 ng/mL RANKL cultured at 24 h (B) or 48 h (C), , 40 ng/mL M-CSF and 60 ng/mL RANKL cultured at 24 h (D) and 48 h (E) and a negative control by omitting the primary antibody and staining only the secondary antibody (F). Within images show 50 µm boxes display magnified areas of the bone marrow with positive cell labelling

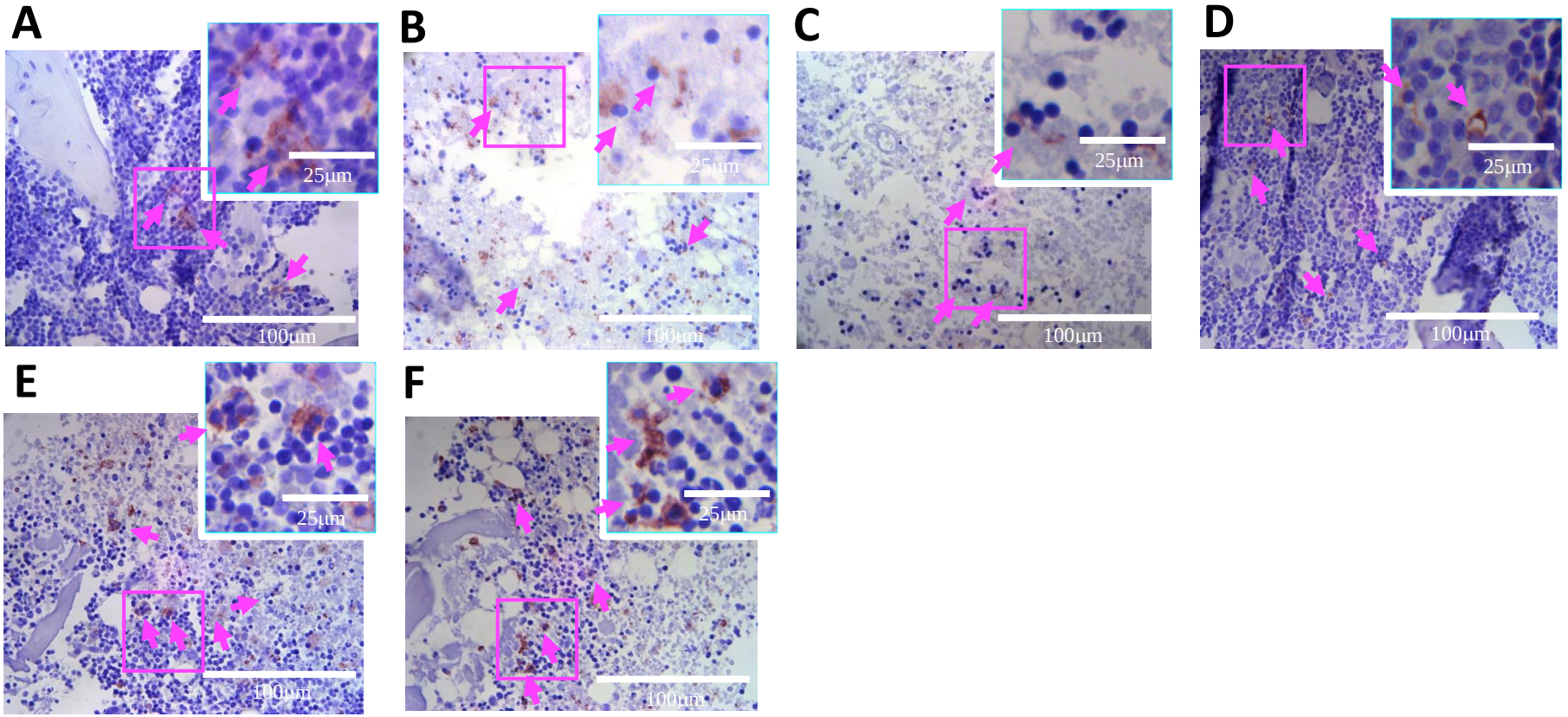

Supplementary Figure 12: Immunohistochemistry staining for CD68 labelled antibodies within the bone marrow Trowell-type cultured femoral slices microinjected with either mixed bone marrow cells (A-C) or αMEM sham injection (D-F) along with supplementation with 20 ng/mL M-CSF and 30 ng/mL RANKL over 48 h compared to uncultured 0 h controls (examples indicated by arrows). Images for mixed bone marrow microinjected slices for; 0 h (A), 24 h (B) and 48 h (C). Images for αMEM media only microinjected slices cultured at 0 h (D) 24 h (E) and 48 h (F). Within images show 50 µm boxes display magnified areas of the bone marrow with positive cell labelling.

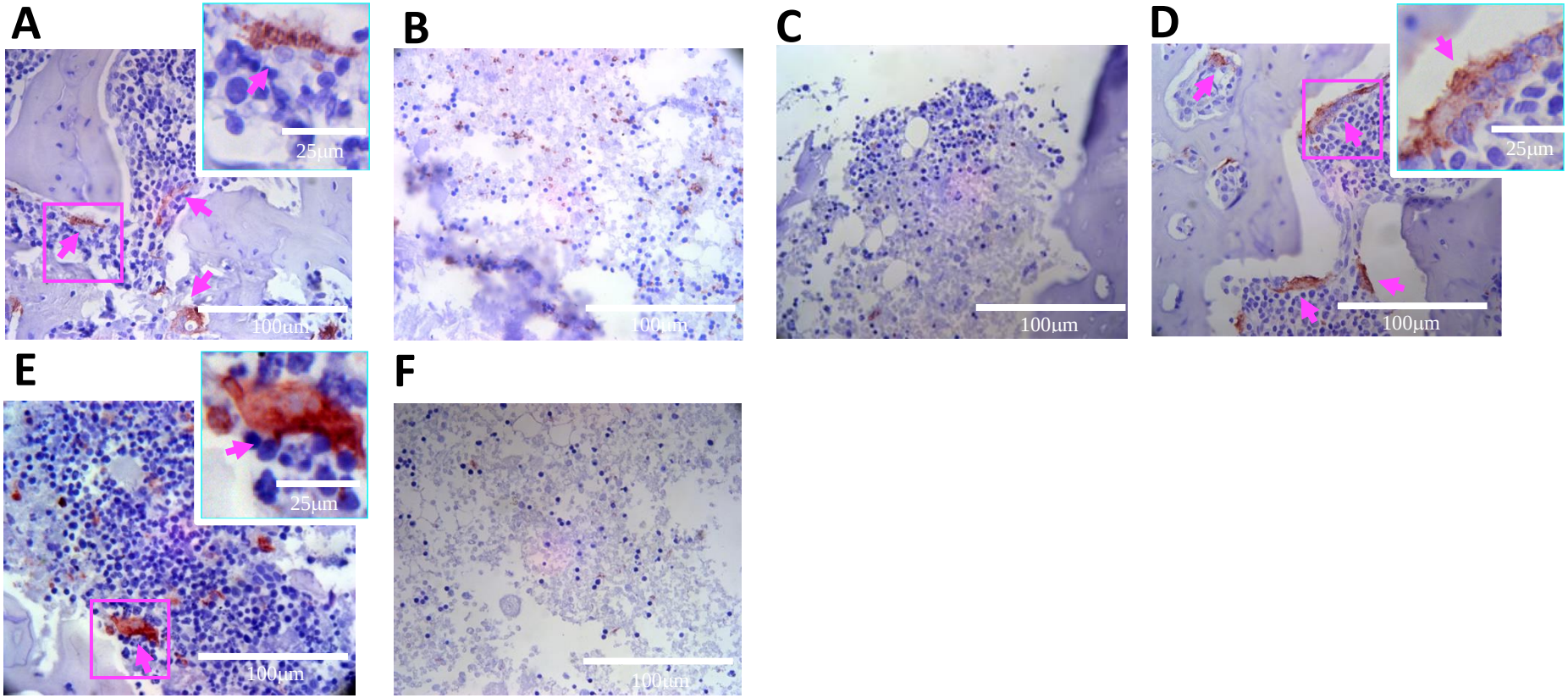

Supplementary Figure 13: Immunohistochemistry staining for CD68 multinucleated cells within the bone marrow Trowell-type cultured femoral slices microinjected with either mixed bone marrow cells (A-C) or αMEM sham injection (D-F) along with supplementation with 20 ng/mL M-CSF and 30 ng/mL RANKL over 48 h compared to uncultured 0 h controls (examples indicated by arrows). Images for mixed bone marrow microinjected slices for; 0 h (A), 24 h (B) and 48 h (C). Images for αMEM media only microinjected slices cultured at 0 h (D) 24 h (E) and 48 h (F). Within images show 50 µm boxes display magnified areas of the bone marrow with positive cell labelling.

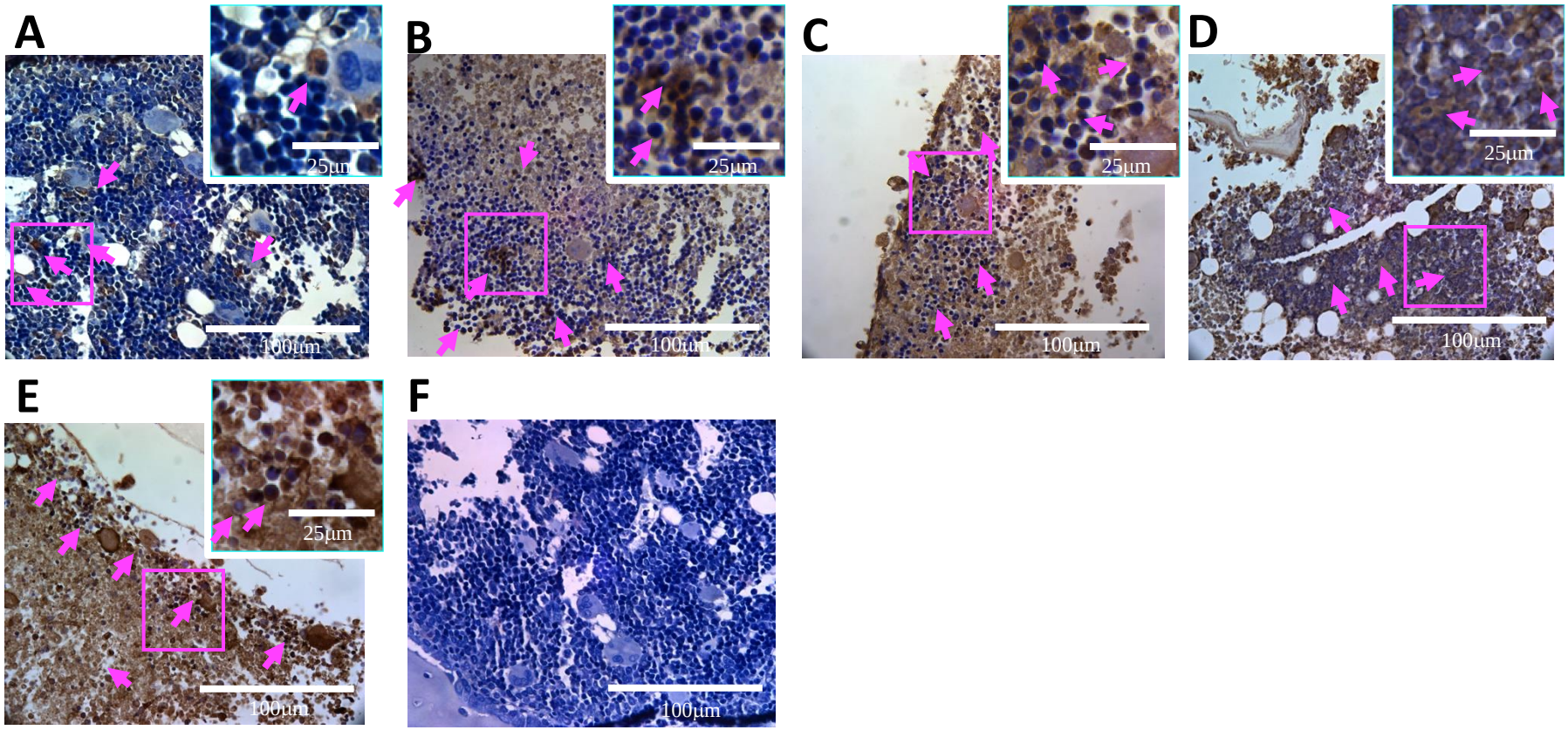

Supplementary Figure 14: Immunohistochemistry staining for CD73 labelled antibodies within the bone marrow of Trowell-type cultures supplemented with M-CSF and RANKL (examples indicated by arrows). 0 h uncultured controls (A), 20 ng/mL M-CSF and 30 ng/mL RANKL cultured at 24 h (B) or 48 h (C), 40 ng/mL M-CSF and 60 ng/mL RANKL cultured at 24 h (D) and 48 h (E) and a negative control by omitting the primary antibody and staining only the secondary antibody (F). Within images show 50 µm boxes display magnified areas of the bone marrow with positive cell labelling.

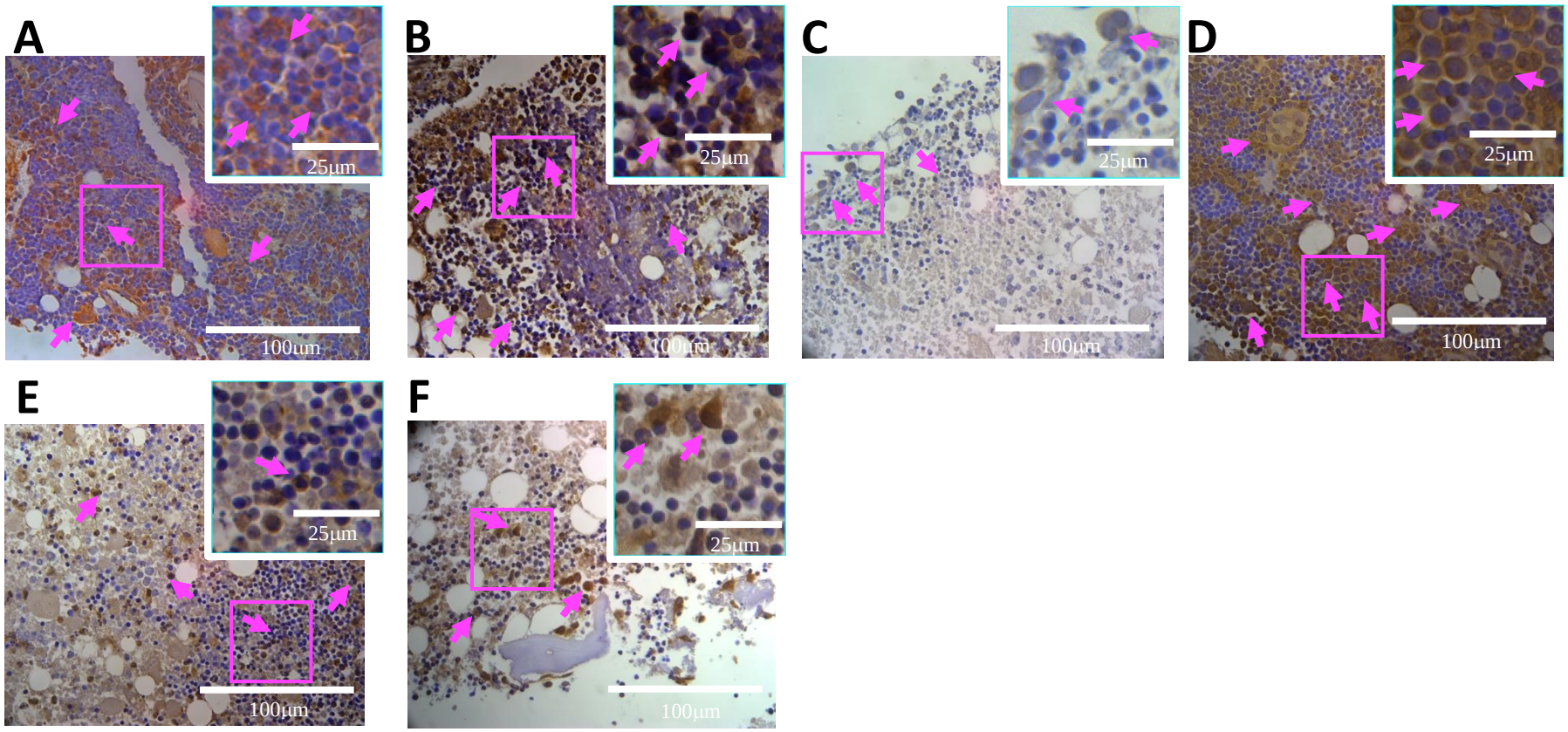

Supplementary Figure 15: Immunohistochemistry staining for CD73 labelled antibodies within the bone marrow Trowell-type cultured femoral slices microinjected with either mixed bone marrow cells (A-C) or αMEM sham injection (D-F) supplemented with 20 ng/mL M-CSF and 30 ng/mL RANKL over 48 h compared to uncultured 0 h controls (examples indicated by arrows). Images for mixed bone marrow microinjected slices for; 0 h (A), 24 h (B) and 48 h (C). Images for αMEM media only microinjected slices cultured at 0 h (D) 24 h (E) and 48 h (F). Within images show 50 µm boxes display magnified areas of the bone marrow with positive cell labelling.

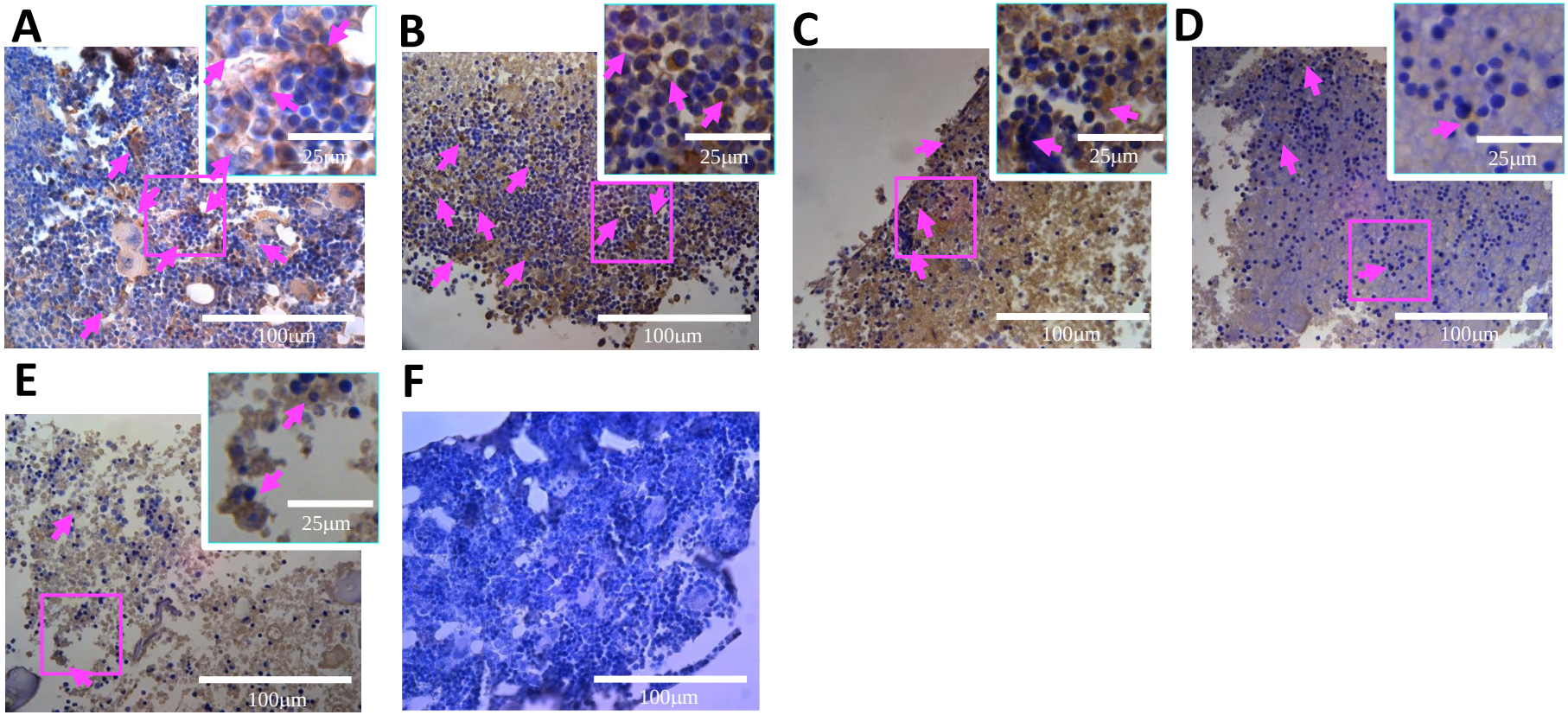

Supplementary Figure 16: Immunohistochemistry staining for CD105 labelled antibodies within the bone marrow of Trowell-type cultures supplemented with M-CSF and RANKL (examples indicated by arrows). 0 h uncultured controls (A), 20 ng/mL M-CSF and 30 ng/mL RANKL cultured at 24 h (B) or 48 h (C), 40 ng/mL M-CSF and 60 ng/mL RANKL cultured at 24 h (D) and 48 h (E) and a negative control by omitting the primary antibody and staining only the secondary antibody (F). Within images show 50 µm boxes display magnified areas of the bone marrow with positive cell labelling.

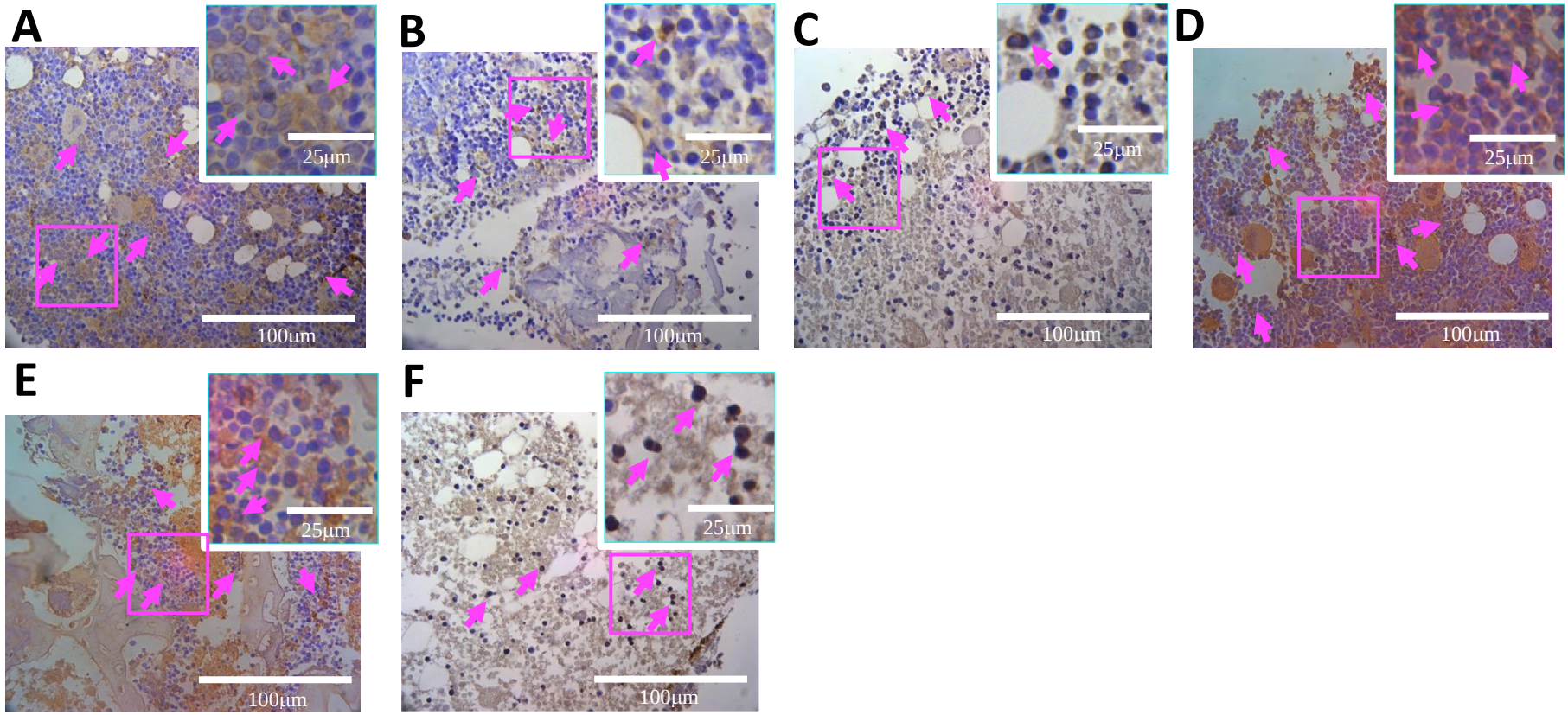

Supplementary Figure 17: Immunohistochemistry staining for CD105 labelled antibodies within the bone marrow Trowell-type cultured femoral slices microinjected with either mixed bone marrow cells (A-C) or αMEM sham injection (D-F) supplemented with 20 ng/mL M-CSF and 30 ng/mL RANKL over 48 h compared to uncultured 0 h controls (examples indicated by arrows). Images for mixed bone marrow microinjected slices for; 0 h (A), 24 h (B) and 48 h (C). Images for αMEM media only microinjected slices cultured at 0 h (D) 24 h (E) and 48 h (F). Within images show 50 µm boxes display magnified areas of the bone marrow with positive cell labelling.

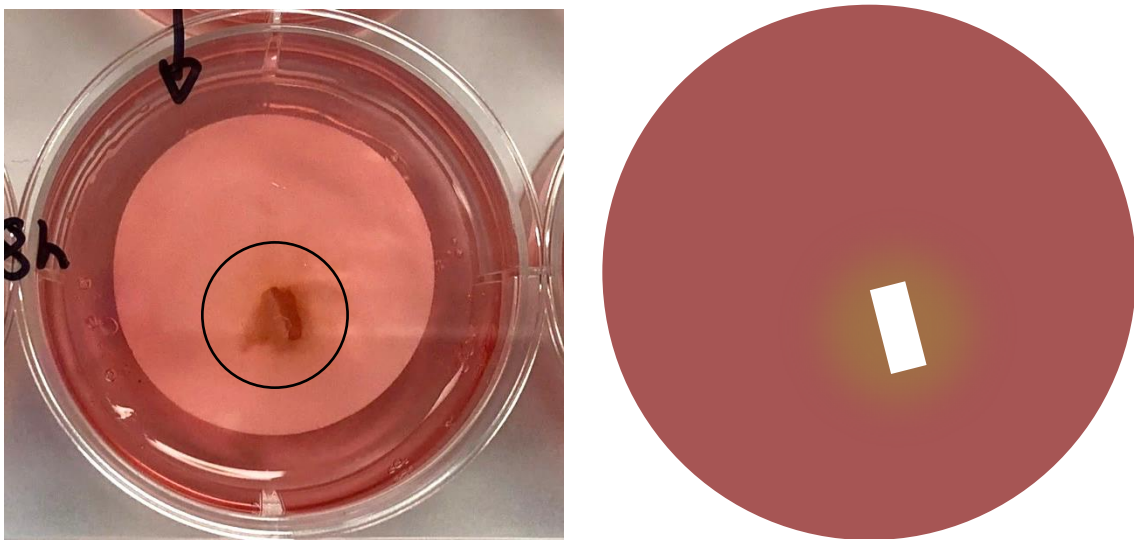

Supplementary Figure 18: Image and graphical illustration of the diffusion of oxygen or nutrients around the bone slice embedded within the agarose gel. Following culture for 24 h and 48 h, a small area surrounding the bone had a slightly acidic pH (yellow circle), this colour change is indicative of hypoxia, where the pH drops when oxygen is low.

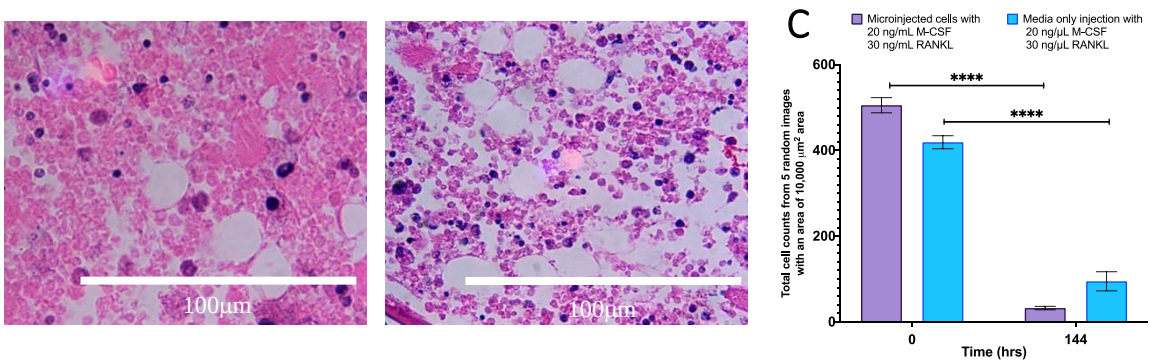

Supplementary Figure 19: Representative image high (x600) magnification and total cell counts of haematoxylin and eosin-stained femoral slices of Trowell-type cultures at 144 h culture supplemented with 20 ng/mL M-CSF and 30 ng/mL RANKL with or without the addition of mixed tibial bone marrow cells. Images indicate loss of cells within the bone marrow cavity along with the retention of pink extracellular matrix-like construct for A) femoral slices with 20 ng/mL M-CSF and 30 ng/mL RANKL with the addition of mixed tibial bone marrow cells and B) femoral slices with 20 ng/mL M-CSF and 30 ng/mL RANKL without the addition of mixed tibial bone marrow cells. C) graphs indicating the total cell counts of 0 h and 144 h cultures, indicating significant loss of cells after 144 h of culture. Error bars display S.E.M with statistical analysis calculated using two-way ANOVA followed by Tukey's post-test. Significant values were only plotted ****$P < 0.0001$.

Appendix II

Supporting documentation for Chapter 4

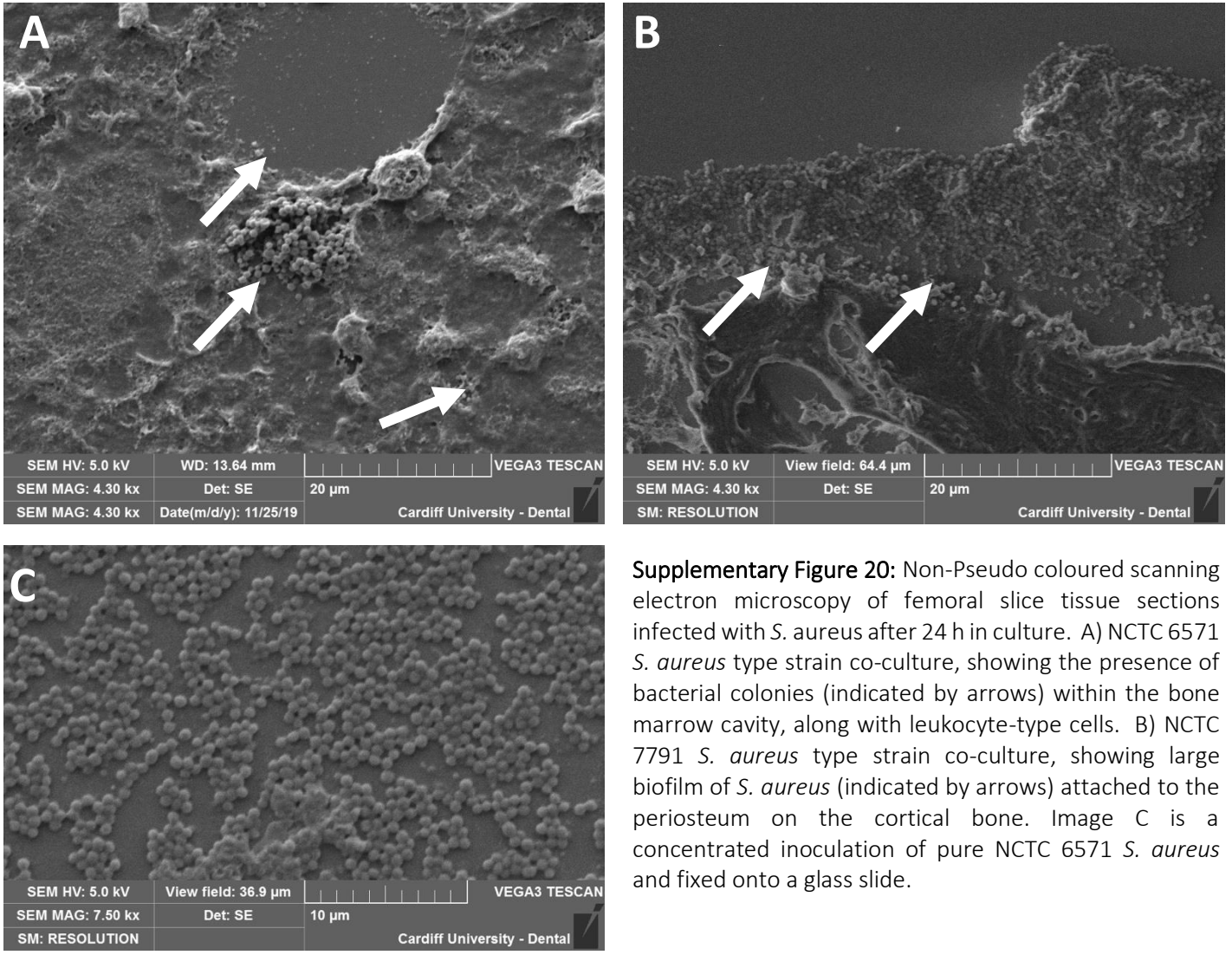

Supplementary Figure 20: Non-Pseudo coloured scanning electron microscopy of femoral slice tissue sections infected with *S.* aureus after 24 h in culture. A) NCTC 6571 *S. aureus* type strain co-culture, showing the presence of bacterial colonies (indicated by arrows) within the bone marrow cavity, along with leukocyte-type cells. B) NCTC 7791 *S. aureus* type strain co-culture, showing large biofilm of *S. aureus* (indicated by arrows) attached to the periosteum on the cortical bone. Image C is a concentrated inoculation of pure NCTC 6571 *S. aureus* and fixed onto a glass slide.